Sixth International Oil Sands Tailings Conference

Edmonton, Alberta, Canada: December 9-12, 2018

U of A Geotechnical Centre

IOSTC

SIXTH INTERNATIONAL

OIL SANDS

TAILINGS CONFERENCE

Edmonton, Alberta
Canada

December 2018

Proceedings of the Sixth International Oil Sands Tailings Conference

9-12 December 2018, Edmonton, Alberta, Canada

Sixth International Oil Sands Tailings Conference

Edited by

Nicholas A. Beier, G. Ward Wilson & David C. Sego

University of Alberta Geotechnical Centre and
Oil Sands Tailings Research Facility

University of Alberta Geotechnical Centre Edmonton, Alberta, Canada

Published by: University of Alberta, Dept. of Civil & Environmental Engineering

ISBN 978-1-55195-426-4
Printed in Canada

FORWARD

It is with great pleasure that we present the **Sixth International Oil Sands Tailings Conference 2018 (IOSTC'18)**. There have been several sweeping changes in the management of oil sands tailings since the First International Oil Sands Tailings Conference held 10 years ago in 2008. **IOSTC'08** offered an industrial and regulatory perspective on the needs for tailings research and management. In response to Directive 074 issued by the Energy Resources Conservation Board (ERCB, now Alberta Energy Regulator (AER)) in 2009, **IOSTC'10** focused on presenting technologies and approaches to meet the provincial regulator's tailings criteria and requirements for the oil sands industry. Two years later, **IOSTC'12** provided a venue to present the Oil Sands Tailings Technology Deployment Road Map prepared by the Consortium of Tailings Management Consultants (CMTC) on behalf of Alberta Innovates – Environment and Energy Solutions (AI-EES) and the Oil Sands Tailings Consortium (OSTC, now Canada's Oil Sands Innovation Alliance (COSIA)). At **IOSTC'14**, Alan Fair provided observation on the development of tailings management from his 30-year career in the oil sands industry, and we debuted the research program from the NSERC/COSIA Senior Industrial Research Chair in Oil Sands Tailings Geotechnique held by Dr. G. Ward Wilson at the University of Alberta**.** At our milestone fifth **IOSTC'16**, we were privileged to have the Alberta Energy Regulator provide a comprehensive overview of what was then its newest regulation, Directive 085.

The aim of **IOSTC'18** is to provide a further exchange of information between the people responsible for managing the oil sands tailings: researchers and providers of tailings management services who have experience with this industry. **IOSTC'18** has received strong support by the authors who have submitted a significant number of manuscripts, the exhibitors who continue to support the conference in these trying economic times and most importantly by our sponsors who recognize the important contribution of this conference to meeting the challenges presented by oil sands tailings to the environment and the viability of this most important Alberta industry.

We want to personally thank members of the OSTRF for their encouragement and support. The conference would not have been possible without the dedication of Vivian Giang, Jen Stogowski, Elena Zabolotnii and especially Sally Petaske who provided so much assistance and leadership.

The technical challenges associated with fluid fine tailings (FFT), including legacy mature fine tailings (MFT), require novel and innovative approaches to ensure the sustainable development and environmental stewardship of Alberta's vast oil sands. It was with this in mind that the session themes and manuscripts were selected for presentation and inclusion in the proceedings. We want to thank our professional colleagues who willingly contributed their technical knowledge, experiences and especially their time to write the manuscripts that make the proceedings of this conference. May you find further insights to enhance your understanding of the current state-of-practice in oil sands tailings management through **IOSTC'18**.

Nicholas A. Beier, G. Ward Wilson and David C. Sego
Co-Chairs, IOSTC 2018 Organizing Committee

Thank you to the following sponsors for their support in making the Sixth International Oil Sands Tailings Conference a huge success:

OSTRF

The UofA Geotechnical Centre

University of Alberta

PLATINUM SPONSORS:

CONETEC

GOLD SPONSORS:

Alfa Laval Inc.

BGC

HAYWARD BAKER WICK DRAINS
A DIVISION OF CYNTECH

THURBER ENGINEERING LTD.

SILVER SPONSORS:

AGAT Laboratories

GREGG
GEOTECH DRILLING - GROUP OF COMPANIES

TABLE OF CONTENTS

SESSION 4: TAILINGS DEPOSIT CHARACTERIZATION

SESSION 5: IMPLICATIONS OF TAILINGS TREATMENT

SESSION 6: TAILINGS CHARACTERIZATION

SESSION 7: UTILIZING NATURE FOR TAILINGS DEWATERING

SESSION 8: REGULATORY

SESSION 9: TAILINGS MANAGEMENT

SESSION 10: PHYSICAL MODELING OF OIL SAND TAILINGS

SESSION 11: TAILINGS TREATMENT PROCESSES

SESSION 12: SAND CAPPING OF OIL SAND TAILINGS DEPOSITS

Session 1

TAILINGS TREATMENT PROCESSES

EFFECTIVE DEWATERING OF FLUID FINE TAILINGS (FFTS) BY IONIC LIQUIDS

Zohrab Ahmadi[1], Paula Berton[1,2], Yuyan He[1], Robin D. Rogers[2] and Steven L. Bryant[1,2]
[1]University of Calgary, Calgary, Canada
[2]CalAgua Innovations Corp., Calgary, Canada

ABSTRACT

We synthesized a series of ionic liquids (IL) initially for dewatering of mature fine tailings (MFT). Cationic and anionic counterparts of IL were modified to impart desired degrees of hydrophobicity and hydrophilicity. The tailored ionic liquid (IL1) is able to destabilize suspended clays and hence cause dewatering quite rapidly after mixing with MFT. A comprehensive study on MFT showed the effect of mixing energy (IL1 and MFT mixture) and various dewatering process such as centrifugation, gravitation, and filtration. The result shows the compatibility of IL1 for process development in the field suggesting a new and effective path for tailing remediation. Herein, we briefly demonstrate the extension to Fluid Fine Tailings (FFT) as the precursor of MFT composite. Formation of large flocs, neutralization of clay particles inferred from zeta potential analysis, and fast water release illustrate the IL1 resilience for variable tailing compositions. This finding is the basis for a novel, rapid, and low energy reclamation process, which suggests further process development for treatment of various oil sands tailings in field applications.

INTRODUCTION

Background

Canada's oil sands represent one of the largest unconventional oil reserves of the world. Currently, the major oil sand extraction methods include surface mining and in situ recovery (Nasr & Ayodele 2005). In mining, hot water is mixed with oil sands ore, hydro transported, followed by flotation separation. This process generates tailings as byproducts, composed of water, bitumen, and solids (mostly sand, enriched in fine and clays). During the mine operation, tailings are stored in containment areas known as tailing ponds. While the larger mineral particles such as sand settle rapidly and form beaches, the composition of negatively charged clays, residue bitumen and fine minerals form a rather stable fluid known as fluid fine tailings (FFT) with variable solid composition. By passage of time a mature form of tailing is formed with around 30% solid which stays stable for long period of time and is known as mature fine tailings (MFT). Based upon the most recent report from Alberta Energy Regulator (AER), in 2016 there are over 30 active ponds from operating oil sands mining projects storing over 1000 Mm^3 of fluid tailings (AER 2018).

Currently, several technologies are used to minimize the volume of produced tailings from oil sands mining extraction, including centrifugation, composite tailing, freeze-thaw drying, and thin lift (Kasperski & Mikula 2011, Proskin et al. 2010). What is common among all these techniques is the necessity of inserting additives to the process (Hripko 2018). The most common industry additive in the tailing remediation is polymer flocculant.

Anionic polyacrylamide (PAM) with high molecular weight is the standard polymer widely used in this industry and hence widely studied (Cong & Pelton 2003, Vedoy & Soares 2015). However, the formed flocs are not coherent and retain considerable amount of water. The presence of a large amount of water decreases the shear strength of composition and hence reclamation is not immediate. Hence, various modification and functionalization of PAM are undertaken to enhance the mechanical properties of the resulting flocs (Li et al. 2017, Reis et al. 2016, Wang et al. 2014).

As alternative, we have designed and synthesized an ionic liquid (ILs, organic salts with melting points below 100 °C (Welton 1999, Wilkes 2002)) for MFT treatment. The tailored IL1 reduces the water content significantly immediately after mixing with MFT. Its interaction with MFT was examined at variable conditions (e.g., concentration of IL1, mixing rates, filtration, centrifugation, gravity settling, etc.) Our investigation on the mechanism of dewatering of MFT in the presence of IL1 shows a novel path of operation which cannot be obtained by polymer or coagulant additions alone.

In addition, the interaction of IL with the water shows that the water holds a proper quality with extremely low suspended particles at optimized conditions.

The tailored IL shows a great potential to replace PAMs in the dewatering process. The rate of water discharge of MFT in the presence of IL1 is orders of magnitudes faster than that of PAM at optimized conditions.

However, even when we have demonstrated its effect for MFT treatment, a question remains whether this IL will also show good performance for FFT treatment. In this work, we aim to compare the performance of IL1 for MFT vs. FFT dewatering treatment.

EXPERIMENTS

Sample Characterization

MFT sample was received from Alberta Innotech (Calgary, AB, Canada), while the FFT sample was donated by a third-party company in Calgary (AB, Canada) and the source of sample is unknown. The composition of MFT and FFT was determined using the Dean-Stark method (Dean & Stark 1920). Water samples of the untreated MFT and FFT samples were obtained after centrifugation (4000 rpm, 10 min) of the samples, followed by filtration using a 0.2 μm filter (Durapore PVDF membrane filter). The filtrate samples were used for pH (Orion Star™ A215, Thermo Scientific™ Calgary, AB, Canada) and conductivity (SevenCompact S220/S230, Mettler Toledo, Mississauga, ON, Canada) determinations and for elemental analysis using an inductively coupled plasma mass spectrometry (ICP-MS, 8900 Triple Quadrupole ICP-MS, Agilent Technologies, Santa Clara, CA, USA).

The statistics of particle size distribution of untreated MFT and FFT were obtained by wet analysis method using Laser Diffraction Particle Size Distribution Analyzer (LD-PSD, Beckman Coulter, LS 13 320).

The electrokinetics of different clays was examined using a Zeta/Nano Particle Analyzer (NanoPlus HD, Particulate Systems, Norcross GA, USA). Original MFT and FFT were diluted to about 0.7 wt% solid in the water for zeta potential measurement. Given that the zeta potential value depends on the viscosity of diluted sample, the viscosity of the diluted samples was measured using a viscometer (DV2T EXTRA, Brookfield AMETEK, Middleboro, MA, USA).

A floor-model powder X-ray diffraction (XRD) instrument (Multiflex, Rigaku, Scottsdale, AZ, USA) was used for minerals and clays characterization on the solid phase of untreated MFT and FFT samples. Samples were dried at room temperature for one week and disintegrated using a mortar and pestle to obtain a fine powder. For data collection, the angle range was from 3 to 70 (2theta), the scan rate was 2 degrees/min, and the voltage, current, and power were 40 kV, 20 mA, and 0.8 kW, respectively. The Jade software (MDI Jade 2010, Version 5.5.5) was used for identification and quantification of the mineral phases.

Tailings Treatment Methods

For the treatment of MFT and FFT with IL1, 100 g of each tailings sample was placed into a baffled beaker (250 mL). Further, 8.4 mmol of IL1 was added; previous work has shown this mass of IL1 produces the maximum water recovery. An overhead mixer stirred (Fisherbrand™, Fisher Scientific, Nepean, ON, Canada) the mixture for 12 min at 500 rpm. The viscosity of the samples increased immediately after mixing, suggesting a quick interaction of IL1. Samples turn to a pasty mixture quite distinct from the thin slurry of the untreated tailings.

Subsequently, water was separated by either centrifugation (Eppendorf™ 5810R, Fisher Scientific) for 5 min at 500, 1600, and 4000 rpm (53, 544, and 3340 x *g*, respectively) or vacuum filtration at room temperature (21 °C). The later was done using a Büchner filtration (Büchner flask and funnel) and a 2.5 μm pore size filter (Whatman). In both methods, water was quantified gravimetrically and kept for quality measurement.

The relative percentage of water released was calculated as the amount of the aqueous phase released divided by the total amount of water in the given amount of the tailings sample.

RESULTS AND DISCUSSION

Samples of MFT and FFT were received and characterized. When their compositions are

compared (Table 1), the first notable difference is observed in the higher amount of bitumen present in MFT, while the solid and water content and pH are similar. The second difference is the conductivity of the samples; the conductivity of the MFT aqueous phase is 10 times higher than that of the FFT, difference generated by the higher concentration of ion, mainly Na^+ and Cl^-, in MFT.

The composition of the solids of the untreated MFT and FFT samples was analyzed using XRD (Table 1) and indicates major difference in minerals and clay minerals in the structures of MFT and FFT. The FFT shows larger amounts of quartz and kaolinite, but much less quantity of illite. The latter has high surface area and surface charge, and its abundance possibly would contribute to the greater stability of MFT compared to FFT.

Table 1. Compositions, water chemistry, and mineralogy of untreated MFT and FFT

	Untreated MFT	*Untreated FFT*
Bitumen (wt%)	5.4	0.5
Solids (wt%)	25.3	31
Water (wt%)	69	69
pH	8.1	8.3
Conductivity (µS)	2.6	0.25
Element (mg/L)		
Na^+	659	40
K^+	15	6
Mg^{2+}	11	7
Ca^{2+}	11	14
Al^{3+}	1	0.03
Cl^-	1260	58
Solid phase (wt%)		
Quartz	30.5	37.5
Kaolinite	27.7	42.3
Illite	35.1	10.8
Siderite	3.9	-
Orthoclase	2.0	5.4
Pyrite	0.8	-
Albite	-	3.9

The particle size of clay minerals and their high surface charge are the key in the stability of the tailing components (Long et al. 2006). A comparison of the statistics of particle size distribution of untreated MFT and FFT (Table 2) indicates that in both cases all the particles present are below 44 µm. Although the mode of the samples is the same, all other values including the d10, d90, mean, and median show differences. Overall, FFT is slightly finer in particle size with mean value of 4 µm as compared with MFT with 9 µm. The zeta potential values for MFT and FFT were -61 and -69 mV, respectively, showing high surface charge in both matrices.

Table 2. Statics of particle size distribution untreated MFT and FFT

PSD (µm)	*Untreated MFT*	*Untreated FFT*
Mean	9	4
Median	6	3.3
Mode	9	9
d10	1.3	0.3
d90	20	9

After the characterization of the samples, the designed and synthesized IL for MFT treatment (IL1) was used to treat FFT at the dosage and mixing conditions optimized for MFT. Hence, IL1 was added to the sample and stirred using an overhead stirrer for 12 min at 500 rpm. After tailings mixing time, the samples were either transferred to centrifugation tubes or transferred to Buchner funnel, for centrifugation or vacuum filtration, respectively. Our previous studies on MFT treatment indicate that water recoveries from gravity settling, centrifugation, and filtration correlate with each other. Hence centrifugation or filtration can be used as quick indicators for efficacy of the ionic liquid. In all cases, an aqueous phase was observed to separate from the treated samples.

The first strategy to separate the phases evaluated was centrifugation. The treated sample was transferred into centrifugation tubes and these were centrifuged at different centrifugation forces (53, 544, and 3340 x *g*) for 5 min (Figure 1). The FFT without treatment (control) releases minimal amount of water at high centrifugation forces. (Note: When untreated MFT was centrifuged, no water was released, even at 3340 x *g*, the highest centrifugation force evaluated in our study.) When both FFT and MFT samples were treated with IL1, water is released at all centrifugation forces. The amount of water released from the FFT and MFT samples in each centrifugation force is similar and increases with the force of the centrifugation.

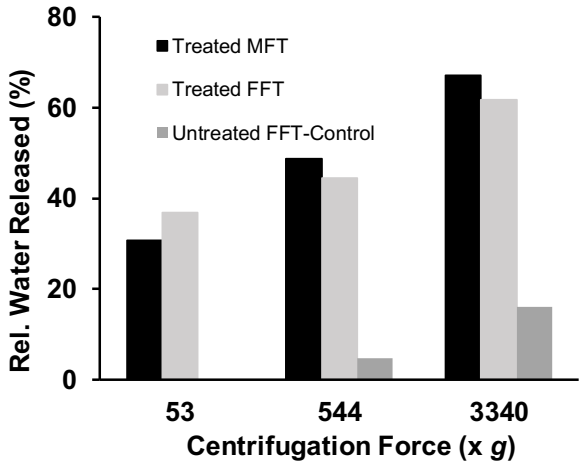

Figure 1. Relative water released (%) from IL1-treated MFT and FFT and from untreated FFT (FFT-control) at different centrifugation forces for 5 minutes

The particle size distribution of the untreated and treated FFT show significant differences (Figure 2). Interaction between FFT solids and IL1 produced flocs an order of magnitude larger than the original particles. Nevertheless, a few particles remained in the treated FFT in the same size range as the untreated particles. Table 3 shows the statistics of particle size distribution. Every measure verifies the substantial shift toward larger particles due to the floc formation in the treated FFT.

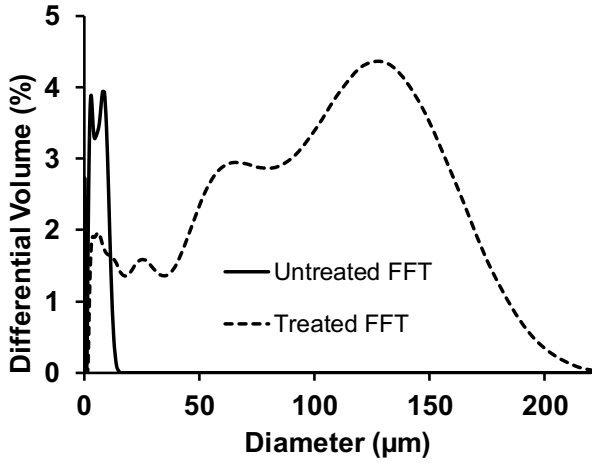

Figure 2. Differential volume particle size distribution of untreated and treated FFT

Table 3. Statics of particle size distribution of untreated and IL1-treated FFT

PSD (µm)	*Untreated FFT*	*Treated FFT*
Mean	4	58
Median	3.3	40
Mode	9	128
d10	0.3	4.1
d90	9	142

The recovered water of the untreated and treated FFT samples was analyzed (Table 4). The first noticeable difference between untreated and treated FFT is the slight increase in the pH of water after treatment by IL1, together with its increase in conductivity. The elemental analysis reveals the changes in the water chemistry. The concentrations of Na^+, K^+, and Mg^{2+} increase in the treated FFT while the Ca^{2+} concentration decreases. The zeta potential of treated FFT is also in accordance with PSD data, decreasing in magnitude to -4.0 mV from -69 mV in untreated FFT. Substantial decrease in the value indicates the capability of IL1 to neutralize the clays surface charges and hence to induce the flocculation of particles. The information gathered from the aqueous phase analysis suggests that cation exchange is taking place during the treatment of the tailings with IL1.

Table 4. Water chemistry of untreated and treated FFT

	Untreated FFT	*Treated FFT*
pH	8.3	9.0
Conductivity (µS)	0.25	1.23
Element (mg/L)		
Na^+	40	281
K^+	6	36
Mg^{2+}	7	41
Ca^{2+}	14	9
Al^{3+}	0.03	0.03
Cl^-	58	86

As second strategy to separate the aqueous phase from the treated MFT and FFT samples, vacuum filtration using a 2.5 µm size filter was carried out (Figure 3). The water recovered was monitored over time for nearly 20 min, until the water discharge was extremely slow. It was observed, as expected, that the largest portion of

water was recovered within the initial few minutes. In comparison, the rate of water released from treated MFT was initially significantly faster than for FFT (first 5 min). However, the amount of water reaches a similar plateau with time (after 15 min): about 55% vs. 60% water released from treated FFT and MFT, respectively. These results illustrate the convenience and speed of dewatering after treatment with IL1 for both MFT and FFT.

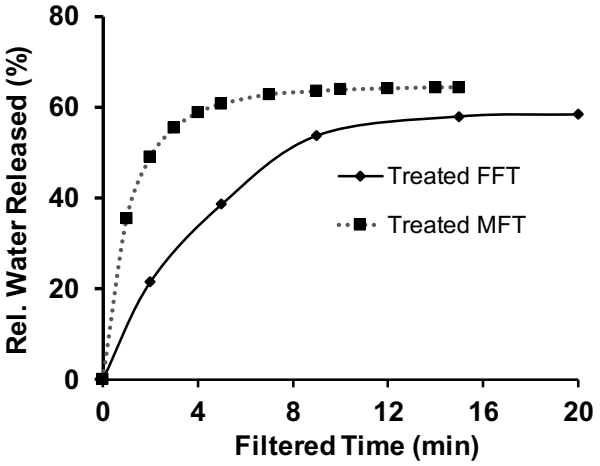

Figure 3. Effect of different times of vacuum filtration on the relative water released from treated MFT and FFT

CONCLUSIONS

In this work, we have demonstrated an efficient dewatering mechanism of FFT using IL1. After treatment with IL1, different strategies can be used to separate the solids, including centrifugation or vacuum filtration. Although the MFT and FFT samples had different bitumen content, mineralogy, particle size distribution, and most importantly, the water chemistry, the IL1 was able to dewater the FFT effectively, just as it did for MFT. This result represents a proof of concept, since the conditions were not optimized for FFT but for MFT. However, even when not optimized for FFT samples, this work demonstrates the great flexibility of our approach to dewater FFT at similar conditions and suggests a wide scope of applicability of IL1 for tailings remediation in oil sands mining operations.

REFERENCES

AER. (n.d.). Tailings Management. http://www.aer.ca/providing-information/by-topic/tailings/tailings-management. Accessed September 19, 2018.

Cong, R. and Pelton, R. (2003). The influence of PEO/poly (vinyl phenol-co-styrene sulfonate) aqueous complex structure on flocculation. Journal of Colloid and Interface Science, **261**(1): 65-73.

Dean, E. W. and Stark, D. D. (1920). A convenient method for the determination of water in petroleum and other organic emulsions. Industrial & Engineering Chemistry, **12**(5): 486-490.

Hripko, R., Vajihinejad, V., LopesMotta, F. and Soares, J. B. (2018). Enhanced flocculation of oil sands mature fine tailings using hydrophobically modified polyacrylamide copolymers. Global Challenges, **2**(3): 1700135

Kasperski, K. L. and Mikula, R. J. (2011). Waste streams of mined oil sands: characteristics and remediation. Elements, **7**(6): 387-392.

Li, S., Liao, Y., Li, G., Li, Z. and Cao, Y. (2017). Flocculating and dewatering performance of hydrophobic and hydrophilic solids using a thermal-sensitive copolymer. Water Science and Technology, **76**(3): 694-704.

Long, J., Xu, Z. and Masliyah, J. H. (2006). Role of illite–illite interactions in oil sands processing. Colloids and Surfaces A: Physicochemical and Engineering Aspects, **281**(1-3): 202-214.

Nasr, T. N. and Ayodele, O. R. (2005, January). Thermal techniques for the recovery of heavy oil and bitumen. In SPE International Improved Oil Recovery Conference in Asia Pacific. Society of Petroleum Engineers (SPE-97488-MS).

Proskin, S., Sego, D. and Alostaz, M. (2010). Freeze–thaw and consolidation tests on Suncor mature fine tailings (MFT). Cold Regions Science and Technology, **63**(3): 110-120.

Reis, L. G., Oliveira, R. S., Palhares, T. N., Spinelli, L. S., Lucas, E. F., Vedoy, D. R., Asare, E. and Soares, J. B. (2016). Using acrylamide/propylene oxide copolymers to dewater and densify mature fine tailings. Minerals Engineering, **95**: 29-39.

Vedoy, D. R. and Soares, J. B. (2015). Water-soluble polymers for oil sands tailing treatment: A Review. The Canadian Journal of Chemical Engineering, **93**(5): 888-904.

Wang, C., Harbottle, D., Liu, Q. and Xu, Z. (2014). Current state of fine mineral tailings treatment: A critical review on theory and practice. Minerals Engineering, **58**: 113-131.

Welton, T. (1999). Room-temperature ionic liquids. Solvents for synthesis and catalysis. Chemical Reviews, **99**(8): 2071-2084.

Wilkes, J. S. (2002). A short history of ionic liquids—from molten salts to neoteric solvents. Green Chemistry, **4**(2): 73-80.

ROBUST LOW DOSAGE TREATMENT ACROSS MULTIPLE OIL SANDS FLUID FINE TAILINGS SAMPLES USING A NEW AMENDMENT

Lizbeth Rostro, Paul A. Gillis, Wu Chen, Michael K. Poindexter and Jason Tubbs
The Dow Chemical Company, Lake Jackson, TX, USA

ABSTRACT

Oil sands surface mining generates fluid fine tailings (FFTs) which are stored in open-air ponds. The solids content of the FFTs is limited to 30-35 wt% due to the formation of a stable colloidal suspension which hinders further consolidation. As a result, FFT treatment strategies with chemical amendments have been developed. These techniques consolidate the FFTs by releasing water from the slurry and thus increase solids content and ultimately soil strength. A novel amendment (XUR) with unique performance attributes has been identified and scaled up from benchtop testing to the filling of 70 m^3 casings. In addition to demonstrating superior dewatering, this additive improves released water quality and lowers the treated FFT yield stress.

Recently, significant progress has been made in understanding XUR's operating ranges (including low dosages), while maintaining superior treatment performance. Laboratory experiments demonstrated that long-term (> 500 hours) monitoring of XUR treated tailings is required to fully capture the performance. This insight enabled significant optimization of the treatment dosage and the reduction of the required mixing intensities. The studies were conducted on a variety of FFT samples ranging in clay content and solids content. The dewatering results revealed the robustness of the XUR amendment to variations in tailings properties at dosages as low as 350 ppm (based on solids).

INTRODUCTION

The extraction of bitumen from oil sands using surface mining has proven to be a viable recovery method. The extraction is completed using the Clark hot water extraction process which creates a significant amount of tailings (Clark 1932, 1944). These tailings streams have been collecting and accumulating since the inception of this technology. It has been determined that these streams are slow to dewater and the consolidation of the solids is more difficult than initially anticipated (Botha 2015, Mikula 1996, van Olphen 1963). As such, the volumes of these tailings continues to grow (Camp 1977, Kasperski 1992).

The fluid fine tailings (FFT) are a stable clay-containing slurry. The stability of the suspension leads to difficulties in the consolidation of the solid particles (BGC 2010, Sobkowicz 2009). To encourage the dewatering process, several mechanical methods have been developed and some scaled up to commercial size operations (Oil Sands Tailings Technology Deployment Roadmaps 2012). These include centrifuges and thickeners. These strategies often require the use of chemical amendments to aid in the release of water from the slurry (Mohler 2014). These amendments often serve as coagulants or flocculants and in some applications a blend of both provide the best performance. Although the amendments are key in the ultimate treatment process, there is still a need for further improvement (Vedoy 2015).

During the evaluation of new amendments, multiple parameters should be considered. It is important that the tests be designed to mimic the final application. For example, it is important to consider the measurement timeframes when evaluating the performance of new amendments. For some treatment processes, like thickeners or centrifuges, the initial dewatering performance is critical; however, for end-pit lakes, the long-term performance is the most significant (Holden 2014). In addition to water release, it is important that the amendment does not alter the water chemistry (Allen 2008). The water will eventually be released back into the environment and it is a critical part of the remediation directive (Alberta Energy Regulator 2016). Furthermore, the transportability (rheology and shear tolerance) of the treated material strongly influences the feasibly of an amendment in the field. During the development of any amendments, all of these issues should be considered in order to identify the best amendment for each application.

Dow used high-throughput screening methods to identify amendments for the remediation of tailings (Mohler 2012). The most promising candidates from the screening process were scaled up 150 mL – 2 L

scales, and the dosages and shear rates were varied (Gillis 2013). These efforts identified XUR as a shear and dosage tolerant amendment and enabled testing at larger scales. Specifically, FFT was treated with XUR and 3 meter tall geocolumns and 10 meter tall casings were filled (Poindexter 2015; Stianson 2016a, 2016b). The results demonstrated superior dewatering and high release water quality. Following these studies the laboratory efforts shifted to optimize the dosage and mixing requirements for XUR (Poindexter 2016). The reduction in dosage did not affect the water release chemistry or the long-term dewatering (>500 hours). This work demonstrates the effect of shear and XUR dosage on the short and long term dewatering for a variety (solids and clay content) of tailings.

EXPERMENTIAL

All tailings samples discussed here were received in 275 gallon totes from Alberta, Canada and stored in an outdoor storage area. Prior to conducting tests with XUR, the FFT sample was thoroughly homogenized. Each tote was mixed using a combination of manual and overhead mixing for a period of time ranging from 2-8 days. The manual mixing was achieved with a combination of a paint mixer and gardening tools. The ITM 7000 Tote Mixer was used at 175 rpm. Both methods focused on dispersing any solids on the bottom or in the corners of the totes. Any residual clumps of solids would increase sample variability. This would make it challenging to compare results within a tote. In addition, a wire screen (1/2”) was used during the sample distribution process to remove any large particles (e.g., rocks, debris). The homogenization was deemed complete once successive samples gave constant MBI and solids content values and there were no tailings detected at the bottom of the totes. The homogenization step has been critical in obtaining consistent data throughout all experimental runs. After homogenization, the totes were distributed into five 55 gallon containers using the bottom spout on the totes.

Dewatering Experiments

The tailings were treated using a processing skid comprising of a tailings pump, a flocculant pump and a proprietary dynamic mixer. The flocculant was always used at a loading of 0.4 wt% in process water. The dynamic mixer was run at rotational speeds ranging from 0-1500 rpm. Each experimental set used approximately 40 gallons of FFT. The treated tailings flowed through the dynamic mixer and a 1” line before being collected in 5 gallon containers. The containers were placed on laboratory benchtops and monitored for several months. During this time, the samples were not perturbed in any manner while solids settled and consolidated. The solids content of the treated material were calculated based on the mudline height.

Tailings Characterization

Four FFT samples were analyzed prior to testing (Table 1). The solids content was measured using a Mettler Toledo HB433-S halogen moisture analyzer. The clay content was also measured using methylene blue index (MBI). The MBI values are reported in units of meq MB/100 grams of Clay (Omosoto 2008).

Table 1. Initial solids content and clay content of the tailings samples

Sample	Wt %	MBI
FFT 1	40.7	8.8
FFT 2	29.3	9.0
FFT 3	32.0	8.2
FFT 4	36.8	7.5

Data Analysis

The effect of the amendment will be detailed for short-term and long-term timeframes. The short-term performance describes the properties measured within the first 24 hours of settling and the long-term performance describes the performance beyond 500 hours.

RESULTS AND DISCUSSION

Case 1: Effect of Dosage on Dewatering Performance

A strong emphasis has been placed on the performance attributes of the new amendment XUR. Specifically, the focus is to minimize the dosage while maintaining good dewatering performance. It was previously reported (Poindexter 2016) that neither long-term dewatering performance nor release water chemistry were affected by the dosage reduction. However, the treatment dosage has a strong influence on the initial dewatering rates (Kuvadia 2017). This work

expands upon these previous observations and highlights the resilience to shear of XUR-treated tailings.

The first study was focused on understanding the effect of dosage on the short-term dewatering performance of XUR. Dosages ranging from 350-1000 ppm were used to treat FFT1. Figure 1 illustrates the effect of dosage on the initial dewatering rates. These values were measured during the first 24 hours. Two very important conclusions can be gleaned from this study: 1), the dosage has a strong influence on the initial dewatering rate; and 2), the mixer agitation speed does not effect on the short-term performance.

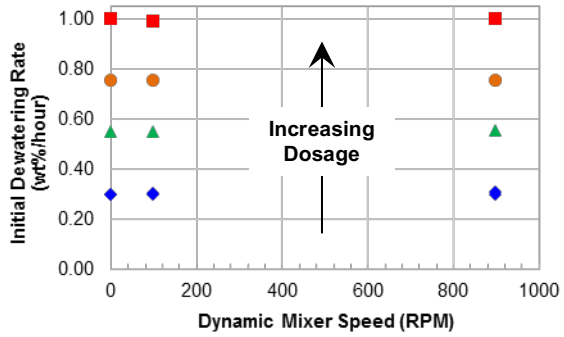

Figure 1. Initial dewatering rates for FF1 treated at a range of XUR dosages and mixer rotational speeds

The dewatering rates for low dosages are 0.29 wt%/hour and can increase by a factor of 4 by increasing the flocculant loading. The effect is likely due to the influence of polymer dosage on the floc size that is formed during the treatment process. Specifically, as the dosage increases, the size of the flocs increase resulting in faster initial settling. This is an important consideration for treatment strategies that require fast dewatering. Therefore, for applications like thickeners and centrifuges, the treatment dosage will be higher than what is required for deep deposits. Preliminary laboratory data suggests dosages greater than 350 ppm are needed for thickener and centrifuge applications.

Secondly, the mixing intensity (rpm) does not affect initial dewatering rates. This suggests that the flocs that are formed are shear tolerant. The interactions between the amendment and the suspended solids are strong enough to form structures that are not broken up at the shear rates generated in the dynamic mixer. The shear tolerance exemplified by XUR would allow for the treatment and transportation of tailings without any subsequent detrimental effects on dewatering performance. This is important as distances between treatment locations and depositions can be several hundred meters to several kilometers. This property of XUR-treated tailings will be of great importance for field implementation.

The results above pertain to short-term performance. However, treated tailings are placed on beaches, in ponds, or into end-pit lakes, and this material could reside there for long periods of time (decades). Laboratory scale work should also consider these longer time frames. The initial large-scale XUR work was at higher dosages (1500 - 1900 ppm) and relatively high rotational speeds in the proprietary dynamic mixer. The process was initially optimized using only short-term results. During these tests, the relatively high dosages and intense blending were required. After the earlier studies were completed, the focus shifted to understanding the long term effects of XUR on treated tailings. From this work, the team learned that monitoring samples for longer time periods allowed for further dosage and mixing optimization.

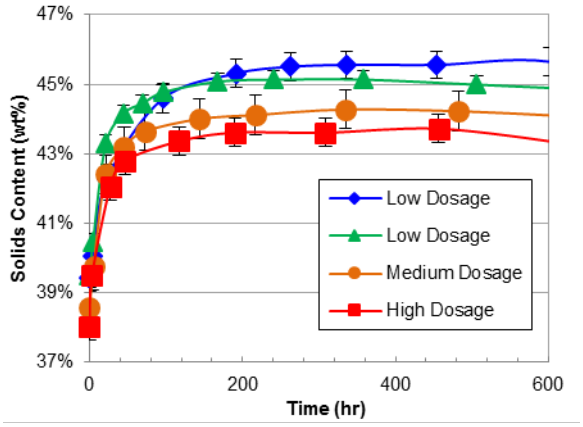

Figure 2. Long-term dewatering data for FFT1

Dewatering curves for XUR-treated FFT1 are depicted in Figure 2. Each colored curves represents averaged solids content from samples processed using 3 dynamic mixer speeds: 0 rpm, 100 rpm, 900 rpm. The small error bars for each data point establish that there is an insignificant effect of mixer speed on dewatering. The long-term performance indicates that there is a slight reduction in performance at the higher dosages; the highest dosage produced the lowest final solids content. This effect is likely caused by the entrapment of water within the floc structure. The larger floc size enables more rapid initial dewatering

at the cost of entrapping water and resulting in a slight reduction in the final performance. Although previous results have shown an insignificant dosage effect, some FFT samples show a slight performance reduction at higher dosages (Kuvadia 2017).

In addition to the direct economic benefit of using less flocculant, lower dosages also reduce the water addition requirements for treatment and lessen the deposition area footprint. Lower dosages mean less flocculant solution and thus less water will be introduced into the FFT. This reduces the operation cost associated with water handling. Furthermore, the deposition area/volumes are used more effectively, reducing the cost of earthworks. This secondary effect is a result of reducing the amount of water added to the tailings during the treatment process. As such, a deposit can be filled with more tailings rather than a significant volume of water.

Case 2: Effect of FFT Properties

Next, several FFT samples were treated with a low XUR dosage and both the short-term and long-term performance were monitored. Here, FFT2, FFT3 and FFT4 were used. These tailings samples vary in initial solids and clay content as detailed in Table 1. Figure 3 highlights the initial dewatering rates for these samples. All the samples were treated at low dosages and at several mixing intensities. Interestingly, the dewatering rates for these samples are all higher than the low dosage rate for FFT1. Specifically, the rates for FFT2 and FFT3 are comparable to the higher dosages shown in Figure 1.

The primary difference among the samples are the initial solids content (Table 1). FFT2 and FFT3 have the lowest initial solids content therefore have the most water to release. On the other hand, FF4 and FF1 have higher solids content and less water to release. The trend shown in Figure 3 indicates that one should expect higher initial dewatering rates for samples that lower initial solids content. These results do not support the idea of diluting tailings prior to treatment in order to obtain higher water release rates. In fact, work presented in 2017 by Kuvadia et al., demonstrated that this would result in a lower final solids content. This illustrates that higher water release rates (for diluted FFT) is simply the removal of the added water and not the water in the original FFT.

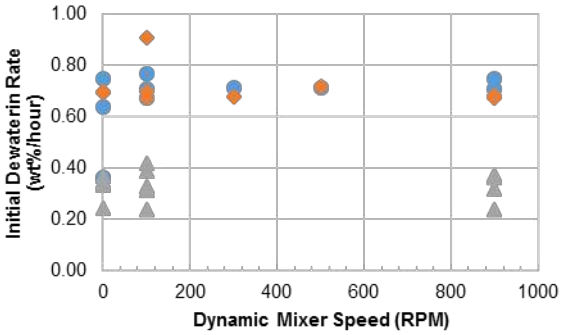

Figure 3. Initial dewatering rate as a function of dynamic mixer speed for FFT2, FFT3, FFT4. All FFT samples were treated at low dosages and the conditions were run at least three times. Circle – FFT2; diamond – FFT3; triangle – FFT4

The long-term dewatering performance was also monitored for these samples. These data are plotted in Figure 4 using a logarithmic scale in order to differentiate between the FFT samples. The samples were monitored for more than 3,000 hours, and the performance for all samples was satisfactory (increase of at least 10 wt% solids). The performance was very consistent among the different data sets and between the different mixing intensities. Additionally, samples FFT2 and FFT3 had similar properties and hence the performance was very similar. Similarly, FFT4 had similar long-term performance as FFT1. Tailings properties have a strong influence on the dewatering performance of XUR; however, it is encouraging that XUR performed well across different FFT samples.

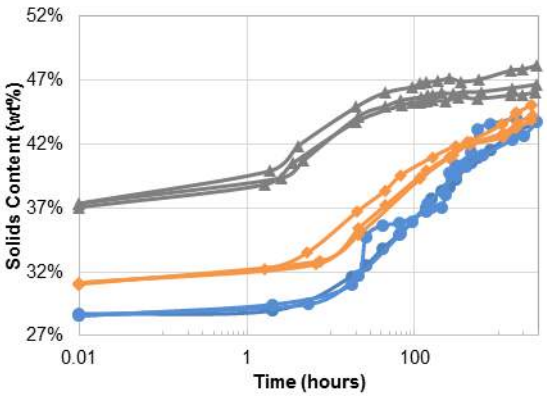

Figure 4. Long-term dewatering performance for FFT2, FFT3, and FFT4. Circle – FFT2; diamond – FFT3; triangle – FFT4

CONCLUSIONS

The dewatering performance of XUR for short and long timeframes was evaluated for multiple FFT samples. The FFT samples were treated with XUR at dosages ranging from 350-1000 ppm. The treatment dosage had a strong influence on the initial dewatering rate, while the mixing intensities did not show an effect. Treatment strategies that require fast initial dewatering rates should consider higher (>350 ppm) dosages. Low XUR treatment dosages are suited for deep deposits or end-pit lakes. Furthermore, the evaluation at long timeframes (> 500 hours) suggests that there is only a slight dosage effect on performance. The higher dosages are more effective at releasing water faster but ultimately obtain slightly lower final solids content. Lastly, the initial solids content of the tailings also had a strong influence on the initial dewatering rates observed.

REFERENCES

Alberta Energy Regulator. (2016). Directive 85. Fluid Tailings Management for Oil Sands Mining Projects. Release date: July 14.

Allen, E. W. (2008). Process Water Treatment in Canada's Oil Sands Industry: I. Target Pollutants and Treatment Objectives. Journal of Environmental Science, **7**, 123-138.

BGC Engineering Inc. (2010). Oil Sands Tailings Technology Review. Oil Sands Research and Information Network, University of Alberta, School of Energy and the Environment, Edmonton, Alberta. OSRIN Report No. TR-1.

Botha, L. and Soares, J. B. P. (2015). The Influence of Tailings Composition on Flocculation. Canadian Journal of Chemical Engineering, **93**, 1514-1523.

Clark, K. A. and Pasternack, D. S. (1932). Hot Water Separation of Bitumen from Alberta Bituminous Sand. Industrial & Engineering Chemistry, **24**: 1410-1416.

Clark, K. A. (1944). Hot-Water Separation of Alberta Bituminous Sand. Transactions of the Canadian Institute of Mining & Metallurgy, **47**: 257-274.

Camp, F. W. (1977). Processing Athabasca Tar Sands – Tailings Disposal, Canadian Journal of Chemical Engineering, **55**: 581-591.

Gillis, P. A., Moore, J. S., Poindexter, M. K., Witham, C. A., Chen, W., Singh, H., Mohler, C. E. and Atias, J. (2013). The Effects of In-line Static Mixer Flow Loop Operational Parameters on Flocculant Performance in Mature Fine Tailing Samples. Tailings and Mine Waste Conference; Banff, Alberta, November 3-6, pp 137-146.

Holden, A., McKenna, G., Fan, X. and Biggar, K. (2014). The Potential Impact of Different Types of Tailings on Water Quality and Quantity Reporting to Oil Sands End Pit Lakes: A Preliminary Modeling Exercise. 4th International Oil Sands Tailings Conference; Lake Louise, Alberta, pp 359-367.

Kasperski, K. L. (1992). A Review of Properties and Treatment of Oil Sands Tailings, AOSTRA Journal of Research, **8**: 11-53.

Kuvadia, Z., Poindexter, M. K., Gillis, P. A., Rostro, L., Chen, W. and Tubbs, J. (2017). Statistical Data Mining Approach to Improve Understanding of Flocculant Dewatering of Fluid Fine Tailings. Sixth International Oil Sands Tailings Conference; Banff, Alberta; November 5-7, pp 710.

Mikula, R. J., Kasperski, K. L., Burns, R. D. and MacKinnon, M. D. (1996). Nature and Fate of Oil Sands Fine Tailings, in Suspensions: Fundamentals and Applications in the Petroleum Industry, Advances in Chemistry, Schramm, L. (ed.), Washington, DC, pp 677-723.

Mohler, C. E., Poindexter, M. K., Atias, J., Chen, W. and Witham, C. A. (2012). Development of Flocculants for Oil Sands Tailings using High-Throughput Techniques. 3rd International Oil Sands Tailings Conference; Edmonton, Alberta; December 2-5, pp 113-120.

Mohler, C., Poindexter, M. K., Acevedo, C., Sanders Jr., T., Meyers, G., Reinhardt, C., Chen, W., Singh, H. and Atias, J. (2014). Clay-Flocculant Interactions in Developing Next Generation Flocculants for Oil Sands Fluid Fine Tailings Management. 4th International Oil Sands Tailings Conference; Lake Louise, Alberta, pp 437-445.

Oil Sands Tailings Technology Deployment Roadmaps. (2012). Report to Alberta Innovates – Energy and Environment Solutions. Volume 1 Project Summary.

Omotoso, O. and Morin, M. (2008). Methylene Blue Procedure: Sludges and Slurries, CanmetENERGY – Devon, Natural Resources Canada.

Poindexter, M. K., Gillis, P. A., Moore, J. S., Tubbs, J., Mahood, R. and Freeman, G. (2015). Geotechnical Column Evaluation of New Flocculant Technology for Dewatering Oil Sands Mature Fine Tailings. Tailings and Mine Waste Conference; Vancouver, British Columbia, October 25-28, pp 490-499.

Sobkowicz, J. C. and Morgenstern, N. R. (2009). A Geotechnical Perspective on Oil Sands Tailings. 13th International Conference on Tailings and Mine Waste, Banff, Alberta, pp. xvii-xli.

Stianson, J., Mahood, R., Fredlund, D. G. and Sun, J. (2016a). Large-Strain Consolidation Modeling to Determine Representative Tailings Consolidation Properties from Two Meso-Scale Column Tests. Fifth International Oil Sands Tailings Conference; Lake Louise, Alberta; December 4-7, pp 40-50.

Stianson, J., Mahood, R., Thomas, D., Song, J. and Li, L. (2016b). A Shell Tailings Consolidation Casing Experimental Pilot Project (TCCEPP). Fifth International Oil Sands Tailings Conference; Lake Louise, Alberta; December 4-7, pp 432-441.

van Olphen, H. (1963). An Introduction to Clay Colloid Chemistry for Clay Technologists, Geologists, and Soil Scientists. Interscience, New York.

Vedoy, D. R. L. and Soares, J. B. P. (2015). Water-Soluble Polymers for Oil Sands Tailing Treatment: A Review. Canadian Journal of Chemical Engineering, **93**: 888-904.

PRETREATMENT OF OIL SANDS TAILINGS WITH LIME TO ENHANCE THICKENING PROCESSES

Nikolas Romaniuk[1], Jesse Fox[2], Jared Leikam[2] and Mike Tate[3]
[1]Graymont Inc., Calgary, Canada
[2]Graymont Inc., Salt Lake City, USA
[3]Graymont Inc., Genoa, Ohio, USA

ABSTRACT

Thickeners play an important role in many commercial oil sands tailings treatment processes. Separation of solids from tailings process water by flocculation increases tailings density and reduces tailings volume, which are necessary to comply with government regulations and achieve reclamation goals. Reuse of hot process water from the thickener overflow can save energy in the bitumen extraction process, provided water quality is acceptable. Unfortunately, current thickener operations require high levels of dilution and long residence times to effectively dewater oil sands tailings despite the use of long chain polyacrylamide polymers as process aids. Additionally, polyacrylamide flocculation can have difficulties capturing some of the fine clay particles, resulting in poor release process water with high turbidity. These fine clay particles settle slowly, if at all, so extremely large thickeners are required. Our study focuses on the use of small doses of lime, between 600 to 1,000 ppm calcium hydroxide on a slurry basis, as a pretreatment for polyacrylamide flocculation of dilute fluid fine tailings. Compared to polyacrylamide flocculation alone, a lime pretreatment is shown to improve fines capture and release water quality, nearly eliminating turbidity at low soluble calcium concentrations. Lime pretreatment to polyacrylamide flocculation also demonstrates a faster rate of fines settling and higher final solids content when compared to alum and gypsum pretreatments. The mechanism of the enhancement appears to be in part a result of coagulation, due to charge neutralization of clay surfaces that enhances dewatering, and from the improvement of water quality, which may enhance polymer performance.

INTRODUCTION

Oil sands surface mining operations in Alberta use modified versions of the Clark Hot Water Extraction process to extract bitumen, a highly viscous petroleum product, from oil sands ore with water and caustic addition which result in tailings, a mixture of water, clay, sand and residual bitumen. The most troublesome of the oil sands tailings are fine clays, which segregate from coarse sand rich minerals in whole tailings upon beach deposition. These fine clays, as well residual bitumen, collect in tailings ponds as fluid fine tailings (FFT) that slowly settle and generally resist consolidation beyond 30 to 40% solids and are unamiable for remediation (Kasperski 1992, Scott 1985). For instance, remediation of FFT to support and uplands ecosystem requires a shear strength of about 20 kPa, which could require FFT be dewatered to approximately 75-80% solids content (McKenna 2016). The oil sands operator's inventory of FFT in now exceeds 1.2 billion cubic meters and represent an increasing environmental risk to the Athabasca region and economic risk for the operators (AER 2018).

Methods to treat and prevent of FFT have been studied extensively but have yet to provide a cost-effective solution (Boswell 2012). Many high-performance FFT treatment technologies rely mechanical solid/water separations, such as centrifuge, thickeners, or filtration, that assisted with chemical additives (McMinn 2017, Renard 2016).

High performance thickeners are currently used by multiple oil sands operators as means to rapidly densify fine extraction tailings and produce low turbidity water that could be reused in the extraction process. Operators treat tailings with chemical additives to facilitate efficient thickening; however, to attain high clarity in release water large thickeners with long residence times may be required. Feed to thickeners can range from 3-10% solids. Tailings solids levels of the underflow can reach over 40% solids. Thickener underflow could be deposited as "thickened tailings" which may consolidate further over time. Alternatively, increasing the solids content of tailings could be beneficial for mechanical dewatering processes like pressure filtration.

The most common chemical additives are partially hydrolyzed polyacrylamide (HPAM) polymers which are used as flocculants. These flocculants act by absorbing the small clay particles onto the polymer which yields large flocs that settle easier due to changes in density and allow for quick initial release of water; however, the HPAM flocculants often fail to achieve complete capture of all fine clays, especially many of the smallest clays with the largest surface areas. Additionally, HPAM flocculants have additionally been shown to have trouble dewatering beyond 50-60% solids content (Vedoy 2015), since the HPAM flocculants collect the clay particles rather than changing the surface properties of the clays to facilitate dewatering. A further concern is that the HPAM flocculated solids are fragile and can break down during transportation.

Inorganic coagulants, such as hydrated lime [$Ca(OH)_2$], alum [$Al_2(SO_4)_3$], and gypsum [$CaSO_4$], provide multivalent cations in solution that can bind to clay particles and neutralize surface changes and results in coagulation of fine clays as larger agglomerates. These agglomerates are held together through cation bridges, generally provided by soluble cationic calcium or aluminum ions which exchange with other cations, such as sodium, on the clay surfaces (Ching 1994, Lane 1983, Little 1995). Unlike flocculants, solution chemistry is very important as it will determine how much of the active multivalent cation is available for cation exchange, as the multivalent cations may associate with bicarbonate or sulfate compounds which will decrease their chemical activity. Coagulants can also have beneficial effects beyond clay modification such as water quality improvements (Tate 2016). Although coagulants can be very effective to provide clear release water and greatly improve dewatering, they do not provide quick dewatering in slurries composed of only fine (<45 micron) clays, such as FFT, due to their low permeability and when used on their own. By themselves, coagulants may be unamenable in systems relying on rapid settling, like thickeners.

Coagulants and flocculants can be used together to take advantage of both mechanisms, the improvement of water quality and clarity from coagulants and quick rate of settling from flocculation. Previous investigations of slaked lime treatment before flocculants demonstrated improvement in release water quality (Hamza 1996); however, the study did not determine slurry pHs and dissolved ion concentrations after lime addition. Previous investigation by our group have demonstrated that the optimal lime additive to FFT in laboratory scale experiments is hydrated lime as a 5% mass in water slurry (Tate 2017). This study investigates a similar approach, but is updated to understand how three common coagulants, hydrated lime, alum, and gypsum, can be used as a pretreatment to a modern HPAM flocculant, envisioned for use in a high-throughput thickener.

EXPERIMENTAL DESIGN

Evaluating coagulants as a pretreatment for polymer flocculation in thickening processes was performed using a stand pipe style test with a diluted FFT. Polymer selection and dosing were performed by FLSmidth at their Salt Lake City laboratories as a component of a previous test program (Rahal 2018).

Materials

The FFT used in the experiments was analyzed for solids content, bitumen content and MBI as shown in Table 1.

Table 1. FFT Properties

Bitumen Content	Mineral Content	Water Content	Solids Content	MBI
% Mass	% Mass	% Mass	% Mass	
1.5	28.4	70.3	27.5	12.2

The hydrated lime, $Ca(OH)_2$, used was high calcium from Graymont's Indian Creek quarry. The alum, $Al_2(SO_4)_3$, was purchased from British Drug Houses as an octadecahydrate. The gypsum, $CaSO_4$, was purchased from Hi Valley Chemical as a hemihydrate. The partially hydrolyzed polyacrylamide (HPAM) polymer was A3331 obtained from SNF.

Methods

The experiments were completed at Graymont's central laboratory in Salt Lake City, Utah, USA. Ca^{2+}, Na^{+}, K^{+}, Mg^{2+}, Al^{3+}, and S were analyzed using a PerkinElmer optima 7300 ICP-OES. Cl^{-}, CO_3^{2-}, and SO_4^{2-} were analyzed using a Thermo Scientific Dionex ICS-2100 ion chromotographer. pH was analyzed on a Thermo Scientific Orion 920A+ ISE pH meter. Particle size was analyzed on a Cilas 1190 laser diffraction PSA. Absorbance was measured using a Thermo Scientific Genesys 10s,

absorbance is reported as relative absorbance units (AU).

All coagulant doses are calculated on a mass basis of the total mass of dilute slurry.

Coagulant and Flocculant Preparation. All coagulants (hydrated lime, alum, and gypsum) were prepared as 5% mixtures in distilled water by mass. The hydrated lime generates a slurry that must be resuspended before addition, gypsum and alum dissolved in solution without requiring remixing. The polymer was prepared as a 0.5 g/L mixture. Polymer was added to a concentration of 250 g/ton of dried solid in the FFT.

Preparation of Simulated Process Water. A simulated process water was prepared by dissolving salts ($CaCl_2$, $MgCl_2$, Na_2SO_4, KCl, $NaHCO_3$) to achieve a water chemistry similar to oil sands process water. The simulated process water is then adjusted with either HCl or NaOH to adjust pH to 8.2.

Preparation of Dilute FFT Slurry. FFT was homogenized using an overhead mixer for approximately 30 minutes using an overhead mixer and then subsampled with mixing. The FFT was diluted to 3% solids in simulated process or oil sand process water by mass either directly in a 1 L graduated cylinder, for individual tests, or as a batch in a 20 L pail. Diluted FFT prepared in a 20 L batch must be homogenized for about 5 minutes with an overhead mixer before subsampling with mixing. The ionic composition of the process water in the dilute FFT was determined by centrifuging a sample of slurry to remove solids, syringe filtration at 0.2 microns, and analyzed with a combination of ICP-OES and ion chromatography methods. The ionic composition of the two dilute FFTs prepared is shown in Table 2.

Table 2. Dilute FFT Water Chemistry Properties

Dilute	Ca^{2+}	Na^{+}	K^{+}	Mg^{2+}	Cl^{-}	SO_4^{2-}	H_2CO_3	HCO_3^{-}	CO_3^{2-}	pH
FFT	mg/L	mg/L	mg/L	mg/L	mg/L	mg/L	mg/L	mg/L	mg/L	
A	31	263	7	12	90	99	0	498	31	9.1
B	29	354	32	14	178	205	4	246	0	8.2

Initial Coagulant Screening. A 1 L portion of diluted FFT A simulated process water diluted FFT was subsampled into a tared 1 L graduate cylinder. 5% coagulant mixtures (hydrated lime, alum, or gypsum) were then added and mixed in using at least 4 quick full sweeps with a plunger. The polymer (A3331) solution was then added and the dilute FFT was flocculated with 3 slow strokes of the plunger. The amount of time for the mudline to settle to 700 mL was recorded as is the mudline height, as mL, after 30 minutes elapsed. The pH of the Release water was measured, and samples of the release water were removed using a syringe and analyzed in a spectrophotometer for absorbance at 750 nm.

Sweep Experiment with Hydrated Lime and Alum. A 1 L portion of diluted FFT B was subsampled into a tared 1 L graduate cylinder. 5% coagulant mixtures (hydrated lime or alum) were then added and mixed in using at least 4 quick full sweeps with a plunger. The pH of the slurry was recorded, and a subsample was removed for water chemistry analysis. The polymer (A3331) solution was then added and the dilute FFT was flocculated with 3 slow strokes of the plunger. A sample of the release water was removed using a syringe and analyzed in a spectrophotometer for absorbance at 750 nm.

RESULTS AND DISCUSSION

The effectiveness of the coagulants as pretreatments for flocculation was assessed by evaluating release water clarity and settling performance, both settling rate and final settled volume. The release water clarity demonstrates decreased turbidity caused by suspended fines and dissolved organics, which is the key variable to demonstrate effective coagulation. The water clarity qA assessed by the absorbance of light at 750 nm by spectrophotometer where low absorbance indicates lower turbidity. The settling rate, measured as time for the mudline to settled to 0.7 of normalized height, and final settled volume, measured at 30 minutes of settling, were determined to assess the impact of the coagulant on the flocculation by the HPAM polymer. The ideal coagulant pretreatment for flocculation will demonstrate a low absorbance at 750 nm while maintaining a quick time to reach 0.7 normalized height and settle significantly at 30 minutes.

The initial coagulant screening tests compared the effectiveness of hydrated lime, alum, and gypsum with a broad sweep of doses. Both hydrated lime and alum appear to outperform gypsum for decreasing absorbance, as shown in Figure 1, where both hydrated lime and alum achieve less than 0.1 AU, whereas gypsum only reaches about 0.2 AU; however, all coagulants performed better than no coagulant which had an absorbance of 1.23

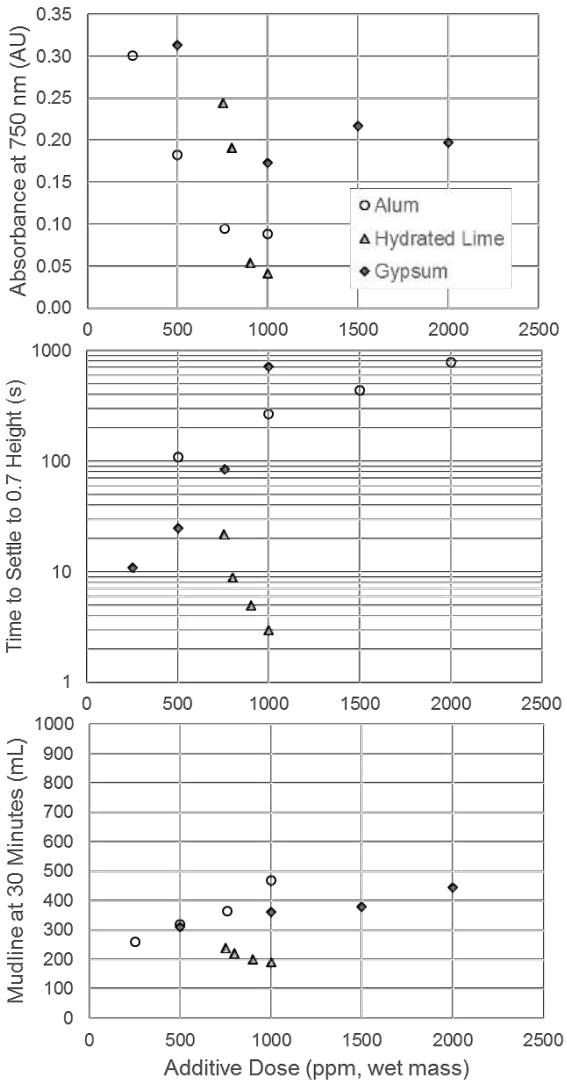

Figure 1. Initial Investigation of the Effects of Alum, Hydrated Lime, and Gypsum Coagulants as Pretreatments to HPAM Flocculation

Table 3. Point Matrix for Evaluation of Coagulants to Assist Polymer Flocculation

Score	Absorbance	Settling Rate	Settled Height
	AU	Seconds	mL
0	>0.4	>100	>400
1	0.2-0.4	50-100	400-300
2	0.1-0.2	10-50	300-200
3	<0.1	<10	<200

AU. Figure 1, also demonstrates that, when achieving optimal water clarity, gypsum and alum both exhibit poor settling rates, where alum required at least 84 seconds and gypsum required at least 270 seconds, to reach 0.7 normalized height. Hydrated lime demonstrated rapid settling, reaching 0.7 normalized height at 4 seconds or coagulant was used it was impossible to determine the time to settle to 0.7 normalized height; however, this speed is expected to be quick, likely about 2 seconds. Lime additionally demonstrated better settling at 30 minutes, while maintaining water clarity, with settled volume of 190 mL, when compared to either alum or gypsum, with settled volumes of 365 mL and 360 mL, respectively. The lowest settled volume of 155 mL was seen using no coagulant.

The initial screening tests were evaluated using a scoring matrix assigning points based on absorbance, speed of settling, and final settled volume as shown in Table 3. To place emphasis on the importance of high water clarity the points awarded to absorbance were doubled in the calculation of total points. The highest point scoring doses for all coagulants are presented in Table 4 where both hydrated lime performed best, followed by alum, no additive, and gypsum. The results indicated that hydrated lime and alum deserved further study.

The second round of experiments investigated hydrated lime and alum over a larger sweep of doses, every 50 ppm from 550 to 1000 ppm for hydrated lime and every 200 ppm from 200 to 1,000 ppm for alum. The results of the absorbance, settling rate, and settled volume are presented in Figure 2. Lime and alum both demonstrated absorbance at 750 nm below 0.1 AU starting at 750 ppm for hydrated lime and 800 ppm for alum, confirming that both coagulants are effective at capturing fine clays and organics and promoting high water release clarity. However, hydrated lime appears to provide significantly superior settling rates and final settled volumes when compared to alum at doses with good water clarity. Interestingly, the sweep of doses between 650 and 1,000 ppm for hydrated lime formed a U-shape for time to settle to 0.7 normalized height and settled volume at 30 minutes with notable minima representing the quickest settling times and lowest settled volumes, where 750 ppm appears to produce both the quickest settling rate and lowest settled volume.

The benefits of using a coagulant like hydrated lime and alum results from the multi-valent cations they contribute to the water chemistry that can act to

neutralize surface charges and link particles. Hydrated lime is only able to generate soluble calcium at elevated slurry pH of 10.9 after the calcium hydroxide has reacted with the alkalinity, as shown in Figure 3. The mechanism of this reaction is shown in Figure 4, where in Equation 1 calcium hydroxide initially reacts with sodium bicarbonates to generate insoluble calcium carbonate and sodium hydroxide, increasing pH. As the pH increases sodium hydroxide will react with the remaining bicarbonates to yield sodium carbonate (Equation 2), which can also react with calcium hydroxide and produce insoluble calcium carbonate and sodium hydroxide (Equation 3). Once there are no carbonates remaining, calcium hydroxide can dissociate to release free calcium as well as hydroxide (Equation 4). Alum does not contain any calcium in its structure; however, no soluble aluminum was observed in the water chemistry of any of alum treatments in this study. Instead alum is shown to both increase soluble calcium and decrease available carbonate while lowing pH in Figure 3. These observations can be explained by the reaction in Figure 4, where aluminum sulfate reacts with water to form insoluble aluminum hydroxide and sulfuric acid (Equation 5), lowering pH. The generated sulfuric acid can then reaction with either calcium bicarbonate (Equation 6) or carbonate (Equation 7) to generate calcium sulfate, also known as gypsum, and carbon dioxide gas, which bubbles out of the system resulting in the loss of carbonate alkalinity. The calcium sulfate can then provide soluble calcium to the system as well as sulfate (Equation 8). As the pH lowers below 6.5 monovalent aluminum dihydroxide [$Al(OH)_2^+$] becomes soluble and may cation exchange on clay surfaces to release soluble calcium. It is only below a pH 6 that the multivalent aluminum monohydroxide [$Al(OH)^{2+}$] and soluble aluminum [Al^{3+}] are available for linking particles (Pernitsky 2006). For both hydrated lime and alum, calcium appears to be a principle multivalent cation responsible for coagulation.

To further investigate the nature of hydrated lime and alum dose effects on settling rate and settled volumes the data was analyzed to as a function of soluble calcium concentration, as this is providing the coagulative properties. This analysis, shown in Figure 5, demonstrates the best settling properties at a soluble calcium concentration of 32 mg/L that for both hydrated lime (750 ppm) and alum (200 ppm); however, hydrate lime provides superior water clarity compared to alum (0.025 versus 0.337 AU). The results suggest that 800 ppm of alum is

Table 4. Evaluation of Coagulants Pretreatments

Coagulant	No Additive		Hydrate Lime		Alum		Gypsum	
Best Dose (ppm)	n/a		1000		750		1000	
Absorbance (AU | pts)	1.23	0	0.04	3	0.01	3	0.17	2
Settling Rate (s | pts)	2*	3	3	3	84	1	270	0
Settled Height (mL | pts)	155	3	190	3	365	1	360	1
Total Points**		6		12		8		5

* Settling of rate of no additive was estimated
** Total Points = (Absorbance Points)*2 + Settling Rate Points + Settled Height Points

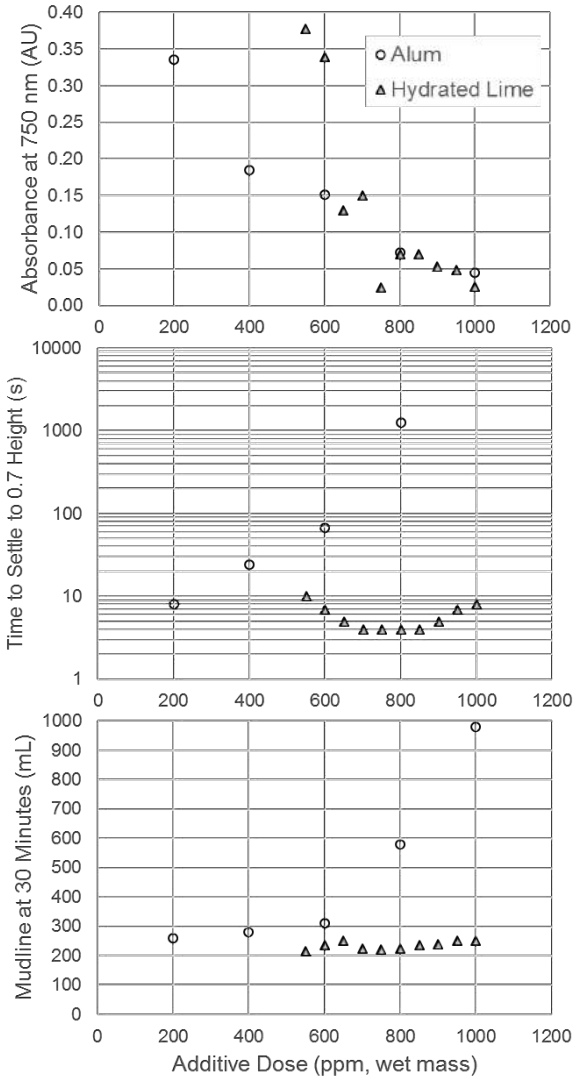

Figure 2. Detailed Sweep of the Effect of Hydrated Lime as a Coagulant Pretreatment to HPAM Flocculation with Comparison to Alum

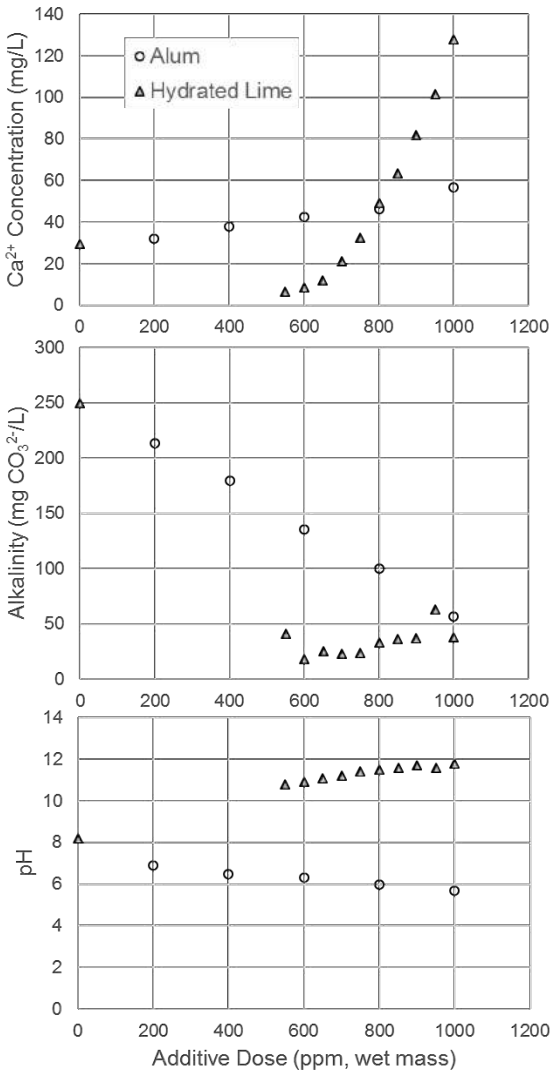

Figure 3. Effect of Hydrated Lime and Alum Treatment of a Dilute FFT Slurry on Calcium Concentration, Alkalinity, and pH

required to reduce turbidity with a soluble calcium concentration of 46 mg/L, but any increases above 200 ppm of alum result in significant decline settle rate and increase in settled volume. The decrease in performance of settling properties with increases alum dose was also observed in the initial screening, where its behavior shows similarities to gypsum in Figure 1. The similarities between alum and gypsum are most likely a result of in-situ generation of calcium sulfate by alum. There is also a much smaller decline in settling rate and increase in settled volume as hydrated lime increases calcium concentration; however, the effects are negligible compared to those observed with alum.

Hydrate Lime ($CaOH_{(2)}$)

$$Ca(OH)_{2(aq)} + NaHCO_{3(aq)} \rightarrow CaCO_{3_{(aq)}} + NaOH_{(aq)} + H_2O \quad (1)$$

$$NaOH_{(aq)} + NaHCO_{3(aq)} \rightarrow Na_2CO_{3(aq)} + H_2O \quad (2)$$

$$Ca(OH)_{2(aq)} + Na_2CO_{3(aq)} \rightarrow CaCO_{3_{(aq)}} + NaOH_{(aq)} + H_2O \quad (3)$$

$$Ca(OH)_{2(aq)} \rightarrow Ca^{2+}{}_{(aq)} + 2OH^{-}{}_{(aq)} \quad (4)$$

Alum ($Al_2(SO_4)_3$)

$$Al_2(SO_4)_{3(aq)} + 6H_2O \rightarrow 2Al(OH)_{3(s)} + 3H_2SO_{4(aq)} \quad (5)$$

$$H_2SO_{4(aq)} + Ca(HCO_3)_{2(aq)} \rightarrow CaSO_{4(aq)} + 2CO_{2(g)} + 2H_2O \quad (6)$$

$$H_2SO_{4(aq)} + CaCO_{3(s)} \rightarrow CaSO_{4(aq)} + CO_{2(g)} + H_2O \quad (7)$$

$$CaSO_{4(aq)} \rightarrow Ca^{2+}{}_{(aq)} + SO_4{}^{2-}{}_{(aq)} \quad (8)$$

Figure 4. Reaction Mechanisms of Hydrated Lime and Alum to Generate Soluble Calcium

The effect of increasing calcium concentration appears to improve water clarity and decrease the flocculant performance. Improvements to water clarity appear to be the result of decreased turbidity from the removal of fine clay particles and organics by the divalent calcium ion, likely due to charge neutralization and agglomeration of these particles which facilitates their capture during flocculation with polymer. Hydrated lime appears to be able to achieve this coagulation at a lower soluble calcium concentration than alum. As calcium concentrations rise the flocculation performance declines, possibly due to bivalent calcium creating linkages inside the polymer and collapsing its structure into a ball; however, this consequence is most severe for alum as it required higher soluble calcium to achieve effective water clarity. Additionally, the coagulation by alum appears to be far worse for the settling properties compared to hydrated lime as a calcium source – this significant difference cannot be explained by the current study and merits further investigation. Hydrated lime was able to provide excellent release water clarity with only minor decreases in settling performance.

CONCLUSIONS

This study investigated the potential benefits of using hydrate lime, alum, or gypsum as a coagulant before flocculation of dilute FFT slurries. Initial screening demonstrated that both hydrated lime and alum were able to provide significantly improve water clarity compared to the control while maintaining a reasonable settling rate and dewatering volume, vastly outperforming gypsum. A second study investigated hydrated lime and alum in further detail, including water chemistry analysis

which demonstrated that soluble calcium appears to be the cation responsible for coagulation with hydrated lime and alum. While both hydrated lime and alum were able to achieve high water clarity, hydrated lime achieved this high clarity at a lower calcium concentration and therefore was able to provide significantly better settling rate and settled volumes compared to alum. In these experiment, hydrated lime was the superior coagulant pretreatment for this HPAM polymer flocculation of FFT and deserves further study to understand potential benefits in oil sands tailings thickener processes.

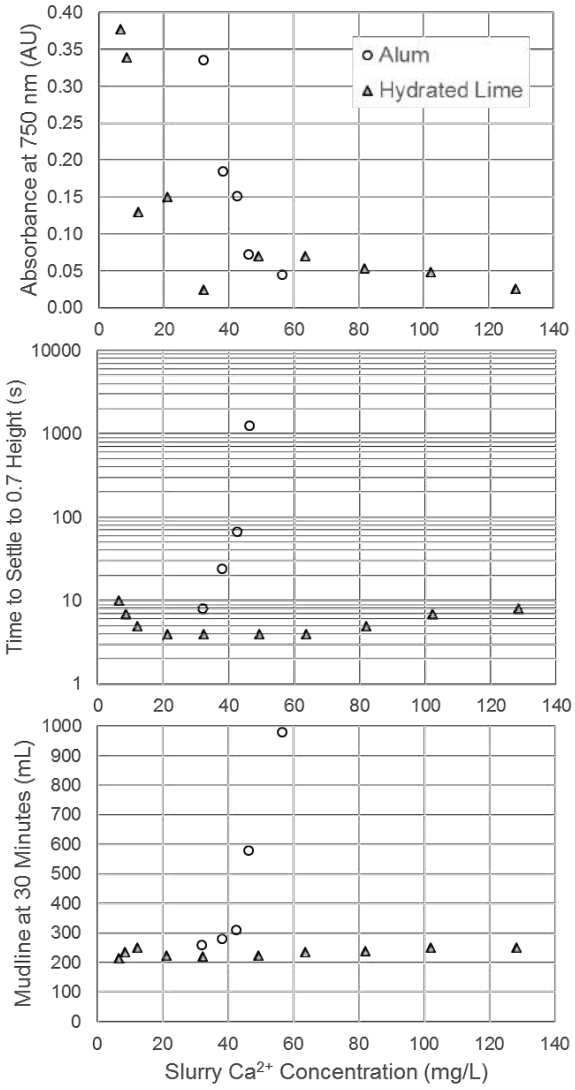

Figure 5. Effect of Soluble Ca^{2+} Concentration on Settling Rate for Hydrated Lime as a Coagulant Pretreatment to HPAM Flocculation with Comparison to Alum

REFERENCES

Alberta Energy Regulator (2018). State of Fluid Tailings Management for Mineable Oil Sands, 2017.

Boswell, J., Sobkowicz, J. and Davachi, M. (2012). Oil Sands Technology Development Roadmap. Project Report, **5**.

Ching, H. W., Elimelech, M. and Hering, J. (1994). Dynamics of Coagulation of Clay Particles with Aluminum Sulfate. Journal of Environmental Engineering, **120**(1): 169-189.

Hamza, H., Stanonik, D. and Kessick, M. (1996). Flocculation of Lime-Treated Oil Sands Tailings. Fuel, **75**: 280-284.

Kasperski, K. (1992). A Review of Properties and Treatment of Oil Sands Tailings. AOSTRA Journal of Research, **8**: 11.

Lane, S. (1983). Lime Coagulation and Stabilization of Total Oil Sands Tailings. Petroleum Society of Canada Annual Technical Meeting, May 10-13. Banff, AB, Canada.

Little, D. N. (1995). Handbook for Stabilization of Pavement Subgrades and Base Courses with Lime. The Lime Association of Texas.

McKenna, G. Mooder, B., Buton, B. and Jamieson, A. (2016). Shear Strength and Density of Oil Sands Fine Tailings for Reclamation to a Boreal Forest Landscape. Proceedings of Fifth International Oil Sands Tailings Conference, pp. 130-153.

McMinn, N., Gramlich, B. and Stephens, G. (2016). The MFT Centrifuging Experience. Proceedings of Fifth International Oil Sands Tailings Conference, pp. 313-317.

Pernitsky, D. and Edzwald, J. (2006). Selection of Alum and Polyaluminum Coagulants: Principles and Applications. Journal of Water Supply, **55**: 121-141.

Rahal, K., Fox, J., Leikam, J., Tate, M. and Romaniuk, N. (2018). Impact of Calcium Hydroxide on the Equipment and Process of Oil Sands Tailings Treatment. To be presented at Tailing and Mine Waste 2018.

Renard, D., Zahabi, A., McMullan, J., Sakahuni, G., Liu, Y., Hickson, S., Esmaeili, P., Cavanagh, P., Lenart, J., Loman, P., Dela Rosa, E., Huculak, T., Jara, R., Baier, K., Medrano, J., Mirza, J., Najafi, A. and Clark, J. (2016). Thickening and Reflocculation Pilot Plant. Proceedings of Fifth International Oil Sands Tailings Conference, pp. 270-279.

Scott, J., Dusseault, M. and Carrier, W. (1985). Behaviour of the clay/bitumen/water sludge system from oil sands extraction plants. Applied Clay Science, **1**: 207-218.

Tate, M., Leikam, J., Scott, J. D., Mehranfar, M., Romaniuk, N. and Ozum, B. (2016). (2016). Impacts of Calcium Compounds on Oil Sands Water Chemistry. Tailings and Mining Waste 2016.

Tate, M., Leikam, J., Fox, J. and Romaniuk, N. (2017). Use of calcium hydroxide as a coagulant to improved oil sands tailings treatment. Tailings and Mining Waste 2017.

Vedoy, D. and Soares, J. (2015). Water-Soluble Polymers for Oil Sands Tailing Treatment: A Review. Can J Chem Eng, **93**: 888-904.

Session 2

NUMERICAL MODELLING

FRAMEWORK FOR CONSOLIDATION OF UNCONVENTIONAL MATERIALS

Silawat Jeeravipoolvarn and Sam Proskin
Thurber Engineering Ltd., Calgary, Canada

ABSTRACT

Consolidation testing and analysis have been utilized to measure consolidation properties and design for various materials worldwide. For most naturally occurring materials, the application of the test and analysis are straightforward and provide results appropriate to engineering designs. For unconventional materials such as tailings, their young ages, complex compositions and deposition configurations often make their consolidation prediction complex and evolving. The mining application of the consolidation information demands increasing accuracy for essential dyke raise, material planning and regulatory reporting purposes. This type of material and operation require an in-depth appreciation of the overall objectives, background theory, laboratory testing, supporting analytical tools and their limitations. This paper presents an example of a framework with practical application for estimating tailings volume changes. The implementation of the framework in the early stages of a project would provide an effective and sensible approach to improving tailings consolidation predictions for mine tailings planning.

INTRODUCTION

The application of soil consolidation was recognized in Mesopotamia in the fifth millennium B.C. when the Sumerians constructed new buildings on the site of old structures – applying the technique of preloading as it is known today (Schiffman 2001). Modern consolidation testing for soils and slurries, its mathematical treatment and engineering framework have been around since the early 20th century (Terzaghi 1923, 1924; Gibson et al. 1967). This modern framework has been utilized in various types of projects worldwide including foundations of structures and large land reclamation projects. Successes and failures of these works have taught geotechnical, foundation and civil engineers to be mindful of what is underneath.

For naturally occurring materials, the analysis of the consolidation problem is mature involving the estimation of material properties along with appropriate analytical tools and design combined with calibration through field measurements. This is not the case for unconventional materials such as tailings – with variety of physical and chemical compositions, young (by geological standards) and undocumented histories. Tailings deposits challenge the design engineers attempting to predict tailings rate of consolidation accurate enough for materials management and mine planning. In the outset, this might sound like a daunting task. The working solution is, however, already available and lies in the history of the development of the geotechnical engineering discipline. This paper presents a multiscale framework for geotechnical analysis for tailings consolidation.

Challenges of Unconventional Materials

For typical civil engineering projects, natural occurring soils are composed of quartz, clays and other rock forming minerals reflecting natural crustal abundances. Pore fluids within soil and rock generally are in chemical equilibrium with a well-documented set of chemical compositions. Their particle gradation, fabric and structure are related to their weathering and depositional environment developed over geological time frames of millions of years. In situ foundation soils are investigated by drilling/sampling, cone penetration test (CPT) or standard penetration test (SPT). Soil samples can be recovered to obtain consolidation parameters from one-dimensional consolidation testing. Reliable foundation design for such deposits is a routine practice for most of the world. The consolidation settlement prediction of the Bangkok International Airport deviated less than 1% from the actual (Bergado et al. 2002) showing an example of the reliability in settlement predictions for large civil engineering projects.

For typical oil sands mining operations, the mined material consists of quartz sands, clay shales, limestones, clays, semi-solid bitumen and pore water. The mined oil sands are then subjected to

crushing, grinding and flotation processing to separate the bitumen from the solids. The pore fluid chemistry is amended with caustic, coagulant, flocculant, and other process related chemicals. These compositions are known to vary during the life of mine as the ore body changes and process refinements are made to enhance bitumen extraction and tailings dewatering. The tailings – with their high initial water content – are forming complex deposits as their composition changes and different types of tailings are discharged over different areas. The common goal for such material is to accelerate settlement during deposition therefore maximizing the tailings containment capacity and water recovery; and minimizing the settlement after the end of filling. Tailings height prediction deviation of within ±20% from the actual has been documented in Table 1 and Figure 1. These "unconventional" materials are typical day-to-day routine tasks for tailings engineers and planners.

These prediction results, of course, span a variety of material types and projects. One thing they have in common is the simple performance indicator of the deposit height with time. It is observed in Table 1 that in some cases the prediction accuracy is comparable to civil engineering projects, while for others the error is non-trivial.

To understand the sources of error in the predictions, the following simplified key considerations shall be examined:

1. The contained materials (i.e. tailings):
   a. Dewatering mechanism (and analysis method for it)
      i. Stokes settling
      ii. Hindered sedimentation
      iii. Segregation
      iv. Consolidation
      v. Secondary compression
      vi. Others (e.g. flow, thixotropy, channelization, evaporation, evapotranspiration, biological, wicks etc.)
   b. Material information (and how the information is obtained)
      i. Initial condition (e.g. solids, particle size, mineralogy, chemistry, specific gravity)
      ii. Material behaviour (e.g. compressibility and hydraulic conductivity)

2. The containment structure and foundation:
   a. Boundary condition (e.g. foundation material type, and ground water table)
   b. Geometry (e.g. containment width, height, side slope, other structures within the containment, etc.)

3. Activities (previous, present and future)
   a. Processing
   b. Filling
   c. Dredging
   d. Others that could impact the behaviour (e.g. capping, decanting, flowing & sliding, etc.)

These considerations are important to establish a dependable prediction framework. For example, in the case of dewatering mechanism, the focus should be on selecting the most influential ones on a case by case basis. The following are two examples of the challenges associated with the "unconventional" materials.

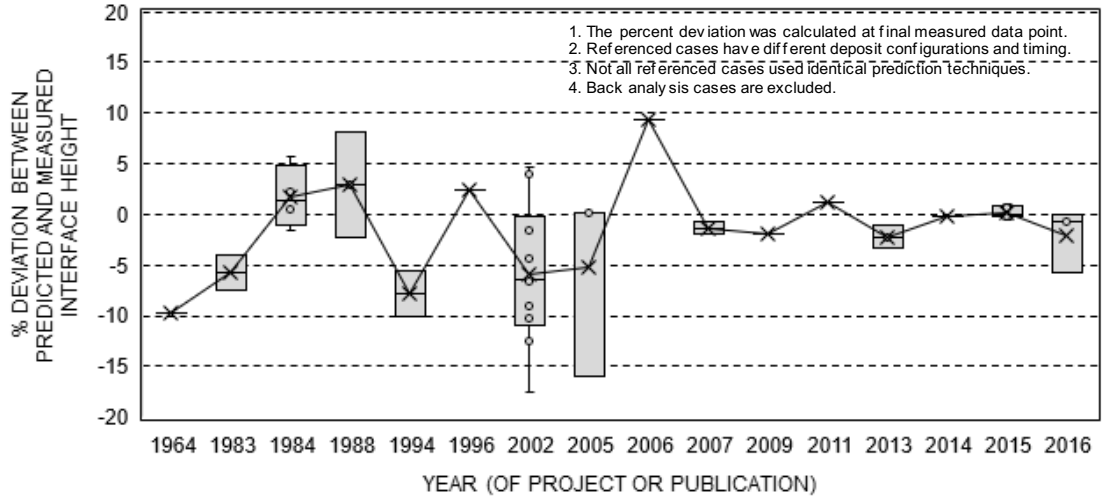

Figure 1. Percent deviation between predicted and measured interface height with time

Table 1. Unconventional materials – prediction vs. observed

Name	Material	Project scale	% Deviation	Reference
Suncor Pond A 1977 data - accreting pond	Oil sands fluid fine tailings	Commercial	-8%	Yong et al. (1983)
Suncor Pond B 1977 data - stagnant pond	Oil sands fluid fine tailings	Commercial	-4%	Yong et al. (1983)
Test Area 1, Seagirt Marine Terminal	Dredged materials, Baltimore	Field test	-2% to 2%	Krizek and Somogyi (1984)
Test Area 2, Seagirt Marine Terminal	Dredged materials, Baltimore	Field test	0% to 6%	Krizek and Somogyi (1984)
Disposal sites, Toledo, Ohio	Dredged materials	Commercial	-10%	Krizek and Somogyi (1984)
10 m standpipe test on MFT (1988)	Oil sands fluid fine tailings	Pilot lab test	-2% to 8% (3% median)	Pollock (1988)
Bitumen free centrifuge test	Bitumen free oil sands fine tailings	Lab test	2%	Eckert et al. (1996)
Syncrude CT prototype field deposit	Composite tailings	Field test	0% to 4%	Pollock et al. (2000)
Sidere	River sediment, Belgium	Lab test	-17% to 5% (-7% median)	Bartholomeeusen et al. (2002)
Phosphatic mine tailings evaporation	Phosphatic tailings	Field test	-2% to -1%	Znidarcic (2007)
10 m standpipe test on MFT (2009)	Oil sands fluid fine tailings	Pilot lab test	-16%	Jeeravipoolvarn et al. (2009)
10 m standpipe test on MFT-sand mix (2009)	MFT-sand mix 52% fines	Pilot lab test	0%	Jeeravipoolvarn et al. (2009)
10 m standpipe test on MFT-sand mix (2009)	MFT-sand mix 18% fines	Pilot lab test	0%	Jeeravipoolvarn et al. (2009)
Syncrude ILTT lab standpipe	In-line thickened tailings	Lab test	-2%	Jeeravipoolvarn (2010)
Syncrude ILTT field deposit	In-line thickened tailings	Field test	9%	Jeeravipoolvarn (2010)
Suncor centrifuge test	Oil sands fluid fine tailings	Lab test	1%	Znidarcic et al. (2011)
Evaporation standpipes	Thickened oil sands tailings	Lab test	-1 % to -3% (-2% median)	Jeeravipoolvarn et al. (2013)
Treated fine tailings standpipe test	Treated fluid fine tailings	Pilot lab test	0%	Moore et al. (2014)
Centrifuge prototype - TT-50	Thickened tailings, 50% fines	Lab test	0%	Sorta (2015)
Centrifuge prototype - TT-60	Thickened tailings, 60% fines	Lab test	1%	Sorta (2015)
Centrifuge prototype - AL-7.5	Albian FFT from 7.5 m depth	Lab test	1%	Sorta (2015)
Centrifuge prototype - AL-15	Albian FFT from 15 m depth	Lab test	0%	Sorta (2015)
Centrifuge prototype - FSMT	Fines and sand mixture tailings	Lab test	0%	Sorta (2015)
10 m standpipe test on MFT (2005)	Oil sands fluid fine tailings	Pilot lab test	-1%	Krishna et al. (2015)
Evaporation of fine tailings - deep stack	Oil sands fluid fine tailings	Field test	0%	Vardon et al. (2016)
Evaporation of fine tailings - thick multi lift	Oil sands fluid fine tailings	Field test	-1%	Vardon et al. (2016)
Evaporation of fine tailings - thin multi lift	Oil sands fluid fine tailings	Field test	-6%	Vardon et al. (2016)
Caustic oil sands tailings standpipe test	Caustic oil sands fine tailings	Lab test	-5%	Jeeravipoolvarn et al. (2017)
Non-caustic oil sands tailings standpipe test	Non-caustic oil sands fine tailings	Lab test	-10%	Jeeravipoolvarn et al. (2017)

Notes: 1. The percent deviation was calculated at final measured data point. Complete comparison can be found in the references.
2. Referenced cases have different deposit configurations and timing.

The first example is settlement and pore water pressure dissipation with time under a constant vertical effective stress for an unconventional material (Figure 2). The primary consolidation by the excess pore water pressure occurs rapidly. After the primary consolidation, secondary compression leads to considerable settlement (comparable to the primary stage) even though there is no measurable excess pore water pressure. If one conducts the large strain consolidation test for such material without measurement of excess pore water pressure, one might be perplexed by the slow compression regardless of its high hydraulic conductivity. This is an example of "dewatering mechanism" consideration.

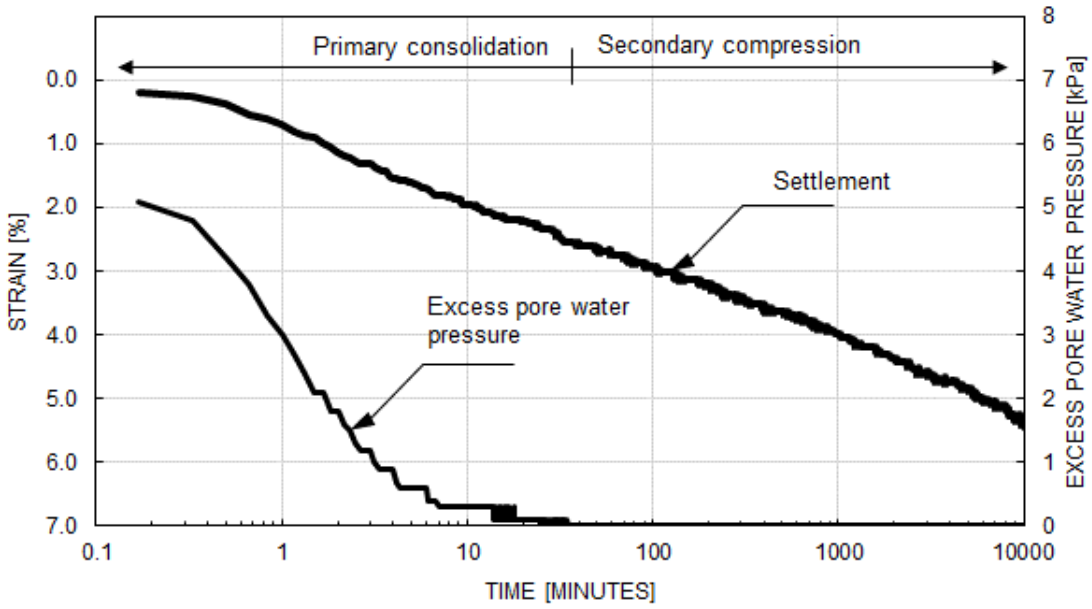

Figure 2. Excess pore water pressure and settlement of unconventional tailings (Thurber's files)

The second example is a layered deposit (Figure 3, Esposito and Nik, 2012) representing an example of variable "pond filling activities". Although this type of deposit layering can be found in nature but not so common that one has to analyze them for every layer or as a whole under a large strain condition. Questions for this type of deposit might include:

- What type of constitutive relationships are applicable to each layer?
- Are there three-dimensional effects?
- Can a simplification be made while maintaining sufficient of accuracy?

These questions help forming a sensible and practical solution of the overall system.

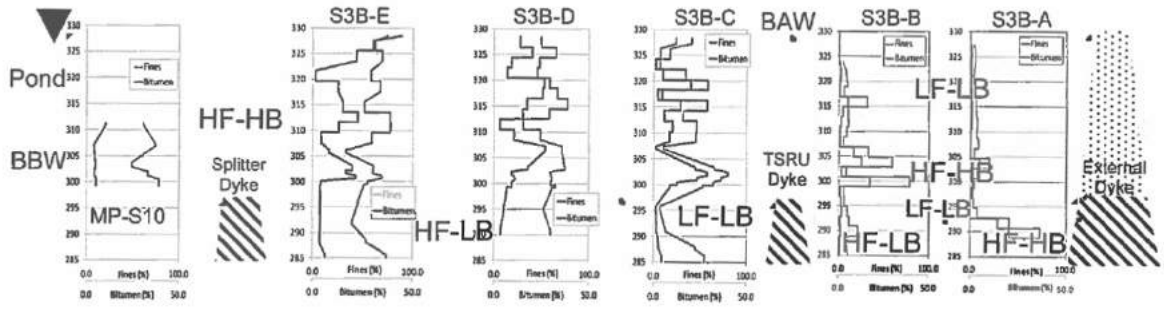

Figure 3. Complex layering in a deposit (Esposito and Nik 2012)

Multi-scale Framework for Consolidation Analysis

A design engineer has to adopt an approach for consolidation analyses that are consistent with the data available and risk approach. Figure 4 proposes a multiple-scale framework for consolidation analysis. In this approach there are three options:

1. Theoretical projection
2. Empirical projection
3. Theoretical-Empirical projection

Theoretical Projection

This method uses index data, laboratory data or both to obtain soil parameters and apply them to consolidation analysis. The risks may not be well known or understood as analyses are not supported by actual field behaviour and information. For known materials the risk can be low when such methodology has been previously applied; and experience and know-how have been well developed. However, the method could post high risk for tailings with limited laboratory or field experience. Design engineers may have to resort to using very conservative parameters that could lead to overestimates of tailings volume requirements and is subsequently considered wasteful. The method requires relatively small time and budget to complete.

Empirical Projection

This method uses index data (or other rapid testing) with field scale data to directly develop a performance base empirical correlation. The empirical projection can be reliable for known materials with given fixed conditions. However, the method can be a risk for unknown materials because an empirical formula is based on parameters which may or may not control the key performance; and conditions which may or may not stay the same as the mine operations progresses through its life span. The method typically requires an experienced engineer with good understanding of site operations, and strong theoretical and field experience to set out the work. The method also needs a considerable development time into the actual operation to permit a reliable performance based empirical correlation.

The theoretical and empirical projection methods are valuable tools but will not be discussed further in this article.

Theoretical-Empirical Projection

The theoretical-empirical projection is based on integrated theoretical and empirical approaches – evolved from the consolidation theory development method (Terzaghi 1956) and the observational method described by Peck (1969). The geotechnical observational approach is a proven approach to managing the risk for natural soils that could be adapted to unconventional materials such as tailings.

In Figure 4, during the planning stage, a design engineer develops a list of potential dewatering mechanisms based on available geotechnical information. With the list of mechanisms established, the engineer sets the objectives of the work and selects the key considerations for the framework. Expert inputs are highly recommended during this stage. The list of properties of the tailings which may have a significant influence on their performance under stress and a list of required testing and interpretation methods of the properties must be established as an outcome of this stage. Once completed, the work flow continues on the flow diagram in Figure 4, and descriptions in Table 2.

During the microscopic stage, basic information is gathered to develop a database of basic material parameters (e.g. particle size, water chemistry, Atterberg limits, etc.). This database is used as “tailings specification” to screen material and see if the tailings remains within the specification during the operation. The microscopic tests must be selected and performed in a way that they relate to the key performance parameters (i.e. settlement vs. time) in a simple and rapid manner. Tailings outliers (those not meeting specification) shall require a performance or field scale evaluations in the next stage.

In the macroscopic stage, engineering design information is obtained systematically using standard and/or advanced testing methods. The results will be used to prepare working hypotheses for design. Macroscopic tests must be conducted in the way that the material is expected to go through in the actual and/or the extreme conditions. A design engineer should invite expert inputs from the planning stage and apply his/her ingenuity to setup the tests depending on the goal of the clients and their risk tolerance. The engineer must also be aware of how the results will be used in within the analytical or empirical senses – i.e. the laboratory data must be supported by a proper design tool.

Limitations should be noted, not only in the analytical but also in laboratory test data (often that observed behaviour is perceived as the truth which is not always the case). In essence, the macroscopic stage provides a working hypotheses design, an initial projection, and a basis for comparison to the field performance.

In the field scale, the engineer will select the key performance indicators (KPI) and their measurement methods. One needs to compare the field behaviour with the working hypotheses design. Re-design / calibration / correction / additional laboratory work might be required depending on the level of the acceptable accuracy. Quality control and quality assurance are also recommended during the stage, the engineer shall set out QA and QC programs to regularly monitor the field behaviour (KPI) as well as key fundamental considerations (selected during the planning stage). Contingencies should be developed from the micro and macro stages to anticipate substantial deviations observed in the field scale from the working hypothesis design to mitigate the associated risks to mine operations. The theoretical-empirical method, when properly applied, offers economic and risk mitigation advantages. Flexibility is built into the approach in a way that one could select to perform certain tasks at certain time depending on the requirement.

GOING FORWARD AND MAJOR DEVELOPMENT REMARKS

Temporal and spatial variability create uncertainties in the fate of most tailings – changes in ore grade, extraction methods, processing, aging, tailings operations, climate-change etc. The history of consolidation has evolved from basic observation to advanced instrumentation and mathematics. Advances in laboratory testing, geotechnical instrumentation, and the understanding of the theory and the realization of the actual behaviour are combined into the geotechnical multiscale framework – one of such is given in Figure 4.

With the right objectives and in-depth understanding of each working components, the given framework allows time and complex variables to be economically evaluated through laboratory testing, field observation and data analysis. To this end, some notable developments during the last decade in the field of tailings consolidation in Canada are listed below:

- Development of new chemicals, biological, and mechanical processes for favourable dewatering behaviour of oil sands tailings.
- Advances in laboratory testing:
  - Beam centrifuge consolidation test at the University of Alberta that allows a prototype simulation of long-term consolidation to be conducted in a matter of days.
  - Optimized large strain consolidation (LSC) test – an optimized test setup for higher productivity.
  - Seepage Induced Consolidation (SIC) test – a faster consolidation test method using seepage force on soft materials.
  - Restricted Flow Consolidation (RFC) test – a faster consolidation test method with continuous constitutive relationship measurement.
  - Rapid Centrifuge Consolidation (RCC) test – a rapid consolidation assessment / screening / monitoring tool.
  - Soil water characteristic curve and constitutive relationships determination for high water content material.
- Advances in tailings consolidation analysis:
  - 2D and 3D self-weight consolidation
  - Time dependent constitutive relationship (e.g. creep)
  - Environmental dewatering (freeze-thaw, evaporation, and evapotranspiration)
  - Numerical analysis of layered deposit by homogenization and layered approaches
  - Laboratory numerical analysis (RFC, RCC and beam centrifuge)
  - Statistical analysis for consolidation (probabilistic, database, etc.)

We believe significant opportunities exist in taking advantages of these developments by incorporating them into the multiscale geotechnical framework and enhancing the reliability of consolidation analyses of tailings deposits.

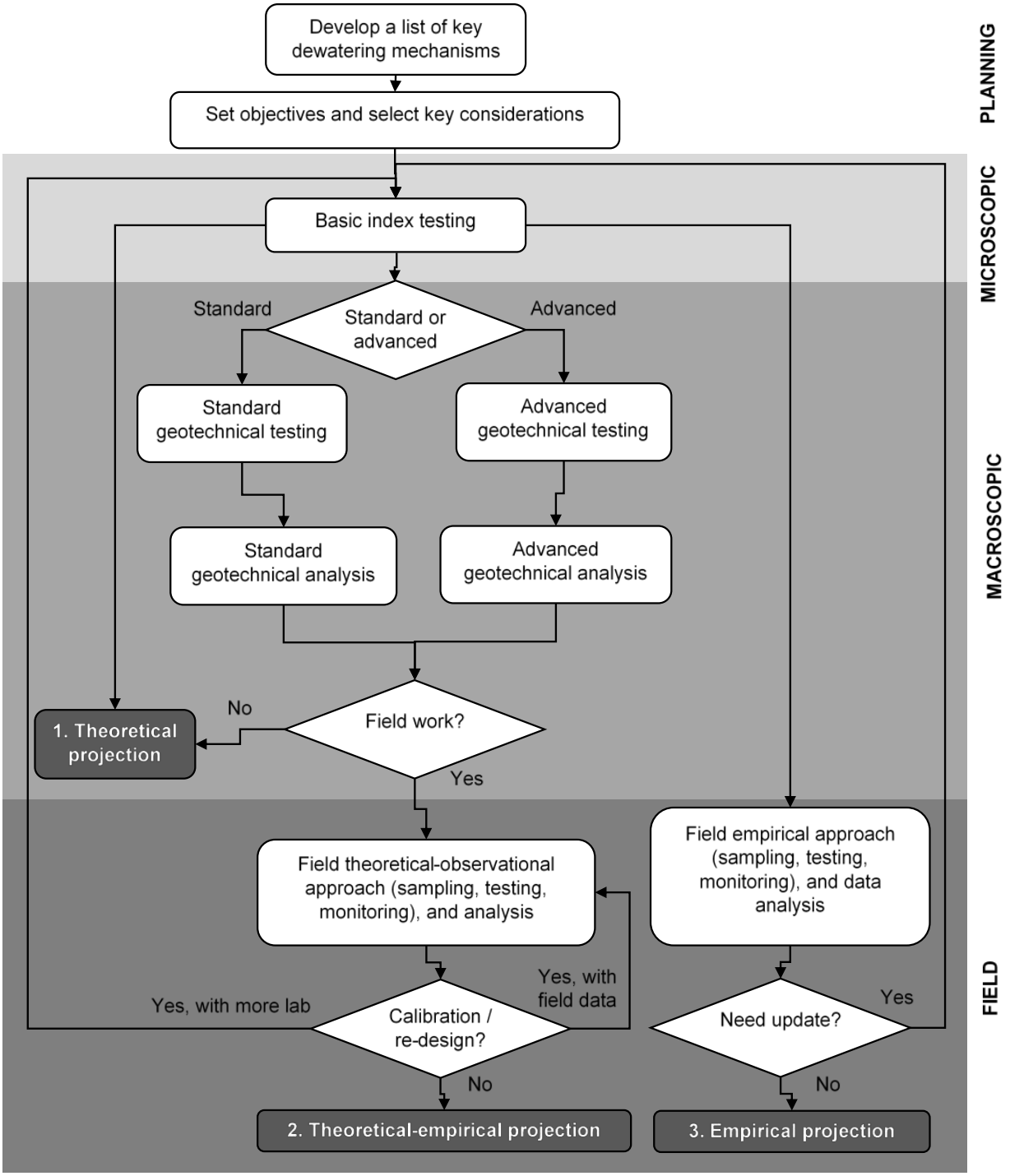

Figure 4. Example of geotechnical multi-scale framework for consolidation analysis

Table 2. Multiple scale work tasks - objectives, test method and outcome

Scale	Objectives	Test method selection / frequency	Outcome	Remarks
Microscopic (or laboratory index properties)	• Identify fundamental changes that might cause changes in engineering properties • Obtain initial design parameters based on index information	• **Quick and simple test** method allows database development and statistical treatment. • **Focus on test method that affects the key performance behavior** and avoid unjustified scientific curiosity. • Perform the test regularly but guided by the mining and related fundamental changes.	• A database of fundamental parameters representative of a whole deposit – tailings specifications. • A quality control tool to feed information to the designer and alert if the fundamental compositions of the material has changed.	• Recent studies on the use of bench-top centrifuge could allow a more focused screening / monitoring • Non-standardize testing could provide mixed signals
Macroscopic (or laboratory performance parameters)	• To study the engineering parameters for uncharacterized materials. • To obtain engineering parameters for design under a laboratory-controlled environment. • Option to do both standard and advanced geotechnical testing and analyses. • To explore unfavorable conditions, expect the unexpectable and plan of actions	• Engineering test for quantitative engineering parameters, quality assurance • **Must be conducted in the way that the material is expected to go through in the real case**. Extreme conditions can be conducted to develop working boundaries. • **Must aware of how the data will be used** with what models / simulations / assumptions. • Advanced (custom) testing method may be required for special circumstances.	• Engineering design parameters to feed into a theoretical analysis. • The use of theoretical analysis provides estimate of field behaviour in various possible conditions.	• Laboratory performance work typically is too expensive to generate data sets sufficient for statistical analysis. • Non-standardize testing could provide mixed signals. The design engineer shall request for repeatability / reproducibility.
Field	• To track the actual behaviour and compare to the design. • To refine / calibrate the prediction if required.	• **Key performance must be identified and measured with time.** • **Must be aware of changing conditions and working hypotheses.** • Typical measurements include: settlement, excess pore water pressure dissipation, void ratio reduction.	• Actual global behaviour. • Reality feedback to the design and laboratory performance section • Allow back analysis / prediction refinement.	• Care and diligent are required in the field to capture the right type data properly and adequately. • Key physics must be implemented for proper back analysis.

ACKNOWLEDGEMENT

Thurber Engineering Ltd., Calgary for their financial support in the preparation of this article.

REFERENCES

Bartholomeeusen, G., Sills, G. C., Znidarcic, D., Van Kesteren, W., Merckelbach, L. M., Pykes, R., Carrier, W. D., Lin, H., Penumadu, D., Winterwerp, H., Masala, S. and Chan, D. (2002). Sidere: numerical prediction of large-strain consolidation. Geotechnique, **52**(9): 639-648.

Bergado, D. T., Balasubramaniam, A. S., Fannin, R. J. and Holtz, R. D. (2002). Prefabricated vertical drains (PVDs) in soft Bangkok clay: a case study of the new Bangkok International Airport project. Canadian Geotechnical Journal, **39**: 304-315.

Esposito, G. and Nik, R. (2012). Fines capture in a long tailings beach at the Shell Muskeg River Mine External Tailings Facility: Hydraulic and depositional aspects. Third International Oil Sands Tailings Conference, Edmonton, AB, Canada, December 2-5, 2012.

Jeeravipoolvarn, S., Scott, J. D. and Chalaturnyk, R. J. (2009). 10 m standpipes test on oil sands tailings: long-term experimental results and prediction. Canadian Geotechnical Journal, **46**: 875-888.

Jeeravipoolvarn, S. (2010). Geotechnical behaviour of oil sands in-line thickened tailings. Ph.D. thesis, University of Alberta, 431p.

Jeeravipoolvarn, S., Gidley, I., Moore, T. and Tran, D. (2013). A finite strain consolidation model with evaporation: actual evaporation and unsaturation correction approach. Proceedings of Tailings and Mine Waste Conference 2013, November 3-6, Banff, AB, pp. 277-286

Jeeravipoolvarn, S., Miller, W., Scott, J. D., Kabwe, L. and Wilson, G. W. (2017). Modeling Effect of Bitumen Extraction Processes on Oil Sands Tailings Ponds. Journal of Civil Engineering and Architecture, **11**: 48-59.

Krishna, C., Fredlund, M., Lu, H. and Xu, L. (2015). Benchmarking of Large Strain Consolidation, Sedimentation, and Creep Process for Oil-Sands Tailings. Tailings and Mine Waste Conference 2015, Vancouver, BC, 12p.

Krizek, R. J. and Somogyi, F. (1984). Perspectives on modelling consolidation of dredged materials. Sedimentation consolidation models: predictions and validation: In proceeding of a symposium R. N. Yong and F. C. Townsend Eds, ASCE, New York: 296-332.

Moore, T., Zhang, C., Moffett, R. and Odle, J. (2014). Self-weight consolidation of Particlear-treated tailings in a 10 metre column. Paste 2014, Vancouver, BC, June 2014.

Peck, R. B. (1969). Advantages and limitations of the observational method in applied soil mechanics, Ninth Rankine Lecture, Geotechnique, **19**(2): 171-187.

Pollock, G. W. (1988). Large Strain Consolidation of Oil Sand Tailings Sludge. M.Sc. Thesis, University of Alberta, 276p.

Pollock, G. W., McRoberts, E. C., Livingstone, G., McKenna, G. T. and Matthews, J. G. (2000). Consolidation behaviour and modelling of oil sands composite tailings in the Syncrude CT prototype. Tailings and Mine Waste 2000.

Schiffman, R. L. (2000). Theories of Consolidation. March 2001. University of Colorado Press.

Sorta, A. (2015). Centrifuge modelling of oil sands tailings consolidation. PhD thesis, University of Alberta, Edmonton Alberta, Canada, 315p.

Terzaghi, K. v. (1923). Die Berechnung der Durch-lassigkeitsziffer des Tonnes aus dem Verlauf der hydrodynamischen Spannungserscheinungen. Akad. Wiss. Wien. Math-naturw. Klasse **132**(3/4): 125-128.

Terzaghi, K. (1924). Die Theorie der hydrodynamischen Spannungserscheinungen und ihr erdbautechnisches Anwendungsgebiet. Proceedings of the international congress for applied mechanics, 288-294. Delft.

Terzaghi, K. (1956). Letter to Skipper, The Terzaghi Library, Norwegian Geotechnical Institute, Norway.

Vardon, P. J., Yao, Y., van Paassen, L. A. and Frits van Tol, A. (2016). Consolidation and atmospheric drying of fine oil san tailings: comparison of blind simulations and field scale results. Fifth International Oil Sands Tailings Conference, Lake Louise, AB, Canada, December 4-7, 2016.

Znidarcic, D. (2007). Soil and Water: The Essence of Soil Mechanics, Proceedings of the Suklje's Days Symposium, Slovenian Geotechnical Society, June 15-16, Strunjan, Slovenia, pp.5-25.

Znidarcic, D., Miller, R., van Zyl, D., Fredlund, M. and Wells, S. (2011). Consolidation Testing of Oil Sand Fine Tailings, Tailings and Mine Waste '11 Conference Proceedings, November 6-9, Vancouver, BC, ISBN: 978-0-88865-815-9, pp.251-257.

CREEP AND STRUCTURATION IN TAILINGS AND IN NATURAL CLAYS

Sunchao Qi, Muhammad Asif Salam and Paul H. Simms
Carleton University, Ottawa, Canada

ABSTRACT

There is now evidence that time dependent phenomena, such as creep and structuration, may affect predictions of large strain consolidation, in at least some types of oil sands tailings. Creep is commonly modelled through the concept of rate dependent compressibility. Three such models have been incorporated into the UNSATCON deposition simulation platform, and generally give similar results. Structuration is not generally incorporated into consolidation modelling. However, there exists much experimental data concerning structuration behaviour in natural clays. These are reviewed, and it appears that structuration behaviour exhibited in some flocculated FFT samples are not atypical of clay behavior. Therefore, observations on the change in the compressibility curve due to structuration in natural clays may help tailings engineers bound estimates of structuration and its effect in tailings deposits.

INTRODUCTION

Evidence of creep and thixotropic behaviour in oil sands tailings as well as natural clays is reviewed in a companion paper at this conference (Salam et al. 2018b). Suffice to say there is considerable body of work on these phenomena in FFT (Jeeravipoolvarn 2010, 2009, Miller 2010, Scott et al. 2013), and even larger body of work in natural clays, including for instance, Burland's Rankine Lecture (Burland 1990).

The practical relevance of creep and thixotropy is that they potentially modify the compression behaviour of a tailings deposit over the long term. Hence, the compression behaviour in deeper deposits with long consolidation times may underperform with respect to current expectations.

Creep in Natural Clays

Many clays exhibit a viscous component to their deformation, such that they continue to deform under a constant load or effective stress. This viscous component is evident in rate dependent compressibility curves, which must be accounted for in engineering applications involving long-term settlements of soft clays. For example, the construction of Kansai International Airport in Japan and similar projects involving construction of other artificial islands on clays (Watanabe et al. 2012).

The rate dependency of compression is often treated by considering that the location of the compressibility curve is dependent on strain rate (Leroueil 2006). At typical example of rate dependent behaviour for a natural clay is shown in Figure 1.

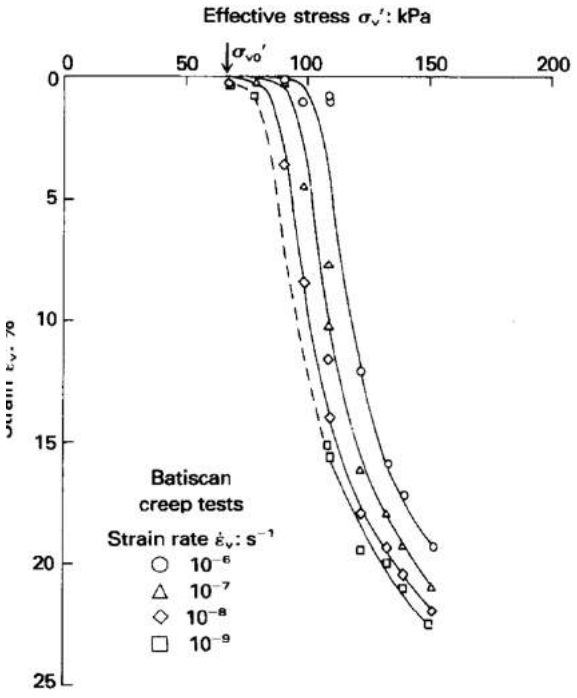

Figure 1. Typical strain rate dependence observed in natural clays (from Leroueil et al. 1985)

Data of the type presented in Figure 1 can be normalized with respect to an apparent pre-consolidation pressure that is related to strain rate. Watanabe et al. (2012) proposed a simple

relationship to relate the apparent pre-consolidation pressure and strain rate:

$$ln\frac{p_c^{'}-p_{cL}^{'}}{p_{cL}^{'}} = c_1 + c_2\dot{\varepsilon}_{vp} \quad (1)$$

In which p'_{cL} is a reference pre-consolidation pressure, p'_c is the actual preconsolidation pressure as a function of strain rate, $\dot{\varepsilon}_{vp}$ is the strain rate, c_1 and c_2 fitting coefficients.

Watanabe et al. (2012) analyzed data from around the world, and found strong agreement with many data sets, as shown in Figure 2. It can be seen that the shift in apparent compressibility due to rate effects is relatively well bound, between 0.7 and 1.5 of a reference pre-consolidation pressure.

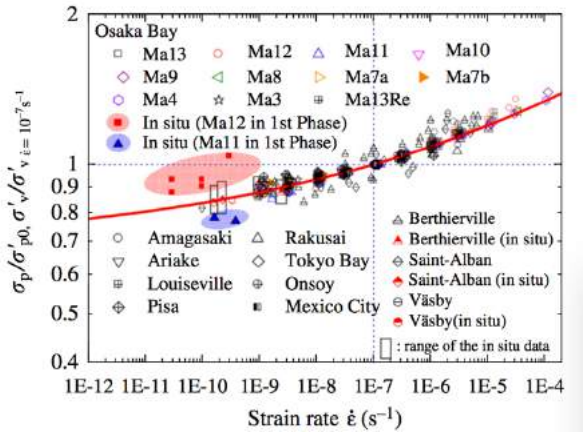

Figure 2. Variation in apparent pre-consolidation pressure with strain rate in large data set on clay compressibility (Watanabe et al. 2012)

It should be noted in the literature that there is some dispute as to the magnitude of creep during primary consolidation. The authors believe that the implications of creep to oil sands tailings deposition are largely independent of that dispute.

Structuration (Thixotropic Hardening / Ageing)

Structuration in natural clays is the process whereby a reconstituted or remolded natural clay, recovers its pre-consolidation pressure or stiffness over time, subsequent to being "destructured by the reconstitution process". Structuration is similar to thixotropy, the latter describing the recovery of strength rather than stiffness in a remolded or reconstituted soil. Soil mechanics is usually concerned with field materials that are already in their fully structured state, whereas with tailings the material has yet to reach this state. However, knowledge of the difference between the compressibility of remolded / reconstituted soils and their natural intact compressibility may assist tailings engineers in arriving at useful estimates of how the compressibility curves of tailings might change over time.

Burland (1990) compared compressibility characteristics between reconstituted and natural clays using a normalized void index, I_v:

$$I_v = \frac{e-e_{100}^{*}}{e_{100}^{*}-e_{1000}^{*}} \quad (2)$$

where $e_{100,1000}$ * denotes the void ratio at 100 kPa or 1000 kPa vertical effective stress from the compressibility curve of the reconstituted soil. For reconstituted natural clays, Burland (1990) found that I_v for many reconstituted natural clays fell on a unique line. However, consolidation data from intact or *in-situ* measurements of compressibility fell above this line, as shown in Figure 3. The line passing through the data in Figure 3 for intact clays is labeled the Sedimentation compression line.

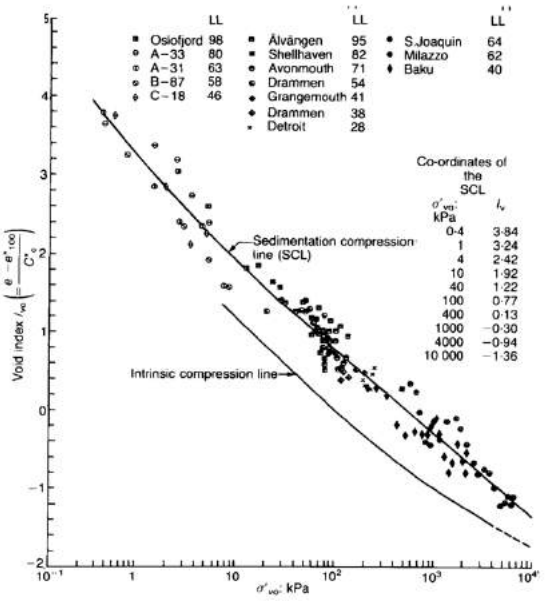

Figure 3. Difference between compressibility of in-situ or intact natural clays and the compressibility of reconstituted specimens (Burland 1990)

For a given void ratio or void index, the load borne by natural clays ranged from about twice to almost an order of magnitude higher for the natural clays compared to the reconstituted specimens. Burland (1990) gives examples of clays differing from this trend, in particular, highly cemented clays where precipitation of ferric hydroxides led to substantially poorer compressibility than indicated by Figure 3.

Creep and Structuration in a Polymer Amended FFT

Both creep and thixotropy have been reported in unamended FFT samples (Jeeravipoolvarn et al. 2009, Miller 2010). Miller (2010) presented some evidence of structuration, as an explanation to differences in the compressibility curves in 1m and 2 m high columns.

Salam et al. (2017, 2018) studied long term behaviour in short (0.1 m) replicate columns of polymer flocculated FFT (fFFT). 600 ppm of a high molecular weight anionic polymer was mixed into FFT at 32% solids. Details of the experimental setup and tailings preparation are given in another paper submitted to this conference (Salam et al 2018b). The behaviour is summarized in this paper in terms of dewatering and pore-water pressure data, as well as compressibility curves obtained from oedometer tests performed on samples cut from the replicate columns.

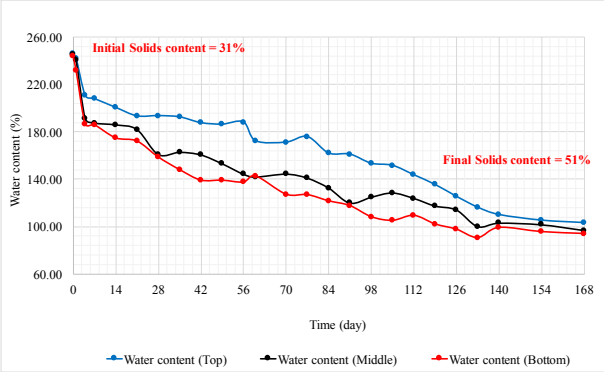

Figure 4. Dewatering of 0.10 m tall single drainage columns

The water content data is shown in Figure 4 occurs under submerged conditions, due to flux of water from the tailings up to the surface (the bottom boundary is sealed and the accumulated surface water is not decanted). Pore-pressure data variations are small after the first week. Nevertheless the bulk of volume change occurs almost continuously at the middle and bottom 1 cm of the sample, while the top 1 cm experiences most volume change after 50 days. The reduction in the top 1cm and the development of a more uniform profile with depth in density is characteristic of creep behaviour.

Some of these replicate columns were used to prepare oedometer samples, which were tested in oedometer cell modified for pore-water pressure measurement. The oedometer results are compared with compressibility inferred from a 0.5 m column test and from a large strain consolidation test (LSC) on a similar material.

One aspect to note is that compressibility does not change past 112 days – which is close to the end of creep recorded in the replicate samples, shown in Figure 4.

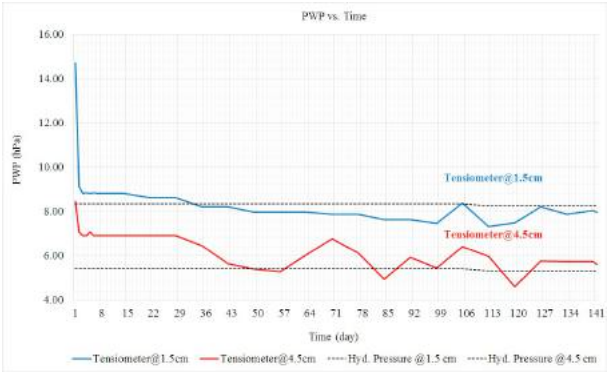

Figure 5. Pore-water pressure (1 hPa = 1cm) in the 0.10 m high single drainage columns

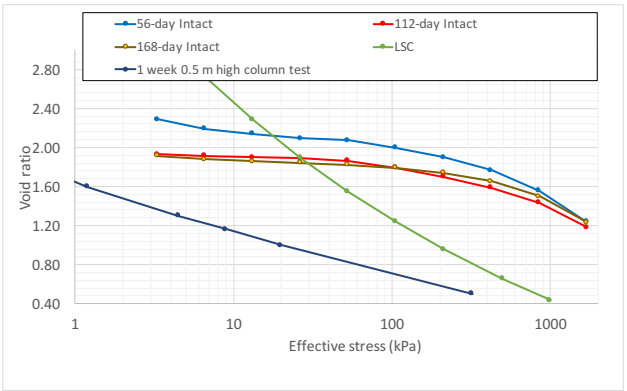

Figure 6. Compressibility curves on differently aged samples

The relationship between early age compressibility and late age compressibility in the tailings is similar to the difference between reconstituted and natural

or intact / in-situ clay response. The shape of the curves of the tailings is similar to that of many clays, and example from Burland (1990) is given in Figure 7.

Other aspects of interest include the rate of creep after the aged sample has been loaded. Figure 8 and 9 give examples of settlement and pore-pressure measurements in an oedometer.

In Figure 8, which is for a loading step well-below the apparent pre-consolidation pressure, the magnitude of secondary compression is very low, almost undetectable. This is similar to many tests on clays, where the observed rate of creep is low or undetectable for an over-consolidated soil. Indeed, preloading with a surcharge is sometimes used to reduce creep in clays (Alsono et al. 2000). However, near or exceeding the pre-consolidation pressure, the magnitude of secondary compression is measurable. In Figure 9, for a load of 105 kPa, the secondary compression would be an additional change in void ratio of 0.095 over 10 years and 0.105 in 100 years.

Also of note in Figure 9 is the temporary flattening in the pore-water pressure measurements at about 10,000 s. This can be explained by the transitioning of the sample from over-consolidated to normally consolidated states. As the sample transitions, part of the sample become normally consolidated, which causes a relatively large release of water, and hence slows down the rate of pore-water pressure dissipation. Again, this is a behaviour commonly seen in compression tests in soft clays (Leroueil et al. 1980).

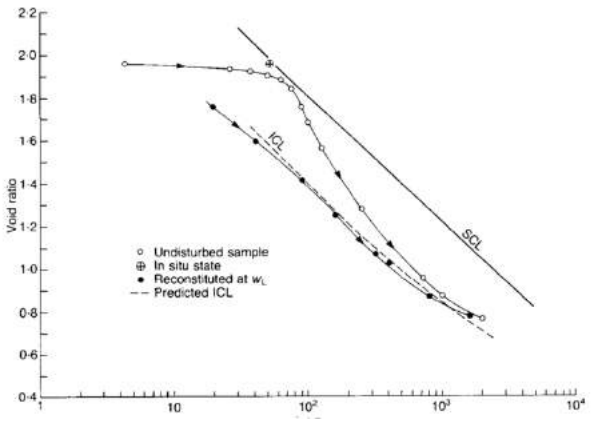

Figure 7. Example of compression curves from a single reconstituted or intact soil (Burland 1990)

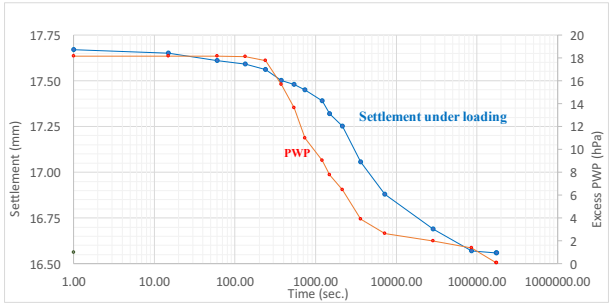

Figure 8. Settlement and pore-water pressure in a loading step from 3.3 to 6.6 kPa in sample aged for 168 days

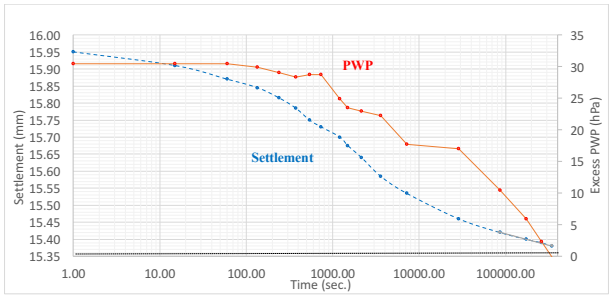

Figure 9. Settlement and pore-water pressure in a loading step from 53 to 106 kPa for the sample aged for 168 days

Handling the Uncertainty Over Time-Dependent Effects

The authors are pursuing two approaches to assist tailings deposition planers to quantify creep and structuration. The first is to incorporate creep and structuration effects directly into large strain consolidation modelling. Using the UNSATCON platform, the authors have incorporated three commonly used creep models (Leoni et al. 2008, Rowe and Hinchberger 1998, Yin and Graham 1994). These models handle the rate-dependency of the compressibility curve discussed under the “creep” section of this paper. Emergent from all these models is a shift in the location of the compressibility with strain rate: the lower the strain rate, the longer time available for creep, the lower void for a given effective stress.

Figure 10 gives an example of the influence of creep is shown for a hypothetical simulation of a 10 m deposit, with and without creep. The model employed in this simulation for creep is the Vermeer model (Leoni et al. 2008). Examples of the use of the Yin and Graham model with UNSATCON are reported in Qi et al. (2017).

Two important observations that will be reflected in real observations of deposit behaviour are the differences in density profiles with depth and the relative development of pore-water pressure and effective stress. In Figure 10 a and b, colours move from dark blue through to red over time. It can be seen in the simulation with creep, that the deposit has a more uniform distribution of density with depth. Though the total volume change is greater in the simulation with creep over the same time period (4.5 m compared to 5 m without creep), the rate of volume change is initially greater in the simulated deposit without creep. This is because creep tends to impede pore-water pressure dissipation.

The latter behaviour is also evident in the pore-pressure profiles. Without creep, the gradient of pore-water pressure with depth steepens over time, as a substantial amount of pore-water dissipation occurs towards the bottom of the deposit. With creep, pore-water pressure dissipation is suppressed, and therefore the pore-pressure gradient flattens, mirroring the change due to total stress only. Both these characteristics will appear in deposits if creep is a relevant phenomenon.

These models use two material parameters to characterize creep. One parameter is slope of the compression curve after primary consolidation in *e* versus log σ'_v space, the other is a parameter related to rate. The former parameter is conventionally extracted from compression test data, while the second can be calibrated to the same data using the existing creep models.

Structuration, however, is not commonly simulated in the soil mechanics literature, and the authors at the time of writing have not settled on a satisfactory way to model this phenomenon. However, an alternative approach to handle uncertainty in settlement predictions due to structuration is to consider existing empirical comparisons between structured and reconstituted clays. Liu and Carter (1999) reviewed twenty case studies where data on reconstituted and natural soil compressibility data were available. Of potential use to the tailings community is that almost 90% of the pre-consolidation pressures measured in the natural soils were less than 200 kPa. Also, Liu and Carter (1999) proposed a parameter for the increase in void ratio above the value given by the reconstituted soil. They define a parameter, S, to characterize the differences in the compressibility curve between a reconstituted and structure soil. S is given by the increase in void ratio above the reconstituted compressibility curve divided by the natural

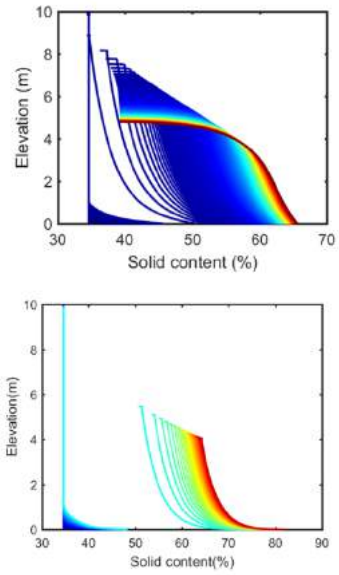

Figure 10a. Solids content in predictions of dewatering of a 10 m deposit of polymer amended FFT, with (bottom) and without (top) creep

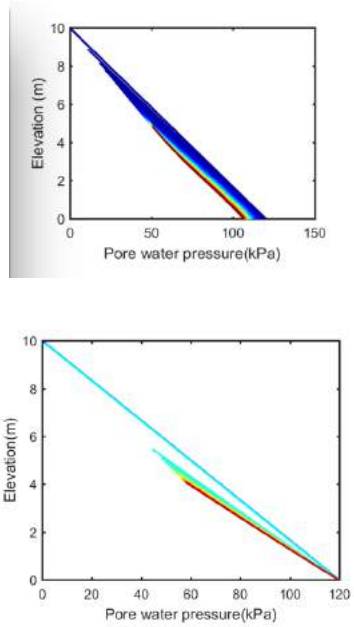

Figure 10b. Pore-water pressure profiles in simulation of a 10 deposit, with (bottom) and without (top) creep

logarithm of the vertical effective stress. When applied at the pre-consolidation pressure, 90% of S values fall below 0.2, while the median value was

0.12. The concept is illustrated in Figure 11, where $\Delta e = S \ln \sigma'_v$ at the pre-consolidation pressure.

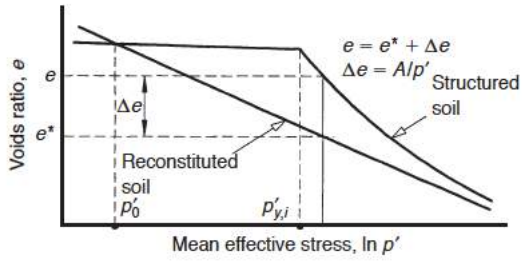

Figure 11. Scheme for analyzing differences in reconstituted and natural clays proposed by Liu and Carter (1999)

If we apply this concept to the data in Figure 6, we find for a pre-consolidation pressure of 100 kPa, there is a difference of 0.6 in void ratio between the reconstituted (which we take to be the LSC results) and structured compressibility curve, which gives an S value of 0.13. Therefore this polymer amended FFT does not appear to be atypical in its degree of structuration, compared to natural clays.

DISCUSSION

Creep and changes in the compressibility relationship due to structuration are well-known to bear substantially on the settlement of natural clays, and have implication for strength development. They also appear to bear on the compression behaviour on at least one fFFT material, reported extensively on by Salam et al. (2017, 2018).

Whether these phenomena are important to other oil sands tailings types can perhaps be readily established through field sampling of intact specimens or in-situ testing of existing deposits or field trials.

In the absence of other information, the known behaviour of natural clays as to creep and structuration could be used to limit uncertainty. For example, the known variability in rate dependent compressibility presented in Figure 2 for worldwide clays is helpful to quantify the limits of creep, while the data from Burland (1990) and Liu and Carter (1999) should be useful to bound structuration.

The authors have defined the LSC test data rather than the very short term compressibility deduced from a short column test as representative of the reconstituted state for the fFFT samples. This is because the authors are aware that very dramatic changes to floc size occur over 48 hours in this sample, even after deposition (Khattak et al. 2018). Therefore the authors judge that the compressibility from the column test is not really representative of any intrinsic state of the tailings.

What is clear is that the compressibility of these tailings is initially greater at earlier times. Therefore, deposition plans that results in shorter drainage paths (slow rates of rise or relatively thin lifts, wick drains etc) would give better better dewatering performance, for similar tailings. The authors have observed this behaviour, even when modelling consolidation-desiccation in physical simulations of multilayer deposition (Qi et al. 2016): Initially 0.35 m thick lifts of fFFT were more compressible than 0.5 m lifts during the initial consolidation phase of the experiments.

SUMMARY AND CONCLUSIONS

Creep and structuration in a fFFT sample prepared with a high molecular weight anionic polymer were compared with creep and structuration behaviour observed in natural clays. It the case of creep, there exist models to describe simultaneous consolidation-creep effects, which can be applied to tailings. The authors are not aware of a current method to incorporate structuration into large strain consolidation simulations.

The likely change in the compressibility curve of a give tailings deposit, however, can be potentially estimated using the existing literature on soft clay soils. Quantifying the degree of structuration in one fFFT suggests that structuration in fines dominated tailings is not atypical of structuration in natural clay deposits. Field measurements of compressibility in field tailings deposits would also help reduce uncertainty as to the magnitude of structuration effects on compressibility.

ACKNOWLEDGEMENTS

This study was funded through NSERC Grant 429272–11 held by the third author and sponsored by Canada's Oil Sands Innovation Alliance (COSIA).

REFERENCES

Alonso, E. E., Gens, A. and Lloret, A. (2000). Precompression design for secondary settlement reduction. Geotechnique, **50**(6): 645-656.

Burland, J. B. (1990). On the compressibility and shear strength of natural clays. Géotechnique, **40**(3), 329-378.

Jeeravipoolvarn, S. (2010). Geotechnical behaviour of in-line thickened oil sands tailings (Ph.D. thesis). The University of Alberta, Edmonton, Alberta.

Jeeravipoolvarn, S., Scott, J. D. and Chalaturnyk, R. J. (2009). 10 m standpipe tests on oil sands tailings: Long-term experimental results and prediction. Can. Geotech. J., **46**: 875-888.

Jeeravipoolvarn, S. (2005). Compression behaviour of thixotropic oil sands tailings (Master's thesis). The University of Alberta, Edmonton, AB.

Leroueil, S., Perret, D. and Locat, J. (1996). Strain rate and structuring effects on the compressibility of a young clay. In Measuring and modeling time-dependent soil behavior (pp. 137-150). ASCE.

Leroueil, S., Le Bihan, J. P. and Tavenas, F. (1980). An approach for the determination of the preconsolidation pressure in sensitive clays. Can. Geotech. J., **17**(3): 446-453.

Leoni M., Karstunen, M., Vermeer, P. A. (2008). Anisotropic creep model for soft soils. Géotechnique, **58**: 215–226.

Leroueil, S. (2006). The isotache approach. Where are we 50 years after its development by Professor Šuklje? (2006 Prof. Šuklje's Memorial Lecture). In: Proceedings of the 13th Danube-European Conference on Geotechnical Engineering, Ljubljana 2006, pp. 55–88.

Leroueil, S., Kabbaj, M., Tavenas, F. and Bouchard, R. (1985). Stress–strain–strain rate relation for the compressibility of sensitive natural clays. Géotechnique, **35**:159-180.

Liu, M. D. and Carter, J. P. (1999). Virgin compression of structured soils. Geotechnique, **49**: 43-57.

Khattak, M., Salam, A. M. and Simms, P. (2018). Image processing for studying flocculation in fluid fine tailings. Proceedings of GeoEdmonton 2018, 71st Canadian Geotechnical Conference. Edmonton, AB.

Miller, W. G. (2010). Comparison of geoenvironmental properties of caustic and non-caustic oil sand fine tailings (Ph.D. thesis). The University of Alberta, Edmonton, AB.

Rowe, R. K. and Hinchberger, S. D. (1998). The significance of rate effects in modelling the Sackville test embankment. Canadian Geotechnical Journal, **35**(3): 500-516.

Salam, A. M., Simms, P. H. and Örmeci, B. (2018). Structuration in polymer amended oil sands fine tailings. Proceedings of GeoEdmonton 2018, 71st Canadian Geotechnical Conference. Edmonton, AB.

Salam, A. M., Simms, P. H. and Örmeci, B. (2018). Evidence of creep and structuration in polymer amended tailings. Submitted to IOSTC 2018.

Salam, A. M., Simms, P. H. and Örmeci, B. (2017). Investigation of creep in polymer amended oil sands tailings. Proceedings of GeoOttawa 2017, 70th Canadian Geotechnical Conference. Ottawa, ON.

Scott, J. D., Jeeravipoolvarn, S., Kabwe, L. K., Wilson, G. W. and Sorta, A. (2013). Properties which affect the consolidation behaviour of mature fine tailings. Proceedings of the 17th international conference on tailings and mine waste, Banff, AB.

Watanabe, K., Udaka, K., Nakatani, Y. and Leroueil, S. (2012). Long-term consolidation behaviour interpreted with isotache concept for worldwide clays. Soils Found., **52**: 449-464.

Yin, J. H. and Graham, J. (1994). Equivalent times and one-dimensional elastic viscoplastic modelling of time-dependent stress-strain behaviour of clays. Canadian Geotechnical Journal, **31**(1): 42-52.

NUMERICAL MODELING OF TAILINGS FLOW, SAND SEGREGATION AND SAND CO-DEPOSITION: LATEST DEVELOPMENTS AND APPLICATIONS

A. M. Talmon[1,2], J. L. J. Hanssen[1], D. S. van Maren[1,2], P. H. Simms[3], L. Sittoni[1], J. A. Th. M. van Kester[1], R. E. Uittenbogaard[1], J. C. Winterwerp[2] and C. van Rhee[2]
[1]Deltares, The Netherlands
[2]Delft University of Technology, The Netherlands
[3]Carleton University, Ottawa, Canada

ABSTRACT

Since 2016 Deltares collaborates with COSIA and IOSI, the Technical University of Delft and lately with Carlton University to improve numerical prediction and theoretical understanding of tailings deposition flow and segregation, to best characterize tailings deposits under different potential deposition scenarios (e.g. tailings properties, cell geometry, subaereal or subaqueous, etc). Deltares has since continuously improved the open source numerical model Delft3D[1] including rheology and sand settling physics specific for tailings. Since 2016, this numerical model has been utilized to conceptually simulate: the flow and sand settling behavior of tailings with various rheological properties during beach deposition; the interaction or co-deposition of different tailings types; the deposition of sand above and within a fine tailings deposits.

Currently Deltares is: 1) upgrading this research code to the open source version of Delft3D, with possible use of its Graphic User Interface (GUI); 2) in collaboration with Paul Simms at Carleton University, modifying a thixotropy equation for 3D implementation to simulate time-dependent rheological behavior; and 3) exploring three dimensional deposition model performance (already included in the numerical model but not yet tested for tailings).

The latest results of these new developments and a trajectory forward will be presented, together with practical potential application of the model to oil sands tailings management.

[1] https://www.deltares.nl/en/software/delft3d-4-suite/; https://oss.deltares.nl/web/delft3d

INTRODUCTION

Background Literature and Processes of Non-Newtonian Slurries

Understanding and predicting the deposition behavior of tailings or slurries is critical for the mining and dredging industry, as well as for land reclamation and coastal or inland safety. Thousands of cubic meters of tailings are produced and deposited in tailings basins every day; land is being reclaimed for human developments or coastal protection at faster pace and in more remote areas; mud slides, caused by natural disaster or manmade structure failures, kill people every year. Since 2015 Deltares, in partnership with Canadian Industry (COSIA and IOSI) and Canadian and Dutch academic institutions (The Technical University of Delft and Carleton University), is leading the development of numerical tool, Delft3D-slurry (D3Ds) to predict flow and segregating behavior of non-Newtonian slurries, with focus on (oil sands) tailings management. At the same time, Deltares is evaluating the opportunity to utilize this same tool for mud slide prediction related to dam failure or meteorologically induced.

The flow and segregating behavior of thickened slurries (i.e. thickened, centrifuge, non-segregating tailings) is determined by the rheological properties (i.e. yield stress *and* viscosity) of the carrier fluid (i.e. fines – water – residual bitumen mixture), the shear rate (i.e. flow velocity and discharge conditions), and the properties of the coarse sand fraction (Deltares 2017, Hanssen 2017, van Es 2016). Sand settles faster in high shear regions, and accumulates in proximity of the bed (i.e. beach), Figure 1. Sand increases the viscosity and yield stress of the slurry reducing the flow velocity locally, and likely promoting the development of morphological features (i.e. channels or lobes).

Previous publications present the background objective, approach and theory of this research and development trajectory (Deltares 2017; Sittoni et al. 2016, 2017; Talmon et al. 2016; van Es 2017). We refer the reader to these publications for in detail description of the theoretical background. In this paper we focus on a summary overview of recent concrete applications of D3Ds to typical (oil sands) tailings management questions. In this overview, when applicable we reference additional literature that gives more in depth details of a specific application.

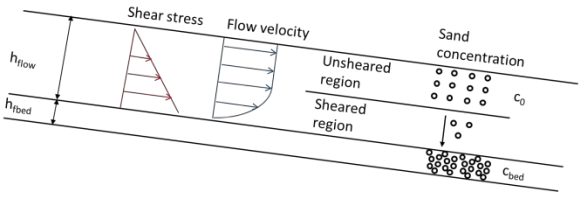

Figure 1. Schematic of flow and segregation processes thick slurries flowing down a beach

Delft3D-slurry

Numerical prediction of thick slurry flow and segregating behavior are based on the numerical tool D3Ds. D3Ds is developed embedding non-Newtonian and sand settling specific processes to the open source Delft3D. Delft3D is a hydrodynamic, sediment transport and water quality numerical model developed by Deltares offered in open source to a vast user community (order of thousands of members) and utilized in hundreds of applications world-wide.

Three slurry (i.e. tailings) specific rheological analytical models and two sand settling formulations were added to Delft3D-FLOW obtaining D3Ds (Hanssen 2017). D3Ds can simulate three dimensional (shallow water) non-Newtonian laminar flow and shear induced sand settling. D3Ds includes the Graphic User Interface (GUI) of Delft3D, which facilitates model setup, as well as output visualization software (Figure 2). Specific non-Newtonian slurries parameters are added to the output of D3Ds to facilitate judgment of model performance and to plot typical tailings properties.

D3Ds is therefore suited to simulate:

1. Tailings flow and deposition on beaches and underwater for non-Newtonian tailings types of various composition and rheological behavior;

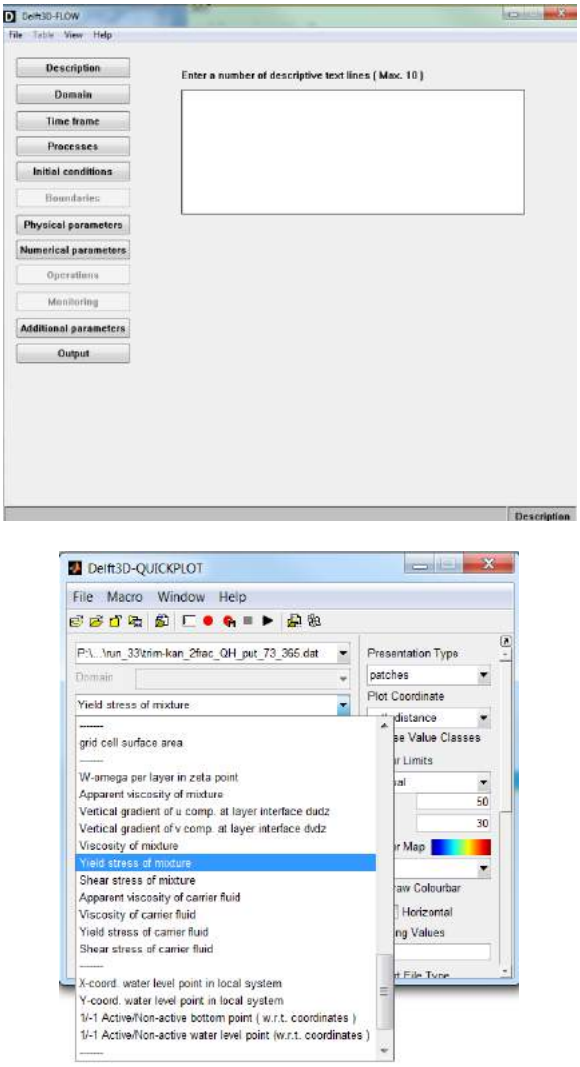

Figure 2. D3Ds GUI (top) and output visualization software (bottom) with dedicate non-Newtonian slurries parameters

2. Sand settling and fines segregation;
3. Intermixing of the tailings flow with other slurries or fluids.

POTENTIAL APPLICATIONS AND ADDED VALUE OF D3Ds

Typical tailings management applications of D3Ds include:

- Prediction of depositional flow characteristics and optimization of deposit geometry and beach slope;

- Optimization of tailings discharge: flow rate and solids content; composition (i.e. coarse/fines; on/off spec.); pipe locations and relocation;
- Design of mixing and co-mixing operations of various tailings types, e.g. coarse tailings discharge onto a thickened fine tailings deposit, or co-deposition of different lines;
- Enhancement of fines capture in the beach above or below water;
- Design and simulation of mine closure scenarios;
- Design, interpretation and scale-up of flume tests; design and interpretation of deposition pilots; and evaluation of multiple deposition scenarios in parallel and support of flume tests and pilot tests (i.e. decreasing the need for multiple flume tests or pilot tests, which can be modelled numerically).

All these applications offer potentially significant cost efficiencies in current operations and future liability. While exact quantification of such cost reductions is operator and site specific and requires information not available to the authors, we can conceptually list concrete potential added value of utilizing D3Ds as:

- Control of beach slope with optimization between cost of raising dikes and maximization of deposit capacity;
- Minimization of cost for fluid fine tailings re-handling;
- Minimization of cost for additional (long term) treatment, such as capping, thickening, etc;
- Decrease cost (and safety risk) for relocating pipes, or mechanical re-handling tailings on beaches;
- Improve learnings and allow for model-based extrapolation from flume tests and field trials, which will: minimize the required number and scale of such trials; optimize data collection and analysis; and improve accuracy. The cost of each flume test is at least one order of magnitude larger than the equivalent numerical study. The cost of each field pilot test is likely two orders of magnitude larger than the equivalent numerical study. A combined physical (i.e. flume or field pilot) and numerical study offers more robust, accurate and widely applicable results at about half the price (with most of the cost related to the physical part).

RECENT APPLICATIONS OF DELFT3D AND D3Ds

In this section, we briefly illustrate selected applications of Delft3D and D3Ds that are directly or indirectly related to (oil sands) tailings management. With Delft3D we model Newtonian carrier fluid, with D3Ds we model non-Newtonian sand settling processes.

Development of Deltaic Deposit – Delft3D

This application simulates the development of a river delta in 3D, with tracking deposit composition (e.g. sand and fines, from van der Vegt, 2018). As explained in Sittoni et al. (2016) deltaic deposits are physically equivalent to deposition of coarse or diluted tailings (e.g. Newtonian), when tracking of sand and fines distribution allows computation of fines capture. This application is setup with standard Delft3D. Figure 3 shows the developing delta topography and the corresponding particle size distribution along a cross section of the deposit for varying incoming particle size distribution. Fines are trapped under the sand or within the sand skeleton in the beach. From these outputs fines capture can be computed in post-processing. Tailings basins are expected to show similar behaviour as these river deltas (Sittoni et al. 2016), when sediment is discharged from a pipe (instead of an incoming river) and within a tailings basin (instead of ocean).

Development of Beach Deposit in Tailings Basin – Delft3D

This simulation is similar to the deltaic application described above, but developed to simulate discharge of whole tails in a conceptual tailings basin (Sheets et al. 2014). Tailings are discharge from two pipes. A similar behavior of fines trapped under coarse tailings is observed, with greatest mix of sand and fines between the two discharges (Figure 4).

Flow and Sand Settling of Non-Newtonian Thick Tailings – D3Ds

The newly developed D3Ds is implemented to simulate flow and settling behavior of thick tailings (e.g. non-Newtonian) flowing along a beach cross section. Figure 5 shows discharge of initially uniform tailings along a 400 m beach. Consistently with Figure 1, sand settles from high shear region towards the beach. The plug flow at the higher part of the flow remains uniform. The produced fines flow into the pond. These figures illustrate clearly the new developments included in D3Ds (i.e. non-Newtonian physics and sand shear settling).

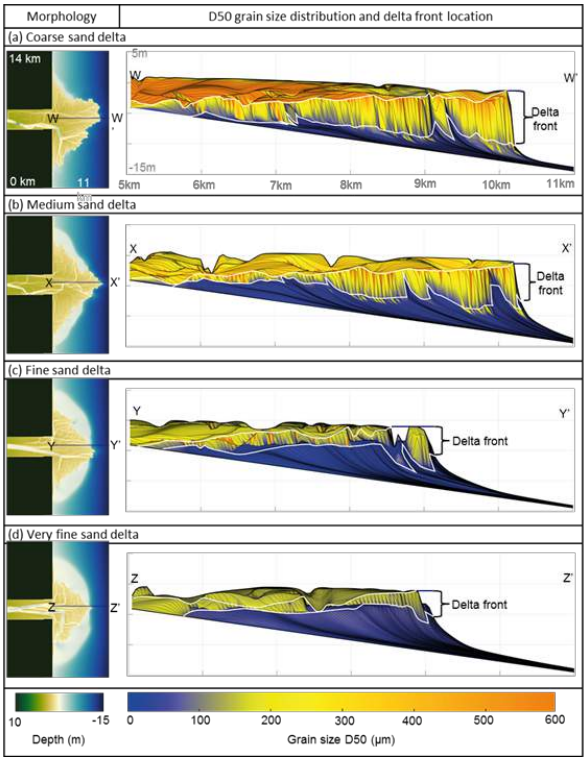

Figure 3. Simulation of deltaic deposition. Figures "a" through "d" vary in particles size composition at discharge, from coarse to fines. Warm colours (red) show sand, cold colours (blue) show fines

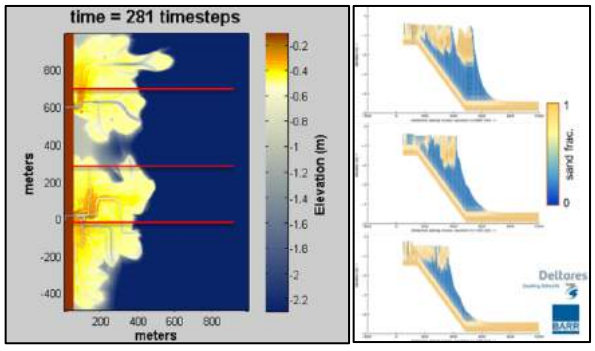

Figure 4. Left: top view of tailings deposition from two pipes into a water filled conceptual tailings basin. Colours represent elevation. Right: distribution of sand (brown) and fines (blue, calculated as 1 – sand) along the three cross-sections highlighted in red in the left figure

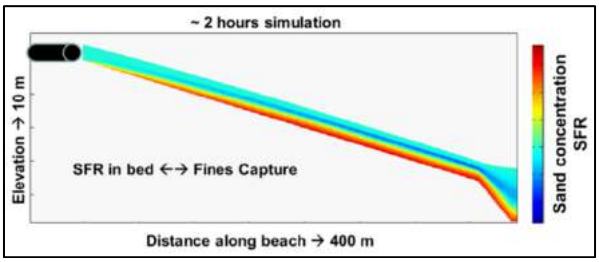

Figure 5. Cross sectional view of deposition of initially uniform segregating tailings along a 400 m beach. Colours represent SFR

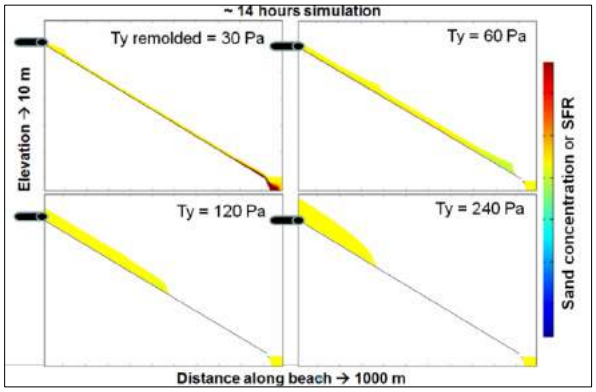

Figure 6. Flow and sand settling behavior of four different slurries with varying rheological properties (yield stress = 30, 60, 120, 240 Pa). Colors represents SFR

Effect of Rheological Properties on Depositional Flow and Sand Settling – D3Ds

As explained in the introduction and in the references associate to this paper, the rheological properties of thick tailings determine the flow (i.e. flow thickness and runout time and distance) and sand settling behavior. Figure 6 illustrates concept D3Ds simulations of four tailings slurries characterized by different rheological properties. As expected stronger slurries show shorter runout distance, thicker flow and less sand settling.

Subsequent Deposition of Different Tailings Types – D3Ds

D3Ds was conceptually utilized to evaluate subsequent deposition of two tailings types. Fresh tailings were deposited above aged (i.e. deposited the previous day) thicken tailings to evaluate displacement or mixing. These simulations are performed with two subsequent pours of tailings

with different rheological properties that were modified offline. At this stage on-line time dependency is not included in D3Ds. This is a potential follow-up development. Figure 7 shows that fresh tailings flow above aged tailings with small displacement. These simulations are conceptual as knowledge and formulations of mixing and erosion processes of non-Newtonian tailings are still being developed and tested.

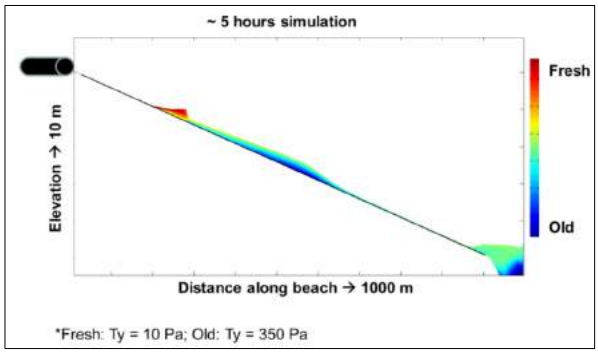

Figure 7. Example of tailings subsequent discharge co-deposition: red represents fresh tailings, blue old tailings (blue), and green mixing between old and fresh tailings

Deposition of Sand Above and Within Fine Tailings Deposit – D3Ds

D3Ds was conceptually applied to assess the fate of coarse tailings when discharged above a centrifuge cake deposit. D3Ds showed partial mixing of coarse tailings with the existing cake, as well as density current of mostly coarse tailings migrating near the bottom of the deposit (Figure 8). The results of these simulations agreed well with field data. All details of this application are reported in Ansah-Sam et al. (2016). This application shows the general potential of D3Ds to evaluate mixing of coarse tailings in existing fines deposit, assessing where coarse tailings would stop and the resulting properties of the deposit as far as strength of the mixed layer for example. This technology can be seen as an alternative to capping or to evaluate the consequences should capping not be successful.

Fine Tailings, Single Discharge Three Dimensional Application – D3Ds

Since 2018, D3Ds is being tested in three dimensions. Figure 9 shows a simple constant

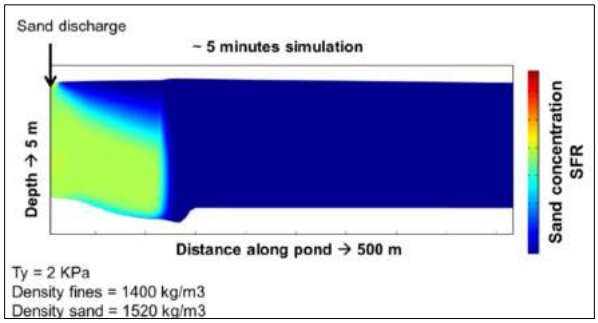

Figure 8. Deposition of coarse tailings (top left corner of the basin under the arrow) above a tailings basin filled with centrifuged tailings (blue = centrifuge tailings, not water). Coarse tailings penetrate and mix with the centrifuged tailings (green)

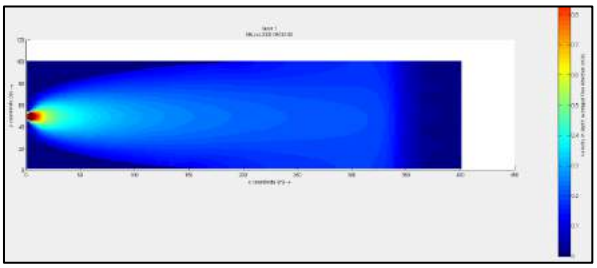

Figure 9. 3D simulation of fine tailings (no sand) along a beach. Top view. Colour is flow velocity

discharge of thickened tailings along a 100 m wide and 400 m long beach, seen from above. A roughly symmetric expanding flow forms, as expected from theoretical non-Newtonian behavior. No channels or other morphological features are observed.

Fine and Coarse Tailings, Two Points Discharge, Three Dimensional Application – D3Ds

This application represents the latest results of D3Ds at the time of this paper. In this applications, fine and coarse tailings (SFR = 2) are discharged from two different discharge points with different discharge rates (1 and 2 m^3/s). Figure 10 shows flow velocity and Figure 11 sand concentration (or SFR) at the beach. These results clearly show the difference in discharge rates between the two pipes. More interestingly however, these results show the development of complex morphological features, with lobes turning into what resembles alternating channels as deposition continues. This

appears to indicate the critical role of sand settling in leading to defined and variable morphological features.

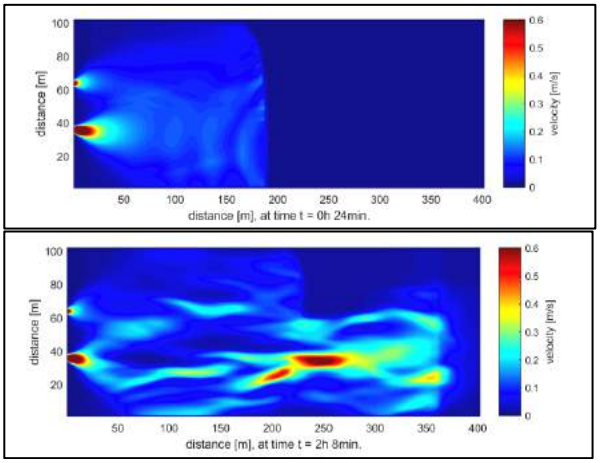

Figure 10. 3D simulation of mixed fine-coarse tailings discharged from two pipes. Bottom pipe has double the flow rate as the top pipe. Top view. Colour is flow velocity. The top figure is 24 min and the bottom figure is 2h 8 min after beginning of discharge

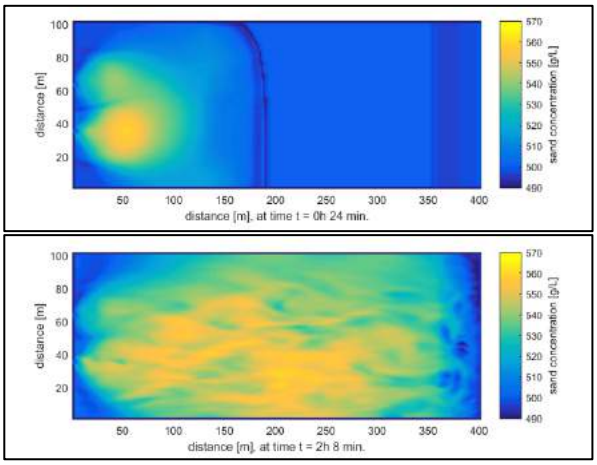

Figure 11. 3D simulation of mixed fine-coarse tailings discharged from two pipes. Bottom pipe has double the flow rate as the top pipe. Top view. Colour is sand concentration. Yellow is high SFR. The top figure is 24 min and the bottom figure is 2h 8 min after beginning of discharge

DISCUSSION AND CONCLUSIONS

Deposition of diluted and thick tailings (i.e. fines – sand slurries) is a complex discipline with numerous knowledge gaps and research questions open. However, deposit composition, fines capture and beach slope have significant impact on daily tailings basin management and implication on closure landscape.

D3Ds is the single process based three dimensional model to the knowledge of the authors that can predict non-Newtonian flow and sand settling behavior. This paper shows an overview of applications of D3Ds to concrete (oil sands) tailings management questions. When the current limitations and applicability of model are well taken into account, D3Ds can be utilized for engineering assessment of tailings flow, settling and co-mixing.

Many remain the knowledge gaps and processes that are not included or yet verified in the model. The authors therefore recommend continuing the development and validation of the model by setting up a robust research and development trajectory aside to utilizing the current model version to assess operator specific engineering applications. This approach would ensure a continuous feedback between industry needs and development priorities, with a model that continues to improve in accuracy and processes while it's being used in engineering and operation practice.

The development trajectory should focus on three major pillars:

1. Fundamental flow behavior: thixotropy and rheology;
2. 3D morphological features: channels, lobes, beach slope;
3. Near field phenomena.

Item 1 is essential for accurate simulation of flow and sand settling behavior in materials with fines, and it is specifically important in oil sands tailings. This allows prediction of deposition of tailings with time-dependent rheological behavior (e.g. thixotropy); co-deposition or mixing of tailings with different rheologies (e.g. on and off spec. tailings); assessment of the effect of various polymeric amendments on depositional behavior and deposit geometry; prediction of NST or eNST performance; and estimates of water release and densification during deposition. This item is also important to distinguish transition from slurry to soil mechanics regimen (and possible need to transition to a soil mechanics-based model). At the

time of this paper an analytical thixotropy model is developed for implementation in D3Ds, but not yet embedded in the model. Preliminary analytical computations suggest that thixotropy alone would generate migrating channels, in a similar manner as sand settling appears to be doing (Figure 10). Yet, numerous knowledge gaps remains in this field, for example the rheological properties resulting from mixing tailings with different rheology or effect of bitumen on rheological properties.

Item 2 extrapolates deposition to three dimensional processes, necessary to predict actual (large scale) deposition operations. This allows predicting the flow and spread of a beach deposit and beach formation including sand settling; design, analysis and scale up of flume tests or field trials; predicting beach slope; simulating specific filling scenarios to optimize pipe locations and discharge rates; computing fines capture along subaerial or subaqueous beaches at various user-specified cross sections and depths. Preliminary 3D simulations show the potential of D3Ds to estimate sand settling and morphological feature in three dimensional. The driving processes behind the various morphological features (i.e. channels or lobes), being this for example thixotropy, sand settling or turbulent / laminar transition, are still not well understood. Similarly holds for processes of erosion in non-Newtonian tailings.

Item 3 is dedicated to near-field phenomena to evaluate the effect of discharge strategy (e.g. single pipe discharge, plunge pool, multiple spigots, diffuser) on flow characteristics, deposit geometry and composition, and fines segregation or sequestration. This item is not yet investigated in detail as part of this development trajectory. Field evidence shows however that the discharge type and tool may have significant influence on the flow and segregating behavior near the discharge point. The intense dynamics of near-field flow may be addressed better with a specific hydrodynamic near-field model (e.g. OpenFOAM) rather than D3Ds. In this case, it is important to assure integration of a near-field model with D3Ds to capture the appropriate spatial and temporal scale, and any changes in the slurry properties resulting from near-field effects.

These items include a combination of fundamental research, laboratory testing, model development and verification. It is the ultimate intent that all new processes and analytical models (equations) will be included in D3Ds (or an accompanying near-field model) and delivered to the industry for application.

REFERENCES

Ansah-Sam, M., Sheets, B., Langseth, J., Sittoni, L. and Hanssen, J. (2017). Delft3D modeling of Sand Placement on an Oil Sands Treated Tailings Deposit. Tailings and Mine Waste 2017, Banff, Canada.

Deltares. (2017). A Research Trajectory Towards Improving Fines Capture Prediction: Verification, Application and Improvement of Delft3D-Slurry – Phase I. COSIA#: 40-TE0028-16-145-0. TKI#: DEL035.

Hanssen, J. L. J. (2016). Towards improving predictions of non-Newtonian settling slurries with Delft3D: theoretical development and validation in 1DV. MSc Thesis, Delft University of Technology.

Sheets, B., Wagner, T., Swenson, J., Horton, J., Langseth, J., Sittoni, L., Walstra, D. J. R., Winterwerp, J. C., Uittenbogaard, R., van Kester, J.A.Th.M. and Talmon, A. M. (2014). Muddy river deltas as analogues for oil sand tailings beaches: improving fines capture and operational efficiency with tailings beach deposition modeling. Proc. 4th Int. Oil Sand Tailings Conference, IOSTC, Lake Louise, Canada, pp.397-405.

Sittoni, L., Talmon, A. M., Hanssen, J. L. J., van Es, H. E., van Kester, J.A.Th.M., Uittenbogaard, R. E., Winterwerp, J. C. and van Rhee, C. (2016). Optimizing tailings deposition to maximize fines capture: latest advance in predictive modeling tools. 5th Int. Oil Sand Tailings Conference, IOSTC, Lake Louise, Canada.

Sittoni, L., Talmon, A. M., Hanssen, J. L. J, van Es, H. E., van Kester, J.A.Th.M., Uittenbogaard, R. E., Winterwerp, J. C. and van Rhee, C. (2017). One step further towards prediction of tailings deposition flow and sand segregation. Where we are, and what comes next. COSIA Innovation Summit, Calgary, Canada.

Talmon, A. M., Hanssen, J. L. J, Winterwerp, J. C., Sittoni, L. and van Rhee, C. (2016). Implementation of Tailings Rheology in a Predictive Open-Channel Beaching Model. Paste 2016, Santiago, Chile, ISBN 978.956.9393-47-1.

van der Vegt, H. (2018). From fluvial supply to delta deposits. Simulating sediment delivery, transport and deposition. PhD Thesis, Technical University of Delft.

van Es, H. E. (2017). Development of a numerical model for dynamic deposition of non-Newtonian slurries. MSc Thesis, Delft University of Technology.

INTEGRATION OF MINE-TO-MILL PRODUCTION PLANNING STRATEGY FOR OIL SANDS MINING AND WASTE DISPOSAL

Ahlam Maremi and Eugene Ben-Awuah
Laurentian University, Sudbury, Canada

ABSTRACT

For oil sands mining, the production schedule must be integrated simultaneously with in-pit and ex-pit dyke construction scheduling. In-pit dykes are constructed in the mined-out areas concurrently with the advancement of the pit phase mining. The mined ore that exceeds the plant capacity is stockpiled for a limited duration and the topmost layer of the overburden is used for land reclamation. Organic Rich Solids (ORS) which represents about 5 w% of the total ore and negatively affects the bitumen recovery is used as a predictor for ore processability. In this research, a theoretical and conceptual mine planning framework based on Mixed Integer Linear Goal Programming (MILGP) for oil sands production scheduling and waste management is presented. Robust constraints that control the annual tonnage fluctuation for material mined and processed over the mine life are introduced in the model. The model generates an integrated mine plan with a waste management and stockpiling strategy over the mine life that maximizes the Net Present Value (NPV) of the operation. The results show a 2% overestimation of NPV arising from not taking into consideration the impact of ORS on bitumen recovery during mine planning.

INTRODUCTION

Open pit mine planning optimization aims to provide the plant with ore at full capacity subject to a variety of production, grade blending and pit slope constraints (Whittle 1989). Oil sands mining of the McMurray formation (MMF) is studied and used as a case study. The Pleistocene unit is the topmost layer of the deposit. It contains muskeg (reclamation material). The Clearwater formation overlies the MMF. Both the Pleistocene and Clearwater formation are referred to as overburden. The MMF contains bitumen, the element of interest. Devonian carbonates mark the end of the oil sands formation (Masliyah 2010).

Oil sands mining operations result in different types of material: ore, interburden (IB), overburden (OB), reclamation material (RM) and waste. Material with a bitumen grade of 7% or more are classified as ore according to Directive 082 (Alberta Energy Regulator 2016). Processing the ore results in huge amounts of tailings. Tailings coarse sands (TCS) is used for dyke construction and tailings slurry is deposited in the disposal areas created with dykes.

Any ore material that has a bitumen grade less than 7%, known as interburden, are reclassified based on the fines content. Material with fines content less than 50% will be used for dyke construction; otherwise, it will be sent to the waste dump. Overburden will be used either for roads or dyke construction if it meets the fines requirement. Muskeg will be stockpiled and used to reclaim the land at the end of mine life. Any material that does not meet the requirements of ore, dyke materials or reclamation material is classified as waste and will be sent to the waste dump.

There are three significant aspects in oil sands waste management: greenhouse gas emissions; environmental challenges due to the toxicity of the tailings; and space limitations increasing the need for in-pit tailings containment (Devenny 2009).

Directive 085 (Alberta Energy Regulator 2017) issued by the Alberta Energy Regulator (AER) requires oil sands operators to periodically publish their waste disposal and tailings plans publicly (Ben-Awuah and Askari-Nasab 2013, McFadyen 2008). Figure 1 shows a conceptual mining model, which includes an oil sands deposit area to be mined and simultaneously used as an in-pit tailings storage facility. It should be mentioned that the final pit block model is divided into pushbacks. The material intersecting a pushback and a bench is known as a mining-panel. Each mining-panel contains a set of mining-cuts and is used to control the mine production operation sequencing. Mining-cuts are clusters of blocks within the same mining bench that are similar in terms of location, grade, rock type and the shape of mining-cuts created on the lower bench. As mining advances in the

specified direction, the in-pit tailings dyke footprints are released for dyke construction.

This research seeks to develop a mine planning theoretical framework that maximizes the NPV of an oil sands mining operation and minimizes waste management cost using Mixed Integer Linear Goal Programming (MILGP) model. The proposed MILGP model aims to determine:

- The sequence of extracting ore, reclamation and dyke materials to maximize the NPV of the project;
- The destination of reclamation and dyke materials to minimize the extra mining cost for land reclamation and dyke construction;
- A reclamation strategy for the ore that is stockpiled for a limited duration;
- A mine-to-mill production planning strategy that uses Organic Rich Solids content (ORS) to determine ore processability.

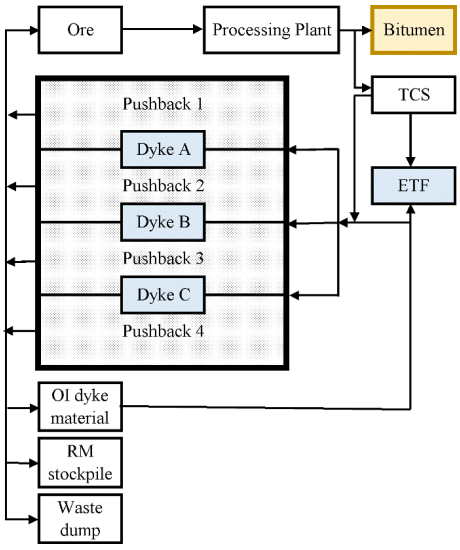

Figure 1. Conceptual model for mining and waste management strategy (modified after Ben-Awuah and Askari-Nasab 2013)

The next section of this research gives details on oil sands processing and ORS, and is followed by a section presenting processing recovery calculations using ORS. The paper then highlights the theoretical mathematical programming formulation and explains the implementation of the MILGP model framework. A case study is presented prior to the section containing the research conclusions.

OIL SANDS PROCESSING AND ORGANIC RICH SOLIDS

In oil sands mining, Clark Hot Water Extraction process (CHWE) is used to recover bitumen from the ore deposit (Masliyah 2010). CHWE process depends on the surface characterization of solid particle in the ore matrix. Measurements of fines (<45μm) are used to predict the processability of the ore, however, it is not always effective. It has been found that certain solid fractions known as Organic Rich Solids (ORS) still exist even after the treatment of oil sands by multiple extraction toluene. These ORS comprise about 5% of the total ore, and potentially affect the processability of oil sands (O'Carroll 2002, Sparks et al. 2003). During the bitumen separation process, ORS carry any associated bitumen into the aqueous tailings, thus reducing overall bitumen recovery. In this sense, these solids are considered to be active and their associated quantity per ore can be estimated, thus, a better predictor for ore processability than the traditional use of bitumen ore fines content (O'Carroll 2002). O'Carroll (2002) noted that loss in bitumen recovery is associated with higher ORS content in the ore. The Bitumen to ORS ratio increases with higher bitumen content that implies the ratio has potential for use as an index in the characterization of oil sands ores.

PROCESSING RECOVERY CALCULATIONS

Recovery Calculations Based on Directive 082: Alberta Energy Regulator

For oil sands mining, the recovered volume of bitumen from the mining and processing operations, is specified by Directive 082 (Alberta Energy Regulator 2016). The processing recovery equals to 90% if the average bitumen content is 11% or greater, otherwise it is determined by Eq. (1) (Alberta Energy Regulator 2016):

$$RECOV_{AER} = -2.5 * (BIT)^2 + 54.1 * (BIT) - 202.7 \quad (1)$$

Recovery Calculations Based on Organic Rich Solids

ORS associated with oil sands ore is modeled from O'Carroll (2002). An exponential correlation exists between bitumen and ORS as can be seen

in Eq. (2) with a coefficient of determination (R-squared) of 62.6%. For the ultimate pit block model in our case study, ORS ranges from 0 to 2.60% with an average of 0.88%. The processing recovery for ore is also modeled from O'Carroll (2002) as can be seen in Eq. (3) (with R^2 of 99.8%). Bitumen recovery is plotted against BIT:ORS ratio and a raising trend is noted. Recovery levels off at 90% for BIT:ORS ratio of 8 and more (Figure 2). The ORS recovery is used to calculate revenue from the sale of bitumen.

$$ORS = 3.8145 \times e^{-0.094 \times Bit} \quad (2)$$

$$RECOV_{ORS} = -0.02 \times (\frac{BIT}{ORS})^2 + 0.33 \times (\frac{BIT}{ORS}) - 0.38 \quad (3)$$

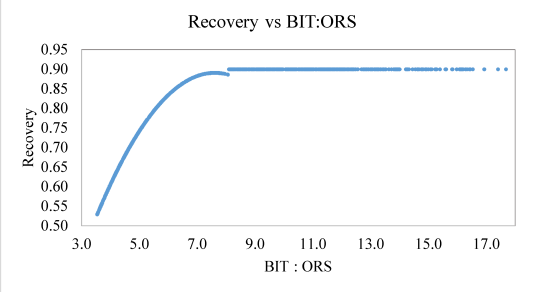

Figure 2. Recovery vs. BIT to ORS ratio

Subsequently, a case study with two scenarios is examined using the proposed MILGP model. Both scenarios use tonnage fluctuation constraints to achieve the mining and processing targets as part of the production scheduling optimization process with a limited duration stockpiling strategy for ore. The first scenario uses processing recovery calculated from the AER equation to determine the revenue while the second scenario uses processing recovery calculated from the ORS equation. MATLAB (Mathworks 2017) is used for coding the mathematical programming formulation and the resulting optimization problem is solved with a large-scale optimization solver IBM/CPLEX (ILOG 2012). This solver uses a branch and cut algorithm which is a hybrid of branch-and-bound algorithm and cutting plane methods to solve the optimization problem (Wolsey 1998). The effect of ORS on the ore processability compared to the processing recovery recommended by AER is investigated.

MILGP THEORETICAL MODEL FORMULATION

The strategic production schedule considers the time and sequence of extracting ore, reclamation material, RM, overburden, OB, interburden, IB, and waste blocks, as well as determining their destinations from a predefined UPL. The proposed MILGP model is capable of considering multiple mining locations, multiple pushbacks and different types of materials. The stockpiled oil sands ore will be reclaimed in a limited duration controlled by the planner to avoid the risk of oxidation, which can affect the efficiency of the processing recovery. Stockpiling is for the mined ore that exceeds the plant capacity in any given year. The MILGP model is subject to different constraints that control the mining operation. It is assumed that: 1) when a mining-panel is scheduled, all the mining-cuts within this mining-panel are extracted uniformly; 2) when modeling the relationship between the mining-panels and mining-cuts, the planner has access to all the mining-cuts within each mining-panel; 3) the stockpiling strategy is considered in the optimization problem for extra ore that exceeds the mill capacity and stockpile bins are available for each period; 4) the exact amount of ore sent to the stockpile in period t will be reclaimed after the stockpiling duration controlled by the planner. The notations used in the formulation of the oil sands long-term production planning and waste management framework can be found in the list of nomenclature in the Appendix.

Modeling of Economic Mining-Cut Value

The notion of economic mining-cut value is based on ore parcels within mining-cuts which could be mined selectively. The profit from mining a mining-cut is a function of the value of the mining-cut based on the processing destination and the costs incurred in mining, processing, and dyke construction at a specified destination. Based on the value of the mining-cut and the costs incurred during mining and processing operations, the discounted profit from each mining-cut equals to the discounted revenue obtained by selling the final product contained in mining-cut *k* minus the discounted costs. For a mining-cut, if there are valuable elements, its discounted economic value if it is sent from the mine to the processing plant ($dm_k^{d,t}$) or from the stockpile to the processing plant ($ds_{k,sp}^{d,t}$) is given by Eqs. (4) and (5), respectively. Eqs. (6) to (12) define the parameters used in Eqs. (4) and (5).

$$dm_k^{d,t} = rm_k^{a,e,t} - dw_k^{l,t} - dmu_k^{d,t} - dob_k^{d,t} - dib_k^{d,t} - dt_k^{d,t} \quad (4)$$

$$ds_{k,sp}^{d,t} = rs_k^{a,e,t} - dw_k^{l,t-ts} - dmu_k^{d,t-ts} - dob_k^{d,t-ts} - dib_k^{d,t-ts} - dt_k^{d,t-ts} \quad (5)$$

$$rm_k^{a,e,t} = \sum_{e=1}^{E} o_k \times g_k^e \times rp_{avg}^{a,e} \times \left(p^{e,t} - sc^{e,t}\right) - \sum_{e=1}^{E} o_k \times pc^{a,e,t} \quad (6)$$

$$rs_k^{a,e,t} = \sum_{e=1}^{E} o_k \times g_k^e \times rp_{avg,sp}^{a,e} \times \left(p^{e,t} - sc^{e,t}\right) - \sum_{e=1}^{E} o_k \times pc^{a,e,t} - \sum_{e=1}^{E} o_k \times pc_{sp}^{a,e,t} \quad (7)$$

$$dw_k^{l,t} = (o_k + mu_k + ob_k + ib_k + w_k) \times mc^{l,t} \quad (8)$$

$$dmu_k^{d,t} = mu_k \times muc^{d,t} \quad (9)$$

$$dob_k^{d,t} = ob_k \times obc^{d,t} \quad (10)$$

$$dib_k^{d,t} = ib_k \times ibc^{d,t} \quad (11)$$

$$dt_k^{d,t} = t_k \times tc^{d,t} \quad (12)$$

$$Max \sum_{l=1}^{L}\sum_{j=1}^{J}\sum_{d=1}^{D}\sum_{sp=1}^{SP}\sum_{a=1}^{A}\sum_{e=1}^{E}\sum_{t=1}^{T}\left(\sum_{\substack{k\in MK_p \\ p\in Mp_j}}\left(rm_k^{a,e,t} \times x_k^{a,t} + rs_{k,sp}^{a,e,t} \times c_{k,sp}^{a,t} - dw_p^{l,t} \times y_p^{l,t}\right)\right) \quad (13)$$

MILGP Model for Optimizing Production Schedule

The objective function of the MILGP model for oil sands long-term production planning and waste management is defined by Eq. (13). Eq (13) maximizes the NPV of the mining operation using the continuous decision variables $y_p^{l,t}$, $x_k^{a,t}$ and $c_{k,sp}^{a,t}$ to model mining, processing from mine and processing from stockpile respectively. Continuous decision variables are used to allow for fractional extraction of mining-panels and mining-cuts in different periods for different locations and destinations.

Tonnage fluctuation constraints defined by Eqs. (14) and (15) are introduced in the proposed MILGP model to control the mining and processing targets. These constraints control the consecutive periodic fluctuation of the tonnage mined and tonnage processed. For material mined, the sum of deviations between two consecutive years should be less than or equal to a set deviation tonnage, D_m , allowed for mining. For material processed, the sum of deviations between two consecutive years should be less than or equal to a set deviation tonnage, D_p , allowed for processing. The mine planner controls the parameters D_m and D_p . The planner also controls when to start and finish applying these constraints. Eqs. (14) and (15) can be used for a controlled ramping up in the first years and ramping down in the last year. Eq. (15) includes stockpile ore reclamation. If there is no reclamation, set the ore reclamation variable in Eq. (15) to zero.

The importance of these special constraints is that, the planner does not need to set mining and processing targets. The optimizer uses the set periodic tonnage fluctuation parameters to determine the mining and processing targets. These constraints provide varying practical production schedule options for mine planners.

$$\sum_{t=1}^{T}\left(\sum_{p\in MP_j}\left(o_p+mu_p+ob_p+ib_p+w_p\right)\times\left(y_p^{l,t+1}-y_p^{l,t}\right)\right)\le D_m \tag{14}$$

$$\sum_{t=1}^{T}\left(\left(\sum_{\substack{k\in MK_p\\ p\in Mp_j}}\left(x_k^{a,t+1}+\sum_{sp=1}^{SP}c_{k,sp}^{a,(t-ts)+1}\right)-\left(x_k^{a,t}+\sum_{sp=1}^{SP}c_{k,sp}^{a,t-ts}\right)\right)\times o_k\right)\le D_p \tag{15}$$

Constraints that control ore stockpile tonnages are presented in Eqs. (16) and (17). These equations control the amount of ore sent to stockpile sp in period t. The material sent to the stockpile in period t are reclaimed in period $t+ts$. The planner controls the upper and lower capacity limits for stockpile bins and the stockpiling duration, *ts*.

Ore bitumen grade blending constraints ensure the extracted ore sent to either processing destination a or to stockpile sp in period t meets the grade quality requirements. Eqs. (18) and (19) represent inequality constraints that control the limiting ore bitumen grade sent from the mine and stockpile to the processing plant. Eqs. (20) and (21) represent inequality constraints that control the limiting ore bitumen grade sent from the mine to the stockpile.

Eqs. (22) and (23) represent inequality constraints used to control the limiting grade of ore fines sent from the mine and stockpile to the processing plant. Eqs. (24) and (25) represent inequality constraints used to control the limiting grade of ore fines sent from the mine to the stockpile.

$$\sum_{sp=1}^{SP}\sum_{k=1}^{K}o_k\times s_k^{sp,t}\le\overline{os}^{sp,t} \tag{16}$$

$$\sum_{sp=1}^{SP}\sum_{k=1}^{K}o_k\times s_k^{sp,t}\ge\underline{os}^{sp,t} \tag{17}$$

$$\sum_{p=1}^{P}\sum_{k\in MP_p}g_k^e\times o_k\times\left(x_k^{a,t}+c_{k,sp}^{a,t-ts}\right)-\overline{g}^{a,e,t}\sum_{p=1}^{P}\sum_{k\in MP_p}o_k\times\left(x_k^{a,t}+c_{k,sp}^{a,t-ts}\right)\le 0 \tag{18}$$

$$\underline{g}^{a,e,t}\sum_{p=1}^{P}\sum_{k\in MP_p}o_k\times\left(x_k^{a,t}+c_{k,sp}^{a,t-ts}\right)-\sum_{p=1}^{P}\sum_{k\in MP_p}g_k^e\times o_k\times\left(x_k^{a,t}+c_{k,sp}^{a,t-ts}\right)\le 0 \tag{19}$$

$$\sum_{p=1}^{P}\sum_{k\in MP_p}g_k^e\times o_k\times s_k^{a,t}-\overline{g}^{a,e,t}\sum_{p=1}^{P}\sum_{k\in MP_p}o_k\times s_k^{a,t}\le 0 \tag{20}$$

$$\underline{g}^{a,e,t}\sum_{p=1}^{P}\sum_{k\in MP_p}o_k\times s_k^{a,t}-\sum_{p=1}^{P}\sum_{k\in MP_p}g_k^e\times o_k\times s_k^{a,t}\le 0 \tag{21}$$

$$\sum_{p=1}^{P}\left(\sum_{\substack{k\in MK_p\\ p\in MP_j}}o_k\times fn_k^e\times\left(x_k^{a,t}+c_{k,sp}^{a,t}\right)\right)-\overline{fn}^{a,t,e}\sum_{p=1}^{P}\left(\sum_{\substack{k\in MK_p\\ p\in MPj}}o_k\times\left(x_k^{a,t}+c_{k,sp}^{a,t}\right)\right)\le 0 \tag{22}$$

$$\underline{fn}^{a,t,e}\sum_{p=1}^{P}\left(\sum_{\substack{k\in MK_p\\ p\in MPj}} o_k\times\left(x_k^{a,t}+c_{k,sp}^{a,t}\right)\right)-\sum_{p=1}^{P}\left(\sum_{\substack{k\in MK_p\\ p\in MP_j}} o_k\times fn_k^e\times\left(x_k^{a,t}+c_{k,sp}^{a,t}\right)\right)\le 0 \tag{23}$$

$$\sum_{p=1}^{P}\left(\sum_{\substack{k\in MK_p\\ p\in MP_j}} o_k\times fn_k^e\times s_{k,sp}^{a,t}\right)-\overline{fn}^{a,t,e}\sum_{p=1}^{P}\left(\sum_{\substack{k\in MK_p\\ p\in MPj}} o_k\times s_{k,sp}^{a,t}\right)\le 0 \tag{24}$$

$$\underline{fn}^{a,t,e}\sum_{p=1}^{P}\left(\sum_{\substack{k\in MK_p\\ p\in MPj}} o_k\times s_{k,sp}^{a,t}\right)-\sum_{p=1}^{P}\left(\sum_{\substack{k\in MK_p\\ p\in MP_j}} o_k\times fn_k^e\times s_{k,sp}^{a,t}\right)\le 0 \tag{25}$$

$$Min\sum_{l=1}^{L}\sum_{j=1}^{J}\sum_{d=1}^{D}\sum_{sp=1}^{SP}\sum_{a=1}^{A}\sum_{e=1}^{E}\sum_{t=1}^{T}\left(\sum_{\substack{k\in MK_p\\ p\in Mp_j}}\begin{bmatrix}\left(dmu_k^{d,t}\times v_k^{d,t}\right)+\left(dob_k^{d,t}\times z_k^{d,t}+dib_k^{d,t}\times u_k^{d,t}+dt_k^{d,t}\times q_k^{d,t}\right)\\ +P_1\left(PN_1\times dv_1^{-,l,t}\right)+P_2\left(PN_2\times dv_2^{-,a,t}\right)\\ +P_3\left(PN_3\times dv_3^{-,d,t}\right)+P_4\left(PN_4\times dv_4^{-,d,t}\right)\end{bmatrix}\right) \tag{26}$$

MILGP Model for Optimizing Reclamation and Dyke Material Schedule

The objective function of the MILGP model that minimizes reclamation material cost and dyke construction cost as part of the waste management operation can be formulated using the continuous decision variables $v_k^{d,t}$, $z_k^{d,t}$, $u_k^{d,t}$, and $q_k^{d,t}$. These variables are used to model RM, OB, IB and TCS dyke material requirements respectively, for all dyke construction destinations. Other continuous deviational variables, $dv_1^{-,l,t}$, $dv_2^{-,a,t}$, $dv_3^{-,d,t}$, and $dv_4^{-,d,t}$ are defined to support the goal functions that control RM, OB, IB and TCS dyke materials. In the objective function, these deviational variables are minimized. There is also deviational penalty cost and priority parameters in the objective function used to model the focus of mine management in the presence of multiple conflicting goals. The deviational penalty cost parameters PN_1, PN_2, PN_3, and PN_4 penalize the NPV for any deviation from the set goals. The priority parameters, P_1, P_2, P_3, and P_4 are used to place emphasis on the most important goals. In general, the deviational penalty cost and priority parameters are set up to penalize the NPV if the set goals and most important goals are not met. The objective function for minimizing the reclamation material and dyke construction costs is represented by Eq. (26).

There are tonnage targets for reclamation material and dyke material for dyke construction destinations. Eqs. (27) to (30) represent all required goal functions for RM, OB, IB and TCS respectively. The negative allowable deviation from the set RM, OB, IB and TCS goals are controlled by the planner using the $dv_1^{-,d,t}$ $dv_2^{-,d,t}$, $dv_3^{-,d,t}$ and $dv_4^{-,d,t}$ decision variables.

$$\sum_{p=1}^{P}\left(\sum_{k\in MP_p}\left(mu_p\times v_p^{d,t}\right)\right)+dv_3^{-,d,t}=MUg^{d,t} \tag{27}$$

$$\sum_{p=1}^{P}\left(\sum_{k\in MP_p}\left(ob_k\times z_k^{d,t}\right)\right)+dv_4^{-,d,t}=OBg^{d,t} \tag{28}$$

$$\sum_{p=1}^{P}\left(\sum_{k\in MP_p}\left(ib_k\times u_k^{d,t}\right)\right)+dv_5^{-,d,t}=IBg^{d,t} \tag{29}$$

$$\sum_{p=1}^{P}\left(\sum_{k\in MP_p}\left(cs_k\times q_k^{d,t}\right)\right)+dv_6^{-,d,t}=CSg^{d,t} \tag{30}$$

Eqs. (31) and (32) represent inequality constraints used to control the limiting grade of interburden dyke material fines sent from the mine to dyke construction destinations.

$$\sum_{p=1}^{P}\left(\sum_{\substack{k\in MK_p\\ p\in MP_j}} ib_k \times fn_k^{ib} \times u_k^{d,t}\right) - \overline{fn}^{d,t,ib}\sum_{p=1}^{P}\left(\sum_{\substack{k\in MK_p\\ p\in MPj}} ib_k \times u_k^{d,t}\right) \le 0 \tag{31}$$

$$\underline{fn}^{d,t,ib}\sum_{p=1}^{P}\left(\sum_{\substack{k\in MK_p\\ p\in MPj}} ib_k \times u_k^{d,t}\right) - \sum_{p=1}^{P}\left(\sum_{\substack{k\in MK_p\\ p\in MP_j}} ib_k \times fn_k^{ib} \times u_k^{d,t}\right) \le 0 \tag{32}$$

MILGP Model General Constraints

Mining-Panels Extraction Precedence Constraints

Five precedence constraints presented in Eqs. (33) to (37) are used to define the precedence extraction sequence for each mining panel p based on its spatial location. These equations use the binary integer decision variable b_p. Specifically:

- Eq. (33) defines the vertical mining precedence. The set $IP_p(Z'')$ represents the set of immediate mining-panels that are above mining-panel p.
- Eq. (34) defines the horizontal mining precedence. The set $IH_p(Z')$ represents the set of immediate mining-panels in the specified horizontal mining direction.
- Eq. (35) defines the pushback mining precedence. The set $MP_j(H'')$ represents the set of mining panels in the predecessor pushback.
- Eq. (36) ensures that mining-panel p can only be extracted if it has not been extracted before.
- Eq. (37) ensures that once the extraction of a mining-panel starts in period t, this mining-panel is available for extraction during the subsequent periods.

$$b_p^t - \sum_{c=1}^{c}\sum_{m=1}^{t} y_{u_1}^{c,m} \le 0, \quad u_1 \in IP_p(Z'') \tag{33}$$

$$b_p^t - \sum_{c=1}^{c}\sum_{m=1}^{t} y_{u_2}^{c,m} \le 0, \quad u_2 \in IH_p(Z') \tag{34}$$

$$b_p^t - \sum_{c=1}^{c}\sum_{m=1}^{t} y_{u_3}^{c,m} \le 0, \quad u_3 \in MP_j(H'') \tag{35}$$

$$\sum_{c=1}^{c}\sum_{m=1}^{t} y_p^{c,m} - b_p^t \le 0 \tag{36}$$

$$b_p^t - b_p^{t+1} \le 0 \tag{37}$$

Decision Variables' Control Constraints

In the MILGP model, all decision variables used to control mining, processing, stockpiling, reclamation material, dyke materials and goal deviations are continuous variables. Inequality Eq. (38) makes sure that all the material mined as ore, and all reclamation and dyke materials extracted from the mining-cuts k belonging to mining-panel p in period t are less than or equal to the total material mined from mining-panel p in period t from any mining location. Eq. (39) ensures that the total fractions of ore mined from a mining-cut is less than or equal to one. Eq. (40) ensures that the fraction of ore extracted and sent to the stockpile must be equal to the fraction of ore reclaimed from the stockpile after the stockpiling duration. Eq. (41) ensures that the fraction of TCS dyke material produced from processed ore is less than or equal to the total fractions of ore sent to the processing plant in each period. Eq. (42) ensures that the fractions of mining-panel p extracted and sent to different destinations in different periods is less than or equal to one. Eq. (43) ensures that the fractions of reclamation material extracted from the mine and sent to all destinations in different periods is less than or equal to one. Eqs. (44) to (46) ensure that the total fractions of dyke materials extracted from the mine (OB and IB) or generated from the processing plant (TCS) and sent to all destinations in different periods is less than or equal to one.

$$\left[\sum_{d=1}^{D}\sum_{sp=1}^{SP}\sum_{a=1}^{A}\sum_{\substack{k\in MK_p\\ p\in MP_j}}\begin{pmatrix} o_k\times x_k^{a,t}+o_k\times s_{k,sp}^{a,t}\\ +mu_k\times v_k^{d,t}+ob_k\times z_k^{d,t}+ib_k\times u_k^{d,t}\end{pmatrix}\le\sum_{l=1}^{L}\sum_{p\in MP_p}\left[y_p^{l,t}\left(o_p+mu_p+ob_p+ib_p+w_p\right)\right]\right] \quad (38)$$

$$\sum_{a=1}^{A}\sum_{sp=1}^{SP}\sum_{t-1}^{T}\left(x_k^{a,t}+s_{k,sp}^{a,t}\right)\le 1 \quad (39)$$

$$\sum_{a=1}^{A}\sum_{sp=1}^{SP}\sum_{t=1}^{T}\left(c_{k,sp}^{a,t}-s_{k,sp}^{a,t-ts}\right)=0,\quad t-ts\ge 0 \quad (40)$$

$$\sum_{d=1}^{D}\sum_{t=1}^{T}q_k^{d,t}\le\sum_{a=1}^{A}\sum_{t=1}^{T}x_k^{a,t}+\sum_{sp=1}^{SP}\sum_{t=1}^{T}c_{k,sp}^{a,t} \quad (41)$$

$$\sum_{d=1}^{D}\sum_{t=1}^{T}y_p^{d,t}\le 1 \quad (42)$$

$$\sum_{d=1}^{D}\sum_{t=1}^{T}v_p^{d,t}\le 1 \quad (43)$$

$$\sum_{d=1}^{D}\sum_{t=1}^{T}z_p^{d,t}\le 1 \quad (44)$$

$$\sum_{d=1}^{D}\sum_{t=1}^{T}u_p^{d,t}\le 1 \quad (45)$$

$$\sum_{d=1}^{D}\sum_{t=1}^{T}q_p^{d,t}\le 1 \quad (46)$$

Non-Negativity Constraints

Eqs. (47) and (48) ensure that the decision variables for mining, processing, stockpiling (ore sent to and reclaimed from stockpile), RM, OB, IB, TCS dyke material as well as deviational decision variables are non-negative.

$$y_p^{l,t},\ x_k^{a,t},\ s_{k,sp}^{d,t},\ c_{k,sp}^{a,t},\ v_k^{d,t},z_k^{d,t},\ u_k^{d,t},q_k^{d,t}\ \ge 0 \quad (47)$$

$$dv_1^{-,l,t},dv_2^{-,a,t},dv_3^{-,d,t},dv_4^{-,d,t},dv_5^{-,d,t},dv_6^{-,a,t}\ \ge 0 \quad (48)$$

IMPLEMENTATION OF THE MILGP FRAMEWORK

This section documents the application of the developed MILGP model for an oil sands dataset. Whittle software (Gemcom Software International 2015b), which is based on 3D LG algorithm (Lerchs and Grossmann 1965) is used to generate the optimized pit limit. The optimized pit shell from Whittle serves as a guide in designing the final pit in GEMS software (Gemcom Software International 2015a). The blocks within the final pit design are used as input data for the MILGP model for subsequent integrated long-term production scheduling and waste disposal planning.

As mentioned in Section 1 organic rich solids (ORS) comprises of about 5% of the total ore and it reduces overall bitumen recovery by carrying any associated bitumen into the aqueous tailings (O'Carroll 2002, Sparks et al. 2003). In this sense, ORS is considered to be active and might be a better predictor for ore processability than the traditional use of ore bitumen and fines contents. This ORS recovery is calculated based on the BIT:ORS ratio. Subsequently, the bitumen recovery is calculated based on the bitumen content. It is noted that the recovery calculated based on AER requirements is always greater than or equal to the recovery calculated based on ORS content. The recovery difference ranges between 0.0 and 4.0% for lower bitumen grades (<11%) (Figure 3).

The developed MILGP model has two robust constraints which control the periodic tonnage fluctuation of mining and processing material. The tonnage fluctuation constraints eliminate the need to directly set a mining and processing target. It requires the mine planner to set an acceptable cumulative periodic tonnage fluctuation throughout the mine life, together with any production ramp up or ramp down requirements. The optimizer then determines the appropriate mining and processing targets that meets the tonnage fluctuation requirements. The cumulative periodic tonnage fluctuation value also controls the maximum possible mining and processing capacities indirectly. The tonnage fluctuation constraints provide varying practical production schedule options for mine planners. Two years stockpiling duration is used. This MILGP model generates a smooth and practical production schedule, a NPV with known limits of optimality and is easy to setup with more flexibility for the mine planner.

Two implementation scenarios highlighting different aspects of the developed MILGP model are

run, including: 1) determining the mining and processing annual targets as part of the production scheduling optimization process and not as an input; 2) determining the NPV based on the revenue generated from AER recovery (Scenario 1) as compared to ORS recovery (Scenario 2).

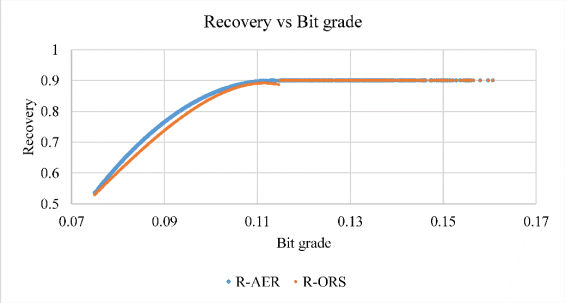

Figure 3. Recovery vs bitumen grade

CASE STUDY

For this case study, to create mining-panels, the ultimate pit was divided into four pseudo pushbacks. Blocks in each mining-panel were clustered into mining-cuts using hierarchical clustering algorithm (Tabesh and Askari-Nasab 2011). Two implementation scenarios are investigated. The deposit is to be scheduled for 8 years for the processing plant, reclamation and dyke construction destinations. Summarized information on the oil sands deposit final pit design is presented in Table 1. Table 2 shows the economic parameters and operational capacities for production scheduling. The economic data are extracted and compiled based on (Ben-Awuah and Askari-Nasab 2013). The stockpiling duration is set at 2 years. The upper and lower bounds of ore bitumen grade is 16.0/7.0 wt%. The upper and lower bounds of ore fines percent is 30.0/0.0 wt%. The upper and lower bounds of IB dyke material fines percent is 50.0/0.0 wt%. The model is implemented on a Lenovo Think Pad computer with i5 Core at 2.2 GHz and 8.0 GB of RAM.

In Scenarios 1 and 2, the mining and processing capacities are not required to be set. The mine planner decides on an acceptable cumulative periodic tonnage fluctuation throughout the mine life for the mining and processing operations and allows the optimizer to determine the mining and processing limits that meets the cumulative periodic tonnage fluctuation value. The planner also controls how many ramping up years is allowed at the beginning of the operation and how many ramping down years is allowed at the end. In this case study, 1-year ramping up is allowed at the beginning and 1-year ramping down is allowed at the end. The cumulative periodic tonnage fluctuation value indirectly controls the maximum possible mining and processing capacities. The focus is to achieve a smooth processing rate throughout the mine life and generate a uniform production schedule that generates the highest NPV.

Table 1. Oil sands reserve characteristics

Description	Value
Total tonnage of material (Mt)	182.23
Total ore tonnage (Mt)	88.44
Total TCS tonnage (Mt)	66.33
Total OB tonnage (Mt)	18.02
Total IB tonnage (Mt)	20.05
Total RM tonnage (Mt)	7.05
Number of blocks	2,523
Number of mining-cuts	155
Number of mining-panels	22
Number of benches	6

Table 2. Economic parameters and operational capacities

Parameter (unit)	Value
Mining cost ($/tonne)	4.60
Processing cost ($/tonne)	5.03
Ore re-handling cost ($/tonne)	0.50
Selling price ($/bitumen %mass)	4.50
TCS dyke material cost ($/tonne)	0.92
OB dyke material cost ($/tonne)	1.38
IB dyke material cost ($/tonne)	1.38
RM mining cost ($/tonne)	0.50
Cumulative periodic mining tonnage fluctuation (Mt)	50.00
Cumulative periodic processing tonnage fluctuation (Mt)	30.00
Mining recovery fraction (%)	100.00
Discount rate (%)	10.00
RM capacity (Mt/year)	1.42
OB capacity (Mt/year)	2.50
IB capacity (Mt/year)	2.40
TCS capacity (Mt/year)	9.00
Stockpiling duration (years)	2

Case Study: Scenario 1

In Scenario 1 for this case study, the overall NPV generated, including the reclamation and dyke material costs is $ 1,499.3 M. The results of the production schedule are presented in Table 3 and Figures 4 and 5.

Table 3. Production schedule (Scenario 1)

Period	Average bitumen grade (wt%)	Material mined (Mt)	Material processed (Mt)
1	8.32	25.00	0.89
2	10.55	25.00	13.85
3	11.53	25.00	13.85
4	10.97	25.00	13.85
5	10.86	25.00	13.85
6	11.10	25.00	13.85
7	11.21	25.00	13.85
8	10.90	6.90	4.43

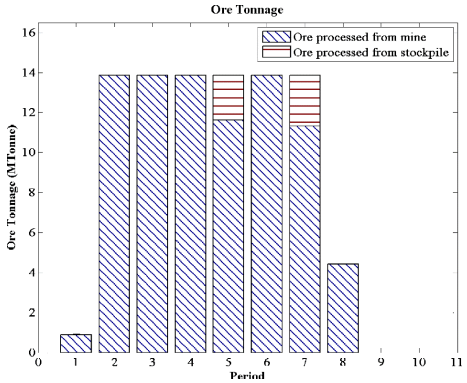

Figure 4. Processing schedule (Scenario 1)

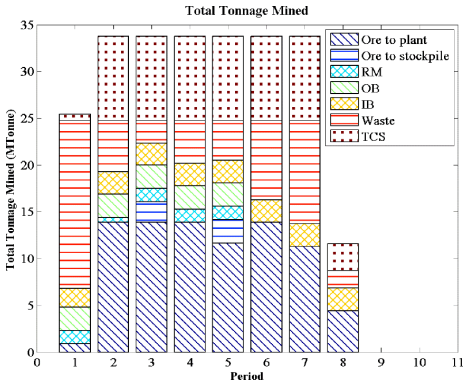

Figure 5. Mining schedule (Scenario 1)

Case Study: Scenario 2

In Scenario 2 for this case study, the overall NPV generated, including the reclamation and dyke material cost is $ 1,468.2 M. The results of the production schedule are presented in Table 4 and Figures 6 and 7.

Table 4. Production schedule (Scenario 2)

Period	Average bitumen grade (wt%)	Material mined (Mt)	Material processed (Mt)
1	8.32	24.78	0.89
2	10.57	24.78	13.80
3	11.53	24.78	13.80
4	10.98	24.78	13.80
5	10.85	24.78	13.80
6	11.09	24.78	13.80
7	11.25	24.78	13.80
8	10.90	8.43	4.45

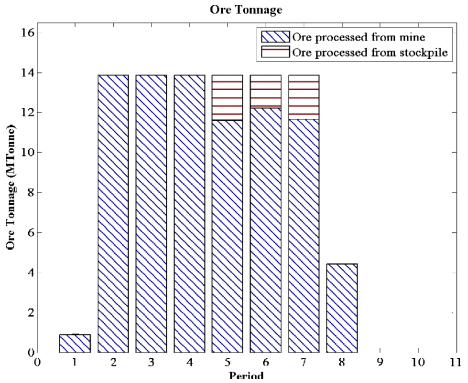

Figure 6. Processing schedule (Scenario 2)

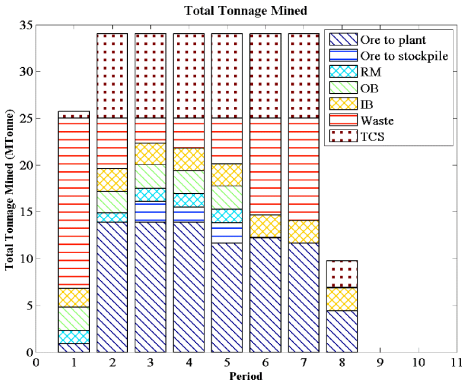

Figure 7. Mining schedule (Scenario 2)

DISCUSSION OF RESULTS

The performance of the MILGP model in Scenarios 1 and 2 is analyzed based on: NPV, mining and processing production targets, bitumen grade profile, and smoothness and practicality of the generated schedules. Both scenarios generate smooth schedules for mining, processing, reclamation and dyke materials. Figure (7) shows a plan view of the pit showing periods of extraction for level 310 m. In Scenario 1, more material is

mined and processed compared to Scenario 2. The average bitumen head grade is slightly different due to the amount of material processed and the use of the stockpile material. The overall NPV generated from Scenario 1, including the reclamation and dyke material cost, is 2% higher than the overall NPV generated from Scenario 2. There are two reasons that explain the differences in the generated NPV. The primary reason is that, the AER recovery is always higher or equal to the ORS recovery. Secondly, more ore is processed in Scenario 1 due to higher revenues resulting from the AER recovery. The average bitumen head grade is slightly different due to the difference in mining and processing schedules, and stockpile reclamation in different periods. The total material mined in Scenario 1 and 2 are the same (181.9 Mt), while the total material processed is slightly different. The model generated a uniform production schedule for OB, IB and TCS dyke material over the 8 periods in both scenarios. This ensures the effective utilization of the mining fleet and processing plant throughout the mine life. The main advantage of using the robust tonnage fluctuation constraints is that, they are easy to set up and there is no need to decide on the periodic mining and processing targets. The only inputs required is how much total deviation is allowed throughout the mine life and if there is any production ramp up or ramp down requirements. These constraints provide varying practical production schedule options for mine planners.

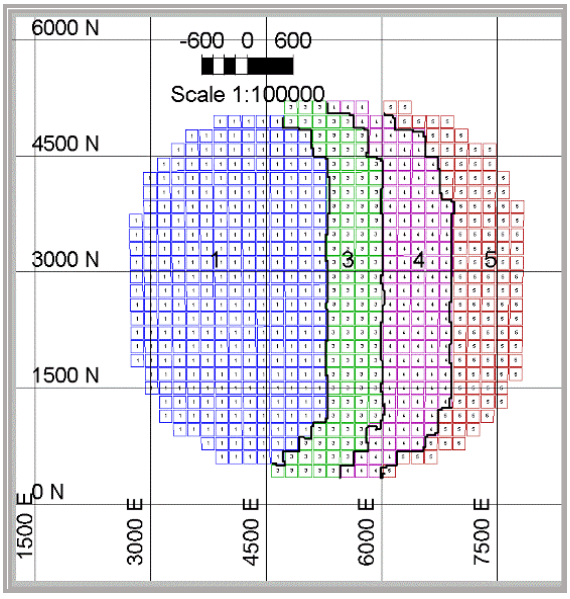

Figure 8. Mining sequence at level 310 m with west–east mining direction (Scenario 1)

CONCLUSIONS AND FUTURE WORK

The MILGP model for oil sands long-term production planning involves the interactions of the objective function, the goal functions and the constraints in an optimization framework to achieve the research objectives. The MILGP model uses tonnage fluctuation constraints for mining and processing. The constraints are easy to set up and do not require the periodic mining and processing targets. This provides robust and practical production schedule options for mine planners. The model generates a strategic production schedule for ore, reclamation and dyke materials for a case study in two scenarios. For both scenarios, the MILGP model illustrates how production scheduling with limited duration stockpiling strategy for ore can be effectively integrated with waste disposal planning and reclamation material stockpiling in oil sands mining. Based on dyke construction requirements, schedules are generated to provide the required dyke materials to support engineered dyke construction that will help in reducing environmental impacts. This schedule gives the planner flexible control over dyke materials and provide a solid platform for effective dyke construction and waste management planning. The MILGP framework integrates a mine-to-mill production planning strategy that uses organic rich solids (ORS) content to estimate bitumen recovery.

The next step of this research will integrate determination of tailings cell sizes and locations in the MILGP framework for waste management. This will ensure sufficient and timely in-pit tailings containment areas are made available for backfilling. Thus, impacting directly the profitability and environmental sustainability of oil sands mining operations.

REFERENCES

AER. (2016). Directive 082 - Operating Criteria: Resource Recovery Requirements for Oil Sands Mine and Processing Plant Operations.

AER. (2017). Directive 085 - Fluid Tailings Management for Oil Sands Mining Projects.

Ben-Awuah, E. and Askari-Nasab, H. (2013). Incorporating waste management into oil sands long term production planning. Transactions of the Institution of Mining and Metallurgy, Section A, **122**(1): 33-45.

Devenny, D. W. (2009). Overview of oil sands tailings. Calgary: Alberta Energy Research Institute.

Gemcom Software International. (2015a). Gemcom GEMS (Version 6.7.1). Vancouver: Gemcom Software International Inc.

Gemcom Software International. (2015b). Whittle strategic mine planning software (Version 4.5.5). Vancouver: Gemcom Software International Inc.

ILOG, IBM. (2012). CPLEX reference manual and software (Version 12.5). Pullman, WA, USA: ILOG S.A. and ILOG Inc.

Lerchs, H. and Grossmann, I. F. (1965). Optimum design of open-pit mines. Transactions of the Canadian Mining and Metallurgical Bulletin, **68**: 17-24.

Masliyah, J. (2010). *Fundamentals of oilsands extraction*. Edmonton: University of Alberta.

Mathworks, Inc. (2017). MATLAB Software (Version 9.2 (R2017a)) [Software]: Mathworks Inc.

McFadyen, D. (2008). Directive 074. Calgary: Energy Resources Conservation Board.

O'Carroll, J. B. (2002). Factors affecting bitumen recovery from oil sands. National Library of Canada = Bibliothèque nationale du Canada, Ottawa.

Sparks, B. D., Kotlyar, L. S., O'Carroll, J. B. and Chung, K. H. (2003). Athabasca oil sands: effect of organic coated solids on bitumen recovery and quality. Journal of Petroleum Science and Engineering, **39**(3): 417-430.

Tabesh, M. and Askari-Nasab, H. (2011). Two stage clustering algorithm for block aggregation in open pit mines. Transactions of the Institution of Mining and Metallurgy, Section A, **120**(3): 158-169.

Whittle, J. (1989). The facts and fallacies of open pit design. North Balwyn, Victoria, Australia: Whittle Programming Pty Ltd.

Wolsey, L. A. (1998). *Integer programming*. New York: J. Wiley.

LIST OF NOMENCLATURE

$a \in A, A = \{1.....,A\}$	Index for possible processing destination.
$d \in D, D = \{1,.....,D\}$	Index for possible destinations for materials.
$e \in E, E\{1,....,E\}$	Index for elements of interest in each mining-cut.
$j \in J, J = \{1,.....,J\}$	Index for pushbacks.
$k \in K, K = \{1,.....,K\}$	Index for mining-cuts.
$l \in L, L = \{1,.....,L\}$	Index for possible mining locations (pits).
$p \in P, P = \{1,.....,P\}$	Index for mining-panels.
$sp \in SP, SP = \{1,....,SP\}$	Index for possible stockpiles in the model.
$t \in T, T = \{1,....,T\}$	Index for the scheduling periods, years.
$ts \in TS, TS = \{1,....,TS\}$	Index for possible stockpiling durations, years.
$dm_k^{d,t}$	Discounted economic mining-cut value obtained by extracting mining-cut k and sending it to destination d in period t.

$rm_k^{a,e,t}$ Discounted revenue obtained by selling the final products within mining-cut k in period t if it is sent to processing destination a, minus the extra discounted cost of mining all the material in mining-cut k as ore from location l and processing at destination d.

$dw_k^{l,t}$ Discounted cost of mining all the material in mining-cut k in period t as waste from location l.

$dmu_k^{d,t}$ Extra discounted cost of mining all the material in mining-cut k in period t as muskeg reclamation material at destination d.

$dob_k^{d,t}$ Extra discounted cost of mining all the material in mining-cut k in period t as overburden dyke material for dyke construction at destination d.

$dib_k^{d,t}$ Extra discounted cost of mining all the material in mining-cut k in period t as interburden dyke material for dyke construction at destination d.

$dt_k^{d,t}$ Extra discounted cost of mining all the material in mining-cut k in period t as tailings coarse sand dyke material for dyke construction at destination d.

$ds_{k,sp}^{d,t}$ Discounted economic mining-cut value obtained by extracting mining-cut k and sending it to stockpile sp and reclaiming it to destination d in period t.

$rs_k^{a,e,t}$ Discounted revenue obtained by selling the final products within mining-cut k from stockpile sp in period t if it is sent to destination a in period t, minus the extra discounted cost of processing and re-handling.

$dw_k^{l,t-ts}$ Discounted cost of mining all the material in mining-cut k in period $t-ts$ as waste from location l.

$dmu_k^{d,t-ts}$ Extra discounted cost of mining all the material in mining-cut k in period $t-ts$ as muskeg reclamation material at destination d.

$dob_k^{d,t-ts}$ Extra discounted cost of mining all the material in mining-cut k in period $t-ts$ as overburden dyke material for dyke construction at destination d.

$dib_k^{d,t-ts}$ Extra discounted cost of mining all the material in mining-cut k in period $t-ts$ as interburden dyke material for dyke construction at destination d.

$dt_k^{d,t-ts}$ Extra discounted cost of mining all the material in mining-cut k in period $t-ts$ as tailings coarse sand dyke material for dyke construction at destination d.

o_k, o_p Ore tonnage in mining-cut k and mining-panel p

g_k^e The required average head grade of element e in ore portion of mining-cut k.

$rp_{avg}^{a,e}$ Proportion of element e recovered (processing recovery) if it is sent from the mine to processing destination a.

$rp_{avg,sp}^{a,e}$ Proportion of element e recovered (processing recovery) if it is sent from the stockpile to processing destination a.

$p^{e,t}$ The selling price of element e in present value terms per unit of product.

$sc^{e,t}$ Selling cost of element e in present value terms per unit of product.

$pc^{a,e,t}$ Extra cost in present value terms per tonne of ore for mining and processing at processing destination a in period t.

$pc_{sp}^{a,e,t}$ Extra cost in present value terms per tonne of ore for stockpiling at stockpile sp and processing at destination a in period t.

mu_k, mu_p Reclamation material tonnage in mining-cut k and mining-panel p.

ob_k, ob_p OB dyke material tonnage in mining-cut k and mining-panel p.

ib_k , ib_p	IB dyke material tonnage in mining-cut k and mining-panel p .
w_k , w_p	Waste tonnage in mining-cut k and mining-panel p .
$mc^{l,t}$	Cost in present value terms of mining a tonne of waste in period t from location l .
$muc^{d,t}$	Cost in present value terms per tonne of RM at destination d .
$obc^{d,t}$	Cost in present value terms per tonne of OB dyke material for dyke construction at destination d in period t .
$ibc^{d,t}$	Cost in present value terms per tonne of IB dyke material for dyke construction at destination d in period t .
t_k , t_p	TCS dyke material tonnage in mining-cut k and mining-panel p .
$tc^{d,t}$	Cost in present value terms per tonne of tailings coarse sand dyke material for dyke construction at destination d in period t .

Session 3

TAILINGS MANAGEMENT

EUREKA! I HAVE THE SOLUTION TO OIL SAND TAILINGS – NOW WHAT?

Andrea Sedgwick, Heather Kaminsky and Jean-François Bouffard
Northern Alberta Institute of Technology, Edmonton, Canada

ABSTRACT

Introducing new technologies in the oil sands tailings segment is a daunting task fraught with many barriers and is difficult to navigate for entrepreneurs and multi-national companies alike. The experience is often frustrating, filled with dead ends, false starts, confounding results, failed pilot studies, and most importantly, wasted capital. Compounding matters is the inherent complexity of oil sands tailings necessitating considerable resources and time to learn and understand how to best apply any novel tailings technology.

This paper will summarize the publicly available information on the current tailings technologies used in the oil sands industry along and the key areas for innovation while considering unique business aspects of oil sands. This summary will help innovators understand the current tailings landscape to better understand where their solution would have the best chance of success. In addition, the paper will discuss some of the key questions and methods to answer questions that a technology provider may be required to answer before bringing their technology to market. These questions include:

- Where is the best fit for the product?
- Is your testing regime appropriate?
- Is your data of high enough quality?
- How does your technology fit and react to existing processes?
- How robust is your technology?

All of these considerations are used by oil sands companies to determine the suitability of new technologies for evaluation and potential commercial deployment.

INTRODUCTION

Background

The production of synthetic crude oil results in large volumes of waste material made up of connate and process water, sand, silt, clay, residual bitumen and diluent, and inorganic and organic by-products of the extraction process (Allen 2008, Bedair 2013). These materials are stored in manufactured tailings storage facilities, on-site, until they are reintegrated into the natural environment and reclaimed. Recent Alberta Energy Regulator (AER 2018) reports indicate that over 1,200 million m^3 of Fluid Fine Tailings (FFT), a tailings slurry comprised of fine clay particles with solids contents ranging from 24 to 52 wt% (AER 2017, Kaminsky and Omotoso 2016, Masliyah et al. 2011). Fine tailings behavior is dominated by the activity of the clay content, prohibiting the consolidation of the material into trafficable deposits. The tailings management framework outlines the goal for fluid tailings treatment and on-site direct placement (Government of Alberta 2015). Under this scenario, placed treated tailings require monitoring, and the physical and chemical characteristics of the materials must be managed in order to achieve the desired performance criteria.

In alignment with the Tailings Management Framework, the Government of Alberta's Alberta Energy Regulator has implemented Directive 085 (2017) for progressive reclamation to ensure that all fluid tailings associated with a project are ready to reclaim (RTR) ten years after the end of mine life. Oil sands companies have explored a variety of tailings treatment technologies to achieve the regulated goals. Technologies that have been applied differ across operators owing to the variation in the mined ore grade and type of the extraction processes. Technologies currently employed include physical and/or mechanical methods, natural processes, chemical amendments, and co-disposal mechanisms (AER 2018). Such technologies are expected to speed up the transformation of tailings slurry into trafficable deposits, ready for reclamation, allowing operators to overcome the following tailings deposition challenges: lack of strength, lack of stability and lack of structure. Most tailings research, to date, has been focused on achieving end products that are geotechnically stable.

Table 1. Novel tailings technologies used by major oil sands operators in the mineable oil sands (summarized from AER Directive 085 decision summaries)

Mine Site	Tailings Technologies in Use to Meet Directive 085
Suncor - Millennium	• In-line flocculation, thin lift drying, and rehandling (TRO) • In-line flocculation and stacking • PASS (in-line flocculation and coagulation with in-pit deposition, followed by water capping at end of mine life (524 Mm^3))
Syncrude - Mildred Lake	• Composite Tailings (gypsum treated middlings, mixed with coarse sand) • Centrifuge treatment of FFT • Water capping of untreated FFT
Syncrude - Aurora	• Composite Tailings (gypsum treated middlings, mixed with coarse sand) • Water capping of 188 Mm^3 of untreated FFT
CNUL - Muskeg River mine	• Composite tailings (discontinued in 2018) • Thickeners with co-deposition
CNUL - Jackpine Mine	• Thickening of middlings with placement in a mixed deposit • Centrifuge treatment of FFT
CNRL - Horizon Mine	• Selective mine planning (MFTRMP) (reduced fines mined) • Non segregated tailings (NST) (thickening middlings and mixing with coarse sand) • Enhanced NST (adding MFT to thickener along with middlings) • CO_2 injection of tailings to pond • Water capping of untreated FFT
Imperial - Kearl	• Thickening of middlings with secondary inline chemical treatment of thickener underflow prior to deposition • Water capping of 125 Mm^3 untreated FFT

There are still uncertainties in: the selection of optimal tailings treatment technologies, the quantity of treated tailings that can be integrated into a landscape, and the optimal location of treated tailings within a reconstructed soil profile. Large time and cost savings would be achieved if treated tailings could both meet the desired strength and be integrated into the reclaimable environment directly, without capping (Caldwell 2017).

WHAT A NEW TECHNOLOGY VENDOR NEEDS TO KNOW

Barriers to Entry

Many technology vendors approach the oil sands industry with a traditional oil and gas culture, mentality and business model. However, it is useful to remind ourselves that oil sands mining is a very unique subset of the sector, creating various barriers to entry for new technology. For example, traditional oil and gas, including enhanced oil recovery operations, typically have multiple operating wells in one geological play. These wells offer a fairly inexpensive entry point for many new technologies. At times, customers can pilot a technology at one well without jeopardizing production at other wells. This relatively low risk and low-cost entry point means that new technologies can be introduced and adopted in reasonably short order.

In contrast, oil sands mining facilities follow a typical mining approach. That consists of very few, large scale operations with very large outputs. These facilities are costly operations, often worth billions $CAD. This facilities cost combined with the isolated nature of oil sands deposits means fewer entry points for new technology when compared to the traditional oil and gas market.

Large, integrated facilities create barriers from an operational risk point of view. Mining is a business built upon efficiencies, where small process changes can create significant cost to these large operations (see Table 2). This ties directly to tailings technology as the water from tailings treatment makes up a portion of the 85% of water that is recycled back into bitumen extraction (Tetra Tech 2017). The extraction plant recovery can be sensitive to water chemistry changes depending on a variety of factors (examples: Cuddy 2000, Masliyah et al. 2011, Yang and Sedgwick 2014). Therefore, oil sands facility operators are often reticent to implement even simple technologies with unknown effects on extraction processes.

Table 2. List of operating oil sands mine facilities and approximate outputs (adapted from Oil Sands Magazine, 2018)

Operator	Froth Treatment	Capacity (bbl/day)
Canadian Natural		
Horizon	Naphthenic	294,000
Muskeg River	Paraffinic	155,000
Jackpine	Paraffinic	100,000
Imperial		
Kearl	Paraffinic	220,000
Suncor		
Base Plant*	Naphthenic	150,000
Millenium	Naphthenic	180,000
Fort Hills	Paraffinic	194,000
Syncrude		
Mildred Lake	Naphthenic	150,000
Aurora†	Naphthenic	225,000
* Froth from Steepbank		
† Froth to Mildred Lake		

Where is the Best Fit for the Product?

There are several tailings streams in the oil sands. Knowing where your technology fits, is very important. Understanding if the new technology fits best for centrifuge tailings or paraffinic froth treatment tailings is typically a revelation for new technology providers, however it is essential to be able to perform the proper testing and determine the right business plan.

If a new technology provider doesn't have this understanding, it can cause some major challenges due to cost of developing the new technology. If the initial path is not applicable, more data will have to be generated on the new business case otherwise it becomes difficult for the industry to adopt the technology.

As mentioned above, tailings streams available for treatment can include: fresh sand tailings, fresh fine tailings, naphthenic froth treatment tailings, paraffinic froth treatment tailings, thickener underflow, and fluid fine tailings (from pond). Not every technology is appropriate for all types of tailings. Additionally, the same technology can be used to achieve different outcomes which depend on the goals of the end user. For instance, using a thickener to produce hot recycle water vs high density underflow. There also may be a more immediate need to deal with certain tailings streams vs. others. For example, fresh sand tailings can be used for a variety of purposes, therefore it is not typically seen as a "problem" for the industry. Coarse tailings are reasonably geotechnically stable and easy to reclaim. In order for reclamation to occur, coarse tailings must be capped or covered with a salvaged reclamation material (e.g., peat mineral mix) in sufficient depth. Without this cover, coarse tailings have little moisture holding capacity. That being said, coarse tailings are very low on the priority list for tailings treatment.

In contrast to fresh tailings, fluid fine tailings have been accumulating for years and must be managed due to the large inventories. One of the methods used currently for treating fluid fine tailings is flocculation. Flocculated FFT are created through the mixture of fine tailings enhanced with a coagulant and/or flocculant to increase the yield stress of the fine tailings. This generates a material with a greater available water holding capacity than most soils. These materials are initially extremely wet, and if the surface dries out completely, a water infiltration barrier is created on the surface similar to the Bnt horizon of Solonetzic soils in southern Alberta (i.e., poor seedbed and inhospitable to vegetation growth and establishment). Also, fine tailings, even when flocculated, creates extremely soft landscapes that are not geotechnically stable enough to conduct reclamation activities unless intensively capped or dewatered further.

Matching a technology to the appropriate tailings application can save a new technology provider a lot of time and money. Each tailings application has a different testing methodology and providing proof of the validity of a technology using the wrong test could lead a technology provider down a more expensive path to commercialization.

Is Your Testing Regime Appropriate?

For ease of adoption, a new tailings technology must ultimately help the oil sands industry meet the criteria required for regulatory mandated reclamation purposes. The end goal for all tailings processes is to provide a reduction in volume and a basis for a reclaimable landscape.

An ideal solution for fluid tailings streams is generally something that mixes easily with the slurry, reacts with the solids to make them easily separable from water, allowing the ideal amount of water to be released and immediately recycled yet allows the remaining material to be pumped with low wear and low pumping energy for the distances required. It would then uniformly fill the deposit according to the deposit design criteria and instantly release the targeted amount of water once placed

in the deposit. This would leave all the solids in the deposit and perfectly clear water with a water chemistry mimicking that of softened river water coming off. This ideal is difficult to achieve and in reality it requires trade-offs or disruptive technologies. How these tradeoffs are made will depend on the site. For example, one company may prioritize the strength of the final deposit whereas another may prioritize the capture of naphthenic acids.

Even if a technology achieves these objectives it may not be implemented if it is not sufficiently robust or doesn't reduce the volume of tailings in the desired time frame. It is essential for a new technology provider to understand where the technology could be used (one site or several sites) and ensure that the data that they are collecting captures all of the key performance indicators that are in their target market.

Is Your Data of High Enough Quality?

Oil sands companies expect that a certain amount of rigor has gone into "proving" that a technology is applicable in oil sands. Even if that technology has been adopted in other mining applications, it must have enough information to ensure that it is applicable in oil sands. Often this requires a good Design of Experiments (DOE) where a sufficient number of experiments are performed that the results are statistically linked to a single variable or known combination of variables. In most cases, this means that tests are done in triplicate within a DOE.

If the technology is at the pilot stage, then there must be enough time run per condition to get a feasible amount of data. In this case, a large number of samples are required. Typically, at least one third of the overall pilot budget should be considered for sample collection and analysis. This often seems like a large amount of money, however it has been noted by industry personnel that multi-million dollar pilots have been run which did not produce any conclusive results due to the lack of DOE and statistically relevant data. It is essential to run the data through statistical analysis to determine if the variables or interaction of variables have an impact on the treatment.

How Does Your Technology Fit and React to Existing Processes?

A large amount of water (>85 wt%) is recycled back to the extraction plant (Tetra Tech 2017) from the tailings ponds. Water chemistry is very important to effectively recover oil from the sands (Masliyah 2011), therefore the type of tailings treatment is important. For example, certain types of electrical processes can release Ca or Na from the clays, causing an increase in those ions which can be detrimental to the extraction process in some conditions. For example, assuming a 300,000 bpd facility, a one percent change in recovery can decrease production by more than 3,000 bpd which works out to one million barrels per year. It is important to consider these impacts and their effect on a return on investment calculation.

Another consideration is if the new technology results in an overall increase of carbon dioxide emissions. In a complex plant environment, industry may be very reluctant to increase carbon dioxide emissions even if the technology gets them closer to their reclamation goals. Therefore, testing of carbon dioxide emissions may need to be part of the validation program.

By understanding the existing processes and ensuring a proper test plan is followed, a new technology provider will ensure that answers to questions industry might have are available. This often results in a quicker path to deployment.

How Robust is Your Technology?

In some industries, the particle size is kept within a proscribed tolerance for the plan to operate properly. However, in oil sands the particle size distribution of the tailings can vary. If the technology is appropriate on fluid fine tailings, it has to be able to handle a variety of ratios of sands, fines and clays, water and bitumen. This mixture can change significantly within an hour timeframe (Kaminsky and Omotoso 2016) therefore the more robust a technology is, the more favorable it will be seen. The key to this is testing on a wide variety of fluid fine tailings.

For the business case, it is also important to test tailings from a variety of sites. Typically, each oil sands pond has different water chemistry characteristics. Therefore, if a technology wants to be applicable across various sites, it must be able to prove that it is robust enough to handle different water chemistries.

Paraffinic versus Naphthenic Froth Treatment

There are two types of froth treatment processes used by the oil sands industry at this time: paraffinic and naphthenic. They produce two very different

types of tailings. Paraffinic froth treatment tailings consist of fine minerals and clays, asphaltenes and a very small amount of maltenes in a large portion of water. The fine minerals and clays often bind loosely with the asphaltenes to make an asphaltene agglomerate. However, some of those clays and ultrafines are still separated from the asphaltenes and make up a good portion of the fluid fine tailings. It has been proven that these asphaltene agglomerates act like larger size particles and settle quite easily. Naphthenic froth treatment tailings do not have asphaltenes due to the use of a different type of chemical (diluent). Both froth treatment tailings have a very small percentage of solvent (0.3% vol./vol) or diluent (less than 0.4% vol./vol) in the tailings (Tetra Tech 2017). Some technologies will handle asphaltenes better than others, therefore this factor should be taken into account.

Interestingly, the type of froth treatment does have some effect on the tailings. Solvents or diluents actually provide a good source of food for bacteria naturally found in the tailings, therefore certain kinds of tailings treatments may see gas generation occur. This leads to two issues: 1) gas emissions (industry is interested in decreasing gas emissions from ponds) and 2) “fluffing” of the tailings. Fluffing of the tailings results in a loss of room in the tailings pond for deposition. A technology that has either of these two phenomena (although they typically go together from our experience) may have a more difficult time being adopted in oil sands.

Intellectual Property

The ownership of technology and associated intellectual property (IP) is often a barrier to deployment of new technologies in any domain. The same is true for oil sands. Generally speaking, IP consists of patents, data, trademarks, trade secrets plans, processes and other elements that can be used to describe a technology. It can be divided into two categories, background IP and resultant IP. Background IP is largely historical and is what companies bring to the table at the beginning of a working relationship. For example, a technology provider with a new chemical additive brings all of their historical IP on the product to the oil sands operator, who in turn has background IP on their own internal processes, etc. Background IP is usually not a barrier to engagement.

Where conflict generally occurs is during the negotiations of IP developed as a result of a partnership. For example, if the two aforementioned companies share costs on the testing of a new chemical tailings treatment. The project outcomes lead to a new process or method for applying the chemical. In such a case there is potential conflict on the matter of IP ownership and the resultant commercial opportunities, as both parties may have a legitimate claim on the new developments.

There are several practices that can be implemented during the development of a new tailings technology. One suggested practice is to establish what elements of the technology fall in the public domain and are therefore off the table to IP claims. This helps establish a playing field where there is some clarity on where there are potential starting points for conflict. To avoid conflict, cash rich organizations may choose to handle all costs and development internally as long as possible, thereby delaying the potential for conflict. Conversely, cash poor organizations may negotiate away a portion of their IP rights to oil sands companies as part of a joint venture on developing the technology. Importantly, at some point almost any tailings technology provider will need to concede some portion of their IP in order to complete the final validation of their technology through the fact that the customer sites are each appreciably different and are controlled by oil sands companies.

Samples

Technology developers are often surprised by the availability of tailings samples. The core assumption is that as an abundant waste product, tailings should be inexpensive and a plentiful resource for technology providers to access. In practice however, the reality is very different.

At a minimum, tailings are in remote deposits with restricted access. Seasonality must be considered as samples cannot be collected in winter. Collection requires vacuum trucks or specialized equipment with high mobilization costs. Large batches of tailings must then be homogenized before being split into smaller subsamples, usually either 1 cubic meter totes or smaller 20-liter buckets. This also requires specialized capabilities maintained by few organizations. In order to manage sample costs, most organizations plan their sample collection during field season. For these reasons, it is suggested that technology developers secure samples well in advance of their experimental program. It is possible that samples provided by oil sands mines will require a contract between both parties outlining the limitations for use of the samples.

For small quantities, InnoTech Alberta maintains a tailings sample bank in Edmonton. Samples are available in 20-liter (5 US Gallon) pails for a fee. Samples can be ordered online at: https://innotechalberta.ca/mature-fine-tailings-sample-bank-request-form/. In October of 2018, the cost for one pail was $700 CAD (approx. $540 USD).

Due to the barriers associated with obtaining samples, many developers have adopted seemingly innocent practices to save on costs. Unfortunately, these can have sub optimal impacts. For example, it can be tempting to re-use samples multiple times to save costs. The downside is this may cause biases in your data, harming your repeatability. For this reason, we suggest using tailings samples once, before disposing of them.

As tailings streams can vary depending on their origin, background process, and collection method, samples should be characterized prior to use. Common methods and their output are listed in Table 3. These will represent valuable metadata on your sample and useful for interpreting the results obtained using your technology. Without this metadata, operators have no baseline to interpret the results and will generally require you to do another set of tests or worse, completely ignore what you have generated. The reason for this is that FFT is highly variable even within a single pond or site and will respond differently to treatments depending on the clay content, solids content and water chemistry (Kaminsky and Omotoso 2016).

Table 1. Suggested tailings sample characterization methods

Method	Characterization
Dean and Stark (on tailings containing bitumen)	Determine composition of sample (bitumen, water and solids content)
Oven drying (on tailings containing no bitumen)	Determine composition (Water and solids content)
Particle size distribution	
Methylene Blue Index (MBI)	Determine clay content and activity
Water Chemistry	pH, conductivity, TDS, Total Organic Carbon, Total Inorganic Carbon, Major anions and cations
Rheology measurement	Yield Stress

Site Access

As a technology matures and advances along the technology readiness levels, it will eventually require scaled up trials. These are typically an order of magnitude larger in terms of product throughput which are only economically feasible on site.

Oil sands mines and their tailings ponds are located in remote areas with limited access. Furthermore, tailings ponds can be hazardous environments, requiring training and operating procedures to work in and around. Site access is often limited to a few trusted operators with specific qualifications and certification programs in place. This has created a barrier to access for many technology developers not deeply embedded in oil sands operations.

Industry will often ask for testing to be performed by third party laboratories, or consultants to ensure that the data is relevant (the methods that are followed are industry accepted), before moving to an on-site test.

Scale Up

Oil sands mining produces fluid fine tailings in a ratio of approximately 1 barrel of FFT per barrel of bitumen produced (AER 2018). As stated earlier, the Alberta Energy Regulator estimates that there are currently 1.2 billion cubic meters of untreated tailings, with stockpiles expected to continue growing for the foreseeable future. This volume of material is significant, with few parallels elsewhere in the world. The scale of operations can also be surprising to new technology developers. Quite often, over 26,000 tph of tailings (coarse and fine) report to the tailings pond (Tetra Tech 2017). This is a significant amount, when new technology providers propose treating fresh, whole tailings. For example, if there is a technology that requires whole tailings (sands and fines size fractions), then the tonnages that are relevant are in the 10s of thousands tonnes per hour.

For this reason, many technology developers put an emphasis on scaling up their technology very early on in the development process. However, it is very important to not rush to a pilot stage and to ensure that the scale up factors and variables are known. This means that in some cases, computational fluid dynamics is required. Other methods can be a systematic movement in size based on data gathered at each phase. By doing this work at smaller volumes, the technology can be tested on a wider variety of variables and the variables can be

tested in less complex configurations. This leads to a greater chance of success.

In addition, it is important to understand the impacts of these scale or technology development costs. For reference, recall that 20 Liters of oil sands tailings from a sample bank is approximately $700. If a technology requires 10 liters of tailings per test run, each run will cost as much as $350 for sample. Larger scale technologies requiring volumes up to 1 cubic meter can expect to pay up to $10,000 per sample run. Factor these costs by the appropriate number of experimental replicates, and it becomes apparent that tailings technology at even relatively small scales can be costly in terms of sample costs.

When designing your technology development plan, it is suggested to consider the impact the scale of experiment can have on your testing. Instead of focusing on larger scale, quasi pilot demonstrations with high costs, it is often preferable to perform smaller scale experiments to validate assumptions prior to scale up. This method is more agile, nimble and often more cost-effective approach which allows for a more methodical scale up as the technology progresses.

Technology Readiness

Technology readiness is a measure of how close any particular technology may be to deployment in the field. It is typically highly subjective and dependent on many factors, therefore making it difficult to evaluate. However, technology developers are often asked to self-assess their Technology Readiness Level (TRL). TRL was originally developed by NASA (Mankins 1995) as an integrated technology planning and management tool to assess flight worthiness of new systems. In oil sands, a modified TRL scale published by Alberta Innovates is often used (Table 2).

As TRLs were developed with a narrow scope and application in mind, they often work best for technologies with a narrow scope and within niche applications. This can cause problems for technology developers trying to attract interest for their offerings. For example, a technology may be commercially deployed in another domain outside of oil sands. In such a case, it is tempting to categorize a technology as being at a high TRL level however it is our suggestion is to resist this temptation. The complexities associated with oil sands tailings often means that technologies do not “port over” to a similar level in the oil sands tailings domain.

Table 2. Technology Readiness Levels (adapted from Alberta Innovates, 2018)

TRL1	Basic principles of concept are observed and reported.
TRL2	Technology concept and/or application formulated.
TRL3	Analytical and experimental critical function and/or proof of concept.
TRL4	Component and/or validation in a laboratory environment.
TRL5	Component and/or validation in a simulated environment.
TRL6	System/subsystem model or prototype demonstration in a simulated environment
TRL7	Prototype ready for demonstration in an appropriate operational environment
TRL8	Actual technology completed and qualified through tests and demonstrations
TRL9	Actual technology proven through successful deployment in an operational setting.

Industry Experience

Commercialization of new technologies in the oil sands market is not for the faint of heart. Technology adoption cycles in the market are long (typically 10 years or longer) and take considerable time and resources to accomplish. Companies inexperienced in the industry typically struggle this. Developing a reputation as a serious and worthwhile party can be time consuming. This struggle is faced by large multinationals as well as smaller startups and SMEs.

Successful companies often include some form of oil sands industry experience on their technical team or their management team. The right people can help a company navigate the myriad technologies, companies, personalities and even acronyms that create barriers to entry. Companies without this experience are encouraged to seek it out in the form of service providers or by hiring appropriate team members early in the process.

Brownfield versus Greenfield Application

A key mistake that technology developers make is not recognizing the difference between Brownfield and Greenfield oil sands mining operations. They can be defined as:

Brownfield site. Existing, operating oil sands mines as described in Table 2. These are typically large-scale facilities with high replacement costs.

Greenfield site. Planned or unbuilt facilities and expansions. These are typically less bound by legacy infrastructure. If future mines proceed, they may use new techniques. Typical development cycles are on the order of 10 plus years.

The primary contrast between the two types of sites is based upon the adoption cost of technologies. Brownfield sites are established, with significant in place infrastructure. Technologies that significantly impact existing operations or would replace existing processing streams are generally considered too expensive in terms of capital cost and opportunity costs from lost production. As such brownfield sites are generally more receptive of technologies that are incremental or supplementary to their existing process and operations. Successful commercial deployment requires that technology providers develop a deep understanding of the client's business model and operational context.

Greenfield sites, by virtue of not already having a large capital investment, are conceptually open to new technologies and different processes. They are a proverbial "Blue Ocean". However, the market is considerably more difficult to predict. At the time of this writing, there is only one planned oil sands mine submitted for approval, the Teck Energy Frontier mine. If approved, Frontier will likely operate like most existing mines. Less defined opportunities exist in unannounced mines however the timeframe to commercialize the technology is on the order of decades.

Business Model

The business model is critical to the successful commercial deployment of any new technology. A poor business model introduces risk and can make otherwise good technologies fail. Unfortunately, technically driven entrepreneurs often emphasize technology development at the detriment of their business model. This is understandable in the early stages of development but should be rectified at the later TRLs.

A sound business model will allow a potential customer to easily evaluate the economic value of investing in a new technology. The methods of doing this are highly variable and include: payback period (the time it takes to recoup an investment), Return on Investment (the percentage return on a dollar spent), and Net Present Value (the present value of dollars invested in a technology). In order to be successful, technology developers are advised to understand the economic decision method their potential clients use in order to tailor their business model to the client. Pricing of a new technology should reflect this fact.

Beyond pricing, other aspects of the business model are important. For example, what warranties or guarantees of performance are required? Will after sales service be needed? Will the operator require new staff to operate the technology, or will this be offered by the vendor? Mindful consultation with potential clients and careful consideration of these details will help facilitate the commercial adoption of the technology.

CONCLUSION

There is a lot to know when new technology providers are entering into the oil sands industry. We have provided some of the main pieces to the puzzle of oil sands technology development, however this is only a portion of the complexity of the field. It is important for new technology developers to talk to the right people and gain insight into the oil sands industry before pitching their technology to the oil sands companies. Understanding where your technology fits into the complexities of the oil sands industry will help you navigate through the business and will decrease the frustrations often felt by those entering into the field unaided.

REFERENCES

Alberta Energy. (2013). Alberta's oil sands: January fact-sheet. Government of Alberta, Edmonton, Alberta.

Alberta Energy Regulator. (2017). Fluid Tailings Management for Oil Sands Mining Projects.

Alberta Energy Regulator. (2018). Mineable Oil Sands Fluid Tailings Status Report 2016.

Alberta Energy Regulator. (2017). Decision 20171025A: Suncor Energy Inc; Application for Operational Amendment and Base Plant Tailings Management Plan.

Alberta Energy Regulator. (2017). Decision 20171218A: Canadian Natural Resources Limited; Application for Operational Amendment and Base Plant Tailings Management Plan.

Alberta Energy Regulator. (2018). Decision 20180523A: Canadian Natural Upgrading Limited; Application for Muskeg River Mine Tailings Management Plan.

Alberta Energy Regulator. (2018). Decision 20180523B: Canadian Natural Upgrading Limited; Application for Jackpine Mine Tailings Management Plan.

Alberta Energy Regulator. (2018). Decision 20180613A: Syncrude Canada Ltd; Application for Aurora North Tailings Management Plan.

Alberta Energy Regulator. (2018). Decision 20180716A: Imperial Oil Resources Limited; Application for Kearl Management Plan.

Alberta Innovates. (2018). Technology Readiness Levels. Available at: https://albertainnovates.ca/wp-content/uploads/2018/05/Technology-Readiness-Levels.pdf

Allen, E. (2008). Process water treatment in Canada's oil sands industry: I. Target pollutants and treatment objectives. Journal of Environmental Science, **7**: 123-138.

AMEC Environment & Infrastructure. (2013). Beach Fines Capture Study.

Beier, N. and Sego, D. (2008). Dewatering of Oil Sands Tailings Using Cross Flow Filtration. 61st Canadian Geotechnical Conference and 9th joint IAH-CNC Groundwater Specialty Conference, Edmonton, Alberta, September 22-24, 2008.

BGC Engineering Inc. (2010). Oil Sands Tailings Technology Review. OSRIN, (July).

Caldwell, J. (2017). Covers for Tailings, Heap Leach Pads, and Waste Rock Dumps. Tailings and Mine Waste Conference 2017. Lake Louise, Canada. Short course.

Canadian Association of Petroleum Producers (CAPP). (2018). Canada's Oil Sands.

Cuddy, G. (2000). Empirical studies on the relationship between process water chemistry and oil sands processability (Syncrude Canada Ltd.), in "Problem Ores. 1st Extraction Fundamentals Seminar", CONRAD, Ft. McMurray.

Government of Alberta. (2015). Lower Athabasca Region Tailings Management Framework for the Mineable Athabasca Oil Sands.

Hollander, E. and Omotoso, D. (2017). Introduction to oil sands clays: clays impact on bitumen extraction processes. Clay Minerals Society Workshop, Edmonton, Alberta, Canada.

Kaminsky, H. A. W. and Omotoso, O. (2016). Variability of Fluid Fine Tailings. Proceedings of the fifth International Oil Sands Tailings Conference (IOSTC), Lake Louise, Canada.

Kasperski, K. L. (2001). Review of research on aqueous extraction of bitumen from mined oil sands. Natural Resources Canada, CANMET-WRC, Devon, Canada.

Kasperski, K. L. and Mikula, R. J. (2003). Water treatment in oil sands: a novel approach to calcium control. In Proceedings of Corrosion 2003 Conference, San Diego, California, pp 7.

Mankins, J. C. (1995). Technology Readiness Levels, A White Paper. NASA Advanced Concepts Office, Office of Space Access and Technology, 6 pages

Masliyah, J., Czarnecki, J. and Xu, Z. (2011). Handbook on Theory and Practice of Bitumen Recovery from Athabasca Oil Sands. Vol. 1: Theoretical Basis. Kingsley, Calgary.

Sanford, E. C. (1983). Processability of Athabasca oilsand: interrelationship between oilsand fine solids, process aids, mechanical energy and oilsand age after mining. CJChEng, **61**(4): 554-567.

Sanford, E. C. and Seyer, F. A. (1979). Processability of Athabasca tar sand using a batch extraction unit: the role of NaOH. CIM Bull, 164-169.

Tetra Tech. (2017). Development of a Static Oil Sands Mine and Extraction Reference Facility.

Yang, X. and Sedgwick, A. (2014). Investigation of interburden dilution on oil sand processability. SPE Heavy Oil Conference-Canada, Calgary, Alberta, Canada.

CANADA MEETS THE WORLD: HOW OIL SANDS TAILINGS MANAGEMENT KNOWLEDGE AND TECHNOLOGIES ARE APPLIED IN EUROPE AND BEYOND, AND VICE VERSA

L. Sittoni[1,2], E. M. M. van Eekelen[1,3], F. van der Goot[1,4] and H. E. Nieboer[1,5]
[1]EcoShape, The Netherlands
[2]Deltares, The Netherlands
[3]Van Oord Dredging and Marine Contractors, The Netherlands
[4]Royal Boskalis Westminster N.V., The Netherlands
[5]Witteveen + Bos, The Netherlands

ABSTRACT

Oil sands fluid fine tailings, thickened tailings or sand–fines tailings mixtures have a lot of similarities with natural mud, sand–mud mixtures and soft soils commonly found in estuarine and coastal areas. While the specifics of oil sands operations are certainly different, the physics and physical processes at the basis of tailings treatment technologies (especially in the direction of tailings basins closure), and sediment management for land reclamation or coastal defense are very similar.

In various regions of the world sediment management is becoming a critical matter for sustainable development: coastal regions and river banks are eroding exposing towns to more recurrent flooding; coastal development activities demand for large quantities of sediment as building material, or development of harbors for access to remote coastal regions. Similarly to fluid fine tailings management and tailings basin closure, these challenges indicate that smart, integrated and technologically advanced sediment (and tailings) management is critically necessary.

With this in mind, EcoShape initiated the Living Lab for Mud (LLM) initiative. The LLM includes five pilots project in the Netherlands and Indonesia where innovative fine sediments knowledge and technologies are developed and tested in the field. These projects include utilizing dredge and natural sediments to: build islands for enhancing biodiversity; produce construction material for dykes reinforcement; and enhance the development of wetlands, salt marshes and mangroves. Similarly to oil sands tailings management, the underlying physic and processes at the basis of these pilots include: flocculation, dewatering and strength development (i.e. sedimentation, consolidation, drying and ripening); fines resuspension, fate and trapping; interaction of sediments with biota; and socio-economic aspects.

Not too dissimilar from the Canadian Oil sands Innovation Alliance (COSIA), EcoShape (www.ecoshape.org) is a Dutch consortium created to develop, collect and disseminate pre-competitive innovative knowledge and technologies based on the Building with Nature (BwN) approach. EcoShape unifies research institutes (Deltares and Wageningen University and Research), consultants (Witteveen en Bos, Arcadis, Royal Haskoning – DHV, HKV), contractors (Boskalis, Van Oord, IHC) and government agencies (Dutch Ministry and Municipalities).

This paper presents the LLM initiative and gives a general overview of these pilot projects, highlighting the similarities in knowledge, (numerical) tools and technologies with oil sands tailings management and tailings basins closure. This presentation has the ambition to continue inspiring international collaboration and knowledge exchange between Canada, Europe and beyond.

INTRODUCTION

Based on the assumption of general and fundamental similarities between Canadian Oil sands tailings and natural mud, this paper describes a selected numbers of international, Dutch-based experience and pilot projects, where knowledge partly developed in oil sands research is utilized for the beneficial nature-based use of natural mud. This paper intends to demonstrate that collaborative pre-competitive knowledge development and dissemination approaches are similarly developed in Canada and in the

Netherlands. This paper therefore pledges for even closer international collaboration.

Canadian Oil Sands Tailings Challenges

One of the largest challenges of Canada's oil sands is the production of large volumes of slow dewatering oil sands tailings during bitumen extraction (Martin and Davids 2000). Oil sands operators are required to comply with Alberta Energy Regulator (AER) requirement to manage fluid tailings (FT) volumes during and after mine operation in order to manage and decrease liability and environmental risk resulting from the accumulation of fluid tailings on the landscape. FT management should be achieved while balancing environmental, social, and economic needs (AER, Directive 85).

FT are a mixture of process water, sand, silt, clay and residual bitumen. During deposition or as part of tailings management processes sand is often separated from the rest of the tailings generating fluid fine tailings (FFT). FFT is at the core of the oil sands tailings management challenge. FFT has very poor dewatering (i.e. settling and consolidation) properties largely caused by the bitumen extraction process which disperses the clay fraction.

Independently or through COSIA, the industry is investing significant resources to develop effective technologies to minimize production and treat legacy of FFT[1]. The key objective is to reclaim FFT into boreal landscape soon after mine life. Example technologies include (a combination of):

- Flocculant treatment, generally synthetic anionic polymers;
- FFT centrifugation with large centrifuges;
- Atmospheric drying of FFT with subsequent deposition and drying of thin FFT layers;
- Non-segregating tailings, mixing sand and fines before deposition, and avoiding segregation of sand and FFT during deposition;
- Co-mixing, mixing coarse and fine tailings during deposition or within existing deposits;
- Capping, covering existing deposits with a layer of sand of other lighter material;
- Deposition of treated FFT in deep mine-pit deposits;
- Biological (nature-based) methods, such as enhancing dewatering through vegetation, worms, bacteria.

This collaborative research and technology development at pre-competitive stage is funneled via COSIA. COSIA was launched in 2012 with all largest oil sands companies contributing to fund and co-develop innovative technologies with focus on accelerating the pace of improvement the environmental performance of Canada's oil sands[2]. COSIA includes four Environmental Priority Areas (EPAs): greenhouse gases (GHG), land, water and tailings.

While the clay fraction of FFT has undergone dispersive treatment during the bitumen extraction process, FT presents many similarities with natural mud. Therefore the knowledge that is developed in Canadian oil sands is applicable to many other challenges in muddy areas world-wide. Vice versa solutions from international experience can be effectively imported in oil sands when appropriately adapted to the peculiarity of the oil sands tailings and the needs of the industry.

Worldwide Mud Challenges

Throughout the world, different coasts, shores, lakes, and rivers have to deal with excess sediment or sediment shortages. The natural balance between the erosion and deposition of sediment is disrupted by human interventions such as dams in a river, port developments in an estuary and dredging activities for the maintenance of existing ports and waterways. Disruption of the natural balance creates areas of sediment starvation (i.e., coastal erosion) and areas of sediment abundance (i.e., siltation in harbors), Winterwerp and Wang (2013), Winterwerp et al. (2013), Vörösmarty et al. (2003), and Brils et al. (2017). Human developments and natural ecosystems are directly affected by this sediment unbalance, with implication on industrial activities (e.g. navigation, logistic and tourism industry); space for living, flood safety and impact of climate change (e.g. loss of coastal areas and more frequent flooding) and food security (e.g. loss of productivity).

Optimizing sediment management by integrating human developments into the natural sediment cycle is one of present days' greatest challenges

[1] https://www.cosia.ca/initiatives/tailings#projects

[2] https://www.cosia.ca/about

as well as greatest opportunities. Sediment is therefore potentially a precious resource, not a waste.

Worldwide, various initiatives and programs exist that focus on the development and testing of sustainable and nature-based approaches for optimizing sediment management and reuse. The Central Dredging Association (CEDA) started a Working Group on Beneficial Use of Sediments in 2017[3], which collected the latest case studies and listed the most important worldwide initiatives regarding beneficial use of natural (and contaminated) sediments in an Information and a Position paper soon to be published.

THE LIVING LAB FOR MUD, ECOSHAPE AND BUILDING WITH NATURE

The Living Lab for Mud (LLM)[4] is managed by the consortium EcoShape – Building with Nature in The Netherlands[5]. EcoShape is a Dutch consortium that unifies many of the most important Dutch private (i.e. engineering and contractor), research institute and academic organizations, NGO and public entities of the Dutch water sector. The objective of EcoShape is to collaboratively develop, demonstrate through pilots, and publically share precompetitive BwN knowledge and solutions for water-(and dredging) related challenges. While different in the organizational details, EcoShape is not too dissimilar from COSIA.

BwN means proactively utilizing the ecological, physical and socio-economic system integral ingredient of an engineering solution (De Vriend et al. 2015, De Vriend & Van Koningsveld 2012). In coastal defense setting it may mean utilizing vegetation to trap sediments and decrease the impact of a storm on the dike, rather than increasing a concrete dike. It may also mean taking advantage of the too high turbidity of a river and harbor siltation to dredge and ripen these sediments to produce clay soil to strengthen and broaden dikes. BwN also means to incorporate local governance and stakeholder engagement and sustainable business models.

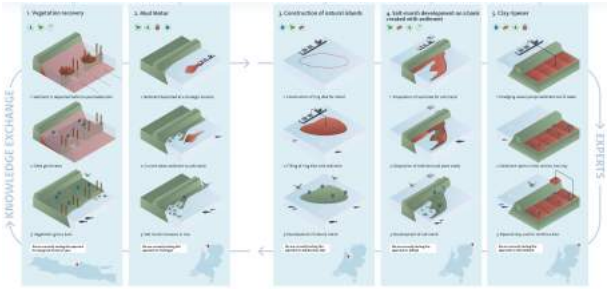

Figure 1. Representation of the 5 LLM concepts. The LLM concepts are tested in five pilot projects. From left to right: Vegetation recovery in eroding coastal areas, Pilot Building with Nature Indonesia; Strategic disposal of dredge sediment for salt marshes development, Pilot Mud Motor; Construction of natural islands from natural dredge sediments, Pilot KIMA Marker Wadden; Develop salt marshes from sand and mud, Pilot Marconi; Producing clay soil from dredge sediments, Pilot Kleirijperij. Generic knowledge regarding fine sediment physics, project implementation and governance is developed within each pilot. The knowledge and experts network are shared across the pilots. Image by EcoShape, 2017

The main objective of the LLM is to develop, show and share innovative knowledge, technologies and techniques regarding the sustainable use and re-use of fine sediments (i.e. mud) based on the BwN approach (EcoShape 2017). The LLM is a real big living lab. It links five mud and BwN based concepts which are tested in five full-scale EcoShape managed specific pilot projects in The Netherlands and Indonesia (Figure 1). In these pilots we “learn-by-doing”. Innovative mud based solutions are tested to: reduce flood risk and increase resilience to climate change; enhance ecosystem restoration and nature development; improve water quality; transform sediment into alternative building material and improve the navigability of waterways. The LLM extrapolates and exchange generically applicable concepts from existing specific pilots.

The LLM pilots apply the principle of BwN. It is the ambition of the authors, of EcoShape and its partners, to apply the knowledge developed with the LLM in practice and to extend the LLM experts

[3] https://www.dredging.org/ceda/working-groups
[4] https://www.ecoshape.org/en/projects/living-lab-mud/
[5] https://www.ecoshape.org

network both nationally and internationally, since estuaries, coastal areas and inland waters, as well as various industry activities (e.g. oil sands) elsewhere in the world face similar sediment or tailings management challenges and opportunities.

THE LIVING LAB FOR MUD PILOTS

The LLM includes five pilots as described in Figure 1. These pilots transition through:

- Trapping suspended fine sediments to enhance vegetation recovery (Pilot Building with Nature Indonesia in Demak, Indonesia)[6];
- Strategic disposal of dredged material to encourage salt marsh or wetland development (Pilot Mud Motor Koehoal salt march development in Harlingen, The Netherlands)[7];
- Construction of natural islands with fine dredge material within sand dikes (Pilot KIMA Marker Wadden, The Netherlands)[8];
- Develop salt marshes at different percentages of sand and mud content and through planting vegetation (Pilot Marconi, The Netherlands)[9];
- Producing clay soil through ripening fine dredge material (Pilot Kleirijperij, The Netherlands)[10].

These pilots cover the full range between: fines in suspension, fluid, consolidated and ripened mud; and between maximizing BwN with very limited human intervention and more involved human activities. These pilots integrate physical understanding of mud dynamics, ecology and vegetation science, innovative operational know-how on handling and constructing with very soft mud, and often complex innovative multi-party and multi-agency public-private-academic collaboration. When the world “tailings” is substituted to the world “mud” in the chapter above, the parallel with oil sands tailings management is apparent. Some of the EcoShape partners actively participate in oil sands research and development and engineering projects. Significant experience, knowledge and tools that are developed in oil sands projects are utilized in the LLM pilots, and vice versa.

In this paper we present in more details those pilots where the correlation between LLM knowledge development and application is mostly intertwined with oil sand applications. These are: 1. Kleirijperij; 2. Marker Wadden; and 3. Marconi. These pilots are all currently in execution with preliminary results fresh of the press. In this paper we present a general introduction to these pilots and the most important results to date. For additional information and background of all pilots, we refer to previous publications (van Eekelen et al. 2017) and to the EcoShape website referenced in the footnotes of each pilot. For a description of the full EcoShape Program and all EcoShape pilots we refer to van Eekelen et al. (2018).

Pilot Kleirijperij

The Pilot Kleirijperij is located at Delfzijl, on the west side of the Eems-Dollard estuary, which borders The Netherlands and Germany. Since a few decades, the turbidity in the Ems River has been increasing due to an increase in suspended sediments concentration (van Maren et al. 2015). This leads to an increase in required maintenance dredging for the harbors in the Ems Estuary, such as Delfzijl. At the same time, the clay that is needed to maintain or strengthen the dikes in the area is bought and brought in from distant locations.

In the pilot Kleirijperij sediment is dredged from the harbor channel of Delfzijl and the nature area Breebaart. It is directly transported on land across the dike and deposited into 24 departments in two locations, covering about 22 ha. The size of the departments varies but is in the order of 100 m x 100 m. The mud is deposited in one or two cycles with a total initial thickens in the order of 1.5 m. There it is allowed to ripen for three years into clay soil. The objective of this pilot is to test different ripening strategies to determine efficient and cost-effective delivering of dike quality clay. Ripening strategies include different thickness, mixing with fresh water, overturning and mixing, and vegetation planting. At its termination in 2021, the pilot will have to deliver 70,000 m^3 of clay for use in a demonstration project of the green dike concept ‘Brede Groene Dijk’ (Van Loon et al. 2015). This dike has a grass-covered embankment with a slope that is less steep than in regular embankments in the Netherlands. If successful, the pilot will be scaled up in the future to extract up

[6] https://www.ecoshape.org/en/projects/building-with-nature-indonesia/
[7] https://www.ecoshape.org/en/projects/mud-motor/
[8] https://www.ecoshape.org/en/projects/marker-wadden/
[9] https://www.ecoshape.org/en/projects/saltmarsh-development-marconi-delfzijl/
[10] https://www.ecoshape.org/en/projects/clay-ripening-pilot-project/

to 1 million cubic meter of dredge material form the Eems-Dollard.

While ripening dredged material or fine tailings is not new, for the first time this pilot aims to produce clay from dredge sediments that meets the requirements for application in Dutch dikes. Simultaneously, this pilot contributes to decreasing the turbidity of the Ems River and improving its water quality. The Kleirijperij pilot represents therefore an attractive win-win opportunity which harnesses BwN processes such as evaporation and consolidation and ripening, to turn excess dredged sediment into a resource, by creating clay soil for dikes.

Dutch legislation requires clay for dikes of a specific class (determined mainly by the Atterberg Limits and water content), a maximum salt and organic content. During ripening, the dredged mud needs to lose water and decrease its salt and organic content. A monitoring program, laboratory test and numerical modeling are associated to this pilot, to predict and continuously verify its performance. In the field, measurements are taken: during deposition; regularly throughout the year; and in detail one per year. During deposition, online measurements were taken for density and general dredge material characterization. During ripening, mud level is regularly measured with settling plates and fiber optic measurements. The latter is an innovative method to monitor mudline and mud density being tested in parallel in the pilot and in the lab. Drainage water is also measured from the sand drains. Each year in September, an extensive field monitoring investigation is carried out, through analysis of in-situ sediment samples. In parallel to the field pilot, settling columns, Seepage Induced Consolidation and permeability tests are carried out in the lab to assess and predict dewatering performance. An extensive literature study to collect pre-existing knowledge was performed before the pilot. Numerical modeling development and specific lab testing are foreseen dedicate to understanding and predicting ripening.

At the time of this paper (summer 2018), deposition is completed in Delfzijl while construction has begun in Breebaart. Deposition in Delfzijl took place in two subsequent events. A first event started on April 5th, 2018 (official opening of the pilot), and a second event in July. The cells were filled with a height of 0.4-1.6 m. The initial density of the dredged material was slightly below

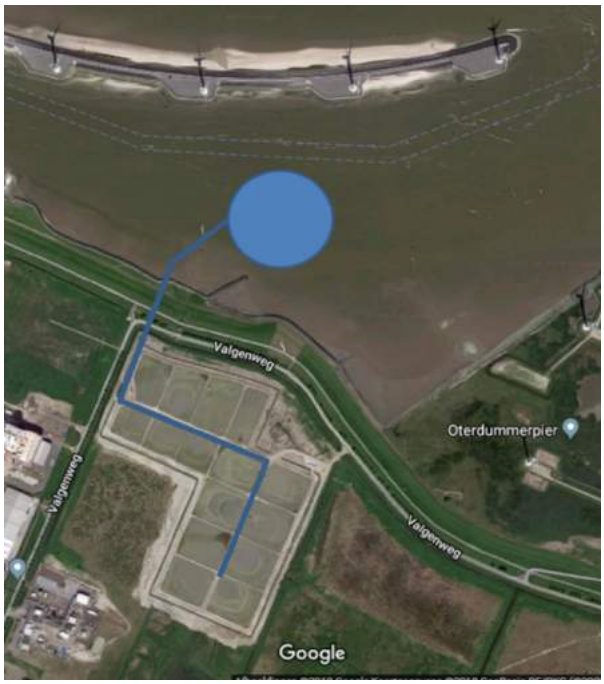

Figure 2. The Kleirijperij site of Delfzijl seen from Google maps about two months after deposition of the first layer. 15 cells are filled with dredged sediment coming from the entrance channel of the Delfzijl harbor (blue circle, approximate location) and transported directly to the cells with a pipeline (blue line)

Figure 3. Image of one cell of the Kleirijperij taken on 16th of August (day 135), therefore about one month after the second layer was deposited. Photo EcoShape

1,200 kg/m^3. The overlying water was drained from the cells about two weeks after deposition. Soon after drainage, a crust formed on top of the deposited mud (Figure 3).

Preliminary measurements indicated dewatering rates in line with theoretical expectations, with faster dewatering rates in thinner deposits and with underlying drain. To facilitate dewatering, the crust was broken mechanically. Under the crust, the mud was still rather fluid, except in the cell with a thickness of deposited mud of 0.4 m, that showed very rapid dewatering. In June 2018 a second layer was deposited.

The Kleirijperij project is a collaboration between EcoShape, the Province of Groningen, the water authority 'Hunze en Aa's', the Delfzijl port authority Groningen Seaports, nature organization Groninger Landschap and the Dutch Ministry of Infrastructure and Water Management. The project partially financed by the Waddenfonds and the Dutch National Flood Protection Program HWBP. This pilot is part of the larger ED2050 program[11], which includes various pilots in the Eems-Dollard region with the same objective of improving the natural and economical value of the Region.

Oil sands experience with atmospheric fines drying was used to develop the filling and monitoring strategy of the pilot. Biological treatment methods will include vegetation and possible worms, techniques that are currently investigated in oil sands research by EcoShape partners Deltares together with Canadian partners (e.g. NAIT). The fiber optic tool is being developed and tested in this pilot to monitor mud – water – air interface and density profile development. This same tools is being considered for installation in oil sands tailings ponds.

Pilot Marker Wadden (KIMA)

Lake Marken in the center of the Netherlands is one of the largest freshwater lakes in Western Europe. Since the lake was artificially closed off from Lake IJssel, its ecological status has deteriorated severely due to a significant increase of the turbidity caused by re-suspension of fines. The nature conservation organization Natuurmonumenten and the Dutch government have joined forces with the ambition of improving the natural habitat in Lake Marken by decreasing suspended fines concentration. A potential strategy includes the excavation of deeper sediment traps that favor natural settling and sedimentation of fine particles and inflow of possible fluid mud. The trapped sediment can be utilized as part of the building material to create an archipelago of marsh islands: the so called Marker Wadden, which is intended to become a "bird paradise". The Marker Wadden intends to demonstrate that fine sediments can be used as a construction material for land reclamation, dike reinforcement and soil improvement. This ambition is in line with the Kleirijperij project described above, and therefore similar to turning FFT deposits into reclaimable landscape.

Figure 4. Aerial view of Marker Wadden under construction, April 2018. To the left of the the island, three smaller cells, where part of the KIMA research program will be executed. Photo by Natuurmonumenten

After the construction of a ten-hectare trial island in 2014, the construction of a 600-hectare island began in 2016. Part of the island is opened for the public in 2018. The development of the Marker Wadden is monitored closely to improve understanding of how to build with mud (in oil sands terms, how to dewater and achieve strength and bearing capacity in fine deposits) as a form of BwN. Enclosed by sandy ridges, fines (clay and silt) sediments are deposited in the Marker Wadden to establish a productive marsh landscape.

The Marker Wadden project includes a construction project and a pilot knowledge development project associated to it. The knowledge development project (Kennis Innovatie programma Marker Wadden, KIMA) is designed to deliver generic as well as directly applicable knowledge to the construction project present and future phases, but without interfering directly with it. Questions are brought from the operational project to the research program and vice-versa knowledge and innovative products are delivered to the project (and to the community), without having the research program to interfere with operational logistics and schedule of construction.

[11] https://www.eemsdollard2050.nl/

KIMA is carried out in collaboration between the operational department of Dutch Ministry for Infrustructure and Water (Rijkswaterstaat), Natuurmonumenten, Deltares and EcoShape, therefore in collaboration between Government, NGO, academia and research, and private partners.

KIMA specifically focus on:

1. Fundamental and applied research, and scaling-up to engineering solutions regarding:
   - Building with mud and sand (physics)
   - Development of ecological systems (ecology)
   - Adaptive Governance (socio-economics)
2. Field monitoring of the Marker Wadden;
3. Knowledge and data management, and dissemination.

Challenges, knowledge and tools developed in the Marker Wadden are potentially similar to those developed in various oil sands applications, especially related to tailings basin closure and reclamation, or in-pit lake management. The same numerical consolidation tool developed and utilized in oil sands tailings consolidation estimates is utilize to predict final topography of the Marker Wadden islands. Similar concepts of dewatering through vegetation studies in the oil sands are also implemented in the Marker Wadden. The KIMA program will offer the opportunity to study the continuous process of (hindered) settling or sedimentation, consolidation and ripening, and to develop and tests numerical tool and monitoring methods to quantify it. This same tool will allow improvement of performance of oil sands consolidation estimates to closure landscape.

Pilot Marconi

The Marconi pilot is located near the Kleirijperij Pilot, therefore along the Eems-Dollard. The Marconi Pilot is also part of the Eems-Dollard 2050 Program. The larger objective of this pilot is to improve the natural and economical value of the water front of the town of Delfzijl. This pilot includes the modification of the waterfront with improving its safety against climate change and sea level rise and at the same time providing areas for recreation and nature development.

EcoShape is responsible for a smaller portion of this project, which focuses on understanding and monitoring optimal conditions for salt marsh development. Different percentage of fine sediment is mixed with sand to provide the substrate for vegetation development. The initially sandy substrate is subdivided in ten different sections (Figure 5). In each section different percentage of fines and sand are mixed (5% - 20% and 50%). In some sections vegetation is planted. For about three years these sections will be monitored to track vegetation development as well as morphological changes. The overall idea of this pilot is to learn how to effectively establish a salt marsh, how vegetation develops in time and the effectiveness of the vegetation to trap sediment and self-sustain itself. The EcoShape part of the project will begin on November 1st, 2018. Therefore there are no data currently available.

Figure 5. Infographic representing the development of salt marshes in front of the Delzijl harbor entrance channel (top), and the design of the Marconi salt marsh with the specific subdivision in different compartments with different fines content to be mixed in sand (5 – 20 – 50%), green represents sections where vegetation will be planted (bottom)

This project may connect with oil sands application as far as opportunity for vegetation establishment in sand / fines substrates, which are typical of sand beaches or sand rich deposits. Vegetation may potentially be implemented also in combination with thin lift, so enhance fines capture and speed up dewatering. Similar concepts are currently under development in The Netherlands to utilize thin lifts to slowly raise dikes, or in USA by the Corps of Engineers to restore wetlands.

CONCLUSIONS

This paper shows that the fundamental underlying physical processes, predicting and monitoring methods behind atmospheric fines drying and making clay soil for dikes from dredge material, predicting and monitoring consolidation in of FT in deep deposits and final settlement of natural sediments in natural islands, or understanding the optimal condition for vegetation growth in tailings and in sand-mud soil are generally similar.

It is unneglectable that oil sand tailings present specific peculiarities especially related to the very poor dewatering likely caused by the clay treated with dispersant additives to facilitate the bitumen extraction process, and to the presence of residual bitumen in the tailings. These are important peculiarities that need to be considered when working in the oil sands and applying methods imported from different regions and environments.

When these peculiarities are considered, the world outside the oil sands offers a vast experience of knowledge and engineering solutions, and opportunities to co-development and co-funding that should be exploited for continuing improving the sustainable management of oil sands tailings and the mining industry in general.

The international experience in dealing with sediment (read also tailings) management is directing further and further toward a nature-based (e.g. BwN), beneficial reuse and circular economy approaches, centered on sustainable development. International collaboration and exchange of knowledge is central to these developments.

The LLM we presented in this paper is developed in this direction. The LLM currently includes five pilots, located in the Netherlands and Indonesia, and it is connected to the most important international programs and initiatives related to sustainable and beneficial sediment management.

Some of the experience, tools and monitoring methods acquired in oil sands research and engineering projects was instrumental in the design and success of these pilots. Therefore numerous pilots carried out by the oil sands industry, mostly under the COSIA umbrella, that connect the four COSIA EPAs (tailings, land, GHG and water), and that are directed in improving the sustainable development of the industry, offer a great opportunity for international collaboration.

Thus, we must close this paper with the ambition and the invitation to add at least a Canadian (oil sands) pilot to our LLM.

REFERENCES

Alberta Energy Regulator. (2017). Directive 85: Fluid Tailings Management for Oil sands Mining Projects. Release Date October 12, 2017.

Brils, J., de Boer, P., Mulder, J. and de Boer E. (2014). Reuse of dredged material as a way to tackle societal challenges. Journal of Soils and Sediments. DOI 10.1007/s11368-014-0918-0.

De Vriend, H. J. and Van Koningsveld, M. (2012). Building with Nature: Thinking, acting and interacting differently. EcoShape, Building with Nature, Dordrecht, the Netherlands.

De Vriend, H. J., Van Koningsveld, M., Aarninkhof, S. G. J., De Vries, M. B. and Baptist, M. J. (2015). Sustainable hydraulic engineering through Building with Nature. Journal of Hydro-environment Research, **9**: 159-171.

EcoShape. (2017). Living Lab for Mud. Infographic flyer produced by EcoShape. https://www.ecoshape.org/uploads/sites/2/2017/10/EcoshapeA3A4-GB-4-4versie1.pdf

Martin, T. E. and Davies, M. P. (2000). Trends in the stewardship of tailings dams. Proceedings of Tailings and Mine Waste ’00, Fort Collins, January, Balkema Publishers, pp.393-407.

van Eekelen, E. M. M., Sittoni, L., van der Goot, F. and Nieboer, H. E. (2018). Building with Nature: More than 10 Years of Pre-competitive Knowledge Development. WODCONXXII, Shanghai, China.

van Eekelen, E. M. M., Sittoni, L., van der Goot, F., Nieboer, H. E., Baptist, M. J., Boer, J. and Tonneijck, F. M. (2017). The Living Lab for Mud: Integrated Sediment Management Based on Building with Nature Concepts. CEDA Dredging Days 2017, Rotterdam, The Netherlands.

van Loon-Steensma, J. M., Schelfhout, H. A., Broekmeyer, M. E. A., Paulissen, M. P. C. P., Oostenbrink, W. T., Smit, C., Cornelius, E-J. and Jolink, E. (2014). Nadere verkenning Groene Dollard Dijk. ISSN 1566-7197.

van Maren, D. S., Van Kessel, T., Cronin, K. and Sittoni, L. (2015). The impact of channel deepening and dredging on estuarine sediment concentration. Continental Shelf Research, **95**: 1-14. 1 March 2015.

Vörösmarty, C. J., Meybeck, M., Fekete, B., Sharma, K., Green, P. and Syvitski, J. P. (2003). Anthropogenic sediment retention: major global impact from registered river impoundments. Global and planetary change, **39**(1): 169-190.

Winterwerp, J. C. and Zheng, B. W. (2013). Man-induced regime shifts in small estuaries - I: theory. Springer-Verlag Berlin Heidelberg. doi: 10.1007/s10236-013-0662-9.

Winterwerp, J. C., Zheng, B. W., van Braeckel, A., van Holland, G. and Kösters, F. (2013). Man-induced regime shifts in small estuaries—II: a comparison of rivers. Springer-Verlag Berlin Heidelberg. doi: 10.1007/s10236-013-0663-8.

A NEW PROTOCOL TO ASSESS THE QUALITY OF TAILINGS FLOCCULATION/COAGULATION: A COLLABORATION TO IMPROVE TAILINGS TREATMENT AT SUNCOR ENERGY

Ardalan Sadighian[1], Adrian Revington[1], Heather Kaminsky[2], Benito Moyls[3], Yunhui Li[2] and Oladipo Omotoso[1]
[1]Suncor Energy Ltd., Calgary, Canada
[2]Northern Alberta Institute of Technology, Edmonton, Canada
[3]Coanda Research & Development, Edmonton, Canada

ABSTRACT

Suncor Energy Ltd. (Suncor), Coanda Research & Development (Coanda) and NAIT Centre for Oil Sands Sustainability (COSS) have worked together over the years on testing and evaluation of new polymeric tailings treatment technologies and processes via a standardized protocol with a clear set of metrics. This standard methodology using a 4-inch cup was developed by Suncor early in the research on flocculation of mature fine tailings (MFT) by adapting a waste water jar tester. This has led to the screening of over 44 different flocculants for use within Tailings Reduction Operations (TRO) by Suncor, of which 4 polymers have passed the evaluation. After passing the 4-inch cup screening a 2-inch diameter pipe loop pilot and field validation at 12-inch diameter scale were performed. The 4-inch cup method was replaced by an automated flocculation method, which was designed by Coanda to increase the repeatability of flocculation and understand the fundamental properties of MFT and polymer mixing. Extensive testing of this "Floccumatic" has demonstrated that the automated flocculation can capture the scaling effects and is sufficient to predict field performance, eliminating the need for the 2-inch trials.

Building on this collaborative success Suncor, Coanda & COSS have worked together to update the 4-inch cup evaluation method to replace it with the floccumatic. This paper outlines the ways that floccumatic screens and evaluates potential chemistries for dewatering applications in oil sands tailings.

INTRODUCTION

TRO was developed as a treatment method for fluid fine tailings by Suncor in 2008. The objective of this technique was to develop a technology that would get to a reclamation ready product within a single season and was a step change from other technologies available at the time as it eliminated the need for large, capital intensive process vessels.

The TRO process has two stages, in the first stage MFT and a polymer are mixed together and the resulting chemical reaction releases water through a flocculation process. In the second stage the flocculated MFT is spread over a beach in a thin lift to evaporate the water that isn't released by the chemical reaction. Once the lift has dried sufficiently an additional lift is placed on top. This is a summer only activity and the rate of dewatering from evaporation varies through the year, the peak is in June-August, May and September have a reduced rate and April and October are the shoulder seasons. The technology has the potential to use freeze thaw in the March or late October time period. The TRO process can be split up into four different processes: In Pond removal, Flocculation and conditioning systems, Depositional Systems and Environmental dewatering (Figure 1).

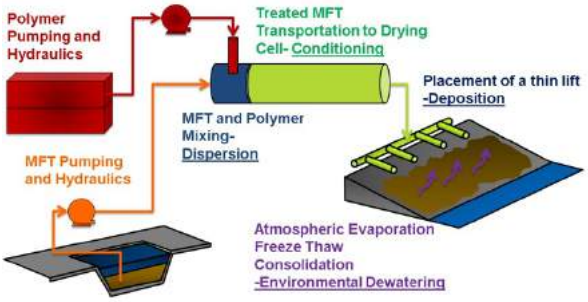

Figure 1. Schematic and Definitions of TRO Technology

TRO SCREENING PROTOCOL

To support the continuous improvement of the TRO technology Suncor developed a screening method

Table 1. 2012 Process for Qualifying Alternative Chemistry

Step	Program	Description
1	Gate 1-Pre-Screening of available chemicals	Suncor Provides MFT information and minimum criteria for dewatering. Vendors conduct pre-screening of their products, and select up to 5 chemicals as the primary candidates.
2	Stage 2-Screening at NAIT	Suncor tests vendor's primary chemical candidates using Suncor's standardized lab techniques. This testing will be conducted by Suncor at NAIT research facilities in Edmonton, and are head-to-head comparison tests with Suncor's current chemical. Vendor representatives are invited to participate. Chemicals which exceed the performance of Suncor's current incumbent may be selected for continued testing at Suncor's discretion.
3	Stage 3A-Testing on Coanda Rig	Suncor tests best chemical from Gate 2 for suitability in pipe reactor at the Coanda facility in Edmonton, AB. At this stage focus will be placed on the chemical's suitability for field operations including effectiveness in pipe reactors, rheology and water release characteristics, beach flow parameters, and drying characteristics. Data from these tests will go towards the design of full scale field trials of select chemicals at Suncor's discretion.
4	Stage 3B-Testing on TRO Test cell	Suncor tests successful chemical in a full scale field trial.

based on basic water treatment techniques and visual assessment, and modified it over time to take advantage of new learnings of process fundamentals understood through Research & Development (R&D). This process was applied to the screening of new polymer chemistries starting in 2012. The screening protocol is as follows.

Overall Chemical Evaluation Program

The chemical evaluation program was run through Suncor's stage/gate evaluation process. In order for a chemical to reach the stage of full field trials, it had to pass through each of the gates outlined in Table 1.

The time frame for a successful chemical to make it through all four steps in this protocol was 18 months, as field trials typically require a winter season to properly design the construct in order to best assure an effective and representative test. The protocol identified four chemicals that have been field tested and tested in the 2" rig at Coanda and represent an improvement on polymer A3338 which was the incumbent superior polymer for six years.

Gate 2 – Screening at NAIT: 4" Cup Technique

The 4" cup technique (Figure 2) was developed by Suncor in 2009; it uses a paddle mixer system that is limited to 320 rpm. This technique named the "fast-slow" technique is a manual technique and requires extensive training in order to obtain comparable results. The technique is named the fast slow as the polymer is injected at 320 rpm until the material looks visibly thick, once this occurs the mixer is turned down to 50 rpm and is stopped when the technician observes water release.

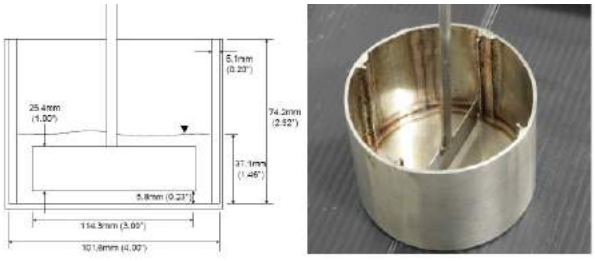

Figure 2. 4" Cup Device

The 4" cup technique has been used to screen and evaluate new potential polymers for TRO application at NAIT COSS. The testing is a five stage process. The current incumbent polymer is tested alongside the new polymers as a bench

mark. All the testing will be carried out in triplicates by 2-3 technicians and in total ~200 flocculation tests will be performed for each new polymer tested.

The five stages are outlined below:
1. MFT characterization and Polymer concentration determination;
2. Chemical reactivity test;
3. Water release potential test;
4. Mixing and conditioning parameter evaluation;
5. Drying test.

Gate 2 – Stage 1 MFT Characterization and Concentrations Determination of Tested Polymer

MFT is characterized on Dean & Stark (D&S) for the composition (Dean and Stark 1920), methylene blue index (MBI) for the clay content (Kaminsky 2014), particle size distribution (PSD) for the fines%, and water chemistry. Process water is characterized for major anions and cations. Typical MFT has a clay to water ratio (CWR) (Equation 1) of ~0.35-0.4 as removed from the pond and during testing MFT will be used as is as well as after dilution. The MFT is diluted using process water to 0.2 and 0.3 CWR. The dynamic yield stress and static yield stress of as received MFT, 0.2 feed CWR sample, and 0.3 feed CWR sample are measured. All the rheograms are expected to fit Bingham model.

Equation 1. Clay to Water Ratio (CWR) Calculation

$$CWR = \frac{wt\%\ clay\ in\ solids \times wt\%\ solids\ in\ MFT}{wt\%\ water\ in\ MFT}$$

The concentrations of the tested polymers are determined by the viscosity properties of the polymer solutions. Each polymer is prepared to the concentrations of 0.1 wt% to 1.0 wt% and tested to determine the consistency index using a rheometer and Power Law Model. Based on past experience provided by Suncor, a consistency index of 1000-1500 cp range is a good match for mixing the polymer into the MFT. Three concentrations of each polymer in this range of consistency index are chosen for further assessment.

Gate 2 – Stage 2 Chemical Reactivity Test

Chemical reactivity testing is conducted on diluted MFT (5 wt% solids) using the cylinder mixing method outlined in Figure 3. The polymer solution is prepared at 0.1 or 0.2 wt% using process water. A 500 mL graduate cylinder with 500 mL of diluted MFT is injected with 0.5-2 mL of polymer solution and inverted 10 times to mix the polymer. The polymer injection and inversion is repeated until a reaction is observed and flocs start forming. If there is no reaction at a flocculant dose > 3000 g/tonne of clays the polymer probably cannot flocculate solids in MFT. Once flocs have formed, the mudline height is recorded as a function of time every 10-30 seconds until there is no change in the interface for a period of 10 minutes. The release water is then separated from the sediment by pouring the water and sediment onto an 18 mesh sieve, followed by 3-hour drainage.

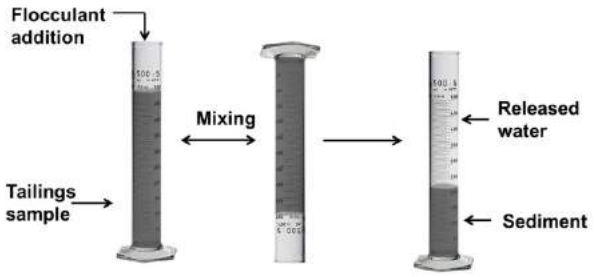

Figure 3. Cylinder Mixing Method for Stage 2 Test

This test uses diluted MFT to determine flocculation potential of the polymer on the specific minerals involved. The key performance indicators (KPIs) are settling rate and volume of supernatant released. In order to pass this stage these KPIs need to be of the same order of magnitude as the reference polymer, and the clarity of the release water must meet or exceed that from reference polymer for the same test.

Gate 2 – Stage 3 Water Release Potential at High Slurry Density

In this stage the polymer is injected as a titration method (Figure 4). Each feed CWR tailings (0.4, 0.3 and 0.2) are tested by three concentrations of polymer determined in Stage 1. During the flocculation test, 1-3 mL of polymer solution is added into the tailings at high mixing speed (~200-320 rpm), the mixer cycled down between 0 and high rpm in a pulse-like fashion. The process is repeated until all of the 1-3 mL of polymer solution is mixed into the MFT. If no water release is observed, another 1-3 mL of polymer solution is added and the pulse fashion mixing is repeated until water release is observed. Alternatively expert technicians can set the rpm at 320 rpm and inject

slowly and consistently to get the same results. The flocculated tailings are then placed on an 18 mesh sieve for 24 hours to drain for measurement of the net water release (NWR). The percentage of 24-hr NWR is calculated based on Equation 2. The solids% in the flocs after 24-hr draining is measured and the CWR is calculated – with the assumption that there is no preferential segregation of the clays.

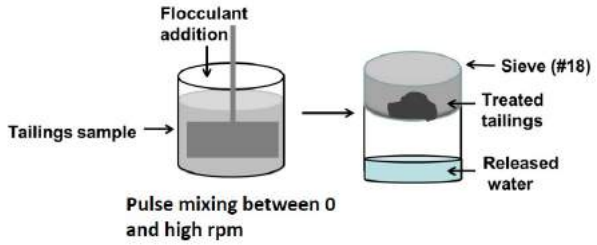

Figure 4. Stage 3 Titration Method of Polymer Addition using Pulse Mixing

Equation 2. Volumetric 24-hr NWR calculation

$$NWR = \frac{(volume\ of\ released\ water - volume\ of\ polymer\ solution)}{volume\ of\ water\ in\ MFT} \times 100$$

This stage is to determine whether the polymer can produce dewatering when treating MFT with high density. The KPIs in this step are that the NWR at each feed CWR tailings meets or exceeds NWR from properly dosed reference polymer. The optimal concentration of the tested polymer for each feed CWR (0.2, 0.3 and 0.4) tailings and the approximate dosage of the polymer will be determined and used for further assessment.

Gate 2 – Stage 4 Mixing and Conditioning Parameter Evaluation

This stage determines the polymer's sensitivity to dispersal and shear conditioning, utilizing NWR and CWR in flocs as key parameters. Each feed CWR tailings (0.4, 0.3 and 0.2) are flocculated by the concentration of polymer determined in Stage 3. In stage 4, two steps are carried out to evaluate mixing and conditioning parameters. (1) NWR conditioning test: a single shot injection of polymer is performed from an under-dosed condition (less water release) to an optimal dosed condition (maximum water release) and then to over dosed condition (less water release). (2) Rheology conditioning test: the optimal dose from step 1 is taken and the yield stress is measured at set mixing time internals.

Step 1: NWR conditioning test. NWR conditioning test is also called the "fast slow". The polymer is added at once in one shot while the tailings are mixed at high speed as presented in Figure 5. Once the entire polymer is dispersed homogeneously in the tailings, the speed is lowered to low speed. The mixture is mixed at low rpm until flocs are formed and water release is observed. The high and low mixing speeds for different feed CWR tailings may vary, Table 2 gives a typical example. The speed is chosen to avoid over and under shearing during the flocculation process.

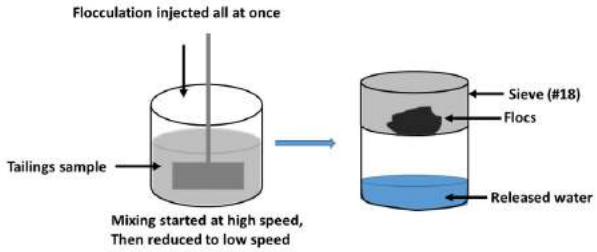

Figure 5. Stage 4 One Shot Injection Method of Polymer Addition

Table 2. The High and Low Speeds for Different Feed CWR Tailings

	Feed CWR Tailings		
	0.2	**0.3**	**0.4**
High mixing speed (rpm)	200	300	320
Low mixing speed (rpm)	20	30	50

The tests use the best NWR dosage and polymer concentration from Stage 3 as a dosing starting point and then increase and/or decrease the dose to determine the best working dosage range for the polymer. Typically the dosage increase/decrease from Stage 3 test is by 100-200 g/tonne on a clay basis. Typically at least 5 tests are carried out: two with under-dose, two with overdose, and one with optimal dose. Additional higher or lower doses are added if the expected pattern NWR is not observed (lower at under-dose, peak at optimal dose, and lower at overdose). The expected dosing curve is shown in Figure 6. The dose results in this step are a reasonable indicator of the dosage requirements in the field.

The KPIs in this step are the NWR and CWR in flocs after 24 hours draining meeting and exceeding those from properly dosed reference polymer at tested feed CWR tailings.

Step 2: Rheology conditioning test. The optimal dose in step 1 is used for the one shot Rheology test. The optimal dosage of the polymer solution is

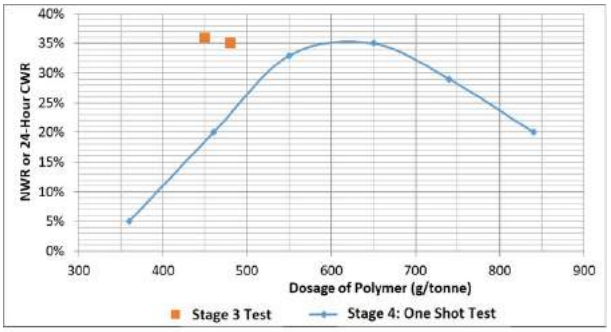

Figure 6. Expected Data Output (Dosing Curve) from One Shot Test

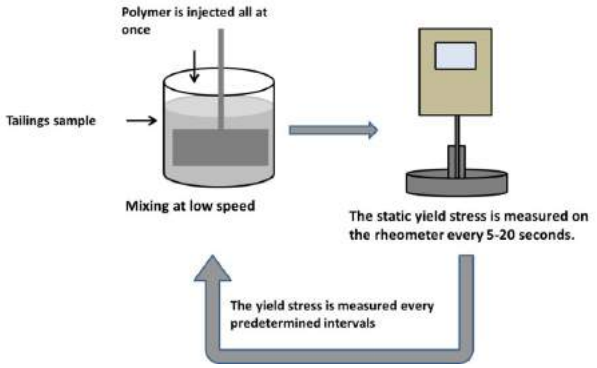

Figure 7. Stage 4 One Shot Rheology Test

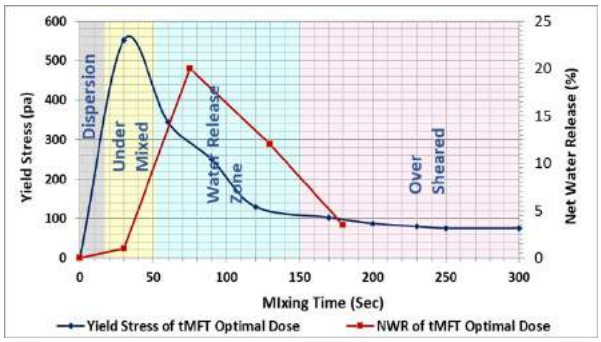

Figure 8. Expected Output from Stage 4 One Shot Rheology Test

injected into the MFT at high mixing speed. Mixing is stopped once a gel-like MFT is observed and the static yield stress is then measured using a Brookfield DVIII HB Rheometer. The sample is mixed at low mixing speed for a certain time (5-20 seconds) before stopping the mixer. Then treated tailings are carefully transferred into a 250 mL glass beaker and the yield stress measurement is repeated. The treated tailings are then transferred back to the mixing vessel and mixed again. The process of mixing at low mixing speed and yield stress measurement is repeated until there is no flocs structure visually observable, the sample resembles non-flocculated tailings, and the static yield stress values do not change with mixing. The water release is observed visually and recorded for each repetition cycle. The high and low mixing speeds used in this step are consistent with the step 1 NWR conditioning test. The procedure of rheology condition testing is illustrated in Figure 7. The expected output from the stage 4 rheology conditioning test is presented in Figure 8.

The reason for performing the rheology test is to identify how the polymer reacts with the MFT. The rheological evolution of flocculated thick fine tailings includes four zones: (1) a dispersion zone where a flocculant is well dispersed into the MFT; (2) floc build up/under mixed zone where the yield stress increases and reaches a peak; (3) floc break down/water release zone where the yield stress decreases and water is released from the flocculated materials; (4) over sheared zone where the flocs are totally broken down to a similar state to the initial MFT. In the earlier test the technician is looking for the water release zone only, while this test is to attempt to determine if the polymer will work in a TRO system, i.e. will the yield stress be the same (impact on pump sizing) and will the point of water release be the same (impact on pipe length setup after the injector) (Revington 2016). Camp numbers for the pipe model are calculated by multiplying the average shear rate G against mixing time Δt, according to Equation 3.

Equation 3. Equation Developed for Camp Number

$$Camp\ Number = G\Delta t$$

G = average shear rate, and Δt = mixing time

To demonstrate the premise that Camp Number can be applied to treated tailings material once the polymer has been adequately dispersed and remains homogeneous, one would expect the yield stress breakdown for post dispersion mixing at low mixing speed to only differ by a factor of mixing time when a high speed mixing is applied. This is important because in this test the mixing rpm may vary depending the technician's ability to spot the water release zone. In order to compare different CWR MFTs the same data can be converted to a ratio of reduced versus initial yield stress ratio (Equation 4).

Equation 4. Yield Stress Ratio Equation Which Allows Yield Stress to Be Compared Non-dimensionally

$$Yield\ Stress\ Ratio\ = \frac{Measured\ Yield\ Strength\ (Pa)}{Peak\ Yield\ Strength\ (Pa)}$$

The rheology test determines the polymer's sensitivity to the shear conditioning utilizing the strength of the flocs as a key parameter. For these tests the polymers are evaluated to determine if (1) the product achieves peak yield stress in the same or shorter time than the reference polymer; (2) the time/energy range of optimal flocculation is at or wider than the reference polymer; and (3) the yield stress values at dewatering onset and breakdown are at or below the yield stress for the reference polymer.

Gate 2 – Stage 5 Drying test and strength gain

In the drying test (Figure 9), the optimal dosage achieved in NWR conditioning test is used to flocculate enough tailings, using the one-shot test, to fill the drying vessel (Sieve #18). The vessel is not covered and the loss of water to drainage and evaporation is measured over time after every 24 hours until the sample reaches equilibrium moisture content. The static yield stress is also measured each day.

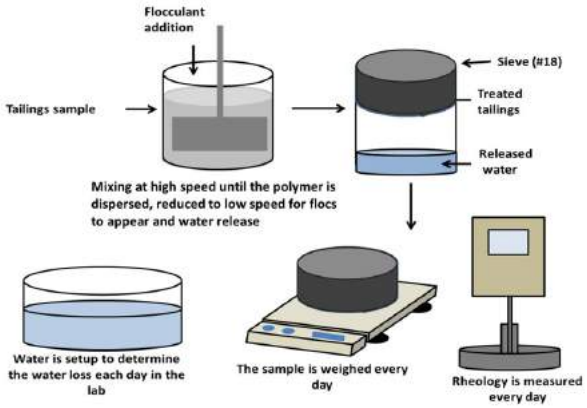

Figure 9. Stage 4 Drying Test

Two pans of water are also setup next to the samples, as shown in Figure 10, to aid in the determination of the wt% solids gain at 100% of potential evaporation and to compare actual evaporation (AE) to potential evaporation (PE). AE is the mL of water being released from the drying treated MFT. PE is the mL of water released from the water pan with the same area of sample.

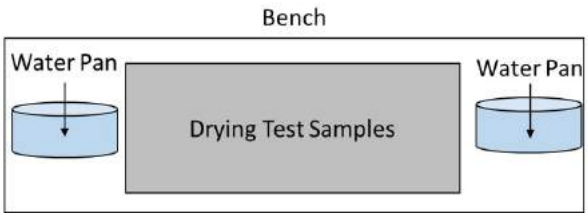

Figure 10. Drying Test Samples and Two Pans of Water Setup

A non-dimensionalized drying curve is generated in order to compare samples since the water evaporation for each sample would be different due to the location in the lab. For example, Figure 11 shows that polymer C dried the fasted throughout the drying test, followed by polymer B. The non-dimensionalized drying curves (Figure 12), however, show that all the polymer-treated MFT dried at similar rates. The different drying rates are likely due to the different locations on the bench resulting in different water evaporation rates. The KPI of the drying test is that the tested polymer-treated tailings dry at or faster than the reference polymer and the strength gain is at or greater than 5 KPa at 75% solids by weight (Based on directive 74 target).

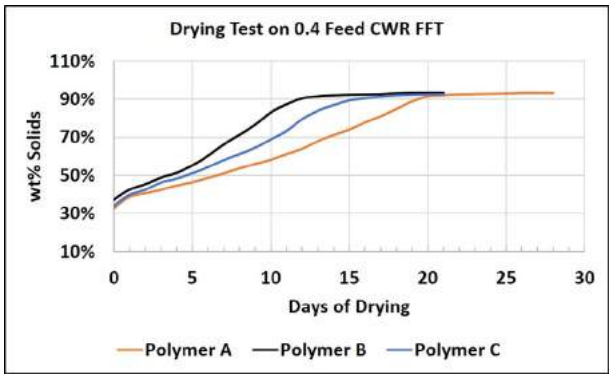

Figure 11. Drying curves of polymer treatment on 0.4 feed CWR MFT

Polymer evaluation criteria. A 5-point scale is used for polymer evaluation as shown in Table 3. The total score of the tested polymer will be compared with the reference polymer and used to determine whether the new polymer will be evaluated using a 2" line lab pilot at Coanda.

Table 3. The Criteria of 5-Point Scale for Polymer Evaluation

Chemical	Water Quality		Stage 3 24-hr CWR		Stage 4 24-hr CWR		Stage 4 24-hr Dose	
	Specification	Score	Specification	Score	Specification	Score	Specification	Score
Incumbent	Incumbent	1	Incumbent	1	Incumbent	1	Incumbent	1
Tested Polymer	Clarity is ≥ incumbent +/- 2	1	CWR is incumbent +/- 0.02	1	CWR is incumbent +/- 0.02	1	dosage is incumbent +/- 100 ppm	1
	Clarity is < incumbent-2	0.5	CWR >0.5	0.5	CWR is > incumbent +0.02	2	dosage is <1700 ppm and CWR >0.5	0.5
	Clarity is <4	0	CWR <0.5	0	CWR >0.55	0.5	dosage is >1700 ppm	0
					CWR <0.55	0		

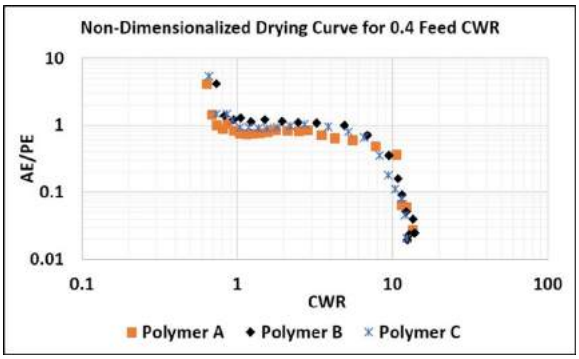

Figure 12. Non-dimensionalized drying curves of polymer treatment on 0.4 feed CWR MFT

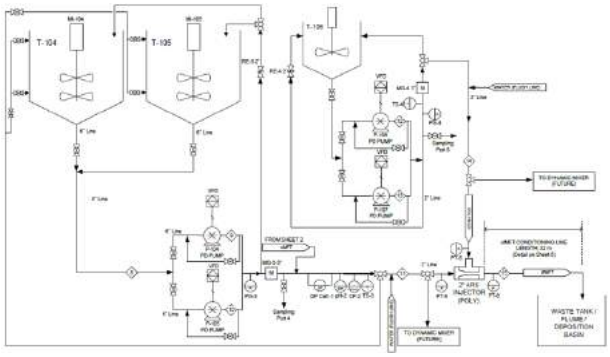

Figure 13. Schematic of In-Line Injection Apparatus (prep system and entire pipeline not shown)

Gate 3A – Testing at Coanda: 2" In-line Lab Pilot

A semi-continuous in-line injection apparatus was first constructed for flocculation testing in 2007 and has since been upgraded to accommodate higher throughput and pressure as well as multiple chemical addition. A basic rig schematic is shown in Figure 13. The rig includes slurry prep and feed systems, two chemical additive prep and feed systems (ie: polymer flocculant and/or coagulant), lab-scale TRO-style static injectors, suitable piping for injecting testing up to delivery pressures of 350 psig at total flows reaching 1500 lpm, with the discharge into a deposition basin or flume. This setup is configurable to enable semi-continuous injection of polymer into MFT flowing through a 2" or 4" test section, with all process streams being independently controlled and metered using a dedicated DAQ and control system. The pipeline downstream of the static injector is equipped with various on-line monitoring instrumentation such as flow meters, static and differential pressure transducers, as well as pH and conductivity sensors.

Unlike an impeller system, where mixing is due to turbulence generated by the impeller, in-line mixing is largely driven by turbulence generated from the bulk MFT flow – often characterized by the dimensionless Reynolds number. As the MFT flow varies, so does the mixing performance of polymer into MFT. In order to quantify this variation across the expected TOE, polymer dosage sweep experiments are run in the 2" line at select low, mid-range and high MFT flow rates for each polymer. Experiments are executed in a sequential manner in order to minimize MFT consumption, often starting at the lowest dosing condition and monotonically increasing as per the experiment specifications. For one polymer screening experimental series (3-5 dosage sweep tests), timeframes are in the order of 1-2 weeks.

The following outlines the typical steps of an in-line flocculation dosage sweep test:

1. Pump MFT through a 0.25” filter to remove debris and into the MFT prep system.
2. If required, dilute MFT to the desired CWR using PEW. Once adequately homogenized in the prep system tanks, the target CWR is checked by measuring the diluted MFT’s moisture content and the undiluted MFT BMW and MBI data already inhand, assuming no clay segregation occurred during the process thus far.
3. Once the desired CWR has been achieved, MFT is transferred from the prep system to the feed system tanks.
4. The flocculation test begins with the MFT and polymer being injected into the pipeline through a Suncor AR5 static injector at predetermined set points to achieve appropriate mixing and dosing conditions.
5. Once both MFT and polymer flows are stable, and once a complete pipeline retention time has elapsed, sampling of flocculated MFT (fMFT) begins along the pipeline downstream of the static injector.
6. Once sampling has completed, the polymer flow is adjusted to obtain the next desired dosing condition. Upon system stabilization, sampling along the pipeline commences again, and the process is repeated until all polymer dosages have been tested.

Figure 14 shows 24-hour CWR and CST results from all pipeline samples of a 2” in-line dosage sweep, obtained from a NWR procedure. These, along with rheological and on-line pressure measurements are used to further evaluate incumbent polymers and aid in the prediction of a polymer’s performance across the various stages of the flocculation process (dispersion, undermixed, water release and over sheared). Due to uncertainties in both scale up from batch impeller driven mixing systems used in initial chemical screening, and the often variability inherent in field-scale testing, results from in-line tests are utilized to finalize a polymer selection prior to field-scale testing.

Ultimately, the chemical screening protocol at bench-scale will be developed sufficiently to reduce the reliance on lab-scale in-line testing and allow a more streamline evaluation process that utilizes fewer material and calendar days to complete.

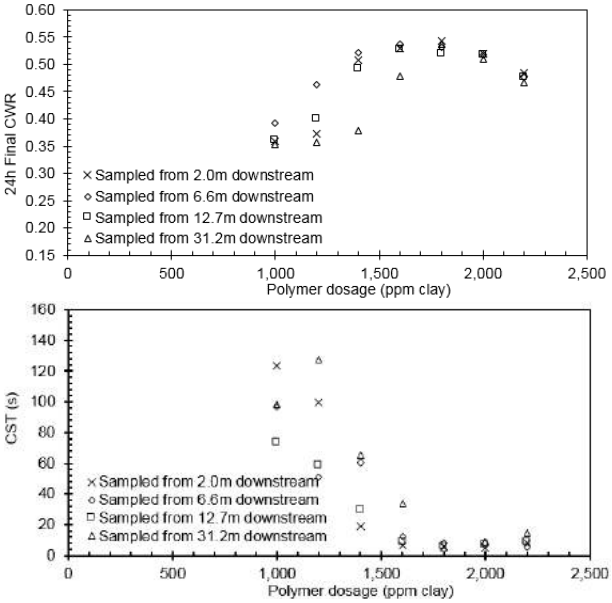

Figure 14. 0.3 CWR MFT flocculation performance at different polymer dosages

IMPROVEMENTS TO SCREENING PROTOCOL

Lab Scale Dewatering Tests Evaluation

The 4” cup technique uses an 18 mesh sieve to measure the 24-hr NWR, and takes another ~12 hours to measure the solids content in the flocs by heating at an oven. The 18 mesh sieve works well only for large flocs. Polymers producing small flocs provide poor results as the flocs pass through the sieve along with the water. The sieves with smaller pore size are not able to drain the released water effectively due to the water tension. Since the dewatering degree is a major KPI, this issue puts chemicals with a smaller floc size at a significant disadvantage which may not be justified by field performance. Additionally, the net water release method hadn’t been critically examined to evaluate its sensitivity and reproducibility. Therefore, several methods of evaluating dewatering were tested at NAIT COSS: these included NWR, settling, capillary suction time (CST), and specific resistance to filtration (SRF).

Settling Test. Since settling tests are a common way to evaluate dewatering, the applicability of this method to TRO style flocculation was evaluated. Pouring polymer-flocculated MFT into different containers and recording the mudline height at

several points for the first day and once per day for 7 days. After 7 days settling, the total amount of released water and the solids content of the flocs were measured. 250 mL, 500 mL and 1000 mL graduated cylinders were tested along with 500 mL beakers. It was found that the large flocs hampered settling in the graduated cylinders due to wall effects, while the large surface area of the glass beaker resulted in uneven solid surface, so it was not able to measure the mudline height accurately. In addition, Water was trapped in the flocs, so the final solids content in the flocs were not repeatable. Therefore, this method of settling tests is not recommended for the polymer screening of thick slurries which form large flocs.

CST Test. The CST is derived from the time taken to draw a known volume of filtrate from suspension by the capillary suction pressure generated from standard CST filter paper. CST test is simple and inexpensive, since it does not require an external source of pressure or suction. CST is designed to test homogenous and well mixed slurry samples. Results on inhomogeneous materials vary depending on the subsampling to the CST cell and are not reproducible by different operators. Suncor had used CST technique to study the flocculated oil sand fine tailings. For flocculated MFT showing large flocs it is recommended to use only release water for CST testing, rather than flocs or the mixture of flocculated materials. For material with small flocs the full flocculated sample can be used. Figure 15 shows the CST tests tried on three types of A3338-flocculated materials at the optimal dosage: (1) the flocculated materials were kept in 4" cup for 20 min to allow the water release and then the mixture of flocs and water (mostly flocs) were subsampled into the CST cell for testing; (2) the flocculated materials were kept in the 4" cup for 60 minutes to allow the water release, followed by pouring onto an 18 mesh sieve for 1 min to collect the release water and (3) flocs. It was found that the CST values on the released water only were most repeatable (narrower error bar) compared to the testing on flocs only and mixture of flocs and released water.

The CST dosage curve (Figure 16) of testing on released water obtained from A3338-flocculated MFT was normalized according to Equation 5. The normalized 24-hr CWR in flocs were also plotted for comparison. The dosage curve from the CST results were consistent with the 24-hr NWR dosage curve. Both CST and 24-hr NWR results are able to provide the optimal dosage range of the testing polymer.

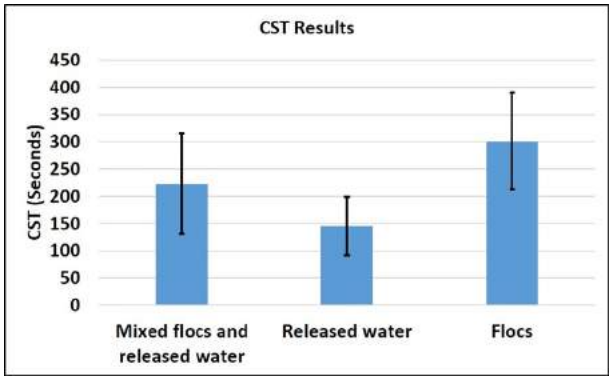

Figure 15. CST Results on A3338-Treated MFT at Optimal Dosage: Mixture of Flocs and Released Water, Released Water only, and Flocs only. Error Bar: Standard Deviation

More investigation on CST test is required to rate one polymer against another.

The CST dosage curve (Figure 16) of testing on released water obtained from A3338-flocculated MFT was normalized according to Equation 5. The normalized 24-hr CWR in flocs were also plotted for comparison. The dosage curve from the CST results were consistent with the 24-hr NWR dosage curve. Both CST and 24-hr NWR results are able to provide the optimal dosage range of the testing polymer. More investigation on CST test is required to rate one polymer against another.

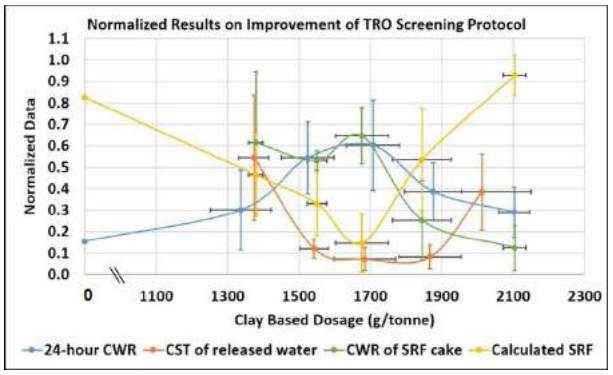

Figure 16. Normalized results of 24-hr NWR, CST, and SRF testing on A3338-Treated MFT. Error Bar: Standard Deviation

Equation 5. Calculation of Normalized Value

$$Normalized\ Value = \frac{current\ value - Minimum\ value}{Maximum\ value - Minimum\ value}$$

SRF Test. It is a standard test used primarily to assess the filtration resistance drilling muds. This test has also been used to screen the filtration performance of tailings for the potential application to pressure filtration. NAIT used a modified SRF setup by inserting a piston cylinder in between the gas and the sample (Li et al. 2018). This allows the same gas pressure to be applied to the sample but removes the limitation on dewatering time due to cracking which usually happens during the SRF test.

Figure 16 shows the normalized SRF results of A3338-treated MFT. The MFT samples were flocculated by polymer A3338 using the one-shot testing method and the flocculated samples were kept in the 4" cup for 60 minutes to allow the water release, followed by a 60-minute filter press under 100 psi. With 60 minutes filter press, the solids contents/CWRs in the filtration cakes are comparable with those in the flocs obtained by 24-hr NWR method. The SRF results on a dosage curve were consistent with the 24-hr NWR results. The calculated SRF values were able to differentiate the optimal dosage from under dose and overdose.

In all, both CST and SRF methods can be used in the TRO polymer screening, but CST testing on the released water of flocculated tailings is recommended to replace the 24-hr NWR method for screening dosage sweep tests due to its fast, inexpensive, and repeatable technique. SRF testing is recommended to compare total water release between polymers – especially where their floc size may vary significantly. However, one should note that CST is inherently less reliable and should only be used as initial screening tool.

Floccumatic

To automate the mixing method developed with the 4" cup and increase the screening protocol's robustness a new proprietary semi-automated mixing device termed the Floccumatic was developed. The device consists of an engineered flocculation vessel, computer controlled chemical injection system and an overhead mixer stand assembly capable of monitoring the torque exerted on the impeller shaft over the course of a flocculation test. Figure 17 shows the Alpha version of the Floccumatic mixing device.

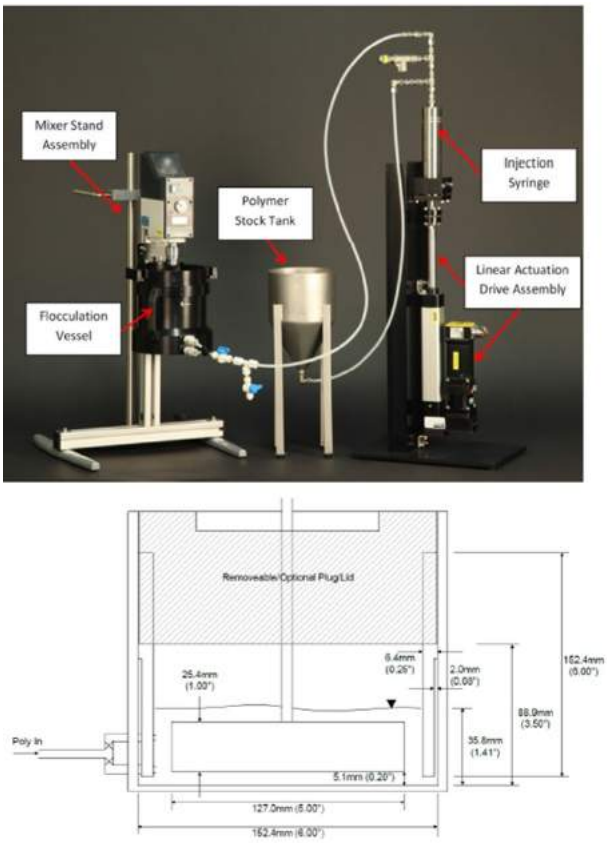

Figure 17. Version 1 (Alpha) Floccumatic Device

By monitoring the impeller shaft torque over time ('torque trace'), the various stages of the flocculation process (dispersion, undermixed, water release and over sheared) can be precisely monitored and identified in real-time – refer to Figure 19. The engineered flocculation vessel along with the controlled mixer and injection system increase testing repeatability through reduction of operator variability, reducing the need for a significant amounts of replicate tests. Impeller rpm and polymer injector conditions are often specifically manipulated to isolate mixing conditions of interest to aid in the evaluation of polymers for MFT flocculation and translation of bench-scale results to an in-line system.

While using the Floccumatic apparatus, the following procedure is typically followed:

1. Weigh the pre-determined amount of MFT into the flocculation cup so that 650 ml of MFT is in the cup based on the MFT's density
2. Install the flocculation vessel onto the mixer assembly and pre-shear the MFT for 1 minute at 600 rpm to remove thixotropic effects that may

be present due to the handling of the MFT sample prior to testing.

3. Once the minute of pre-shearing is completed, the mixer speed is adjusted to the target rpm for the test (300 rpm typical) and then polymer solution is injected into the vessel at a predetermined rate (50 ml/s typical).
4. The mixer stopping time varies between tests and is dictated by the progression of the mixing/chemical reaction between the polymer and MFT. In polymer dosage sweep tests, the stopping time is determined to be the point at which rapid water release occurs for a given sample. This is identified by monitoring the materials' thickness over the flocculation test through the torque imparted on the impeller shaft. Once the peak or max torque is reached, the operator continues to mix the material until the torque has reduced by approximately ~ 30-50% the peak value. For mixing time series tests, similar to those previously described for the 4" cup method, the mixing time is varied to capture data in each of the mixing zones (polymer dispersion, under mixed, water release, over sheared).
5. At the end of a flocculation test, the material is transferred to a sieve for NWR processing while a small amount is used for CST. If performing a mixing time series test, another sub-sample of material is utilized to measure static and Bingham rheology parameters for each mixing zone – this data is then used to populate a pipe model for assessing pipeline pressure drop and dewatering, while also outputting input parameters for subsequent beach-flow cell utilization estimates.

Figure 18 shows typical 24-hour CWR and static yield for a mixing time series test, while Figure 19 shows the torque trace corresponding to the ~ 22 second sample from Figure 18 – stopping times for the 22 second test and others are identified using a black star.

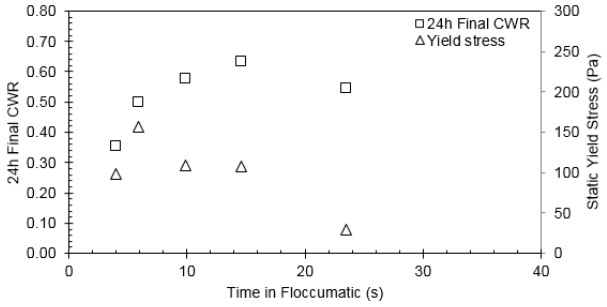

Figure 18. 0.3 CWR MFT Floccumatic dosage sweep performance data

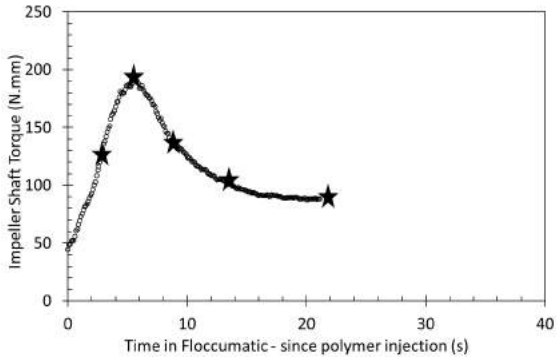

Figure 19. 0.3 CWR MFT Floccumatic mixing series torque trace from 22 sec test in Figure 18

CONCLUSION AND FUTURE WORK

Chemical screening is somewhat cumbersome, expensive and long in duration. The shortest development time from the laboratory to field test is 18 months. There are a large number of chemicals proposed by various vendors for tailings treatment, and it would be advantageous to revamp the current process and create a more efficient and streamlined screening protocol. The present work focus on fundamentals required for such protocol and will result in a new and improved chemical screening protocol for Suncor in 2019.

REFERENCES

Allen, E. (2008). Process water treatment in Canada's oil sands industry: I. Target pollutants and treatment objectives. Journal of Environmental Science, **7**: 123-138.

Beier, N. and Sego, D. (2008). Dewatering of Oil Sands Tailings Using Cross Flow Filtration. 61st Canadian Geotechnical Conference and 9th joint IAH-CNC Groundwater Specialty Conference, Edmonton, Alberta, September 22-24, pp 8.

Dean, E. W. and Stark, D. D. (1920). A convenient method for the determination of water in petroleum and other organic emulsions. Ind. Eng. Chem., **12**: 486-490.

Kaminsky, H. (2014). Demystifying the methylene blue index. International Oil Sands Tailings Conference, Banff, Alberta, Canada.

Li, Y., Kaminsky, H., Romaniak, N. and Tate, M. (2018). Filter Press Modification to Assess Dewatering Performance of Fluid Fine Tailings. International Oil Sands Tailings Conference. Edmonton, AB, Canada.

Revington, A. (2016). Screening of Alternative Chemicals for Application in MFT Drying. Suncor Internal Report.

CONVERTING RENDERING WASTE TO VALUE-ADDED PRODUCTS FOR OIL SANDS TAILINGS TREATMENT

Heather Kaminsky[1], Yuki Gong[1], Paolo Mussone[1],
Birendra Adhikari[2], Jesse Yuzik[2], Mike Chae[2] and David Bressler[2]
[1]Northern Alberta Institute of Technology, Edmonton, Canada
[2]University of Alberta, Edmonton, Canada

ABSTRACT

Every year, more than 300,000 metric tonnes of waste bovine material from the rendering industry are landfilled or incinerated. Recent experimentation has proven that aqueous thermal hydrolysis is an effective method to eliminate any potential risks to human health associated with these materials while simultaneously generating peptide building-blocks that can be converted to higher value materials for industrial applications. This paper assesses the performance of the developed polymers to date for dewatering of kaolinite and fluid fine tailings, starting with the unrefined peptides and moving to chemically-modified derivatives that possess enhanced flocculation qualities. This work is the result of a collaboration between two NAIT applied research centers and the Bressler lab at the University of Alberta. The work aims to develop and validate cost effective biodegradable additives that can provide similar initial dewatering capabilities as the incumbent polymer flocculants. The bio-based flocculants studies in this work can also serve as a potential nutrient source for vegetation, which could better enable the use of vegetation as a secondary dewatering technique.

INTRODUCTION

Oil sands extraction in Alberta employs the Clark Hot Water Extraction process (CHWE), which produces fine fluid tailings (FFT) at a rate of 0.1 m3 per tonne of processed sand. These tailings are stored in large ponds, and covered an area of about 77 square kilometers by 2013. The CHWE process relies on both the dilution of the ore and elevation of the pH to promote bitumen recovery and decrease slurry viscosity; however, this processing results in fine tailings that have poor settling and consolidation behavior (Mikula et al. 1996). There are currently 1,100 Mm3 of fluid fine tailings stored in tailings ponds (Alberta Energy Regulator 2016). This fluid inventory poses significant risks as the fluid is primarily stored behind man made dykes which have the potential for failure and have been recognized as a global concern (UN Environment 2017). Government regulations, such as the Alberta Energy Regulator's Directive 085 (Alberta Energy Regulator 2017) outline requirements for tailings ponds closure, which put significant business pressure on oil sands mine operators. As a result, oil sands companies and their suppliers are continually looking for improvements in tailings technology. The goals of these technologies are to treat the tailings such that they can be placed in their final location in the closure landscape on a trajectory towards reclamation (Alberta Energy Regulator 2017).

All of the oil sands operators currently use polymer flocculants to treat at least a portion of their tailings. The polymer treatments are effective at rapidly increasing the sediment solids content to ~50 wt% from ~30 wt%. This allows the release of supernatant containing <0.5 wt% total suspended solids which can be recycled back through the extraction process thus reducing the need for fresh water. The treated sediments are then placed in deposits and allowed to consolidate or dry depending on the treatment plan. While the current treatments can be considered "ready to reclaim" the time frame for reclamation of these treated sediments is on the order of decades to centuries.

One option being investigated for potentially significantly increasing the speed of reclamation is to use biodegradable polymers which could provide a source of nutrients to plants and microbes native to the boreal ecosystem. If the polymers can provide the same initial water release benefits while subsequently providing a nutrient source, they could be used in combination with native vegetation to significantly increase the speed of dewatering and the progression towards final reclamation.

The Canadian Food Inspection Agency (CFIA) defines Specified Risk Materials (SRM) as "the skull, brain, trigeminal ganglia (nerves attached to the brain), eyes, tonsils, spinal cord and dorsal root ganglia (nerves attached to the spinal cord) of cattle aged 30 months or older; and the distal ileum (portion of the small intestine) of cattle of all ages." There are presently four approved disposal methods for these materials, including incineration, landfilling, and alkaline or thermal hydrolysis. The latter option has been identified over the last decade as a possible processing pathway to simultaneously eliminate the risk of prion contamination in the environment and generate higher value materials for industrial application from recovered protein.

EXPERIMENTAL CONDITIONS

SRM Hydrolysis

A thermal hydrolysis protocol (180^{0}C, ≥1200 kPa, ≥40 mins in an enclosed pressure vessel) developed by Bressler lab at the University of Alberta and approved by CFIA was used for hydrolysis of SRM. Recovery of hydrolyzed protein (peptides) from the hydrolysate consisted of extraction with water followed by centrifugation, filtration, washing with hexane, and freeze or spray drying of the aqueous hydrolysate; which is a typical protein recovery protocol being practiced in Bressler lab. The process of centrifugation and filtration removes the insoluble materials (mostly bones), and hexane washing removes any residual lipid and/or long chain fatty acids produced as a result of lipid hydrolysis. In this study, however, two samples of SRM peptides were provided to the Centre for Oil Sands Sustainability (COSS) laboratory: one before lipid removal omitting the hexane washing step (Defined as Crude SRM peptides) and one after lipid removal by hexane washing (Defined as Pure SRM peptides). The purpose of using the crude peptides is to investigate if the hexane washing step can be omitted for this target application, thus making the peptides recovery process more benign. The protein content of crude peptides was identified as 89% and the protein content of the purified peptides was identified as 91%. The material received by COSS was stored in the freezer between uses to avoid degradation with time.

Synthetic Process Water

Synthetic process water was created to mimic the dispersing water chemistry present in oil sands ores. This water was used to create artificial tailings with kaolinite as well as to dilute the fluid fine tailings. 180L of process water was created to ensure sufficient process water for all of the required tests.

The synthetic process water consisted of the salts dissolved in distilled water as shown in Table 1. To facilitate dissolution, the salts were dissolved in a small quantity of water first and then added to the remaining distilled water. Sodium bicarbonate was dissolved separately from the other salts and was added to the water first.

Table 1. Synthetic process water recipe

Salt	Mass added to 180L (g)
CaCl2.2H2O	9.9
MgCl2.6H2O	15.1
KCl	5.1
NaCl	98.1
NaHCO3	161.1
Na2SO4	79.8

The solution pH was adjusted prior to use via dropwise addition of 10 wt% hydrochloric acid or 10 wt% sodium hydroxide until the desired pH was achieved when measured with a pH meter. Due to the buffering capacity of the process water, the pH was adjusted on the morning of the tests rather than in advance. Finally, gypsum (0.75g into 2.4L of process water) was added to the pH adjusted water prior to mixing with the kaolin substrate. Initial screening work was conducted on at pH 5, 6, 7, 8 and 9. Based on the initial screening work, three target pH's were used for the bulk of the testing: 8, 8.5 and 9. These pH's were selected as representing not only a typical range for oil sands tailings but also the range where the kaolinite substrate had the slowest settling rate and therefore the most need of an additive.

Kaolinite clay - Polygloss 90 manufactured by Kamin LLC was selected as the primary test substrate. This material has a relatively high specific surface area for kaolinite at 22 m^2/g and therefore is one of the commercial products most similar to oil sands kaolinite. The kaolinite was mixed with process water to create a 4%

weight/weight slurry. The slurry was allowed to mix for 30 minutes and hydrate for an hour before use.

In addition, a single fluid fine tailings (FFT) sample was selected to check if the results of the kaolinite were repeatable on a true tailings sample.

The FFT were tested using Dean and Stark analysis (D&S) (Dean & Stark 1920) to determine the bitumen, solids and water content of the FFT. The dean stark extracted solids from the FFT and the as received polygloss were tested to determine the methylene blue index (MBI) (Currie et al. 2014) (Kaminsky 2014), and particle size distribution (PSD) analysis (COSIA FMWG Fines Method 2016) at COSS.

A commercial flocculant (Flopam A3338 produced by SNF) was used as a control. The polymer comes as a dry powder and must be made into an aqueous solution prior to use (this is called polymer make down in industrial terms). The polymer was dissolved in deionized water to a 0.5 w/w% solution kept in a cool dark place for up to two weeks. The solution was further diluted on a daily basis to a 0.02 w/w% solution prior to use with the substrates. This is similar to industrial practice where polymer is made into a mother solution at 0.5-2% and then further diluted prior to use. The dilution is done to reduce the viscosity of the solution allowing for better mixing.

After hydration of the kaolinite slurry the pH was measured. The slurry was then mixed with a Phips & Bird gang mixer for 5 minutes to ensure complete suspension of all solids. Immediately after mixing, 250g of the slurry was then poured into a 250mL graduated cylinder for each test.

Peptides were weighed out using an analytical balance into an anti-static weigh boat. Despite these precautions the weight of freeze-dried peptides added is only accurate to 2 decimal places as there were challenges with the SRM powder sticking to the weigh boat or floating away during transfer. The required weight was calculated on a mass of solid pure peptides to mass of mineral solids basis. Thus, the mass of the crude peptides required was calculated as 2% more than the mass of the pure SRM needed as it contains 2% less protein than the pure. The peptides were added in dry powder form and mixed with a plunger (moving at a rate of 1 plunge per second) 20 times. After plunging, the cylinders were allowed to settle for 48 hours (this is an industrial practice adapted for COSS testing).

The interface height was recorded at 0 min, 2 min, 5 min, 10 min, 30 min, 1 hour, 2 hours, 24 hours and 48 hours. The pH of the supernatant was measured with a pH meter after 2 hrs of settling.

As received FFT was diluted with synthetic process water to achieve a final solids content of 8.9 wt%. The diluted sample was mixed for 30 minutes with an overhead mixture to ensure complete homogenization (COSS practice based on industrial experience). 250g of the diluted material was weighed out into a 250mL graduated cylinder for each test.

SRM was weighed out using an analytical balance into an anti-static weigh boat. The required weight was calculated on a mass of protein to mass of solids basis. The peptides were added in the dry powder form and mixed with a plunger. Two rates of mixing were tested – vigorous mixing for 60 seconds and 20 plunges at 1 second/plunge. After plunging the cylinders were allowed to settle for 72 hours.

The interface height was recorded at 0 min, 2 min, 5 min, 10 min, 30 min, 1 hour, 2 hours, 24 hours, 48 hours, and 72 hours. The pH of the supernatant was measured with a pH meter after 2 hrs of settling.

After the required settling times the cylinders were dismantled. The final volume of the sediment and supernatant were recorded. The middle 50mL of supernatant was removed by pipetting and the color and clarity of the supernatant were measured. The total suspended solids (>0.45 μm) of the supernatant was measured by filtering the supernatant through a 0.45 μm nylon membrane filter and then measuring the dry weight of solids trapped on the filter. The remaining supernatant was removed by pipetting to minimize the disturbance of the sediment layer. The remaining sediment was decanted out of the cylinder and homogenized. A subsample was dried to determine the total solids content of the sediment.

A test series was conducted to evaluate the effect of mixing speed, peptides dosage, and solution pH on the settling of the two substrates. The tests were conducted in triplicate and the order of the tests were randomized to minimize any influence of ordering on the results.

RESULTS AND DISCUSSION

The baseline characterization of the FFT and kaolinite used in the testing is shown in Table 2. The kaolinite was fairly fine with a higher than average surface area for kaolinite while the FFT represents material commonly found near the top of an FFT pond. The water chemistry of the As-received tailings is shown in Table 3.

Table 2. Baseline Characterization of FFT and Kaolinite used

Item	Kaolinite	FFT
Bitumen content (wt%)	N/A	1.23%
Solids content (wt%)	100%	24.68%
Water content (wt%)	N/A	73.64%
Bitumen/Solids Ratio	N/A	0.05
MBI (meq/100 g solids)	4.1	14.1
Fines content %	100%	84.2%
pH	N/A	8.2
Conductivity (µs/cm)	N/A	2900 µs/cm

Table 3. Water chemistry of as received FFT used

Cation (mg/L)	**Na**	306
	K	23
	Ca	51
	Mg	19
	Ba	-
	Sr	-
	Fe	-
Anions (mg/L)	**Cl**	138
	HCO_3	393
	SO_4	-
	CO_3	0
	OH	-

Mixing conditions are known to have a critical impact on the performance of commercial polyacrylamide flocculants. This is particularly true when working with more concentrated slurries but can still be important in dilute suspensions.

According to Bourne (2003) there are a series of screening tests that should be conducted to determine if mixing has a significant effect on a system. The first of these tests is adjusting the mixing speed when adding a reagent. If no substantial difference is noted between the two tests then mixing can be determined to be relatively unimportant.

To assess how important mixing is in the system, the settling rates were measured under vigorous mixing (60 seconds vigorous plunging) and gentle mixing (20 plunges with the plunger moved at 1s/plunge).

As shown in Figure 1, mixing energy did have an impact on all the tests conducted including the pure kaolinite control. This makes sense as increased mixing energy imparts more energy into the system, which then helps keep the fine particles suspended for a longer period of time.

This difference in the initial settling rate is most pronounced for the control where the slow mixing has a settling rate of 0.021m/hr compared to 0.0034m/hr for the fast settling, which is a 6.25 fold difference in rate. The difference in the rate was reduced for both the A3338 and the SRM peptides to a 1.18 and 1.15 fold difference, respectively. Although the influence of mixing was the lowest for the SRM-based material it is still significant enough that it is on the same order of magnitude as the A3338 and should be considered in future testing.

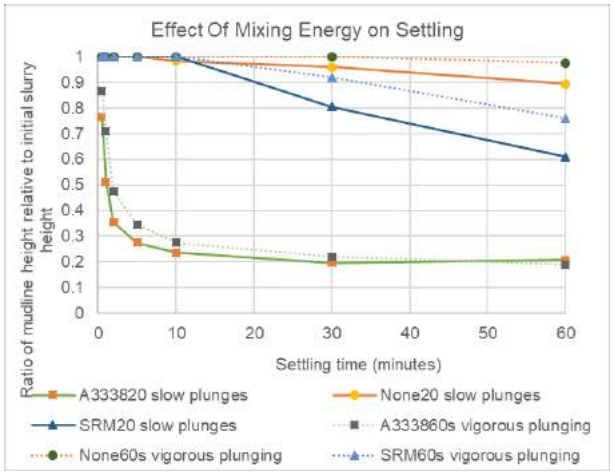

Figure 1. Effect of mixing energy on settling rate

Effect of Dose and pH on Kaolinite Flocculation

As shown in Figure 2 the lowest dosages of the Pure peptides and Crude peptides (1wt%) (small dash lines) showed the lowest influence on settling and were significantly worse than the 3 wt% and 5 wt% additions for pH 8. In both cases the 3 wt%

addition showed the best settling performance relative to the 1 wt% and 5 wt% additions. The difference between 3 wt% and 5 wt% was insignificant and thus a 3 wt% addition may be optimal to maximize impact and minimize the amount of flocculant required. The Crude peptides showed significantly faster settling than the Pure peptides at doses above 3 wt%.

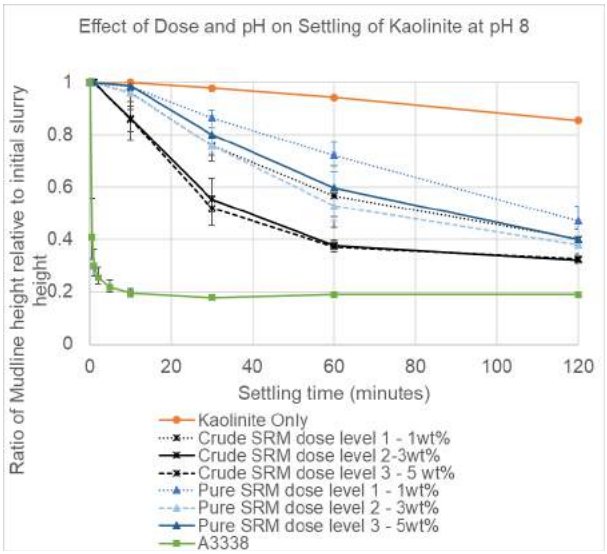

Figure 2. Effect of dosage settling on Kaolinite settling at pH 8

A similar trend was observed for pH 8.5 and pH 9 with the exception that the optimal dosages shifted to 5 wt%.

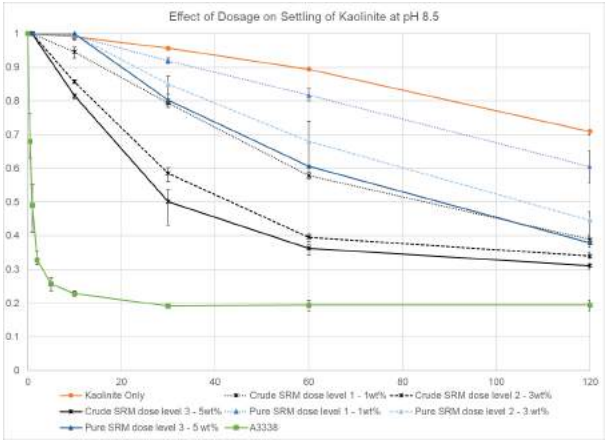

Figure 3. Effect of dosage settling on Kaolinite settling at pH 8.5

Initial Settling Rate

The initial settling rate was calculated over the first two points where settling was observed for each sample. The average initial settling rate for the A3338 treated material was 10 m/hr, which is approximately two orders of magnitude higher than the rest of the results and so was not included in the summary graph shown in Figure 4. As shown in Figure 4 the Crude peptides had a significantly higher settling rate (approximately double) than that of the Pure peptides and the Pure peptides produced a settling rate significantly higher than the untreated kaolinite control. This demonstrates that the Pure peptides were interacting with the solids initiating settling.

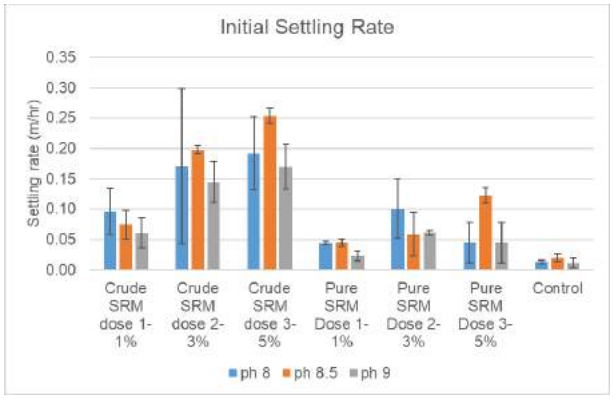

Figure 4. Effect of dosage and SRM type on initial settling rate

Effect of SRM Peptides on pH of Kaolinite Slurries

The pH of the slurry was measured after flocculation. As shown in Figure 5, the SRM peptides significantly impacted the pH of the final slurry with the Crude peptides having the largest influence. To evaluate whether the improvement of settling was purely a pH effect, the settling rate of peptides treated material with an initial pH of 9 was compared to the settling rate of the raw FFT and a pH of 8. In all cases the initial settling rate of the peptides treated material was significantly higher than that of the control treated material, therefore the peptides are acting as more than a simple pH adjustment.

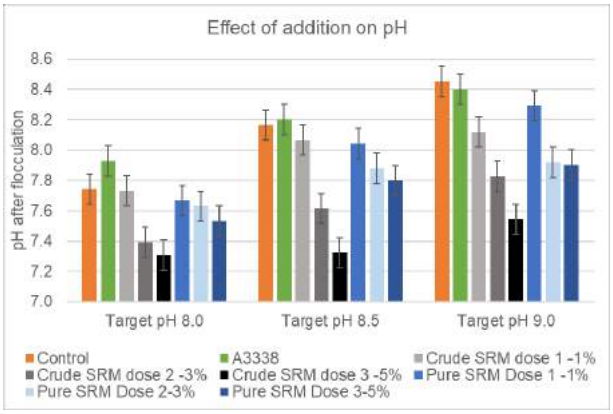

Figure 5. Effect of SRM peptides dosage on tailings pH

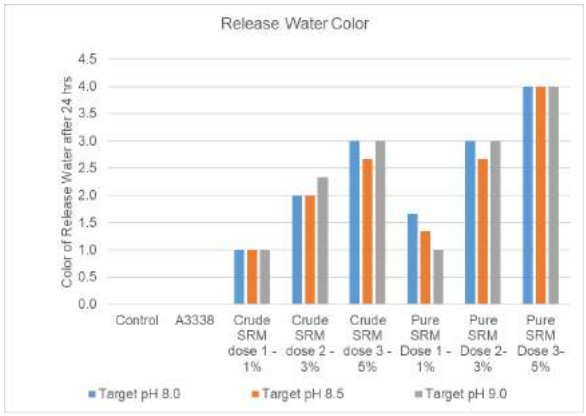

Figure 6. Color of release water after 48 hours of settling (relative scale)

Clarity, Color and Total Suspended Solids of Supernatant

After 48 hours, the columns were dismantled and the water quality and the total suspended solids were determined. The water was qualitatively assessed by clarity wedge. While the water was found to be quite clear in all cases (a clarity off the scale of the wedge – at 46 or greater) a distinct yellow color was noted in the samples treated with SRM peptides. The color of the water was compared and a number assigned from 1 (lightest) to 4 (darkest) yellow. The control and A3338 treated material showed no color in the water, only a pale white due to the residual suspended kaolinite.

As shown from the average values in Figure 6, the color increased with the dose of peptides added, indicating that the reaction between the peptides and the solids was not optimized and a significant amount of the peptides remained in the water phase. The intensity of the color was greatest for the Pure peptides.

Effect of SRM on Settling of FFT

As shown in Figure 7 and Figure 8, the settling rate of the Crude peptides treated FFT was significantly faster than the untreated FFT for the first 2 hrs and comparable to the untreated FFT after 24 hrs of settling. The settling rate of the A3338 treated material was significantly faster than any of the other treatments.

The initial settling rate was calculated over the first two points where settling was observed for each sample. The average initial settling rate for the

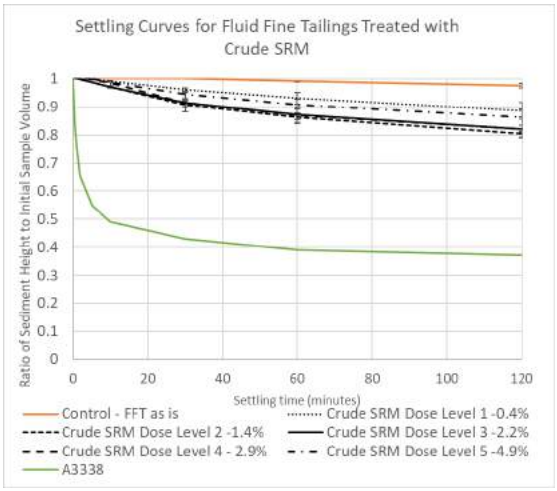

Figure 7. First 2 hrs of Settling for diluted FFT with different treatments

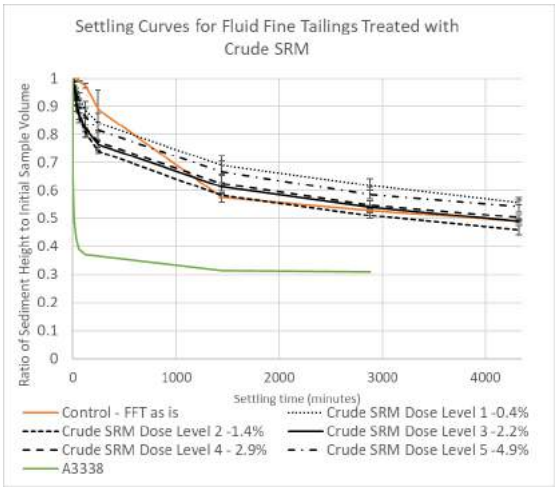

Figure 8. 72 hours of settling for diluted FFT treated with various treatments

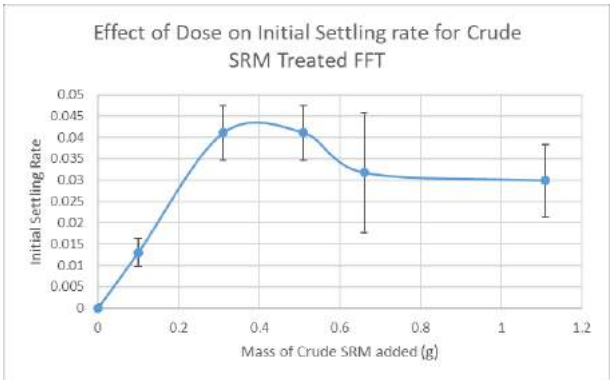

Figure 9. Initial settling rate of crude SRM treated FFT

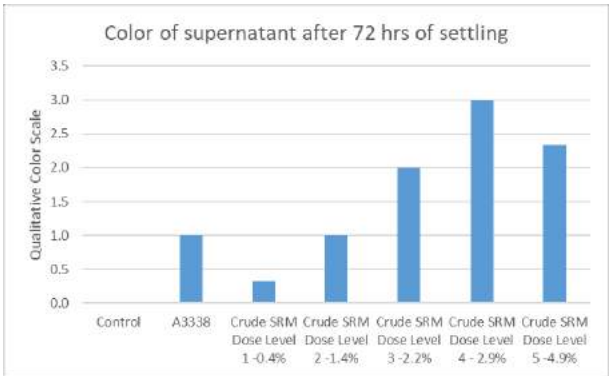

Figure 10. Relative color ranking for release water from treated FFT

A3338 treated material was 4.3 m/h, which is more than one order of magnitude higher than the rest of the results and so was not included in the summary graph shown in Figure 9. As shown in Figure 9 the optimal dose of Crude peptides on the diluted FFT was dose level 2 (1.4%) or 0.31g per column; this works out to a dose of 13600 g/t or ~1.4 wt%. This is almost two orders of magnitude higher than the dosage needed for A3338 (optimal dosage of 180 g/ton for this FFT).

After 72 hours of settling the columns were dismantled and the water quality and the total suspended solids determined. In addition, the water was qualitatively assessed by clarity wedge. The clarity of the water was very high in all cases and the level of suspended solids effectively 0 for all samples except those treated with A3338 where the TSS was 0.01 wt%. As with the kaolinite samples, a faint yellow tinge was observed in the supernatant of the samples treated with peptides. In these samples the A3338 treated material also had a slight color to the water where the water was a light taupe color, which put it at more brown and less yellow than the peptides treated material but with a similar level of intensity as the level 2 dosage for the peptides. The intensity of the color for the FFT release water was similar though slightly lighter than was observed for a similar dose in kaolinite. This lighter result was very interesting as there are other organics present that usually color the water for FFT and so a darker release water color was expected. These other organics include bitumen, humic acids and naphthenic acids.

CONCLUSIONS

The hydrolyzed protein recovered from SRM was able to flocculate both kaolinite and fluid fine tailings. The unrefined product used in these experiments is not able to compete with available commercial products but it shows some potential as an additive, in particular it may provide a nutrient source to microbes and plants.

Further work in the Bressler lab is ongoing to try and modify the product to create a more effective polymer.

REFERENCES

Alberta Energy Regulator. (2016). Mineable Oil Sands Fluid Tailings Status Report 2014 and 2015.

Alberta Energy Regulator (2017). Directive 085. Fluid Tailings Management for Oil Sands Mining Projects. Alberta Energy Regulator.

Bourne, J. R. (2003). Mixing and the Selectivity of Chemical Reactions. Organic Process Research & Development, **7**(4).

Canadian Food Inspection Agency (2018). Annex D: Specified Risk Materials. Retrieved on September 21, 2018. http://www.inspection.gc.ca/food/meat-and-poultry-products/manual-of-procedures/chapter-17/annex-d/eng/1369768468665/1369768518427

COSIA Fines Measurement Working Group. (2016). Unified Fines Method for minus 44 micron material and for Particle Size Distribution February 2016 revision, retrieved from: https://www.cosia.ca/sites/default/files/attachments/COSIA%20FMWG%20Fines%20Method%20February%202016.pdf

Currie, R., Bansal, S., Khan, I. and Mian, H. (2014). An Investigation of the Methylene Blue Titration Method for Clay Activity of Oil Sands Samples. OSRIN – Oil Sands Research and Information Network.

Dean, E. W. and Stark, D. D. (1920). A Convenient Method for the Determination of Water in Petroleum and Other Organic Emulsions. Ind. Eng. Chem., **12**: 486-490.

Kaminsky, H. (2014). Demystifying the Methylene Blue Index. Fourth International Oil Sands Tailings Conference, (pp. 221-229). Banff, Alberta.

Mikula, R., Kasperski, K., Burns, R. and Mackinnon, M. (1996). Nature and fate of oil sands fine tailings: suspensions. Fundamentals and Applications in the Petroleum Industry, **251**: 677-723.

UN Environment. (2017). Mine tailings storage: safety is no accident. A rapid response assessment.

Session 4

TAILINGS DEPOSIT CHARACTERIZATION

REAL-TIME PREDICTION OF OIL SANDS TAILINGS PROPERTIES USING HYPERSPECTRAL OBSERVATIONS

Iman Entezari[1], Benoit Rivard[1], James Sharp[2], P. Sean Wells[3], Mark Styler[2] and Dallas McGowan[2]
[1]University of Alberta, Edmonton, Canada
[2]ConeTec Group, Vancouver, Canada
[3]Suncor Energy Inc., Calgary, Canada

ABSTRACT

Annually, a large number of tailings samples are collected by oil sands mining operators and sent to laboratories for measurement of tailings characteristics. This procedure is not only costly and time consuming, but the laboratory results can be variable, a function of the methods used, and subject to human error. In particular, the repeatability and accuracy of some of the laboratory methods depends significantly on how the samples are prepared and how well the agglomerated clays are dispersed. Therefore, introducing reliable, repeatable, and accurate methods that are fast, cost effective, and capable of estimating tailings characteristics in a wide range of conditions is of great benefit for tailings management. Further, it could significantly reduce the costs and inconsistencies associated with laboratory measurements. In this study, the effectiveness of hyperspectral sensing is assessed for the estimation of tailings characteristics including methylene blue index (MBI), water content, and bitumen content. Hyperspectral observations were collected from 290 tailings samples in their initial saturated condition with a wide range of tailings characteristics. Partial least square (PLS) regression was combined with an iterative stepwise elimination process to select the best wavelengths (bands) and thus best estimator model. Results showed that MBI, water content and bitumen content can be predicted with an accuracy of 1.12 meq/100g, 4.3 wt%, and 0.57 wt%, respectively, using hyperspectral observations collected from saturated samples.

INTRODUCTION

Oil Sands mining operations to extract bitumen from oil bearing sand formations produce large volumes of tailings. Characterization of in-place oil sands tailings is important to assess the tailings dewatering and consolidation performance, to develop more effective measures for tailings management and to monitor their state for reclamation.

In past publications, we investigated the use of hyperspectral sensing for the estimation of several properties of oil sands soft tailings (Entezari et al. 2016a, 2016b, 2017). Spectral models were developed for the quantitative estimation of tailings properties including water content (% water by mass), Methylene Blue Index (MBI), and mineral content, in particular clay and quartz content. The research showed potential use for in-situ and on-site applications, however the established spectral models were developed using a limited number of samples spanning a relatively narrow range of tailings characteristics. In addition, the models developed for MBI estimation were shown to perform best for samples having a moisture content of less than 20 wt%. However, to improve efficiency in the MBI estimation, the models should be adapted to fully saturated tailings and preferably be developed using a larger sample suite.

The main objective of the current study was to develop and calibrate spectral models for the estimation of MBI of wet tailings using a large sample suite. As a secondary objective, models were also developed for the estimation of % water content by mass, and residual bitumen content by mass.

EXPERIMENTAL PROCEDURE

Sample Selection and Description

More than 1000 tailings samples were collected from various Suncor tailings ponds in the summer of 2017. These samples were sent to a commercial laboratory for standard measurement of tailings characteristics. After homogenization, sub-samples were taken for this research. Among these samples, 290 were selected for spectral measurement and model development. These

samples were selected based on the pond, the site location, and the laboratory data to ensure they represented the entire sample population. In other words, efforts were made to select samples showing the widest range of variation in MBI, water content, and bitumen content. Table 1 summarizes the range of variation in MBI, the water content, and the bitumen of the samples selected for spectral measurements and model development. Since the main objective of the research was to develop predictive models for MBI estimation, the 290 samples were selected in a way that they had a uniform distribution across the MBI range to avoid biasing the model performance. The samples were then split into calibration and validation sets, containing 232 and 58 samples respectively. In order to select the validation set, the 290 samples were sorted pond by pond based on their MBI values and every fifth sample was selected to fall into the validation set. This process ensured that validation samples cover a wide range of MBI and represent all the ponds.

Table 1. Summary of the samples' characteristics

MBI (meq/100g)	Water Content (wt%)	Bitumen Content (wt%)
0.48 to 20.56	13.78 to 95.75	0.05 to 10.17

Spectral Measurement

The samples were homogenized at the commercial laboratory, sub-sampled, and shipped in 250ml bottles to the University of Alberta for spectral measurement. Prior to collecting the spectra of each sample, they were shaken for 5 minutes using an industrial shaker to create a homogenous mixture. The sandy samples were also mixed manually with a metal stick. The spectra of the samples were then measured using an analytical spectral device (ASD) covering visible near-infrared (VNIR), and shortwave infrared (SWIR) portion of the electromagnetic spectrum (350-2500 nm). The instrument was equipped with a contact probe fabricated with a sapphire window and an internal light source powered by a 6.5 w quartz-halogen bulb. To collect the spectra of each sample, they were poured into aluminum containers with 2 cm depth and the contact probe was immersed in the sample. Three spectra were collected from each sample and were averaged to calculate the final measurement with an ASD Fieldspec instrument. A Spectralon panel was used for reflectance normalization.

Pre-Processing of Spectra

In order to eliminate the noise at the edges of each reflectance spectrum, the wavelength region was limited to 400-2400 nm. The spectra were also down-sampled to 6 nm intervals to reduce the redundancy of the data and increase the computation performance (ASD delivers the reflectance value at 2151 bands). From these procedures, the number of bands were reduced to 334 bands. Several pre-processing methods on spectra were then examined to explore their impact on the model performance. These included mean vector normalization, first derivative, transformation to absorbance (log (1/R), R is reflectance), and Savitzky-Golay (SG) smoothing filter. Different combinations of the methods were tested (e.g. first derivative + SG filter). A detailed review on these spectral pre-processing methods has been published by Rinnan et al. (2009).

Modelling and Accuracy Assessment

Partial least square (PLS) regression was used for model development. Since the performance of PLS depends on the input bands, an iterative stepwise elimination process was employed to select the optimum bands (most informative bands) for PLS regression. In this procedure, PLS was first calibrated using all 334 bands. Then, the score of variable importance in projection (VIP) was calculated in each iteration and the band with the lowest VIP (least information) was eliminated from the available bands. PLS was re-calibrated with the new bands and the process was repeated until only one band remained. Also, in each iteration, 5 to 30 PLS components were examined to select the optimum number of PLS components. In each iteration, the PLS model was calibrated using the calibration set and the performance of the model was assessed by calculating R-squared and root mean square error (RMSE) values on the validation set. The PLS model that resulted in the highest R-squared and lowest RMSE value on the validation set was selected as the best model for the prediction of the tailings characteristic of interest. It is noted that any errors in the laboratory data will inherently introduce errors in the spectral model. Therefore, the performance of the models developed in this research can only be as good as the laboratory measurements. In other words, the laboratory data is incorrectly assumed to be perfect in order to determine model errors.

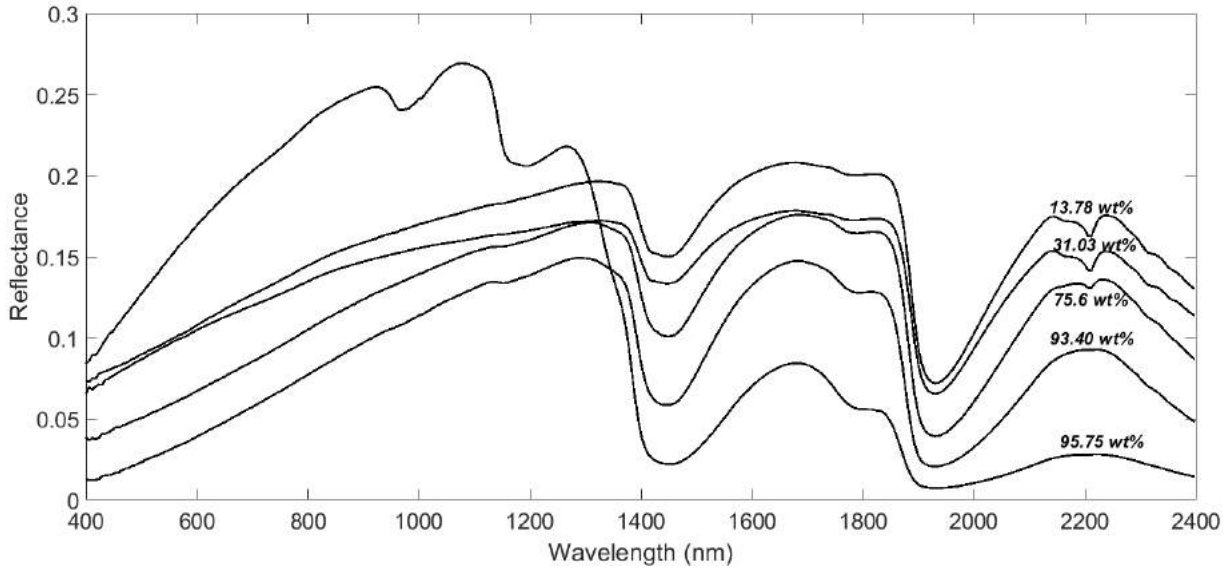

Figure 1. Reflectance spectra types of the tailings samples measured. Water content associated with each sample is shown on each spectrum.

RESULTS

Spectra of Samples

Figure 1 shows spectra of a representative selection of the tailings samples. In general, the samples display similar reflectance spectra. The absorption feature near 1.4 μm is attributed to water or OH overtones, while the 1.9 μm feature is a water combination band. The feature at 2.2 μm is a characteristic clay feature in oil sands tailings spectra. The presence of residual bitumen causes absorption features near 1.7 μm and 2.3 μm and may affect the clay absorption bands as well. In addition to the variation in the depth of the absorption features, it is evident that the slope of the spectra in different wavelength regions also changes with a variation in tailings composition, in particular water content variations.

MBI Estimation Model

For MBI estimation, the best results were achieved using a PLS model with 107 input bands (selected through the stepwise elimination process) and 30 PLS components when the tailings spectra were transformed to absorbance and smoothed with a SG filter. Figure 2a shows the relationship between MBI measured in the laboratory and MBI predicted using the PLS model for both calibration and validation sets. R-squared and RMSE were 0.94 and 1.12 (meq/100g), respectively, using the validation set.

Water Content Estimation Model

It was observed that the combination of first derivative and SG filter to pre-process the input spectra led to the best results in PLS regression for water content estimation. The relationship between estimated and measured water content is shown in Figure 2b. A PLS model with 73 bands and 29 components resulted in the best R-squared and RMSE on the validation set (R-squared = 0.96, RMSE = 4.3 wt%).

Bitumen Content Estimation Model

Similar to the case of water content estimation, the best pre-processing method was observed to be applying a first derivative followed by SG filter on the input spectra. The highest R-squared and lowest RMSE for the estimation of residual bitumen content of tailings were achieved for a PLS model with 71 bands and 25 components. R-squared and RMSE were observed to be 0.91 and 0.57 wt%, respectively.

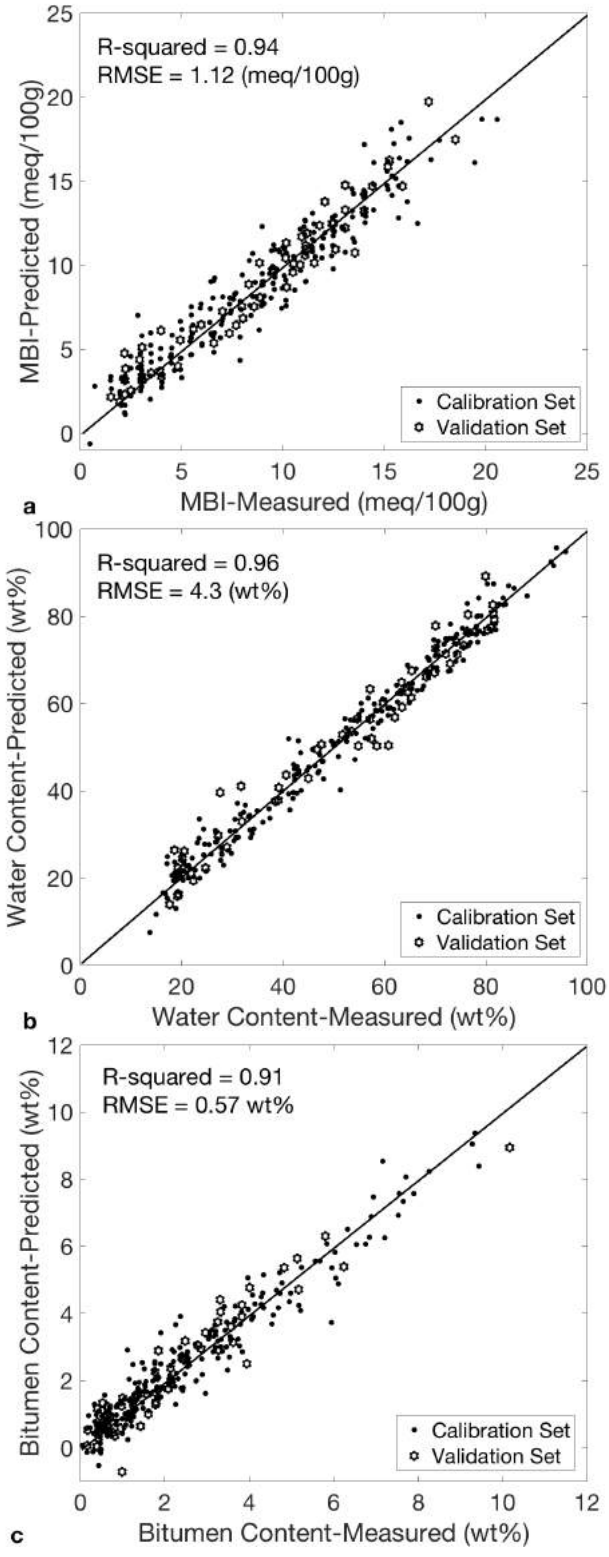

Figure 2. Relationship between measured and predicted (a) MBI, (b) water content, and (c) bitumen content

CONCLUSIONS

This research examined the use of hyperspectral sensing in the estimation of some tailings characteristics. The work conducted here on 290 tailings samples showed that hyperspectral observations can be highly correlated to tailings properties that include MBI, water content, and bitumen content. The results showed that MBI can be predicted with an accuracy of 1.12 meq/100g while the contents of water and bitumen can be estimated with 4.3 and 0.57 wt% errors, respectively. Although these errors are generally higher than published laboratory measurements, they are sufficiently accurate enough for many applications and for investigating tailings behaviour. A key advantage of spectral models is that they provide rapid (within minutes) and repeatable predictions that are less prone to human errors. Consequently, the use of hyperspectral technology for tailings characterization can enable the oil sands operators and service providers to quickly analyze the tailings on-site to provide a near real-time assessment of the tailings properties. This would significantly reduce the operational costs associated with sample collection, transportation, and laboratory analysis. Timely, repeatable, and sufficiently accurate measurements of tailings properties such as MBI and water content may be of great benefit for establishing best practices in tailings management.

ACKNOWLEDGEMENTS

The funding of this project was provided by Mitacs, ConeTec, and Suncor Energy Inc.

REFERENCES

Entezari, I., Rivard, B., Lipsett, M. G. and Wilson, G. W. (2016a). Prediction of water content and normalized evaporation from oil sands soft tailings surface using hyperspectral observations. Canadian Geotechnical Journal, **53**(10): 1742-1750.

Entezari, I., Rivard, B. and Lipsett, M. G. (2016b). Estimation of methylene blue index in oil sands tailings using hyperspectral data. Canadian Journal of Chemical Engineering, **95**(1): 92-99.

Entezari, I., Rivard, B., Geramian, M. and Lipsett, M.G. (2017). Predicting the abundance of clays and quartz in oil sands using hyperspectral measurements. International Journal of Applied Earth Observations and Geoinformation, **59**: 1-8.

Rinnan, A., Van der Berg, F. and Engelsen, S. B. (2009). Review of the most common pre-processing techniques for near-infrared spectra. TrAC Trends in Analytical Chemistry, **28**: 1201-1222.

A METHOD FOR AUTONOMOUS BATHYMETRIC SURVEYING USING AN AMPHIBIOUS ROBOT

Nicolas A. Olmedo and Michael G. Lipsett
Copperstone Technologies Ltd., Calgary, Canada

ABSTRACT

Bathymetric surveying determines the volume contained in ponds and identifies subsurface structures. Workers in boats generally conduct surveys manually with simple tools for measuring the depth at a location that is measured by GPS. Depth can be measured using probes, ultrasound, or sonar. With contact instruments, the survey data can be collected while moving along a path that covers the pond surface with a pre-selected maximum spacing between locations. This approach is labour-intensive, prone to measurement error, and can pose some risk to personnel when the littoral zone is difficult to access. Radio-controlled boats are problematic when access is limited, there are mud zones near the surface that may strand the boat, or there are obstacles in the water such as trash or bitumen mats. In this work, a new system is presented for autonomously surveying a pond. The system comprises an amphibious platform with a set of screw rollers (scrolls) for locomotion over land and water, an automatic control system for navigation, a communication system for remote control, and a sensing and data acquisition system for recording geo-referenced depth measurements. Results are presented for system commissioning tests; and field trials at an operating mining facility are described.

INTRODUCTION

Environmental monitoring of areas affected by industrial operations, such as fluid waste deposits, is key for sustainability and eventual reclamation of the site. Fluid waste (tailings) from mining operations and from raw material processing facilities needs to be monitored for (i) improving the performance of mining processes (Lipsett 2014), (ii) timely feedback to improve remediation efforts (Hold 1993), (iii) environmental monitoring (Plumlee 1994), and legislative compliance (Wills 2016).

Geotechnical sampling and measurements campaigns can help identify hazards, minimize long-tem storage of material and improve reclamation (Lipsett 2009). Currently, environmental surveys, including geotechnical campaigns, are conducted manually (Beier 2013), and are limited to areas made accessible to workers or areas that large manned vehicles can navigate. There are risks associated with equipment sinking and some operations may put personnel at risk.

Bathymetric surveying is necessary to calculate the volume contained in water-capped deposits and to profile subsurface structures. Manual surveys from boats are costly, and are only possible on deposits with docks, or traversable beaches. Typically, the varying nature of tailings deposits and unstable littoral zones are a challenge for boat operators.

These challenges can lead to costly and intermittent monitoring of accessible areas, and insufficient monitoring of inaccessible areas. Additionally, human surveying is labour-intensive, and prone to measurement error. Recently, unmanned systems have been developed to provide access to traditionally difficult terrains and reduce the risk of injuries to workers. Robotic systems have been developed to aid human workers in collecting samples and estimating soil properties (Olmedo 2016a). Wheeled and tracked ground robots have been tested on deposits that have developed a crust to collect samples and estimate soil properties. These measurements were limited to the bearing strength of the deposits, 15kPa.

Amphibious robots have been developed to provide access to very rough terrains and water (Olmedo 2016b). The unmanned amphibious robots have been used to deploy geotechnical tools and specialized payloads for tailings characterization and reclamation activities. Screw-drive robots have been used to measure shear strength, install wick drains, broadcast sees, and plant seedlings in previously inaccessible terrain (Olmedo 2017). Key unique design and control

elements allow these robots to move over hard ground, deformable terrain, snow, and water, making them a highly versatile platform for challenging environments.

Bathymetric surveys have been conducted with remote controlled (RC) boats, which carry sonars and a Global Positioning System (GPS) to collect geo-referenced depth measurements. These systems are challenging to deploy in deposits that have an inaccessible littoral zone. Typically, workers cannot approach the water line to manually drop the boats in the water. Shallow deposits may pose a risk of the RC boats getting stuck. In some deposits, shallow areas located far from the shoreline may also pose a risk of getting stuck.

This paper presents the design and preliminary field trials of an autonomous amphibious robot designed specifically for unsupervised long-endurance bathymetry that provides easy access to rough terrain.

SYSTEM DESCRIPTION AND FUNCTIONALITY

An amphibious robot developed for bathymetric surveys (CST-AR0) is shown in Figure 1. The platform employs a modified screw-drive locomotion method. A screw-drive (amphirol) robot is an unmanned system propelled by counter-rotating Archimedean screws (scrolls).

This propulsion mechanism provides a number of operating advantages, such as the ability to traverse both water and solid ground and side-to-side mobility. The scrolls are sealed, to make the robot buoyant. Typically, two counter-rotating scrolls have been used (Olmedo 2016b), but two pairs of counter-rotating scrolls with opposite pitch have been shown to provide significant advantages in mobility.

Based on observed performance in previous field trials, the dual-scroll configuration works well on soft terrain and on liquid; but two scrolls presents difficulties for control when turning on hard ground that is prone to excessive slip. A four-scroll system allows for forward motion in soft material & water as well as side-to-side rolling movement with high turning manoeuvrability when traversing solid ground (Figure 2). The system must be able to deliver both high torque for ground motions in rough terrain, and fast motion to propel through water. To accomplish this, the current design has direct-drive electric servomotors that actuate each of the four scrolls.

Figure 1. CST-AR0, Alberta, Canada

Figure 2. CST-AR0 moving through the transition between water and a sandy beach, Alberta, Canada

For ease of manufacture for operations primarily in water with little chance of extended driving on rough hard ground, the scrolls are made of plastic by additive manufacturing, with metallic inserts and mating flanges for structural integrity. Each 3D-printed plastic scroll is coated with epoxy to prevent leaking of water into the scrolls. While this fabrication method is cost effective, it is not very durable.

The structure of the UGV is a simple ladder frame. For the demonstration prototype, the frame is constructed primarily from t-slot extruded aluminum. Overall dimensions of the vehicle are approximately 1 m x 1.5 m x 0.5 m and it has a

mass of 55 kg. Controller electronics and power supplies, including lithium-ion batteries, are mounted in watertight enclosures above a polycarbonate splashguard. Motor controllers accept inputs from an autopilot or manual commands through a microcontroller. Under automatic control, geo-positioning is achieved using a GPS receiver into a PixHawk autopilot, which delivers motion commands to the microcontroller.

Depth is measured with an Airmar DT800 NMEA 2000 (CAN-based) ultrasonic depth sensor, mounted at the front of the rover slightly submerged to reduce the influence of air entrainment on the transducer. The autopilot sends telemetry information that is displayed on a laptop to act as a ground station. Manual control is achieved through a commercial Taranis radio control transmitter with digital telemetry capability.

Telemetry, including GPS information and depth measurements is recorded on board the rover, as well as on the ground station. The ground station is used to configure the robot, for real time data visualization, and debugging; but the ground station is not necessary for autonomous operation.

PERFORMANCE TRIAL RESULTS

The rover performance was assessed on a range of ground conditions and in water.

Rolling on land was done on grass and sand. Gravel and sharp rocks were avoided to prevent damage to scrolls due to impacts. Manoeuvrability was good, with the rover able to make tight radius turns while rolling. The motors delivered sufficient torque to be able to shear saturated sand, but not clay-loam soil. Maximum linear velocity on land was approximately 2 m/s.

Screw motion on water was successful, with top speed of about 1.8 m/s, excellent manoeuvrability, and no tipping during turns (Figure 3). There was no ingress of water into the scrolls or electronics enclosures. Transitioning from water to sand beach was successfully done under manual control while rolling. More durable scrolls would allow for transition while scrolling. The speed control mode allowed the scrolls still in the water to spin to create a drive force while the scrolls on sand rolled (and spun at times) to drive up onto the beach (Figure 2).

Figure 3. CST-AR0 water performance tests, Alberta, Canada

Peak power consumption was about 6kW at maximum speed. Two 24 V 2.5 kWh Li-ion batteries were connected in parallel to supply power. Battery life was monitored during operations to ensure that the rover did not stop from a loss of power unexpectedly. Most operations were conducted at less than half of the peak power consumption. The robot can achieve and endurance of 10km with the current battery capacity. The robot can carry up to four times the current battery mass if necessary.

BATHYMETRIC SURVEY TRIALS

A pond mapping scenario was identified at a Canadian mineral processing facility. The pond of interest has a sandy edge (littoral zone) that is inaccessible; and there are shallow zones in the middle of the pond that prevent manual surveys with conventional boats. For these reasons, an amphibious platform is necessary to access the entire pond. A teleoperation approach is possible for navigating around the pond; but an autonomous system was much preferred.

The survey was set up with a sequence of waypoints in a rastered geometry with a home position and a set of straight parallel lines for the rover to pass by as it traced the pattern. Each new line of surveying was beside the previous line segment. Spacing between waypoints was approximately 15 m to allow good coverage of the pond; and a different spacing specification could easily be defined. For wavy conditions, the pitch and roll angles of the rover could be used to

calculate the actual depth at a particular location; but testing was done with no significant waves and so this feature was not necessary.

The autopilot required tuning to reduce oscillations and overshooting, especially when the rover was navigating without RTK GPS. The configuration software of the PixHawk allowed real-time visualization of the navigational accuracy and the path of the rover, while also displaying the depth, which helped with tuning.

MAPPING RESULTS

A trial bathymetric survey of a natural pond is shown in Figure 4. The results of geo-reference depth measurements on the pond are presented below. The CST-AR0 conducted an autonomous survey with a grid spacing of 15m. For larger, multi-kilometer area ponds, a spacing of 50m is suggested. An example of a planned trajectory is presented in Figure 5. The robot navigated at a speed of approximately 0.9 m/s, and collected depth measurements at 1Hz. These parameters are configurable.

The resulting map of the survey is presented in Figure 6. The measured depths were recorded between 1 and 4 meters. The data recorded was interpolated linearly to create the continuous heat map in Figure 6. Other possible interpolation methods can be used, including cubic and nearest point hold. The graphs were generated using the open source Matplotlib packages (Hunter 2017).

Using an RTK GPS can mitigate sources of error in localization. Typically, the base stations for RTK GPS need to be setup in advance in order to have reliable, accurate, position references. Sources of error in depth measurements can be reduced by correcting for pitch and roll angles of the robot, in case of waves and wind, as well as by using more than one sensor in the platform. Additionally, multi-beam and multi-frequency sensors are available to increase measurement accuracy and precision.

FUTURE WORK

While the commercial prototype performed very well, several improvements are being implemented. A payload is in development for collecting a set of water samples. A payload has been tested for automatically collecting a surface soil sample; and a related system has been developed for vegetation sampling, such as peat moss. A more durable structure and scrolls are in development for commercial service duty. At the littoral zone between water and shore, individual scroll control will be used for improved transition between fluid and solid ground, allowing a scroll in each zone to move at a speed that delivers good torque to move up onto the shore. A simple scroll cleaning mechanism has been designed for conditions with sticky mud to prevent the scrolls from accumulating material on the scrolls. For long surveys, a larger battery payload can be installed, but also easily removed for carrying the machine. Metal printing is being investigated for fabricating the scrolls.

Figure 4. CST-AR0 conducting a bathymetric survey, Alberta, Canada

Figure 5. Planned trajectory for surveying part of a natural pond with 15m spacing

Figure 6. Measured pond depth. Scale in meters

ACKNOWLEDGEMENTS

James Yuen of Copperstone Technologies provided input to drive train design, and participated in field trials. Stephen Dwyer of Copperstone assisted with sensor interfacing and autopilot tuning.

REFERENCES

Beier, N. A., Wilson, G. W., Dunmola, A. and Sego, D. C. (2013). Impact of flocculation-based dewatering on the shear strength of oil sands fine tailings. Canadian Geotechnical Journal, **50**(9): 1001– 1007.

Holm, L. A. (1993). Strategies for remediation. Geotechnical Practice for Waste Disposal, pp. 289–310, Boston, MA: Springer US.

Hunter, J. D. (2007). Matplotlib: A 2D graphics environment. Computing In Science & Engineering, **9**(3): 90-95.

Lipsett, M. G. and Dwyer, S. (2009). A robotic system to characterize soft tailings deposits. Proceedings of Mine and Tailings Waste Conference 2009, Banff Alberta, November 2009.

Lipsett, M. G., Olmedo, N. A., Rivard, B. and Wilson, G. W. (2014). Robotic Systems for Measuring Properties of Tailings Deposits and Collecting Samples. Proceedings of the Fourth International Oil Sands Tailings Conference, (Lake Louise, AB), Dec. 2014.

Olmedo, N. A. and Lipsett, M. G. (2016a). Design and field experimentation of a robotic system for tailings characterization. J. Unmanned Vehicle Systems. Mar.

Olmedo, N. A., Dwyer, S., Yuen, J. and Lipsett, M. G. (2016b). Amphibious robot for environmental monitoring of oil sand tailings". Fifth International Oil Sands Tailings Conference. Lake Louise, Alberta, Canada. December 4-7.

Olmedo, N. A., Dwyer, S., Yuen, J. and Lipsett, M. G. (2017). Amphibious robot for reclamation work on soft tailings deposits. Tailings & Mine Waste. Banff, Alberta, Canada.

Plumlee, G. S., Smith, K. S. and Ficklin, W. H. (1994). Geoenvironmental Models of Mineral Deposits, and Geology-based Mineral-environmental Assessments of Public Lands. Tech. Rep. Open-File Report 94-203.

Wills, B. A. and Finch, J. A. (2016). Tailings Disposal. Wills' Mineral Processing Technology, pp. 439– 448, Elsevier.

CHARACTERIZING SOFT OIL SAND TAILINGS BY GAMMA CONE PENETRATION TESTING

Mark Anthony Styler, Dallas McGowan and Jamie Sharp
ConeTec, Fort McMurray, Canada

ABSTRACT

Piezocone Penetration Testing (CPTu) is performed by pushing an instrumented conical-shaped probe into the subsurface at 2 cm per second. CPTu performed in oil sand tailings containment facilities provide a continuous profile of measurements from the pond surface through the recycle water, across the mud-line, through the fluid tailings, across the hard bottom, through the soil-like tailings, and into the natural ground. Passive-gamma, and other, modules can be attached behind the cone probe to respond to in-situ concentrations of natural radioisotopes. In this paper we show how the Gamma Cone Penetration Test (GCPTu) results can be used to measure the mud-line and hard bottom depth. We show how the GCPTu results can be used to estimate the total unit weight of fluid tailings and that this estimate is confirmed by adjacent laboratory results. We also show that the passive-gamma measurements are strongly correlated to the total fines content. GCPTu profiles can be interpreted to develop cross-sections of tailings units (recycle water, fluid tailings, soil-tailings), to investigate time-dependent phenomena by comparing successive CPT profiles, and to investigate ongoing tailings management operations. This paper does not report on the product of a single experimental testing program, but the result of examining empirical observations made in over 29 years of cone penetration testing in oil sand tailings.

INTRODUCTION

Athabasca oil sands ore is mined and processed to extract bitumen impregnated in the soil. Bitumen is extracted from the ore on site, which creates a waste by-product of tailings. These tailings are a mix of soil particles, water, and residual bitumen. Continued operations at oil sand mine sites requires responsible management, through transportation, storage, treatment, and deposition of the generated tailings by-product.

The purpose of this paper is to share our experience analyzing Gamma Cone Penetration Test (GCPTu) results in oil sand tailings. The GCPTu is one site-investigation tool that can be combined with other tests and sampling campaigns to fully characterize OST tailings facilities.

TAILINGS STORAGE FACILITIES

Oil sand tailings are managed in tailings storage facilities. The whole-stream tailings have high water contents and are typically transported hydraulically. Tailings must be contained to limit the footprint to the mine-site. Tailings storage facilities can be in-pit, where the tailings are deposited in place of previously mined ore and contained within in-pit dykes. Alternatively, external facilities can be constructed where a tailings dam is built above the original ground elevation to contain the tailings.

Tailings management is required to meet operational needs and regulatory requirements. Tailings storage facilities need to have sufficient capacity for the existing tailings and future production. This capacity can be met by constructing new facilities, raising dam crest elevations to increase the volume, or by treating the existing tailings to remove stored water. Oil Sand Tailings regulations, such as the rescinded ERCB Directive 074, the Alberta Tailings Management Framework, and the active AER Directive 085, have been instituted to ensure that these facilities are designed for eventual closure. Current tailings regulations requires annual tracking of the volumes of stored fluid tailings and the quantity of fines in these fluid tailings.

Tailings are dynamic. The discharged tailings can flow, segregate, form a consolidating sediment, or remain suspended in a fluid column. Blight & Bentel (1983) covered the hydraulic deposition of tailings. The discharged tailings can segregate along a forming beach slope angle, with progressively finer tailings settling with distance

from the discharge point. Consoli and Sills (2000) analyzed the simultaneous transportation, consolidation, and sedimentation that occurs in tailings reservoirs. Tailings management needs and regulatory requirements necessitate the investigation and characterization of the contents of these tailings storage facilities. A COSIA working group reviewed current site-investigation techniques used in oil sand tailings facilities (Ansah-Sam et al. 2015).

A typical tailings profile may include a water cap, fluid tailings, and soil-like tailings. The water cap, also called recycle water, has solids contents less than 5%. There is typically a sharp boundary between the water cap and fluid tailings termed a mud-line. The solids content at the mudline rises sharply. Fluid tailings are dominated by fines and have negligible effective stress. The fine grained soil particles may be entirely suspended within the fluid column. A sediment bed forms at the base of the fluid column where the soil-particles are in contact and form a soil-skeleton that develops effective stress. This boundary between fluid tailings and soil-like tailings is termed the “hard bottom”. This hard bottom can increase in elevation due to additional sedimentation, decrease in elevation due to consolidation of underlying soils, or remain essentially constant due to the balance of these phenomenon or the logarithmic-scale of time required for continued sedimentation and consolidation. Soil-like tailings have formed a particle skeleton and the geotechnical behaviour depends on effective stress.

Characterizing the entire profile, from the water cap through the hard bottom, can inform tailings management decisions. The recycle water volume can be returned to bitumen extraction or other uses. The fluid tailings volumes are required for regulatory reporting, and can be dredged and treated to reduce their volumes. Beach and dyke tailings require geotechnical characterization for construction purposes.

CONE PENETRATION TESTING

Piezocone penetration testing (CPTu) is performed by advancing an instrumented probe into the soil at a rate of 2 cm/s. The standard CPTu probe, shown in Figure 1, includes sensors to measure the tip resistance (q_c), friction sleeve (f_s), dynamic pore pressure (u_2), inclination, and temperature at a depth interval of 1 cm, 2.5 cm, or 5 cm. The cone tip resistance requires a systematic correction from q_c to a corrected value of q_t using $q_t = q_c + u_2(1 – a)$ (Campanella et al. 1982).

The CPTu is a geotechnical test that was developed to investigate soils. Published methods to reduce CPTu data are mostly limited to natural soils such as gravels, sands, silts, clays, or organics (e.g. Lunne et al. 1997, Mayne 2007, Robertson & Campanella 1983a, 1983b). The CPTu is used in geotechnical practice to profile soil-types and characterize the geometry of the geotechnical problem. The CPTu is also used to estimate soil-properties for the various identified soil units.

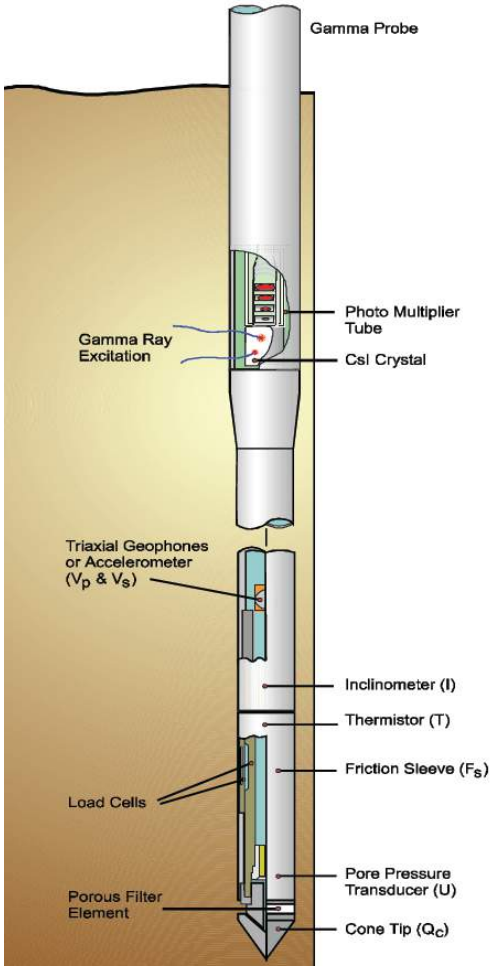

Figure 1. Diagram of Passive Gamma module attached behind a 15 cm² cone probe

AER Directive 085 defines fluid tailings as having solids content greater than 5% and undrained strengths less than 5 kPa. In geotechnical engineering, the undrained strength actually depends on the stress path to failure and different laboratory and in-situ tests result in different undrained strength measurements. The CPTu net penetration resistance is often correlated to the field vane undrained shear strength $(s_u)_{fv}$ (Wroth 1984), and this undrained strength is used to geotechnical analysis and design (Aas et al. 1986, Bjerrum 1974, Larrson 1980).

AER Directive 085 defines the bottom of the fluid tailings profile using a conical drop-probe. This boundary is termed the hard bottom, and depends on the strength of the tailings. This hard bottom will be located at sharp increases in the CPTu net-penetration resistance associated with the development of effective stress and a soil-particle skeleton. It also corresponds to an increase in the viscosity and friction.

The CPTu probe, as shown in Figure 1, includes a piezometer which is used to obtain a measure of dynamic fluid pressure in-situ. This fluid pressure is affected by transient pore pressures generated from cavity-expansion and shear of the soil to accommodate the in-situ probe. The dissipation of these excess pressures can be monitored by suspending cone penetration during a pore pressure dissipation (PPD) test. PPD results can be interpreted to estimate the soil's coefficient of consolidation. Tanaka and Sakagami (1989) performed PPD tests in a deposit undergoing consolidation. The characterized PPD equilibrium profile versus depth agreed with adjacent permanently installed piezometer monitoring.

In recycle water and fluid tailings with negligible effective stress, the measured CPT pore pressure equals the total stress. PPD results in fluid tailings show no dissipation of excess pore pressures.

Gamma Cone Penetration Testing (GCPTu) uses a passive-gamma module attached behind the cone probe, as shown in Figure 1. The module housing contains a scintillating crystal that glows when it is struck by gamma rays. The gamma-module uses a photo-multiplier-tube and associated internal electronics to monitor this scintillating crystal. The observed gamma-ray incidents are counted up and used to calculate the gamma counts-per-second, which is reported in the GCPTu soundings. Quantitative application of gamma measurements requires repeatability between soundings and equipment.

There are three common Naturally Occurring Radioactive Minerals (NORMs). These are natural radioisotopes of Potassium (^{40}K), Thorium (^{232}Th), and Uranium (^{238}U). These three radioisotopes exist in nature due to exceptionally long half-life times of a similar magnitude to the age of Earth. Potassium is in Illite and Feldspar minerals, Thorium is associated with heavy minerals (Ellis 2007), and Uranium is found in uranium salts and organic shale (Ellis 2007). The mineralogical constituents of the bitumen ore remain in the tailings by-product and gamma profiling can identify different tailings units. The gamma measurements in tailings are proportional to the total fines content (weight of fines / total weight) due to the potassium in the Illite mineral. It is not proportional to the geotechnical fines content (weight of fines / weight of solids). The total fines content is proportional to the in-situ concentration of ^{40}K in OST.

The generated gamma rays from these natural sources will interact with matter. This interaction makes it possible to observe gamma rays in-situ. The propagating gamma rays can re-coil, lose energy, and change direction in a process known as Compton scattering. When the gamma ray energy drop below 100 keV, the ray can be extinguished by photoelectric absorption. Gamma rays with energies higher than 1022 keV and split into two rays of 511 keV in a process known as pair-production. Berger (1961) presents table of energy absorption coefficients that averages these three matter interaction effects. For a typical density of tailings a generated gamma ray from ^{40}K may travel from 10-20 cm. This means that the GCPTu gamma profile responds to the same soil measured by the cone penetration test.

CONVENTIONAL TAILINGS PROFILE

GCPTu profiles in OST can include recycle water, fluid tailings, soil-like tailings, and natural ground. The typical measurements in these types of materials can be used to identify the tailings units and to estimate OST properties – such as solids content and fines content.

Recycle Water

GCPTu measurements in OST recycle water produce an easily identifiable profile. First, the corrected tip resistance, q_t, equals the pore pressure u_2. The friction sleeve, f_s, is nearly zero. The pore pressure channel, u_2, increases at approximately 9.8 kPa per m (kN/m^3) in pure water and slightly higher in saline water.

Recycle water has negligible concentrations of natural radioisotopes. The observed passive gamma rates are nearly 0 cps. There can be an increase in gamma rates at the pond surface due to atmospheric radiation. Over a very short depth, the impact of atmospheric radiation is completely shielded by the recycle water.

Mudline

Hitting the mudline typically has no discernable effect on q_t. The friction sleeve, f_s, will still be nearly 0 kPa. The slope of u_2 will begin to deviate from 9.8 kN/m^3; but this change can be nearly imperceptible. The standard cone probe results cannot be used to identify the mudline depth with any degree of confidence.

However, below the mudline the tailings contain a concentration of natural radioisotopes. Therefore, the mudline corresponds with a sharp increase in passive gamma rates. The GCPTu can be used to easily identify the mudline depth.

All gamma ray measurement devices have an efficiency factor that reduces the in-situ concentration of gamma rays to a measured gamma rate. This efficiency factor depends on the module shielding, module electronics, and scintillating crystal geometry and type. By sheer coincidence, the ConeTec passive gamma module shown in Figure 1 has an efficiency factor that produces measured gamma rates approximately equal to the total fines content in fluid oil sand tailings. The mudline definition of 5% solids corresponds to a gamma rate of 5 cps. The mudline depth can be routinely and easily profiled using the GCPTu, however other pond surface geophysical methods are more efficient for large mudline surveys.

Fluid Tailings

In fluid tailings the cone tip resistance will increase with the measured pore pressure. The effective tip resistance, q_t-u_2, will be close to zero. The friction sleeve measurements will also be nearly zero.

The measured pore pressures will equal the total stress in fluid tailings. This has been observed in laboratory tests on sedimentation (Sills 1998). It was also observed in 10 m high standpipe tests on oil sand tailings (Jeeravipoolvarn et al. 2009). Since the u_2 measurements equal total stress, the slope of u_2 versus depth equals the total unit weight of the fluid tailings.

PPD tests can be performed in fluid tailings. These show that the u_2 channel does not dissipate to a hydraulic profile of 9.8 kN/m3 from the pond-surface. The u_2 channel does not dissipate at all because there are no excess pore pressures from shear or cavity expansion to accommodate the cone probe.

This total unit weight, $\gamma_t = du_2/dz$, can be used to estimate the solids content of the fluid tailings using Equation 1. In this equation G_s is the specific gravity of the oil sand tailings particles and can be assumed to equal 2.6; γ_t is the unit weight of water, 9.8 kN/m^3.

$$\frac{Solids(\%)}{100\%} = \left(\frac{G_S}{G_S - 1}\right)\left(1 - \frac{\gamma_w}{\gamma_t}\right) \qquad \textbf{Eq. 1}$$

If the fluid tailings are 100% geotechnical fines, then the estimated solids content also equals the total fines content. The gamma measurements approximately equal the total fines content. Therefore, the difference between the estimate of solids content and the passive gamma estimate of total fines content can indicate the presence of sand in the fluid tailings. Empirical equations, such as the Tailings Behaviour Type, can be developed from compiled datasets of OST constituents and GCPTu results to further refine these interpretations (Ansah-Sam et al. 2015).

The froth-treatment process concentrates minerals containing Thorium-232 and Uranium-238 radioisotopes that naturally occur in the parent ore body. The passive gamma measurements in fluid froth treatment tailings are not proportional to the total fines content. In froth-treatment tailings we measure passive gamma rates that are an order of magnitude larger than conventional OST tailings. While this removes one application of the GCPTu site investigation tool, it adds another. The GCPTu

profiles can be used to easily identify depth-ranges of froth-treatment affected tailings.

Hard Bottom

The hard bottom corresponds to the development of significant effective stresses between the soil-particles. It is identified by a sharp increase in the cone penetration resistance, q_t. It can also occur with a gradual increase in q_t in old thick fines dominated deposits. The hard bottom depth corresponds to an increase in f_s from zero and the generation of transient pore pressures on the u_2 channel.

The net penetration resistance, q_t-σ_{v0}, is used to estimate the undrained vane strength $(s_u)_{fv}$ through an N_{kt} factor such that $(s_u)_{fv} = (q_t-\sigma_{v0})/N_{kt}$. A typical Nkt factor is 15, which means that the undrained strength boundary of 5 kPa would occur when the net penetration resistance exceeds 75 kPa.

Calculating the net penetration resistance requires an estimated profile of total unit weight to calculate the total vertical stress. There are many approaches available to estimate unit weights from CPTu data in natural soils, but they may not be applicable to tailings. In tailings, the total unit weight should be estimated as 9.8 kN/m^3 in the recycle water, equal to the slope of u_2 in fluid tailings, and roughly estimated as 18.3 kN/m^3 below the fluid tailings. From Equation 1, this 18.3 kN/m^3 corresponds to a solids content of 75%. This assumption can be adjusted if alternative information is available from characterized samples or empirical relationships to solids content.

Soil-Like Tailings

Soil-like tailings occur below the hard bottom depth. A soil-particle skeleton has formed and the geotechnical behaviour depends on developed effective stress. CPT responses have net-tip resistances in excess of 75 kPa, friction sleeve measurements above zero, and pore pressure measurements with transient pore pressures that will dissipate to an equilibrium value. This equilibrium value can depend on the hydrostatic pore pressure, any pore pressure flow gradients, and any excess pore pressure due to ongoing consolidation of the deposit. Tanaka and Sakagami (1989) presented PPD equilibrium values in a deposit of clay under consolidation due to the construction of a man-made island. The connected PPD points matched the excess pore pressure profile due to consolidation pressures.

The passive gamma measurements in soil-like tailings are still proportional to the total fines content. However, a smaller fraction of the gamma rays will be sourced from the sand content.

CPTu measurements in soil-like tailings can be used in geotechnical analyses for strength and stability, static liquefaction susceptibility, deformation and consolidation, and other applications.

Natural Ground

CPT results in natural soils can be interpreted using conventional data reduction techniques. Routine techniques to interpret CPTu measurements in natural soils are readily available and not within the scope of this paper.

EXAMPLE GCPTu PROFILES

Two sites were selected and interpreted to demonstrate typical GCPTu observations. These two sites both had a water cap over fluid tailings over soil-like tailings. They did not have froth-treatment affected tailings influencing the passive gamma rates.

Site 1

The GCPTu profile for Site 1 is shown in Figure 2. This test was performed to a depth of 14.7 m. The mudline was crossed at 4.3 m and the hard bottom was crossed at 9.1 m.

The water cap had zero net tip resistance, zero friction sleeve resistance, a u_2 pore water pressure that increased at 9.8 kN/m3, and essentially no gamma rates. Four fluid samples were collected and characterized in a laboratory. These samples had solids contents of 0.01%, 0.06%, 0.00%, and 6.74%. These solids contents were converted to total unit weights, γ_t, using Equation 1 and plotted in the fourth column. The calculated results agreed with the calculated slope of the measured pore water pressure. These four samples had insufficient solids contents for total fines measurements. The passive gamma rate column includes data-points for fines contents. In this plot, we assumed that these points had 100%

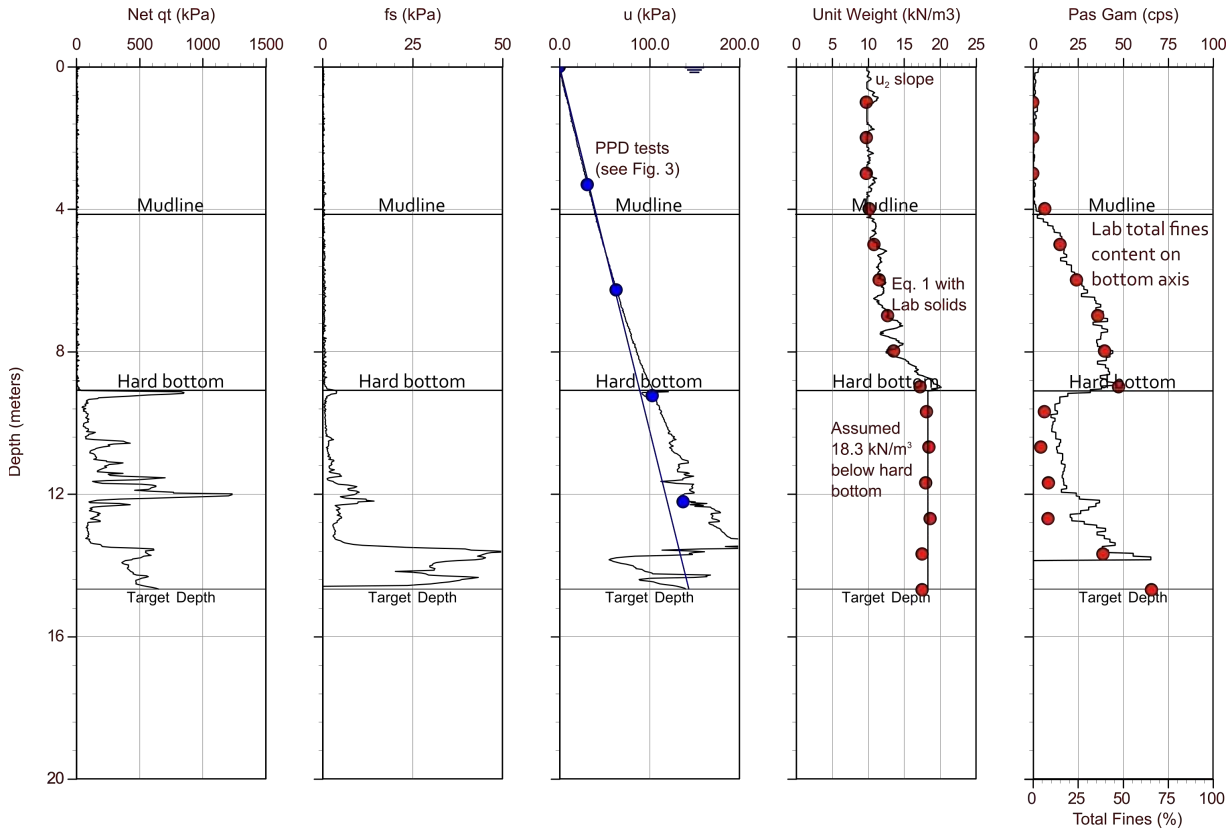

Figure 2. Site 1 GCPTu profile compared to adjacent laboratory characterized samples (red points)

geotechnical fines such that the total fines were equal to the solids content.

The mudline was crossed when the passive gamma rates first exceeded 5 cps. The fluid tailings below the mudline also had nearly zero net tip resistance and zero friction measurements. At the mudline the pore pressure measures begin to deviate from the hydrostatic profile drawn from the pond-surface. Figure 3 shows the results of a PPD test performed at 6.3 m depth. There were no excess pore pressures. The pore pressures in the fluid tailings column equal the total stress under the higher unit weight of the fluid tailings. Five fluid samples were collected and the constituents were measured in a laboratory. The measured solids contents were converted to total unit weights using Equation 1. These total unit weight points are plotted in the fourth column. This fourth column also shows the slope of the u_2 channel versus depth. The GCPTu estimated unit weight is confirmed by these laboratory points. The passive gamma measurements increase to near 40 cps in the fluid tailings. The passive gamma plot also includes points corresponds to the total fines content. As previously mentioned, by sheer coincidence the gamma ray efficiency factor for this passive gamma tool produces gamma rates that almost equal the total fines content.

The total unit weights were set equal to 18.3 kN/m3 when the local slope of the pore pressure channel became non-linear (responding to shear and cavity expansion to accommodate the cone probe). The total unit weights were used to calculate the total vertical stress and net-tip resistance.

The net-tip resistance was used to define the hard bottom depth at 9.1 m. At this depth the net-tip resistance increased from 36 kPa to 825 kPa. Two dissipation tests, also shown in Figure 3, were performed below the hard bottom. The equilibrium pore pressure is increasing at 11.4 kN/m^3 between these two points. The pore water pressure dissipated values greater than hydrostatic, which may be due to excess consolidation pore pressures in an under-consolidated soil and/or a hydraulic gradient driven ground water flow.

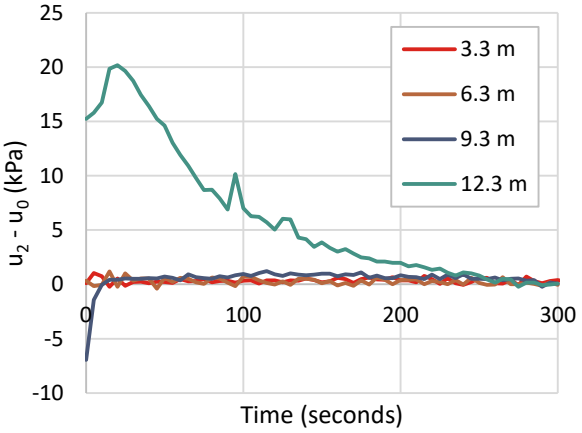

Figure 3. PPD tests performed at Site 1 showing no dissipation in recycle water (3.3 m) and fluid tailings (6.3 m) and dissipation of excess pore pressure below the hard bottom (9.1 m)

The passive gamma measurements below the hard bottom exceed the measured total fines content. Gamma rays are emitted by the sand-fraction of OST, but at a much lower intensity. In these tailings nearly 60% total sands are required to generate an equivalent gamma rate as 10% total fines.

The lab data was compared to the GCPTu interpretations. This lab data was not used in the GCPTu data reduction or interpretation.

Site 2

The GCPTu profile for Site 2 is shown in Figure 4. This test was performed to a depth of 49.0 m. The mudline was crossed at 5.9 m and the hard bottom was crossed at 14.6 m. This GCPTu was performed at a different tailings facility under a different owner than Site 1.

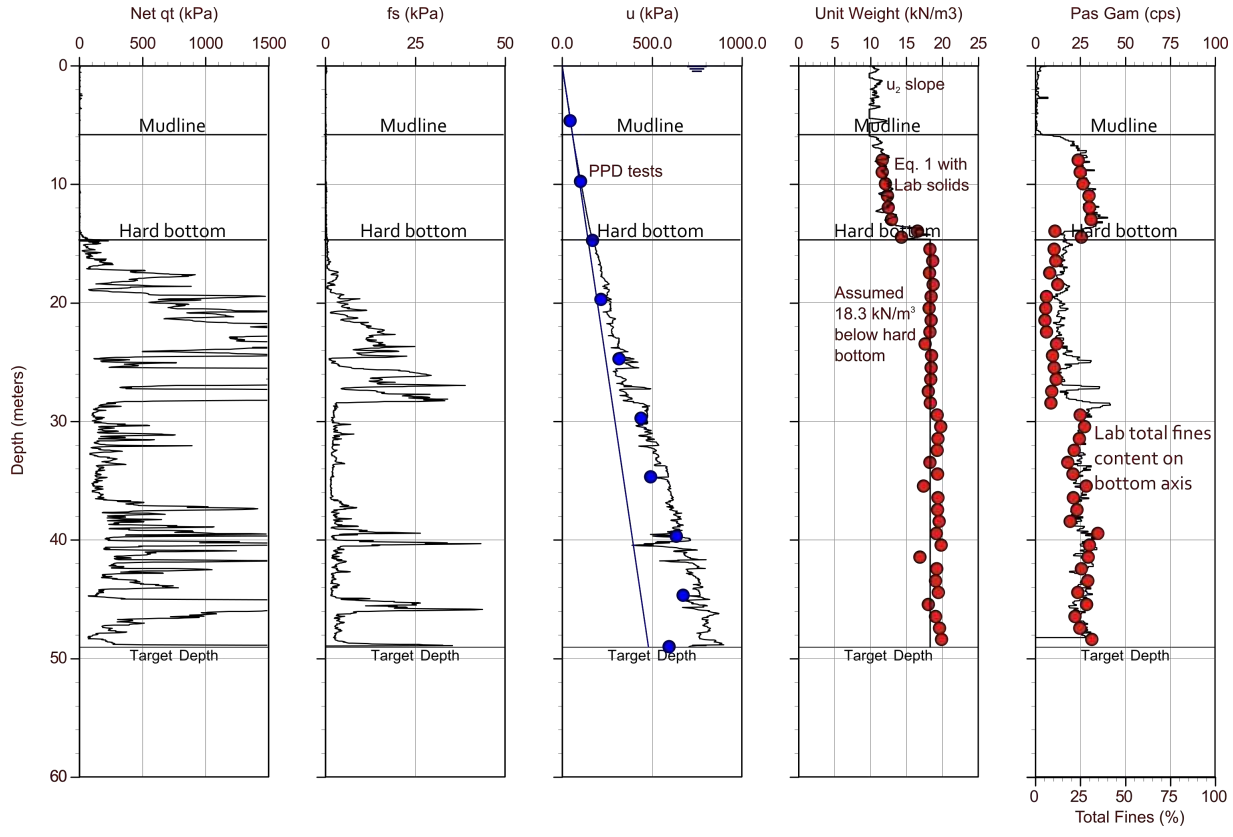

Figure 4. Site 2 GCPTu profile compared to adjacent laboratory characterized samples (red points)

The same criteria used to define the water cap, mudline, fluid tailings, hard bottom, and soil-like tailings were applied to these GCPTu results.

The fourth column includes the laboratory measured solids contents converted to unit weight estimates with Equation 1. These results matched the slope of the pore water pressure through the fluid tailings.

The soil-like tailings had two distinct zones. An upper zone was encountered between the hard bottom and 28.3 m depth. This upper zone had different q_{net}, u_2, and passive gamma measurements than the lower tailings unit below 28.3 m.

CONCLUSION

In this paper we showed that GCPTu profiles can be interpreted to estimate the solids content in fluid tailings using Equation 1. In fluid tailings the pore pressure measurements equal total stress. The increase in total stress with depth equals the total unit weight.

In this paper we showed that the passive gamma rates are proportional to the total fines contents in oil sand tailings. The passive gamma tooling used in the GCPTu probe has an efficiency factor that produces measurable gamma rates almost equal to total fines measurements. More advanced and site-specific empirical relationships can be developed, such as the Tailings Behaviour Type relationships that build upon these underlying correlations.

In this paper we showed how to determine the depth to the mudline and hard bottom from GCPTu profiles.

Two profiles were presented showing typical GCPTu measurements. These results show that the GCPTu measurements can be instructive on both the state and composition of the Oil Sand Tailings. Furthermore, expectations for typical GCPTu results can be used to identify atypical profiles.

REFERENCES

Aas, G., Lacasse, S., Lunne, T. and Hoeg, K. (1986). Use of in situ tests for foundation design on clay. Publication of the Norwegian Geotechnical Institute, **166**:1-15.

Ansah-Sam, M., Binczyk, T., Dobek, C., Geremew, A., Guo, C., Mimura, W. and Weerakone, S. (2015). Guidelines for tailings deposit sampling and measuring tools. COSIA Geostatistical and Deposit Sampling Working Group.

Berger, R. T. (1961). The X- or Gamma-Ray Energy Absorption or Transfer Coefficient: Tabulations and Discussion. Radiation Research, **15**:1-29.

Bjerrum, L. (1974). Problems of soil mechanics and construction on soft clays and structurally unstable soils. Proceedings 8th Internal Conference on Soil Mechanics and Foundation Engineering, Moscow, **3**: 111-159.

Blight, G. E. and Bentel, G. M. (1983). The behaviour of mine tailings during hydraulic deposition. Journal of the South African Institute of Mining and Metallurgy, **83**(4): 73-86.

Campanella, R. G., Gillespie, D. and Robertson, P. K. (1982). Pore pressure during cone penetration testing. 2nd Euro. Symp. on Penetration Testing, Amsterdam, Netherlands.

Consoli, N. C. and Sills, G. C. (2000). Soil formation from tailings: comparison of predictions and field measurements. Geotechnique, **50**(1).

Ellis, D. V. and Singer, J. M. (2007). Well logging for Earth Scientists. Springer.

Jeeravipoolvarn, S., Scott, J. D. and Chalaturnyk, R. J. (2009). 10 m standpipe tests on oil sands tailings: long-term experimental results and prediction. Canadian Geotechnical Journal, **46**: 875-888.

Larrson, R. (1980). Undrained shear strength instability calculation of embankments and foundations on soft clays. Canadian Geotechnical Journal, **16**(1): 591-602.

Lunne, T., Robertson, P. K. and Powell, J. J. M. (1997). Cone penetration testing in geotechnical practice. Blackie Academic and Professional Publishing.

Mayne, P. W. (2007). NCHRP Synthesis 368 on Cone Penetration Testing. Transportation Research Board, National Academies Press, Washington, D.C., 118 p.

Robertson, P. K. and Campanella, R. G. (1983a). Interpretation of Cone Penetration Tests. Part 1: Sand. Canadian Geotechnical Journal, **20**: 718-733.

Robertson, P. K. and Campanella, R. G. (1983b). Interpretation of Cone Penetration Tests. Part 2: Clay. Canadian Geotechnical Journal, **20**: 734-745.

Sills, G. (1998). Development of structure in sedimenting soils. Royal Society of London series – Mathematical, Physical, and Engineering Sciences. pp. 2515-2534.

Tanaka, Y. and Sakagami, T. (1989). Piezocone testing in underconsolidated clays. Canadian Geotechnical Journal, **26**: 563-567.

Wroth, C. P. (1984). The interpretation of in situ soil tests. Geotechnique, **34**(4): 449-489.

USING TECHNOLOGY TO BETTER UNDERSTAND SEEPAGE AT TAILINGS IMPOUNDMENTS

Ryan Blanchard and Val Kofoed
Willowstick Technologies, Draper, UT, USA

ABSTRACT

Preferential seepage flow paths often follow paleochannels, and identifying these seepage flow paths is an expensive and slow process, often characterized by drilling “trial and error” boreholes. A Geophysical technology, applied to the study area in question, along with 3D models are a cost effective and accurate way to identify the seepage flow paths. In this paper, the results from a mine located in Alaska are presented. There was contaminated water flowing from a waste rock dump into a Tailings Storage Facility (TSF). Over fifty wells were drilled in order to understand the flow paths, and a drainage collection trench was installed to divert water from flowing into the TSF. Despite these efforts, the acid rock drainage continued to infiltrate the TSF, causing regulators to get involved. Using MagnetoMetric Resistivity (MMR), Willowstick identified the exact location and depth of thirteen preferential groundwater flow paths. After comparing the locations of the flow paths to pre-mining contours, we determined the contaminated water was following paleochannels. With this information, the mine showed regulators they understood the situation and began targeted remediation.

INTRODUCTION

Preferential seepage flow paths often follow paleochannels, and identifying these seepage flow paths is an expensive and slow process, often characterized by drilling “trial and error” boreholes. Identifying the source and character of seepage is notoriously difficult and has numerous challenges. Engineers often drill several holes by simply guessing the location of the seepage and hoping to intercept water flow paths. This method is expensive and can further impair the integrity of the structure. Alternatively, the MagnetoMetric Resistivity (MMR) method can be used to identify the exact location of preferential groundwater flow paths (Jessop et al. 2018 and Kofoed et al. 2011). The method is based on the following scientific principles:

1. Subsurface water seeping through earthen materials increases the electrical conductivity of the earthen materials through which it flows. Without water, earthen materials are fundamentally electrical insulators while earthen materials saturated by subsurface water flow become excellent electrical conductors. For example, the electrical conductivity of dry earthen materials typically ranges between 10^{-12} and 10^{-17} mho/m. However, in-ground measurements of groundwater conductivity typically range from 10^{-1} to 10^{-8} mho/m—in other words many orders of magnitude higher (Purvance and Andricevic 2000).
2. Whenever an electrical circuit is established a magnetic field is also created.
3. The magnetic field emanates from the electric current. The specific characteristics of the magnetic field are determined by the Biot-Savart Law.
4. The electric current follows the preferential groundwater flow path or the path of least resistance to complete a circuit between two electrodes, which are placed strategically upstream and downstream of the area of investigation, and the water between them is energized with a low voltage, low amperage, alternating electrical current with a 380 Hz frequency.
5. Measuring magnetic field intensity is an accurate method to determine zones of highest conductivity or transport porosity of water, or water bearing zones.

The 380 Hz current creates a distinctive magnetic field that represents the location and character of the groundwater flow occurring between the electrodes (Figure 1).

This magnetic field can be measured from the surface using a Willowstick instrument (specially tuned magnetic receiver, see Figure 2). The instrument has coils in the x, y, and z direction. When an operator decides to make a measurement, the instrument simultaneously measures the magnetic field data from the three orthogonal coils, completes a Fourier Transform

on this data to identify the magnitude of the 380 Hz signal and the magnitude power line frequencies and it merges this data with the GPS data at the specific location. This data is sent to the field computer via Bluetooth. Next, the user can analyze the signal to noise ratio and GPS data and decide whether or not to save the data. Each measurement is completed in eight seconds.

The collected magnetic field data is used to render two- and three-dimensional (2D and 3D) maps and Electric Current Distribution (ECD) models of seepage paths. Through this technique, investigative teams have accurately diagnosed seepage and groundwater problems for over 300 projects in locations around the world.

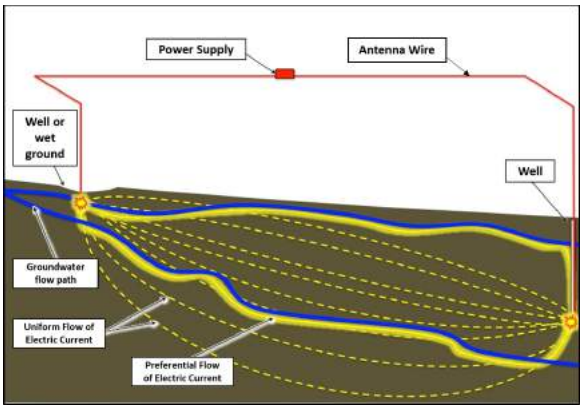

Figure 1. Typical Horizontal Dipole Configuration

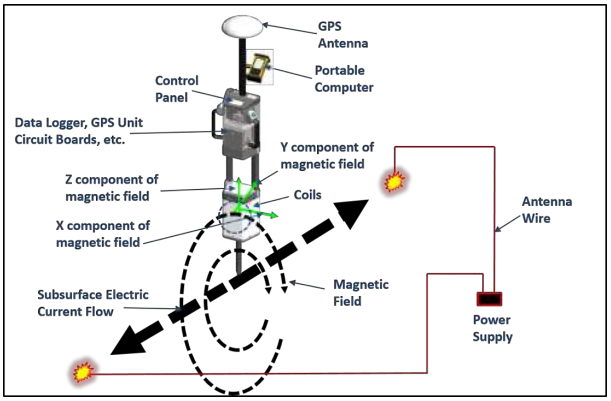

Figure 2. Willowstick Instrument (specially tuned magnetic receiver)

CASE STUDY MINE IN ALASKA

A mine located in Alaska had a waste rock dump and downgradient of it was a tailings pond. The tailings pond provides storage for tailings, waste water and drainage for the mine. Drainage through the waste rock usually has higher contaminant concentrations than the tailings water. It is preferable to collect and treat drainage from the waste rock dump before flowing into the tailings pond. Figure 3 shows a 3D view of the site. The purpose of the investigation, described in this case study, is to identify preferential drainage flow paths bypassing the waste rock dump drainage collection trench to the tailings pond. Figure 4 shows all of the individual study areas.

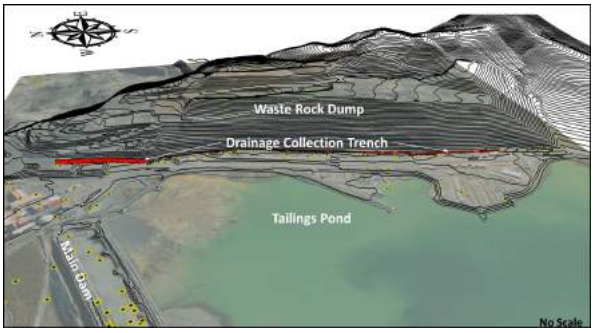

Figure 3. Topography of the survey area (looking East from above) showing the position of the drainage collection trench at the bottom of the waste rock dump

Figure 4. The investigated area is divided into 4 sub-surveys S1 to S4

The field work took about two weeks to complete. Given the length of the drainage collection trench (approximately 1900 m long), four separate survey configurations were employed to energize the different segments of the trench. For every survey an electric current is placed in the ground and the resulting magnetic field is measured using the Willowstick instruments. Figure 5 shows the survey configuration of Survey 3.

Once the field work is completed, the magnetic field is used to create a 3D ECD model. Figures 6 and 7 show slices of the ECD model in plan and profile views, repetitively. The lines in Figure 6 and the tubes in Figure 7 represent preferential flow paths of electric current that pass below the drainage collection trench.

Over fifty wells were drilled in the area of the drainage collection trench, however, the wells alone couldn't provide an explanation of where water bypassed the trench. Figure 8 shows a summary of the investigation. Thirteen preferential flow paths of electric current were identified which were caused by groundwater passing beneath the drainage collection trench. The contours shown in Figure 8 are the pre-mining elevation contours. After comparing the locations of the flow paths to pre-mining contours, we determined the contaminated water was following paleochannels. With this information, the mine showed regulators they understood the situation and began targeted remediation.

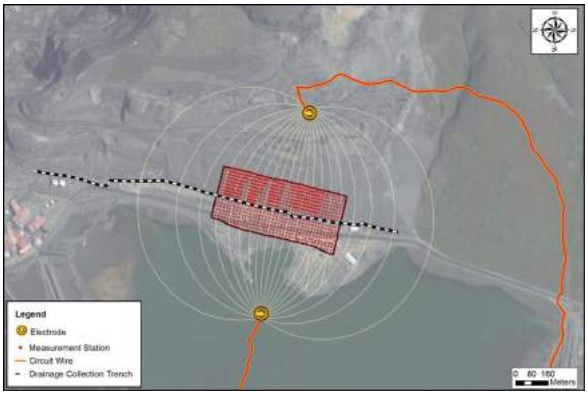

Figure 5. Survey 3 survey configuration with 908 measurement stations

CONCLUSION

The MMR method can be used to identify the exact location of preferential groundwater flow paths without the need to drill "trial and error" boreholes. This method was used at a mine in Alaska to successfully identify water bypassing a drainage collection trench between a waste rock dump and tailings pond. This allowed the mine to show regulators they understood the situation and

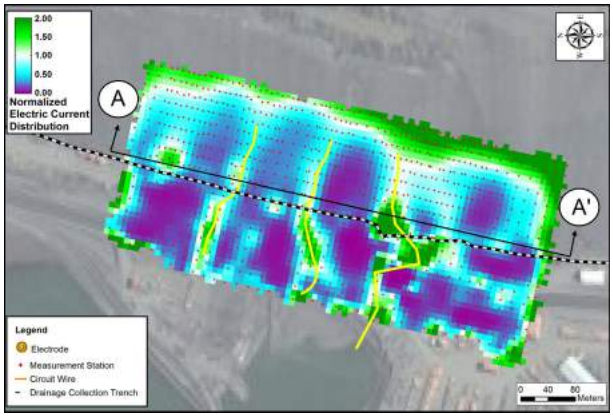

Figure 6. Plan view of Survey 3's ECD model slice

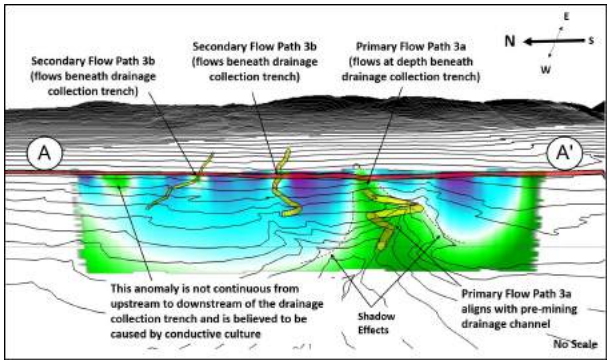

Figure 7. Profile view of Survey 3's ECD model slice

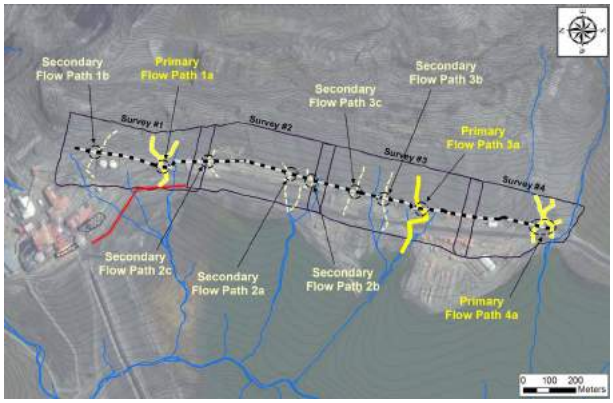

Figure 8. Summary of the investigation.

begin targeted remediation, saving the mine a significant amount of time and money.

REFERENCES

Jessop, M. L., Jardani, A., Revil, A. and Kofoed, V. O. (2018). Magnetometric resistivity: a new approach and its application to the detection of preferential flow paths in mine waste rock dumps. Geophysical Journal International, **215**(1): 222-239.

Kofoed, V. O., Jessop, M. L., Wallace, M. J. and Qian, W. (2011). Unique applications of MMR to track preferential groundwater flow paths in dams, mines, environmental sites and leach fields. International Society of Applied Geophysics, Society of Exploration Geophysicists, The Leading Edge, Special Session: Near Surface Geophysics, **30**: 2.

Purvance, D. T. and Andricevic, R. (2000). On the electrical-hydraulic conductivity correlation in aquifers. Water Resources Research, **36**: 2905-2913.

Session 5

IMPLICATIONS OF TAILINGS TREATMENT

EVIDENCE OF CREEP & STRUCTURATION IN POLYMER AMENDED OIL SANDS TAILINGS

Muhammad Asif Salam, Paul H. Simms and Banu Örmeci
Carleton University, Ottawa, Canada

ABSTRACT

The void ratio-effective stress relationship and the hydraulic conductivity-void ratio relationship are the two most important properties that govern the consolidation characteristics of the oil sands tailings. However, there are other important factors such as creep and thixotropy /structuration, which may affect tailings consolidation behaviour in certain fines dominated. Creep is any change in volume that occurs independent of effective stress changes. Whereas, thixotropy is the time-dependent reorganization of the particles due to the electrochemical forces. Like creep, thixotropy may induce a volume change, but also may manifest as an increase in strength or stiffness (structuration) at constant water content and volume. To investigate the creep and thixotropy in fluid fine tailings treated with the polymer, an experimental study was undertaken using small 10 cm high columns under saturated for several months. Tailings exhibhited large decreases in volume nto associated with changes in effective stress. Tailings also exhibited a time-dependent 'structuration' behaviour, an increase in pre-consolidation pressure over time as determined from oedometer tests.

INTRODUCTION

Some of the advanced tailings treatment technologies, such as in-line flocculation, tank thickening, and centrifugation technique, use polymers to promote flocculation for faster dewatering. Field trials have shown that the application of polymers allow such technologies to increase solids concentration to at least 50% in short-term, usually within days (Matthews et al. 2011, Wells 2011). However, to meet the regulatory standards and to develop a deposit safe and strong enough for reclamation, it is thought that a solids concentration of at least 70% (a gravimetric water content of 43%) is required, which is close to the plastic limit of the material (McKenna et al. 2016). In order to take the tailings deposits to such state, it is an imperative to optimize the tailings deposition and management plans and methods, which again depends on attaining a comprehensive understanding of longer-term dewatering processes such as consolidation and potentially others, such as creep (Salam et al. 2018).

Creep and Thixotropy / Structuration in Oil Sands Tailings

The consolidation of tailings involves the slow settlement of the fine-grained tailings material along with the release of excess pore water pressure and the development of an effective stress within the tailings deposits in response to the self-weight or vertical surcharge from a capping layer (BGC Engineering Inc. 2010). Although void ratio-effective stress relationship and hydraulic conductivity-void ratio relationship are the two most important properties that govern the consolidation behaviour of FFT, creep and thixotropic behaviour of tailings also have been found to influence the consolidation behaviour significantly (Jeeravipoolvarn 2005, Jeeravipoolvarn et al. 2009, Miller 2010).

Creep refers to any change that takes place in volume over time and is independent of changes in effective stress. During creep, the viscous resistance of the soil structure governs the rate at which the soil deforms with time (Sorensen 2006). Such viscous deformation manifests as a time-dependent compressibility curve, and several models in the literature have quantitatively reproduced this effect (e.g., Yin and Graham 1994). Lab-scale experiments conducted over a larger time-scale (e.g., 10-meter standpipe tests conducted at the University of Alberta) showed that a creep compression could take place in tailings deposits over time at a constant effective stress and contribute to the settlement (Jeeravipoolvarn 2005, Jeeravipoolvarn et al. 2009), though this result is somewhat controversial.

Thixotropy refers to a time-dependent reorganization of the fine clay particles due to the electrochemical forces (Mitchell 1960). Skempton

and Northey (1952) attributed the thixotropic effect in the soil to the gradual rearrangement of the particles under the influence of bonding forces and suggested that thixotropy increases mechanical stability. The effects of thixotropy are most evident in the time-dependent strength recovery of clays after remolding at constant density, which has been observed and measured by several researchers in oil sands tailings as well (Jeeravipoolvam 2005, Jeeravipoolvarn et al. 2009). The thixotropic effect has also been found to affect the tailings consolidation behaviour. Typically, due to the very slow dissipation of excess pore water pressure, effective stresses that develop in the tailings ponds are of very low magnitudes. However, at such low effective stresses, the thixotropic behaviour of the tailings material contribute to the development of an over-consolidated structure that affects the rate and magnitude of initial self-weight consolidation (Miller 2010). That's why, the poor dewatering behaviour and the very low rate of consolidation of the FFT are often, in part, attributed to the thixotropic behaviour of tailings (Scott et al. 2013).

Creep and Thixotropy in Clays

The creep and thixotropic behaviour demonstrated by the tailings material have also been observed in many natural clays. Such clays exhibit a time-dependent behaviour called 'structuration', which is typically manifested in a change in the soil microstructure, and an associated increase in apparent pre-consolidation pressure over time. Inherent ageing effects such as thixotropy, inter-particle bonding, and cementation, and viscous effects such as creep have been identified as the processes responsible for such microstructural changes and the subsequent strength development (Burland 1990, Locat and Lefebvre 1986, Sorensen 2006).

Several studies of the effects of structuration on the consolidation behaviour of natural clays have been reported in the literature. Delage et al. (2006) investigated the time-dependent ageing effects in compacted bentonite clay at a constant water content and density by using the mercury intrusion pore size distribution measurements and scanning electron microscopy (SEM) performed on freeze-dried samples. When they compared two SEM images from a clay sample (generated after 1 day and 90 days respectively), they observed significant changes in clay microstructure with time. The appearance has changed, with fewer inter-aggregate pores, and a less clear definition of the individual clay particles, and overall, a more homogeneous aspect (Delage et al. 2006).

Studies of compressibility and shear strength of natural clays revealed that a comparison between the compressibility of the intact and the remolded samples could help in determining the influence of changes in clay microstructure on its compressibility and strength characteristics (Burland 1990, Delage 2010, Locat and Lefebvre 1985). Delage (2010) studied the combined effects of changes in the arrangement of the particles and the inter-particle bonding on the compressibility of the Champlain clay. Delage made a comparison between the one-dimensional compression curves of three intact samples and a remolded sample. He correlated the changes in compressibility to the changes in soil fabric (arrangement of particles) and attributed increased pre-consolidation pressure (yield strength) in the intact samples to the strong inter-particle bonding (Delage 2010). Several researchers reported the phenomenon of structuration in clays based on their findings from the long-term oedometer tests. They observed a significant increase in pre-consolidation pressure, which was thought to be due to the development of bonds between the particles (an ageing effect or thixotropy) that took place over time during the secondary compression or creep (Leonards and Altshaeffl 1964, Leroueil et al. 1996).

The present paper aims to investigate the extent of creep and thixotropic effects in polymer amended tailings from an experimental perspective. The experiments included a combination of long-term column dewatering tests with pore water pressure measurements, advanced rheological tests, fall cone tests, mercury intrusion porosimetry, low/high vacuum SEM, optical microscopy, and oedometer tests. Both consolidation and non-consolidation volume change behaviour of tailings were characterized under the saturated conditions. The implications of creep and thixotropy for the longer-term dewatering and consolidation performance of the polymer amended tailings deposits were discussed based on the findings from the tests. Some of the tests results (partially) were presented before in a paper submitted to the proceedings of the GeoEdmonton 2018 Conference (Salam et al. 2018). However, in this paper, all the results are presented and discussed in totality.

MATERIALS

Oil Sands Tailings

Oil sands tailings samples were collected from a tailings pond in Northern Alberta, Canada, and shipped to Carleton University in Ottawa, Canada. Different laboratory tests and analyses were performed to determine the physical, mineralogical, and chemical characteristics of the raw fluid fine tailings. The initial solids content was 31% and the liquid limit was 60%. The sands to fine ratio (SFR) was 0.25. The clay content obtained from the Methylene Blue Index (MBI) analysis ranged from 28% to 32%. According to the X-ray diffraction (XRD) results, the composition of the clay fraction was 68-72%% Kaolinite and 28-32% Illite. Total Dissolved Solids (TDS) in the pore water collected from the raw fluid fine tailings was 1050 mg/L, electrical conductivity was 1590 micro-S/cm, while the dominant cations were sodium at 340 mg/L. Typical material characteristics of the tailings used are listed in Table 1.

Table 1. Tailings properties

Parameters	Average value
Initial solids content (%)	31
Initial water content (%)	220
Hydrocarbons (%)	1.4
Initial wet density (g/cm^3)	1.20
Initial void ratio	5.1
Specific gravity	2.12
Liquid limit (%)	60.0
Plastic limit (%)	27.0
Plasticity index (%)	33.0

Polymer Stock Solution

An anionic polyamide-based polymer (A3338) was used to prepare the polymer amended oil sands tailings samples. In a plastic weighing dish, 4 g of A3338 polymer (for the preparation of 0.4% polymer stock solution) was weighed using an analytical balance (Fisher Scientific, Sartorius AG Germany, LE225D) and decanted into a 1500 mL glass beaker and completed to 1000 mL with deionized water. The polymer solutions were stirred using a jar tester (Phipps and Bird, USA) at 200 rpm for 5 minutes and at 125 rpm for the following 55 minutes. Then the polymer solution was mixed with a hand blender for 10 seconds and left for maturation for 1 hour.

To prepare the polymer amended tailings, a pre-determined volume of the polymer solution was mixed with the FFT in a 10-liter pail using a mixer set at 250 rpm and the mixer ran for 20 seconds. Both the mixing speed and the duration were kept at optimal points for dewatering, which were determined based on the findings from a combination of CST tests and settlement tests.

METHODS

10 cm tall column experiments were conducted using two (2) different boundary conditions: Single-drainage and double-drainage (Figure 1). The short height was chosen to maximize the influence of creep. Typically, a short column height leads to the development of a low effective stress within the deposited tailings material, and the creep is thought to be one of the main mechanisms behind the deformations that occur at lower effective stresses (Miller 2010).

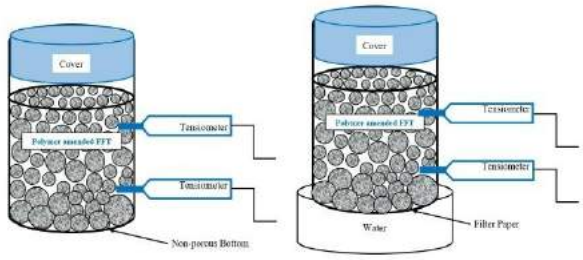

Figure 1. A schematic diagram of the (left) single-drainage and (right) double-drainage column experiments

In single-drainage column experiment, a single lift of polymer amended fluid fine tailings (dosed with 800 ppm of anionic polymer) was deposited in two 14 cm diameter transparent plastic acrylic columns with the material reaching a height of 10 cm inside the columns. Two (2) tensiometers (model T5 from UMS) were installed into one of the columns (at the elevations of 1.5 cm and 4.5 cm respectively) to monitor both positive and negative pore water pressures. The columns were kept covered at the top with the help of a tight lid. The space between the lid and the surface of the deposited tailings was closed to prevent the escape of water vapor.

Like single-drainage column experiment, a single lift of polymer amended FFT (dosed with 800 ppm of anionic polymer) was deposited in two 14 cm

diameter transparent plastic acrylic columns in the case of the double-drainage column experiment. One of the columns was equipped with two (2) tensiometers at the same elevations as the single-drainage column (1.5 cm and 4.5 cm respectively). The only difference between the single-drainage and the double-drainage is that the non-porous bottom in single-drainage columns didn't allow for any drainage, whereas, the tailings in double-drainage columns was rested on a filter paper that allowed for drainage. In both drainage systems, a set of replicate columns was used for measuring the water content at different depths, the changes in water-solids interface height and void ratio, and for providing samples for other tests and analyses.

Additionally, a large transparent plastic column (Dimensions: 17 cm X 22 cm X 50 cm) was used for the dewatering test (Figure 2). FFT mixed with 800 ppm of anionic polymer was deposited in that column. The column was equipped with three (3) T5 tensiometers at three different elevations (5 cm, 15 cm, and 25 cm respectively) for the measurements of pore water pressure. The test was conducted to see whether the phenomena of creep and thixotropy could be observed when the test is conducted on a larger scale.

Figure 2. Column dewatering tests (different boundary conditions and scales)

Advanced rheological tests were performed to examine the mechanical response of the samples to the small-strain shear. The changes in viscoelastic properties were tracked using the Amplitude sweep tests. First, the sample was placed in a cylindrical sample holder in the rheometer (an Anton Paar Physica MCR301 model rheometer with a vane fixture). The vane fixture was then lowered into the sample, and oscillated at a constant frequency, but at increasing maximum values of stress. This allowed for the determination of the elastic modulus, the linear elastic region, the viscous modulus, and the yield stress. A combination of tests was used to measure the recovery of the elastic modulus after shearing.

A fall cone device was used for measuring the changes in the strength of polymer amended FFT based on the measurements of cone penetration.

For both single-drainage and double-drainage systems, the scanning electron microscopy (SEM) images were generated using the samples collected from replicate columns. A Tescan Vega-II XMU SEM device was used for the image analysis. Using the cryo-techniques, the samples were frozen at temperatures less than 173 K and then imaged under low vacuum pressure (50 Pa). SEM images helped to observe the changes in size, shape, and arrangement of the flocs with time. The mercury intrusion porosimetry (MIP) technique was applied to the freeze-dried samples for the pore size distribution measurements. The same samples were used for generating SEM images.

Oedometer tests were performed on the samples collected from the replicate columns to determine their void ratio-effective stress relationships and to track the changes in compressibility. Both undisturbed and remolded samples were tested.

RESULTS AND DISCUSSIONS

Pore Water Pressure and Water Content

In the single-drainage column, the pore water pressure declined rapidly after the deposition. Afterward, the pore water pressure became steady and remained almost at the same values for the first four (4) weeks. Then, the pressure started to decline, but at a very slow rate (Figure 3). To the contrary, the tailings underwent volume change throughout the experiment with the gravimetric water content declining from 245% to 98%.

Water content was measured at an interval of 1 cm throughout the depth of the solids settled in the replicate column. Figure 4 shows the water contents measured at the top, bottom, and middle.

Figure 5 shows how the water content changed at the same elevation with time when there was very little dissipation of excess pore water pressure.

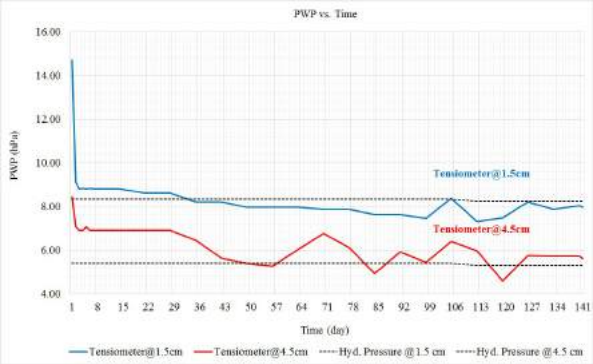

Figure 3. Pore water pressure (in hPa) at 1.5 cm and 4.5 cm (single-drainage)

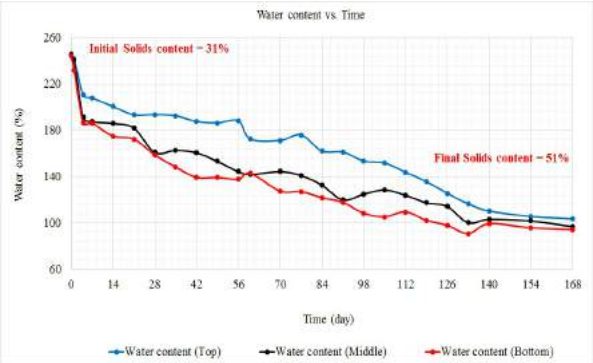

Figure 4. Water contents measured at different heights (single-drainage)

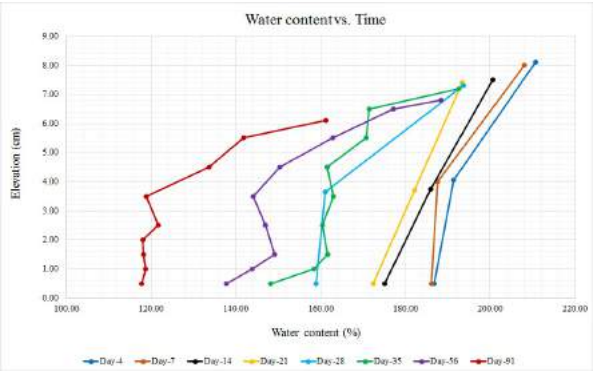

Figure 5. Changes in water content at the same elevation (Single-drainage)

In the double-drainage column, the pore water pressure declined rapidly immediately after the deposition; afterward, it remained almost at the same values for the first two (2) weeks and then started to decline gradually (Figure 6).

During the same period, the dewatering and the volume change experienced by the FFT was

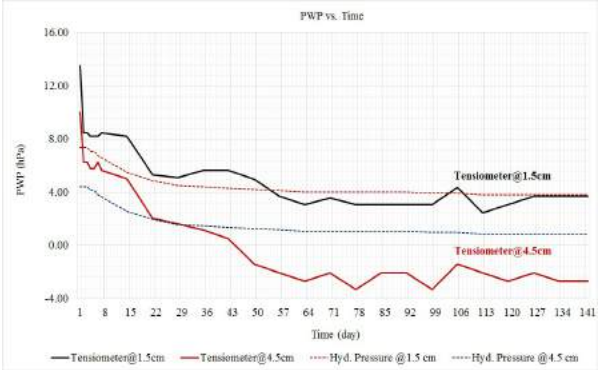

Figure 6. Pore water pressure (in hPa) at 1.5 cm and 4.5 cm (double-drainage)

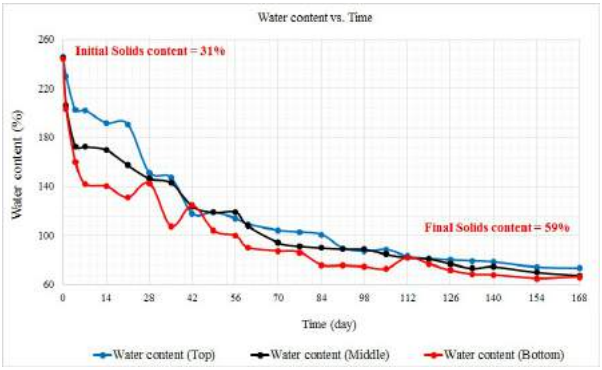

Figure 7. Water contents measured at different heights (double-drainage)

substantial as well as uniform. The water content declined to 70% from the initial water content of 245%. Figure 7 shows the water content measured at the top, bottom, and middle of the solids settled.

In both drainage systems, it was anticipated that the decline in gravimetric water content would diminish with the pore water pressure dissipation becoming negligible. However, something different was observed in these experiments. Especially, in the double-drainage columns, where the substantial and uniform reduction in water content was quite remarkable, which indicated that some processes or mechanisms other than consolidation (such as creep) contributed to this volume change.

The magnitudes of both initial consolidation and the subsequent creep compression in single-drainage columns were not so much as in the double-drainage columns. Different boundary conditions resulted in different rates and magnitudes of settlement. Although the effective stress in the double-drainage samples was slightly

larger (1.2 kPa at the bottom in double-drainage column compared to 0.2 kPa in single-drainage) due to the imposed boundary conditions, samples were subjected to the same effective stress.

Large Column

The pore water pressure measurements showed a steady decline with time for the first five (5) weeks since deposition. During the same period, there was a considerable settlement as the solids settled to a height of 21 cm from the initial height of 35 cm. Besides consolidation, other non-consolidation behaviour (such as creep, sedimentation, etc.) could have contributed to such volume change. Afterward, the pore water pressure declined very little, but the solids still continued to settle, which could be due to the creep (Figure 8 and 9).

Oscillatory Rheometry

Figure 10 and 11 illustrate the results of the Amplitude sweep tests performed on the samples. The x-axis (stress in Pa) denotes the maximum stress during a given oscillation. The maximum stress is successively increased with each oscillation. The resulting deformation in the tailings materials was estimated and expressed in terms of the elastic modulus (G') and viscous modulus (G").

The results from the Amplitude sweep tests demonstrated the changes in a linear elastic range in response to the stresses applied. Such changes are correlated to the changes in material structure since the elastic modulus is strongly dependent on the fabric (Mizani et al. 2017). The region where the elastic modulus is relatively constant represents the true elastic range of the tailings material and the point where G' reduces and G" becomes dominant represents the yield stress.

In the single-drainage columns (Figure 10 and 11), after 84 days, there was a slight increase in the linear elastic region. However, there were considerable increases in elastic modulus (increased to 1250 Pa from 270 Pa) and yield stress (from 150 Pa to 220 Pa). In literature, such

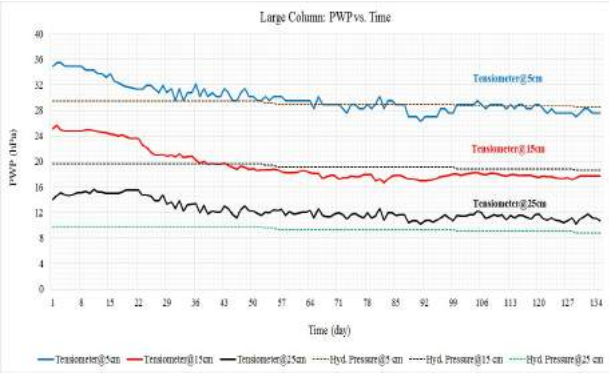

Figure 8. Pore water pressure (in hPa) at 5, 15, and 25 cm of the large column

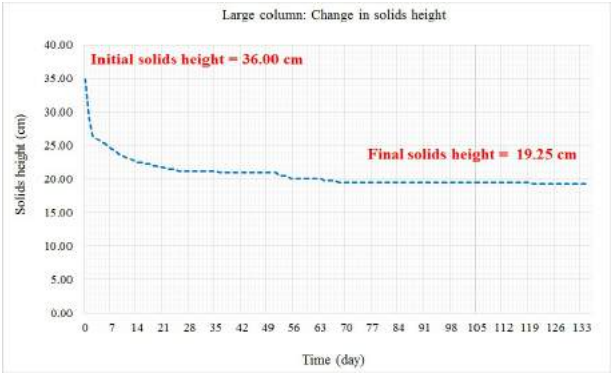

Figure 9. Change in large column solids height

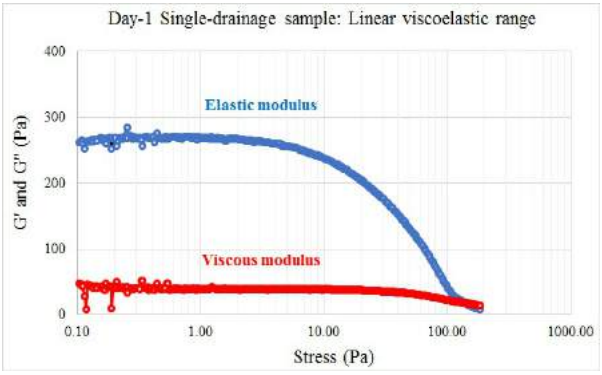

Figure 10. The linear elastic region at 10 rad/s (single-drainage 1-day sample)

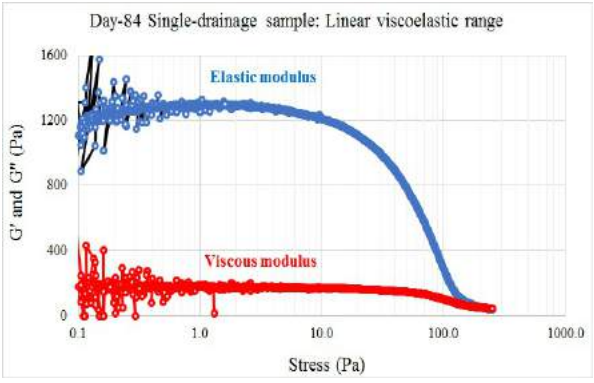

Figure 11. The linear elastic region at 10 rad/s (single-drainage 84-day sample)

an exceptional increase in elastic modulus (with respect to the reduction in void ratio) has been attributed to the structuration effects (such as inter-particle bonding) (Lohani et al. 2001).

A combination of Amplitude sweep tests and Stress growth tests was used to measure the recovery of elastic modulus after the sample had been sheared at a constant strain rate of $0.1s^{-1}$. Figure 12 shows the recovery of G' for the 105-day double-drainage sample immediately after the shearing, and after 30, 60, 120, and 180 minutes of shearing. With time, the percentage of recovery increased. Figure 13 shows how the sample was sheared, and the elastic modulus was measured at specific time intervals, and how the sample recovered most of its pre-shear elastic modulus with time. Such a recovery or strength gain with time was an indication of ageing effects in tailings.

Fall Cone Test

Fall cone test is a commonly used alternative to the Casagrande method for measuring the Atterberg limits. The test can also be used for measuring the undrained shear strength of clays in both undisturbed and remolded conditions. According to Hansbo (1957), when a cone of mass 'm' penetrates a distance 'd' into a clay, the undrained shear strength 's_u' can be expressed by the following equation (Cabalar & Mustafa 2015):

$$s_u = k\frac{mg}{d^2}$$

Where:
s_u = undrained shear strength (in kPa)
k = constant [~1.0 for undisturbed clays (Hansbo 1957); ~0.85 for remolded clays (Wood 1985)]
m = mass of the cone (in gram)
g = gravitational acceleration (9.81 m/s^2)
d = The depth of penetration of the cone in the sample (in mm)

Undrained shear strengths were estimated for both single-drainage and double-drainage replicate columns. Also, the undrained shear strengths of the remolded samples were measured at the same water content. When natural clays are remolded, they lose a portion of their undrained shear strength due to the destruction of the soil structure developed earlier. The sensitivity of a natural clay can be determined by comparing its undrained shear strength in the undisturbed state to its undrained shear strength in the remolded state at the same water content (Sorenson 2006). There are several ways of assessing the degree of soil structure in clays; however, the sensitivity measurement is the most commonly used method among them (Sorenson 2006). Terzaghi (1944) defined the sensitivity (S_t) as (Abuhajar et al. 2010):

$$St = \frac{S_u \text{ Undrained shear strength (undisturbed)}}{S_{ur} \text{ Undrained shear strength (remoulded)}}$$

The sensitivity of the tailings was measured for both single and double-drainage columns at the initial stage of the experiment and plotted against the void ratios (Figure 14). The double-drainage samples showed relatively higher values of sensitivity indicating that double-drainage samples went through more thixotropic hardening. Also, the sensitivity declined at a slower rate in the double-drainage in comparison to the single-drainage.

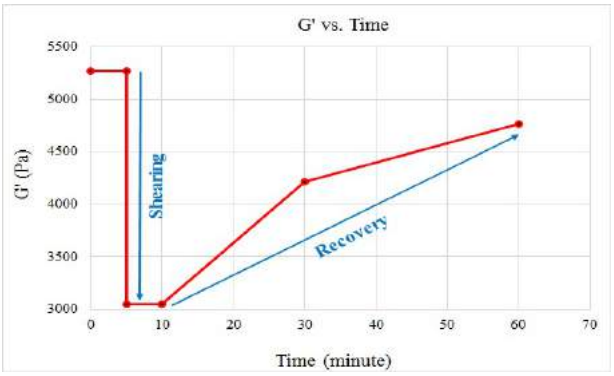

Figure 13. Thixotropic recovery of structure (Double-drainage 105-day sample)

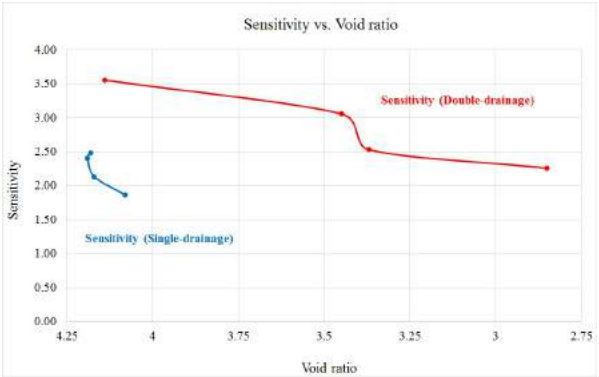

Figure 14. Sensitivity measurements

Oedometer Tests

In the single-drainage experiment, 56-day, 84-day, 112-day, and 168-day samples were used for the oedometer tests, whereas, in the double-drainage experiment, oedometer tests were performed on the 28-day, 42-day, and 70-day samples. The compressibility curves for the 28-day and 42-day double-drainage samples are shown in Figure 15. The 42-day sample was found considerably stiffer in comparison to the 28-day sample. Although there were changes in compressibility with time in both drainage systems, these changes were prominent in the double-drainage samples in comparison to the single-drainage (most possibly, due to the more prominent ageing effects in double-drainage samples, which also have been observed in the rheometry and fall cone tests).

In order to investigate how these changes in compressibility affect the accuracy of final settlement prediction for the tailings deposits, a simple numerical analysis was performed based on Qi's analytical functions for final height estimation (Qi et al. 2018):

$$\text{Final height} = z + \frac{az[z(\gamma_s - \gamma_w)]^b}{b+1}$$

$$\text{Where, } z = \frac{Initial\ height}{Initial\ void\ ratio\ (e_0) + 1}$$

Constants a and b can be estimated by fitting the compressibility curves with a power function:

$$e = a(\sigma')^b$$

Where e and σ' are void ratio and effective stress, respectively. γ_s and γ_w represent the unit weight of solids and water, respectively.

By fitting the compressibility curves (28-day and 42-day) obtained from the oedometer tests with power functions and using Shunchao's equation, as shown above, the final settlements for a 50-meter tailings deposit were calculated (21.12 meter and 22.38 meter, respectively). Evidently, the reduced compressibility and the increased pre-consolidation pressure resulted in different final settlements for the same tailings deposits.

Figure 16 shows the final density profiles predicted on the basis of 28-day and 42-day compressibility curves.

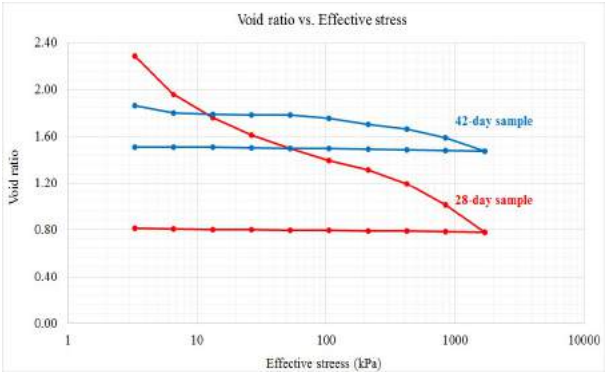

Figure 15. Compressibility curves (28-day and 42-day double-drainage samples)

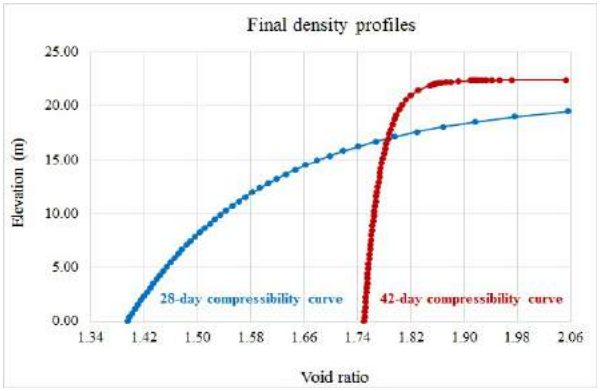

Figure 16. Final density profiles from the compressibility curves

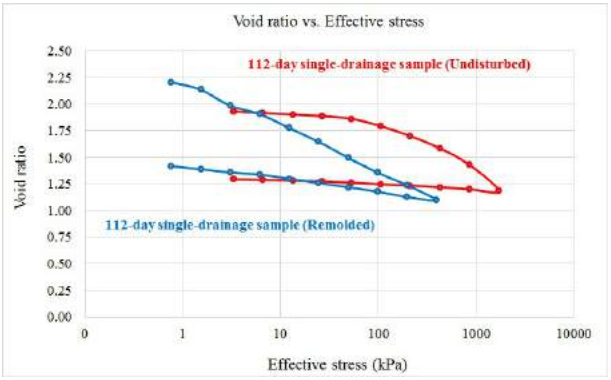

Figure 17. Compressibility from the 112-day single-drainage samples (both undisturbed and remolded)

Oedometer tests were also performed on both undisturbed and remolded samples for the 84-day and 112-day single-drainage and 70-day double-drainage columns. Figure 17 shows the compressibility curves for the 112-day undisturbed and remolded single-drainage samples. Since the

remolded sample went through some 'destructuring', there were changes in its fabric and the inter-particle bonds became weaker. Therefore, the remolded sample demonstrated less resistance to the compaction.

Scanning Electron Microscopy (SEM)

SEM images from the double-drainage column experiment are shown in Figure 18. The samples became relatively less porous as the flocs appeared to grow with time. Overall, the appearance became more compact and homogeneous. Although the single-drainage SEM images displayed the same trend, the changes were not so pronounced as they were in the double-drainage samples. Figure 19 shows the SEM images generated from the freeze-dried samples (prepared from the single-drainage replicate columns). The trend shown by these SEM images is similar to SEM images from the wet samples.

SUMMARY

Overall, the tests results demonstrated that there was considerable deformation after the initial sedimentation and primary consolidation as well as significant strength buildup with time. The pore water pressure and water content profiles showed that there was a considerable dewatering even when the excess pore water pressure dissipation was very negligible. The gravimetric water content declined uniformly throughout the experiment.

The undrained shear strength measurements from the fall cone tests showed that there was a continuous buildup of strength in the initial stages. Also, the degree of structure formation measured in terms of sensitivity showed that a structure was building up and gaining strength with time.

The measurements of elastic modulus from the Amplitude sweep tests indicated that the material increased in strength with time. Since thixotropy is a time-dependent effect, time plays an important role in this thixotropic strength gain. The measurements of recovery of elastic modulus immediately after the shearing and later showed that the material regained its pre-shear strength with time. Such a recovery of elastic modulus (an increase in material strength) explains the ageing effects in tailings, which is due to the thixotropy.

From the microstructural perspective, a qualitative analysis of the SEM images helped to track the changes in tailings fabric with time, which also corroborated the findings from other tests. As the samples became less porous and more compact and homogenous, there were associated changes in macrostructural behaviour: increased yield strength and reduced compressibility.

The changes in the compressibility curves, which were observed during the oedometer tests, indicated that there was a structuration effect taking place leading to an increased pre-consolidation pressure. The aged tailings samples showed considerable stiffness in response to the compression, especially, at relatively low stress levels. The initial flattening of the compressibility curves at low effective stresses could be due to the development of thixotropic strength, which gave the tailings an over-consolidation effect (also suggested by Miller, 2010). This strength buildup was also evident in the results from the fall cone and rheological tests, whereas, the subsequent change in compressibility behaviour (resistance to the compression) was observed during the oedometer tests. Different estimations of final settlement showed how this variation could affect the accuracy of the prediction made by the models.

Since tailings show a delayed compression (creep) and ageing effects with time (thixotropy), a single compressibility relationship would not be adequate to represent the complete consolidation characteristics of a tailings deposit over time and also to predict the final settlement with accuracy. Therefore, instead of using a single compressibility relationship with the large strain consolidation modeling, it would be a more realistic approach to use a set of similar curves that represent the tailings settlement behaviour over a longer-term (also suggested by Jeeravipoolvarn 2005). Such a development would help the oil sands industry in optimizing the dewatering and consolidation efficiency of the tailings treatment technologies and to meet the regulation standards.

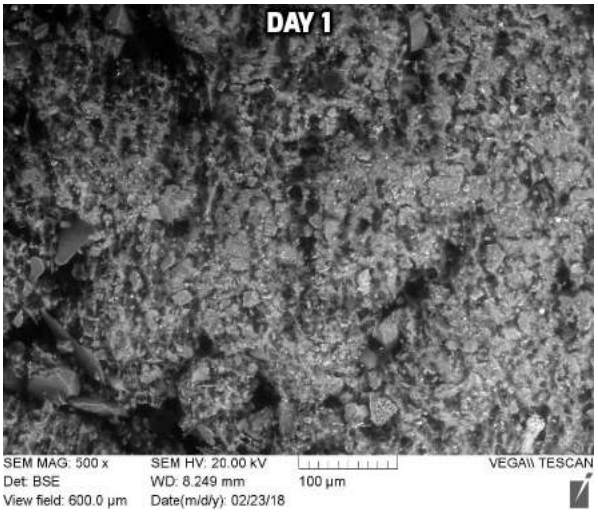

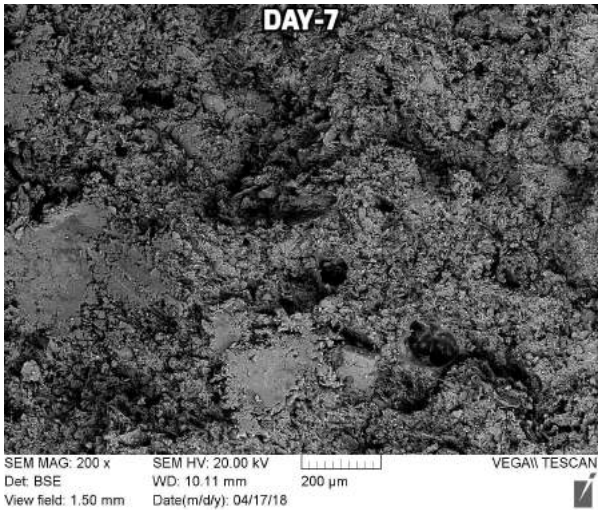

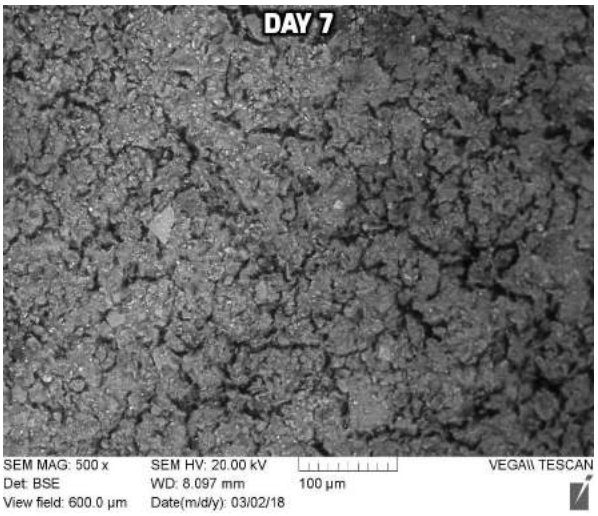

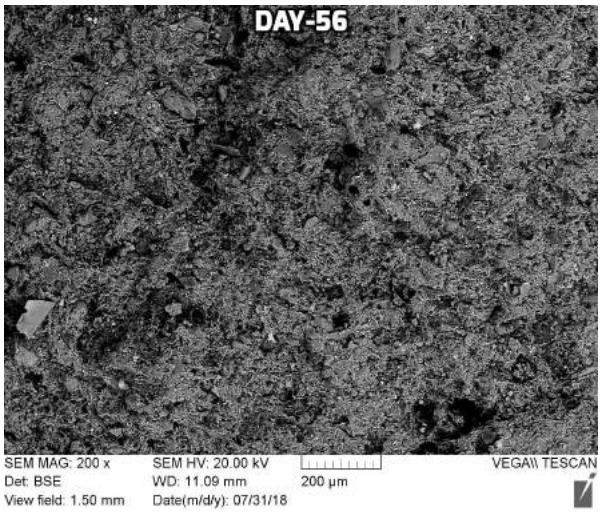

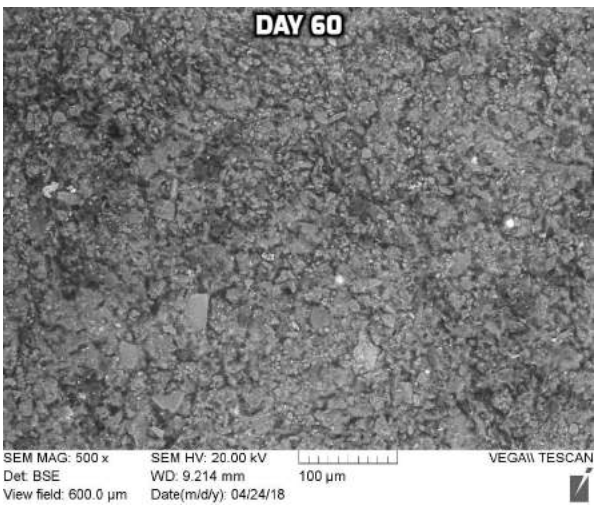

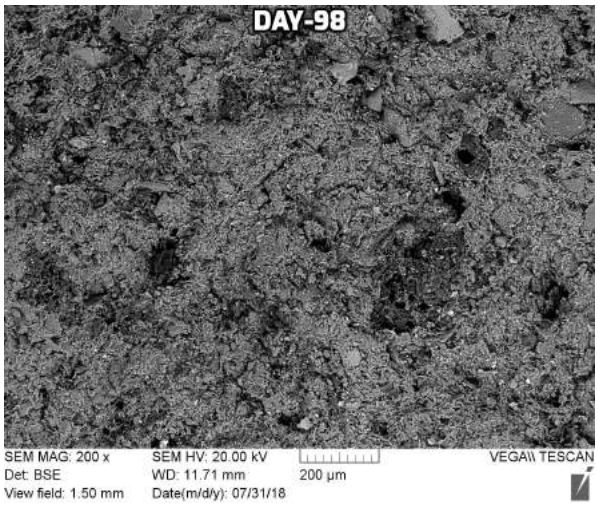

Figure 18. SEM images from the 1, 7, and 60-day double-drainage samples (500X magnified)

Figure 19. SEM images from the 7, 56, and 90-day freeze-dried single-drainage samples (200X magnified)

ACKNOWLEDGEMENTS

This study was funded through NSERC Grant 429272–11 held by the second author and sponsored by the Canada's Oil Sands Innovation Alliance (COSIA).

REFERENCES

Abuhajar, O., El Naggar, M. H. and Newson, T. (2010). Review of Available Methods for Evaluation of Soil Sensitivity for Seismic Design.

Alberta Energy Regulator. (2018). Directive 085: Fluid tailings management for oil sands mining projects. Retrieved from the website: https://www.aer.ca/regulating-development/rules-and-directives/directives/directive-085

Beier, N., Wilson, G. W., Dunmola, A. and Sego, D. (2013). Impact of flocculation-based dewatering on the shear strength of oil sands fine tailings. Canandian Geotechnical Journal, **50**(9): 1001-1007.

BGC Engineering Inc. (2010). Oil sands tailings technology review. Oil Sands Research and Information Network, University of Alberta, School of Energy and the Environment, Edmonton, Alberta. OSRIN Report No. TR-1. 136 pp.

Burland, J. B. (1990). On the compressibility and shear strength of natural clays. Géotechnique, **40**(3): 329-378.

Çabalar, A. F. and Mustafa, W. S. (2015). Fall cone tests on clay–sand mixtures. Engineering Geology, **192**:154-165.

Canadian Association of Petroleum Producers (CAPP). (2018). Canada's oil sands. Retrieved September 2018 from the website: www.canadasoilsands.ca

Delage, P. (2010). A microstructure approach to the sensitivity and compressibility of some Eastern Canada sensitive clays. Géotechnique, **60**(5): 353-368.

Delage, P., Marcial, D., Cui, Y. J. and Ruiz, X. (2006). Ageing effects in a compacted bentonite: a microstructure approach. Géotechnique, **56**(5): 291-304.

Hansbo, S. (1957). A new approach to the determination of the shear strength of clay by the fall-cone test. Royal Swedish Geotechnical Institute.

Jeeravipoolvarn, S. (2010). Geotechnical behaviour of in-line thickened oil sands tailings (Ph.D. thesis). The University of Alberta, Edmonton, Alberta.

Jeeravipoolvarn, S., Scott, J. D. and Chalaturnyk, R. J. (2009). 10 m standpipe tests on oil sands tailings: Long-term experimental results and prediction. Canadian Geotechnical Journal, **46**: 875-888.

Jeeravipoolvarn, S. (2005). Compression behaviour of thixotropic oil sands tailings (Master's thesis). The University of Alberta, Edmonton, Alberta.

Leonards, G. A. and Altschaeffl, A. G. (1964). Compressibility of clays. J. Soil Mech. Found. Div., **90**(SM5): 133-155.

Leroueil, S., Perret, D. and Locat, J. (1996). Strain rate and structuring effects on the compressibility of a young clay. In Measuring and modeling time-dependent soil behavior (pp. 137-150). ASCE.

Locat, J. and Lefebvre, G. (1985). The compressibility and sensitivity of an artificially sedimented clay soil: the Grande Baleine marine clay, Québec, Canada. Marine Georesources & Geotechnology, **6**(1): pp.1-28.

Locat, J. and Lefebvre, G. (1986). The origin of structuration of the Grande-Baleine marine sediments, Québec, Canada. Quarterly Journal of Engineering Geology and Hydrogeology, **19**(4): 365-374.

Lohani, T. N., Imai, G., Tani, K. and Shibuya, S. (2001). Gmax of fine-grained soils at wide void ratio range, focussing on the time-dependent behavior. Soils and Foundations **41**(5): 87-102.

Matthews, J., Dhadli, N., House, P. and Simms, P. (2011). Field trials of thin-lift deposition of amended mature fine tailings at the Muskeg RiveMine in Northern Alberta. Proceedings of the 14th International Seminar on Paste and Thickened tailings, 5–7 April 2011, Perth, Western Australia, pp. 271–280.

McKenna, G., Mooder, B., Burton, B. and Jamieson, A. (2016). Shear strength and density of oil sands fine tailings for reclamation to a boreal forest landscape. Proceedings of the Fifth International Oil Sands Tailings Conference (IOSTC), December 4-7, 2016, Lake Louise, Alberta.

Miller, W. G. (2010). Comparison of geoenvironmental properties of caustic and non-caustic oil sand fine tailings (Ph.D. thesis). The University of Alberta, Edmonton, Alberta.

Mitchell, J. M. (1960). Fundamental aspects of thixotropy in soils. Journal of the Soil Mechanics and Foundations Division, **86**(3): 19-52.

Mizani, S., Simms, P. and Wilson, G. W. (2017). Rheology for deposition control of polymer-amended oil sands tailings, Rheologica Acta, Published Online May 2017, DOI 10.1007/s00397-017-1015-2.

Oil Sands Discovery Centre. (2009). Oil sands overview. Retrieved September 2018 from the website: www.oilsandsdiscovery.com

Orland, K. (2018). 340 Billion Gallons of Sludge Spur Environmental Fears in Canada. Retrieved April 2018 from the website: https://www.bloomberg.com/news/articles/2018-01-16/340-billion-gallons-of-sludge-spur-environmental-fears-in-canada

Salam, A. M., Simms, P. H. and Örmeci, B. (2018). Structuration in polymer amended oil sands fine tailings. Proceedings of the 71st Canadian Geotechnical Conference. Edmonton, Alberta.

Salam, A. M., Simms, P. H. and Örmeci, B. (2017). Investigation of creep in polymer amended oil sands tailings. Proceedings of the 70th Canadian Geotechnical Conference. Ottawa, Ontario.

Salam, A.M., Örmeci, B. and Simms, P.H. (2016). Determination of the optimum polymer dose for dewatering of oil sands tailings using UV–vis spectrophotometry. Journal of Petroleum Science and Engineering, **147**: 68-76.

Scott, J. D., Jeeravipoolvarn, S., Kabwe, L., Wilson, G. W. and Sorta, A. (2013). Properties which affect the consolidation behaviour of mature fine tailings. Proceedings of the 17th International Conference on Tailings and Mine Waste, Banff, Alberta.

Skempton, A. W. and Northey, R. D. (1952). The sensitivity of clays. Géotechnique, **3**(1): 30-53.

Sobkowicz, J. C. (2013). Developments in treating and dewatering oil sands tailings. Proceedings of the 16th Internal Conference on Paste and Thickened Tailings, 17–20 June, Belo Horizonte, pp. 3-20.

Sorensen, K. K. (2006). Influence of viscosity and ageing on the behaviour of clays (Ph.D. Thesis). The University of London.

Wells, P. S. (2011). Long term in-situ behaviour of oil sands fine tailings in Suncor's Pond 1A. Proceedings of the Tailings and Mine Waste 2011, 6-9 November, Vancouver, BC, Canada.

Wood, D. M. (1985). Some fall-cone tests. Géotechnique, **35**(1): 64-68.

Yin, J. H. and Graham, J. (1994). Equivalent times and one-dimensional elastic viscoplastic modelling of time-dependent stress-strain behaviour of clays. Canadian Geotechnical Journal, **31**(1): 42-52.

INFLUENCE OF BITUMEN CONTENT ON FLOCCULATION OF FFT

Heather Kaminsky[1], Yunhui Li[1], Taimur Qureshi[1], Andrea Sedgwick[1] and Kevin Moran[2]
[1]Northern Alberta Institute of Technology, Edmonton, Canada
[2] Titanium Corporation, Edmonton, Canada

ABSTRACT

The role of bitumen in tailings is the subject of much debate within the oil sands industry. One of the challenges is that bitumen content is difficult to separate from other influences such as clay content or process history. This study aimed to assess the specific impact of bitumen removal from Fluid Fine Tailings (FFT) using Titanium Corporation's solvent extraction technology to produce a tailings stream suitable for use in tailings processes targeting a final upland ecosystem such as flocculation and drying In this study several different bitumen removal conditions using Titanium Corporation's process were used to generate FFT with different levels of bitumen content but otherwise identical properties. The technology was able to remove most of the residual bitumen from the FFT, producing a bitumen to solids ratio of 0.02. The "cleaned" FFT, after bitumen removal, required a lower flocculant dosage compared to raw FFT. Cleaned FFT also produced higher solids content in the final flocculated sediment and lower solids content in the released water. The study provides a directional indication that removing bitumen using Titanium Corporation's process can produce quantifiable benefits in tailings treatments that look to create an upland ecosystem as the final reclamation landscape.

INTRODUCTION

The oil sands in northern Alberta, Canada, represent the 3rd largest proven global oil reserve with a bitumen reserve equivalent to 1.6 trillion barrels of oil (Alberta Energy 2013). Bitumen is extracted by the Clark hot water extraction process, leaving behind a combination of sand, silt, clay, water and residual bitumen known as tailings. The tailings in the Athabasca oil sands region covered 1,206 million m^3 by 2016 (AER 2016a), despite past regulatory efforts requiring operators to treat the FFT. In 2016 the Alberta Energy Regulator (AER) released Directive 85 which requires operators to ensure that all fluid tailings are returned to a reclamation ready state ten years after the end of mine life (AER 2016b).

The role of bitumen in tailings is the subject of much debate within the oil sands industry. One of the challenges is that bitumen content is difficult to separate from other influences such as clay content or process history.

Titanium Corporation's (Titanium) previous research demonstrated that their technology is capable of removing bitumen from froth treatment tailings (Moran et al. 2016). They have also gathered some evidence which indicates that the cleaned froth treatment tailings settle faster and require less chemical treatment in thickening experiments.

In this study, the Northern Alberta Institute of Technology (NAIT) Applied Research Centre for Oil Sands Sustainability (COSS) located in Edmonton, Alberta, Canada, in collaboration with Titanium has investigated the residual bitumen removal conditions on FFT and evaluated the impact of the bitumen removal on FFT flocculation parameters.

EXPERIMENTAL

Materials

Two types of FFT from oil sands tailings ponds were characterized by Dean and Stark (D&S) for bitumen, solids, and water (BSW) contents (Dean and Stark 1920), methylene blue index (MBI) and particle size distribution (PSD) (Table 1). The D&S extraction was performed by COSS in the range of 21 to 24 hours to ensure complete removal of bitumen from the solids. The weight percentage of fines in the sample are defined as the particles with a size less than 44 microns.

Table 1. Average MBI, %Fines, D&S data for bitumen, solids and water

Item	FFT-1	FFT-2
Bitumen content (wt%)	7.81	1.23
Solids content (wt%)	32.09	24.68
Water content (wt%)	60.04	73.64
Bitumen/Solids Ratio	0.24	0.05
MBI (meq/100 g solids)	10.6	14.1
Fines content (%)	49.2	84.2

Methods

The study was performed at the Centre for Oil Sands Sustainability's laboratory. Several tests were performed to extract bitumen and solvent to prepare the tailings for further processing. The tailings were then flocculated and parameters measured as noted below.

Bitumen Extraction Using Jet B Solvent

The FFT samples were mixed with Jet B solvent on a shaker table, followed by centrifugation to separate the solvent layer (Jet B containing bitumen and an emulsion or "rag layer" if it existed) from the sediment layer (water and solids). The solvent layer was then removed using a pipette and the sediment layer was labeled "washed FFT".

Distillation of Jet B

The washed FFT was distilled three times to remove the residual Jet B. Water was added between each distillation to maintain water content and to avoid drying out the clays. Based on some investigation, this was the most effective method of removing the Jet B solvent.

Flocculation Test

Pulsed mixing and one-dose mixing techniques (0-320 rpm) were used to flocculate the FFT. Polymer A3338, which is a common baseline polymer used in oil sands tailings flocculation (Li et al. 2016), was used in this experiment. Solids plus bitumen content in floccules (flocs) and solids content in released water were measured by heating the samples in an oven at 110°C overnight.

RESULTS AND DISCUSSION

Determination of the Bitumen Extraction Conditions Using Jet B Solvent

Two types of raw FFT were used in this study and the characterization results are shown in Table 1. FFT-1 was from a tailings pond containing a portion of froth treatment tailings and FFT-2 was from a typical FFT pond. Jet B is a fuel in the naphtha-kerosene region that is usually used for its enhanced cold-weather performance, with similar properties as naphthas produced by oil sands upgraders.

The bench scale bitumen extraction process using Titanium's technology comprised three stages (Figure 1): washing the FFT to generate "washed FFT" by separating bitumen from the FFT sample, distillation to generate "cleaned FFT" by removing the residual Jet B from the washed FFT, and evaluation to characterize the cleaned FFT using the Dean and Stark (D&S) process in order to obtain the quantity of components in the cleaned FFT. The bitumen to solids ratio (B/S) before and after the bitumen extraction process was the key performance indicator (KPI) to evaluate the efficiency of the bitumen removal.

The washing stage included four main steps as shown in Figure 1: mixing uncleaned/raw FFT and Jet B, shaking the mixture to extract the bitumen from the solid phase into the solvent (Jet B) phase, centrifuging the mixture and separating the solid phase from the solvent phase known as diluted bitumen.

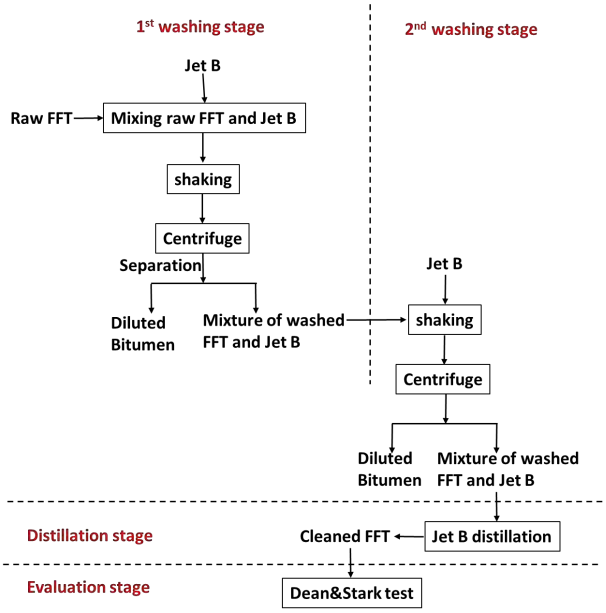

Figure 1. Bitumen extraction process using Jet B solvent

Various shaking times and centrifuge times were investigated and assessed for bitumen recovery efficiency and operating feasibility.

It was found that the residual bitumen of FFT-1 with one-round of washing was lower (0.04) than the initial state (0.24). This represented a high bitumen recovery rate (81% after stage 1, 88% after stage 2) but the very high initial bitumen content of FFT1 meant that the cleaning brought the bitumen

content (Table 2) only to within the low-normal range for FFT (Table 3).

Table 2. Characterization of cleaned FFT-1 using Jet B solvent

	Uncleaned FFT-1	Cleaned FFT-1 with one-round washing	Cleaned FFT-1 with two-round washing
Bitumen content (wt%)	7.81	1.46	0.84
Solids content (wt%)	32.09	36.28	32.35
Water content (wt%)	60.04	61.91	66.07
Jet B content (wt%)	--	0.35	0.73
Bitumen to solids ratio (B/S)	0.24	0.04	0.03
MBI of solids (meq/100 g)	10.6	10.6	9.5

Table 3. 10th, 50th and 90th percentile of bitumen, mineral and B/S ratio for historical pond data (fines>50%) (Taken from Kaminsky & Omotoso 2016)

	Bitumen	Mineral	B/S ratio
D10	0.9	20.7	0.03
D50	2.9	36.2	0.08
D90	5.5	58.3	0.15

Two-rounds of washing showed the B/S decreased to 0.03 which brought the FFT-1 to the very low end (D10) of typical FFT.

This cleaning process was also effective on an FFT with an already low bitumen content. The B/S of the uncleaned FFT-2 was 0.05 and decreased to 0.02 after two-rounds of washing using Jet B (Table 4).

Table 4. The Dean & Stark results of FFT1 and FFT2 after bitumen removal, and bitumen-spiked FFT-2

Sample	S/F	Bitumen (wt%)	Solids (wt%)	Water (wt%)	B/S
FFT1	1	2.78	32.85	59.81	0.08
	0.5	0.71	33.08	61.68	0.02
	0.25	1.09	37.71	56.01	0.03
	0.1	2.01	38.31	53.23	0.05
FFT2	0.5	0.5	27.02	71.38	0.02
	0.25	0.54	26.24	73.53	0.02
	0.1	0.44	22.87	76.99	0.02
Spiked FFT2		1.61	28.11	69.11	0.06

Residual Jet B solvent in the cleaned FFT is economically and environmentally undesirable. In order to remove as much residual Jet B as possible from the cleaned FFT, steam distillation was performed. Water was added periodically to maintain water content. The water was added to avoid drying out the clays which could potentially change the clay's properties and increase losses by having stuff stick to the bottom of the distillation kettle.

Characterization of Cleaned FFT with Different Solvent to Feed Ratio

The effect of different solvent (Jet B) to feed (FFT) ratio (S/F) on the resulting B/S values was determined by D&S (Table 4). While there was some variability in response to S/F ratio observed with the higher bitumen content FFT-1, the B/S value of the cleaned FFT-2 maintained the same value (0.02) with the decrease of the S/F from 0.5 to 0.1. Therefore, in the S/F range that was tested, the amount of Jet B used in the washing stage did not affect the efficiency of bitumen extraction on FFT-2.

Impact of Bitumen Removal on FFT Flocculation

The impact of cleaned FFT-2 with different S/F ratios on the flocculation performance was investigated by dosage curve testing using a one-dose flocculation method (Figure 2). Dosage curve testing is able to provide an insight to the full dosage range and the one-dose flocculation method can provide accurate prediction of the flocculation performance. The key performance indicators (KPIs) of dosage curve testing are the optimal dosage of the flocculant and the solids% in the flocs after 24-hours of water release. The optimal polymer dosage is the dosage that produces the highest solids% in the flocs after 24-hour water release.

The solids plus bitumen content in flocs was measured by oven heating after 24-hour water release of the flocculated FFT. The solids contents in flocs shown in Figure 3 were then calculated by subtracting the bitumen content from the solids plus bitumen content assuming all of the bitumen left in the flocs. The bitumen content in the flocs was calculated according to Equation 1 and the results are shown in Figure 2.

Equation 1. Bitumen Content Calculation in Flocs

$$\text{Bitumen Content in Flocs} = \frac{\text{Weight of FFT} * \text{Bitumen content in FFT}}{\text{Weight of FFT} + \text{Weight of polymer added} - \text{weight of released water}}$$

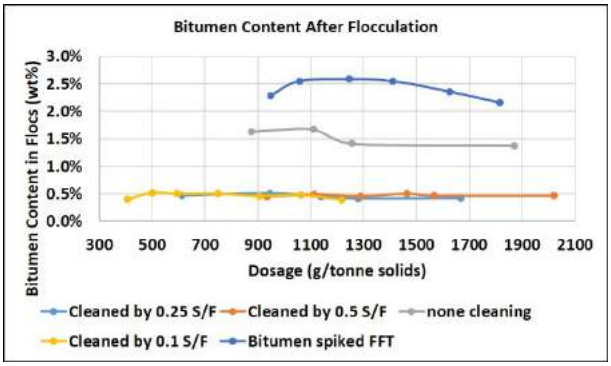

Figure 2. Bitumen Content in Flocs After Flocculation of Cleaned, Uncleaned, and Bitumen Spiked FFT-2

The cleaned FFT-2, obtained by using S/F ratio of 0.5 in washing, showed a wide range of dosage window and a comparable solids% in the flocs after 24-hour water release with the uncleaned FFT-2 (Figure 3 and Figure 4) performance. The cleaned FFT-2 obtained by using an S/F ratio of 0.25, required 25% lower optimal polymer dosage and produced 12% higher solids% in the flocs after 24-hour water release than uncleaned FFT-2 performance. The cleaned FFT-2 by 0.1 of S/F required 60% lower optimal polymer dosage and produced 5 wt% higher solids in the flocs after 24-hour water release than uncleaned FFT-2 performance. The reason why a lower polymer dosage is favorable is due to the lower cost.

The cleaned FFT-2 required a lower optimal polymer dosage than the uncleaned FFT-2 due to the impact of the bitumen in the sample since solids content and clay content showed no significant difference between cleaned and uncleaned FFT-2. In order to confirm the bitumen impact on the flocculation, bitumen-spiked FFT-2 was tested and flocculation performance was compared. Bitumen spiked FFT-2 was obtained by spiking uncleaned FFT-2 with bitumen extracted from the S/F ratio of 0.1 in the bitumen extraction process. The D&S result of the bitumen spiked FFT-2 showed the B/S was 0.06 higher than uncleaned FFT-2 (0.05 of B/S). Figure 4 and t-Test analysis shows that the bitumen-spiked FFT-2 and uncleaned FFT-2 required higher optimal polymer dosage than cleaned FFT-2 samples which have lower bitumen content. The required optimal polymer dosage between bitumen spiked FFT-2 and uncleaned FFT-2 had no statistically significant difference according to the t-Test analysis.

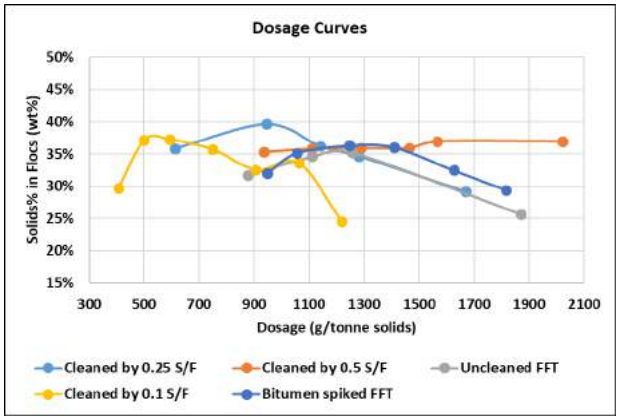

Figure 3. The dosage curves of flocculated cleaned, uncleaned and bitumen spiked FFT-2

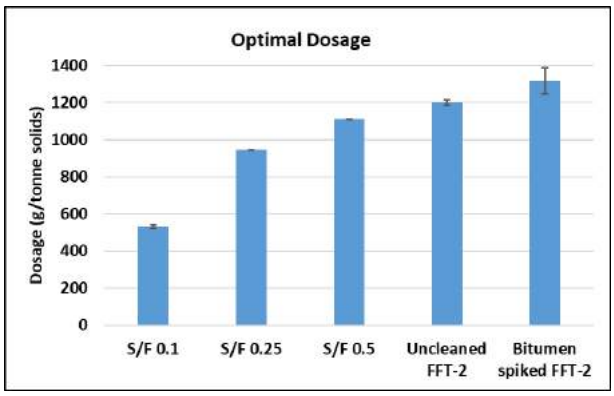

Figure 4. Comparison of the optimal polymer dosage required to flocculate cleaned FFT-2 with different S/F ratios in each washing stage, uncleaned FFT-2 and bitumen-spiked FFT-2. Error bar shows standard deviation amongst flocculation tests performed

Figure 5 shows that the highest solids content in flocs was obtained by the cleaned FFT-2 obtained using an S/F of 0.25. The assumption was that the clays cleaned by a S/F of 0.25 were the most homogeneous active surfaces leading to the best polymer flocculation performance. The bitumen spiked FFT-2 produced comparable solids content in the sediment as uncleaned FFT-2 and cleaned FFT-2 using a S/F of 0.5.

The solids content in the released water was also measured by oven heating after the 24-hour water release of the flocculated FFT (Figure 6). The desired solids content in the released water is less than 0.5 wt%. All of the flocculated samples

produced release water with less than 0.5 wt% solids content at the corresponding optimal dosage. Non-optimal doses resulted in higher solids in the release water.

As with FFT-2 sample, the cleaned FFT-1 required lower optimal polymer dosage than uncleaned FFT-1 and produced higher solids content in the flocs (Figure 7 and Figure 8).

In all conditions cleaned tailings required a lower optimal polymer dosage than the uncleaned ysilinhd and the spiked material required a higher optimal polymer dosage. The best cleaning condition for FFT-2 was found by cleaning with a S/F of 0.1 – showing a 60% reduction in optimal polymer dosage with a 5% increase in solids in the sediment. Cleaning also seemed to increase the polymer dose window.

Impact of Bitumen Removal on FFT Settling

A compressibility standpipe (CS) test under the self-weight stress condition was conducted on uncleaned and cleaned FFT-2. The normalized settling mudline height was calculated according to Equation 2 and plotted in Figure 9.

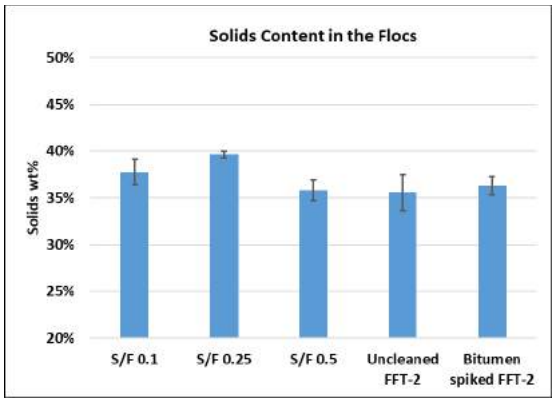

Figure 5. Comparison of solids content in flocs of cleaned FFT-2 with different S/F in each washing stage, uncleaned FFT-2 and bitumen-spiked FFT-2. Error bar shows standard deviation amongst flocculation tests performed

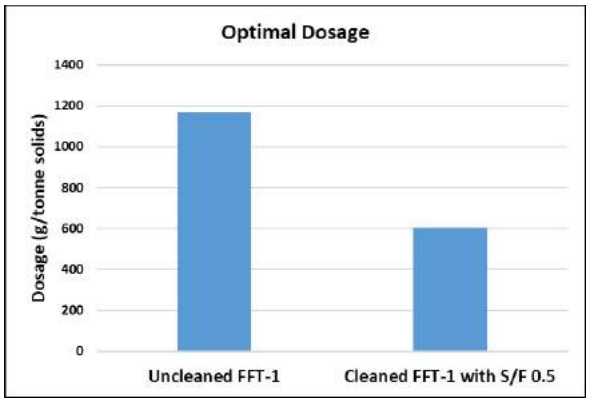

Figure 7. Comparison of the optimal polymer dosage required to flocculate cleaned FFT-1 with 0.5 of S/F and uncleaned FFT-1

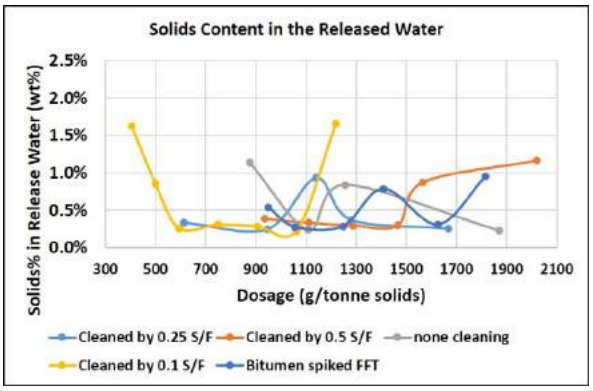

Figure 6. The Solids Content in the Released Water of flocculated cleaned, uncleaned, and spiked FFT

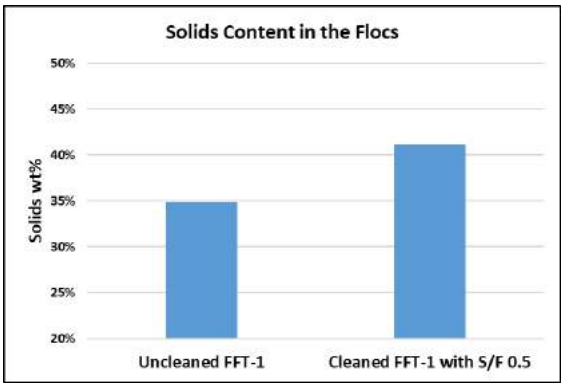

Figure 8. Comparison of solids content in flocs of flocculated, cleaned FFT-1 with 0.5 of S/F and uncleaned FFT-1

Equation 2. Normalized mudline height calculation

$$Normalized\ mudline\ height = \frac{h}{H}$$

Where h is the mudline height at time t, and H is the mudline height at time 0.

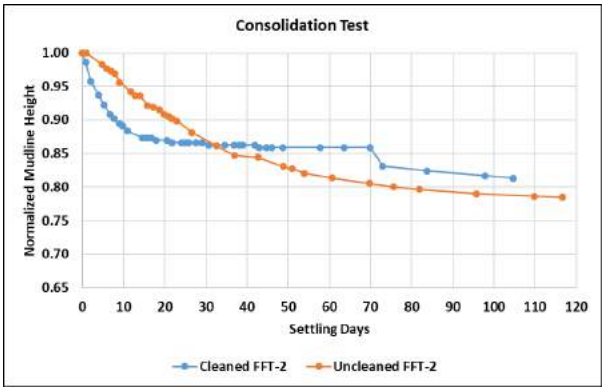

Figure 9. Settling curves of cleaned and uncleaned FFT-2 during the standpipe tests

Cleaned FFT-2 had a higher initial settling rate than uncleaned FFT-2. But after 33 days of settling, uncleaned FFT-2 had a lower mudline height than the cleaned material. With time during settling test, cleaned FFT-2 had cracks occurring, which caused the interface settlement (which had already stopped moving earlier) to move again at ~70 days. This phenomenon was not observed in the uncleaned FFT-2.

CONCLUSIONS

In this study, COSS in collaboration with Titanium, has investigated the bitumen extraction conditions by using Jet B solvent to clean FFT using a lab scale version of Titanium's process to validate the effect of bitumen removal on the FFT flocculation and consolidation. Two types of cleaned FFT, FFT-1 with high bitumen to solids ratio and FFT-2 with low bitumen to solids ratio, were generated and evaluated by lab scale flocculation tests and consolidation tests.

Titanium's cleaning technology was able to remove significant amounts of residual bitumen from FFT, producing a low bitumen to solids ratio of ~0.03. Titanium's cleaning process brought the bitumen content of FFT to the very low end (D10) of typical FFT.

The cleaned FFT improves the flocculation performance by reducing flocculant dosage by 60% compared to that required for uncleaned FFT. Cleaned FFT also showed faster initial settling.

Measurement of solids content and clay content showed insignificant differences between cleaned and uncleaned tailings indicating that the differences in performance are primarily due to bitumen content.

This study provides a directional indication that removing bitumen using Titanium's process can produce quantifiable benefits in tailings treatments that look to create an upland ecosystem as the final reclamation landscape.

ACKNOWLEDGEMENTS

The authors acknowledge the support of the Natural Sciences and Engineering Research Council of Canada (NSERC) and Alberta Innovates.

REFERENCES

Alberta Energy. (2013). Alberta's oil sands: January fact-sheet. Government of Alberta, Edmonton, Alberta.

Alberta Energy Regulator. (2016a). Mineable oil sands tailings status report, 2016.

Alberta Energy Regulator. (2016b). Fluid tailings management for oil sands mining projects.

Dean, E. W. and Stark, D. D. (1920). A convenient method for the determination of water in petroleum and other organic emulsions. Ind. Eng. Chem. **12**: 486-490.

Kaminsky, H. (2014). Demystifying the methylene blue index. Proceedings of The fourth International Oil Sands Tailings Conference, Banff, Alberta, Canada, pp 221-229.

Kaminsky, H. and Omotoso, O. (2016). Variability in fluid fine tailings. Proceedings of The fifth International Oil Sands Conference, Lake Louise, AB, Canada, pp 178-183.

Li, Y., Currie, R., Kaminsky, H., Sedgwick, A. and Qureshi, T. (2016). The effects of flocculation on the methylene blue index. Proceedings of Fifth International Oil Sands Tailings Conference, pp 242-248.

Moran, K., Nelson, S. and Oxenford, J. (2016). New oil sands technology to meet the challenges of climate change and tailings management. World Heavy Oil Congress. Calgary, Alberta, Canada.

INVESTIGATING THE IMPACT OF ALUM ON THE RELEASE WATER OF OIL SANDS MATURE FINE TAILINGS UTILIZING MINERALOGICAL AND CHEMICAL TECHNIQUES

Mitchell Catling[1], Abu Junaid[2], Gavin Freeman[2], Caleb Dusek[1], Coralys Torres López[1], Carlos Silva Gaxiola[1] and Christian Loeschel[1]
[1]BASF Corporation, Tucson, USA
[2]Canadian Natural Resources Limited, Calgary, Canada

ABSTRACT

The bitumen extraction process utilized in the Alberta oil sands is known to generate large volumes of high clay, high fines, mineral tailings as a waste product. This slurry is often stored in large tailings facilities where it begins to slowly settle to ~25-40 %w/w. The material that is produced after about two years of settlement is commonly referred to as mature fine tails (MFT). The dewatering of MFT via the use of anionic copolymers in combination with a pre-treatment of the inorganic coagulant “alum” has been suggested in previous studies and investigations. This study examined the impact of the addition of alum at varying doses and its utilization in combination with conventional and novel polyacrylamide (PAM) technology on the release water (RW) chemistry. The paper highlights correlations between the release water chemistry and the mineral composition of the substrate tested.

This study uses MFT samples from several different sources that have varying levels of clay, differing mineralogy, and changing solids content with a combination of laboratory and field data from BASF and CNRL to draw the conclusions presented in this paper.

INTRODUCTION

Background

The oil sands industry, as well as the Alberta government, has highlighted the need for a tailings solution that enables operators to reduce the large inventory of MFT at their sites in an economical, environmentally friendly, and efficient manner. Most recently, this was outlined in Directive 085 which states that the intention of this regulation is “to minimize fluid tailings accumulation by ensuring that fluid tailings are treated and reclaimed progressively during the life of a project and that all fluid tailings associated with a project are ready to reclaim (RTR) ten years after the end of mine life of that project” (Ellis 2017). How the industry can reach this target has been and continues to be a hot topic and focus of research groups around the world.

A common solution that has been utilized across the industry is the application of conventional and novel PAM flocculants to facilitate the dewatering of the MFT. This technology has been proven to be successful at facilitating volume reduction of MFT and an initial increase in hydraulic conductivity of the treated material. (Znidarcic et al. 2015).

The use of acidified aluminum sulfate solution or “alum” has been documented as a means of improving the dewatering performance of novel and conventional PAM (Pelaez 2016). Alum is a widely used clarification agent employed in water treatment processes globally. Given the highly charged nature of the aluminum cation, it is extremely effective in coagulating or neutralizing excess surface charge of fine particulates, such as those found in wastewater or in MFT. (Ockershausen 1965) One of the main benefits shown has been enhanced clarification of the release water, which can then be recycled back into the extraction process. It has also shown success in isolating bitumen within the settled solids after treatment in combination with a polymer. This has the benefit of helping reduce the volume of water taken from the Athabasca river, which overall, then reduces the total inventory of contaminated process water on site.

This “recycling” of process water does inherently bring with it concerns regarding its quality – namely how it will impact the chemistry of the bitumen extraction (Loganathan 2015). The most common cause for concern is elevated levels of multivalent cations such as Mg^{2+} or Ca^{2+}, which have been shown to greatly depress bitumen recovery (Ding 2006, Sanford 1983). The suggested value at which bitumen recovery drops below 95% was shown to be ~30 ppm of Ca^{2+} (Kasongo 2000). With this in

mind, the calcium level in the process water is carefully monitored in all oil sands operations to ensure that the concentration of this cation does not exceed the recommended levels, thereby negatively impacting bitumen recovery.

With all ideas that are postulated, there must be continued discussion present to assess potential drawbacks as well as positives offered by different tailings solutions, whilst considering the entire operational process and end goal of a "ready to reclaim" landform (Mikula 2012). The main purpose of this study is to investigate how the addition of PAM with and without the addition of alum can impact the release water chemistry (and thus potentially the extraction process) given that from site to site the minerology of the MFT can vary quite substantially (Botha et al. 2015).

EXPERIMENTAL

Mature Fine Tails Characterization

Four separate samples of MFT were provided by CNRL and characterized in Tucson. Each sample comes from different parts of the CNRL operations in the oil sands, with varying feed characteristics. These samples were then homogenized with a Lightnin' overhead mixer and a standard impeller. The analyte values shown for each feed corresponds to results generated by titration and ICP analysis as described in the release water analysis section. The clay content for each feed was determined by methylene blue titration. The full results of this characterization are shown in Table 1.

Sample Preparation

For Part 1 of this investigation, several samples of MFT were treated with doses varying from 0-1700 g/t of either standard anionic PAM or BASF's novel PAM chemistry. For Part 2, a varying single dose of alum solution (0-6000 ppm) was added to fresh MFT samples and then mixed for five minutes at 320 RPM with a flat blade impeller. For Part 3, fresh MFT samples were treated with a varied dose of alum as in Part 2, but after five minutes of mixing, the material was flocculated with a fixed dose of 1200 g/t of either standard anionic PAM or BASF's novel PAM chemistry as this was identified as the optimum dosage for the samples tested.

In each scenario, once the test had been completed, the treated material was placed in a centrifuge tube and centrifuged for 30 minutes at 3500 RPM. This centrate was then carefully collected, centrifuged again at 5000 RPM for 30 minutes to remove fine solids, and finally filtered through 0.2 µm filter paper in a Millipore apparatus.

Release Water Analysis

The filtrate collected from the initial investigation was then taken and analyzed via Inductively coupled plasma-optical emission spectrometry (ICP-OES) with an Agilent 5100 instrument to quantify calcium, sodium, aluminum, iron, potassium, and magnesium concentration. Each sample was also titrated with 1.6M sulfuric acid to determine carbonate/bicarbonate concentration. Sulfate analysis was determined by the barium precipitation reaction, and chloride concentration was determined using a silver nitrate precipitation titration.

X-Ray Powder Diffraction

A small sample of each of the four different MFT samples was taken and prepared for analysis via X-Ray Powder Diffraction at the University of Arizona. These samples were prepared by standard procedures outlined in literature prior to X-ray analysis (Kaminsky 2008). Diffraction was carried out on a Bruker D8 Advanced powder diffractometer (Figure 1) with Cu radiation, 2-90° 2θ, at 0.01 increments, 2 seconds per step. Each pattern was analyzed with the in-house software "Amorphous Profile Characterization" (APC), to determine the identification and quantities of the constituents of the MFT samples at abundance greater than 1%w/w. Data to model the refinements are based from more than 20,000 datasets in the American Mineralogist Crystal Structure Database.

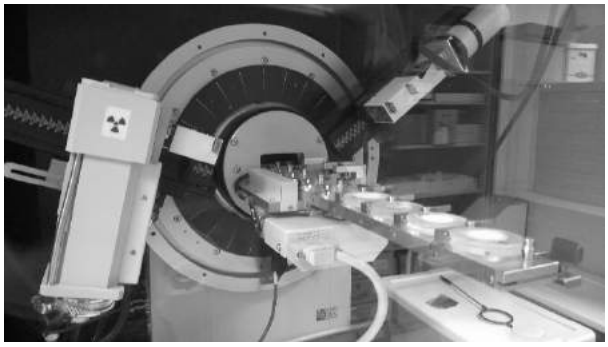

Figure 1. Bruker D8 advanced powder diffractometer

RESULTS AND DISCUSSION

MFT Characterization Results

Full laboratory characterization data for the four different MFT samples used in this investigation is highlighted in Table 1. The samples had solids content between 28.8-37.3 w/w% and MBI values between 6.36-11.87 meq/100 g solids. Most notably, **MFT #1** and **#4** exhibited similar MBI values of ~11.7meq/100g but had significantly different solids content values.

Table 1. MFT Characterization Data

Slurry >	MFT #1	MFT #2	MFT #3	MFT #4
pH	8.2	7.6	7.4	7.8
Density (g/mL)	1.22	1.24	1.20	1.21
Solids Content (%w/w)	30.3	37.3	28.8	35.0
MBI (meq/100 g solids)	11.68	6.36	7.76	11.87
% Clay Content	83.7	45.7	55.7	85.04
CWR	0.25	0.17	0.24	0.25
$[CO_3^{2-}]$ mg/L	<5	<5	<5	<5
$[HCO_3^-]$ mg/L	964	509	778	472
[Al] mg/L	<1	<1	<1	<1
[Ca] mg/L	6.1	24.3	7.3	15.4
[Fe] mg/L	<1	<1	<1	<1
[K] mg/L	15.5	17.4	17.8	17.9
[Mg] mg/L	5.0	15.4	5.8	9.7
[Na] mg/L	997	372	978	376
$[Cl^-]$ mg/L	812	157	676	164
$[SO_4^{2-}]$ mg/L	<50	<50	<50	<50

X-Ray Diffraction Results

Table 2 lists the minerals that were found to fit the profiles in the X-Ray diffraction spectra and their relative abundance. Kaolinite can describe polymorphs of $Al_2Si_2O_5(OH)_4$ and was found at ~26-34 %w/w abundance. Illite was shown to be present with both the 2M1 and 3T polymorphs, at abundances between 30-40 %w/w and 3-7 %w/w respectively, exhibiting different grain sizes and indicating stacking disorders. From this mineral analysis, the bulk chemical composition of each sample was also calculated and is shown in Table 3. As expected, a relatively higher amount of silica was found in **MFT#2**, which was shown to have the lowest MBI (6.36 meq/100 g solids) in Table 1.

Table 2. Mineral Table and Relative Abundance (%w/w)

Mineral >	MFT #1	MFT #2	MFT #3	MFT #4
Quartz	24.73	33.43	24.72	28.75
Kaolinite	34.27	28.53	27.62	26.20
Illite-2M1	35.61	30.09	38.83	39.58
Illite-3T	3.02	5.94	6.57	2.90
Siderite	2.37	2.02	2.26	2.57

Table 3. Bulk chemical composition based on diffraction analysis and ideal chemistries of the component phases (%w/w)

Oxide >	MFT #1	MFT #2	MFT #3	MFT #4
K_2O	4.57	4.26	5.37	5.02
FeO	1.47	1.25	1.40	1.59
Al_2O_3	28.37	25.10	28.34	26.67
CO_2	0.90	0.77	0.86	0.97
SiO_2	58.16	63.01	58.12	60.17
H_2O	6.53	5.61	5.91	5.58

Part 1: Impact of PAM Addition

The release water chemistry was compared for **MFT #2** when treated with a conventional PAM sample as against using BASF's novel PAM. **MFT #2** was selected for this purpose due to its relatively high solids content and low MBI value, which resulted in a simpler slurry to investigate for the first part of this test program. Both polymers are mid-molecular weight charged anionic polyacrylamide copolymers. However, the BASF novel PAM is neutralized with Ca^{2+} instead of the typical Na^+ cation. providing additional polymer adsorption capability during the flocculation step.

The results are shown in Figure 2. The data showed that there was no significant change in the release water calcium level compared to the control (untreated) test, when treated with either the novel or the conventional PAM sample. This indicates that neither the sodium based conventional PAM, or the calcium based novel PAM, contribute to an increase in the release water calcium content when used to treat MFT.

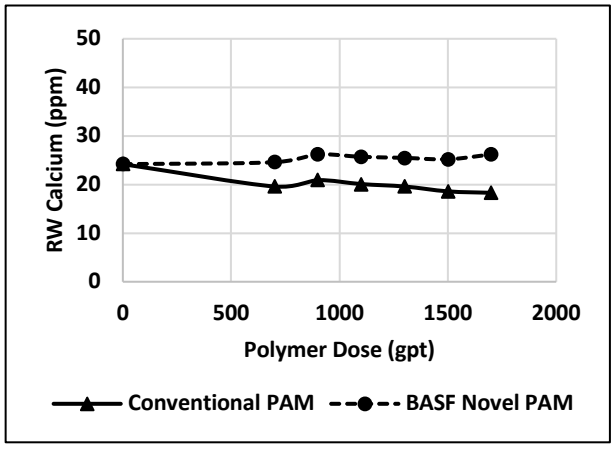

Figure 2. Contrasting calcium content in release water for the two PAM samples

Part 2: Impact of Alum Addition

For the second part of this investigation, the impact of the addition of the acidified alum solution alone was observed. The impact of the levels of Ca^{2+}, Mg^{2+} and K^{+} for all four MFT samples are shown below in Figure 3. From the data it was observed that the concentration of all three cations in solution increased with the increasing dose of alum. The degree to which each cation increased was dependent on the source and mineralogy of the MFT sample. For example, the Ca^{2+} level in the release water for **MFT #1** & **#3** began to rise significantly with alum doses >1500 ppm. However, for **MFT #2** & **#4** a significant increase occurred with doses of alum >800 ppm. This same trend was observed with spikes in both the Mg^{2+} and K^{+} levels at the same doses of alum. Contrasting the

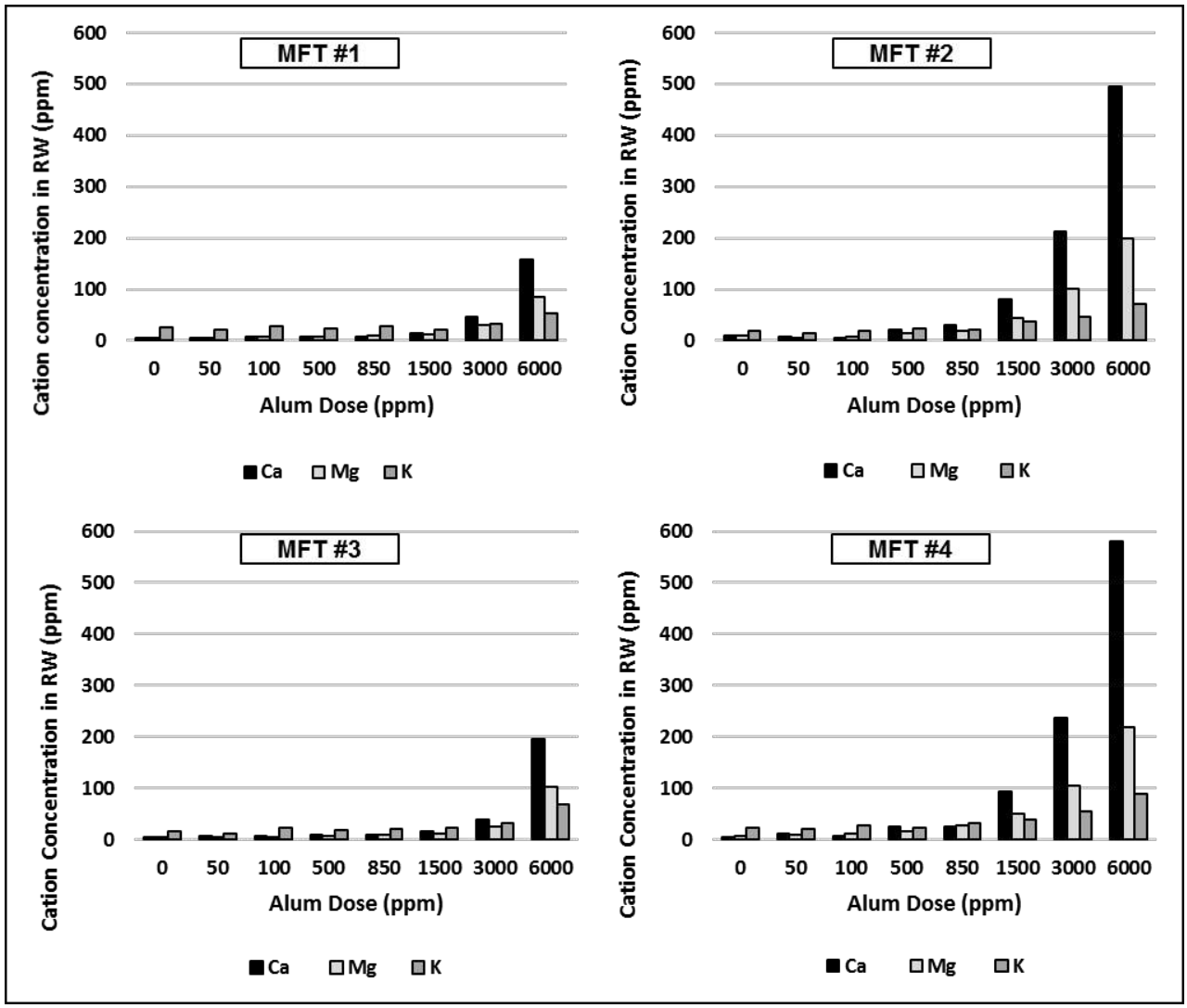

Figure 3. Contrasting RW cation content with increasing alum dose for different MFT samples

mineralogical data presented in Table 2, it was observed that **MFT #2** & **#4** both have elevated levels of quartz in comparison to the other MFT samples (33 and 29 %w/w respectively) in comparison to the ~25 %w/w observed with **MFT #1** & **#3.** All four MFT samples tested all have similar amounts of kaolinite present. The basal siloxane surfaces of kaolinite are believed by many researchers to carry a constant structural charge due to the isomorphous substitution of $Si^{(4+)}$ by $Al^{(3+)}$. Not only this, but charge on the edge of the quartz and kaolinite clay surfaces is brought about by protonation or deprotonation of exposed hydroxyl groups (Eisazadeh 2011). Therefore, the pH of the release water for **MFT #2** was measured to see how it was impacted by the addition of the sulfuric acid and hydroxyl anions present in the aluminum sulfate solution. The results are shown below in Figure 4.

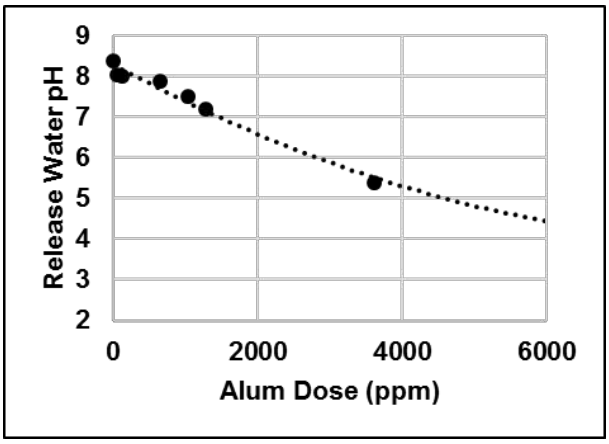

Figure 4. Release water pH for MFT #2 with continued addition of alum

As these minerals are exposed to the pH change imparted by the in the alum, they are also impacted by the presence of the excess cations as shown by the equations below. (M^+ = charged metal cation)

$$Si\text{-}OH \leftrightarrow Si\text{-}O^- + H^+$$
$$Si\text{-}O^- + M^+ \leftrightarrow Si\text{-}O\text{-}M$$
$$Si\text{-}OH + M^+ \leftrightarrow Si\text{-}O\text{-}M + H^+$$

An increase in the $[M^+]$ concentration will push the exchange reaction towards the right. This is because clay minerals have the property of absorbing certain cations and holding them in an exchangeable state (Coulter 1968). The most common exchangeable cations, in order of their affinity for clay surfaces are $H^+ > Al^{3+} > Ca^{2+} > Mg^{2+} > K^+ > Na^+$ (Mikula 2017). This is largely due to ionic radii of the cation present, which will decrease with increased cation charge and lower atomic mass, resulting in a stronger ionic potential. Figure 5 shows the preference based on ionic radii only.

Another factor that relates to this sequential surface interaction is the relative hydration energy of the cation. The potassium ion has a greater affinity for binding to the clay surface largely because sodium has higher hydration energy (-405kJ/mol vs -321kJ/mol), hence sodium tends to be released from the surface of clays during hydration whereas potassium is not. These factors combined influence the thermodynamic balance between ion adsorption and hydration energies.

This would then suggest that the observed increase in release water cation concentrations shown in Figure 3 are as a direct result of a combination of the pH change and cation exchange brought about by the Al^{3+} and H^+ cations having a greater affinity for the charged surfaces present in the MFT mineralogy. That is, the protons and aluminum cations are displacing calcium, magnesium and potassium from the surface of the clay particles.

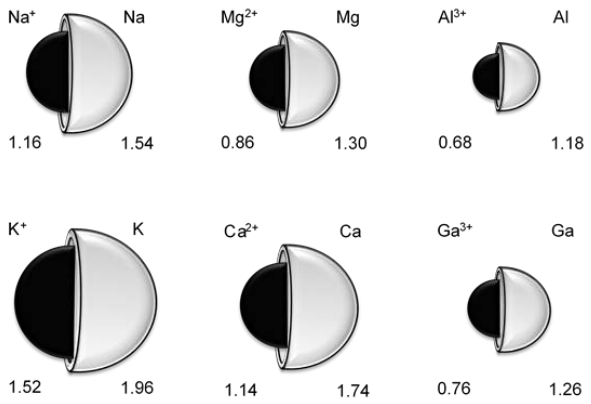

Figure 5. Relative Atomic Radii (A^O) of several elements and their ions

Part 3: Impact of Alum Addition in Combination with PAM

The final part of this investigation sought to investigate what happens to the release water chemistry when the tailings are treated with a combination of alum and PAM, as is done conventionally in field treatment applications. (Ockershausen 1965) The results are shown in Figure 6.

The data shown directly correlates to the data described in Figure 3. All four MFT samples had the

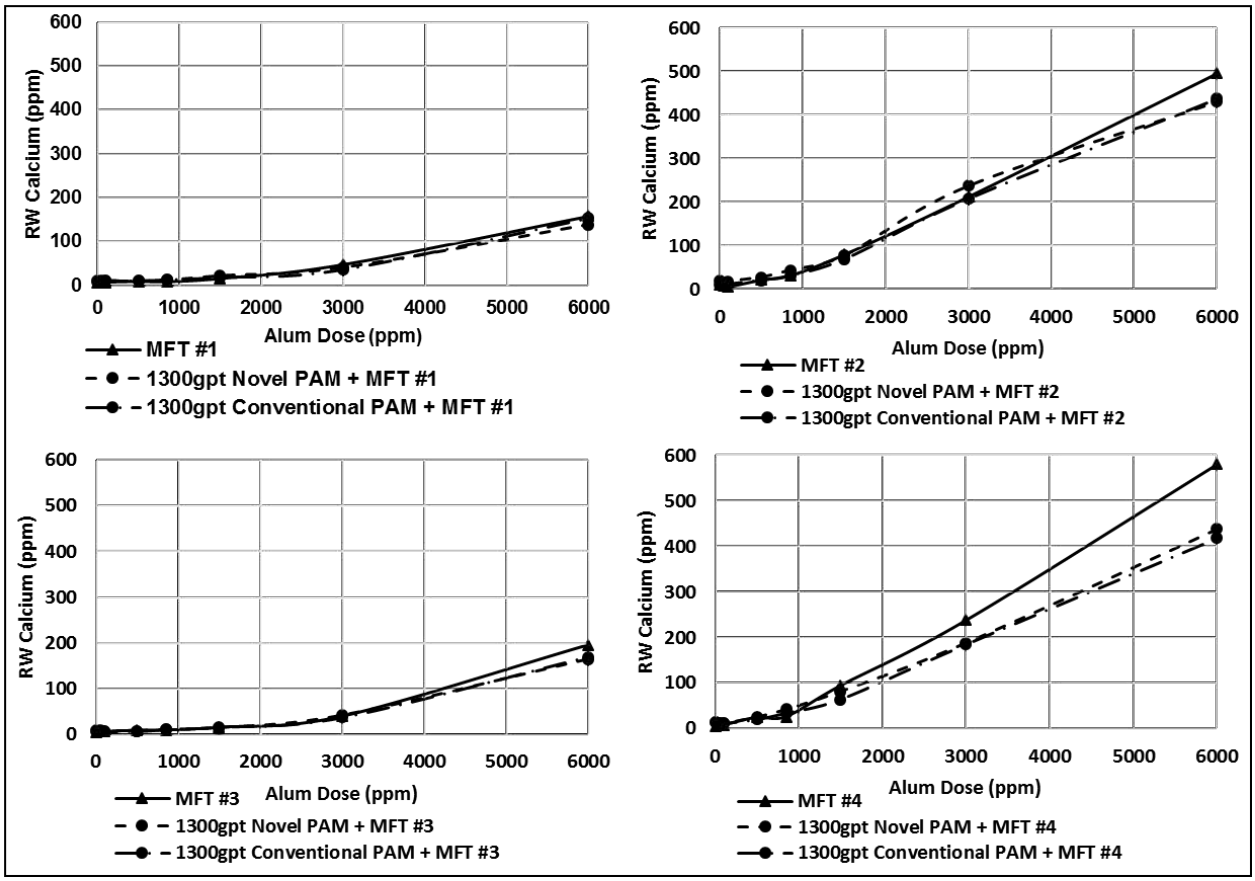

Figure 6. Comparing polymer treated MFT samples RW Ca content with increasing alum dose

same increase in release water cations when exposed to alum in combination with PAM. However, the values observed show very little difference to those seen by using alum alone. This would then indicate that the increase in the release water cations is driven completely by the utilization of alum as a pretreatment coagulant, and not by the use of either a conventional or novel PAM.

There are several potential mechanisms for this to occur, but most likely it is a result of cation exchange occurring prior to the flocculation step. The calcium cation associated with the Novel PAM will most likely be utilized to facilitate the formation of ionic bonds between the flocculant and the mineral surface during the adsorption step. This should then result in the cations being associated with the mineral itself, not impacting the release water chemistry during the dewatering step (Mahmoudkhani 2012). This suggests that in order to limit the increase in release water cations such as Ca^{2+} or Mg^{2+}, great care should be given to dosing of alum and the mineralization of the tailings stream being treated. “Overdosing” of the alum solution will result in a significant increase in the concentrations of these cations, which would make the release water recovered from the tailings less suitable for recycling to the bitumen extraction process.

CONCLUSIONS

The use of the inorganic coagulant alum caused a significant increase in the concentration of soluble calcium present in the release water from dewatered MFT. The probable cause of the observed increase was the displacement of calcium cations by aluminum from solids particle surfaces. This is because the clay normally provides a mineral sink for removing calcium and magnesium from the process water in the operation, as these are retained with the solids in the tailings. The data also suggests that the use of either conventional PAM or novel PAM had no significant effect on the concentration of soluble calcium present in the release water. With these factors in mind, the

utilization of acidified alum as a coagulant in the oil sands should be monitored carefully by operators to ensure that the concentration of multivalent cations in recycled process water does not increase significantly, thereby potentially impacting the bitumen extraction processes.

ACKNOWLEDGEMENTS

BASF would like to thank Dr. Robert Downs for his phenomenal work and assistance with the X-Ray diffraction analysis. This software was programmed by Gordie Downs, an electrical engineering and math student at the University of Arizona and is in use by the CheMin team to analyze the soils of Mars on the NASA rover Curiosity. We also would like to thank CNRL for allowing us to collaborate on this project with them in the spirit of continued collective research.

REFERENCES

Botha, L. and Soares, J. B. P. (2015). The Influence of Tailings Composition on Flocculation. The Canadian Journal of Chemical Engineering, **93:** 1514-1523.

Coulter, B. S. and Talibudeen, O. (1968). Calcium: Aluminum Exchange Equilibria in Clay Minerals and Acid Solids. Journal of Soil Science, **19**: 237-250.

Ding, X., Repka, C., Xu, Z. and Masliyah, J. (2006). Effect of Illite Clay and Divalent Cations on Bitumen Recovery. The Canadian Journal of Engineering, **84**: 643-650.

Eisazadeh, A., Anuar Kassim, K. and Nur, H. (2011). Cation exchange capacity of a quartz rich soil in an acidic and basic environment, Advanced Materials Research, **255-260**: 2766-2770.

Ellis, D. (2017). Directive 085. Fluid Tailings Management for Oil Sands Mining Projects. Alberta Energy Regulator. October 12, 2017. Edmonton, Alberta. pp. 1-4.

Kaminsky, H. (2008). Characterization of Athabasca oil sands ore and process streams. University of Alberta, Edmonton, Alberta, 2008. pp. 50-58.

Kasongo, T., Zhou, Z., Xu, Z. and Masliyah, J. (2000). Effect of Clays and Calcium Ions on Bitumen Extraction from Athabasca Oil Sands Using Flotation. The Canadian Journal of Engineering, **78**: 674-681.

Loganathan, K., Bromley, D., Chelme-Ayala, P. and Gamal El-Din, M. (2015). A hybrid froth flotation-filtration system as a pretreatment for oil sands tailings pond recycle water management: Bench- and pilot-scale studies. Journal of Environmental Management, **161**: 113-123.

Mahmoudkhani, A., Tellakula, R., Watson, P., Fenderson, T., Steward, K. and Wu, Y. (2012). Consolidation of oil sands process tailings by enhanced coagulation - flocculation. IOSTC 2012, Edmonton, Alberta, December 2-5, 2012. pp. 121-132.

Mikula, R. (2012). Evaluation of off the shelf and off the wall tailings treatment technologies: a cautionary tale. IOSTC 2012, Edmonton, Alberta, December 2-5, 2012. pp. 231-236.

Mikula, R. (2017). The Role of Clays in the Performance of Oil-Sands Tailings Management Options. Introduction to Oil Sands Clays. NAIT, Edmonton, Alberta, June 4th, 2017, **22**(8): 164-224.

Ockershausen, R. W. (1965). Use of Alum in Water Plants. Journal of American Water Works Association, **57**(3): 309-313.

Pelaez, M. and Fenderson, T. (2016). Application of Novel Polymer Combined with Inorganic Coagulation for Consolidation of Oil Sands Tailings. IOSTC 2016, Lake Louise, Alberta, December 4-7, 2016. pp. 214-218.

Sanford, E.C. (1983). Processability of Athabasca Oil Sand: Interrelationship Between Oil Sand Fine Solids, Process Aids, Mechanical Energy and Oil Sand Age after Mining. The Canadian Journal of Engineering, **61**: 554-567.

Znidarcic, D., Adkins, S., Utting, L. and Catling, M. (2015). Rheomax® ETD technology, a laboratory study of application performance and associated geotechnical characteristics for polymer assisted tailings deposition of oil sands MFT, Tailings and Mine Waste ‘15 conference proceedings, October 25-28, Vancouver, BC, Canada, pp. 508-520.

Session 6

TAILINGS CHARACTERIZATION

MEASURING SOLIDS CONTENT IN FLUID FINE TAILINGS (FFT) USING A LOW-LEVEL X-RAY RADIATION SOURCE

Bo Yu[1], Wei Wang[1], Felipe Goncalves[1], Priyesh Dhandharia[1],
Andrea Sedgwick[2], Abu Junaid[3], Manisha Gupta[1], R. Fedosejevs[1] and Y.Y. Tsui[1]
[1]University of Alberta, Edmonton, Canada
[2]Northern Alberta Institute of Technology, Edmonton, Canada
[3]Canadian Natural Resources Limited, Calgary, Canada

ABSTRACT

Fluid fine tailings (FFT) are produced after the extraction of bitumen from oil sands, and are composed mainly of water, sands, clay and residual bitumen. X-ray attenuation is a useful technique to measure the variation in density of FFT. Generally, this method is implemented using highly radioactive sources which makes it unsuitable for real-time, large area monitoring such as tailing ponds where several such detectors might be required. In this study, we report the measurement of solid content in tailing samples using an Americium (Am^{241}) source with significantly lower radioactivity equivalent to a level typically released by a smoke detector used in residential buildings and households. Our experiments and simulations were conducted on a number of kaolinite and FFT samples. GEANT4, a Monte Carlo based simulation code to calculate the transmission of radiation through matter, was employed to simulate the results of this study. We observed good agreement between the experimental and simulation results, thus paving the way for a real-time solid content measurement system deployable over large areas.

INTRODUCTION

Canada's oil sands are one of the largest unconventional fossil reserves, constituting 9.6% of the global proven reserves (BP 2018), and 81% of the world's total bitumen reserve (Meyer et al. 2003). With a total estimated deposit of 1.7 trillion barrels, out of which ~165 billion barrels is proven (recoverable using current technologies), it is the world's third largest reserve after Saudi Arabia and Venezuela (Government of Alberta 2018). The production from this valuable resource is expected to increase from 2.8 million bbl/d in 2017 to 3.9 million bbl/d by 2027 (Government of Alberta 2018).

While the economy of Alberta benefits much from the mining of oil sands, some environmental challenges arise from its exploration activities. One of them is the growing volume of stored tailings generated from the extraction of bitumen from the oil sands ore using substantial amounts of water. The tailings inventory is large and increasing each year. In 2013, the ponds covered an area of about 77 square kilometers (Government of Alberta 2013). There are currently 1,100 Mm^3 of fluid fine tailings stored in tailings ponds (Alberta Energy Regulator 2016). Government regulations, such as the Alberta Energy Regulator's Directive 85 (Alberta Energy Regulator 2017) outline requirements for tailings ponds closure.

Proper monitoring of solids settling is essential for tailings pond reclamation. Currently the settling of solids in tailings is primarily monitored by manual sampling along the pond depths and lab analysis which is onerous, not real time and may be misrepresentative due to sampling issues. For better management of fluid fine tailings, a more efficient, dependable and low-cost technique is necessary to monitor the concentration of solid content during the settling process which can help the oil sands producers meet their regulatory requirements.

X- and gamma (γ) -ray attenuation has been widely used for studying environmental samples. Many experimental and theoretical values for physical properties of soil, such as mass attenuation coefficient, density and water content, have been reported over the years (Al-Masri et al. 2013, Costa et al. 2014, De Groot et al. 2009, Pires & Medhat 2016, Taqi et al. 2017). Most of these results were obtained by using high-intensity sources, which are very expensive and harmful. It is impractical to use them for oil sands tailings application as a large number of detectors are required to measure the solid concentration at different depths of the ponds for modeling purposes. In this study a novel method for solid content analysis is proposed using

much weaker X-ray sources while achieving multi-point measurements with reasonable accuracy.

MATERIALS AND METHODS

Sample Collection and Preparation

The kaolinite clays used in this study were obtained from National Resources Canada (NRCAN) and the FFT samples were provided by Canadian Natural Resources Limited's Albian facility. The chemical compositions (except H and O) of each sample were measured by inductively coupled plasma-mass spectrometry (ICP-MS). The atomic number ratios of H and O of dry kaolinite and FFT are both assumed to be 4:9, according to the chemical formula of kaolinite, $Al_2Si_2O_5(OH)_4$. The composition data are shown in Table 1 as percentage of dry solids.

Table 1. Chemical compositions of kaolinite and FFT

Element	wt%	
	Kaolinite	FFT
Al	13.6	6.49
Si	20.5	22.4
Fe	0.457	1.64
Ca	0.362	0.668
K	0.351	1.67
Ti	0.196	0.404
Mg	0.111	0.514
H	1.75*	1.80*
O	62.7*	64.43*

* Calculated Value. For details please refer to MATERIALS AND METHODS section

The kaolinite clay was dissolved in distilled water to make different weight percent (wt%) solutions (10, 20, 30, 40). Two to three drops of 1M NaOH were added to each solution to maintain the pH around 11 in order to reduce the influence of settling. The FFT solutions were prepared by diluting a 41 wt% FFT sample. The volume and mass of each sample were measured by calibrated cuvettes and a high precision balance respectively. The calculated densities are shown in Table 2. The uncertainty of each measurement was estimated at ± 0.02 g/cm^3. During the measurements, all samples were kept in GMPT macro polystyrene cuvettes with dimensions of 45 mm × 12.5 mm × 12.5 mm (outside) and 35 mm × 10 mm × 10 mm (inside).

Table 2. Density of kaolinite and FFT samples

Sample	wt%	Density in g/cm^3
Kaolinite	10	1.07
	20	1.15
	30	1.24
	40	1.31
FFT	10	1.05
	20	1.12
	30	1.22
	40	1.29

X-Ray Attenuation

X-ray attenuation was used to measure the density of kaolinite and FFT samples. When passing an absorber, the attenuation of X-rays follows the Beer-Lambert law as shown in Equation 1:

$$I=I_0\exp(-\alpha x) \quad (1)$$

where I_0 is the incident intensity of X-rays and I is the attenuated intensity after passing through a material of thickness x. The linear attenuation coefficient, α (cm^{-1}), at the incident photon energy, can be written as the product of density and the mass attenuation coefficient, μ_m (cm$^2\cdot$g^{-1}).

$$\alpha=\mu_m\rho \quad (2)$$

The mass attenuation coefficient varies with the energy of the X-ray photon that transmits through the material. In this study, we measured the ratio of two X-ray peaks at 17.8 keV and 59.5 keV using a 0.9μCi Am241 source for different weight percent solid content of kaolinite and FFT. Equations 3 and 4 show the attenuated intensity for 17.8 keV and 59.5 keV X-ray peaks, respectively.

$$I_{(17.8)}=I_{0(17.8)}\exp(-\mu_{m(17.8)}\rho x) \quad (3)$$

$$I_{(59.5)}=I_{0(59.5)}\exp(-\mu_{m(59.5)}\rho x) \quad (4)$$

The 59.5 keV X-ray is produced directly from the alpha decay of Am^{241} (Jaffe et al. 1955), whereas the 17.8 keV X-ray is from the $L_{\beta 1}$ decay of Np^{237} produced by the alpha decay of Am^{241} (Day 1955). The 17.8 keV photon energy is much lower than 59.5 keV photon energy and is attenuated more strongly by the kaolinite and the FFT compared to water. Measuring this extra attenuation provides good sensitivity to the variation of the mass fraction. The 59.5 keV, on the other hand, is not attenuated much by the samples, and therefore acts as a good reference of the source strength. The ratio of the 17.8 keV peak area to the 59.5 keV peak area was used as a monitoring parameter for the variation of the mass fraction of the tested sample. We can then represent the ratio by

$$R = \frac{I_{17.8}}{I_{59.5}} = \frac{I_{0(17.8)}\exp(-\mu_{m(17.8)}\rho x)}{I_{0(59.5)}\exp(-\mu_{m(59.5)}\rho x)}$$

$$= \frac{I_{0(17.8)}}{I_{0(59.5)}}\exp[-(\mu_{m(17.8)}-\mu_{m(59.5)})\rho x] \qquad (5)$$

Experimental Procedures

A schematic layout of the measurement setup is shown in Figure 1. A 0.9μCi Am^{241} source was placed in a plastic disc and then mounted in a polyvinyl chloride (PVC) source holder. The setup was designed to ensure the center of the detector probe and the center of the source face were arranged at the same height. The distance between the source and the detector was 27.5 mm. The intensity of the transmitted X-rays was measured by a cadmium telluride (CdTe) detector (XR-100T-CdTe, Amptek). An amplifier and power source (PX2T, Amptek) was used to power the detector and produce analog signals. A multichannel analyzer (MCA8000A, Amptek) was used to complete the analog-to-digital conversion. Resolution (FWHM) of this system was 0.4 keV at 17.8 keV and 0.8 keV at 59.5 keV, respectively, using 1024 readout channels. The calibration to convert channel number to energy scale was done according to the recommended peak x-ray photon energies of Am^{241} from the International Atomic Energy Agency (IAEA). For each sample, the measurement time was 10 minutes, and each measurement was repeated 5 times to calculate the average and standard deviation of the peak ratios. In between each 10-minute measurement,

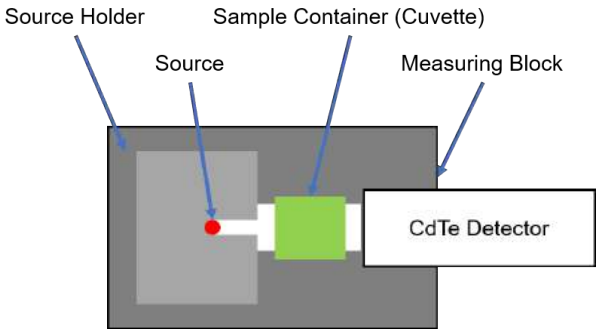

Figure 1. Experimental setup schematic

each cuvette was shaken sufficiently to ensure that the sample was homogenous.

A measured X-ray emission spectrum is shown in Fig. 2(a). Raw recorded data spectra with water and with air in the cuvette at 17.8 keV and 59.5 keV are shown in Figs. 2(b) and 2(c), respectively.

Mass Attenuation Calculation

Mass attenuation coefficients of elements in kaolinite and FFT were obtained from the National Institute of Standards and Technology (NIST) database (Berger et al. 2008) and calculated for 17.8 keV and 59.5 keV by linear interpolation. The results are shown in Tables 3(a) and 3(b). These coefficients result from different cross-sections of interaction between photons and matter, such as photoelectric absorption, coherent scattering and incoherent scattering. The actual attenuation coefficient for a given measurement geometry depends on how much of the scattered X-ray flux is intercepted by the detector. This means that the expected attenuation for our system will be between the photoelectric value and total attenuation value.

This also indicates that the expected peak ratio for our system will be between a minimum value and a maximum value. These two boundary values are defined as

$$R_{max} = \frac{I_{(17.8\ \text{photoelectric})}}{I_{(59.5\ \text{total})}} \qquad (6)$$

$$R_{min} = \frac{I_{(17.8\ \text{total})}}{I_{(59.5\ \text{photoelectric})}} \qquad (7)$$

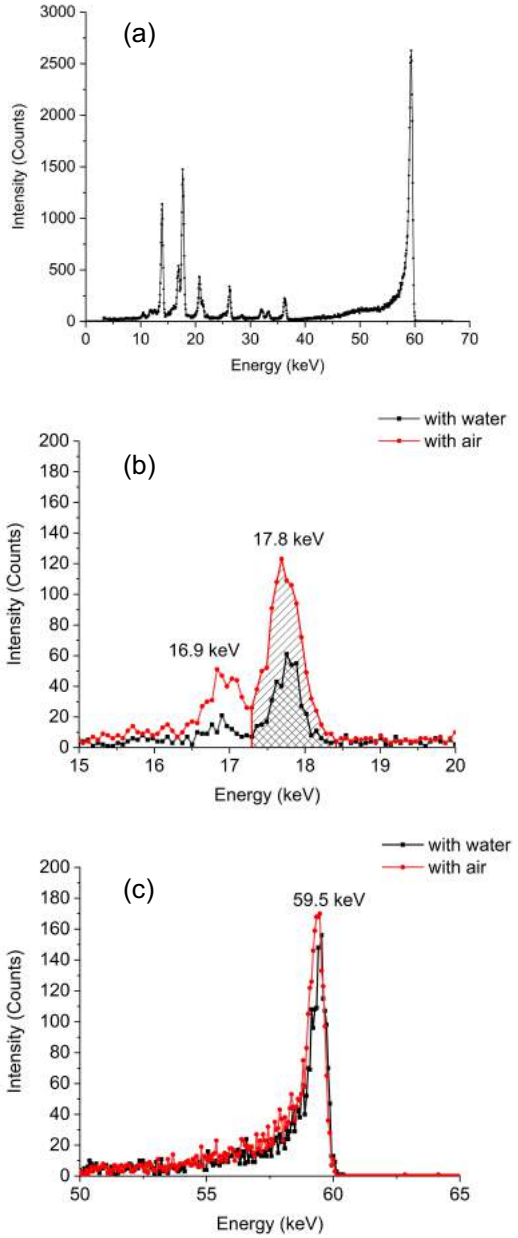

Figure 2. Measured X-ray spectra: (a) X-ray source emission spectrum; (b) spectra of 16.9 keV and 17.8 keV X-rays obtained with water and air in the cuvette taken in a period of 10 minutes with a 0.9 μCi Am^{241} source and (c) spectra of 59.5 keV X-ray obtained with water and air in the cuvette taken in a period of 10 minutes with a 0.9 μCi Am^{241} source

Table 3. Mass attenuation coefficients of elements from NIST

(a) photoelectric absorption

Element	Mass attenuation coefficients (photoelectric Absorption) μ_m in cm^2/g	
	17.8 keV	59.5 keV
Al	5.043	0.09945
Si	6.623	0.1339
Fe	38.77	1.014
Ca	19.84	0.4597
K	16.58	0.3762
Ti	24.06	16.32
Mg	3.975	0.07641
H	4.365×10^{-4}	5.896×10^{-6}
O	1.0214	0.01750

(b) total attenuation

Element	Mass attenuation coefficients (total Attenuation) μ_m in cm^2/g	
	17.8 keV	59.5 keV
Al	5.428	0.2823
Si	7.049	0.3265
Fe	39.50	1.243
Ca	20.42	0.6760
K	17.13	0.5828
Ti	24.66	16.85
Mg	4.344	0.2606
H	0.3725	0.3265
O	1.292	0.1918

The mass attenuation coefficients of kaolinite and FFT can be calculated by

$$\mu_m = \sum \frac{w_i}{100} * \mu_{mi} \quad (8)$$

$$\mu_{m(Sample)} = (w_t/100) * \mu_{m(kaolinite\ or\ FFT)} + ((100-w_t)/100)*\mu_{m(H_2O)} \quad (9)$$

where w_i% and μ_{mi} are the weight percent (Table 1) and mass attenuation coefficient (Tables 3(a) and 3(b)) of the i_{th} constituent element in kaolinite or FFT; w_t% is the weight percent of a solution. The same process can be used to calculate

$\mu_{m(H_2O)}$ when w_t is zero. The results are given in Tables 4(a) and 4(b).

The initial ratio $I_{0(17.8)}/I_{0(59.5)}$ was measured with an empty cuvette (only air inside) as 0.282 ± 0.010. In this study, the thickness of the samples is the regarded as the inside dimension along the direction of the transmitted rays, in this case, 1cm. Using these data, the ratio of transmitted 17.8 keV and 59.5 keV peak areas were calculated and shown in Figs. 3 and 4.

Table 4. Calculated mass attenuation coefficients of samples

(a) photoelectric absorption

Sample		Mass attenuation coefficients $\mu_{m(Sample)}$ in cm^2/g	
	wt%	17.8 keV	59.5 keV
Water	0	0.9069	0.01555
Kaolinite	10	1.120	0.02315
	20	1.334	0.03076
	30	1.547	0.03836
	40	1.760	0.04596
FFT	10	1.179	0.02798
	20	1.451	0.04041
	30	1.723	0.05284
	40	1.995	0.06528

(b) total attenuation

Sample		Mass attenuation coefficients $\mu_{m(Sample)}$ in cm^2/g	
	wt%	17.8 keV	59.5 keV
Water	0	1.190	0.2070
Kaolinite	10	1.407	0.2137
	20	1.625	0.2205
	30	1.843	0.2273
	40	2.061	0.2341
FFT	10	1.466	0.2187
	20	1.743	0.2305
	30	2.020	0.2423
	40	2.298	0.2541

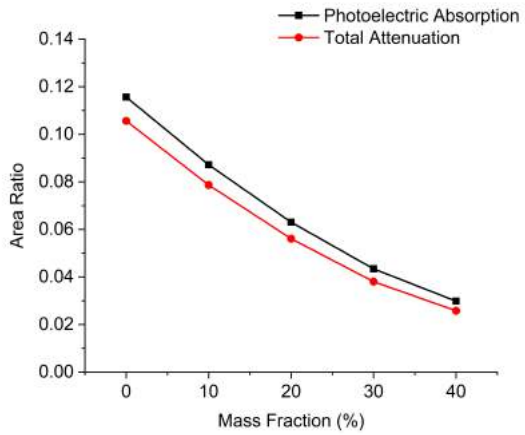

Figure 3. Ratio of transmitted 17.8 keV and 59.5 keV peak areas for kaolinite obtained by mass attenuation calculation

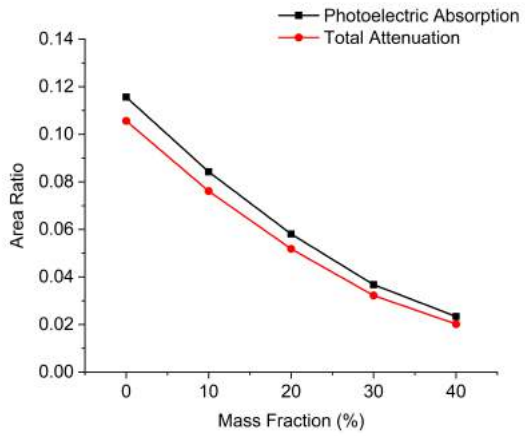

Figure 4. Ratio of transmitted 17.8 keV and 59.5 keV peak areas for FFT obtained by mass attenuation calculation

Monte Carlo simulation by Geant4

Geant4 is a Monte Carlo Simulation toolkit designed to simulate the passage of particles through matter. Here we used Geant4 to model the X-ray attenuation in our system.

In the Geant4 code, the simulation model is constructed to match the actual setup, which is shown as Fig 5. It simply contains an X-ray source, a sample cuvette and an X-ray detector. These three modules are placed respectively in the same optical axis. The photons will be generated by the source, attenuated by the sample, and then collected by the detector.

In the initial simulation step, the X-ray source was simplistically defined as a point source. The beams are all from a single point and are all ejected along the z-axis. Here the area of source and the cone angle of the beams are neglected in the simplified model. For the source spectrum, we used two delta functions in the frequency domain to simulate a source with two monochromatic lines, which represent the two main peaks of the actual source. The spectrum of the source is shown in Fig 6. Here we used the measured ratio of 0.282 for the 17.8 keV to the 59.5 keV lines, to match the measured data of the source.

For the simulation, the same dimensions as in the experimental setup were used to define the cuvette. Regardless of the wall, we assume the effective volume of the cuvette is $10 \times 10 \times 35\ mm^3$ and filled with samples. The measured chemical compositions of kaolinite and FFT samples of different concentrations (weight percent of dry solids) (Table 1) and the measured density values (Table 2) were used for the simulations to define the sample.

The detector was defined as a 3 mm × 3 mm × 1 mm CdTe crystal. It is regarded as an ideal detector, which collects all the X-ray photons that go though its surface. The photoelectric stepping power of the crystal for 59.5 keV photons is 99%. The actual detector in the experimental setup collects most of the X-ray photons incident in each channel. As some photons near the edge of the detector may not deposit all their energy in the detector, using the ideal detector in the simulations may cause some minor deviations from the experimental results.

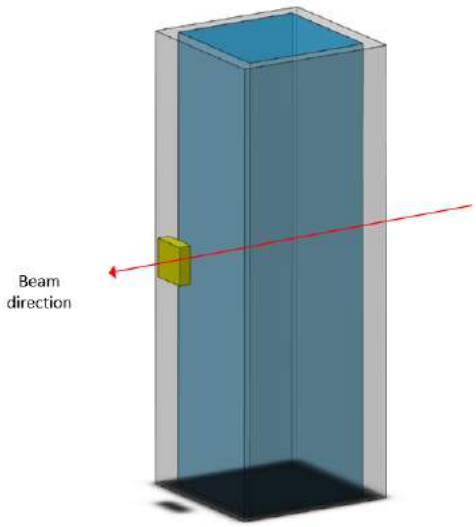

Figure 5. The geometry of Geant4 simulations

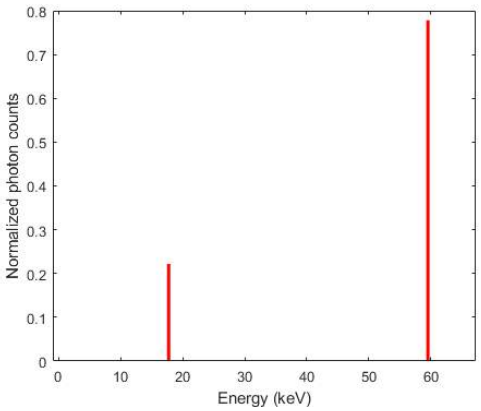

Figure 6. Spectrum of the simulated source

RESULTS AND DISCUSSION

The measured and calculated mass attenuation coefficient peak area ratios are shown in Figs.7 and 8. The measured values are between R_{min} and R_{max}, which agree with our prediction. The experimental peak ratios are much closer to R_{max} compared to R_{min}. This is because the majority of the 59.5 keV photons are attenuated by scattering, while the majority of 17.8 keV photons are attenuated by photoelectric absorption.

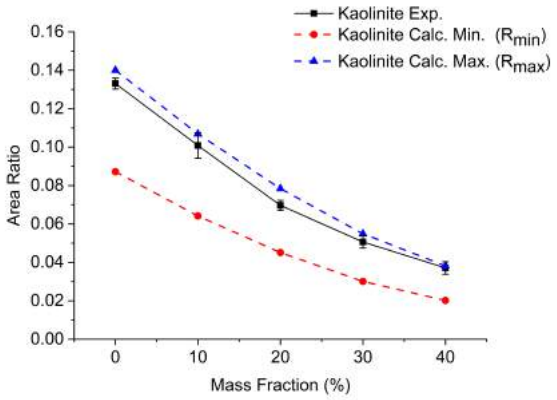

Figure 7. Ratio of measured transmitted 17.8 keV and 59.5 keV peak areas and mass attenuation calculated peak area ratios for kaolinite

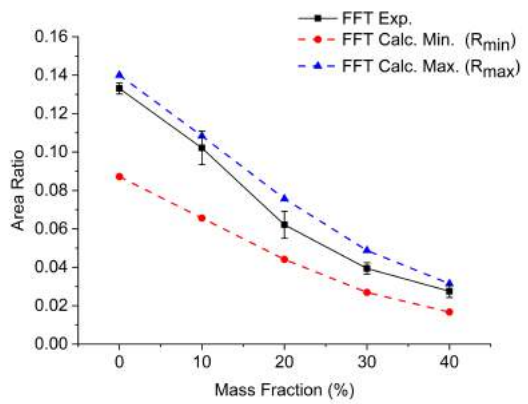

Figure 8. Ratio of measured transmitted 17.8 keV and 59.5 keV peak areas and mass attenuation calculated peak area ratios for FFT

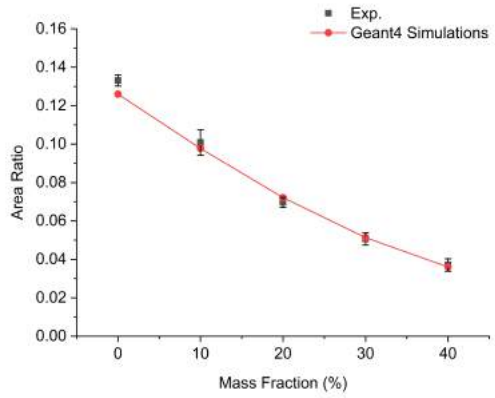

Figure 9. Ratio of measured transmitted 17.8 keV and 59.5 keV peak areas and calculated peak area ratios from GEANT 4 for kaolinite

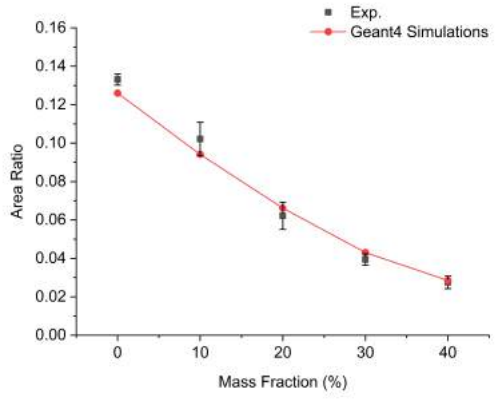

Figure 10. Ratio of measured transmitted 17.8 keV and 59.5 keV peak areas and calculated peak area ratios from GEANT 4 for FFT

Figs. 9 and 10 show the comparison between measured and Geant4 simulated results for the two samples. For 20, 30 and 40 wt%, solid concentrations, they are in reasonably good agreement. However, the measured values tend to be higher than the simulated ones at solid concentrations of 10 wt% and 0 wt% (water). This is possibly caused by additional scattering of X-rays from the sample alignment holder which is not taken into account in the present simulations. This discrepancy is the subject of ongoing studies.

CONCLUSION

In general, good agreement was observed between the experimentally determined peak ratios, the calculated values using mass attenuation coefficients, and the Geant4 simulation results. Based on this, we expect to develop a real-time solid content measuring system using a weak 0.9 μCi Am^{241} source with a reasonable acquisition time which could readily be deployed in large tailings ponds. Studies are ongoing to further optimize the acquisition time, miniaturize the detector setup and reduce the cost of the multichannel analyzer. The discrepancies between the measured and calculated values will also be studied in more detail in the future.

ACKNOWLEDGEMENT

We would like to acknowledge the financial support for this research project by the Natural Sciences and Engineering Research Council of Canada, the Institute of Oil Sands Innovation (IOSI) and Canada's Oil Sands Innovation Alliance (COSIA).

REFERENCES

Alberta Energy Regulator. (2017). Fluid Tailings Management for Oil Sands Mining Projects. *Alberta Energy Regulator Directive 085.*

Alberta Energy Regulator. (2016). *Mineable Oil Sands Fluid Tailings Status Report 2014 and 2015.*

Al-Masri, M. S., Hasan, M., Al-Hamwi, A., Amin, Y. and Doubal, A. W. (2013). Mass attenuation coefficients of soil and sediment samples using gamma energies from 46.5 to 1332 keV. *Journal of environmental radioactivity*, **116**: 28-33.

Berger, M. J., Hubbell, J. H., Seltzer, S. M., Chang, J., Coursey, J. S., Sukumar, R., Zucker, D. S. and Olsen, K. (2008). NIST standard reference database 8 (XGAM). *XCOM: Photon Cross Sections Database*.

British Petroleum Company. (2018). *BP statistical review of world energy*. British Petroleum Company.

Costa, J. C., Borges, J. A. R. and Pires, L. F. (2014). Effect of collimator size and absorber thickness on soil bulk density evaluation by gamma-ray attenuation. *Radiation Physics and Chemistry*, **95**: 333-335.

Day, P. P. (1955). Electromagnetic Spectrum of Am 241. *Physical Review*, **97**(3): 689.

De Groot, A. V., Van der Graaf, E. R., De Meijer, R. J. and Maučec, M. (2009). Sensitivity of in-situ γ-ray spectra to soil density and water content. *Nuclear Instruments and Methods in Physics Research Section A: Accelerators, Spectrometers, Detectors and Associated Equipment*, **600**(2): 519-523.

Government of Alberta. (2013). Oil Sands Tailings. *Fact Sheet Tailings*

Government of Alberta, Energy. (2018). Oil Sands. Retrieved from https://www.energy.alberta.ca/OS/Pages/default.aspx

Government of Alberta, Energy. (2018). Oil Sands 101. Retrieved from https://www.energy.alberta.ca/OS/AOS/Pages/OilSands101.aspx

Jaffe, H., Passell, T. O., Browne, C. I. and Perlman, I. (1955). Gamma and X-Radiation in the Decay of Am 241. *Physical Review*, **97**(1): 142.

Meyer R.F., Attanasi E.D. and Freeman P.A. (2003). Heavy oil and natural bitumen--strategic petroleum resources. Retrieved from http://pubs.usgs.gov/fs/fs070-03/fs070-03.html

Pires, L. F. and Medhat, M. E. (2016). Different methods of mass attenuation coefficient evaluation: Influences in the measurement of some soil physical properties. *Applied Radiation and Isotopes*, **111**: 66-74.

Taqi, A. H. and Khalil, H. J. (2017). An investigation on gamma attenuation of soil and oil-soil samples. *Journal of Radiation Research and Applied Sciences*, **10**(3): 252-261.

OPTICAL SCATTERING TECHNIQUE TO MONITOR SOLIDS CONTENT IN FLUID FINE TAILING (FFT)

Priyesh Dhandharia[1], Wei Wang[1], Yu Wan[1], Bo Yu[1], Andrea Sedgwick[2], Abu Junaid[3], R. Fedosejevs[1], Manisha Gupta[1] and Ying Y. Tsui[1]
[1]University of Alberta, Edmonton, Canada
[2]Northern Alberta Institute of Technology, Edmonton, Canada
[3]Canadian Natural Resources Limited, Calgary, Canada

ABSTRACT

Sub-surface solids content measurement of tailing ponds is essential for its management and land reclamation activities. Currently, solids content is primarily analyzed by manual sampling and offline analytical methods such as gravimetric measurements. In this study, we explore an optical scattering technique to monitor solids content in tailings ponds in real time. Experiments have been carried out with kaolin and fluid fine tailings (FFT) samples with various solids contents using different wavelength laser sources. Measurements were conducted in a calibration ring as well as insert tube, which is designed for deployment in tailing ponds. It was found that certain wavelengths give better responsivity versus the change in the concentration of solid content. However, FFT samples from two different tailing ponds showed different behaviors within those wavelengths. To better understand the dependence of scattering on solids content concentration, Finite Difference Time Domain (FDTD) simulations have also been developed. This technique will allow real-time *in-situ* monitoring of solid content to give both the lateral and depth solid content distributions.

INTRODUCTION

The real-time analysis of solids content and particle size in the tailings pond is important from both environmental and oil-sands extraction points of view (COSIA 2012). From the environmental perspective, the knowledge of solids content will help in water and land reclamation activities, geotechnical stability and ecological development of the reclaimed area. From the oil sands extraction perspective, faster rate of settling means faster recovery and recycling of process water and less land requirement for disposing of the newly generated tailings. Moreover, the risks related to large volumes of tailings in tailings dams may affect the long term stability due to solid content settling issues (UN Environment 2017). Therefore, there is a significant effort from the industry to develop a technology which can increase the settling rate of tailing ponds. Timely information about the solid content and particle size distribution at various depths can provide valuable information on settling and impact the treatment strategies. The current practice to measure the solids content in the ponds is primarily based on gravimetric techniques. To map out the full pond, this technique is time-consuming and can be erroneous due to manual sampling requirement. Real-time *in-situ* optical scattering techniques offers a novel and effective way to monitor the solids content in tailings ponds.

Optical light scattering techniques have been widely used to characterize the size distribution and concentration of particles in solutions (Allen 1990). Dynamic and static light scattering are two techniques widely used in this regard. However, these techniques work for very dilute solutions where single scattering assumptions can be made and not for streams with multiple types of solids like sand, silt and clay. Another method of solids content measurement is turbidity. This method works better when higher concentrations are present. In principle, the concentration of the solids from turbidity measurement can be made provided particle size, shape, etc. are known and the fluid is not contaminated by organics or excess salt. However, in the oil sands, the size and shape are not known as they change as the depth in the pond changes. The particle size is a factor in understanding the geotechnical stability of the pond, therefore adding that information to the solids content would be extremely helpful for the geotechnical and tailings models. A tool to characterize the particle size is Focused Beam Reflectance Measurement (FBRM) which measures the chord length distribution vis-a-vis particle size (Yu et al. 2008). However, the solid content cannot be determined by this technique. There is a strong benefit for development of a system which can determine both solids content and particle size simultaneously. A key factor in developing this new

instrument is that the system must be safe and economical so it can be implemented at multiple locations and depths within the pond for real-time online monitoring.

We have previously presented the solid content analysis of various tailings samples utilizing back-scattered light (Gupta et al. 2012, Ho 2015). It is well known that the scattering from a spherical particle depends on its size (φ) and excitation wavelength (λ). Mie and Tyndall scatterings occur when the excitation wavelength, is approximately equal to the particle size, (i.e., $\lambda/\varphi \sim 1$) or larger than but comparable to the particle size, φ, (i.e., $1 > \lambda/\varphi > 0.1$). Rayleigh scattering occurs when the particle size is much smaller than the wavelength (i.e., $\lambda/\varphi < 0.1$). In tailing ponds the particle size distribution can range from submicron to 100's of micron (COSIA 2012, Mikula et al. 1996). φ <44 μm are considered to be fines which contain clays that take significant time to settle. It has been reported that for solid contents up to 55 wt% the fines content could vary from 50% to 100% (Mikula et al. 1996). Therefore, significant scattering will occur due to the fine particles present in the tailing sample. In our study, probing wavelengths ranging from 405 nm to 980 nm are used. Hence, we can assume that much of the scattering will be in a normal refractive index scattering regime and that some of the scattering will lie in the Mie regime with some scattering transitioning to the Tyndall regime.

To interpret the experimental results, it is important to develop a theoretical understanding about the multiple scattering events. The above discussion based on Mie scattering considers the particles to be spherical in shape. However, the fines in the tailings pond contain clays which have layered structures and their shapes can be significantly different from spherical particles. There are several approaches such as FDTD, recursive T-matrix (Winton et al. 1998), Kubelka-Munk (K-M) theory (Ciani et al. 2005), etc. to understand the scattering mechanism from non-spherical particles. K-M theory can determine the absorption and scattering coefficient as well as penetration depth of electromagnetic radiation, however this approach determines the average properties of the sample assuming broad area illumination. Since our sample particles are mainly non-spherical, FDTD can be used to calculate the scattered intensity of each particle, even if they are in complex shapes (ellipsoid, rough sphere). Then intensity distribution was presented in a spherical coordinate system, where theta is the polar angle, and phi is the azimuthal angle, as shown in Fig 4. (a).

EXPERIMENTAL SETUP

Kaolin samples of different particle size were procured from different sources. The details of the kaolin samples are given in Table 1. The particle size analysis was carried out using Malvern Mastersizer 3000. The pH was determined by pH benchtop meter. Different concentrations of kaolin were prepared by mixing kaolin and deionized water. All the kaolin samples were found to settle very quickly. The pH was adjusted by adding 2-3 drops of 1M Sodium Hydroxide (NaOH) to keep the solution between 8 and 11. This significantly decreased the settling rate of kaolin. FFT samples were received from CNRL's Albian tailings storage facilities in two different batches (1-3 and C1-C6). FFT composition was determined by the Dean & Stark method. The characterization data of the FFT (C1-C6) samples is presented in Table 2. No further treatment of tailing samples was done during the scattering experiment.

For this study, 405, 520, 658, 780, 980 nm wavelengths were used. The laser diodes and photodiodes were procured from Thorlabs. The laser diodes were operated using a FL 500 chip and FL591 driver purchased from Wavelength Electronics.

Table 1. Characterization data of the kaolin samples used in this study

Kaolin Sample #	Particle Size Distribution (μm)		
	Dv 10	Dv 50	Dv 90
1	1.02	5.33	19.4
2	1.57	8.54	31.2
3	1.14	7.61	28.6

Two different experimental setups were used in this study. The first setup comprised of a ring with a Si photodetector mounted at different angles with respect to the laser beam axis (Figure 1a). The sample in a 4 mL cuvette was placed at the center of the ring which was illuminated by a collimated laser diode beam. The diameter of the collimated laser diode beam was 2-3 mm. The angle was measured using the arc formula i.e., $s = r\theta$, where s is the arc length, r is the radius of the ring and θ is the angle subtended by the arc at the center of the ring. To compare the results between different wavelengths, power from the laser diode was also monitored by using a beam splitter. All photodiodes were operated in the linear region. The actual power was measured using either a Thorlab or Newark photometer. A Tektronix oscilloscope, TDS 220, was used to measure the output of the

photodetector. The responsivity of all the photodiodes was calculated by dividing the photodiode current with the measured power. The variation between all the photodiodes was found to be within 10%. Before each reading, baseline measurements comprised of the empty cuvette, water and a Teflon diffuser were recorded. The reading from kaolin and FFT was significantly higher than the empty cuvette and water but lower than Teflon, as expected. For the settling experiment, a 405 nm laser diode was used with 6 beam splitters placed 2 cm apart (Figure 1b). From each beam splitter, ~8% of the light was directed to the settling column. The photodiodes were placed at 20° from the laser beam axis and the output signal was amplified with a transimpedance amplifier (gain = -200 mV/nA). The data was collected using a National Instruments USB 6008 analog to digital converter board. The mentioned heights were measured from the base of the settling column.

Table 2. Characterization data of the FFT samples used in this study

FFT Sample #	Solid Content	Bitumen Content	Water	MBI
1	38.69	4.77	56.53	Not available
2	24.68	1.23	73.64	14.10
3	32.09	7.81	60.04	10.6
C1	20.1	2.4	77.6	6.8
C2	26	2.4	71.8	6.9
C3	29.3	2.4	68.5	7.9
C4	26	2	72.1	8.1
C5	18.2	2.1	79.4	9.3
C6	31.5	1.6	67	11.5

RESULTS AND DISCUSSION

Scattering Measurement

Before investigating the scattering behavior of kaolin and FFT sample, the ring setup was characterized with the diffuser. A perfect diffuser should follow Lambert's cosine law. It was noted that the diffuser followed $cos^n\theta$, where n was determined to be between 1.09 to 1.4 (data not presented), which is in reasonable agreement with the law. After the ring system has been characterized, scattering from two different kaolin samples was studied. The exponent n in $cos^n\theta$ was determined to be between 1.07 to 1.27 for all wavelengths and different kaolin concentrations (data not presented). Figure 2a shows the

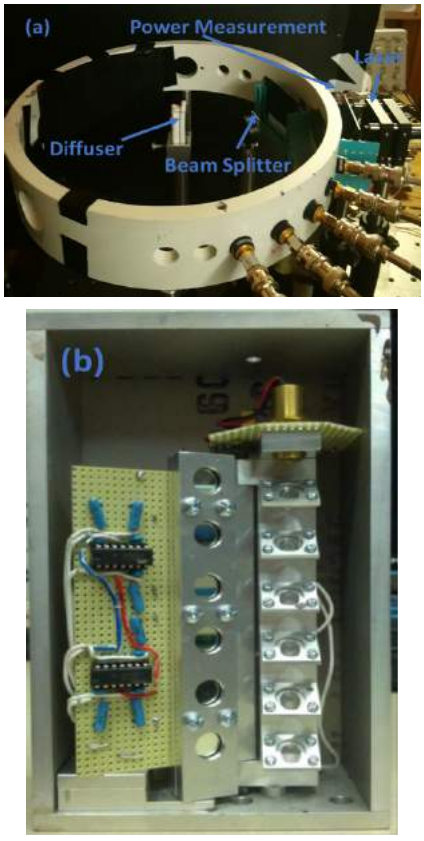

Figure 1. (a) Optical back-scattering characterization setup, (b) Settling experiment setup

scattering (raw data) from Kaolin-2 with 980 nm laser diode. While the back-scattering intensity is maximum at small angle, specular reflection could pose problem. During the experiment, it was found that around 20°, the effect of specular reflection was negligible. Therefore, scattering from both the kaolin samples was compared with the photodetector placed at 21°. To compare the scattering intensity between different wavelengths and samples, normalized scattering intensity was calculated by taking the ratio of scattered power (at a fixed angle) to the input power. Figure 2b and c show the normalized scattering intensity for Kaolin-1 and 2. It is observed that for two different Kaolin we observe different trends with the wavelength. Kaolin-1 demonstrated an increase in the scattering intensity with solids content for all the wavelengths. This is not observed for Kaolin-2. It is expected that with longer wavelength, higher kaolin concentration could be determined. The difference in scattering behavior at 405 nm, between two Kaolin concentrations could be due to particle size distribution. Further studies are required to understand this behavior.

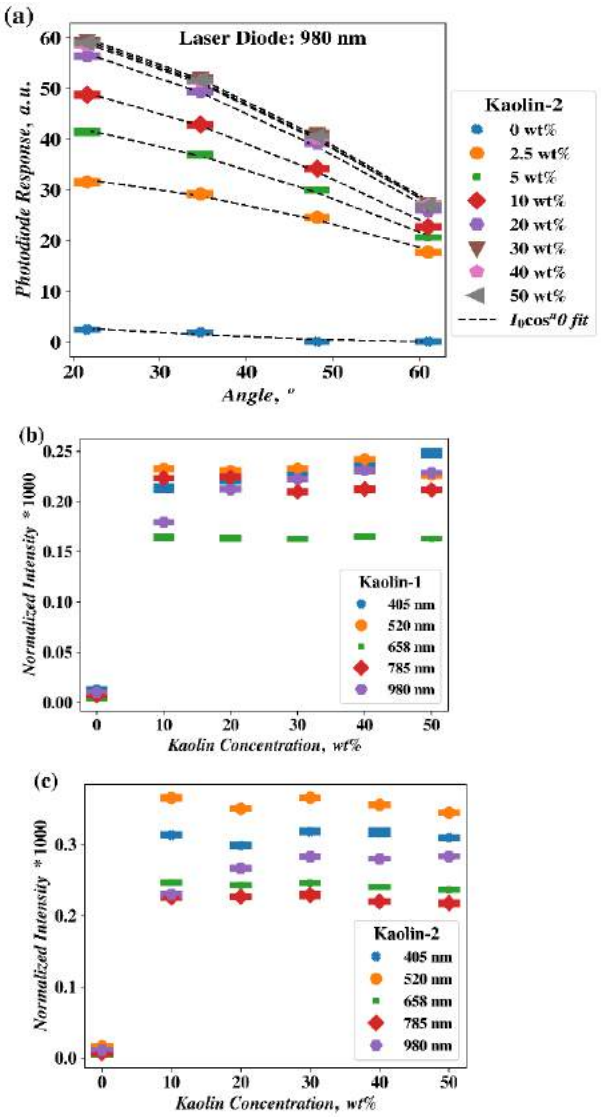

Figure 2. (a) Scattering behavior of Kaolin-2 with 980 nm laser diode and different concentrations; (the normalized scattering intensity of (b) Kaolin-1 and (c) Kaolin-2 at different wavelengths

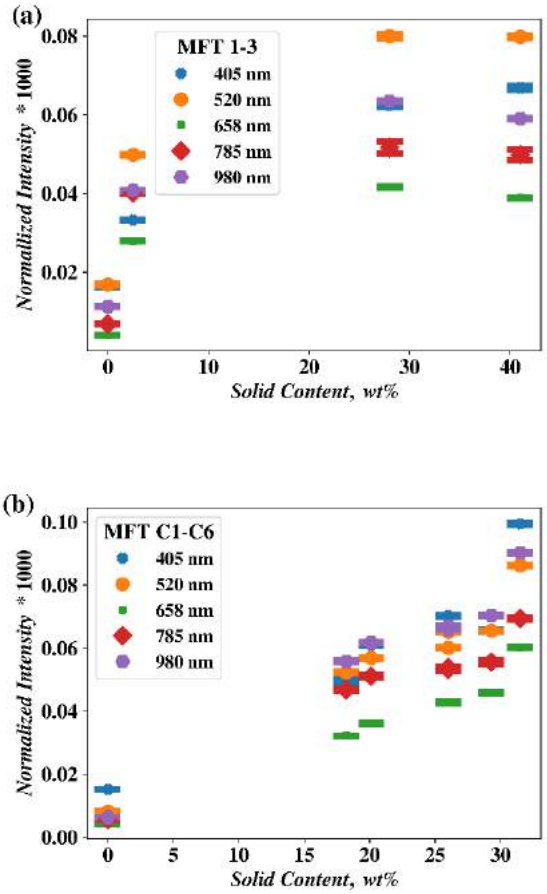

Figure 3. Comparison of scattering from FFT samples obtained for two different sources with different concentration and wavelength (MFT 1-5 in Figure 3a are FFT samples provided from NAIT. MFT C1-C6 in Figure 3b are FFT samples received from CNRL)

From Table 1, Kaolin-1 has a smaller particle size distribution compared to Kaolin-2, therefore, the scattering intensity is expected to be smaller for all the wavelengths. The scattering behavior of the FFT sample was significantly different than the kaolin sample. For instance, the scattering intensity for all of the measured concentrations was found to be lower than kaolin (Figure 3a and b). The exponent n in $cos^n\theta$ was in the range of 0.8 to 2 (data not presented) which varied with wavelength and tailing sample. Also, for all wavelengths the scattering intensity changed with FFT composition. There could be several reasons for the difference between FFT samples and kaolin samples. Firstly, the presence of bitumen can absorb the light which can decrease the scattering intensity. Secondly, the difference in particle size between samples can also influence the scattering intensity. Further experimental studies, as well as simulation, are being carried out to understand the different light scattering behaviours of Kaolin and FFT samples.

FDTD Simulation

The basic principle of FDTD (finite difference time difference) is to discretize the time-dependent Maxwell's equations in the grid system and solve them numerically. FDTD is widely used in for solving electromagnetic (EM) problems. Since optical scattering process can be completely described by

Maxwell's equations, we are conducting FDTD simulations to better understand the physical process of the optical scattering.

Due to the computational limitation the entire real tailings sample cannot be simulated. Hence in the initial step of simulation, we focused more on the system that only included few particles, which can still give some physical understanding of the light scattering process. To demonstrate the FDTD simulation capability, we have simulated a system which includes three Kaolin particles with different shapes. For these simulations optical absorption has been neglected. Figure 4(b) and (c) show the logarithmic intensity versus theta plots for the scattered light at two different values of angle phi. Here we give the result in the form of the far field. The observing distance is set as 2 meters, which is far more than the particle sizes and light wavelength. The ρ and phi values were fixed and scanning was conducted between theta = 0° to 180° to get two far field intensity distribution of the system.

For FFT samples, the presence of bitumen can significantly influence the back-scattering. Further studies to understand the role of bitumen in optical scattering is ongoing. In this study, we have considered a system with only a few particles, whereas the real system will have a large number of particles. Modeling a system with many particles using FDTD will be computationally very expensive. Therefore, we plan to combine Monte-Carlo simulation and FDTD in the future. Additionally, to save the computational time, in future KM theory will be applied to determine the absorption and scattering coefficients as well as the penetration depth of electromagnetic radiation.

Settling Experiment

Apart from the scattering experiments and simulations, settling experiments with kaolin and FFT samples were conducted using the settling setup discussed in the experimental setup section. In the first set of experiments, 30 wt% of Kaolin-3 sample was prepared, and a 405 nm laser diode was used for the study. 405 nm was chosen for these measurements as this particular wavelength has been studied extensively in our earlier work (Gupta et al. 2012). Also, angular measurements on Kaolin-3 sample using the ring setup demonstrated good distinction between the solids contents. The laser diode was operated in continuous mode. Figure 5a shows the settling of kaolin monitored at different heights. It should be noted that employing beam-splitters led to the laser power at each level being reduced by ~8% and hence the scattering response was also expected to be reduced. The scattering response (SR) at any time t and at each level is given as:

$$\begin{aligned} &SR_i(t) \\ &= x\{\frac{L_i}{A_i}Q_{sc}(c_i,\varphi,\lambda,\theta,\dots) \\ &+ \Big(\frac{L_{i-1}}{A_{i-1}}Q_{sc}(c_{i-1},\varphi,\lambda,\theta,\dots) \\ &+ \frac{L_{i+1}}{A_{i+1}}Q_{sc}(c_{i+1},\varphi,\lambda,\theta,\dots)\Big)\cos(\gamma)\} \end{aligned} \qquad \text{Eq. 1}$$

where i is the individual level, x is the multiplying factor due to responsivity of the photodiode, amplifier circuit etc. L_i is the incident light intensity, A_i is the spot area of the incident light, Q_{sc} is the scattering efficiency which depends on particle concentration (c), particle size (φ), wavelength of light (λ) etc. $i-1$ and $i+1$ are the levels above and below level respectively. γ is the angle, subtended by a given level laser spot and the next lower or upper level laser spot, which was calculated to be 32°. Other levels were not included in the calculation, as the subtended angle was >42°, which is greater than total internal reflection angle for plexiglass and air. For the scattering at L_2 (10.5 cm) height, the response was found to be higher than L_1 (12.5 cm) which is due to the contributions from L_1 and L_3. From Eq.1, if Q_{sc} at all levels can be decoupled then the true behaviour of the settling of kaolin or MFT can be deduced. For a well stirred and homogeneously mixed kaolin solution, Q_{sc} is constant for all levels only at the start of the experiment i.e., $t=0$. When we subtract the expected contribution of L_2 from SR of L_1, a value of 0.045 is obtained. The values at L_2, L_3, … etc. are expected to be 0.08 x 0.045, 0.08^2 x 0.045, … etc. respectively. In the calculation, we assumed $x\frac{Q_{sc}}{A_i}$ to be a constant. To verify this, we conducted another round of experiments with the same kaolin solution. In this experiment, the setup was placed 5 cm higher than the previous experiment and we removed the beam splitter from L_2 (Figure 5b). As can be seen from the figure the initial SR value for L_1 is ~0.045 in good agreement with the calculation. If we calculate the expected value for L_2 due to the contributions from L_1 and L_3 with no contribution from L_2 itself (no beam splitter), a value of 0.07 is obtained which is greater than the observed initial value of ~0.055. The observed difference may be due to beam divergence i.e., A_i is increasing with distance from the laser diode. A more sophisticated

analysis procedure including the effect of beam divergence is under development to help properly removing the signal contamination from other levels.

The signal contamination issue can also be mitigated by replacing the beam splitter at each level by a laser diode operating in pulsed mode and only turning on one laser diode at a time. In such a setup many more laser diodes are needed and the output power for each laser diode needs to be characterized.

The next set of settling experiments was conducted with FFT-2 (Figure 6). A slow decrease for light scattering intensity at 18.5 and 16.5 cm can be observed. From this it can be observed that the FFT concentration is reducing at the top of the column. Also, the settling process for the FFT is much slower than the Kaolin. Spikes in Figure 6 could be due to the rapid on and off, of room lights. The stray light issue can be mitigated by adding wavelength filters in front of the photodiodes.

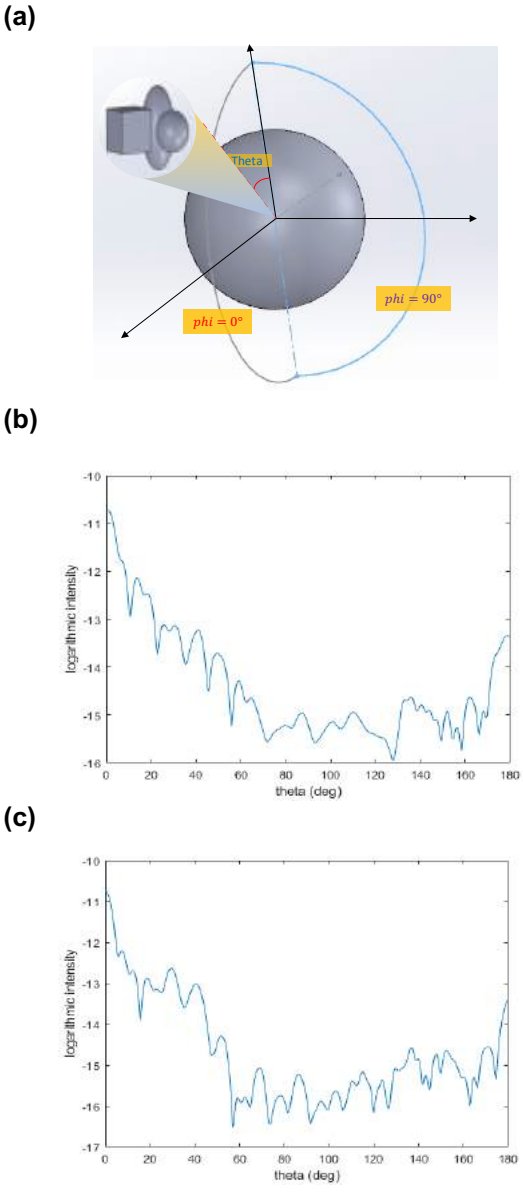

Figure 4. (a) FDTD simulation setup of three kaolinite particles (b) The intensity distribution when fix ρ=2m, φ=0°, and scan θ from 0° to 180° (c) The intensity distribution when fix ρ=2m, φ=90°, and scan θ from 0° to 180°

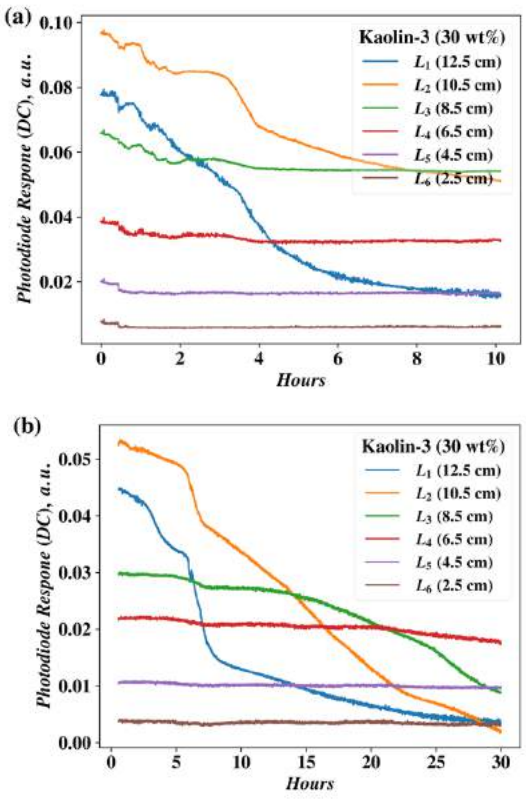

Figure 5. Settling of 30 wt% kaolin-3 (a) with all input coupling beam-splitters, (b) without beam splitter at 15.5 cm (L2). 405 nm laser diode was used in this study. Height was measured from the base of the settling column

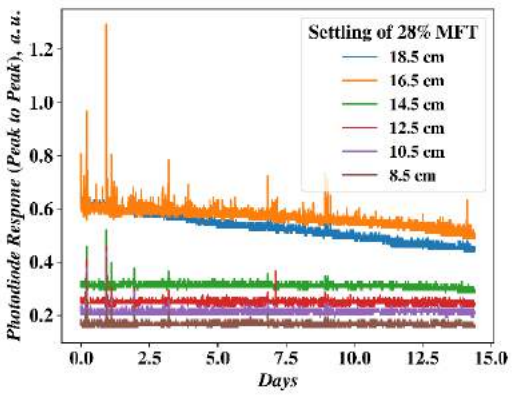

Figure 6. Settling of FFT monitored at different heights using 405 nm wavelength. Height was measured from the base of the settling column

CONCLUSION

The current study pursues a novel real-time optical technique for solids content measurement for tailings slurry. We have conducted angular measurements on different Kaolin and FFT samples to understand the change in the angular scattering intensity along with the solid concentration. From the studies it is quite clear that the light scattering intensity depends strongly on the characteristics of the samples, namely on the particle size and shape, agglomeration, and bitumen concentration. This is further demonstrated by our preliminary FDTD simulations which indicate a strong correlation of scattering intensity with particle size and shape (which will change with agglomeration). Results from the initial settling experiments clearly demonstrate that the light scattering based detection for solid content technique can be extended further by utilising multiple wavelengths. It is expected that this will improve the accuracy of detection and also allow extension of this technique for measurement of solids content >50 %. Thus, we envision the development of an *in-situ,* fast and relatively inexpensive light scattering based instrument for solids content measurement.

ACKNOWLEDGEMENT

We would like to acknowledge the financial support for this research project by the Natural Sciences and Engineering Research Council of Canada, the Institute of Oil Sands Innovation and the Canada's Oil Sands Innovation Alliance. We would like to acknowledge CMC Microsystems for the provision of products and services that facilitated this research, including LabView. We would also like to acknowledge IOSI staff Dr. Xiaoli Tan, Ms. Lisa Brandt, Ms. Brittany McKinnon, and NAIT staff Dr. Heather Kaminsky, Mr. Taimur Qureshi for their technical support.

REFERENCES

Allen, T. (1990). Particle size measurement. London: Chapman and Hall.

Babin, M. and Stramski, D. (2004). Variations in the mass-specific absorption coefficient of mineral particles suspended in water. Limnol. Oceanogr., **49**: 756–767.

Ciani, A., Goss, K.-U. and Schwarzenbach, R. P. (2005). Light penetration in soil and particulate minerals. Eur. J. Soil Sci., **56**: 561–574.

COSIA (2012). Technical Guide for Fine Fluid Management.

Ho, T. T.-S. (2015). Development of compact fluorescent spectrometers and field deployable optical solids content monitoring devices.

Hulst, H. C. and Hulst, H. C. van de (1981). Light Scattering by Small Particles (Courier Corporation). Manisha Gupta, Zhou, Y., Ho, T., Sorta, A., Taschuk, M., Sego, D. and Tsui, Y. Solid Content of Oil Sands Tailings Measured Optically. IOSTC 2012.

Mikula, R., Kasperski, K., Burns, R. and MacKinnon, M. (1996). Nature and Fate of Oil Sands Fine Tailings. In Suspensions: Fundamentals and Applications in the Petroleum Industry, (Washington, DC: American Chemical Society), p. 47.

Mouazen, A. M., De Baerdemaeker, J. and Ramon, H. (2005). Towards development of on-line soil moisture content sensor using a fibre-type NIR spectrophotometer. Soil Tillage Res., **80**: 171–183.

Stenberg, B., Viscarra Rossel, R. A., Mouazen, A.M. and Wetterlind, J. (2010). Chapter Five - Visible and Near Infrared Spectroscopy in Soil Science. In Advances in Agronomy, D.L. Sparks, ed. (Academic Press), pp. 163–215.

Winton, S. C., Sahin, A., Rappaport, C. M. and Miller, E. L. (1998). Comparison of a recursive T-matrix method and the FDTD method for scattering problems in lossy dispersive soil. In Detection and Remediation Technologies for Mines and Minelike Targets III, (International Society for Optics and Photonics), pp. 33–41.

Yu, Z. Q., Chow, P. S. and Tan, R. B. H. (2008). Interpretation of Focused Beam Reflectance Measurement (FBRM) Data via Simulated Crystallization. Org. Process Res. Dev., **12**: 646–654.

UN Environment (2017). Mine Tailings Storage: Safety Is No Accident. GRID-Arendal.

RAPID ESTIMATION OF HYDRAULIC CONDUCTIVITY FOR FLUID FINE TAILINGS

Yagmur Babaoglu, Shunchao Qi and Paul Simms
Carleton University, Ottawa, Canada

ABSTRACT

Accurate estimation of the hydraulic conductivity – void ratio function is important for design of tailings deposition impoundments. This paper describes three new approaches to estimate or measure the hydraulic conductivity function. These are I) improved regression analysis using index properties or compressibility data to determine hydraulic conductivity, using 28 data sets of FFT and amended FFT, II) Direct calculation of hydraulic conductivity from measurements of pore-water pressure and density in a column or other 1D test using the instantaneous profile method adapted for large strain , iii) Estimation through optimization of large strain consolidation solutions, with and without sedimentation, using sedimentation column height data alone. The methods are compared using a previously published study on large columns experiments on thickened oil sands tailings.

INTRODUCTION

The hydraulic conductivity - void ratio relationship (the *k-e* function) is required to calculate settlement rates and strength gain in most fines dominated tailings deposition schemes. Consolidation is not only important to deep deposits but even in thin (or thick) multilayer deposition schemes (Qi and Simms 2018a, Soleimani et al. 2014). Rapid measurement or estimation of the *k-e* function is desirable to accelerate innovation in the oil sands industry by allowing candidate tailings technologies, or modifications to existing technologies, to be quickly evaluated in terms of their long-term dewatering potential.

This paper reviews three methods to estimate the *k-e* function developed by the authors. The first predicts the function using relatively easily measured parameters: the Atterberg limits of the tailings OR their compressibility, and a measurement of hydraulic conductivity at high void ratio. The second uses a variation of the Instantaneous Profile Method (Watson 1966) to allow for direct calculation of hydraulic conductivity from column or any 1-D sedimentation tests (including centrifuge test) from 1D profiles of pore-water pressure and density. The third method allows for robust estimation of the *k-e* function from the same class of tests using only the tailings-water interface; the last method is developed from optimization analysis of large strain consolidation.

Each method is described with examples of application. Finally, all three methods are compared by application to a single example.

DESCRIPTION OF METHODS

Method 1: Estimation From Atterberg Limits or the Compressibility Function

Many correlations of the *k-e* function with Atterberg limits and other basic soil properties abound in the literature. The applicability of these equations to oil sands tailings has recently been reviewed by Babaoglu and Simms (2017, 2018). Babaoglu and Simms (2017) optimized two of these existing equations (Morris 2003, Samaharsinge 1982) using 20 data sets of FFT and amended FFT. The modified Samaharsinge equation is:

$$k = 2\times10^{-12}\left(PI\right)\left[\frac{e^5}{1+e}\right] \quad (1)$$

Despite fair predictions (90% of predictions of individual k(e) measurements fell within 1.5 orders of magnitude of the measured values), Babaoglu and Simms (2017) recommended that these equations were not sufficiently accurate for estimating the k-e function to make reasonable predictions, even for preliminary design of tailings impoundments. Babaoglu and Simms (2017) recommended that predictors that better reflected the state of the tailings at high void ratios would be more appropriate.

Therefore, Babaolgu and Simms (2018) next evaluated the compressibility curve (e -σ'v) itself as a predictor. It seems that both the e - σ'v and *k-e* functions often exhibit very similar shapes. When plotted as function of effective stress, many data sets both functions overlap each other, as in Fig. 1. a, while in others, the curves run parallel to each other.

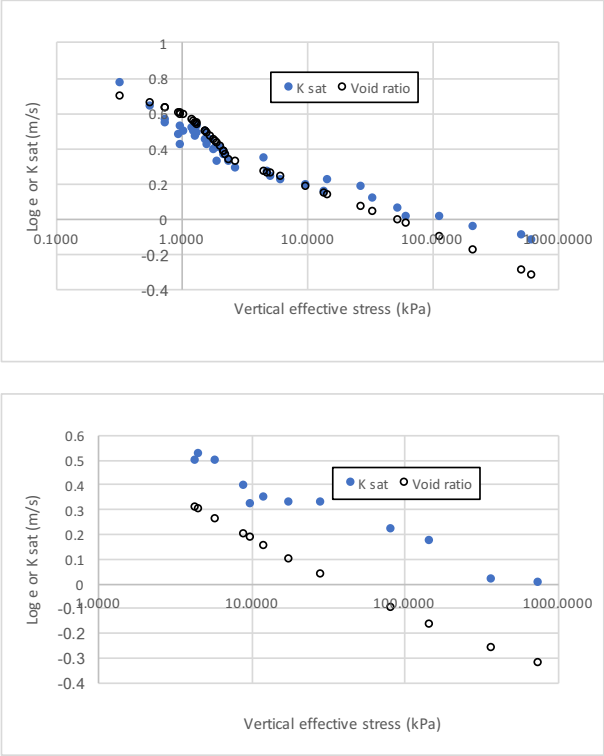

Figure 1. Two examples of correlation between compressibility and hydraulic conductivity functions

From these observations, it was found that the following equation described the *k-e* relationship superior to the Atterberg limit based equations:

$$\log k = \frac{\log e}{A} - B \tag{2}$$

If A and B were dataset specific, 96% of the predicted k values were within 1 order of magnitude of the measured data points (all 400 data points from the 20 data sets). However, using an optimized A and B for all data sets (A=10.3 B=0.2), gave a fairly good agreement, with 81% of predicted k values less than 1 order of magnitude off the measured values. It is interesting to note that when using these A and B values, Equation 2 can be rearranged to give the following power function:

$$k = 3.16^{-11} e^5 \text{ m/s} \tag{3}$$

There are several methods available to estimate *k* values at the initial or during the settlement phase from knowledge of the initial void ratio or at the post-sedimentation void ratio and the velocity of the tailings-water interface (Been and Sills 1981, Pane and Schiffman 1997). Therefore, it is advantageous and practical to correct Equation (3) using a *k* value measured at the initial or some relatively high void ratio, e_0:

$$k = k_{measured\ e_0} \frac{e^5}{{e_o}^5} \tag{4}$$

Similarly, Equation 1 can also be corrected with a single measured value of hydraulic conductivity:

$$k = k_{measured\ e_0} \frac{e^5}{{e_o}^5} \frac{1+e_0}{1+e} \tag{5}$$

The choice of e_0 should be somewhere between the initial void ratio and the post-sedimentation void ratio. The assumption of zero effective stress allows for a straightforward calculation of the hydraulic conductivity (Pane and Schiffman 1997, Been and Sills 1981):

$$k = \frac{(1+e)v_s}{SG-1} \tag{6}$$

where SG is the specific gravity and v_s is the velocity of the tailings-water interface. Equation 6 is theoretically most valid at the start of the any sedimentation test, before any effective stress can develop near the top of the tailings. However, for certain kinds of amended FFT where flocculation is still ongoing during deposition, using a somewhat lower void ratio would be more appropriate, as long as the assumption that the gradient in pore-water pressure near the surface of the tailings is equal to the gradient in total stress can be validated.

When Equations 4 and 5 are compared against the data set, using the measured *k* values at the void ratios close to 2.5, the agreement is much improved and very similar (95% and 92% errors less than 1 order of magnitude.). Babaoglu and Simms (2018) quantified the reliability of these predictors by modelling a 10 m deposit of amended FFT. The range of settlement predictions

based on a very conservative estimate of the errors from this method was relatively small. It is straightforward for practitioners to verify the sensitivity of settlement / consolidation predictions to the inherent error in this method.

To summarize, the method has the following steps:

i) Measure k_0 at either the initial or another relatively high void ratio in a 1D sedimentation / consolidation test. To measure *k* at the initial void ratio, only the sedimentation velocity is needed. To measure at another void ratio, the tailings-water interface needs to be sample for density, and the pore-water pressure needs to be measured close to the tailings-water interface. Use Equation 6.
ii) Predict the full *k*-*e* relationship using Equations 4 and / or 5.
iii) Based on statistical analysis of 28 *k*-*e* data sets, the expected error, conservatively, should increase from near zero at the initial *k* measurement to an order of magnitude by e=1

Method 2: The Instantaneous Profile Method Under Large Strain Conditions

The instantaneous profile method was first proposed by Watson (1966) to calculate the hydraulic conductivity in unsaturated soil. The "Instantaneous profiles" are depth profiles of pore water pressure and water contents at different times. Hydraulic conductivity at different depths and times can be calculated from the gradients in water content and hydraulic head as per the groundwater flow equation:

$$\frac{d\theta}{dt} = k\frac{d^2h}{dz^2} \tag{7}$$

The above equation is based on flow through a constant volume element. However, for saturated conditions with changing density, the same expression remains valid for a constant volume of solids (Fox and Baxter 1997). The volumetric water content θ can be substituted for $e/(1+e)$. For purposes of calculating *k*, the derivative functions can be expressed in terms of finite difference, for example, using a central difference scheme:

$$\frac{\left(\frac{e_{t1}}{1+e_{t1}}\right)-\left(\frac{e_{t3}}{1+e_{t3}}\right)}{t1-t3} = k\frac{h_1+h_3-2h_2}{\Delta z^2} \tag{8}$$

where *k* is $k(z,t2)$, $t2 = (t1 + t3)/2$, h_2 is the head at elevation *z* at time *t2*, h_1 and h_3 are the head values measured Δz above and below *z* at time *t2*. For strict application to large strain conditions, *z* should be the "height of solids" used in formulations of large strain consolidation, rather than a constant elevation or a constant change in elevation. The change in the height of solids can be calculated by knowing the distribution of *e* with depth over time. Alternatively, the height of solids can be assumed to be a constant if the change in the over height of the tailings is small over the time step.

Using Equation 8, *k* can be evaluated at any number of depths and times, given sufficient resolution of the data. The advantage of this method is that the measured *k* values are independent of any assumptions with respect to dewatering mechanism, e.g. sedimentation, consolidation, or creep. The disadvantage is that very high resolution in density or water content measurements are required, or that these can be interpolated with accuracy. Generally pore-water pressures are smoother and can be adequately interpolated.

Method 3: Robust Back-Calculation of k-e From Settlement Data

Qi and Simms (2018c) have performed optimization analysis to fit various 1D column experiments assuming a power law *k*-*e* function, $k=Me^P$. Their analyses are done using sedimentation-large strain consolidation analyses (Sed-LSC) using a piecewise-linear approach (Qi et al. 2017a, 2017b). The compressibility function is obtained from the final density distribution at the end of each column experiments. This exercise had produced a number of methods to robustly estimate *k*-*e*, derived from two findings. Here we present these two findings and show one of the simplest methods for estimating *k*-*e* that follow.

The first finding results from optimization of the *k*-*e* function to measured settlement curves. The optimization exercise is based on a large number (hundreds for each data set analyzed) of Sed-LSC analysis in which the multiplier, *m*, and exponent, *p*, are randomly varied. This large set of analyses produces a distribution of errors, such as shown in Figure 2. The error refers to the distribution of errors between predicted and measured settlement data:

$$\text{Objective}(\boldsymbol{M},\boldsymbol{P}) = \sum_{i=1}^{N}\left(H_{\text{P}}^{i}\text{-}H_{\text{M}}^{i}\right)^{2} \quad (9)$$

where H are the measured and predicted elevations, given N measurements.

Using multiple column experiments, (Bartholomeeusen et al. 2002, Miller 2010, Soleimani et al. 2016) it was always found that the error always reaches a minimum along a line defined by:

$$P = \varpi + \lambda \ln M \quad (10)$$

A point of minimum error that gives a unique *P* and *M* also exists; however, the finding expressed in (10) can be used for much quicker determination of optimal parameters.

The other finding of interest is known to many practitioners who do Sed-LSC analyses, but is not much commented upon in the literature. The finding is that the shape of the predicted settlement curve is independent of the *M* parameter. Varying the *M* parameter scales the results, such that a unique value of settlement is predicted for an infinite set of pairs of M and time, such that (*M* x time) remains constant; if all other parameters, initial conditions, and boundary conditions remain the same. This fact is proven formally in Qi and Simms (2018c). Using these two findings allows for a number of efficient methods to find *k-e* from settlement data. The simplest is as follows:

i) Conduct a 1D test under single drainage conditions.
ii) Measure the settlement and at least one point for pwp analysis.
iii) Once consolidation has effectively finished, sample density in the column with depth.
iv) Use the density distribution and assumed /measured final profile of pore-water pressure to infer compressibility curve.
v) Perform two Sed-LSC analysis, using random pairs of *M* and *P*.
vi) For any measured settlement point, scale each of the two solutions by changing *M* to reproduce that measured point. This gives two sets of *M* and *P* data.
vii) These two sets of *M* and *P* data form a line.
viii) Repeat vi and vii for any of the measured data points, using only the same two initial sed-LSC analysis

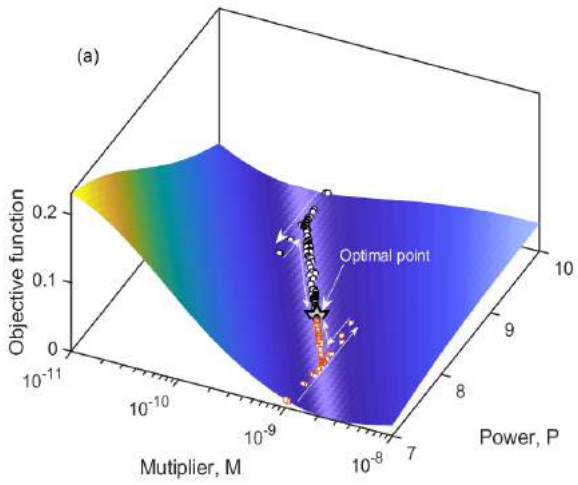

Figure 2. Example Error surface as a function of M and P

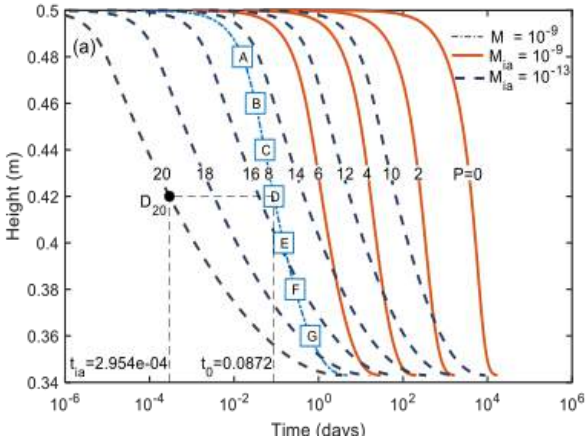

Figure 3. Family of LSC predictions and example of scaling to measured point D

ix) This results in a family of lines in *M* and *P* space. The intersection or near intersection of these lines results in a unique pair of *M* and *P*, which define the *k*-e function.

An example of scaling LSC results is shown in Figure 3, showing scaling of LSC prediction using $M=10^{-14}$ and P = 20. Scaling this curve to D shifts M by the ratio of the time 2.95 x 10^{-4} to 0.0872, producing an M value of 3.4 x 10^{-16}. This pair of *M* and *P* is one point of the line defined with reference to D. Another point could be constructed from the solution for *P*=6 and $M=10^{-9}$, which would produce a *P*=6 and *M*=1.36 x 10^{-8}. These two points associated with D define one line. Shifting

these two solutions for P=20 and P=6 to other points define a family of lines, which intersect to give an optimal solution of k=1e-9 e^8. Figure 4 shows these lines if all of the data points (A through G) are used. However, the method works if only two lines are constructed.

APPLICATION OF METHODS TO THE SAME CASE

The case is one of the column tests presented in the paper "Column Consolidation Testing of oil sands tailings" by Sun et al. (2014). The tests are conducted on thickened oil sands tailings. Density profiles are obtained through gamma ray densiometry and pore-water pressure measurements are made from ports connected to manometers. Sun et al. (2014) report solids content, pore-water pressure, and effective stress profiles over time, from which can be calculated the settlement of the tailings-water interface, the total stress, and the specific gravity. The case used is the data from the C2 columns. The data is replotted in this paper in terms of height, void ratio, and pore-water pressure in Figures 5, 6, and 7.

Application of Method 1

For this case, e_0 is selected as the initial void ratio, (~2.65). The specific gravity, 2.6, is back calculated from the density and height data. The height data over the first 11 days is assumed to be linear. This gives a *k* value of 1.24 x 10^{-6} m/s at e=2.65. The application of Equation 4 and 5 is then straightforward. Equation 4 and 5 are plotted in Figure 10, which shows the predicted *k-e* functions from all three methods.

Application of Method 2

For this case, the hydraulic conductivities were evaluated at Day 88. The pore-water pressure profile at 88 days is used in the right hands side of Equation 8. The void ratio profiles at 60 and 125 days were used to define the fluxes in the left hand side of Equation 8. The data is interpolated using Matlab to depth values every 0.1m. Given the low resolution of the density, Day 88 is probably the best time to apply the analyses, as there is still some deformation, but the magnitude of deformation is substantially less than at the beginning of the test, where there is considerable change in the height of solids.

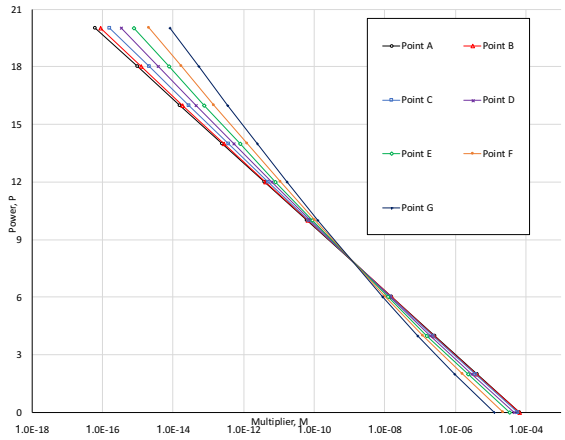

Figure 4. Lines constructed by scaling LSC predictions in Figure 3 to measured points A through G. Intersection of lines defines *M* and *P*

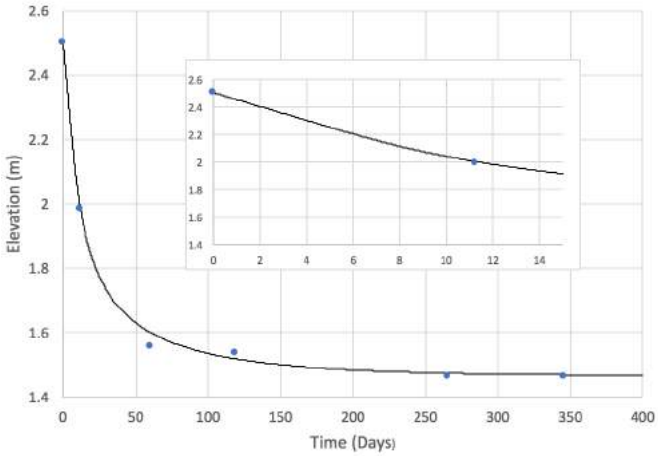

Figure 5. Case Study: Settlement of the tailings water interface, with insert for the first 15 days

Direct application of Equation 8 gives the *k* – elevation profile in Figure 8. This is then converted to *k-e* by associating *z* with the known profiles of *e* at 60 and 120 days and then averaging to estimate the *z* - *e* profile at 88 days. The resulting k-e profile is shown in Figure 10.

Application of Method 3

This method requires the settlement data and the compressibility curve at the final condition. The compressibility curve is extracted from Day 347 data as shown in Figure 9. The data is fit using the analytical for modified power law form derived by

Qi and Simms (2018c), to obtain a compressibility curve e = 1.9 $(\sigma'_v+0.4)^{-0.353}$.

Two large strain consolidation analysis were then employed using two arbitrary k-e curves of *M*, *P* values (10^{-10}, 8) and (10^{-8}, 4). Note no sedimentation was modelled as the upper void ratio appeared to remain close to its initial value. These curves were then shifted to the settlement points at 11 days and 12 5 days. This produced two lines with intersected at *M* = 10^{-8} and *P* = 4.9. This *k-e* function is also plotted in Figure 10.

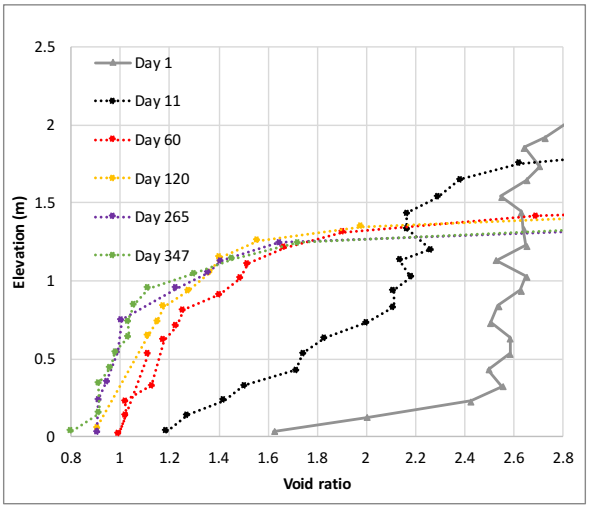

Figure 6. Case Study: Void ratio profiles

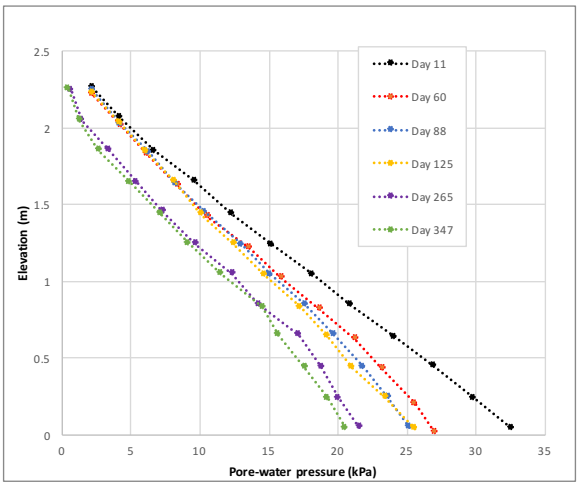

Figure 7.Case Study: Pore-water pressure

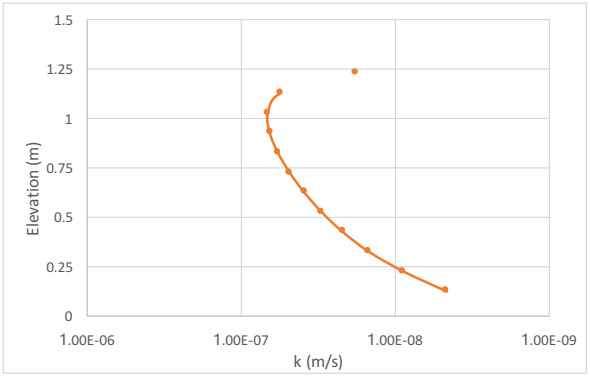

Figure 8. *K* values predicted by Method 2 using pore-water pressure profile at 88 days and void ratio profiles at 60 and 125 Days

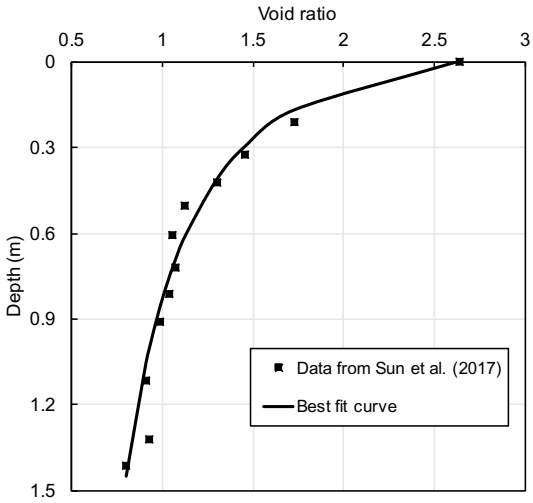

Figure 9. Obtaining the compressibility curve from the final condition of the Case Study

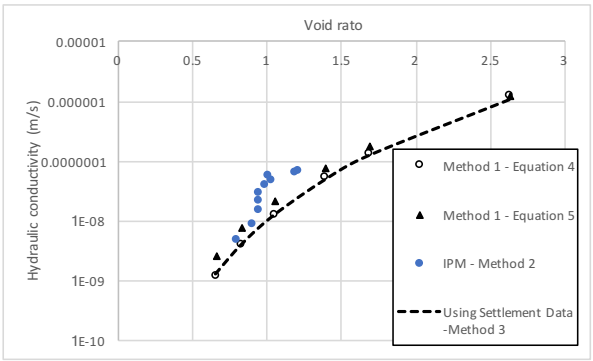

Figure 10. Comparison of predicted *k-e* from all three methods for the case study

COMPARISON OF RESULTS AND DISCUSSION

The agreement between all the methods was quite surprising. Equation 4 and Method 3 gave the closest agreement, almost visually overlapping. This is because the optimized power (4.81) is very close to the power assumed by Equation 4 (5). Also, both Method 3 and Method 1 depend of the settlement curve: Method 3 is based on optimization to the whole settlement curve, while Method 1 uses the initial slope of the settlement curve to determine the *k* value at high void ratio, as per Equation 6.

The only difference between Equation 4 and 5 is the assumed power. However, as both predictions are anchored to the measurement of k at high void ratio, the difference between them is relatively small.

Theoretically, the most valid results should come from the IPM based method, as it is a direct measurement, as opposed to empirical (Method 1), or based on back calculation from Sed-LSC analyses (Method 3). However, it is a "data-hungry" method that requires high resolution in measurements for accuracy. The authors are currently working on several techniques to allow for high resolution of density and / or water content in column tests, which would allow for more accurate application of IPM. Even so, the IPM results for the case study are still quite close to the other predictions, so it appears to be a credible approach.

To demonstrate the accuracy of the predictions, LSC results for the case study are shown for void ratio and pore-water pressure (Figures 11 and 12), using the $k = 10^{-8} \times e^{4.9}$ function obtained from Method 3.

There is very good agreement with measured void ratios but some discrepancies with pore-water pressure that increase with time. This result is also seen when applying predictions using Method 3 to multiple columns studies. This discrepancy is due to the shift in the compressibility function over time, which is noted in both oil sands tailings (Miller 2010, Qi et al. 2018) and other soft sediments (Bartholomeeusen et al. 2002). The evolving compressibility function can be tracked using the paired measurement of density and pore-water pressure – hence the recommendation in Method 3 to measure pore-water pressure at least at one point. When the shifting compressibility function is modelled empirically in Sed-LSC analysis, this results in a somewhat higher optimal *k-e* function, by about half an order of magnitude (Qi and Simms 2018b). Even so, the predicted *k-e* functions without considering the change of compressibility function are reasonably accurate and conservative.

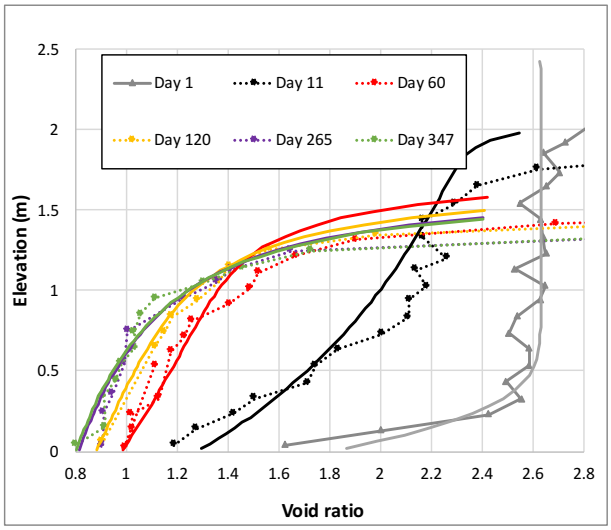

Figure 11. Modelled void ratios using predicted k-e function

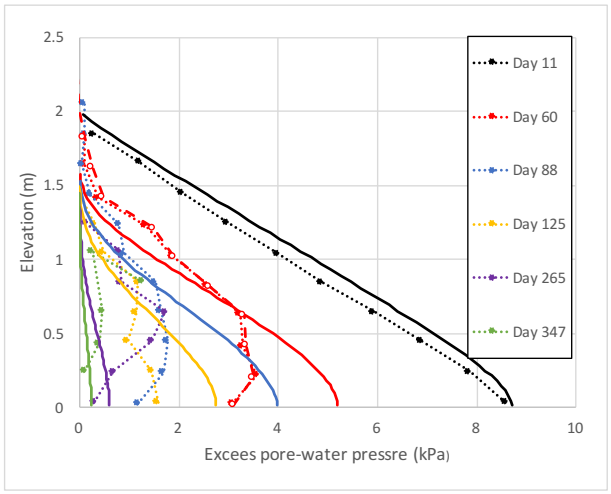

Figure 12. Modelled excess pore-water pressures using predicted k-e function

However, the appropriate compressibility curve to use in a prediction of long term consolidation, say for analysis of a deep deposit, is a very different story, and beyond the scope of this paper. Changes in the compressibility curve over the time

scale associated with deep deposits may be substantial with important implications for final deposit height and settlement rate (Qi et al. 2018).

The *k*-*e* function itself may possibly shift over operational timescales. Field monitoring of hydraulic conductivity, say using IPM, could inform deposit management practices to mitigate this contingency.

SUMMARY AND CONCLUSIONS

Three different methods are proposed to rapidly estimate the *k*-*e* function. To summarize, Method 1 was developed from empirical correlations of basic properties, but resulted in two master equations that use a measurement of k at high void ratio. Method 2 directly calculates hydraulic conductivity from measurements of pore-water pressure and density using in the instantaneous method adapted to high void ratios. Method 3 is based on findings on optimization to settlement curves – this method requires only two LSC analysis using random *k*-e functions in power law form.

The methods were applied to a previously published columns study case on oil sands tailings consolidation. All three methods predicted quite similar results. Method 2 diverged most from the other two methods, probably due to relatively low resolution of density measurements.

The *k*-*e* function obtained by Method 3 was used to simulate void ratio and pore-water pressure profiles for the case study and showed reasonable agreement.

ACKNOWLEDGEMENTS

Funding and personnel support from COSIA and NSERC is gratefully acknowledged. Funding from NSERC comes from a CRD grant supported by COSIA.

REFERENCES

Babaoglu, Y. and Simms, P. (2017). Estimating Hydraulic Conductivity from Simple Correlations for Fine Grained Soils and Tailings. Proceedings of GeoOttawa 2017, 70th Canadian Geotecnical Conference. Ottawa.

Babaoglu, Y. and Simms, P. (2018). Estimating Saturated Hydraulic Conductivity from Compression Curves for Fluid Fine Tailings. Proceedings of GeoEdmonton, 71st Canadian Geotechnical Conference, Edmonton.

Bartholomeeusen, G. Sills, G. C., Znidarcic, D., Kesteren, W. V., Merckelbach, M. D., Pyke, R., Carrier, D. W., H. Lin, Penumadu, D., Winterwerp, H. (2002). Sidere: Numerical prediction of large-strain consolidation. Geotechnique, **52**: 639-648.

Been, K. and Sills, G. C. (1981). Self-weight consolidation of soft soils: an experimental and theoretical study. Geotechnique, **31**(4): 519-535.

Fox, P. J. and Berles, J. D. (1997). CS2: A piecewise-linear model for large strain consolidation. Int. J. Numer. Anal. Methods Geomech., **21**(7): 453-475.

Miller, W. G. (2010). Comparison of geoenvironmental properties of caustic and noncaustic oil sand fine tailings, University of Alberta.

Morris, P. (2003). Compressibility and permeability correlations for fine-grained dredged materials. Journal of waterway, port, coastal, and ocean engineering, **129**(4): 188-191.

Pane, V. and Schiffman, R. L. (1997). The permeability of clay suspensions. Geotechnique, **47**: 273-288.

Qi, S. and Simms, P. (2018). Analysis of dewatering and desaturation of generic field deposition scenarios for thickened tailings, in RJ Jewell & AB Fourie (eds), Proceedings of the 21st International Seminar on Paste and Thickened Tailings, Australian Centre for Geomechanics, Perth, pp. 401-412.

Qi, S. and Simms, P. (2018). Robust methods to estimate large strain consolidation parameters from settlement data. In preparation for submission to Canadian Geotechnical Journal.

Qi, S., Simms, P. and Vanapalli, S. (2017). Piecewise-Linear Formulation of Coupled Large-Strain Consolidation and Unsaturated Flow. I: Model Development and Implementation. ASCE Journal of Geotech. And Geoenv. Eng., https://doi.org/10.1061/(ASCE)GT.1943-5606.0001657

Qi, S., Salam, M. and Simms, P. (2018). Creep and structuration in tailings and natural clays. 2018, IOSTC 2018.

Samarasinghe, A. M. (1982). Permeability and consolidation of normally consolidated soils. Journal of the Geotechnical Engineering Division, **108**(6): 835-850.

Soleimani, S., Simms, P., Dunmola, A., Freeman, G. and Wilson. G. W. (2014). Desiccation and consolidation in thin-lift deposition of polymer-amended mature fine tailings. *Proc. 17th Int. Seminar on Paste and Thickened Tailings*, R. Jewell, A. Fourie, P. S. Wells and D. van Zyl, eds., Australian Centre for Geomechanics, Crawley, Australia, 307-322.

Watson, K. K. (1966). An Instantaneous Profile Method for Determining the Hydraulic Conductivity Unsaturated Porous Material. Water Resources Research, **2**: 709-715.

ASSESSMENT OF THE FLOCCULATION PERFORMANCE OF TAILINGS USING HYPERSPECTRAL IMAGERY

Iman Entezari, Benoit Rivard, Vahid Vajihinejad, G. Ward Wilson,
Joao Soares, Berekat Fisseha and Nicholas Beier
University of Alberta, Edmonton, Canada

ABSTRACT

Flocculation of oil sands tailings is widely used in the oil sands industry to dewater fluid fine tailings. The flocculation performance primarily depends on the flocculant dose as well as the rate and time of mixing. Consequently, the development of techniques that can assess flocculation performance and provide feedback information to adjust the flocculant dose and mixing conditions is essential for optimized commercial implementation of the flocculation process. This paper aims to investigate the potential of hyperspectral imagery to monitor the flocculation performance of tailings. The results show that hyperspectral imagery can potentially be used to detect under-dosed and over-sheared samples. It is however required to examine a wider range of flocculation conditions to calibrate the method and validate the results of this research. The current study represents the initial foundation in the development of a hyperspectral technique for real-time assessment of the flocculation process.

INTRODUCTION

The slow sedimentation and consolidation rate of fluid fine tailings (FFT) is the primary reason that makes the reclamation of tailings a major challenge for oil sands operators. Accelerated dewatering technologies are, therefore, required to treat and reclaim the tailings within a reasonable time frame. In-line flocculating and drying of tailings has been a potential tailings treatment strategy used by several oil sands operators to accelerate dewatering of tailings (COSIA 2012). In this method, tailings are mixed with polymer flocculants so that clay particles form aggregates of large flocs resulting in an improved settling velocity. Once the appropriate polymer flocculant is selected, the effectiveness of the flocculation process depends on optimal flocculant dose and optimal mixing rate and time (Webster et al. 2016). Maintaining the optimum polymer dose and mixing conditions is challenging because these parameters vary with tailing characteristics, such as mineralogy, percentage of fines, and solid content. Therefore, developing instrumentation capable of real-time assessment of the flocculation performance of tailings is essential to ensure the consistent generation of effectively flocculated tailings.

The current study aims to investigate the use of hyperspectral imagery for the assessment of flocculation performance. Hyperspectral imaging systems collect the reflectance of light from a target material as a function of wavelength for every pixel of the image. The output imagery can be used to study chemical composition and physical structure of the target material. In past publications, we have investigated the use of hyperspectral sensing for the estimation of several properties of oil sands soft tailings (Entezari et al. 2016a, 2016b, 2017). Spectral models were developed for the quantitative estimation of tailings properties including water content and the normalized evaporation, clay swelling potential indicated by the Methylene Blue Index (MBI), and mineral content, in particular clay and quartz content. Herein, we investigate whether hyperspectral imagery can be used for the assessment of the effectiveness of tailings flocculation through post-depositional hyperspectral imagery and ensuing image analysis. Small-scale flocculated samples were generated in the laboratory using different flocculant doses and mixing conditions to assess the efficiency of hyperspectral imagery in detecting samples with poor flocculation performance.

EXPERIMENTAL PROCEDURE

The tailings sample used to generate flocculated samples was provided by a major oil sands operator in northern Alberta. The sample had an initial solid content of 42 wt%, bitumen content of 2.57 wt%, MBI of 3.75 meq/100g, and fines content (< 44 μm) of 40 wt%. We then diluted the sample to 30 wt% solid content, from which

flocculated samples were produced (process water from the same mine site was used to dilute the tailings). Trial and error experiments were carried out to determine the optimum flocculant dose and mixing conditions.

Nine flocculated tailings samples were prepared using three flocculant doses and three mixing conditions. Accordingly, flocculation doses of 1000 ppm (under-dosed), 1200 ppm (optimum-dosed), and 1400 ppm (over-dosed) were examined. For each dose, three different mixing times and rates were tested: 60 s × 420 rpm (optimum-sheared), 120 s × 420 rpm (partially over-sheared), and 60 s × 550 rpm + 60 s × 750 rpm (fully over-sheared). An anionic commercial polymer, A3338 (SNF), was used as the flocculant and the flocculant solution was prepared at 0.2% (w/w) concentration using deionized water.

The following procedure was used for mixing the tailings with the flocculant solution to prepare the flocculated samples. First, 100 g of diluted tailings was poured into a beaker with a 7 cm diameter and allowed to stir for 2 minutes at a mixing rate of 450 rpm using a propeller shape three-blade impeller (5 cm diameter) to ensure full dispersion of slurry. Then, a determined amount of flocculant solution was injected into the sample using a pipette, while the sample was mixed under the mixing conditions described above. After stopping the mixer, the quality of the prepared flocculated sample was assessed through visual assessment of aggregated floc size and the sample was immediately poured into a pan for acquiring the spectral imagery. Hyperspectral imagery was collected using the SisuROCK imaging system. The output data consisted of 256 reflectance images (i.e. spectral bands) measured from 1000 to 2500 nm with a spectral resolution of ~6 nm and a spatial resolution of ~1 mm per pixel. The spectral images were analyzed with the objective of developing spectral metrics enhancing the texture of the samples and ultimately revealing differences between the flocculated samples. Band ratio analysis was employed to find a band ratio from the available band set revealing the most texture in the samples imagery and improving the contrast between the flocculated samples produced under different conditions.

A threshold-based segmentation was applied on the established band ratio image to highlight different image domains and support the assessment of samples based on their textural properties and spectral contrast. Such segmented color imagery can potentially be used for automated detection of textural differences between flocculated samples as discussed below.

RESULTS

Observations of Flocculation Performance

The 1000 ppm dose was observed to be insufficient to produce a good flocculated sample and resulted in relatively poor dewatering. The condition of 60 s × 420 rpm and 1200 ppm flocculant dose yielded the best flocculated sample (large aggregates of ~ 1 cm). At the 1400 ppm flocculant dose, although a large floc size was observed (~1 cm), the flocculated sample seemed to be over-dosed as it looked jelly-like. By increasing the mixing time (120 s x 420 rpm), the three samples became fully or partially over-sheared, as excessive shear reduced the aggregate size. For all three doses, the flocculated samples had smaller floc size compared to samples produced with mixing conditions of 60 s x 420 rpm. For a mixing condition of 60 s × 550 rpm + 60 s × 750 rpm (total mixing time of 120 s), the samples were generally observed to be fully over-sheared. In particular, samples conditioned with 1000 ppm and 1200 ppm looked completely over-sheared under this mixing condition and almost no aggregated flocs were observed.

Image Analysis Results

Figure 1 compares photos of the samples flocculated under different conditions and shows the equivalent false color composite image of these samples generated using three bands in the shortwave infrared (SWIR).

From band ratio analysis, the ratio between the 1678 nm and 1930 nm bands was found to reveal differences amongst samples flocculated at different conditions (Figure 2). In Figure 2, the dark and bright pixels are associated with the low and high band ratio values, respectively. In this figure, some samples show high brightness with little spatial variability or contrast (for instance, 1000 ppm and 120 s × 420 rpm), while others are darker and display high contrast, defined by a range of dark circular domains observed against a brighter background (for instance, 1200 ppm and 60 s × 420 rpm). The texture variation captured by this band ratio appears to be sensitive to differences in surface micro-topography (comparing the band

ratio image with the sample optical photos (Figures 1 and 2)). It is evident that where larger flocs are formed as a result of a better flocculation process, more contrast and texture is observed in the band ratio imagery. In other words, dark circular domains in Figure 2 correlate with the presence of larger flocs on the sample surface. Figure 2 indicates that tailings samples treated with 1000 ppm of flocculant are not as well textured as samples treated with higher doses. These samples appear brighter than samples treated with doses of 1200 ppm or 1400 ppm since they lack large flocs. When the flocculant dose is increased to 1200 ppm, the texture varies with mixing conditions. The sample mixed at 60 s × 420 rpm is the most textured flocculated sample while the texture decreases with increasing mixing time. As the mixing time and rate increase, the samples are more sheared because relatively more floc breakage occurs than floc formation and thus less texture is observed. A similar trend is observed for the samples treated with a flocculant dose of 1400 ppm. Therefore, it is concluded that when the samples are under-dosed or over-sheared, less texture is observed in the established band ratio image and the overall brightness of the sample images is increased. It is however noted that we could not determine over-dosed samples from the band ratio imagery. To develop an automated technique to detect under-dosed and/or over-sheared samples, a threshold-based segmentation was applied to the established band ratio image to classify the samples based on their textural properties. In the resulting classified band ratio image (Figure 2), under-dosed and/or over-sheared samples display a greater relative abundance of yellow pixels with respect to red and blue pixels. Therefore, the high relative percentage of yellow pixels can be indicative of under-dosed and/or over-sheared samples.

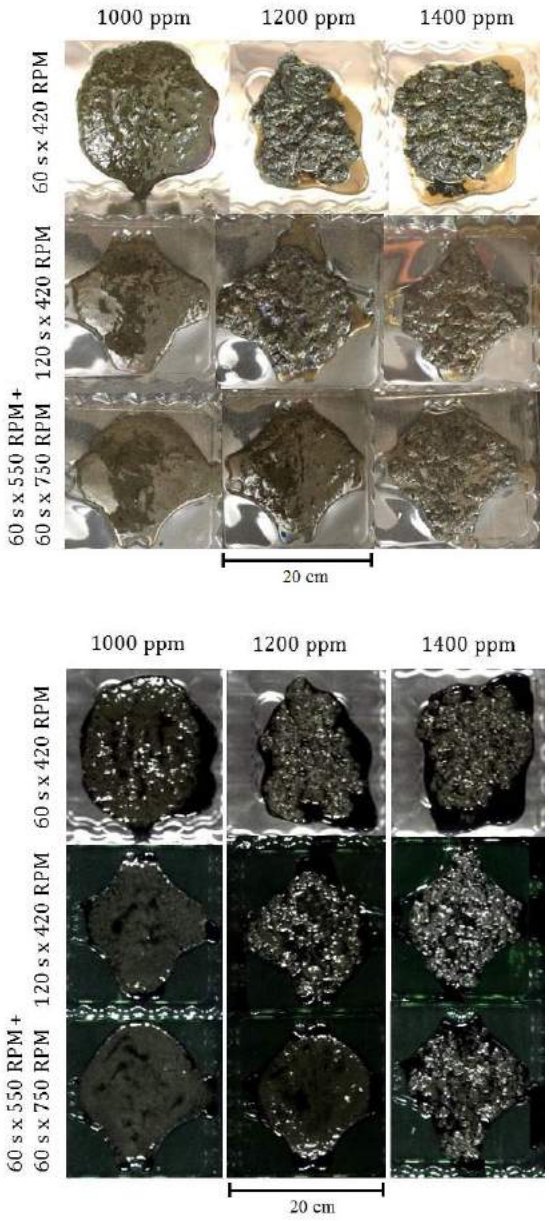

Figure 1. (Top) photographs of the flocculated samples. (Bottom) a false color composite image (R = 2150 nm, G = 2200 nm, B = 2350 nm) of the flocculated samples showcasing low overall reflectance and contrast (thus a near black and white appearance)

CONCLUSIONS

The potential of hyperspectral imagery to assess the effectiveness of the flocculation performance of tailings was examined through spectral measurements and ensuing image analysis for flocculated tailings samples generated in the laboratory. The results showed that a ratio of bands at 1678 and 1930 nm is an effective spectral metric to enhance the texture of the flocculated samples and reveal differences amongst samples. The variation in the surface micro-topography of the samples appeared to be the main factor deriving the variation in the texture captured by the 1678 and 1930 nm band ratio. More texture was observed when larger flocs were formed as a result of a better flocculation process. This study has shown that although it is feasible to

detect under-dosed and/or over-sheared samples using hyperspectral imagery, further flocculation tests are required to calibrate the method, validate the results, and ultimately develop online instrumentation for real-time assessment of flocculation performance.

ACKNOWLEDGEMENTS

The authors would like to thank the National Science and Engineering Research Council (NSERC), Canada's Oil Sands Innovation Alliance (COSIA) and Alberta Innovates for their financial support of this research. The authors acknowledge that the material presented in this paper has been submitted for publication to the Canadian Journal of Chemical Engineering.

REFERENCES

Canada's Oil Sands Innovation Alliance. (2012). Oil sands tailings technology deployment roadmaps. Report to Alberta Innovates–Energy and Environment Solutions.

Entezari, I., Rivard, B., Lipsett, M. G. and Wilson, G. W. (2016a). Prediction of water content and normalized evaporation from oil sands soft tailings surface using hyperspectral observations. Canadian Geotechnical Journal, **53**(10): 1742-1750.

Entezari, I., Rivard, B. and Lipsett, M. G. (2016b). Estimation of Methylene Blue Index in Oil Sands Tailings Using Hyperspectral Data. Canadian Journal of Chemical Engineering, **95**(1): 92-99.

Entezari, I., Rivard, B., Geramian, M. and Lipsett, M. G. (2017). International Journal of Applied Earth Observations and Geoinformation, **59**: 1-8.

Webster, S. E., Brown, W. A., Derakhshandeh, B., Dubash, N., Gomez, C. and Veenstra, C.N. (2016). A comprehensive control scheme for dynamic inline flocculation of oil sands tailings. Fifth International Oil Sands Tailings Conference (IOSTC 2016), Lake Louise, AB, Canada, 4-7 December 2016.

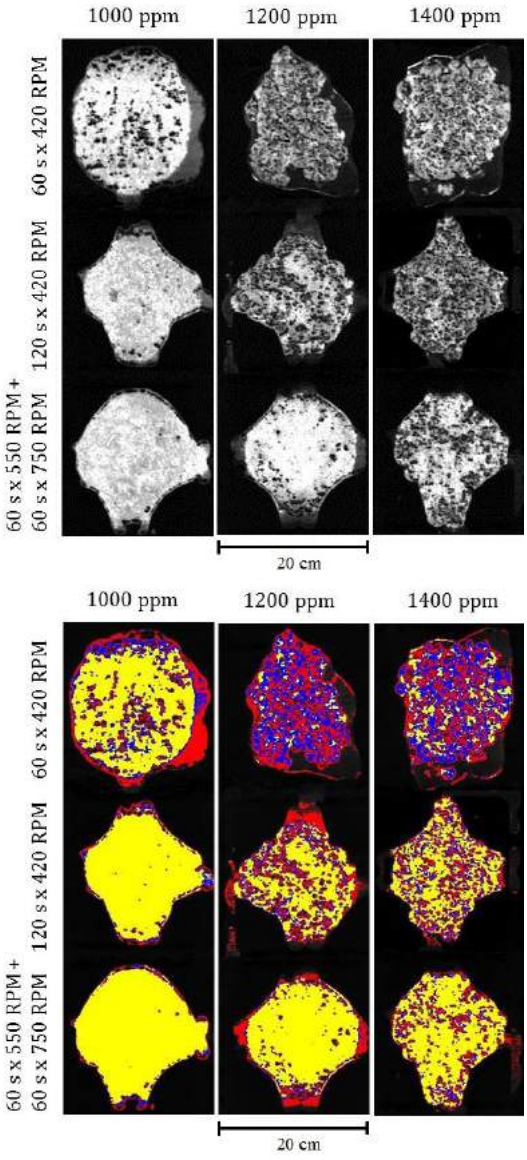

Figure 2. (Top) band ratio image (band ratio of bands at 1678 and 1930 nm) of the flocculated samples produced to reveal texture. (Bottom) classified band ratio image of the flocculated samples produced to assess the effectiveness of flocculation and to detect under-dosed/over-sheared samples. This image was created by assigning red, blue, and yellow colors to pixels with band ratio values of 1.5-2.5, 2.5-3.5, and 3.5 and higher, respectively. Band ratio values below 1.5 were associated with background materials (e.g. containers and imaging system platform) and were masked

Session 7

UTILIZING NATURE FOR TAILINGS DEWATERING

DESIGN OF LANDFORM ELEMENTS FOR OIL SANDS MINE RECLAMATION

June Pollard[1] and Gord McKenna[2]
[1]J. Pollard Consulting, Edmonton, Canada
[2]McKenna Geotechnical Inc., Delta, BC, Canada

ABSTRACT

Landform design is the multidisciplinary design process that builds mining landforms and landscapes to meet agreed upon land use goals and performance objectives. Such work starts even before mining begins, carries on through mine development and operation, and continues through closure and beyond to guide post-mining stewardship of the land. It allows mining companies, regulators, and local communities to progressively reclaim the land with confidence, managing costs, risks, and liabilities, to create beneficial landscapes.

Landform elements are a component of a landform design at a scale large enough to be featured on detailed design drawings; typically, tens of metres. Some elements are exquisitely designed. Some are field-fit. Many of these elements are constructed on tailings drainage basins, on sand or coke capped beaches, so many overlie soft tailings deposits. Examples of landform elements include swales, mounds, outlets, watershed berms, vegetation patches, meandering toe creeks, islands and wildlife enhancements such as snags, rockpiles etc. All provide efficient and practical solutions to complex reclamation problems and each performs specific functions to meet the overall goals and objectives of a landform design. Each member of the landform design team, which comprises geotechnical, mining, surface water, groundwater, soil, vegetation, wildlife, and regulatory specialists will play a role in design of these elements.

The paper outlines the concept of landform elements and provides examples of landform elements for mine reclamation for two common mining landforms (tailings facilities and surface watercourses). The paper focusses on landform elements for oil sands landforms and landscapes.

INTRODUCTION

Mine closure and reclamation planning are undertaken at a variety of nested scales: region, mine lease/ landscape and mining landform (Table 1). Historically spatial scales smaller than landform have been referred to as a multitude of terms; macro-topography, meso-topography, micro-topography, patch are examples. Much of the landform design effort is logically focussed at the mining landform scale (for example, a single dump, an end pit lake, or a tailings facility). From recent

Figure 1. Common mining landforms and landform elements

work designing and reclaiming mine sites, the authors recognized the practicality and usefulness of cataloguing “landform elements” (Pollard and McKenna 2018); defined as all features smaller than the landform scale. The list of elements includes, for example, ridges, swales, wetlands, patches, trails, and signage.

This paper starts by providing background on landforms and landform design and then describes and defines the concept of the landform elements within this context. To illustrate the concept further, worked examples where landform elements are identified for two oil sands landforms, oil sands tailings drainage basins and surface watercourses are provided. Finally, the use and opportunity for landform elements in design (generic design opportunities) and as communication tools in end land use planning are discussed.

MINING LANDFORMS AND LANDFORM DESIGN

Mining landforms are distinct topographic and operational units that together comprise a reclaimed mining landscape (McKenna 2002). Landform design is the collaborative and multidisciplinary effort to create mining landforms and closure landscapes that are constructed and reclaimed to meet specific design goals and objectives, create land for targeted end uses, and reduce risk, costs, and liabilities. Mining landscapes and landforms are designed to specific goals, design objectives, and design criteria using a design basis memorandum (DBM) approach (Ansah-Sam et al. 2016). Many of these goals and objectives are defined by regulatory approval requirements.

Table 2 describes typical oil sands landforms identified from closure plans from the region. These distinct landforms have individual design, regulatory requirements and functions which all work in tandem to achieve the landform goals and objectives. In undertaking a closure landscape level design, all areas of the mining lease should be allocated to one of these landform (or management) units. The rigour in assigning all areas of the lease to a landform, safeguards against spatial areas of the site not being incorporated into the topographic design. It also safeguards against spatial areas being omitted when considering, predicting and modelling flow of water, groundwater, trucks, monitoring, wildlife, for example, through the closure landscape.

There is a temporal scale to landform design work; in the period from pre-disturbance, mining, production, bulk overburden placement or tailings infilling, and through to reclamation a specific area of the site may be used for a number of different mining activities. An example is an area of a site which may be stripped, mined to a mined-out pit, infilled with tailings and then reclaimed as an End Pit Lake. For clarity when the term, ‘landform’ and ‘landform design’ is used in this paper it is for the design and construction of the structure as it is intended to be in its reclaimed post-closure state. Hence the non-inclusion of intermediate mining structures such as mined out pits in Table 2.

Table 1. Landform design scales

Design scale	Representative dimension, m	Description and examples
Regional	100,000	A grouping of mines in a valley or region *Regional plan, cumulative effects assessment*
Lease / landscape	10,000	A single mine lease / property. More generally: everywhere you can see from a particular point on the land (the Renaissance definition) *Life of mine plan, mine closure plan, landscape ecology*
Landform	1,000	A single mine facility: dump, mined out pit, stockpile, tailings facility *Dump design, dam design, landform design*
Landform elements	1 to 100	Specific designed physical subcomponent of a mining landform *Wetland, hummock, berm, rock pile*

Adapted from McGreevy et al 2013; McKenna et al 2013; Eaton et al 2014; Turner & Gardner 2015. It is proposed that “landform elements” replace the macro-, meso-, and microtopography nomenclature previously employed for features smaller than 100m in scale.

Table 2. Typical Oil Sands Mining Landforms

Landform Type	Description
Tailings Dyke	A terraced hillslope that acts as a dam to store tailings. Tailings dykes are typically constructed with a combination of compacted interburden, overburden, or most commonly, tailings sand. The slopes are typically terraced and contain diagonal access ramps for access. Constructed swales gather and transport surface water runoff. *Examples: Suncor Tar Island Dyke, Syncrude Boundary Dyke*
Tailings Drainage Basin	A tailings drainage basin is a plateau created through hydraulic deposition of tailings sand (to form beaches) and soft tailings (that is contained in the central area). For design and management, it is usually more practical to consider the tailings drainage basin as a separate landform unit from the tailings dyke or pitwalls that contain the soft tailings. The basin is constructed to shed water to a single armoured outlet. For both in-pit and ex-pit tailings drainage basins, the resulting topography forms a topographic high in the closure landscape with ridges and mounds around the perimeter to form uplands surrounding a central wetland complex in the middle. *Examples: Syncrude MLSB, Suncor Pond 1/ Wapisiw Lookout, Albian Muskeg River External Tailings Facility*
Overburden Dump	Overburden dumps are terraced hills created to store overburden materials. They can be comprised of a variety of materials; glacial deposits including saline-sodic clay-shale overburden, quaternary fluvial deposits and/or reject bedrock formations (for example lean oil sands). Most overburden dumps have large plateaus (which may be mounded to shed water or dished to direct surface water to a central swale) and steep terraced slopes which often comprise a large proportion of the footprint. *Examples: CNRL MRM Dump 2C, Albian Syncrude S4 Dump / Gateway Hill, Suncor MD9*
End Pit Lake (EPL)	CEMA (2012) provides the following description: *"an engineered water body, located below grade in an oil sands post-mining pit. It may contain oil sands by-product material and will receive surface and groundwater from surrounding reclaimed and undisturbed landscapes. EPLs will be permanent features in the final reclaimed landscape, discharging water to the downstream environment"* *Examples: Syncrude Base Mine Lake (BML), Suncor Demonstration Pit Lakes*
Surface water drainage system	Drainage ditches, swales, creeks and streams which move water through the reclaimed landscape to the external environment. This landform also includes the associated banks, riparian, flood zones and offset corridors which accompany these watercourses. Most surface water drainage systems, on oil sands leases, have been planned and had a high level of design but have not been constructed.
Plant site	Flat topographic and accessible areas which contain all the plant site facilities and associated mining processing facilities (ponds, tanks etc.). *Example: Suncor Base Plant, various laydown areas in the region*
Landfills	Various types of landfills are constructed on each lease, most of which are terraced hillslopes with compacted overburden and interburden containing various types of wastes and byproducts. Examples: *Syncrude FGD Landfill*
Reclamation stockpile	Temporary hills comprised of uncompacted peat and other reclamation materials. *Examples: Syncrude NT1 Dump, Jackpine Reclamation Material Stockpile 7a*
Borrow pits	Shallow basins and mounds as remnants of gravel, sand, or clay extraction. The resulting landform is often comprised of hummocky hills with low flat wetlands. *Example: Poplar Creek gravel pits, Susan Lake gravel pit.*
Reservoirs	Ponds and lakes created to store or divert water, or as fish-compensation. Many were former natural lakes that were raised by dams. Others are lined facilities. Example: *Poplar Creek Reservoir, Kearl Muskeg Lake*

LANDFORM ELEMENTS

Definition of Landform Element

A landform element is a specific physical subcomponent of a mining landform that is designed and constructed to allow the landform to meet the design goals and objectives. Such elements are typically large enough to be featured on a detailed design drawing and be built with mine reclamation equipment, typically at the 1m to 100m scale. Examples are pit walls, haul roads, berms, wetlands and snags.

A list of landform elements for reclamation of metal, coal, and oil sands mines is presented in Pollard and McKenna (2018). The list includes 97 different landform element types and is being added to over time. As follow-up to this work, landform design guidance specific to oil sands have been reviewed against the overall list (CEMA 2005, 2012, 2014). Lists for landform elements for two different oil sands specific landforms; an oil sands tailings drainage basin and surface water drainage systems are discussed in the following sections.

The definition of landform elements is a deceptively simple concept. Landform elements are already being designed as part of landform designs, in reclamation work, and as part of life-of-mine closure plans. In the following two sections, the authors have selected and described two oil sands landforms; oil sands tailings drainage basins and surface water drainage systems, and then, to describe the concept, provided a list of landform elements and some illustrated examples from reclaimed sites. The usefulness of these lists in design is described in the final section of this paper.

Landform Elements for an Oil Sands Tailings Drainage Basin

A description of and oil sands tailings drainage basin is described above in Table 2. Typical design constraints for the landform design include the low shear strength of soft tailings, the need for geotechnical stability, freeboard requirements, significant predicted settlement for the final closure surface, closure drainage requirements (the need to construct outlets specifically) and poor trafficability (Ansah-Sam et al. 2016, McKenna et al. 2016). As part of recent work reclaiming tailings drainage basins, we have documented typical landform elements included in the landform design and the resulting list of elements is included as Table 3. Figure 2 is an illustration of an oil sands tailings drainage basin landform where identifiable landform elements have been labelled.

Landform Elements for Surface Water Drainage Systems

A surface water drainage system is a type of landform associated with a watercourse (swale, ditch, creek, stream or river) and its associated banks, riparian zone and floodplain offsets. These watercourses can be existing natural waterbodies or those designed and constructed as part of a closure drainage network. Surface watercourses themselves, excluding wetlands and lakes, can be divided into three broad categories; swales and vegetated waterways, geotechnical/operational watercourses, and reconstructed streams and creeks. Table 4 provides a description of these watercourses. A list of landform elements associated with these landforms is presented in Table 5.

Table 3. Landform Elements for Oil Sands Tailings Drainage Basin

Watershed berm (bund)	Spillway	Access roads - haul road, light vehicle road
Ridge	Pond (Sedimentation, water treatment, outlet)	Access controls – fence, barrier rocks, gate, moat
Mound or hummock	Inlet	Trail
Microtopography mounds	Island	Boardwalk
Depression/ Hollow	Peninsula	Laydown, pad, parking lot
Containment berm	Reclamation cover	Culvert
Cover	Vegetation patch	Sign
Stockpile	Brush pile	Lookout
Dam	Rock pile	Water treatment facility
Dam crest	Snag / wildlife tree	Pump house
Cap	Nesting box	Pipeline
Upland zone	Remnant stand	Power line
Riparian zone	Vegetation island	Monitoring instrumentation
Wetland (marsh, fen, bog, open-water wetland, swamp)	Shelterbelt	Research plot
Central swale	Buildings – visitor centre, village, maintenance sheds, office	
Outlet channel		

Figure 2. Landform Elements – Oil Sands Tailings Drainage Basin (Suncor Wapisiw Lookout)

Table 4. Oil Sands Surface Watercourses

Surface Watercourse		Description
Vegetated waterways and swales		Swale (no defined bed and banks) which provides erosion protection by distributing flow over the full width of the watercourse minimizing the occurrence of concentrated flow paths. (Ade et al. 2011) *Examples: Wapisiw Lookout, Sandhill Fen, W1 Dump swales*
Reconstructed streams and creeks (alluvial channel)	Lowland Stream	Slope of less than 0.5%, slow channel flow impeded by beaver dams, fallen trees, debris and muskeg accumulations. Has well defined bed and banks. Surrounded by lowlands vegetated with low grasses and shrubs. Attractive to beaver dams. (Ade et al. 2011) *Examples: Lower Poplar Creek*
	Upland Stream	Slope of 0.5 to 5%, fast channel flow, bed material of permeable gravels, cobbles and material as large as boulders. Well defined bed and banks. Surrounded by upland forests. (Ade et al., 2011) *Examples: Coke Cell 5 outlet channel*
Geotechnical and operational watercourses		Mine site ditches designed to drain water from the toes of structures or access routes. Often designed for a defined flow. (Note: Unless specifically removed or redesigned these structures may be present in the final closure landscape.) *Examples: Toe ditches, haul road drainage, operational sumps*

Table 5. Landform Elements for Surface Water Drainage Systems

Watershed berm (bund)	Vegetation patch	Access roads - haul road, light vehicle road
Mound	Brush pile	Access controls – fence, barrier rocks, gate, moat
Microtopography mounds	Rock pile	Trail
Depression/ Hollow	Snag / wildlife tree	Boardwalk
Spillway	Nesting box	Laydown, pad, parking lot
Central swale	Corridor	Bridge
Sedimentation pond	Remnant stand	Culvert
Attenuation pond	Vegetation island	Ford
Water treatment pond	Vegetation patch	Sign
Outlet pond	Creek	Lookout
Containment berm	Confluence	Water treatment facility
Diversion channel	Bench (bankfull)	Pump house
Levee	Meander bend	Pipeline
Cover	Oxbow	Power line
Stockpile	Point bar	Monitoring instrumentation
Retaining wall	Pool	Test pond
Upland zone	Step pool	
Riparian zone	Plunge pool	
Wetland (marsh, fen, bog, open-water wetland, swamp)	Riffle section	
	Bank stabilization	
Lake	In-stream structure – cross, j-hook and rock vanes	* *Drainage network elements adapted from USDA (2007).*
Inlet		
Outlet	Flow control structure – low head dam, weir, pier	
Reclamation cover		

DESIGN OF OIL SANDS LANDFORM ELEMENTS

Landform elements should be easily identifiable in a landform design drawing or report as individual functional components of the landform design. The level of detail for the design of each element will vary significantly. Some elements require a detailed engineering design; for example, dams, cap, or a water treatment plant and need professional sign-off, for example where geotechnical stability, surface water drainage, or cover performance may be impacted. Some elements will be shown on a plan view map as part of the landform design and may have a standardized 'off the shelf' design; for example, a watershed berm. Some landform elements will be field fit; for example, small mounds for roughening of an upland slope.

A significant opportunity in the use of landform elements as a concept is the option to develop and test generic designs, where appropriate. For example, Eaton et al. (2014) have developed a framework for generic design of wildlife enhancement features. Their work provides an example of a generic design of snags -- dead vertical wildlife trees installed in the reclaimed landscape using a telephone-pole installation rig to provide habitat for cavity nesting birds and perches for raptors. The framework provides details for design based on available information in a concise table, and a program for testing the efficacy of the element. This generic design template could be applied to other landform elements.

Some ideal candidates for generic design of oil sands landform elements are rockpiles, wetland islands, mounds of different shapes and sizes, toe creeks. The use of generic designs presents an opportunity to monitor and research the performance of these designs and consequently improve on the designs over time. Gathering and sharing of the generic designs for landform elements through a book or website may be useful in this respect to advance knowledge. This has already been completed for the larger elements such as wetlands (CEMA 2014) and is a model which can be covered with a smaller level of effort and scope for other smaller elements. A tabular format such as that used in Eaton et al. works well for this scope and detail of design information. For low cost or low risk elements, designs based on judgement can be tested and improved over time.

LANDFORM ELEMENTS AS COMMUNICATION TOOLS

The landform elements presented in this paper also represent a tool for communication for an overall landform design with stakeholders, regulators, management, operators and others. Landform elements presented in a visual format could become a tool for discussion related to end land use planning with these interested parties; describing the landform design at a smaller scale, what landform elements could be included and what that would they be like and what roles they serve. This is an opportunity for this concept which could be developed further. Figure 3 demonstrates some landform elements as stand-alone illustrations for this purpose.

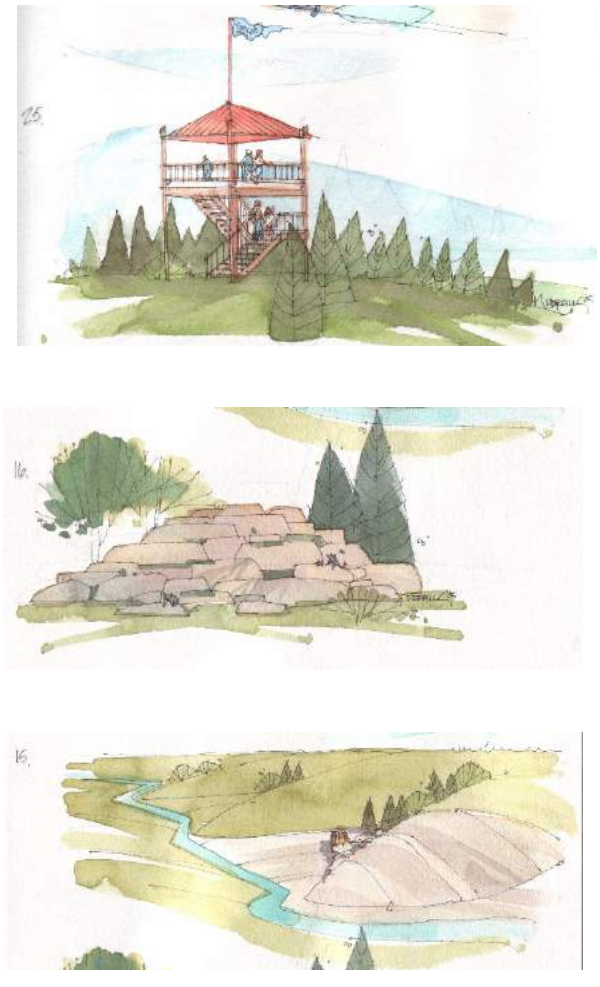

Figure 3. Individual landform elements drawn as communication tools (tower, rock pile and mound)

SUMMARY

This paper provides definition of a new landform design scale of landform element for those features on a landform which are less than 100m in size and form part of an overall landform design. The development of this concept provides a final framework for scales in Landform Design and closure planning; Region, Landscape, Landform and Element (Table 1). The paper provides background on Landform design in the oil sands region, definition of the term 'landform element' and illustrates the concept using examples of landform elements for two oil sands landforms, Oil Sands Tailings Drainage Basins and Surface Water Drainage Systems. Practical uses of the concept are provided in a discussion of the design of landform elements, including the merits of generic designs for some elements, and the potential opportunity for the use of this scale for communication in End Land Use Planning.

REFERENCES

Ade, F., Sawatsky, L., Beersing, A. and Fitch, M. (2011). Geomorphic design of alluvial channels for oil sands mine closure. Mine Closure Conference 2011. Alberta, Canada.

Ansah-Sam, M., Hachey, L., McKenna, G. and Mooder, B. (2016). The DBM approach for setting engineering design criteria for an oil sands mine closure plan. Fifth International Oil Sands Tailings Conference, December 4-7. Lake Louise, Alberta. University of Alberta Geotechnical Group, Edmonton. 11p.

CEMA. (2014). Guidelines for Wetland Establishment on Reclaimed Oil Sands Leases (3rd Edition). Cumulative Environmental Management Association. Fort McMurray. 494p.

CEMA. (2005). Landscape Design Checklist, Revised RSDS Government Regulator Version. May 2005. Landscape Design Subgroup of the Cumulative Environmental Management Association, Fort McMurray. 8p.

CEMA. (2012). Oil Sands End Pit Lakes Guidance Document. Cumulative Environmental Management Association Fort McMurray. 494p.

Eaton, B. R., Fisher, J. T., McKenna, G. T. and Pollard, J. (2014). An Ecological Framework for Wildlife Habitat Design for Oil Sands Mine Reclamation. OSRIN Report No. TR-67. Oil Sands Research and Information Network, University of Alberta. Edmonton. 83p.

Golder. (2008). Geomorphic characterization and design of alluvial channels in the Athabasca Oil Sands Region. Consultant's report for Canadian Oil Sands Network for Research and Development and the Department of Fisheries and Oceans. Golder Associates. Calgary.

McGreevy, J., McKenna, G., An, R. and Scordo, E. (2013). Regional mine closure plans – the next improvement in closure planning. Tailings and Mine Waste 2013 Conference. Banff. Nov 3-6. University of Alberta Geotechnical Centre, Edmonton. p627-636.

McKenna, G. and Cullen, V. (2008). Landscape design for soft tailings deposit. Tailings and Mine Waste 08 Conference. Vail, Colorado. 10p.

McKenna, G., Abbott, R., Nahir, M., O'Kane, M., Seto, J. and Straker, J. (2015). Post mine land uses for northern mines. The Northern Latitudes Mining Reclamation Workshop: Reclaiming the North. September 2015. Juneau, AK. PowerPoint slide deck. 26p.

McKenna, G., Mooder, B., Burton, B. and Jamieson, A. (2016). Shear strength and density of oil sands fine tailings for reclamation to a boreal forest landscape. IOSTC International Oil Sands Tailings Conference. Lake Louise. Dec 4 to 7. University of Alberta Geotechnical Group. Edmonton.

McKenna, G., An, R., Scordo, E. and McGreevy, J. (2013). Toward effective closure planning: From progressive reclamation to sustainable mining. Tailings and Mine Waste '13. Proceedings of the Seventeenth International Conference on Tailings and Mine Waste, November 3-6, Banff. University of Alberta Geotechnical Centre, Edmonton. p615-625.

McKenna, G. T. (2002). Landscape engineering and sustainable mine reclamation. PhD Thesis. Department of Civil and Environmental Engineering. University of Alberta. Edmonton. 660p.

McKenna, G. (2009). Techniques for creating mining landforms with natural appearance, Proceedings of Tailings and Mine Waste '09 Conference. Banff, Alberta. November 1-4. The University of Alberta Geotechnical Centre, Edmonton.

Pollard, J. and McKenna, G. (2018). Landform elements for mine reclamation. British Columbia Mine Reclamation Symposium (BCTRCR) Conference. Williams Lake, BC.

Turner, M. G. and Gardner, R. H. (2015). Landscape ecology in theory and practice: pattern and process. Second edition. Springer. New York. 482p.

USDA. (2007). Stream Restoration Design. National Engineering Handbook Part 654. United States Department of Agriculture. Natural Resources Conservation Service. Washington DC. 660p.

Illustrations by Derrill Shuttleworth. Gabriola Island, BC. http://dshuttleworth.ca

DEVELOPMENT OF BACTERIAL INOCULUM FOR THE PROMOTION OF PLANT GROWTH ON TAILINGS MATERIAL

Victoria Collins, Amanda Schoonmaker, Heather Kaminsky, Andrea Sedgwick, Chibuike Chigbo and Paolo Mussone
Northern Alberta Institute of Technology, Edmonton, Canada

ABSTRACT

Current oil sands tailings dewatering technologies fail to produce trafficable materials for deposition or are cost prohibitive. The goal of this project is to demonstrate the integrated use of native boreal plant species and indigenous selected bacteria cultures capable of degrading residual hydrocarbons and organic acids, while fixing nitrogen in the soil as tools to further accelerate the transformation of oil sands tailings into a reclaimed soil. This project is articulated in two phases, Phase 1: upscaling bacterial culture on a suitable substrate, and Phase 2: growth of slender wheatgrass and sandbar willow on fluid tailings inoculated with the bacterial culture.

During Phase 1 we evaluated the following materials as substrates: activated carbon, diatomaceous earth (DE), and biomass-derived fly ash. We investigated microorganisms enriched from the following tailings sources: Canadian Natural Muskeg River Mine, Syncrude Mildred Lake Settling Basin (MLSB), and two cultures using thickened tailings and tailings centrifuge cake provided by Imperial Oil and Canadian Natural, respectively. We evaluated substrate cultures by measuring methane production as a proxy for microbial metabolism, hydrocarbon concentration, and acetylene reduction as an indicator of nitrogen-fixation. In these trials, Syncrude and Canadian Natural enrichments grown on DE produced the most methane. While hydrocarbon degradation results were inconsistent, Canadian Natural cultures grown on DE were found to have the highest acetylene reducing activity. Based on these results, Canadian Natural enrichment on DE was selected for implementation in Phase 2, beginning June 2018.

INTRODUCTION

Background

Bitumen is extracted from mined oil sands ores using the modified Clark hot water extraction process. Hot water, caustic agents, dispersants, and diluents are employed to separate and recover bitumen from clays (Chalaturnyk et al. 2002). Following diluent recovery, the remaining tailings slurry is pumped into settling ponds for water recovery and storage. These tailings are composed of water, sand, silt, clay, salts, and organic residues. Once in the ponds, the coarse sands quickly fall out of solution, however the remaining materials form a stable suspension that can take years to reach 30 wt% solids. Further consolidation may take decades (Chalaturnyk et al. 2002). Several treatment technologies have been developed to speed dewatering, these include the use of organic and inorganic flocculants and coagulants, centrifugation, and settling aids such as calcium sulfate (Allen 2008). While treatments are effective, implementation at industrial scale is costly and producing trafficable tailings for dry landscape reclamation has remained challenging.

In 1998, a greenhouse study by Silva suggested that certain plant species may be able to grow in tailings (Silva 1999, Silva et al. 1998). Moreover, these plants could dewater the materials while increasing the shear strength in the root zone. This approach provided several benefits such as increased bearing capacity, increased matrix suction and water release through evapotranspiration, potential degradation of organic acids, and CO_2 respiration at relatively low cost (Silva 1999, Silva et al. 1998). However, many plant species were adversely affected by highly saline conditions and efficacy was limited by the relatively shallow roots of grass species.

Tailings can be limited in essential nutrients such as nitrogen (Collins et al. 2016), which is required for plants growth. Other factors such as salinity and hydrocarbons (Allen 2008), can decrease survival of newly established plants (Huang et al. 2004, Nadeem et al. 2013). Plant growth promoting microorganisms can provide nitrogen for plant growth, enhance survivability by degrading stress hormones associated with drought and salinity, produce growth hormones, and assist in the biodegradation of organic contaminants (Ahemad

and Kibret 2014, Bashan 1998, Khan 2005, Vessey 2003, Zhuang et al. 2007). Nadeem et al. (2013) found that inoculating wheat plants grown in naturally saline soil with cultured plant growth promoting bacteria increased seed germination, plant growth, yield, and overall nutrient content including nitrogen, phosphorous and potassium. The authors suggested the inoculated bacteria were capable of degrading 1-aminocyclopropane-1-carboxylate (ACC), the precursor to the plant stress hormone ethylene. Bacteria capable of degrading ACC have been found to promote root elongation and increase nutrient uptake in the presence of heavy metals (Belimov et al. 2001), and hydrocarbon contamination when co-cultured with hydrocarbon degrading bacteria (Khan et al. 2013). Some bacteria including certain *Bacillus* sp. *Pseudomonas* sp. and *Rhizobiaceae* also produce indole-3-acetic acid (IAA), a plant hormone that influences growth. Grobelak et al. (2015) found inoculating grasses with IAA producing bacteria increased shoot and root elongation. Root elongation provides multiple benefits. Rhizodeposition of root exudates increases with root biomass development, thereby feeding the microbial community and expanding the bacterial population in root zone (Juhanson et al. 2007). Enhanced root growth (thereby greater root surface area for nutrient absorption) may be advantageous in nutrient deficient tailings.

Bacteria for bioremediation or bioaugmentation have been well studied and are commercially available, however bacterial amendments applied *in-situ* have traditionally been prone to failure or unpredictable results (Thompson et al. 2005, and references therein). Challenges such as high salinity, heavy metal content, pH, nutrient availability, competition, and toxins present in the amended materials can inhibit microbial growth and nullify potential benefits. Bacteria well adapted to environmental conditions can be employed to overcome these obstacles. Endogenous bacteria can be enriched from the source materials (Salem et al. 2003), or enrichment cultures from materials with similar environmental conditions and known functions can be developed (Nasseri et al. 2010). However, enrichment conditions are highly controlled and environmental shock can still be a concern, therefore the development of a biofilm based inoculum is desirable. Biofilms are highly resilient and serve to protect the microbial community from environmental factors and enable environment dependent metabolic activities. This includes anaerobic nitrogen fixation in the presence of oxygen (Lee et al. 2014, Wang et al. 2017). Growth matrix substrates play a key role in promoting biofilm development. For example, bacteria attach more rapidly to non-polar surfaces due to interactions with the cell wall. This activity has been observed on hydrophobic materials such as plastic and Teflon (Donlan 2002). Biofilms have also been cultured on biochar as a potential alternative to sand and soil wastewater filters (Dalahmeh et al. 2018). Porous or rough surfaces also increases bacterial colonization due to the reduction of shear forces and higher surface area (Donlan 2002).

The objective of this study was to identify a metabolically active bacterial source capable of nitrogen fixation that could persist in oil sands tailings. A variety of carrier substrates (activate carbon, fly ash and diatomaceous earth) were also evaluated to further optimize the vigor of the microbial community and better ensure its survival once inoculated into a tailing-plant root rhizosphere. Activated carbon and wood-based fly ash were selected for evaluation based on hydrophobicity, high surface area, and literature suggesting activated carbon promotes biofilm formation and bioremediation (Caldeira et al. 1999, Koch et al. 1991, Scott et al. 1995). Diatomaceous earth was also chosen for evaluation based on high surface area, low cost, and silica based composition as sand is used as a matrix for biofilm development in wastewater treatment (Dalahmeh et al. 2018).The findings from this investigation were utilized for the second phase of work in this project, which comprised a multi-factor growth experiment with two native species grown in 1.0 m columns of tailings.

MATERIALS AND METHODS

Chemicals, Materials, and Gasses

Acetylene (scientific grade), 30% CO_2/70% N_2 (scientific grade), and all other gasses (certified standard 4.8 or higher) were purchased from Praxair (Mississauga, Ontario). All chemicals were reagent grade or higher from Fisher Scientific (Toronto, Ontario). Thickened tailings and centrifuge cake were provided by Imperial Oil and Canadian Natural, respectively. Syncrude and Canadian Natural media based enrichment cultures were established using methods previously described (Collins et al. 2016) to increase the proportion of bacteria capable of hydrocarbon degradation and nitrogen fixation in tailings (unpublished data). Substrates diatomaceous earth

and activated carbon were purchased from Red Lake Earth (Kamloops, BC), and Alfa Aesar (#3330236), respectively. Fly ash substrate was obtained from a pulp and paper mill in Alberta and was composed primarily of volatile carbon and silicates. Substrates were selected based on the literature, which suggested non-polar, porous, and high surface area substrates promote biofilm development (Donlan 2002).

Primary Cultures

Cultures were prepared in 125 mL bottles (DWK Life Sciences Wheaton, #219755) with open top butyl septa caps (DWK Life Sciences Wheaton, #240680). Due to the varying densities of substrates, culture composition was established by volume to include 35 mL of each substrate. Substrates were as follows; 20 g diatomaceous earth, 25 g of ground fly ash, and 11 g of activated carbon powder. Media was added to a final volume of 75 ml. Bottles with media and substrate were autoclaved, sealed, exposed to vacuum to remove air, then flushed for 5 min with 30% CO_2 balance N_2 prior to addition of reducing agent. Cultures were then inoculated with 1 mL tailings or enrichment culture.

Nitrogen deficient methanogenic culture media was prepared as described in Collins et al. (2016) where methanogenic media recipe containing salts, trace metals, phosphate buffer, reducing agent, and anaerobic indicator (Fedorak and Hrudey 1984, Holowenko et al. 2000) was prepared with nitrogen containing components either substituted or omitted. The following modifications were made; the final concentration of the anaerobic indicator resazurin, was 0.5 mg L^{-1}, and 1 g L^{-1} cysteine was used as the reducing agent in lieu of sodium sulfide. Media and substrates were prepared and autoclaved aerobically before anaerobic preparation described above. Following inoculation and two days incubation in the dark, cultures were amended with 230 mg L^{-1} toluene and 500 mg L^{-1} filter sterilized citrate (777.6 mg L^{-1} trisodium citrate).

This two factor study examined bacterial cultures and growth substrates in combination. Cultures originated from previously developed enrichment cultures (Syncrude, Canadian Natural) or were developed through enrichment of the tailings under evaluation in this study (centrifuge cake, thickened tailings). Substrates included activated carbon, diatomaceous earth, fly ash, and methanogenic media alone. Sterile negative controls for substrates were established without bacterial inoculum, and sterile controls for inoculum were established in media alone without substrate. All treatments were prepared in triplicate.

Secondary Cultures to Evaluate N_2 Fixation

Secondary cultures were established for the acetylene reduction assay as acetylene can negatively impact the metabolism of methanogens (Sprott et al. 1982). For active cultures, 10 mL volume was extracted via needle and syringe at day 55 and transferred to a sterile 16 mL Hungate tube (Chemglass Inc, #420801) that had been previously sealed and flushed with sterile 0.22 µm filtered CO_2/N_2 gas. Cultures were amended with an additional 100 mg L^{-1} citrate to promote metabolism and sterile filtered acetylene was added to the headspace for a final concentration of 1.5 vol% (~4 µmol). Ethylene was measured at day 0 and day 19.

Substrate Characterization

Specific surface area was determined by using the Brunauer–Emmett–Teller (BET) single point method on a Monosorb Quantachrome surface area analyzer. Samples were degassed under heat and inert gas flow (30% He balance N_2 gas mixture: 15-20 psi, 100% N_2: 5 psi, glass sample cells). Surface area was measured in triplicate and corrected for ambient temperature and pressure. To determine the particle size of diatomaceous earth, samples were dispersed in water and sonicated then analyzed on a Horiba LA-950 laser diffraction particle size instrument.

Conductivity and pH were determined by combining substrates with water in centrifuge tubes at the ratio present in cultures (47 vol%; see Primary Cultures) and shaken for 20 min at speed 6 on a VWR standard analogue shaker. Solids were removed by centrifuge (7,000 x g, 20 min) and liquids were analyzed for conductivity (EC) and pH using Barben 551 analytical liquid conductivity sensor and Mettler Toledo seven compact meter, respectively.

SEM samples were prepared by adhering substrate to carbon adhesive tabs on mounting stubs and sputtering with gold-palladium alloy. Images were taken on a Tescan Vega3 scanning electron microscope.

Chemical Analyses

Gas chromatography analyses were performed using an Agilent Technologies 7890A GC System equipped with CTC autosampler and heating block, flame ionization detector (FID) and thermal conductivity detector (TCD). Moles of methane were determined by injecting 0.5 mL culture headspace into a 10 mL headspace autosampler vial and analyzed on GC-FID (column: DB-VRX, 1.2 mL min^{-1} He). Ethylene concentration was analyzed similarly using 0.2 mL headspace from secondary cultures on GC-TCD (column: HP-PLT/Q, 5 mL min^{-1} He). Headspace pressure was monitored using a digital pressure gauge (DPG1000B ± 15.00PSIG-5, MOD-TRONIC Instruments Limited, Brampton, ON) equipped with luer-lock fitting and needle. All gas chromatography data were quantified using external standards, and sterile controls were used as blanks to account for substrate induced background noise.

Culture pH in Table 1 was determined using pH strips (VWR BDH35312.607, BDH35310.601).

Data Analysis

Statistical significance was determined using single and two factor ANOVA as noted in captions with Tukey HSD post-hoc test. Assumptions of equality of varience and normality were checked using skew and kurtosis, and Levene's test. Data was analyzed in Real Statistics Resource Pack software (Release 5.4). Copyright (2013–2018) Charles Zaiontz. www.real-statistics.com.

RESULTS AND DISCUSSION

Bacteria grown on diatomaceous earth had produced significantly more methane compared to all other treatments ($p = 3.4 \times 10^{-17}$) by day 62 indicating this substrate promoted the highest metabolic activity (Figure 1). Previously established enrichment cultures, Canadian Natural and Syncrude, also produced methane faster than tailings inoculum, thickened tailings and tailings centrifuge cake. Methane concentrations present in the headspace of these cultures were significantly higher at day 54 ($p = 8.3 \times 10^{-5}$).

Despite the lower surface area (compared to other substrates; Table 1), diatomaceous earth promoted higher microbial metabolism in cultures. SEM images in Figure 2 demonstrate particle size and size distribution in substrate materials. Although fly ash and activated carbon provided rough and porous surfaces suitable for biofilm development, the visibly diverse array of porous, textured structures representing the fossilized remains of diatoms in diatomaceous earth may have provided more suitable anchor points for cell attachment. High conductivity (EC) of fly ash and high pH in fly ash cultures may have inhibited growth on the substrate compared to diatomaceous earth, which had a pH of approximately 7 in culture media. Conductivity could not be accurately measured in activated carbon however, pH 8 would not have negatively affected growth as process water in tailings ponds is slightly alkaline (Allen 2008). Therefore, enhanced metabolic activity observed in diatomaceous earth relative to activated carbon is less clear but may have been related to surface chemistry. Activated carbon has a complicated surface chemistry relative to the SiO_2 and calcium bentonite based diatomaceous earth used in this study (Li et al. 2002). Essential culture components such as organic carbon sources, nitrogen fixed by the initial inoculum community, and trace nutrients, could have been sorbed to the active surface limiting nutrient access and decreasing overall growth. Calcium bentonite in diatomaceous earth may have also played a role in promoting metabolism as calcium is an essential nutrient for cellular processes (Dominguez 2004).

Table 1. Candidate bacteria carrier substrate physical properties. SD indicates one standard deviation of the mean (n=3 for BET analyses)

BET	Mean Specific Surface Area ($m^2\ g^{-1}$)		SD
Diatomaceous Earth	28.3		1.1
Fly Ash	51.3		1.8
Activated Carbon	>200		-
	pH		**EC**
	Substrate	Culture	($ms\ cm^{-1}$)
Diatomaceous Earth	5.4	7	1.7
Fly Ash	12.7	13	62.4
Activated Carbon	9.0	8	-
Particle Size	Mean (µm)		SD
Diatomaceous Earth	10.2		7.4

Toluene concentration was also monitored to determine if cultures were metabolizing toluene to methane but data were inconsistent across treatments and no trends could be established (data not shown). However, biogeneic methane

production from the degradation of toluene and citrate is well established in the literature. Both Collins et al. (2016) and Li (2010) clearly demonstrated the metabolism of citrate to methane in oil sands tailings communities alongside an absence of methane production in controls without citrate. Similar observations have been reported for toluene amendments in tailings cultures (Laban et al. 2015).

To confirm the presence of nitrogen fixing activity, an acetylene reduction assay was conducted. The acetylene molecule is similar in structure to N_2, which allows the nitrogen fixing enzyme, nitrogenase, to bind and reduce acetylene to ethylene. Fly ash cultures were omitted due to low metabolic activity, growth inhibiting conductivity and high pH. Ethylene production was significantly higher in diatomaceous earth cultures compared to media ($p = 0.0015$) and activated carbon treatments ($p = 0.0009$; Figure 3A). Amongst culture inoculum sources, Canadian Natural had the highest mean average for nitrogen fixing potential, however the difference was not statistically significant (Figure 3B).

In Phase 2, bacteria on substrate materials were inoculated into the root zone of plants in oil sands tailings to promote plant growth, survival, and vigor over one growing season. As such, the most metabolically active bacteria-substrate combination was desired. Canadian Natural bacterial culture established on diatomaceous earth facilitated the highest metabolic activity and high mean average by comparison for potential nitrogen fixation activity. While Canadian Natural was not statistically more active than Syncrude cultures, Canadian Natural enrichment cultures are known to contain several pant growth promoting genera including *Rhizobium*, *Pseudomonas*, *Bacillus* and *Burkholderia* as previously described (Collins et al. 2016). This combination of factors suggested Canadian Natural grown on diatomaceous earth was the most suitable inoculum for Phase 2. Compilation and analysis of Phase 2 work is ongoing but the preliminary observations are promising as there are clear visual differences in leaf morphology present in the treatment where bacteria was introduced (Figure 4).

CONCLUSIONS

The results of this study suggest Canadian Natural on diatomaceous earth has the highest probability of fixing nitrogen for the promotion of plant growth as compared to other treatment combinations examined here. However, community composition and substrate community effects were not addressed. In the future, further insight into the community composition would inform inoculum selection as organisms known to promote plant growth through pathways other than nitrogen fixation may be present. Substrate selection may also enrich or decrease the proportions of these bacteria and merits further consideration.

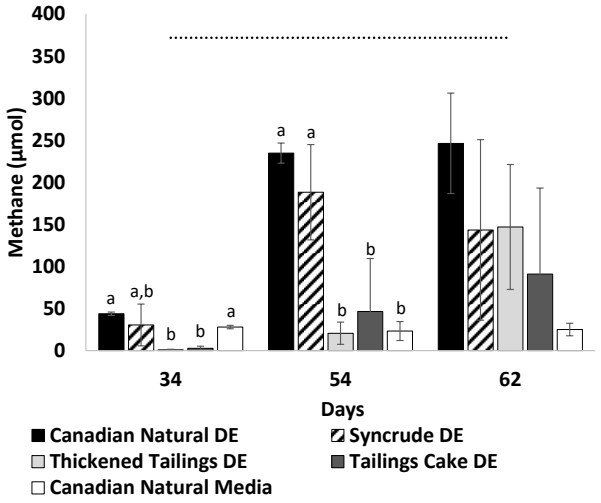

Figure 1. Mean methane production in cultures incubated for 62 days. DE: Diatomaceous earth. Treatment Canadian Natural Media refers to Canadian Natural bacteria enrichment culture in media without substrate. Treatments (fly ash, activated carbon, Syncrude media, thickened tailings media, tailings cake media, and heat killed sterile controls) with methane yield below 20 µmol by day 62 are not shown. Error bars represent 95% confidence interval (n=3), line indicates approximate theoretical methane production from citrate and toluene (372 and 377 µmol, respectively; Symons and Buswell 1933). Statistical significance determined at day 34 and 54 using single factor ANOVA due to low or absent methane in other substrate cultures. No significance was observed at day 62. Within each time point, different letters between treatment means indicate a statistically significant difference ($\alpha < 0.05$)

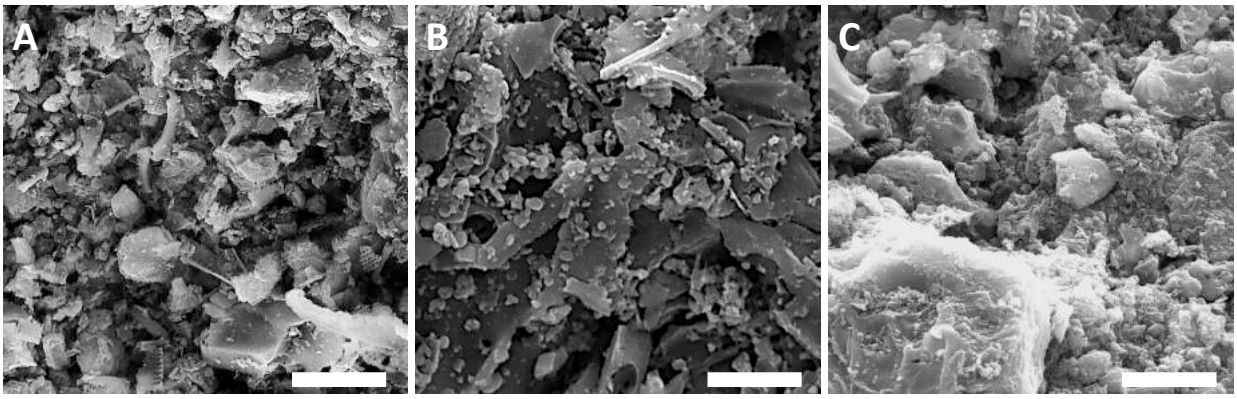

Figure 2. Scanning electron micrograph of substrate materials. A: Diatomaceous earth, B: Fly ash, C: Activated carbon. White bar represents 20 µm

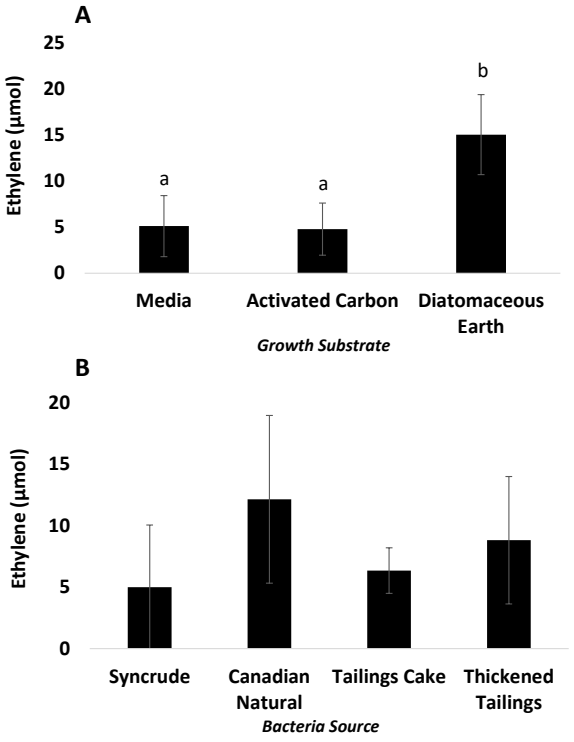

Figure 3. Mean acetylene reduced to ethylene by A: substrate material and B: bacteria source. Treatments that did not produce measurable quantities of ethylene are not shown. Error bars represent 95% confidence interval (n=3). Statistical significance determined using two factor ANOVA and post-hoc test, no significant differences were observed amongst bacteria sources. Different letters between treatment means indicate a statistically significant difference ($\alpha < 0.05$)

REFERENCES

Ahemad, M. and Kibret, M. (2014). Mechanisms and applications of plant growth promoting rhizobacteria: Current perspective. J. King Saud Univ. - Sci., **26**: 1–20.

Allen, E. W. (2008). Process water treatment in Canada's oil sands industry: II. A review of emerging technologies. J. Environ. Eng. Sci., **7**: 499–524.

Bashan, Y. (1998). Inoculants of plant growth-promoting bacteria for use in agriculture. Biotechnol. Adv., **16**: 729–770.

Belimov, A. A., Safronova, V. I., Sergeyeva, T. A., Egorova, T. N., Matveyeva, V. A., Tsyganov, V. E., Borisov, A. Y., Tikhonovich, I. A., Kluge, C., Preisfeld, A., Dietz, K.-J. and Stepanok, V. V. (2001). Characterization of plant growth promoting rhizobacteria isolated from polluted soils and containing 1-aminocyclopropane-1-carboxylate deaminase. Can. J. Microbiol., **47**: 642–652.

Caldeira, M., Heald, S. C., Carvalho, M. F., Vasconcelos, I., Bull, A. T. and Castro, P. M. L. (1999). 4-Chlorophenol degradation by a bacterial consortium: Development of a granular activated carbon biofilm reactor. Appl. Microbiol. Biotechnol., **52**: 722–729.

Chalaturnyk, R. J., Scott, J. D. and Özüm, B. (2002). Management of Oil Sands Tailings. Pet. Sci. Technol. **20**: 1025–1046.

Figure 4. Preliminary observations. Left: Treatment without bacteria inoculum, Right: Treatment with bacterial inoculum

Collins, C. E. V., Foght, J. M. and Siddique, T. (2016). Co-occurrence of methanogenesis and N2 fixation in oil sands tailings. Sci. Total Environ., **565**: 306–312.

Dalahmeh, S., Ahrens, L., Gros, M., Wiberg, K. and Pell, M. (2018). Potential of biochar filters for onsite sewage treatment: Adsorption and biological degradation of pharmaceuticals in laboratory filters with active, inactive and no biofilm. Sci. Total Environ., **612**: 192–201.

Dominguez, D. C. (2004). Calcium signalling in bacteria. Mol. Microbiol., **54**: 291–297.

Donlan, R. M. (2002). Biofilms: Microbial life on surfaces. Emerg. Infect. Dis., **8**: 881–890.

Fedorak, P. M. and Hrudey, S. E. (1984). The effects of phenol and some alkyl phenolics on batch anaerobic methanogenesis. Water Res., **18**: 361–367.

Grobelak, A., Napora, A. and Kacprzak, M. (2015). Using plant growth-promoting rhizobacteria (PGPR) to improve plant growth. Ecol. Eng., **84**: 22–28.

Holowenko, F. M., MacKinnon, M. D. and Fedorak, P. M. (2000). Methanogens and sulfate-reducing bacteria in oil sands fine tailings waste. Can. J. Microbiol. **46**, 927–937.

Huang, X. D., El-Alawi, Y., Penrose, D. M., Glick, B. R. and Greenberg, B. M. (2004). A multi-process phytoremediation system for removal of polycyclic aromatic hydrocarbons from contaminated soils. Environ. Pollut., **130**: 465–476.

Juhanson, J., Truu, J., Heinaru, E. and Heinaru, A., (2007). Temporal Dynamics of Microbial Community in Soil During Phytoremediation Field Experiment. J. Environ. Eng. Landsc. Manag., **15**: 213–220.

Khan, A. G. (2005). Role of soil microbes in the rhizospheres of plants growing on trace metal contaminated soils in phytoremediation. J. Trace Elem. Med. Biol., **18**: 355–364.

Khan, S., Afzal, M., Iqbal, S. and Khan, Q. M. (2013). Plant-bacteria partnerships for the remediation of hydrocarbon contaminated soils. Chemosphere, **90**: 1317–1332.

Koch, B., Ostermann, M., Höke, H. and Hempel, D. C. (1991). Sand and activated carbon as biofilm carriers for microbial degradation of phenols and nitrogen-containing aromatic compounds. Water Res., **25**: 1–8.

Laban, N. A., Dao, A. and Foght, J. (2015). DNA stable-isotope probing of oil sands tailings pond enrichment cultures reveals different key players for toluene degradation under methanogenic and sulidogenic conditions. FEMS Microbiol. Ecol., **91**: 1–12.

Lee, K. W. K., Periasamy, S., Mukherjee, M., Xie, C., Kjelleberg, S. and Rice, S. A. (2014). Biofilm development and enhanced stress resistance of a model, mixed-species community biofilm. ISME J., **8**: 894–907.

Li, C. (2010). Methanogenesis in oil sands tailings: An analysis of the microbial community involved and its effects on tailings densification. University of Alberta.

Li, L., Quinlivan, P. A. and Knappe, D. R. U. (2002). Effects of activated carbon surface chemistry and pore structure on the adsorption of organic contaminants from aqueous solution. Carbon N. Y., **40**: 2085–2100.

Nadeem, S. M., Zahir, Z. A., Naveed, M. and Nawaz, S. (2013). Mitigation of salinity-induced negative impact on the growth and yield of wheat by plant growth-promoting rhizobacteria in naturally saline conditions. Ann. Microbiol., **63**: 225–232.

Nasseri, S., Kalantary, R. R., Nourieh, N., Naddafi, K., Mahvi, A. H. and Baradaran, N. (2010). Influence of bioaugmentation in biodegradation of PAHs-contaminated soil in bio-slurry phase reactor. Iran. J. Environ. Heal. Sci. Eng., **7**: 199–208.

Salem, S., Berends, D. H. J. G., Heijnen, J. J. and Van Loosdrecht, M. C. M. (2003). Bio-augmentation by nitrification with return sludge. Water Res., **37**: 1794–1804.

Scott, J. A., Karanjkar, A. M. and Rowe, D. L. (1995). Biofilm covered granular activated carbon for decontamination of streams containing heavy metals and organic chemicals. Miner. Eng., **8**: 221–230.

Silva, M. J. (1999). Plant dewatering and strengthening of mine waste tailings. University of Alberta.

Silva, M. J., Naeth, M. A., Biggar, K. W., Chanasyk, D. S. and Sego, D. C. (1998). Plant Selection for Dewatering and Reclamation of Tailings. J. Am. Soc. Min. Reclam., 104–117.

Sprott, G., Jarrell, K., Shaw, K. and Knowles, R. (1982). Acetylene as an inhibitor of methanogenic bacteria. J. Gen. Microbiol., **128**: 2453–2462.

Symons, G. E. and Buswell, A. M. (1933). The Methane Fermentation of Carbohydrates. J. Am. Chem. Soc., **55**: 2028–2036.

Thompson, I. P., Van Der Gast, C. J., Ciric, L. and Singer, A. C. (2005). Bioaugmentation for bioremediation: The challenge of strain selection. Environ. Microbiol., **7**: 909–915.

Vessey, J. K. (2003). Plant growth promoting rhizobacteria as biofertilizers. Plant Soil, **255**: 571–586.

Wang, D., Xu, A., Elmerich, C. and Ma, L. Z. (2017). Biofilm formation enables free-living nitrogen-fixing rhizobacteria to fix nitrogen under aerobic conditions. ISME J., **11**: 1602–1613.

Zhuang, X., Chen, J., Shim, H. and Bai, Z. (2007). New advances in plant growth-promoting rhizobacteria for bioremediation. Environ. Int., **33**: 406–413.

EVALUATING THE POTENTIAL TO ESTABLISH PLANTS TO AID IN DEWATERING OF AN ATMOSPHERIC FINE DRYING TAILINGS DEPOSIT AT MUSKEG RIVER MINE

Amanda Schoonmaker[1], Dani Degenhardt[2] and Trevor Floreani[1]
[1]Northern Alberta Institute of Technology, Peace River, Canada
[2]Canadian Forest Service, Natural Resources Canada, Edmonton, Canada

ABSTRACT

In principle, it is possible to use plants as a mechanism to de-water fluid tailings deposits as their roots can extend well beyond the surface and absorb water and release into the atmosphere through transpiration. This project set out to evaluate the establishment and de-watering potential of native and non-native plants at the Muskeg River Mine (MRM) in an atmospheric fines drying (AFD) tailings deposit where a surface crust had developed.

Fall rye (*Secale cereale* L., a winter annual grass) and slender wheatgrass (*Agropyron trachycaulum* (Link) Malte ex H.F. Lewis, a perennial native grass) were seeded in September 2016 and May 2017. Two woody species (balsam poplar [*Populus balsamifera* L.] and sandbar willow [*Salix exigua* Nutt.]) that were previously planted in 2015 were also evaluated. Volumetric water content (VWC), temperature, and matric suction in replicate experimental plots were tracked *in-situ* throughout the 2017 growing season. Vegetation percent cover, leaf area, and above- and below-ground biomass were measured. Solids content was determined from tailings root core samples.

Overall, spring seeded grasses resulted in higher vegetation cover than fall seeded grasses and fall rye had higher vegetation cover than slender wheatgrass. More than 95% of root mass was located in the top 40 cm depth of tailings. Sandbar willow and balsam poplar both survived, but sandbar willow was generally superior in both survival and growth. Over the course of the experiment, the control, fall rye, and slender wheatgrass treatments showed a significant reduction in VWC at 15 cm depth relative to starting conditions in June, with the greatest change in fall rye treatments. Matric suction at 30 and 45 cm depth increased in all vegetated treatments with the greatest suction in the fall rye treatment. There was a significant positive relationship between above-ground plant biomass and solids content at all sampling depths, though mean solids content by treatment (seeded or control) showed little effect. This study has demonstrated that it is possible to establish multiple grass species, as well as a native shrub, on treated mine tailings and that plant growth may enhance the moisture reduction in the upper 45 cm of these tailings.

INTRODUCTION

Tailings are a waste by-product of synthetic crude oil production. They consist of connate (water originating from pore space in sedimentary rocks), processed water, sand, silt, clay, residual bitumen, and inorganic and organic by-products (Allen 2008, Bedair 2013, Lo et al. 2006). Tailings may also include organic phenols, naphthenic acids, polycyclic aromatic hydrocarbons, naphtha and paraffinic diluents as well as heavy metals, salts and alkaline substances (Quagraine et al. 2005). Based on fluid tailings volume reporting to AER, in 2015, there was approximately 1,134 million m^3 of fluid tailings in the Lower Athabasca Region with an increase of 58.8 million m^3 from 2014.

Sufficiently consolidating (and de-watering) tailings to allow human and vehicular traffic is the greatest geo-technical challenge for tailings ponds. As the surface of treated tailings (i.e. atmospheric fine drying (AFD) processed tailings or centrifuge processed tailings) dries, it creates a hydrophobic layer on the surface that reduces further subsurface evaporation. This is a primary limitation with many de-watering techniques currently employed in the oil sands or that are under development. In nature, plant roots are designed for and are highly effective at the extraction of soil pore water. In principle, plant roots have the ability to penetrate the hydrophobic surface and pull moisture from the subsurface of a tailings deposit and which can then be transpired by the plant to the atmosphere. The use of plants to de-water tailings has shown early promise where a number

of plant species have demonstrated survival and persistence on mine tailings (Naeth and Wilkinson 2002, Renault et al. 2003 & 2004, Silva 1999, Wu 2009 & 2015). However, knowledge gaps still exist with respect to the broader use of native and non-native species to dewater tailings, with respect to seed deployment, seedling establishment methods, potential short term toxicological or nutrient availability constraints, survivability over multiple years and how to combine the use of plants with natural freeze-thaw cycle (BGC Engineering 2010) and other dewatering processes employed by the industry, such as AFD or centrifugation.

The objective of this study was to evaluate the field establishment potential and de-watering potential of native and non-native plant species in an AFD deposit at Muskeg River Mine (MRM) from 2016 to 2017.

MATERIAL AND METHOD

Test Cell Material

This experiment was established at cell #10 located at the MRM within the lower AFD cell. Background information on test cell material is summarized below:

- AFD is composed of fluid fine tailings (FFT) dredged and/or pumped from MRM external tailings facility and mixed with an anionic flocculent polymer prior to pouring into drying cells.
- Cell #10 was poured in October 2014, and solids content determined in November 2014 indicated a mean value of 43%. The cell was graded at 2% from north to south to promote drainage and runoff with spill boxes installed at the south berms to siphon off excess water.

Vegetation and Fertilizer Treatments

In June 2015, a grass seeding trial was initiated in Cell #10 to evaluate the establishment of native (slender wheatgrass) and non-native (fall rye and barley) grass species; the results of this work were presented previously (Yucel et al. 2016). A subset of the original plots were re-seeded in 2016 and 2017 to fall rye and slender wheatgrass as the original seeding rate did not yield sufficient vegetation cover. In addition to evaluating grasses, in September 2015 balsam poplar and sandbar willow seedings were planted within a 5 x 5 m subplot in the NW corner of each of the 20 x 20 m experimental plots (0.5 m spacing, 121 plants per plot). The balsam poplar and sandbar willow seedlings were propagated from cuttings collected within the mine lease. Overall, there was a total of 72 treatment plots (20 x 20 m) within the 3 hectare experimental area in Cell #10. The detailed experimental design of seeding treatment implemented from 2015-17 is illustrated in **Figure 1**.

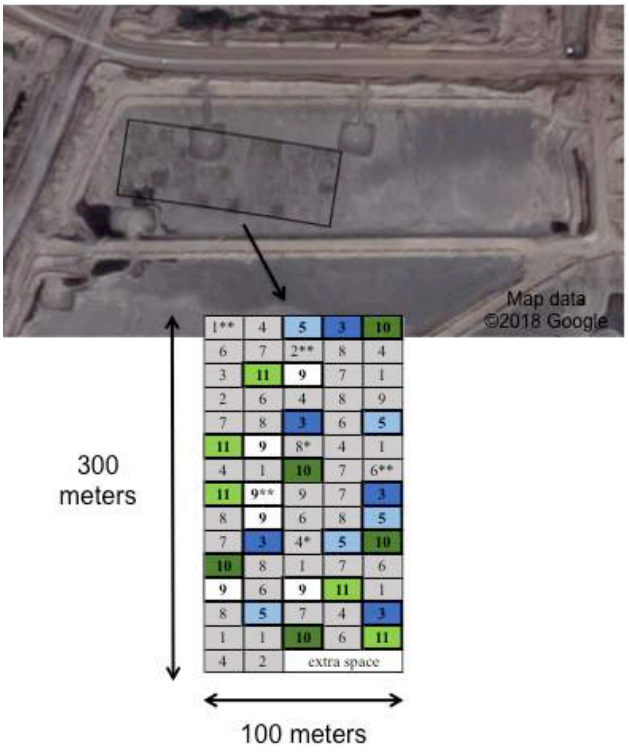

Figure 1. Aerial image of lower AFD (atmospheric fine drying) test area at cell #10 located at the CNRL Muskeg River Mine (MRM) with diagram showing layout and position of treatment area implemented in 2015-2017. The original seeding work completed in 2015 is shown in grey while the test plots seeded in 2016 and 2017 are shown in blue and green with control (non-seeded) in white. Individual treatment plots were 20 x 20 m. Grass seeding treatments were fall 2016 sown fall rye (5) or slender wheatgrass (3), spring 2017 sown fall rye (10) or slender wheatgrass (11) and no-seeding control (9). * denotes willow or poplar seedling planting in September 2015

To increase the overall plant availability of nitrogen (N), as determined to be insufficient from soil nutrient analysis, fertilizers were applied on the entire experimental area: a starter blend (29-59-14) in May 2015 at a rate of 225 kg ha^{-1} and, in August 2015, urea (46-0-0) at a rate of 150 kg ha^{-1}. In addition, for the plots seeded in 2016, 150 kg ha^{-1} of urea was applied concurrently with seeding, as well as a second fertilizer application in May 2017 at a rate of 75 kg ha^{-1} of urea. For the plots seeded in 2017, 150 kg ha^{-1} of urea was applied across the entire plot concurrently with seeding, while 5,000 kg ha^{-1} of alfalfa pellets (Western Alfalfa Milling Co Ltd, Norquay, Saskatchewan) were applied within a 5 x 5 m subplot in the NW corner of each of the 20 x 20 m experimental plots.

Monitoring

In-situ monitoring of temperature and volumetric water content (VMC), as well as water potential (matric suction) were tracked throughout the growing season in 2017 using 5TE and TEROS 21 sensors (Meter, formerly Decagon [sensor name was MPS-6], Washington, USA) connected to an EM50 data logging station (Meter, formerly Decagon, Washington, USA).

Logging stations and instrumentation sensors were placed at the center of ten plots: four in the control plots, four in the 2017 seeded fall rye and slender wheatgrass plots and two in the 2016 seeded slender wheatgrass plots. Sensors were installed by excavating the tailings to 50 cm depth and inserting the sensors into the adjacent undisturbed tailing profile. After the sensors were installed, the hole was backfilled with tailings, while grass seed and fertilizer were uniformly placed over the disturbed tailings. The 5TE sensors (measuring VWC and temperature) were placed at 15, 30 and 45 cm depths and TEROS 21 sensors (measuring matric suction) were placed at depths of 30 and 45 cm. In some locations, individual sensors became disconnected from the logging station (discovered at the time of instrument removal in September 2017), in this situation, the partial data collected from the sensors was removed from the data set presented.

Data Measurement and Sample Collection

Vegetation percent (%) cover (estimated by visually determining the % of area covered by vegetation in a 0.5 x 0.5 m quadrat) was determined at seven locations within each 20 x 20 m experimental plot. Two additional vegetation cover estimate points were included within the 5 x 5 m subplots where alfalfa pellets were broadcasted. Of the seven locations assessed, the one with the highest vegetation cover was selected for detailed assessment of above- and below-ground vegetation. The following information was collected for the detailed assessment:

- Above-ground biomass (within the 0.5 x 0.5 m quadrat) was collected for total biomass determination.
- Adjacent to the quadrat, leaves were sampled and collected in a plastic bag for the determination of leaf area in the lab. One composite sample was collected for each species.
- One composite tailings sample made up of two tailings sample cores (5 cm diameter) taken at 0-10, 10-20 and 20-30 cm were used to determine below-ground biomass analysis.

In addition to the monitoring conducted at each experimental plot, additional assessment was done in the following three plots: 2017 spring-seeded slender wheatgrass and fall rye plot, 2016 fall-seeded slender wheatgrass plot and control plot. The assessment included all of the parameters described above as well as the tailings sampling to 100 cm depth for every 20 cm interval.

Where data logging stations were located, vegetation % cover was also determined by taking 4 point estimates with a 0.5 x 0.5 m quadrat (total cover estimate over a 1 x 1 m area with the data logger as the center point). Additional information including total live count and height of each living plant was also collected at each of the woody species plots.

Lab Analysis

Above-ground plant biomass was initially air-dried in the lab and then uniformly dried at 70 °C to weight constancy. Total plant biomass was determined to the nearest 0.1 g, but in cases where the sample was very small (< 1 g), a different scale was used and the weight was measured to the nearest 0.0001 g. The leaf subsamples were stored at -4 °C to preserve leaf shape prior to analysis. For determination of leaf area, individual leaves from each of the four sample types (as described earlier), were placed on a flatbed scanner and WinFOLIA™ software was used to estimate the leaf area from the scanned image. The scanned leaves were then dried at 70 °C and weighed to the nearest 0.1 g. The ratio of leaf area:leaf mass was used to

estimate leaf area of all plots where above-ground leaf mass had been harvested.

Tailings sample cores were stored at -4 °C to preserve roots until processing. To determine solids content, samples were thawed and 3 to 5 subsamples were extracted from different locations within the core's profile, resulting in 1.5-5.0 g (wet mass) of tailings. Samples were immediately weighed and dried at 105 °C, until mass constancy and weighed again for dry mass. Solids content (%) in the tailings was calculated as dry mass divided by wet mass and multiplied by 100.

To determine below-ground biomass from soil cores, the cores were soaked in a container of water overnight to allow the tailings to soften, easing separation of the root from the tailings and reducing root breakage and fragmentation. Following soaking, the whole sample was placed in a stand mixer to break up clods of tailings. Roots were then separated from the sample by washing through a series of soil sieves (#18 [1.0 mm opening], #60 [0.25 mm opening] and #120 [0.12 mm opening]). Root samples were oven dried at 70 °C overnight and weighed to the nearest 0.0001 grams.

Data Analysis

Data was analyzed using R statistical software (R Core Team, 2017). One-way ANOVA (function *lm*) was performed to test for differences in:

i. vegetation-related parameters (vegetation cover, plant biomass or leaf area index (LAI)) between species and timing of seeding;
ii. effects of alfalfa pellets on vegetation cover; and
iii. for differences between non-vegetated and vegetated treatments on tailings properties (VWC, matric suction and solids content). When significant ($p \leq 0.05$) differences were detected, treatments were separated with a post-hoc (Tukey or Dunnet's) multiple comparison test using lsmeans function (Lenth 2017).

Simple linear regression (SLR, function lm) models were fit to predict relationships between vegetation % cover and plant biomass to tailings parameters (VWC, matric suction and solids content). Model assumptions were checked with diagnostic plots of fitted and residual values, as well as a histogram of residuals.

RESULTS AND DISCUSSION

Vegetation Development: Grasses

Spring seeding resulted in significantly higher vegetation cover for fall rye ($p < 0.001$, **Table 1**) but not for slender wheatgrass, though the mean estimate was still higher on average ($p = 0.1324$, **Table 1**). For fall rye, this was in large part due to the fall rye being a winter annual species as such, the fall seeding treatment would have grown vegetatively through September 2016 and during the spring in 2017 growth would have been in seed production, rather than biomass production. For the spring seeded fall rye, there was also a longer period of vegetative growth (June to September). As slender wheatgrass was a perennial species (lives for 2+ years), higher cover in the fall seeding treatment was expected as the individual plants would have been larger, however this was not the case. The lack of observed difference in slender wheatgrass may be attributable to lower emergence with fall seeding compared to spring seeding. Furthermore, the establishment of fall-sown slender wheatgrass was very patchy, some of the seeds had migrated off of the study plots, which contributed to an overall lower cover within the plots. Spring seeded fall rye also showed significantly higher vegetation cover when compared with spring seeded slender wheatgrass ($p = 0.0031$, **Table 1**), while there was no significant difference between species for fall seeding ($p = 0.3413$, **Table 1**). Although the pattern was similar to that observed in vegetation cover, there was no statistical difference in LAI and above-ground or below-ground biomass between fall rye sown in spring and slender wheatgrass sown in spring or fall (**Table 1**). Therefore, measurements of vegetation cover alone should be taken with a degree of caution when making comparisons between species.

Table 1. Mean vegetation cover (all 7 transect points per plot) and mean vegetation cover, leaf area index, above and below-ground biomass for the highest vegetation cover points measured in replicate fall rye (FR) and slender wheatgrass (SWG) by of seeding date (fall or spring) [n=4-5]. SE is one standard error of the mean. Different letters beside treatment means (within treatment parameters) indicate a statistical difference between means (α < 0.05)

	All transect points		High cover sampling points							
	Vegetation cover (%)		Vegetation cover (%)		Leaf area index		Above-ground biomass (g)		Below-ground biomass (g)	
	mean	SE	mean	SE	mean	SE	mean	SE	mean	SE
FR fall	3[a]	2	9[a]	4	-	-	-	-	21.1	14.1
FR spring	22[b]	3	39[b]	4	0.7	0.1	82.9	17.7	64.9	12.6
SWB fall	6[a]	2	18[a]	4	0.5	0.1	61.0	17.7	27.5	12.6
SWG spring	11[a]	2	21[a]	4	0.4	0.1	50.2	17.7	19.6	12.6

Table 2. Vegetation cover (cover), leaf area index (LAI), above- and below-ground biomass for deep (1.0 m depth) sampling points [n=1]

	Cover (%)	LAI	Above-ground biomass (g)	Below-ground biomass (g)
SWG spring	45	0.9	1108.8	112.9
SWG fall	80	3.7	452.8	190.6
FR spring	85	2.8	334.4	219.6

Approximately 50% of the total roots observed in the upper 30 cm of the deposit were located in the 0-10 cm depth, with 20-25% of roots at 10-20 cm depth and less than 20% roots at 20-30cm depth (**Figure 2**). There was some variation in the mean proportion of roots by depth between fall rye and slender wheatgrass; a greater proportion of roots were at the 20-30 cm depth class for slender wheatgrass compared with fall rye. As slender wheatgrass is a perennial species, it must be able to persist for multiple years, and investing in deeper root development may be an advantageous trait. Although most of the root sampling and analysis occurred only to 30 cm depth, a deeper sample depth (to 100 cm) was conducted in three vegetated treatment locations, as well as a non-vegetated control (**Figure 3a**). These sampling points validated that roots found in the top 40 cm represents over 95% of all roots found in the 100 cm profile. Although less than 5% of all roots were located below 40 cm, roots were present even at the lowest sampling depth interval of 80-100 cm. These deep sampling points represent the likely maximum rooting depth (after 1-2 growing seasons) for these species, as sampling points were selected based on the maximum quantity of aboveground vegetation. This is well illustrated by the vegetation parameters shown including vegetation % cover, LAI, shoot biomass and root biomass (**Table 2**), all of which were substantially higher than the mean estimates obtained across the study (**Table 1**).

Alfalfa pellets (providing a secondary form of nitrogen) were evaluated in a 5 x 5 m subplot within the larger seeding plots to ascertain if improvements in vegetation growth could be demonstrated with an organic form of nitrogen. Although there was no significant difference in vegetation cover in either fall rye (p = 0.1294) or slender wheatgrass (p = 0.333) with/without the pellets, vegetation cover was on average consistently higher for both species when tailings were amended with alfalfa pellets (**Table 3**). As these pellets were surface broadcasted (not incorporated), they may not have had sufficient time to effectively redistribute into the rooting zone of the tailings as the surface of this deposit was typically very dry due to evaporative processes.

Table 3. Mean vegetation cover of FR or SWG (both spring sown) with or without addition of alfalfa pellets (pellet, no pellet). SE is one standard error of the mean. Different letters beside treatment means (within treatment parameters) indicate a statistical difference between means (α < 0.05)

	Vegetation cover (%)	
	mean	SE
FR no pellet	22	4
FR pellet	34	6
SWG no pellet	11	2
SWG pellet	15	3

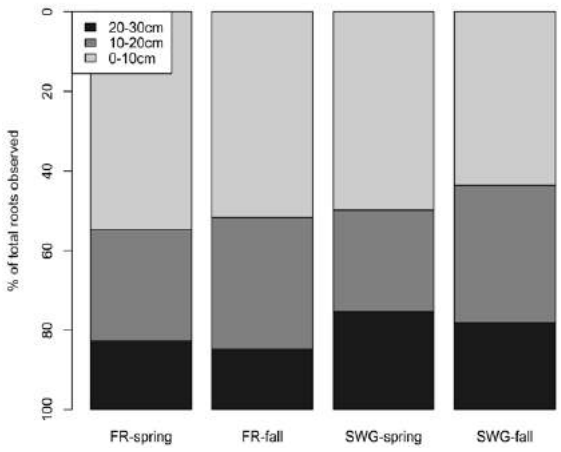

Figure 2. Mean proportion of roots observed in the 0-30 cm depth range for fall rye (FR) and slender wheatgrass (SWG) sown in the fall (late August 2016) or spring (May 2017)

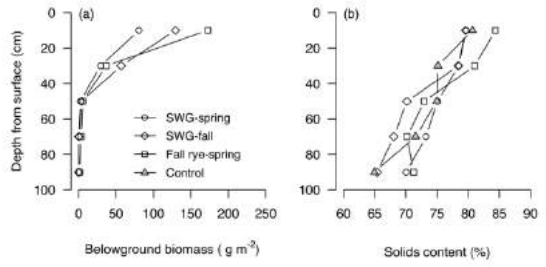

Figure 3. (a) Below-ground biomass and (b) solids content (%) profiles with tailings depth from surface for the single deep sampling points of slender wheatgrass (SWG) and fall rye sown in fall 2016 or spring 2017

Vegetation Development: Woody Species

Sandbar willow and balsam poplar both persisted in the tailings deposit after two growing seasons though survival and growth in sandbar willow was superior to that of balsam poplar and due to limited number of surviving plants in balsam poplar (0-15% survival within each of the four experimental plots it was planted into), only the quantitative results for sandbar willow are shown (**Figure 4**). Sandbar willow was planted into one of six plot types that were seeded to grasses (barley, fall rye or slender wheatgrass) in 2015 (**Figure 1**). Interestingly, survivorship of sandbar willow was increased by two-folds (~45%) on plots where the agronomic grasses (fall rye or barley) were never established (**Figure 4a**). This observation tentatively suggests that the agronomic grasses may have some allelopathic impact (i.e. chemical inhibition of one plant by another) on sandbar willow development. Barley has been documented to interfere with or suppress the growth of other herbaceous plants, as well as inhibit algae development in aquatic systems by the release of allelochemicals from roots and decomposing shoots (Kremer and Ben-Hammouda 2009). Fall rye is also noted to contain allelochemicals (Barnes and Putnam 1986, Yenish et al. 1995), and this has been documented in successful suppression of weeds (Akemo et al. 2000). Allelochemicals can continue to leach from plant tissue even once a plant has died, therefore the effects of allelopathic plants may persist for some time. Of further interest, total height sandbar willow was also greatest (up to 1.5 m) where slender wheatgrass was present and actually lowest (<0.5m) in the plot where no vegetation had ever been established (**Figure 4b**). It is difficult to discern if there is a synergistic effect between slender wheatgrass and sandbar willow through a microbial association, or if the environmental conditions (i.e. drier surface soil due to the presence of the perennial grass) were more favorable to willow growth and development.

The difference in growth and survival between the sandbar willow and balsam poplar may be at least partially attributable to seedling quality. Sandbar willow seedlings were generally larger and exhibited better root development, while the balsam poplar seedlings were smaller in comparison (<15 cm height) with underdeveloped root plugs that were prone to disintegrate during handling and planting. Poor seedling stock can contribute to the decline in the survivorship of out-planted seedlings. In a challenging environment, such as a tailings deposit, establishing healthy and vigorous seedlings will invariably better facilitate the establishment success of that species.

Vegetation Impacts on Tailings Properties

The impact of vegetation on tailings property was clearly observed as the growing season progressed along with the development of vegetation cover. Temperature at all tailings depths tended to decrease relative to non-vegetated controls. This difference was even observable at the 45 cm depth and was detectable by July of the monitoring year (**Table 4**). The presence of growing vegetation likely created shading effects at the tailings surface.

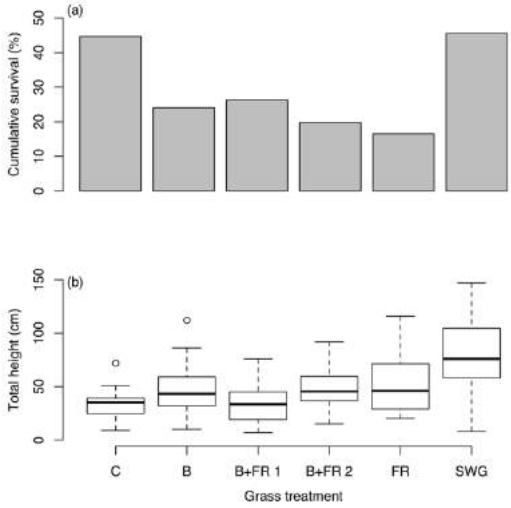

Figure 4. Sandbar willow (a) survival (n=121 plants established in each treatment) and (b) boxplots of total height after two growing seasons. The error bars indicate the maximum and minimum values, the boxes indicate the first and third quartile and the thick black line the median value. The x-axis shows the grass vegetation treatment each plot was planted within where C = control, B = barley, FR = fall rye and SWG = slender wheatgrass

Table 4. Mean monthly temperature at instrumentation stations in non-vegetated control and spring sown fall rye (FR) and slender wheatgrass (SWG) plots. SD indicates one standard deviation of the mean (n=3-4)

	June		July		August		September	
Treatment	mean	SD	mean	SD	mean	SD	mean	SD
15cm depth								
Control	17.7	1.0	22.0	0.8	20.8	0.4	18.8	0.2
FR	16.6	0.5	19.5	0.8	18.9	0.6	17.6	0.4
SWG	17.7	0.9	21.4	0.7	19.7	0.3	17.8	0.1
30cm depth								
Control	16.7	0.4	20.9	0.3	20.3	0.1	18.5	0.0
FR	15.5	0.8	18.7	1.1	18.5	0.9	17.3	0.7
SWG	16.2	0.9	20.0	0.6	19.3	0.3	17.6	0.4
45cm depth								
Control	15.7	0.4	19.9	0.3	19.8	0.1	18.1	0.2
FR	15.0	0.4	18.2	0.6	18.4	0.7	17.2	0.6
SWG	15.1	0.4	18.8	0.4	18.6	0.2	17.2	0.3

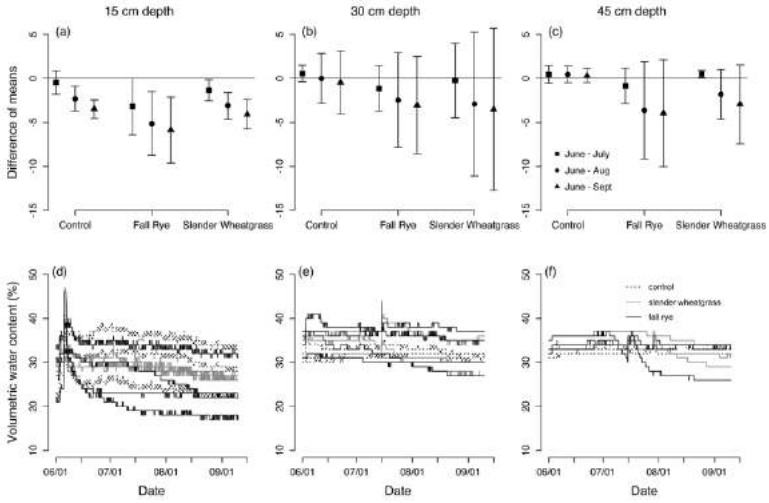

Figure 5. Volumetric water content differences of means relative to June for instrumentation stations at (a) 30 cm and (b) 45 cm depths for non-vegetated control and spring sown fall rye and slender wheatgrass. Daily volumetric water content from June 1 – September 10, 2017 at (c) 30 cm and (d) 45 cm depths. Vegetation cover surrounding the sensor stations ranged from 14 – 33% in slender wheatgrass and 30 – 68% in fall rye

From the onset of monitoring, VWC varied between locations, regardless of treatment. Due to this variability, VWC measurements were averaged by month and the change in VWC over time (utilizing the monthly mean in June as a baseline) was assessed rather than comparisons of the absolute values between treatments. At 15 cm depth, the control, fall rye and slender wheatgrass treatments showed significant declines in VWC relative to starting conditions in June (**Figure 5**). The largest magnitude of the difference was in the fall rye treatment; the decline in VWC was detectable for both grass species in July (though not significantly different from control until August). At the lower depths (30 and 45 cm) there were no statistically different changes in VWC over the growing season detected across treatments. Regression of VWC with vegetation % cover showed no relationships at 15 and 30 cm depths, and a weak (non-significant, p = 0.055) negative relationship during the month of August and September at the 45 cm depth (data not shown).

VWC measures the volume of water in soil while matric suction measures the negative pore water pressure, or how tightly water is held in the soil pores. The impacts of vegetation on VWC content may be subtle, but the presence of vegetation had a more striking effect on matric suction at both 30 and 45 cm depths (15 cm was not monitored), with increases in matric suction in the vegetated plots detected as early as July 1st and July 15th at 30 and 45 cm depths, respectively (**Figure 6c,d**). The largest matric suctions were observed in locations with fall rye, but slender wheatgrass still showed large differences as the season progressed. Interestingly, fall rye sensor stations sharply increased in suction and then remained relatively constant from mid-August to September while suction in the slender wheatgrass plots steadily increased throughout the entire growing season (**Figure 6c,d**). The difference in matric suction between the two vegetated treatments may be reflective of the annual (fall rye) versus perennial (slender wheatgrass) life forms, species specific capabilities to extract tightly bound pore water and the maximum carrying capacities for site occupancy in vegetation as fall rye generally had higher cover than slender wheatgrass (**Table 1**). Seasonal and temporal changes in matric suction were also expressed as mean differences from June (**Figure 6a,b**) where both species exhibited clear monthly changes in suction (increasing suction relative to June) compared with the control where no measurable change was detectable (**Figure 6a,b**). The degree of increase in matric suction was greater at 30 cm depth (likely associated with higher root density, **Figures 2-3**) than at 45 cm depth (**Figure 6c,d**). Differences in matric suction between individual measurement stations was associated with increasing vegetation cover (**Figure 7**) as the monthly mean suction in August increased linearly (at both sampling depths).

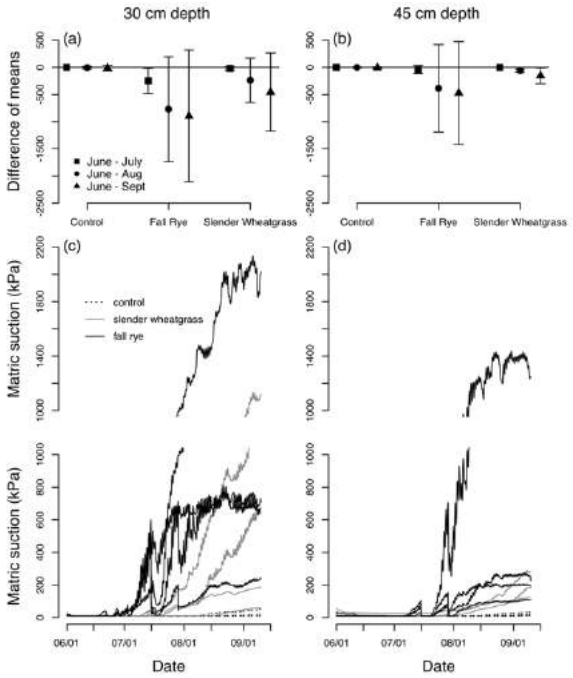

Figure 6. Matric suction differences of means relative to June for instrumentation stations at (a) 30 cm and (b) 45 cm depths for non-vegetated control and spring sown fall rye and slender wheatgrass. Daily matric suctions from June 1 – September 10, 2017 at (c) 30 cm and (d) 45 cm depth

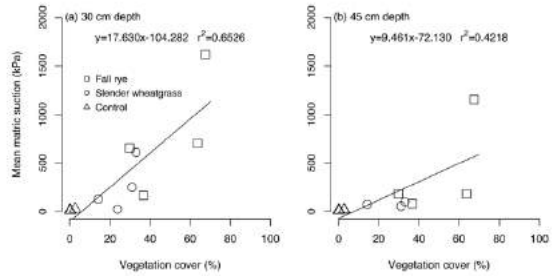

Figure 7. Mean matric suction (August) as a response to mean vegetation cover for all instrumentation stations at (a) 30 cm and (b) 45 cm depths. Regression lines are shown for those relationships where a significant effect was detected (α < 0.05)

Table 5. Mean solids content by vegetation seeding treatment (fall [2016] or spring [2017] seeding and fall rye [FR] or slender wheatgrass [SWG]) and at three depth intervals: 0-10 cm, 10-20 cm and 20-30 cm depths. SE indicates one standard error of the mean (n=4-6 replicate plots per treatment). * Indicates where significant differences (α < 0.05) between control (non-vegetated) and grass-seeding treatments were detected

	0-10 cm depth		10-20 cm depth		20-30 cm depth	
	mean	SE	mean	SE	mean	SE
Control	82.3	1.3	75.8	1.1	75.3	1.0
FR fall	82.3	2.2	77.3	1.3	75.2	1.2
FR spring	87.1	2.0	79.7	1.2	79.9*	1.1
SWG fall	84.7	2.0	78.2	1.2	78.4	1.1
SWG spring	82.3	2.0	78.8	1.2	76.6	1.1

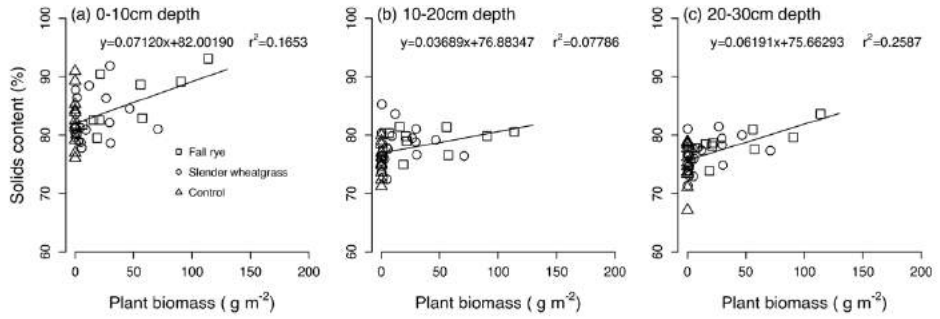

Figure 8. Relationship between solids content and belowground (root) plant biomass by 10 cm depth increments. Regression lines are shown for those relationships where a significant effect was detected (α < 0.05)

Although solids content was not statistically different at majority of the sampling depths (0 to 30 cm) and vegetation treatments measured, there was a detectable difference between the non-vegetated control and the spring-seeded fall rye treatment at 20-30 cm (**Table 5**). Examining solids content in greater detail through regression analysis of plant biomass illustrated a significant positive relationship between plant biomass and solids content at all sampling depths (**Figure 8**). The difference in results between examination of means, rather than regression, illustrated the importance of plant size (leaf and root development) on the eventual quantity of extracted water from tailings. Increasing vegetation cover would also have increased canopy interception thereby reducing the quantity of precipitation reaching the tailings surface during the summer period.

CONCLUSIONS AND FUTURE WORK

This study demonstrated the possibility of growing grass and shrubs on treated tailings as a dewatering mechanism on the upper 45 cm of tailings. Below are suggestions for future work to further pursue in biological tailings dewatering mechanism to improve deposit strength, and eventually facilitate tailings reclamation:

- **Species selection:** The selection of the appropriate perennial herbaceous and woody species is imperative for vigorous growth that would eventually lead to the greatest dewatering potential. In this study, fall rye increased in cover the fastest and appeared to have the greatest impact on drying of AFD tailings. The benefits of perennial species, such as slender wheatgrass, would exceed annual species if the plants are expected to dewater tailings over more than one growing season. The results from this study also showed that sandbar willow exhibits great promise in this respect within individual plants reaching up to 1.5 m height after only two growing seasons.

- **Species mixtures:** Due to the difference in root systems between herbaceous and woody species, the optimal mixture of fibrous fine roots from grasses (or forbs), coupled with deeper roots from woody species are likely to be the most effective combination for de-watering tailings. Further work to better understand potential allelopathic interactions between agronomic species and woody species, such as sandbar willow, is warranted. More insight into potentially beneficial or mutualistic relationships (such as rhizospheric interactions) between sandbar willow and slender wheatgrass, or other native grasses, would be invaluable to optimize plant growth on tailings.

- **Managing nutrition:** Nutrition has been previously cited (Wu 2009) as a management challenge and was evident throughout this study. The field trial attempted to address the nutrient issue by utilizing amendments (alfalfa pellets) and surface broadcasting inorganic fertilizers (urea). While the cost of alfalfa pellets may be greater (if applied based on total N ha^{-1}) compared to inorganic fertilizers, the benefits of amendments may be more persistent than inorganic fertilizer, as loss of N through volatilization as ammonia gas is high especially at low surface moisture conditions. Although the results from the alfalfa pellets treatments were not statistically different, the data did show a

positive trend. More work is warranted in the application of alfalfa pellets (or other organic amendments) in order to explore their utility, not only terms of boosting nutrition, but also for logistics as organic applications do not volatize and could preclude multiple fertilizer applications.

ACKNOWLEDGEMENTS

We would like to kindly acknowledge the financial support of Canadian Natural Resources Ltd and to thank the many staff and contractors that have been engaged in this work since its inception.

REFERENCES

Allen, E. (2008). Process water treatment in Canada's oil sands industry: I. Target pollutants and treatment objectives. Journal of Environmental Science, **7**: 123-138.

Akemo, M. C., Regnier, E. E. and Bennett, M. A. (2000). Weed suppression in spring-sown rye (*Secale cerea*le): Pea (*Pisum sativum*) cover crop mixes. Weed Technology, **14**: 545-549.

Barnes, J. P. and Putnam, A. R. (1986). Evidence for allelopathy by residues and aqueous extracts of rye (*Secale cereale*). Weed Science, **34**: 384-390.

Bedair, O. (2013). Engineering challenges in the design of Alberta's oil sands projects. Practice periodical on structural design and construction, **18**: 247-260.

BGC Engineering Inc. (2010). Oil sands tailings technology review. Oil Sands Research and Information Network, University of Alberta, School of Energy and the Environment, Edmonton, Alberta. OSRIN Report No. TR-1. 136pp.

Decagon Devices Inc. (2016). 5TE Water content, EC and temperature sensor, Operator's Manual. Version: March 11, 2016 – 11:55:57. Pullman, Washington. 26 pp. http://manuals.decagon.com/Manuals/13509_5TE_Web.pdf [last accessed January 18, 2018]

Decagon Devices Inc. (2017). MPS-2 & MPS-6 Dielectric water potential sensors, Operator's Manual. Version: July, 10, 2017 – 16:08:16. Pullman, Washington. 27 pp. http://manuals.decagon.com/Manuals/13755_MPS-2and6_Web.pdf [last accessed January 18, 2018]

Kremer, R. J. and Ben-Hammouda, M. (2009). Allelopathic Plants. 19. Barley (*Hordeum vulgare* L). Allelopathy Journal, **24**: 225-242.

Lenth, R. (2017). emmeans: Estimated Marginal Means, aka Least-Squares Means. R package version 1.0. https://CRAN.R-project.org/package=emmeans

Lo, C. C., Brownlee, B. G. and Bunce, N. J. (2006). Mass spectrometric and toxicological assays of Athabasca oil sands naphthenic acids. Water research, **40**: 655-664.

Naeth, M. A. and Wilkinson, S. R. (2002). Greenhouse emergence and establishment of selected plant species in consolidated tailings. Prepared for Suncor Energy Inc. Edmonton, Alberta. 19 pp.

Quagraine, E. K., Peterson, H. G. and Headley, J. V. (2005). In situ bioremediation of naphthenic acids contaminated tailing pond waters in Athabasca oil sands region--demonstrated field studies and plausible options: A review. Environmental Science and Health, **40**: 685-722.

Renault, S., MacKinnon, M. and Qualizza, C. (2003). Barley, a potential species for initial reclamation of saline composite tailings of oil sands. Journal of Environmental Quality, **32**: 2245-2253.

Renault, S., MacKinnon, M. and Qualizza, C. (2004). Suitability of altai wildrye (*Elymus angustus*) and slender wheatgrass (*Agropyron trachycaulum*) for initial reclamation of saline composite tailings of oil sands. Environmental Pollution, **128**: 339-349.

Silva, M. J. (1999). Plant dewatering and strengthening of mine waste tailings. PhD thesis, Department of Civil and Environmental Engineering, University of Alberta.

Wu, S. (2009). A greenhouse study of selected native plant species for dewatering CT. MSc thesis, Department of Civil and Environmental Engineering, University of Alberta.

Wu, S. (2015). Soil and vegetation properties on reclaimed oil sands in Alberta, Canada: a synthetic review. Faculty of Forestry, University of British Columbia. 52pp.

Yenish, J. P., Worsham, A. D. and Chilton, W. S. (1995). Disappearance of DIBOA-glucoside, DIBOA, and BOA from rye (*Secale cereale* L.) cover crop residue. Weed Science, **43**: 18-20.

Yucel, K., Schoonmaker, A., Degenhardt, D., Kaur, J., Khadka, B. (2016). Utilization of plants to dewater and stabilize mature fine tailings. IOSTC Conference proceedings, Lake Louise, AB.

EVALUATION OF STRENGTH ENHANCEMENT AND DEWATERING TECHNOLOGIES FOR A SOFT OIL SANDS TAILINGS DEPOSIT

William Smith[1], Erin Olauson[1], Jack Seto[2], Amanda Schoonmaker[3],
Reza Moussavi Nik[4], Gavin Freeman[5] and Gord McKenna[6]
[1]BGC Engineering Inc., Calgary, Canada
[2]BGC Engineering Inc., Edmonton, Canada
[3]Northern Alberta Institute of Technology, Peace River, Canada
[4]Formerly at Canadian Natural Resources Limited, Calgary, Canada
[5]Canadian Natural Resources Limited, Calgary, Alberta
[6]McKenna Geotechnical Inc., Vancouver, Canada

ABSTRACT

One requirement for the successful placement of a granular cap on soft tailings deposits is sufficient strength of the deposit surface. As part of its closure and reclamation research efforts, Canadian Natural Resources Limited (Canadian Natural) has been monitoring the strength and density changes over time of soft, deep, fine oil sands tailings deposits. In a recent pilot-scale field trial, Canadian Natural constructed a 30 m wide by 60 m long test cell at its Albian Sands operation and filled it to a depth of 4.65 m with centrifuged-dewatered fluid fine tailings (CFFT) in January 2016. In 2017, strength enhancement technologies were implemented within the test cell, including the installation of vertical wick drains, the seeding and planting of native slender wheatgrass (*Elymus trachycaulus*) and native sandbar willow (*Salix interior*), and pumping ponded water from the deposit surface. The tailings properties measured since deposition are presented, along with an evaluation of the relative performance of these strength enhancement options approximately six months after implementation.

INTRODUCTION

Oil sands tailings are generated in large volumes by the extraction of bitumen from surface mines in northeastern Alberta, Canada. Deep fluid fine tailings (FFT) deposits pose a tailings management and closure challenge due to their low strengths, low densities, low permeabilities and slow consolidation behaviour (McKenna et al. 2016).

Oil sands operators have developed and implemented numerous tailings technologies to improve the strength and density of oil sands tailings. One such method is the flocculation and processing of FFT through a solid-bowl centrifuge to produce centrifuged fluid fine tailings (CFFT) (COSIA 2012).

One method to allow for further reclamation activities with terrestrial equipment is to place a granular cap on the deposit surface (Pollock et al. 2010).

To evaluate the potential to cap CFFT deposits, Canadian Natural designed and constructed the Centrifuge Test Cell in the fall of 2015 and filled it with CFFT in January 2016. A geotechnical site investigation was conducted in the summer of 2016 to evaluate the potential for capping with tailings sand; at this time, the crust was 0.1 m thick with an average undrained shear strength of 5 kPa, and was considered insufficient to support the desired minimum 0.5 m thick cap. Several strength enhancement and dewatering technologies were then implemented within the test cell in March, June and July 2017. One area of the deposit was left unamended as a control zone. The deposit settlement, density, and shear strength were measured before and after these strength enhancement technologies were implemented to compare performance.

CENTRIFUGE TEST CELL

The test cell (see Figure 1) was excavated with 2H:1V slopes on the north, west, and south sides and a 1H:1V slope on the east side. The test cell is approximately 30 m wide by 60 m long at the crest; the berms and excavation form approximately 5.3 m of containment depth. A 60 mil, white, single-sided textured high-density polyethylene (HDPE) liner was installed along the base and side slopes of the test cell, isolating the cell hydrogeologically. The cell has no outlet; precipitation and

consolidation water that pond on the deposit surface are managed by pumping. A floating dock system was installed in March 2017 to allow for deposit access for sampling and testing.

Prior to tailings deposition, two vertical power poles were installed within the cell and instrumented with vibrating wire piezometers (VWPs) and total pressure cells to measure changes in effective stress, and a sonic ranger to measure the deposit height with time.

The cell was filled with approximately 4,000 m^3 of CFFT to an initial thickness of 4.65 m from January 28 to 30, 2016. CFFT samples were collected during cell filling at the end of the discharge pipe for index testing. Twelve settlement plates were installed across the deposit surface in March 2017 and were surveyed monthly.

STRENGTH ENHANCEMENT AND DEWATERING TECHNOLOGIES IMPLEMENTED

Three technologies were implemented at the Centrifuge Test Cell to increase the strength and density of the CFFT: wick drain installation, vegetation planting, and periodic removal of surface water.

The test cell was divided into different zones, as shown in Figure 1. Each zone featured different combinations of amendment technologies, while a control zone was left unamended to compare against. The amended zones consisted of different types of vegetation, wick drains and a combination of wick drains and vegetation. Amendments were applied both in the centre of the deposit over its full depth, and along the side slopes where the tailings depth varied. The unamended control zone was left over the side slopes and the centre of the deposit. The design of these technologies is discussed below.

Wick Drains

Wick drains are prefabricated, band-shaped units that consist of a grooved core wrapped within a filter jacket. They provide an upward drainage path for excess pore water pressure within soft compressible soils. This enhances dewatering and accelerates the consolidation process, leading to an increase in tailings strength and density (Fellenius 2017).

Mebra-Drain MD-88 wick drains were installed in winter conditions in March 2017 using a custom system mounted on an Argo amphibious vehicle (Figure 2). A total of 193 wick drains were installed at approximately 1 m triangular spacing over a 9 m by 16 m area, to depths of approximately 3.5 m below the frozen tailings surface.

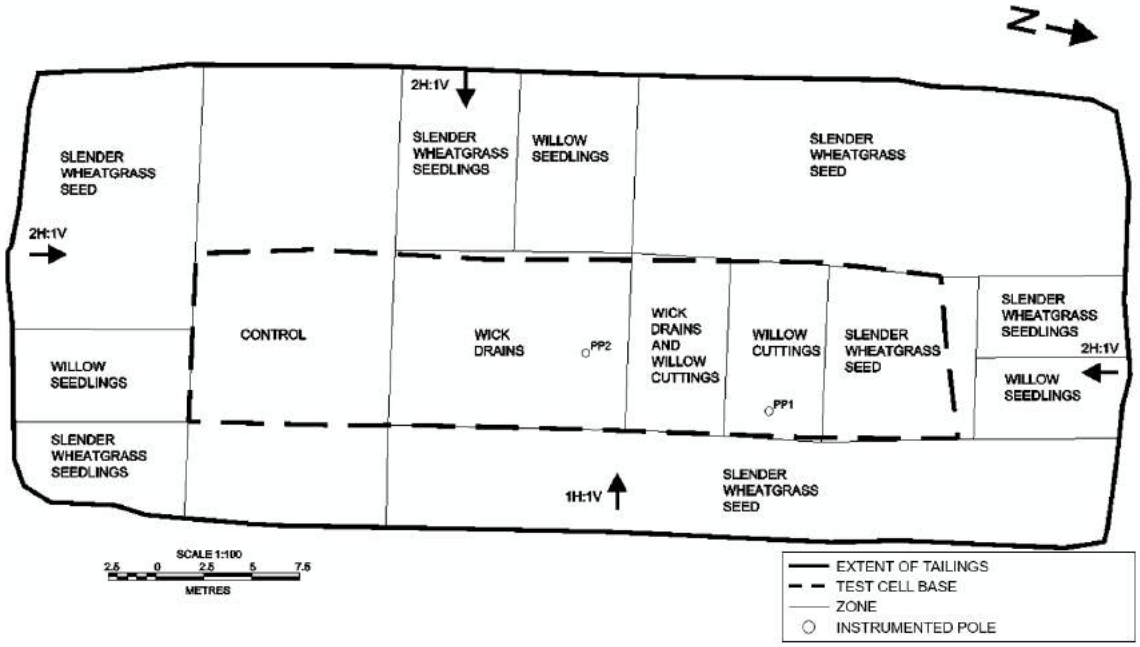

Figure 1. Centrifuge Test Cell layout

Figure 2. Argo-mounted wick drain deployment system

Vegetation

Plants have been shown to dewater and strengthen tailings through evapotranspiration, by increasing matric suction. There is also some mechanical reinforcement of the tailings by the plant roots (Silva 1999).

After greenhouse trials of several plant species, two species were selected as the primary focus of the study: slender wheatgrass (*Elymus trachycaulus* (Link) Gould ex Shinners ssp. *trachycaulus*) and sandbar willow (*Salix interior* Rowlee). Three types of plant material were tested: seeds, unrooted hardwood cuttings, and rooted seedlings (see Table 1).

The vegetation was planted in two phases using various methods as shown in Figure 3. In March 2017, dormant sandbar willow cuttings were harvested, and the cut end exposed to atmosphere was painted with white latex paint to reduce desiccation and allowed to briefly dry. The following day, willow cuttings were inserted vertically into holes hand-drilled into the frozen deposit at approximately 25 cm by 25 cm spacing.

In June 2017, slender wheatgrass seed was surface broadcast both by hand and by a custom-built unmanned amphibious rover (Olmedo and Lipsett 2016) mounted with a 55 L plastic hopper and a remote-controlled rotating disc. Sandbar willow and slender wheatgrass seedlings were planted both by hand and by the rover mounted with a conveyor belt that dropped pre-loaded seedlings onto the deposit and tracked over them twice to embed root plugs within the CFFT.

Figure 3. Different vegetation installation methods used at the Centrifuge Test Cell

Table 1. Installation details for slender wheat grass (grass) and sandbar willow (willow)

Vegetation Type	Approx. Application Rate (per hectare)
Willow cuttings	160,000 stems
Willow seedlings	160,000 stems
Grass seed	700 kg
Grass seedlings	160,000 stems

The entire deposit except for the control and wick drain zones was fertilized with Urea pellets (150 kg ha^{-1}), 13-26-6 Quick Start turf fertilizer (150 kg ha^{-1}), and alfalfa pellets (5000 kg ha^{-1}). Fertilizer was spread manually and by the rover.

Surface Water Removal

Removal of surface water exposes the upper CFFT to atmospheric conditions, leading to tailings

strength increase through desiccation by evaporation and freeze-thaw effects (COSIA 2012). It also facilitates growth of plant species that dewater and strengthen the deposit crust.

Snowmelt, precipitation and consolidation water collect on the test cell surface because the downward and lateral drainage is impeded by the HDPE liner and the lack of a cell outlet. Surface water can only be removed either by pumping or evaporation.

In 2016, the deposit was pumped once after snowmelt, once during the site investigation, and once before winter freeze up, a total of approximately 350 m^3 of water. In 2017, the deposit was pumped once after snowmelt and twice during the summer, a total of approximately 200 m^3 of water.

SITE INVESTIGATION AND LABORATORY METHODS

Three main geotechnical site investigation programs were carried out at the Centrifuge Test Cell in August 2016, June 2017, and September 2017, involving sampling, laboratory testing and in-situ strength testing. A vegetation investigation was carried out in September 2017 in conjunction with geotechnical work involving vegetation assessment, sampling and laboratory testing. A small geotechnical site investigation was carried out in October 2017 involving in-situ strength testing. The tests and sampling methods used in these site investigations are described below.

Geotechnical Sampling and Laboratory Testing

Shallow sampling (<0.5 m depth focusing on the CFFT crust) and deep geotechnical sampling (up to 4.2 m depth) of the CFFT were carried out. Shallow samples were collected using a hand auger, and deep sampling was carried out using a Parky Piston Sampler.

Laboratory testing of samples involved geotechnical (oven dried) moisture content tests according to ASTM D2216, where the bitumen was not removed prior to testing (to determine solids content including bitumen), but also included Dean-Stark analyses (to determine oil-water-solids content), Atterberg limit testing (to determine liquid limit, plastic limit and plasticity index), specific gravity, and hydrometer testing (to determine grain-size distribution).

Geotechnical In-Situ Strength Testing

Two methods were used to measure the undrained shear strength of the CFFT: ball penetration testing (BCPT) and hand vane shear testing (hVST). To calculate soil properties from BCPT, it is assumed to have full-flow movement around the ball. The high projected area of the ball used (150 cm^2) results in high measurement resolution in soft soils. The measured ball tip resistance is corrected using the dynamic pore pressure (u_2), the shaft and ball areas, and the total stress at the measurement point, and converted to an undrained shear strength using an empirical correlation (Weemees et al. 2006). An N_{ball} factor of 11 was used (COSIA 2015).

Hand vane shear testing (hVST) was carried out using one of three different rectangular vane sizes depending on the CFFT strength: 19 mm diameter by 28 mm height, 33 mm diameter by 50 mm height, or 65 mm diameter by 135 mm height. Testing consisted of inserting a four-bladed vane into undisturbed soil, and then rotating it from the surface at a specified slow and constant rate. The maximum torque required to bring the cylindrical shear surface to failure was used to determine the peak undrained shear strength. At all depths greater than 0.15 m, the skin friction of the extension rods was corrected by measuring the torque using a dummy shaft with no vane, and subtracting this from the shear force measurements.

Vegetation Assessment, Sampling and Testing

A 55 m by 21 m sampling grid with 200 points was laid out across the deposit at approximately 3 m intervals for vegetation assessment, sampling, and geotechnical testing. Approximately 25% of the points were selected for vegetation sampling, representing all zones and ranges of vegetation surface cover. Survival was also assessed in seedling planted zones.

At each vegetation sampling location, a photograph was taken, the total aboveground leaf mass was clipped from a 0.5 m by 0.5 m area to determine aboveground biomass and two tailings sample cores (5 cm diameter by 30 cm deep) were collected to determine belowground biomass.

Laboratory testing included aboveground biomass measurements, where total plant dry weight was

determined after oven drying to 70°C. Belowground biomass was determined by weighing oven dried (70°C) roots that had been separated and washed from the tailings cores.

RESULTS

Index and Grain Size Testing Results

Results from laboratory testing (excluding solids content measurements) are summarized in Table 2. The CFFT is classified as a clay with high plasticity. Hydrometer tests were conducted on samples after removing the bitumen (COSIA 2016). Fines and clay contents show the CFFT is almost all fines and is composed of approximately 20% clay-sized particles.

Table 2. Laboratory Testing Results

Parameter	Bitumen Included	Range of Values (Average)	# of Tests
Bitumen Content (%)	-	0.8-2.3 (1.6)	39
Liquid Limit (%)	Yes	71-90 (80)	16
Plastic Limit (%)	Yes	22-29 (24)	16
Plasticity Index (%)	Yes	43-66 (57)	16
Specific Gravity	Yes	2.37-2.55 (2.47)	17
Hydrometer Fines Content (<45 µm) (%)	No	97-99 (98)	7
Hydrometer Clay Content (<2 µm) (%)	No	9-32 (22)	7

Changes in Deposit Thickness

The sonic ranger installed on the power pole in the willow cutting zone indicates the deposit has decreased in thickness in the centre by 84 cm, from an initial thickness of 4.65 m on January 30, 2016 to 3.81 m on October 31, 2017 before the deposit froze and snow started to impact the readings.

The settlement plates installed in various central zones and measured from April 28 to September 19, 2017 show that the control zone and the seeded grass zone settled 9 to 18 cm while the wick-drain zones settled 19 to 23 cm.

Solids Content Results

Solids content in this paper refers to the mass of solids plus mass of bitumen divided by the total slurry mass based on the geotechnical (oven dried) moisture content tests. The initial average solids content of the slurry was 47%. Figure 4 shows the changes in solids content with depth over time.

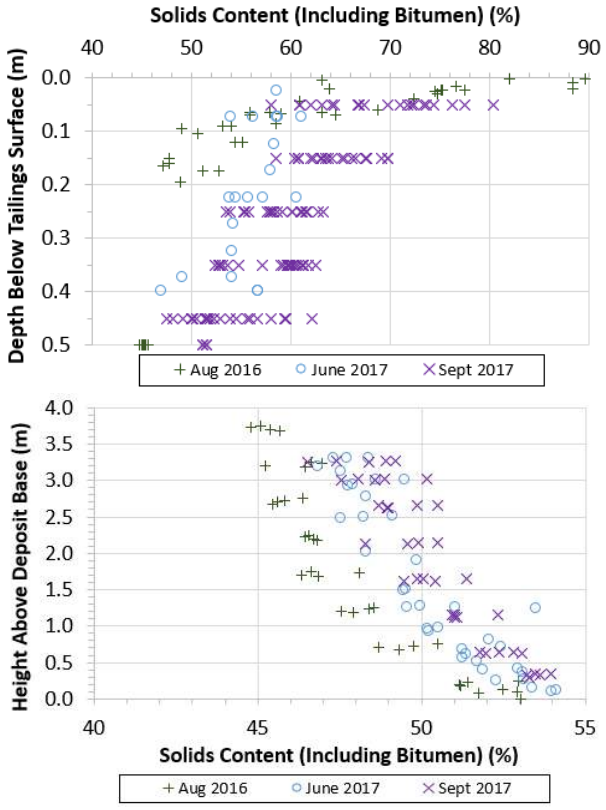

Figure 4. Changes in tailings density (solids content) at the centre of the deposit over time

In August 2016, the upper approximately 0.10 m was dry and unsaturated due to evaporative drying, resulting in the formation of a crust denser than the underlying CFFT. In June 2017, solids contents in the upper 0.40 m showed an increase from August 2016, suggesting that freeze-thaw effects led to crust thickening. The upper 0.10 m was saturated in June 2017 and showed lower solids contents than measured in August 2016, indicating that the crust is sensitive to rewetting. In September 2017, the solids contents in the upper 0.40 m of the deposit increased further due to evaporative drying.

In August 2016, CFFT in the lower 2 m of the deposit had a slightly higher solids content than the

tailings above. This may be due to depositional processes (accumulation of denser material near the base of the deposit with the lighter, wetter material staying near the top) or due to post-depositional densification. This process could not be confirmed since sampling at depth was not carried out immediately following deposition. Between January 2016 and September 2017, the solids content of the CFFT below the upper 0.5 m had increased minimally from 47% to 50%.

Pore Pressure Measurements

The pore pressures measured by VWPs at the two instrumented poles show a decreasing trend after cell filling, due to a combination of a decrease in the deposit thickness (and corresponding decrease in hydrostatic pressure) and settlement due to tailings densification.

To understand whether consolidation settlement is occurring, the total stress and pore pressure within the deposit can be compared, as consolidation occurs due to an increase in effective stress (equal to the total stress minus the pore pressure). Total stress measurements, calculated total stress values from CFFT density, and average pore pressure measurements are compared in Figure 5 for the time just after filling (February 2016) and during the September 2017 site investigation.

The calculated total stresses within the tailings column (using solids contents and deposit height), are very similar to pore pressure and total stress

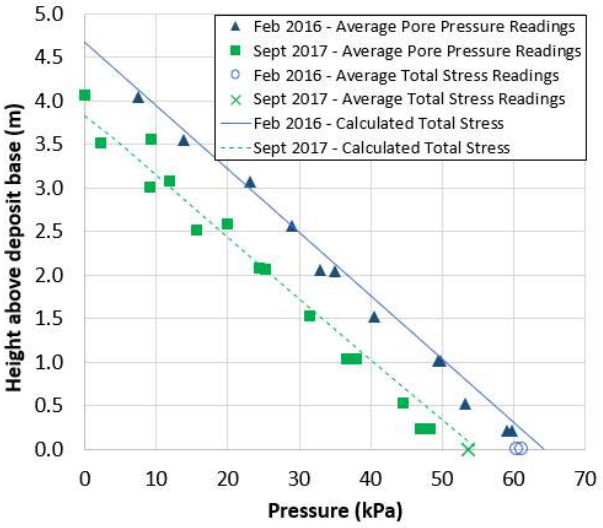

Figure 5. Total pressure and pore pressure profiles in February 2016 and September 2017

measurements in both February 2016 and September 2017, suggesting there has been little to no effective stress developed in the tailings since the cell was filled. But while excess pore pressure dissipation is not seen in the CFFT, the change in height and increase in solids content indicate that settlement due to densification is occurring.

Undrained Shear Strength Results

Figure 6 shows the peak undrained strength profiles measured by BCPT and hVST in the middle of the deposit. The peak undrained shear strength of the crust is higher than the underlying tailings, as expected. Typical crust peak strength measured by hVST in September 2017 (in drier, unsaturated conditions) are 5 kPa but can be as high as 40 kPa. The crust strength is sensitive to rewetting, as the maximum hVST measurement taken in October

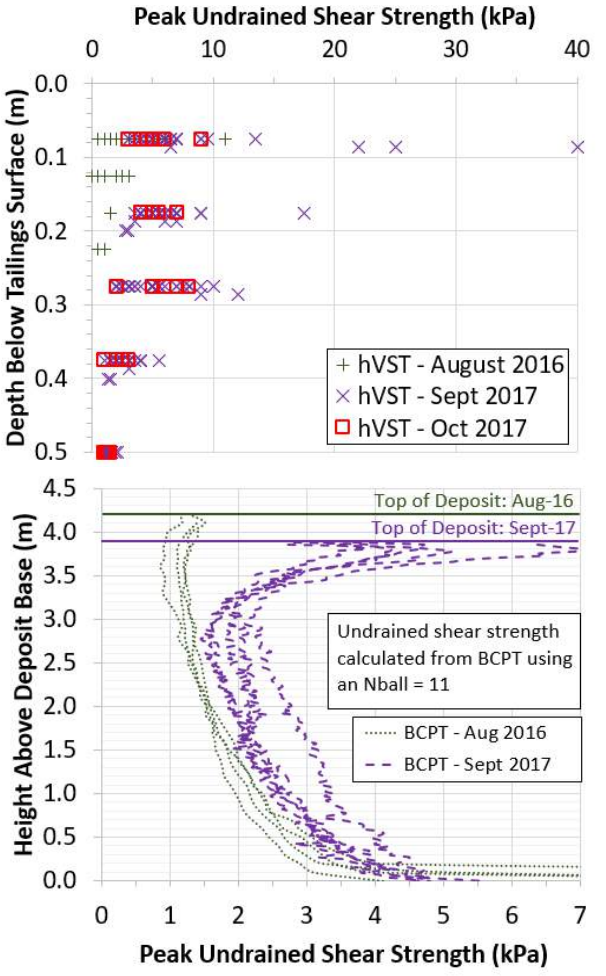

Figure 6. Peak undrained strength profiles measured in the central area of the deposit

2017 in saturated conditions dropped to 9 kPa, 31 kPa lower than the maximum measurement taken in September 2017.

The peak undrained shear strength of the CFFT below the crust remains low. It has increased from an average of approximately 1.5 kPa in August 2016 to 2.5 kPa in September 2017.

DISCUSSION ON STRENGTH ENHANCEMENT AND DEWATERING TECHNOLOGIES

Impact of Wick Drains

Wick drain zones showed an average 0.2 m of settlement between April 28 and September 19, 2017, which was slightly higher than the other central zones of the test cell that settled an average of 0.15 m.

The solids content profile below the crust from September 2017 testing are compared for wick zones with other central zones in Figure 7. The average solids content in the wick zones was 51% as compared to 50% in the other central zones, indicating minor CFFT densification. The solids contents in the wick zones are slightly higher than the other zones in the top 2.5 m of the deposit, with the difference decreasing below this depth.

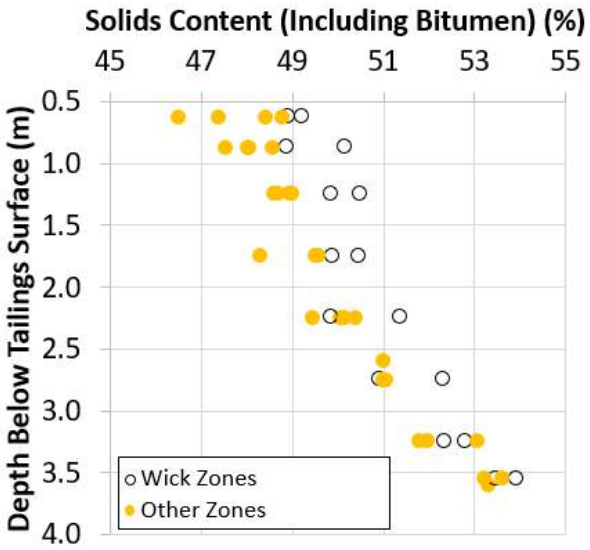

Figure 7. Solids content values in September 2017 in the central zones below the top 0.5 m

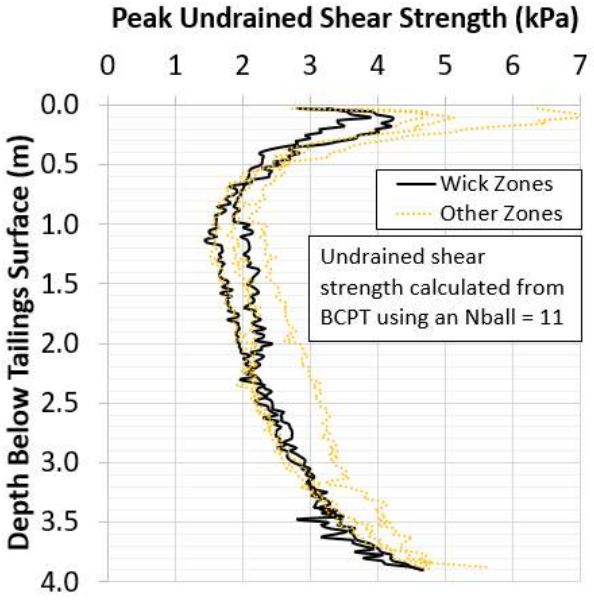

Figure 8. Undrained shear strengths measured by BCPT in September 2017 in the central zones

The undrained shear strengths measured by BCPT in September 2017 shown in Figure 8 were lower at surface in the wick drain zones compared to the other central zones, likely due to a higher phreatic surface, and similar strengths at depth.

Impact of Vegetation

To understand the success of vegetation growth on the CFFT, the effects of the cell configuration and the liner must be discussed. The central portion of the deposit is the low point in the cell, as the settlements are greatest where the CFFT is the thickest. Precipitation and release water flows towards the centre, creating prolonged flooding conditions; the middle of the cell was flooded for six weeks from April to May 2017, and three weeks through June 2017.

The rooted sandbar willow and slender wheatgrass seedlings installed in June 2017 by hand showed high survivorship (99%) regardless of the surface moisture conditions. Seedling planting using the amphibious rover was successful only where the CFFT surface was very soft and moist, where the roots could be physically embedded into the tailings. Where the surface was dry, plant mortality was high as root plugs quickly desiccated due to exposure and due to lack of substrate contact.

Nine weeks of flooding in the middle of the deposit through the spring led to lower survivorship of winter-planted sandbar willow cuttings (<50% in the wettest zones versus >90% where flooding was not prolonged). Three weeks of flooding after June installation led to patchy growth in seeded slender wheatgrass especially towards the centre of the deposit. Although sandbar willow was seen to be tolerant of periodic flooding once established, the unrooted cuttings appeared to be more sensitive during the establishment phase compared to rooted seedlings.

Slender wheatgrass is a species capable of growth in a wide array of environmental conditions (Dobb and Burton 2013) but was not able to withstand prolonged flooding during establishment. In general, seed-based establishment of slender wheatgrass was superior to hand-planting in drier areas of the deposit as vegetation coverage values were generally higher.

Figure 9 presents plots of peak undrained shear strength measured by hVST, solids content and root biomass plotted versus depth for various tailings thicknesses (for the thickest tailings in the central portion of the test cell, to the thinnest tailings along the side slopes). Locations with almost no (control), low (<60 g m^{-2}) and high (>90 g m^{-2}) aboveground biomass are shown.

The peak undrained shear strength of the CFFT is greatest on the side slopes of the deposit, likely due to a combination of lower tailings thickness and the configuration of the cell, where the phreatic surface is deeper on the side slopes than in the middle (lowest portion) of the deposit.

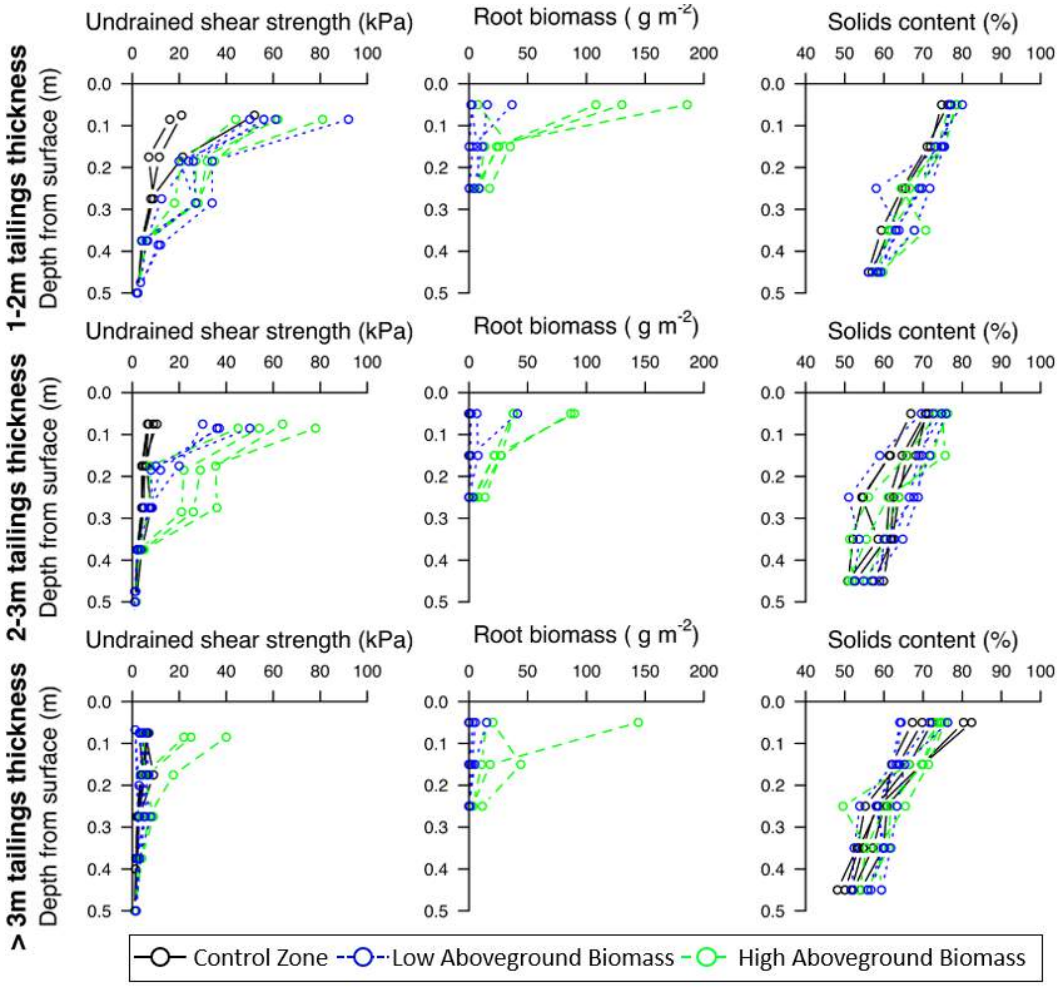

Figure 9. Peak undrained shear strength determined by hVST, root biomass and solids content (including bitumen) profiles to 0.5 m depth at different CFFT thicknesses. Locations with no (control), low (<60g m^{-2}) and high (>90g m^{-2}) aboveground biomass values are shown

The plots show increasing plant biomass is associated with an increase in peak undrained shear strength as compared to the control zone at all tailings deposit depths. The positive association between plant biomass and peak undrained shear strength decreases with increasing tailings thickness towards the centre of the deposit. Increasing plant root biomass is also associated with a slight increase in solids content at 1 to 2 m tailings thickness, but this trend becomes less apparent with increasing tailings thickness.

In summary, after one growing season, the vegetation increased the strength of the CFFT at the very top of the deposit, with this effect most apparent at low tailings thicknesses. At tailings thicknesses of 1 to 3 m, the peak undrained shear strength in areas with high aboveground biomass ranges from typical values of about 20 to 80 kPa, versus values of about 10 to 50 kPa measured in the control zone. However, below 30 cm depth, the vegetation did not increase shear strengths.

Impact of Surface Water Management

Surface water management was found to be important to the dewatering and strength gain of the CFFT, as the lower the water table was in the deposit, the greater the measured solids contents and undrained shear strengths. Since the crust strength and density was seen to be sensitive to rewetting, and vegetation in flooded areas had lower survivorship, effective surface water management at the Centrifuge Test Cell is determined to be important for maintaining ideal vegetation growing conditions (for the species in this study) and maximizing the CFFT exposure to atmospheric conditions.

CONCLUSIONS

After 21 months of monitoring and three site investigations at the Centrifuge Test Cell, the CFFT deposit has settled by around 20% of its original thickness, and solids contents at depth have increased by approximately 3%. However, pore pressure measurements indicate that little to no effective stress gain has occurred. A crust has developed over two years to around 40 cm thickness due mainly to freeze-thaw action, surface water removal, and evaporative drying, and crust strength values have increased to an average of 5 kPa in the centre of the deposit. High undrained shear strength values in the unsaturated crust are quickly lost when rewetted.

Six months after wick drain installation, the difference between the wick drain zones and other central deposit zones is small. In the wick drain zones, the CFFT surface is 0.05 m lower, the strength is similar, and the solids content is 1% higher than the other central zones, suggesting that CFFT dewatering due to wick drains at a 1 m triangular configuration did not significantly accelerate over this time period.

After one growing season, the vegetation installed in the Centrifuge Test Cell led to an up to fourfold increase in the undrained shear strength of the top 30 cm of the deposit. However, due to the cell configuration, vegetation survivorship was low in flooded areas, leading to less strength gain in the central (thickest) portion of the deposit. This highlights the importance of an effective surface water removal program, which also enhances drying and strength gain. Alternatively, native plant species that are more adapted to prolonged flooding (wetland species) may be an option. In a single growing season, slender wheatgrass seed was deemed the superior approach to establishing dense vegetation cover as long as the deposit was kept dry; sandbar willow did not produce the same quantity of biomass in the same time period but over a longer time frame (two to five years), may show more dewatering.

The deposit will continue to be monitored and investigated, to assess the relative performance of the installed strength amendment options over a longer time period.

ACKNOWLEDGEMENTS

The authors would like to thank the following:

- ConeTec Investigations Ltd. (ConeTec) for developing and implementing the custom Argo-mounted wick drain deployment system. Thanks to ConeTec for also conducting all BCPT and deep sampling at the Centrifuge Test Cell.
- Copperstone Technologies Ltd. for the development and deployment of the custom-built unmanned amphibious rover used for vegetation and fertilizer installation.
- O'Kane Consultants Inc. (OKC) for installing instrumentation and carrying out data processing.
- Golder Associates Ltd.'s Calgary laboratory for their geotechnical testing services.

REFERENCES

ASTM. (2015). Standard Test Method for Field Vane Shear Test in Saturated Fine-Grained Soils. ASTM Standard D2573/2573M. American Society for Testing and Materials, West Conshohocken, PA.

ASTM. (2010). Standard Test Method for Laboratory Determination of Water (Moisture) Content of Soil and Rock by Mass. ASTM Standard D2216-10. American Society for Testing and Materials, West Conshohocken, PA.

COSIA (Canada's Oil Sands Innovation Alliance). (August 30, 2012). Technical Guide for Fluid Fine Tailings Management. Canadian Oil Sands Innovation Alliance, Calgary, AB.

COSIA. (June 2015). Guidelines for Determining Oil Sands Fluid Tailings Volumes. Canadian Oil Sands Innovation Alliance, Calgary, AB.

COSIA. (February 2016). Unified Fines Method for minus 44 micron material and for particle size distribution. Canadian Oil Sands Innovation Alliance, Calgary, AB.

CTMC (Consortium of Oil Sands Tailings Management Consultants). (June 29, 2012). Oil Sands Tailings Technology Deployment Roadmaps Project Report. *Report Prepared for* Alberta Innovates – Energy and Environment Solutions and the Oil Sands Tailings Consortium, Edmonton, AB.

Dobb, A. and Burton, S. (2013). Rangeland Seeding Manual for British Columbia. B.C. Ministry of Agriculture, Sustainable Agriculture Management Branch, Abbotsford, B.C.

Fellenius, B. (2017). Basics of Foundation Design. Pile Buck International, Inc., Vero Beach, Florida.

McKenna, G., Mooder, B., Burton, B. and Jamieson, A. (2016). Shear strength and density of oil sands fine tailings for reclamation to a boreal forest landscape. *In* Fifth International Oil Sands Tailings Conference (IOSTC), Lake Louise, Alberta, 4-7 December 2016. University of Alberta Geotechnical Group, Edmonton. pp.130-153.

Olmedo, N.A. and Lipsett, M.G. (2016). Design and field experimentation of a robotic system for tailings characterization. Journal of Unmanned Vehicle Systems, **4**: 169-192. doi: 10.1139/juvs-2015-0034.

Pollock, G. W., Liu, X., McRoberts, E. C., Williams, K., Wells, P. S. and Fournier, J. (2010). Suncor Oil Sands Tailings Pond Capping Project. *In* Tailings and Mine Waste '10 Conference, Vail, Colorado, 17-20 October 2010. CRC Press, Boca Raton, Florida.

Weemees, I., Howie, J., Woeller, D., Sharp, J., Cargill, E., and Greig, J. (2006). Improved techniques for in situ determination of undrained shear strength in soft clays. *In* Sea to Sky Geotechnics, Proceedings of the 59th Canadian Geotechnical Conference, Vancouver, B.C., 1–4 October 2006. BiTech Publishers Ltd., Richmond, B.C., pp. 89–95

.

EFFECTS OF SURFICIAL SEASONAL WEATHERING ON CENTRIFUGED OIL SANDS TAILINGS

Umme Salma Rima and Nicholas Beier
University of Alberta, Edmonton, Canada

ABSTRACT

The combined effect of freezing-thawing-drying and wetting cycles are the most prevalent natural impacts that can contribute to the reclamation of the fluid fine tailings. Laboratory experiments demonstrate that the centrifuged oil sands tailings (having a solids content of 53%) subjected to repeated freeze-thaw and drying-wetting cycles causes substantial dewatering and accompanying increase in undrained shear strength at the surface. The objective of this paper is to establish an enhanced understanding of the volume change and engineering behavior of the tailings deposits exposed to surficial seasonal weathering. A one-dimensional closed system freezing test was carried out in the laboratory for five consecutive freeze thaw cycles to simulate the winter and spring seasons at three different temperature gradients. The alternate evaporation and subsequent rainfall infiltration were simulated through multiple drying-wetting cycles between each of the freeze-thaw cycle. The results suggest that the combined effect resulted in an increase of solids content to a range of 80%- 89% with an associated shear strength of more than 110 kPa at the surface after five freeze-thaw and drying-wetting cycles. The increase in solids content was found significant in each of the drying-wetting cycles while the effect of the freeze thaw on thaw strain and solids content enhancement reduced gradually after the first cycle. However, the sample subjected to a lower temperature gradient deviated from the gradual reduction in thaw strain and resulted in an overall increase in thaw strain and solids content.

INTRODUCTION

Mining and mineral processing generate the production of waste by-products including finer grained slurries known as “fluid fine tailings”. Finding ways to get the fluid fine tailings to accelerate consolidation and to gain in shear strength within a reasonable time is critical to improving overall reclamation performance. Of the several technologies to improve the trafficability and strength properties of the tailings surface, the centrifuge technology along with the use of additives has demonstrated promising results and is now considered commercially operational (Mikula et al. 2008). However, maximizing water removal from the existing treated centrifuged tailings deposit is nevertheless challenging. Therefore, the effect of seasonal weathering (repeated freeze-thaw cycles, summer drying and precipitation) can be considered as a further process of water removal so a deposition strategy can be defined. Cyclic freeze-thaw- drying process is believed to form a desiccated surface crust that can cause a potential increase in strength with time. The increase in strength due to settlement has the potential to provide a surface layer capable of retaining a thinner layer of capping material to support the reclamation efforts. The study described in this paper was developed to see whether the seasonal weathering is effective in forming a surface crust capable of gaining strength. Understanding the development of a surficial crust is required to evaluate potential capping and reclamation scenarios and ultimately to guide the design and construction of reclamation cover systems on deep tailings deposits.

MATERIAL

The material tested consisted of flocculated centrifuged tailings sample that was treated with flocculants created from proprietary material. The investigated tailings were composed of about 48% non-clay minerals comprising predominantly quartz (40%) and about 52% clay minerals comprising mainly of kaolinite (36%) and illite (15%). The tailings had residual bitumen content of about 5.7%. The laboratory investigations including index properties, solids mineralogy and pore water chemistry were conducted using standard ASTM procedures and specialized test methods.

RESEARCH METHODOLGY

The laboratory testing consisted of two components: five cyclic freeze thaw and five drying wetting cycles. The drying-wetting tests were performed between each of the freeze-thaw cycle to investigate the combined effect of freeze-thaw-drying-wetting cycles on the investigated tailings.

Cyclic Freeze-Thaw Tests

In order to simulate the winter and spring season, a one-dimensional closed system freezing test was conducted in the laboratory with three centrifuged samples at three different temperature gradients. The top boundary temperatures were set at -15°C, -10°C and -5°C, respectively while the bottom temperature stayed at 0°C throughout the test. The boundary conditions resulted in three different temperature gradients of 0.083°C/mm, 0.056°C/mm and 0.028°C/mm, respectively. The freeze thaw cells were adopted to accommodate samples with an initial height of 18 cm and diameter of 10 cm. The boundary temperatures were applied through the base plate of the cell at the bottom and the freezing cap at the top connected to the temperature control systems (two temperature baths). The cells were wrapped with insulation to minimize the thermal conduction. Each of the samples were allowed to freeze for 96 hours followed by thawing continued for another 72 hours. The experiments were carried out in a walk-in freezer where the temperature was maintained between 0°C and 1°C. The detailed experimental procedure was explained in Rima and Beier (2018, in press). Upon thawing, undrained shear strength was measured at the near surface (measured at the depth of 15 mm from the surface) using a manual vane shear apparatus.

Cyclic Drying-Wetting Tests

Upon post-thawing, each of the samples were exposed to atmospheric drying followed by a re-wetting event in order to simulate the summer drying and rainfall event, respectively. The drying cycle of each sample was continued for a week at the room temperature (≈20°C) followed by a single day wetting event where the amount of water lost during the drying cycle was re-introduced as distilled water. Upon re-wetting, the samples underwent second phase of drying cycle for another week to understand the drying behavior of the tailings prior to and after rainfall event. Undrained shear strength was measured simultaneously on a daily basis throughout the drying-wetting cycle to track the changes in strength. After the measurements, each of the cells along with the samples were returned to the freezer and another cycle of freeze-thaw was continued. Overall, five cycles of freeze-thaw-drying-wetting event-drying after wetting event were carried out in the laboratory for each of the sample (at three different temperature gradients) for a period of consecutive three months.

Sectional Analysis

After the five cycles of freeze-thaw-drying-wetting tests were terminated, the samples were sectioned into five equal parts of approximately 2 cm in height to determine the solids content profile.

RESULTS

Table 1 summarizes the material properties and water chemistry of the investigated centrifuged tailings.

Table 1. Base Properties of Centrifuged Tailings

Characteristics	Value
Water content, w (%)	89
Solids content, s[1] (%)	53
Bitumen Content (%)	5.7
Specific Gravity	2.24
pH	8.7
Electrical Conductivity (µs/cm)	3560
SAR[2]	27
USCS Classification	CH

[1] $s = 1 / (1 + w)$

[2] $SAR = \frac{[Na^+]}{\sqrt{\frac{[Ca^{2+}+Mg^{2+}]}{2}}}$

The water content was measured to be 89% corresponding to a solids content of 53%. The presence of bitumen resulted in low G_s= 2.24 compared to typical sedimentary clays. The pH was measured to be 8.7 that falls within the typical range of pH (8.0 - 8.8) for oil sands tailings in order to facilitate bitumen extraction from the solid particles. The electrical conductivity was measured to be 3560 µs/cm, which is typical for fine grained soils (100 µs/cm - 10,000 µs/cm), as reported by Mitchell and Soga (2005). Sodium Adsorption ratio (SAR) of the investigated centrifuged tailings was calculated to be 27, the value of which suggested

high likelihood of dispersed (SAR> 20) microstructure by Miller et al. (2010). The detailed solids mineralogy and pore water chemistry results were explained in Rima and Beier (2018, in press) and hence, not repeated here.

Figure 1 summarizes the thaw strain measured upon thaw after each freeze thaw cycle for each of the samples subjected to three different temperature gradients. To account for the volume change of the thawed tailings, the thaw strain was calculated on the basis of change in height prior to and after thawing divided by the total frozen height in each cycle.

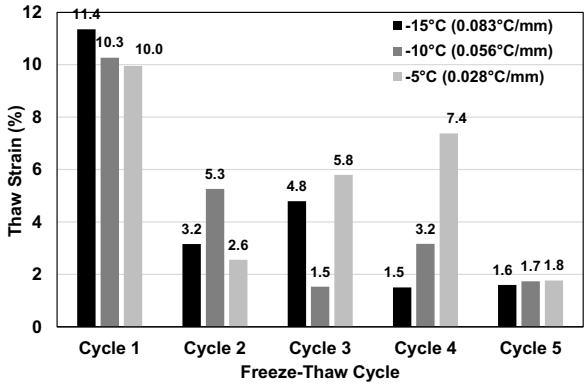

Figure 1. Thaw Strain Diagram at each Freeze-Thaw Cycle

The highest thaw strain was observed at the first cycle for each of the samples subjected to three different temperature gradients. The effects of thaw strain became less significant in the subsequent cycles for the samples subjected to temperature gradients of 0.083°C/mm and 0.056°C/mm, due to the water depletion resulting from cyclic drying-wetting between each freeze-thaw cycle. On the contrary, lower temperature gradient (0.028°C/mm resulting from -5°C at top and 0°C at bottom) as compared to the other two boundary conditions led to higher thaw strains due to the significant increase in volume change with increasing number of cycles. The total thaw strains for the three samples were not reported in this study since each freeze-thaw cycle was partitioned from one another due to the drying-wetting cycle.

Figure 2 illustrates the cumulative increase in average solids content after each seasonal cycle. Based on the change in height and computed thaw strain, the average solids content after each freeze-thaw cycle was calculated using the following equations:

$$\frac{\Delta H}{H} = \frac{\Delta e}{1+e_0} \quad [1]$$

$$s\,(\%) = \frac{100}{e/G_s+1} \quad [2]$$

where, ΔH is the change in height after thaw, H denotes the total frozen height just before thaw, Δe is the change in void ratio, e_o is the initial void ratio, e is the void ratio after thaw, $s(\%)$ is the average solids content and G_s is the specific gravity of the tailings.

Similar to the solids content computation after each freeze-thaw cycle, average solids content after each drying wetting cycle was computed based on the change in mass loss during evaporation and mass gain during rainfall event divided by the initial mass of dry soil.

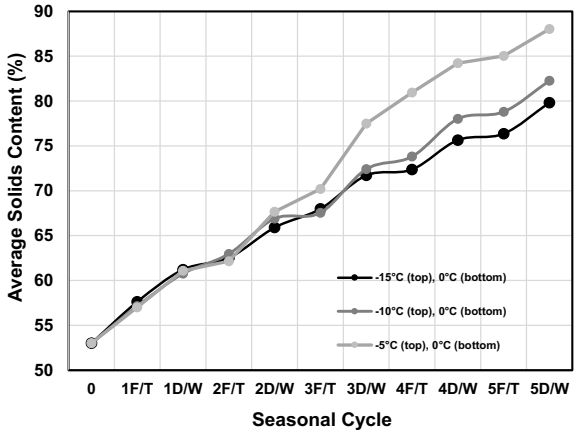

Figure 2. Computed Average Solids Content versus Number of Seasonal Cycles

The data trend shows that the higher average solids content was computed, on the lower temperature gradient sample (0.028°C/mm), to be 88% after five cyclic freeze-thaw and drying-wetting cycles.

Figure 3 shows the undrained shear strength measured at the near surface (15 mm from the top) at each seasonal cycle. The increase in undrained shear strength is more significant and pronounced for the sample subjected to lower temperature gradient (0.028°C/mm) as compared to the other two boundary conditions. The strength at this gradient exceeded 110 kPa in its fourth seasonal cycle and the sample started behaving like a hard soil. On the contrary, the sample with a temperature gradient of 0.056°C/mm exceeded

110 kPa at the final drying-wetting cycle. The data trend for the higher temperature gradient (0.083°C/mm) sample indicates that it would take multiple numbers (more than five) of seasonal cycles to behave like a hard and stiff soil. After five freeze-thaw and drying-wetting cycles, the undrained shear strength was measured to be 35.6 kPa for this gradient sample.

Figure 4a through 4c show the computed average solids content and measured shear strength progression over time for the samples subjected to three different temperature gradients of 0.083°C/mm, 0.056°C/mm and 0.028°C/mm, respectively. After five cycles of freeze-thaw and drying-wetting, the final water content in all the samples were reduced to less than half their initial values indicating a significant volume of water was released during five seasonal cycles. The near surface shear strength gradually increased with cyclic freeze-thaw and atmospheric drying-wetting from non-measured value to a value of higher than 110 kPa after five cycles for the samples with temperature gradients of 0.056°C/mm and 0.028°C/mm, and 35.6 kPa after four cycles for the sample with higher temperature gradient of 0.083°C/mm, respectively. Upon re-introduction of the evaporated water to simulate the rainfall event after each drying phase, the sample underwent re-wetting allowing an increase in water content with an associated shear strength reduction. The samples almost completely lost its strength each time these had been affected by the wetting event.

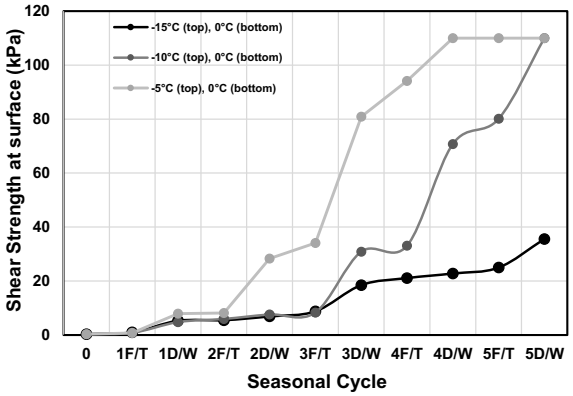

Figure 3. Measured Shear Strength versus Number of Seasonal Cycles (measured at a depth of 15 mm)

However, Figure 4a shows that the near surface shear strength of the sample with lower temperature gradient deviated from being affected by rainfall event after 4th drying cycle when the average solids content exceeded 84%. Similarly, Figure 4b shows that the sample with a temperature gradient of 0.056°C/mm remembered its stress history once the average solids content exceeded 82% at its fifth cycle and as a result, the near surface shear strength remained unchanged (>110 kPa) from getting affected by the wetting event. The average solids content for the sample subjected to a temperature gradient of 0.083°C/mm (as shown in Figure 4c) was

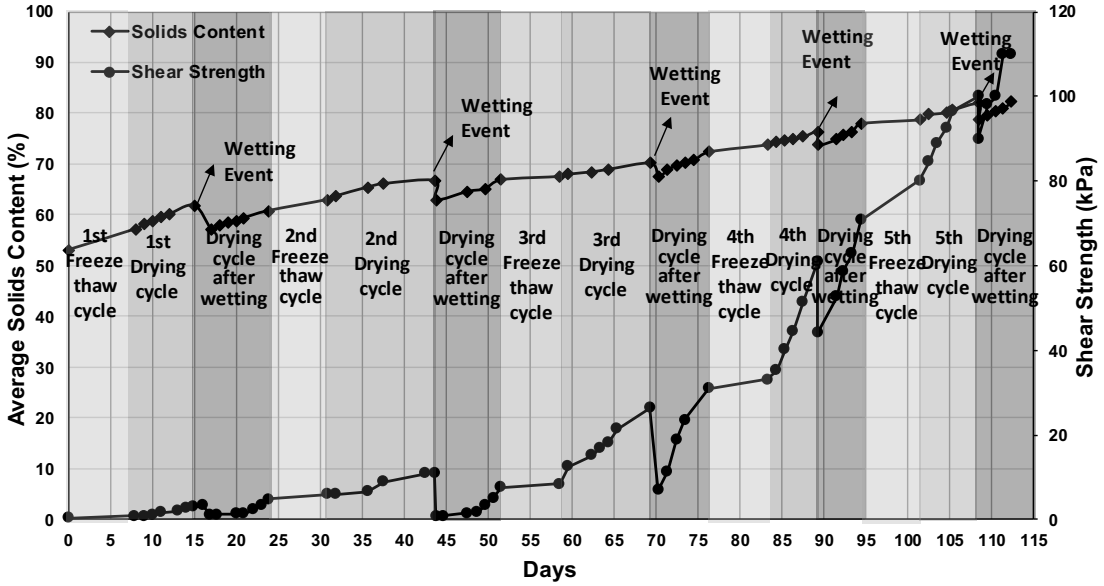

Figure 4a. Average Solids Content and Shear Strength Progression over Time at a Temperature Gradient of 0.028°C/mm

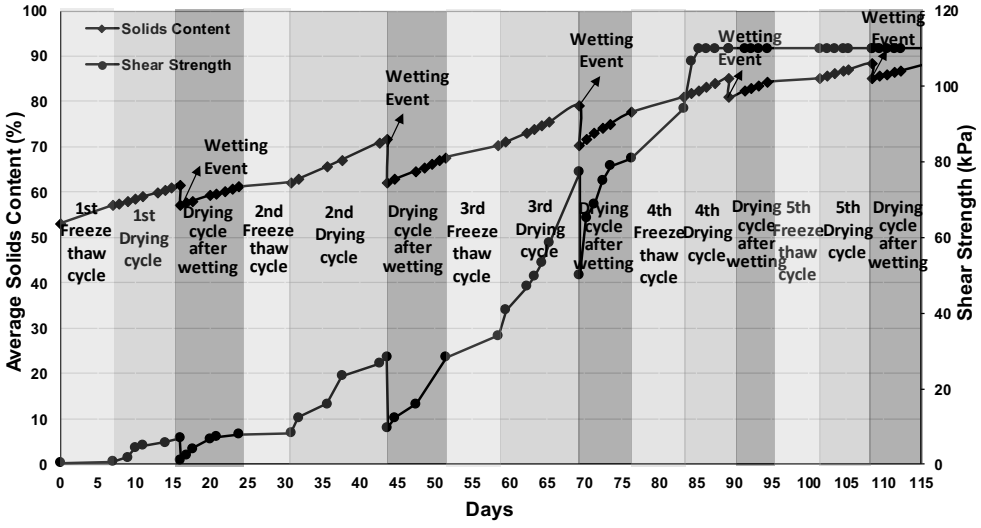

Figure 4b. Average Solids Content and Shear Strength Progression over Time at a Temperature Gradient of 0.056°C/mm

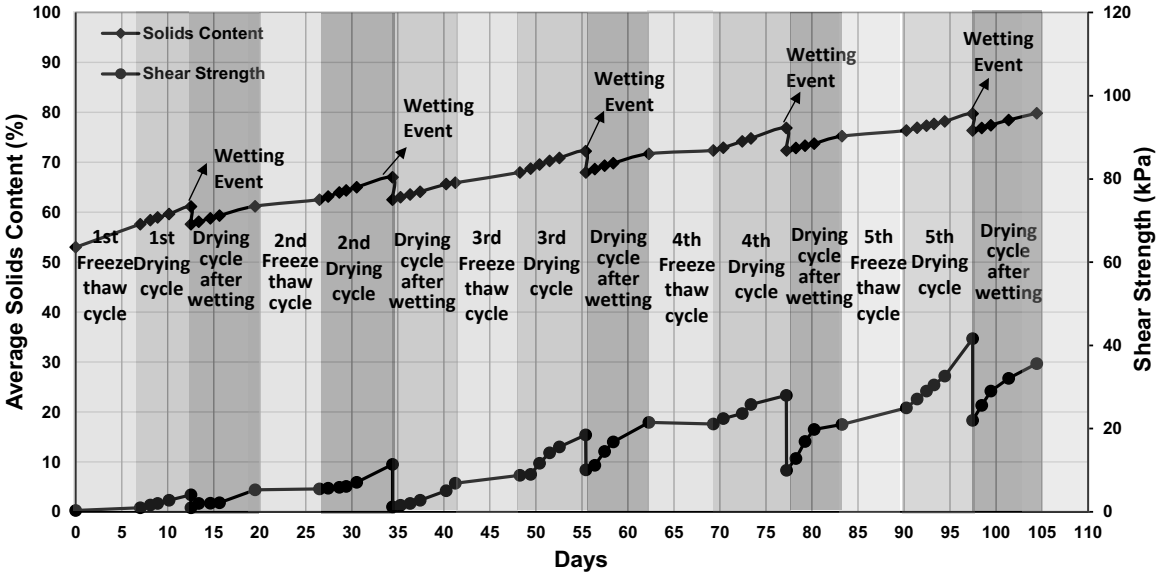

Figure 4c. Average Solids Content and Shear Strength Progression over Time at a Temperature Gradient of 0.083°C/mm

computed to be 76% with an associated undrained shear strength of 35.6 kPa after five cycles of freeze thaw and drying-wetting phase.

Figure 5 shows the measured final solids content profile and was compared with the initial solids content (53%) prior to testing. The sample subjected to higher temperature gradient (0.083°C/mm) was not reported here since the lab testing is currently in its seventh cycle to investigate the total cycles required for this sample to behave like a soil like the other two temperature boundary conditions. The laboratory measured results corroborated well with the average solids content values calculated from the thaw strain during freeze thaw and the loss of mass during atmospheric drying (as shown in Figure 4a to 4c). The figure shows that the sample subjected to lower temperature gradient (0.028°C/mm) resulted in a higher overall solids content (84%) with the

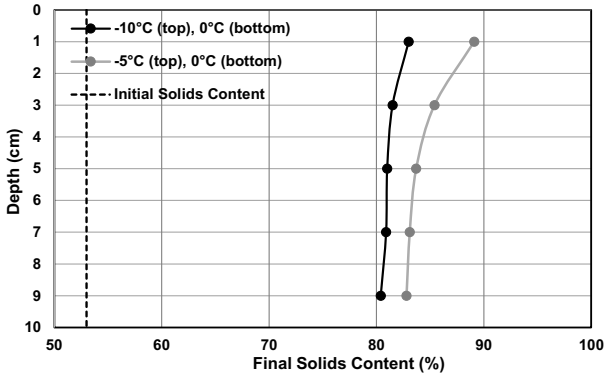

Figure 5. Measured Solids Content Profile within One Dimensional Freezing Cell

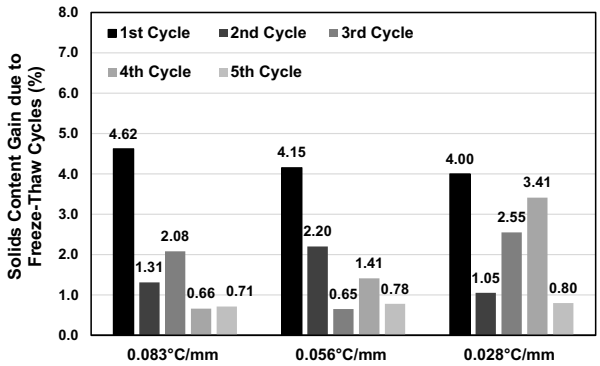

Figure 6. Average Solids Content Gain by Freeze-Thaw Cycles

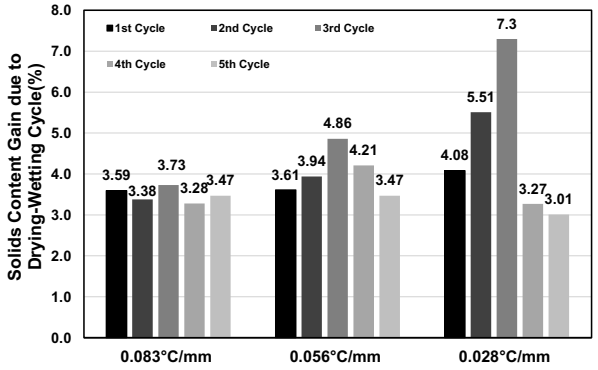

Figure 7. Average Solids Content Gain by Drying-Wetting Cycles

highest value recorded in the surface (=89%). Similarly, the sample subjected to a temperature gradient of 0.056°C/mm resulted in an overall solids content of 81% with an associated higher solids content of 83% at the surface.

Figure 6 shows the average solids content gain from cyclic freeze-thaw dewatering and Figure 7 shows the average solids content gain from cyclic-wetting drying phase over five seasonal cycles. Overall, evaporation dewatering contributed higher gain in solids content compared to the freeze-thaw consolidation in the lab. Average solids content gain with respect to the entire sample profile due to freeze-thaw dewatering declined with each subsequent freeze thaw cycle for two of the three temperature gradient samples (0.083°C/mm and 0.056°C/mm). On the contrary, the average solids content gain from atmospheric drying-wetting cycles did not follow any trend since it depends on the meteorological parameters.

DISCUSSION

The measured thaw strain as shown in Figure 1 shows that each of the samples experienced the largest thaw strain at its first cycle. During freezing, water migration took place in upward direction (top down freezing) towards the freezing front due to the suction generated beneath the front that causes the unfrozen soil to contract followed by a significant volume reduction (Nixon and Morgenstern 1973). Thermal contraction also contributed to this volume reduction (Othman and Benson 1992). In the closed system freezing, the migrated water from within the tailings causes the formation of three-dimensional reticulate network of ice lenses that eventually becomes conduit channels for upward water migration and forms a metastable soil structure upon thawing (Beier and Sego 2009, Proskin et al. 2012). The volume of water released during freeze-thaw cycles was attributed directly to the increase in solids content and subsequent gain in shear strength. However, the volume reduction upon melting became less significant with subsequent cycles due to the loss of moisture caused by the intermediate drying-wetting cycles and thus, led to a lower thaw strain. Nevertheless, the sample subjected to lower temperature gradient (0.028°C/mm) continued to release a significant volume of water beyond second freeze-thaw cycle and this can be attributed to its temperature boundary condition. Lower temperature gradient is expected to lead to greater moisture content reduction since it allows the freezing front to advance slower and thereby, attracts more unfrozen water towards the front by suction (Knutsson et al. 2016). In addition to this, the contribution of polymer is believed to maximize the depth of moisture reduction. During multiple

freeze-thaw processes, polymer is subjected to high shear stresses. This tends to increase the collision probability between the particles with polymer, and thus, the stability of polymer can be disrupted (King et al. 1969). The optimum flocculation of polymer is highly dependent on pH and the conductivity of tailings particles and the change in pH is, in turn, highly dependent on the changes in temperatures. Lower pH and higher ionic concentration facilitate polymer adsorption which, in turn, causes double layer compression and results in increase in solids content (Mitchell and Soga 2005). Apart from volume reduction due to freeze-thaw cycles, it can be hypothesized that polymer may have a contribution to further dewatering. The effect of multiple freeze thaw cycles on pH and electrical conductivity of the identical sample was illustrated in Rima and Beier (2018, in press) and thus, was not repeated here.

Figure 2 and Figure 3 illustrate the effect of seasonal cycles (freeze-thaw cycles and drying-wetting cycles) on the average solids content and gain in surface shear strength, respectively. As expected, computed average solids content and measured shear strength of the investigated samples were all improved through cyclic freeze-thaw-drying process. It is important to note that the solids content and in-situ strength enhancement is dependent on the efficient removal of free melt water accumulated at the surface. Once exposed to the atmosphere, thawing of frozen tailings in spring and atmospheric drying in summer season contributes to the increase in solids content and shear strength, provided adequate drainage is ensured (Beier and Sego 2009). Since water has a greater heat capacity as compared to the tailings particles, effective water removal from the surface through efficient drainage system is paramount to maximize the freezing depths. The higher freezing depths facilitates higher moisture migration and thus, a higher solids content and undrained shear strength at the surface is expected. However, both the computed average solids content (as shown in Figure 2) and undrained shear strength (as shown in Figure 3) corroborated well with the finding that lower temperature gradient led to higher moisture reduction and higher increase in undrained shear strength.

Figure 4 illustrates the effects of seasonal weathering contributing to the change in solids content and shear strength over time. As discussed earlier, freeze-thaw process facilitates formation of a three-dimensional reticulate network of ice lenses which eventually develops larger pores and promotes dewatering upon thawing (Proskin et al. 2012). On the other hand, evaporation drying promotes surface desaturation that contributes to the volume shrinkage and cracking (Innocent-Bernard 2013). The formation of surface cracks increased the surface area for evaporation that eventually disrupted the sample integrity and accommodated rainfall. As a result, evaporation was never ceased during the formation of crust, albeit it may have affected by the accumulation of salt at the surface which was visually observed during the test. Each drying cycle improved the strength properties by two times higher as compared to each freeze-thaw cycle. As expected, the sample subjected to lower temperature gradient (0.028°C/mm) exhibited higher shear strength and exceeded a value of higher than 110 kPa at the starting of 4^{th} drying cycle. Upon drying, the induced wetting event caused re-wetting of surface that led to the dissolution of salts and appearance of large number of new microcracks. As a result, the heterogeneity of the sample was intensified, and the sample almost completely lost its shear strength at the surface. The drying after re-wetting event, therefore, exhibited lower solids content and subsequent lower shear strength as compared to the initial drying phase of each cycle. However, the treated centrifuged tailings sample underwent transition from slurry to solid as the solids content of the tailings exceeded 80% at the surface. In this stage, the sample started to become unaffected by the wetting phase due to the presence of surface crust. The sample subjected to lower temperature gradient (Figure 4a) developed a surface crust with an associated shear strength of over 110 kPa at its 4^{th} initial drying cycle. The collapse of this developed crust was not observed due to re-wetting of the sample. As a result, the sample retained relatively higher solids content (computed value >84%) and the strength remained unchanged (>100 kPa) after an initial drop on the day of wetting. Conversely, the sample with a temperature gradient of 0.056°C/mm (as shown in Figure 4b) reached to an average solids content exceeding 80% at its fifth after drying cycle (after 5^{th} cycle wetting event) with an associated undrained shear strength of over 110 kPa. Therefore, this sample could not remember its stress history throughout its 5^{th} seasonal cycle. The dewatering and strength gain performance for the sample with a higher temperature gradient (0.083°C/mm) is critical to seasonal weathering and the sample was not able to reach to an average solids content exceeding 80% after fifth drying cycle. This sample is far below the

transition phase from slurry to solid with an associated shear strength of 35.6 kPa. Therefore, the number of cycles required for this sample from slurry phase to solid state is currently under investigation in the laboratory. However, the final solids content profile of the samples (as shown in Figure 5) correlated well with the computed average solids content values. The higher solids content crust (89% at the surface for the samples subjected to temperature gradients of 0.028°C/mm) with shear strengths over 110 kPa, though relatively thin of approximately 2 cm, appeared to form low permeability zones that impeded infiltration and formed a separate zone from the underlying relatively lower solid content regions. Conversely, the crust was less distinguishable and less pronounced for the sample with a temperature gradient of 0.056°C/mm, thus, the sample behaved more uniform as evident in Figure 5 (less variation in solids content throughout the profile).

Figure 6 and Figure 7 illustrate the relative contributions of freeze-thaw cycles and drying-wetting cycles towards sample dewatering. Each of the samples experienced the largest solids gain (4.25% gain on an average) in its first freeze-thaw cycle. Afterwards, the volume reduction due to freeze-thaw process became insignificant. Conversely, the contribution of evaporation drying-wetting cycles is predominantly dependent on the metrological parameters including air temperature, relative humidity and wind speed (Newson and Fahey 2003). Therefore, the contribution of drying-wetting cycles was varying depending on the time period of the laboratory testing. On an average, the gain in solids content from each evaporation drying-wetting cycle varied from 3.5% to 4%. Overall, drying-wetting cycle was found to be the largest contributor of the solids content gain, followed by freeze-thaw cycle.

CONCLUSION

Cyclic freeze-thaw and drying-wetting tests in the laboratory showed that the undrained shear strength of the treated centrifuged tailings can be increased by simply exposing the tailings to the atmosphere. The thaw strain and the subsequent increase in solids content and undrained shear strength during freeze-thaw cycle is predominantly dependent on the temperature gradient, freezing rates and the number of freeze-thaw cycles, provided melt water is removed. On the other hand, drying wetting cycles are affected by the metrological properties in the field. The drying-wetting phase contributed to the largest solid content gain (4.25% solids content gain on an average) followed by the freeze-thaw cycles (approximately 2% gain with respect to the entire profile). The combined five freeze-thaw-drying-wetting cycles were able to develop a surface crust with a solids content of over 84% and an associated shear strength of over 110 kPa. Once the sample exceeded this value, it started behaving like a soil and the strength remained unchanged (>100 kPa) even after the wetting event to simulate rainfall. Overall, in an effort to provide a geotechnically stable landscape in a timely manner for colder climate like Western Canada, the physical processes such as freeze-thaw, and drying mechanisms can be considered to further improve the dewatering rate of centrifuged tailings, provided adequate drainage is ensured to allow for the increase in solids content and shear strength through the expulsion of pore water.

ACKNOWLEDGEMENTS

The authors would like to thank the Natural Sciences and Engineering Research Council of Canada (NSERC), Canada's Oil Sands Innovation Alliance (COSIA) and Alberta Innovates – Energy and Environment Solutions for their financial support of this research.

REFERENCES

Beier, N. A and Sego, D. C. (2009). Cyclic Freeze-Thaw to Enhance the Stability of Coal Tailings, Cold Regions Science and Technology, **55**(3): 278-285.

Innocent-Bernard, T. (2013). Evaporation, Cracking, and Salinity in a Thickened Oil Sands Tailings, MASc. Thesis, Department of Civil and Environmental Engineering, Carleton University, Ottawa, ON, Canada.

King, A. P. and Naidus, H. (1969). The Relationship between Emulsion Freeze-Thaw Stability and Polymer Glass Transition Temperature. A Study of the Polymers and Copolymers of Methyl Methacrylate and Ethyl Acrylate, Journal of Polymer Science Part C, **27**(1): 311-319.

Knutsson, R., Viklander, P. and Knutsson, S. (2016). Stability Considerations for Thickened Tailings due to Freezing and Thawing, Proceedings of the 19th International Seminar on Paste and Thickened Tailings, Santiago, Chile: 567-577.

Mikula, R. J., Munoz, V. A. and Omotoso, O. (2008). Centrifugation Options for Production of Dry Stackable Tailings in Surface Mined Oil Sands Tailings Management, Journal of Canadian Petroleum Technology, **48**(9): 19-23.

Miller, W. G., Scott, J. D. and Sego, D. C. (2010). Influence of the Extraction Process on the Characteristic of Oil Sands Fine Tailings, Journal of Canadian Institute of Mining, Metallurgy and Petroleum, **1**(2): 93-112.

Mitchell, J. K. and Soga, K. (2005). Fundamentals of Soil Behaviour, 3rd Edition, John Wiley and Sons Inc., New York, NY, USA.

Newson, T. A. and Fahey, M. (2003). Measurement of evaporation from saline tailings storage, Engineering Geology, **70**(3-4): 217-233.

Nixon, J. F. and Morgenstern, N. R. (1973). The residual stress in thawing soils, Canadian Geotechnical Journal, **10**: 571-580.

Othman, M. A. and Benson, C. H. (1993). Effect of Freeze-Thaw on the Hydraulic Conductivity and Morphology of Compacted Clay, Canadian Geotechnical Journal, **30**(2): 236-246.

Proskin, S. A. (1998). A Geotechnical Investigation of Freeze-Thaw Dewatering of Oil Sands Fine Tailings, PhD Thesis, Department of Civil and Environmental Engineering, University of Alberta, Edmonton, AB, Canada.

Rima, U. S. and Beier, N. A. (2018). Evaluation of Temperature and Multiple Freeze-Thaw Effects on the Strength Properties of Centrifuged Tailings, 71st Canadian Geotechnical Conference, Edmonton, Canada. In press.

Session 8

REGULATORY

COMPLIANCE WITH TMF OBJECTIVES – FACT OR FANTASY – AN INDIGENOUS PEOPLES' PERSPECTIVE

Jim Blum, Independent Consultant
with the support of Margaret Luker and Dan Stuckless, Mikisew Cree First Nation,
Cam MacDonald via Gillian Donald, Fort Chipewyan Métis Local 125,
and Jodi McNeill, Pembina Institute

ABSTRACT

The first regulatory approach to dealing with the dispersed fines resulting from oil sand processing was Directive 074. Compliance was predicated on strength criteria with respect to time. There were some shortcomings; the most obvious being that the Operators were unable to meet the strength requirements.

Directive 085 (D085) was introduced in conjunction with the Tailings Management Framework (TMF) with the intent to control the growth of fluid fine tailings (FFT) – widely perceived as a blight on the landscape. The regulation distinguishes between "new" and "legacy" tailings and specifies allowable profiles within which FFT volumes must fall.

Much of the prescription in D085 is at the discretion of the Operator. The allowable profiles are based on multiples of annual FFT production – as defined by the Operator. FFT is removed from inventory when it meets specified criteria – as defined by the Operator. And in a twist reminiscent of the adventures of Alice in Wonderland – a fluid can become non-fluid – as defined by the Operator.

Reviewing the newly submitted Tailings Management Plans (TMPs) is hampered by lack of transparency and consistency. For example, fines production must be derived from mine ore plans on a mass percentage basis, adjusted by connate water assumptions, reduced by probable beach capture and converted to a volumetric basis using assumed slurry densities.

Many technologies have been incorporated in the plans; but none lead to a dry landscape in a reasonable timeframe. But most damningly – the intent of D085 to constrain the growth of FFT is refuted by studies showing volumes will continue to grow for the next 20 years. This continued growth inevitably prolongs the reclamation timeline.

INTRODUCTION

Disclaimer

The Author is not a spokesperson for the Indigenous Peoples in the area affected by oil sand mining operations. However, he has been engaged by them, principally the Mikisew Cree First Nation, since the fall of 2016 to provide tailings advice. In this capacity, the Author obtained consent from two of the affected Peoples to present a perspective on the extent to which their objectives were being met.

Background

Directive 074 (D074) was introduced with specification that fine tailings be treated to achieve certain strength criteria be within a given time frame. It rapidly became apparent that no Operator could achieve the requirements and the D074 was scrapped. The most positive gain from D074 was that the Operators realized the advantages associated with pooling research knowledge, leading to the development of COSIA (Canada's Oil Sand Innovation Alliance). This was actually a culmination of previous cooperative efforts including the Fine Tailings Fundamentals Consortium, the Canadian Oil Sands Network for Research and Development (CONRAD) tailings group and the Oil Sands Tailings Consortium. However, these groups met on an ad hoc basis in various loaned locations; whereas COSIA has extensive staff and a fixed location.

The TMF was rolled out in 2015, followed by D085 in 2016. This included a presentation at IOSTC 2016 (Tania da Silva – AER). D085 represented the device by which the intent of the TMF would be administered. Objectives espoused included limiting the growth of FFT; coupled with expediting a return to a reclaimed landscape.

A requirement of D085 was that each Operator was required to file a new TMP indicating compliance

with the letter of the D085 and the intent of the TMF. The affected Indigenous Peoples, as accredited stakeholders, or as they prefer, Rightsholders, were entitled to an opportunity to review and make recommendations on the TMPs.

It is important to note that while advances are being made in handling FFT, no fines dominated field scale deposit has been reclaimed.

THE QUESTION

The question most often put to the Author in respect of the work on TMPs is: “what do the Indigenous Peoples want?”

The simple answer is the same thing that all Albertans and all Canadians should want; that the provisions of D085 be enforced in a manner that slows or eliminates the growth of FFT and a speedy return of affected areas to a close approximation to the pre-disturbance landscape. Additionally, as Rightsholders, they want consultation; **and they want their recommendations to be acted on.**

In returning the landscape, it is understood that the Approvals typically refer to an equivalent landscape, not an exact replication. However, this may present fresh problems when site specific uses such as traplines are considered.

The corollary to the previous question is: “what do they not want?” The prime dislike is the potential for a plethora of end-pit lakes (EPLs) or similar, particularly any which contain deposits of FFT.

THE PROBLEMS

FFT Profile

The Pembina Institute has prepared a profile for FFT accumulation based on the approved (or pending) profiles submitted with TMPs under D085. Clearly the total accumulation continues to rise for a number of years, peaking in 2037. There are a number of sharp drops in the accumulated FFT; it is important to understand that these do not represent acceleration in treatment, but rather transfers out of the FFT inventory into pit lakes for water capping.

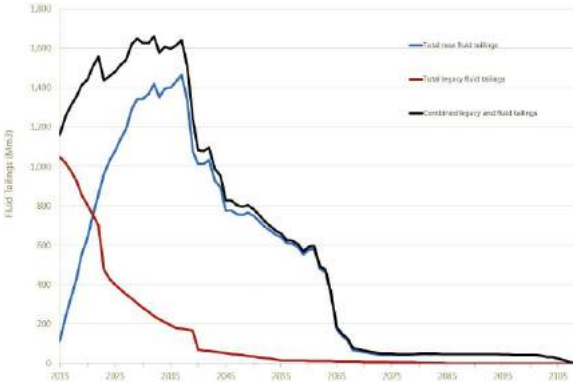

Courtesy of Jodi McNeill (Pembina Institute)

Now refer below to the profile submitted by AER at the last Conference. The graphs are not directly comparable because the Pembina graph is cumulative for all filed TMPs, whereas the AER graph is for a hypothetical mine with legacy tailings. Both charts show new FFT as a blue line and legacy FFT as red. But whereas the black line on the Pembina chart represents the sum of new and legacy FFT; the yellow line on the AER chart is a hypothetical zero treatment line.

The key difference here is that the AER chart envisaged that legacy drawdown should match new FFT production for zero net growth; whereas the Pembina graph based on actual filed and approved profiles shows a steady increase in inventory for another 20 years.

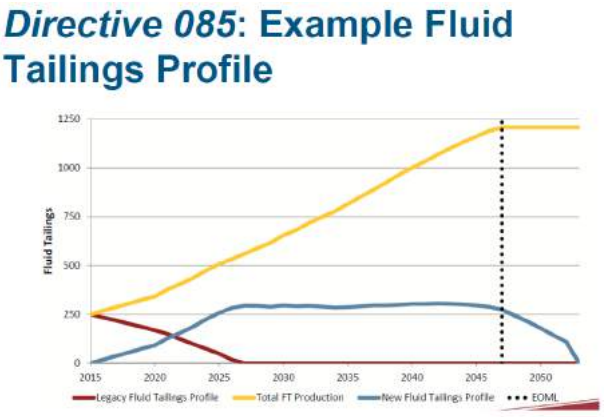

The AER will set thresholds including a profile deviation trigger, total volume trigger, and total volume limit for approved profiles

Features of the AER curves include steady drawdown of legacy FFT commencing with the implementation of D085, a significant zero growth component to the new FFT inventory representing treatment at a rate equal to production, followed by a steady reduction post mine closure. Examination

of the approved TMPs for the 6 operations that have a legacy TMP inventory shows that 5 of them rely on transfers to water-capped deposits with little or no treatment; and that 4 of these transfers occur at or near end-of-mine life.

The Misuse of the RTR Criteria

'Ready to Reclaim' is probably the most compromised term in the TMF and D085. The **intent** of the term is that the designated material is on a trajectory to being reclaimable. However, it is applied in a manner which leads to an alternative interpretation as 'Removed from Inventory'.

FFT is defined in the Regulations as >5% solids by mass and <5kPa undrained shear strength. Many of the submissions include either water-capped FFT or deep fine-grained deposits of treated FFT. The former has a limiting value of about 35-40% solids by mass; the latter is typically deemed RTR at 50-55% solids. This material needs to achieve a solids content of about 75% to reach 5kPa strength. In the case of water-capped material this will never happen. A deep fine-grained deposit will take hundreds of years to achieve this value even with surcharging; while the ongoing deformations may be up to 1/3rd of the depth of the deposit. This is further discussed under deep fines-dominated deposits.

The effect of this is that the Pembina Institute significantly underestimates the actual FFT volumes in future storage; because the RTR criteria as approved by the Regulator **allows fluids to be removed from inventory while still fluid**.

The 'Magic Sand Box'

This section applies to plans based on CT (composite tailings). For the uninitiated this is mix of recycled FFT at say 30% solids, with cyclone underflow tailings (predominantly sand) and gypsum as a coagulant. The ratio of sand to fines in this mix is termed SFR. To achieve a geotechnically competent deposit the proponent suggests a planning basis for an SFR of 4:1.

The proponent submits an ore feed plan for the life-of-mine which averages an SFR of slightly less than 4:1. Some significant portion of the tailings material is used for dike construction and sand capping; let's call this 50%. Experience indicates that this sand will retain some fines at an SFR of about 7:1. The proponent suggests a higher value for fines retention at an SFR of 5.5:1.

There will be a significant sand shortfall for CT production regardless of which value is used. This issue was raised at the Enhanced Review Process for the Aurora TMP. Rightsholders requested that SFR be made part of the RTR criteria. **The request was ignored because the proponent can't possibly meet it.** In arguing against this – the proponent introduced data on existing deposits showing most of the CT material deposited falls in the range 2:1 to 3:1 SFR. The issue here is in part that CT at a lower SFR is likely to gain strength more slowly and be subject to more settlement than CT at a higher SFR. But more importantly, why is a proponent permitted to put forward specifications in a submission which they know to be erroneous? In addition, the COSIA Technical Guide for FFT Management specifies SFR as a Primary Performance Indicator for fines enriched sand deposits.

Lack of Specification

As previously noted, there is a specification for FFT in the Regulations. There are also specifications for the maximum permitted or peak volume of FFT that can be accumulated on a site; and a specification for the maximum volume allowed to remain at the close of mining, to be RTR within 10 years. This latter volume is termed EOML for "end-of-mine life".

These volumes are based on multiples of what is called annual FFT production. Multipliers of 3-10 years for peak and 5 years for EOML are specified. Interestingly, neither the TMF nor D085 indicate just what defines annual FFT production.

Since this annual value is crucial to analysis of TMPs, the Author developed his own formula. This considered the requirement from the suspended D074 which required capture of 50% of fines over and above those which would be expected to be capture in a "normal" tailings operation.

The latter volume is derived from the mass of fines contained within the ore feed taken from the mine plan in any given year. The assumption is made that all these fines are processed with the ore and report with the "whole" tailings stream. It is assumed that in accordance with Industry experience, 55% of these are captured in dikes and/or beaches. The remainder carry on to form FFT. The mass of fines is converted to an FFT volume using 35% solids by weight.

The resulting profile for FFT generation agrees remarkably well (within 10%) of the numbers

supplied in the TMPs. (Note: the Author has reviewed Fort Hills, Frontier, Horizon and Horizon NPE, Aurora North, Kearl, MRM, Jackpine, Suncor and Syncrude MLX).

To date no Operator has challenged the result. This leads to the inevitable conclusion that the derivation is favourable to the Operator! There is an obvious simplification which is that FFT does not reach 35% in the year of formation. However, attempting to rectify this is an unnecessary complication over a 30 or 40-year mine life. A greater issue is when an Operator specifies the capture of FFT as a volume within CT without specifying SFR, thereby rendering the mass of fines incalculable.

A similar problem arises with the expression of tailings profiles in terms of millions of cubic metres of FFT, while expressing mine plans in millions of tonnes of fines. Conversion involves unspecified (by D085) attributes. The calculation is further complicated by the absence of an actual tonnage of fines in the ore feed; instead fines are expressed as a percentage of the mineral; which has to be extricated from the ore tonnage less the bitumen and connate water, which latter item is often not specified.

End-Pit Lakes

The Author recognizes that EPLs are an integral part of a reclamation landscape and provide passive water treatment for surface runoff for the future. Rightsholders do not agree necessarily, as the types of EPLs proposed are not a natural feature of the landscape. The concept that the lakes are needed for treatment of potentially contaminated runoff does not sit well with the end user. An additional concern exists regarding the proximity of some EPLs to the Athabasca River, but the greatest concern is that many of these proposed EPLs are destined to contain either treated or untreated FFT.

The Regulator has not approved EPLs as long term FFT storage facilities as yet. In addition, the Regulations require Proponents to provide an alternative means of disposal of EOML volumes of FFT that do not involve water capping. To date no Application incorporating end-pit lakes for FFT storage has provided such an alternative. AER has picked up on this and has issued requests for such alternate plans to be filed, but within excessive time periods, such as by the end of 2025.

Meanwhile Industry is proceeding with a commercial scale experiments (Base Mine Lake and Demonstration Pit Lake) to show that there may not be detrimental effects from storing water capped FFT indefinitely. From the perspective of Indigenous Peoples, this looks as though the Regulator expects a favourable result from the BML experiment, thereby relieving Industry of the need to comply with the need for an alternate technology.

Insult is then added to injury. One Application proposes to retain the pre-existing Legacy FFT volume throughout the remaining life of the mine. In the interest of accuracy, the FFT volume is drawn down slightly in the first 2 years as a source of densified FFT to be used as feed to a CT plant. Volume reduction of the remainder occurs through a small ongoing increase in solids content.

In the penultimate year of operation, the remaining Legacy FFT is pumped to a second EPL to be water capped. In this way it is made to “disappear” (said Alice). The fact that it is still fluid, and thereby FFT, is ignored because it is now “RTR” (in its final location and ready to be water-capped). It can only be presumed that “treatment” constitutes running it through a pump. While this proves that it is still fluid – the Proponent “doesn’t see it this way”! The Author perceives this as a travesty of the Regulations. AER does not!

This “approved” process circumvents treatment, reclamation, and the limit on EOML volume.

Deep Fines-dominated Deposits

A number of submitted TMPs utilize deep fines-dominated deposits. Typically, these result from either centrifuged or in-line flocculated (ILF) processes. RTR criteria may be 50 or 55% solids by weight. Some of these deposits are intended to be water-capped; others are intended for terrestrial closure; but with no real plan as to how this might be achieved.

This “RTR” material is in fact still fluid. The transition from a regime subject to the laws of fluid mechanics to a regime governed by soil mechanics occurs at an undrained yield strength of about 5kPa – **as specified by the Regulator in D085.** This corresponds to a solids content in the range of 70 to 75% solids by weight; which in turn conveniently translates to about 50% solids by volume. This can be expressed as 1 volume of water to one volume of solids. At the RTR condition, the solids content by volume translates to about 2.5 volumes of water to

one volume of solids. Without entering into a complicated analysis of settlement, it is readily apparent that the overall volume will decrease by about 1/3rd. In the case of a 60-metre-deep deposit, settlement will approach 20 metres, and this will occur over hundreds of years.

In the event that the proponent does succeed in capping the deposit, some settlement will occur as a result of surcharging. However, the "finished" landscape will be subject to considerable deformation over time (again, hundreds of years). Note that Suncor Pond 5, at an SFR > 1:1 has been undergoing surcharging and drainage for about 10 years already. Capping with reclamation material is scheduled to begin in 2035. The proposed deposits have a lower SFR and will be less permeable, leading to longer timelines to reclamation.

Innovation, Industry and COSIA

Innovation, or lack of it, deserves mention. Most of the technologies currently advertised in the TMPs have been around for some time. CT has a 35-year plus life, from concept, through piloting and field trial to full scale implementation. Thickening research began about 30 years ago with the first commercial units commissioned at MRM in 2002, followed by high density units at Horizon. NST was conceptualised during design of MRM, about 20 years ago, but not implemented until Horizon. Centrifuging and In-Line Flocculation each have slightly over 10 years of history behind them.

So what's new. This is hard to uncover as COSIA is not exactly forthcoming. Attendance at the COSIA Technical "Expo" is expensive, not for Indigenous Peoples, but for their consultants, and most of the information is dated. Canadian Natural has hinted at the implementation of selective mining and in-pit extraction; hopefully a paper will appear at this conference. These were both concepts outlined in the Tailings Road Map put out by the consortium of Oil Sands Tailings Consultants (OSTC), also 10 years ago. Tailings filtration by vacuum filter belts (back in the last century), by belt presses and by slotted pipe (both in the last 10 years) have been tested; but have not been implemented.

One promising technology which has been effectively buried within COSIA is thermal drying; which has been presented at previous conferences using 2 similar approaches. The fundamentals use hot exhaust gas from a burner to dry centrifuge cake. The details are in the proceedings. The product is dried to any required moisture content; which is achieved by mixing the 100% dry output with a percentage of feed. The exhaust gas contains all the moisture driven off; which can be condensed to provide hot water. Studies have been performed on both economics, carbon intensity and condensate quality. Indigenous Peoples are aware of these and have requested copies of reports, most recently during the Aurora North Enhanced Review Process; but nothing has been received.

Any attempt to resurrect this technology is stalled by the GHG argument. While this is partially valid; it needs to be considered as part of the solution. The Indigenous Peoples most closely affected by the fine tailings issue are resident in the midst of what is probably the largest CO_2 sink (the boreal forest) in North America. Arguably from their perspective the FFT problem outweighs GHGs. And one proponent is extolling the positive effects of introducing CO_2 into the tailings stream to enhance recycle water clarity! So is CO_2 useful, or not? The CIM Magazine published a recent article on a CO_2 capture technology using hot water as a heat source for the process, suggesting that exhaust from thermal drying could generate a CO_2 stream for injection into a tailings stream.

Another study, carried out by the Civil Engineering Faculty at U of C, addressed addition of commonly available material (termed geopolymers) that can be added to centrifuge cake to improve trafficability. This program has stalled because although U of C considers the results promising, the Intellectual Property is owned by a company no longer active in this area; thus, the IP cannot be released for the work to continue.

The Enhanced Review Process (ERP)

About one year ago an ERP was conducted in Edmonton over a period of 3 days between Rightsholders and Syncrude. The sessions were conducted under the eyes and ears of the Regulator and included court stenographers. It was made apparent at the outset that the forum was for discussions between Rightsholders and the proponent, Syncrude. The Regulator took the position of observer.

A number of arguments arose, in particular: the need for SFR to be a criterion included in the criteria for RTR, the issue of removal of Legacy FFT from inventory in the penultimate year of mining by transfer with no treatment, and the issue of designating material RTR and hence removed from

inventory, while it was clearly still fluid, with no reasonable expectation that this would change.

As stated by AER, they would not engage in these discussions; and subsequently their Approval made no reference to the Rightsholders concerns. It was, therefore, of some interest to note that the recent judgement by the Federal Court of Appeal in the case of Trans Mountain, stated that “the role of the NEB should not have been merely as note takers”. This in part formed the basis for rejection of the Kinder Morgan Project due to inadequate consultation.

SUMMARY

At the time of writing, the Author is unaware of any field scale successful reclamation of a fines dominated deposit.

New FFT inventories continue to rise, predicted by Industry to reach almost 1,500 Mm^3 by 2037.

The peak volume is under-represented as considerable quantities are removed from the inventory while still fluid, often with no prospect of becoming reclaimable as a dry landscape within generations.

SFR, while specified by COSIA as a required performance measure for CT type deposits, is not being incorporated into either TMPs or Approvals, despite Rightsholders requesting this. Consequently, deposits are allowed that will not perform as well as they should.

While FFT production is key to determining allowable FFT profiles, there is no specified method for computing the value. The procedure employed to check volumes provided in TMPs is of necessity rife with assumptions.

End-pit-lakes are utilized in a majority of applications to store residual volumes of FFT over the objections of Rightsholders. Alternative processes are required under the D085 but have not been provided.

Returning the landscape to an equivalent condition, rather than exact, will be problematic where established prior use such as traplines existed.

Deep fines dominated deposits form the basis for a number of submissions, without any consideration as to how these will be capped, and the degree to which settlement will affect the closure landscape. Timelines to revegetation will be excessive.

Industry does not appear to be coming up with any new technologies, while promising alternatives are not being pursued.

The Regulator needs to place more importance on concerns raised by Rightsholders, and engage, and not to fall back to the position of “note taker”.

REFERENCES

Da Silva, T. (2016). Technical Approach to Regulating Fluid Fine Tailings in Alberta. International Oil Sands Conference.

COSIA. (2012, August 30). Technical Guide for Fluid Fine Tailings Management. Section 5.5.1, pp. 5-10.

Lopez-Pachero, A. (2018, September 12). CIM Magazine Innovation rush in the oil sands.

OVERVIEW OF CURRENT STATE OF PRACTICE FOR CLOSURE OF TAILINGS DAMS

Haley L. Schafer, Neeltje Slingerland, Renato Macciotta and Nicholas A. Beier
University of Alberta, Edmonton, Canada

ABSTRACT

The mining process produces slurry wastes known as tailings, which are stored in containment structures called tailings dams. Following mine closure, tailings dams are subject to natural forces as the dam transitions into a landform that is compatible with the natural landscape. This poses a significant technical and regulatory challenge as tailings dams that are designed to be safe during the mine's active life also need to perform safely long after mine operations are finished. Underperformance of these structures can result in significant risks to public and environmental safety, as well as impacts to future land use and economic activities in the vicinity of such structures. To prevent failure of these large structures after mining, their long-term behavior must be understood and incorporated into closure design, ideally from its conception and initial design. Challenges lie in the limited information available regarding how these structures age over time and forecasting loading and environmental scenarios over long time periods (weather events, seismicity, human activity, etc.). Ultimately, the goal of tailings dam closure is to reduce future risk of failure to the environment and public to a degree that is both practical and economical. This paper presents a summary of the current state of practice for closure of tailings dams nationally and internationally.

INTRODUCTION

A number of significant tailings dam failures have occurred over the last six years, including the Obed failure in Alberta in 2013, the Mount Polley failure in British Columbia in 2014, Fundão failure in Brazil in 2015, the Cadia failure in Australia in 2018, and the Cieneguita failure in Mexico in 2018 (Bowker and Chambers 2017, Wise 2018). The consequences of these failures have varied greatly from limited loss of containment to fatalities and extensive contamination. These consequences have also been accompanied by considerable financial losses, loss of social license to operate, and others. Furthermore, the work presented by Bowker and Chambers (2017) suggests that the number and severity of tailings dam or tailings storage facility (TSF) failures are expected to increase.

Overtopping, slope instability, and earthquakes are considered the top three causes for active tailings dam incidents, with additional causes including foundation instability, seepage, structural inadequacies, erosion, mine subsidence, and unknown causes (ICOLD Committee on Tailings Dam and Waste Lagoons 2001). The five tailings dam failures listed previously could be attributed to one or more of these causes. However, root cause analysis of the Mount Polley failure revealed that the root causes of failure were primarily organizational in nature, indicating deficiencies in the safety management system (MEM 2015). In the case of the Obed failure, a similar conclusion can be reached, as the specified operational water level in the pit was exceeded continually throughout operations and a spillway was never constructed despite being specified in the design (Provincial Court of Alberta 2017).

In their evaluation of the underlying causes of tailings dam failures and incidents, the ICOLD Committee on Tailings Dam and Waste Lagoons (2001) noted that it was lack of consistency and attention to detail which led to a high incident frequency. This further highlights the need for robust tailings dam safety management systems and opens a question regarding their implementation and compliance for tailings dams after closure. In this regard, a number of tailings dams in the oil sands have reached or are close to the end of their active service life (OSTDC 2014). These structures are at various stages in closure and some may be attempting to undergo delicensing as dams in the coming years.

Tailings dams in the oil sands industry are complex structures due to a number of key characteristics, including (OSTDC 2014):

- Upstream construction is used extensively. However, construction may occur with a

combination of the upstream, downstream, centreline, and modified centreline methods.
- Dams may be constructed with hydraulically placed tailings or compacted fill from overburden and interburden material, tailings sands, coke, or a combination.
- The type and characteristics of tailings deposited varies greatly and continues to change throughout time technology develops.
- Dams are often constructed on weak foundations resulting in flat slopes and very large structures.

The large size of these structures and the variation in construction method, construction materials, and tailings contained all complicate the design and closure of these structures. Furthermore, earlier structures were designed for operating conditions, with consideration of failure mechanisms that could occur during the mine's active life. As a result, tailings dams in the oil sands industry pose a significant design challenge and can become a public and environmental hazard if not properly managed. In this regard, the regulatory regime needs to promote and facilitate the development of closure strategies that include a robust and sustainable safety management system.

In Alberta, tailings dams are regulated by the Alberta Energy Regulator (AER) under the Water Act and Water Regulation in the Dam Safety Program. The AER's Dam Safety program implements a risk-based approach to dam safety with an emphasis on dam safety management systems (Eaton and Paz 2016). Tailings dams in Alberta adhere to guidelines from the Canadian Dam Association (CDA) and the Mining Association of Canada (MAC). Oil sands operators are required to reclaim tailings ponds, mining sites, and other disturbed land to stable, resilient, functional ecosystems with a land use equivalent to the original landscape (although it may differ) as described in the Tailings Management Framework (Government of Alberta 2015). In this end game scenario, closure occurs and the land is certified such that it is transferred back to the Crown relieving the operator of ongoing obligations and responsibilities indicating a "walk away" scenario (Morgenstern 2012). The fact remains that there have been very few examples of successful walk away scenarios globally. As closure becomes more imminent, the need for clear guidance and regulation becomes more important, including the requirements for a strong safety management system.

This paper provides a review of the current state of practice for closure of tailings dams nationally and internationally. This includes an examination of closure regulations and guidelines from a technical and practicable viewpoint.

STATE OF PRACTICE

Several international and national committees and organizations exist whose aim is to advance the social and environmental performance of mine sites and tailings dams by outlining best available practices (Roberts et al. 2000). Following the best practices outlined by various national and international bodies may be optional, but laws and regulations for TSFs are not. Regulations can take a prescriptive approach which dictate methods and/or quantitative criteria to be achieved. Alternatively, regulations can take a performance-based approach and outline target performance levels to be achieved.

National

Regulations in Alberta, British Columbia (BC), and Saskatchewan will be discussed as well as guidelines from CDA (2014), MAC (2017), and OSTDC (2014). Regulation of dam safety in Canada is a provincial and territorial responsibility (CDA 2014). Guidance on dam safety is further provided by organizations such as CDA, MAC, and the International Committee on Large Dams (ICOLD) with specific reference made in regulations and guidelines to refer to these organizations for guidance on design throughout the life cycle of the dam, including closure (Government of Alberta 2016, MEM 2016, Ministry of Environment 2008). Alberta's proposed updated Dam Safety Guidelines also make reference to OSTDC (2014) for closure guidance. BC and Alberta, unlike Saskatchewan, both have dedicated mining dam safety programs with regulation and guidelines specific to the design of tailings dams, including closure. Al-Mamun and LePoudre (2016) conducted a review of national regulations for closure in the context of tailings dam delicensing.

Currently, the Government of Alberta is working to improve their dam safety regulatory system by issuing new Dam Safety Guidelines following the Mount Polley failure and the Auditor General of Alberta (2015) Report (Government of Alberta 2016). It is expected that the new guidelines will

move away from a prescriptive approach to dam safety noting that selection of appropriate factors of safety (FOS) should be based on careful site specific considerations such as the consequence of failure, uncertainty in material properties and subsurface conditions, implementation of an effective risk management system etc. (Government of Alberta 2016). In BC, mining dams are regulated by the Ministry of Energy and Mines under the Mines Act and the Health, Safety, and Reclamation Code (HSRC). In contrast to expected changes in Alberta, the HSRC specifies minimum design criteria for seismic and flood design, criteria for design slopes, and minimum static FOS with reference made to design in accordance with other guidelines (MEM 2016, 2017). The HSRC code and guidelines also have an emphasis on risk management practices and a tailings management system based on continual improvement using a cycle of planning, implementation, monitoring and surveillance, and review and improvement (MEM 2016, 2017). This commitment to a tailings management framework aligns with the guidance provided by MAC (2017). As discussed, Saskatchewan does not have a formal tailings dam safety program and does not provide information on design of TSFs for operation or closure.

All three provinces require mine operators to submit a reclamation and decommissioning plan for their mine site. Similar to Alberta, the expectation in BC is that the land is reclaimed such that the end land use capability is not less than before the mining operation existed with long-term physical and geochemical stability of the surrounding environment (Government of Alberta 2015, MEM 2017). In Saskatchewan, the objective is to reclaim to a standard that is safe for traditional land use with a condition that is consistent with the surrounding physical and biological environment requiring little or no maintenance (Ministry of Environment 2008).

Despite the lack of a dedicated tailings dam safety program, Saskatchewan has one of the most advanced systems for long-term management of mine sites (including TSFs) through their Institutional Control Program (ICP) (Ministry of Energy and Resources 2009). The ICP is a formal regulatory process for the long-term monitoring and management of provincial lands once a mine operator has fulfilled its decommissioning and reclamation obligations and the site has undergone custodial transfer back to the government (Ministry of Energy and Resources 2009). When the ICP takes control of a site, the control may be active and involve monitoring, surveillance, and remedial works or passive including land use restrictions, maintaining records etc. (Ministry of Energy and Resources 2009). The program will ensure that sites are monitored and maintained in accordance with the monitoring and maintenance plan submitted by the site holder using the funds provided by the site holder (Ministry of Energy and Resources 2009).

CDA (2014), MAC (2017), and OSTDC (2014) all have an emphasis on using risk-based approaches for tailings dam design and operation. The MAC (2017) guidelines emphasize the importance of a tailings management framework for safe, sustainable, and environmentally responsible management of TSFs throughout the entire life cycle, including closure and post-closure, with risk management as a key to success. MAC (2017) notes that long-term liability and risk can be reduced by designing and operating tailings facilities with a long-term view. Aligning with this, CDA (2014) recommends using a risk-based approach for assessing closure strategies especially given the expected time frames (passive care can last for hundreds of years). These lengthy design periods can make it difficult to design for closure due to potentially changing downstream populations, regulatory environments, etc. CDA (2014) provides minimum design criteria for inflow design floods, seismicity, and FOS for different stages in the life cycle with criteria becoming more stringent for the passive care phase. CDA (2014) notes that the designer and owner can increase beyond these levels if they wish to reduce the risk or can go lower if the regulator agrees. The tailings management framework provided by MAC (2017) is designed to be flexible so that it can adapt to changes that occur in the long-term and be used for different sites, owner policies, regulatory requirements, and stakeholders (MAC 2017).

According to CDA (2014) and OSTDC (2014), a dam may be delicensed as a dam if it is transformed into a permanently stable landform where the residual risks for the structure have been reduced to a level compatible with that of natural analogues. This principle aligns with the BC HSRC code which indicates that an operator may be released from permit obligations if the dam can be considered a landform (MEM 2017). In this way, the desired “walk away” condition could be achieved (CDA 2014). OSTDC (2014) provides a framework by which a tailings dam could be

Table 1. Summary of Key Aspects of National State of Practice

Alberta	British Columbia	Saskatchewan	MAC	CDA	OSTDC
• AER Dam Safety Program • Non prescriptive • Requires reclamation & decommissioning plan • Walk away closure • References CDA, OSTDC, ICOLD, MAC	• MEM Dam Safety Program • Prescriptive • Requires reclamation & decommissioning plan • Walk away closure • References CDA, ICOLD, MAC • Specifies minimum design criteria	• No dam safety program • Requires reclamation & decommissioning plan • Institutional Control Program • References CDA	• Risk-based • Tailings management framework • Sustainable development with a long-term view	• Risk-based • Specifies minimum design criteria	• Risk-based • Framework for dam delicensing based on transforming dam into a landform

transformed to a solid earthen structure and delicensed as a dam. This process is based on a performance and risk-based approach. An important element of this process is recognizing that natural areas in the oil sands area undergo geomorphic evolution that can result in slope instability, surface erosion, wave and river erosion, groundwater level fluctuation, fires, etc. (i.e. there is not zero risk in the natural environment) (OSTDC 2014). As such, the solid earthen structure will not have zero risk, but by transforming a structure into a solid earthen structure, the risk is reduced by reducing the consequences and probability of failure (OSTDC 2014). A summary of the key aspects discussed with regard to the national state of practice is provided in Table 1.

International

ICOLD, International Council on Mining and Metals (ICMM), United Nations Economic Commission (UNEC), and the International Standards Organization (ISO) are just a few of the international organizations undertaking work with respect to mine site and tailings dam closure to outline best available practices for mine operators. An overarching objective common to all is “sustainable development”, defined by the Brundtland Report as “development that meets the needs of the present without compromising the ability of future generations to meet their own needs” (World Commission on Environment and Development 1987). In line with this, MAC (2017) states that TSFs should be designed under the assumption that they are permanent landscape features, and ensuring that short-term benefits do not outweigh long-term risks.

A mounting body of evidence regarding the long-term costs of acid rock drainage, surface and ground water contamination, and air pollution resulting from poorly or improperly closed tailings dams has proven a powerful motivator in the industry. Concerns are predominantly related to water quality as physical stability is often assumed to increase over time. However, as DeJong et al. (2015) has noted, the geotechnical state of a tailings dam and its components can be altered over time. The growing expectation globally is that tailings dams be chemically and physically stable for a period in excess of 1000 years (ICOLD Committee on Tailings Dams 2013). This design life necessitates the use of regionally appropriate probable maximum precipitation (PMP) and maximum credible earthquake (MCE) events in geotechnical assessments, but also (and less commonly recognized) the cumulative effects of multiple events. Features such as spillways and surface drainage outlets should be designed with the same attention to detail as failure of these systems could result in failure of the closure landform.

The United States Surface Mining Control and Reclamation Act (SMCRA) (1977) outlines reclamation objectives, as well as construction, maintenance, and reclamation requirements for coal mines across the United States of America (USA). For example, tailings must be stabilized through construction of compacted layers with incombustible and/or impervious materials as necessary, such that they are stable and capable

of regrading to blend with surrounding natural contours (95th US Congress 1977). Ponded water held by a dam is permitted post-closure so long as the dam meets minimum stability criteria, pond size is appropriate to the use, and the water quantity and quality meet discharge criteria (95th US Congress 1977). Coal is primarily used by local power plants in the USA. As a result, while enforcing such an intensively prescriptive act is expensive, the costs can be directly passed to the consumer so as to not impede implementation (Roberts et al. 2000).

A similarly prescriptive reclamation method is exemplified in the Comprehensive Environmental Response, Compensation, and Liability Act (CERCLA), also known as the Superfund Program, introduced in 1980. Superfund has been widely criticized for being prohibitively expensive. The expectation is for sites to be cleaned-up to a pristine condition, regardless of risk or local context (Shanahan 1995). Due to the significant cost associated with this undertaking, only a small segment of sites on the national list have been completed (Shanahan 1995).

Due to the site specific nature of closure challenges, a performance-based approach is more typically chosen by regulators. South Africa requires that all land affected by mining operations be returned "to its natural or predetermined state or to a land use which conforms to the generally accepted principle of sustainable development" (Parliament of the Republic of South Africa 2002, 38.1d). The regulation goes a step further by holding directors of a mining company and members of a close corporation (a parent company, for example) jointly liable for any negative impact to the environment resulting from mining (Parliament of the Republic of South Africa 2002, 38.2). These types of performance-based approaches leave room for innovation and creativity while dictating end results.

In Western Australia, a performance-based approach is also taken; however, they require early and ongoing closure plan submissions, and reporting on TSF reclamation trials and/or research. This approach results in more regulator involvement. TSFs are decommissioned via the Environmental Protection Act (EPA) and TSFs are likely to be issued a "closure notice" requiring additional reporting, monitoring, and/or active maintenance after the dam is delicensed and considered a landform (DMP and EPA 2015). Relinquishment to the state is not typically considered where these closure notices have been issued (ANZMEC and MCA 2000). This system is most similar to the proposed approach in Canada and the Alberta oil sands.

Often in developing nations, no regulation exists; however, this is rapidly changing. Brazil, and in particular Chile, have recently updated their mine closure regulations. Chile now requires chemical and physical stability of all TSFs post-closure (Ministerio de Mineria 2015). In addition to international committee's best practices and government laws and regulations, mining companies may also be bound to the environmental management principles of their financial backers (World Bank and IFC 2002, Equator Principles Association 2013). A mining company operating in a country without regulation may still need to abide by certain social and environmental standards at closure as a result.

Globally, the trajectory in designing for closure of tailings ponds is towards providing physical and chemical stability for a 1000-year design life, such that the definition of sustainable development is met. Delicensing of tailings dams through conversion to an equal or comparable land use capability is typical in most countries with advanced regulation; however, relinquishment remains rare.

DISCUSSION

Nationally and internationally the state of practice for tailings dam closure varies. Regardless, the societal expectation for closure and reclamation is for sustainable mining practices. As discussed, Alberta, Saskatchewan, and British Columbia all have an expectation that the land should be returned to a state similar to the pre-mining land. While Alberta and BC require walk away closure, Saskatchewan has taken measures to develop regulation specific to long-term management of mine sites. In this way, they have developed a path by which companies can relinquish their site responsibilities. It should be noted that site holders do not completely discharge their liability after the site has been transferred to the ICP (Government of Saskatchewan 2009). While the push in global and national guidelines and regulations towards risk-based design and management is promising in allowing the industry to adequately design for closure, there has still been a lack of evidence showing its ability to support the desirable goal of

walk away closure. Morgenstern (2012) indicated that the current proposed walk away end game in the oil sands is likely not fit to achieve the desired goals. At the current time, the only area in the oil sands that has been returned to the Crown is an overburden dump referred to as Gateway Hill. This landform was chosen for its simplicity and the process still took about 10 years (Morgenstern 2012). In light of this, the question is if Alberta should be working towards developing an alternative to the current walk away end game such as the route taken by Saskatchewan which involves relinquishment and a perpetual care strategy. In the author's opinion, the goal for mine closure should be walk away closure; however, failure to plan for scenarios where this might not happen could be considered failure to uphold the public interest, a requirement under the APEGA (2013) Guideline for Ethical Practice.

The incoming changes to the Alberta Dam Safety guidelines are anticipated to have a performance and risk-based approach to dam safety; however, the table of contents provided by the Government of Alberta (2016) indicated that only one page of guidance would be provided on the closure of mining dams with reference made to MAC, CDA, OSTDC, and ICOLD for further guidance. The authors are currently conducting a series of interviews with individuals with experience with tailings dams. The authors asked what the major challenges in tailings dam closure in Alberta are, including the ability to delicense and attain a reclamation certificate. Individuals noted a number of key challenges in Alberta with the primary challenges being the fluid nature of the tailings, the inability to discharge water, the regulator, and long-term projections and time frame. This indicates that clarity is needed from the Alberta regulator on tailings dam closure guidelines and expectations.

The global trajectory for closure design is towards a 1000-year design life. The concept of "in perpetuity" (as presently assumed in Alberta) is difficult to fathom, especially as these structures are constantly evolving due to geomorphic processes. For reference, and in order to appreciate the task-at-hand, the following was happening on our earth roughly 1000 years ago: (1) the *real* Duncan, King of Scotland, was murdered by his cousin "MacBeth", the next King of Scotland; (2) Viking explorer Leif Eriksson discovered North America and named it 'Vinland'; and (3) cliff dwellings were the preferred form of housing in what is presently the state of Colorado (Mesa Verde). What will the future be in another 1000 years?

In terms of design targets and evaluation criteria, "perpetuity" is essentially the same as a 1000-year design life. Both necessitate the use of PMP events, MCE events, and other extremes for design. These are known (or readily determined) values. The remaining challenges are in designing dams that remain stable throughout the cumulative effects of nature over 1000 years, and in integrating climate change, for which reliable projections currently only extend to the year 2100. As shown in Figure 1, the mine life of least one oil sands mine extends beyond this date.

Guidelines and regulations have included the required implementation of a safety management system (SMS) for a number of years now as shown by guidelines provided by organizations such as MAC. SMSs are important throughout the life cycle of a tailings facility, including closure, for failure prevention. In light of the root causes of the tailings dam failures witnessed in the last few years, focus of SMSs may require a shift towards implementation, auditing, training and knowledge transfer, and safety culture. This shift may require changes in the organizational structure for closure to complement the technical expertise (risk managers, social relations experts, etc.). A strong SMS will aid in adapting to the uncertainty associated with the long-term behaviour and management of tailings dams. Alberta's Dam Safety Program expects dam owners to have a dam safety management system that adheres to the guidelines outlined by CDA and MAC (Eaton and Paz 2016). Dam owners are requested to perform a self-assessment on: management commitment to dam safety, emergency readiness, design process, construction process, surveillance process, and if the dam is performing as expected (Eaton and Paz 2016). The AER then assesses the dam safety management system based on management, complexity, records management, and performance (Eaton and Paz 2016). Further research in collaboration between AER and the University of Alberta is ongoing for enhancing the regulator's available tools for assessing the adequacy of operators SMS in light of the characteristics of their storage facilities and foreseeable conditions at and post-closure.

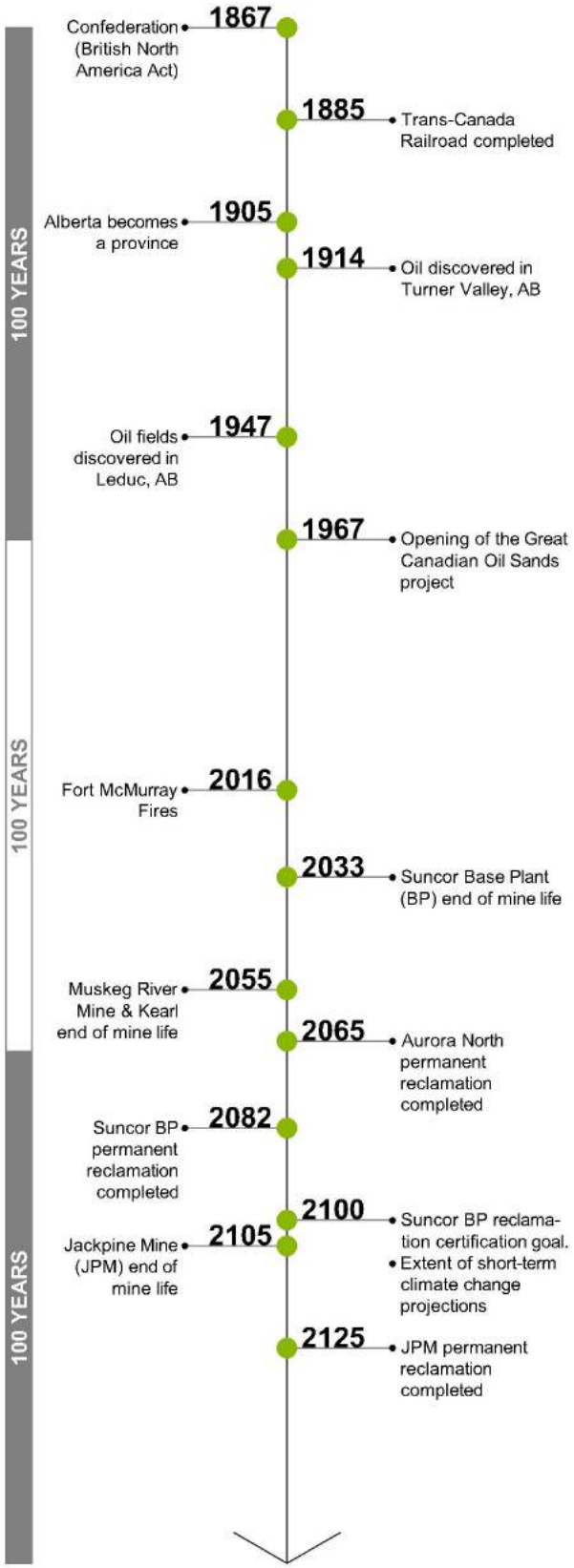

Figure 1. Canadian and oil sands evolution in consideration of 1000-yr design life

SUMMARY

The global expectation of tailings dam closure involves sustainable mining practices. Increasingly, this involves a risk or performance-based approach to closure. The authors' review of best practices nationally and internationally indicates that the following jurisdictions can be learned from:

- Regulatory framework for long-term management in Saskatchewan;
- Western Australia closure guidelines and regulatory review process; and
- Legislative framework in South Africa.

Each of these jurisdictions has a specific characteristic that can be learned from. From a long-term care perspective, Saskatchewan's ICP outlines a perpetual care strategy, including long-term monitoring and management, which may be required in some areas given how rare tailings dam relinquishment is globally (Ministry of Energy and Resources 2009). From a closure planning perspective, Western Australia provides specific closure guidelines outlining minimum expectations and has ongoing closure plan submissions throughout the life of the mine (DMP and EPA 2015). This model emphasizes the importance of regulator guidance and involvement in the closure design process, which should begin at the onset of mining. The legislative framework in South Africa requires that the land is returned to a state that conforms with sustainability principles and holds individuals within a mining company liable for negative environmental impacts (Parliament of the Republic of South Africa 2002).

The need for clarity and strong guidance regarding closure requirements from the regulator is becoming more and more imminent. Alberta is considered a leader in dam safety practices. With some of the largest dams in the world, any failure would be devastating to the industry as a whole. In this sense, nothing but the best is acceptable from a dam safety perspective. Similarly, this attitude must be carried forward to Alberta's approach to tailings dam closure and post-closure safety. Research is ongoing between the AER and the University of Alberta to investigate the long-term behaviour of tailings dams to aid in enhancing and assessing risk management tools for the purposes of tailings dam safety following mine closure.

ACKNOWLEDGEMENTS

The authors would like to thank the Vanier-Banting Secretariat for financial support of this research. The authors would also like to thank Tim Eaton (Senior Advisor, Closure and Liability Branch, AER) for his ongoing support throughout this research.

REFERENCES

95th United States (US) Congress. (1977). Surface mining control and reclamation act (SMCRA), Public Law 95-87, United States Congress, Washington, D.C, USA.

Al-Mamun, M. and LePoudre, C. (2016). Role of Tailings Dam De-licensing (Decommissioning) in the Process of TSF Closure, *In* Proceedings of the CDA 2016 Annual Conference, Halifax, Nova Scotia, 15-20 October 2016.

APEGA. (2013). Guideline for Ethical Practice v2.2. The Association of Professional Engineers and Geoscientists of Alberta (APEGA), Edmonton, Alberta, Canada.

Auditor General of Alberta. (2015). Report of the Auditor General of Alberta, Auditor General of Alberta, Edmonton, Alberta, Canada.

ANZMEC and MCA. (2000). Strategic framework for mine closure, Australian and New Zealand Minerals and Energy Council (ANZMEC) and Minerals Council of Australia (MCA), Canberra, Australia.

Bowker, L. N. and Chambers, D. M. (2017). In the Dark Shadow of the Supercycle Tailings Failure Risk & Public Liability Reach All Time Highs, Environments, **4**(4): 75.

Chambers, D. M. and Bowker, L. N. (2017). Tailings Dam Failures 1915-2017. Available online: http://www.csp2.org/tsf-failures-1915-2017 [accessed 04 January 2018].

CDA. (2013). Dam Safety Guidelines 2007 (2013 edition), Canadian Dam Association (CDA), Ottawa, Canada.

CDA. (2014). Application of Dam Safety Guidelines to Mining Dams, Canadian Dam Association (CDA), Ottawa, Canada.

DeJong, J., Tibbett, M. and Fourie, A. (2015). Geotechnical systems that evolve with ecological processes, Environmental Earth Sciences, **73**(3): 1067-1082.

Department of Mines and Petroleum (DMP) and Environmental Protection Authority (EPA). (2015). Guidelines for preparing mine closure plans, Government of Western Australia.

Eaton, T. and Paz, S. (2016). Alberta Energy Regulator Dam Safety Program, *In* Proceedings of the CDA 2016 Annual Conference, Halifax, Nova Scotia, 15-20 October 2016.

Equator Principles Association. (2013). The Equator Principles III: A financial industry benchmark for determining, assessing, and managing environmental and social risk in projects, Equator Principles Association.

Government of Alberta. (2015). Lower Athabasca Region - Tailings Management Framework for the Mineable Athabasca Oil Sands, Government of Alberta, Edmonton, Alberta, Canada.

Government of Alberta. (2016). Alberta Dam Safety Guidelines and Guidance Documents 2016 Update. Presentation at Alberta Dam Safety Seminar, 11 April 2016. Available online: http://aep.alberta.ca/water/programs-and-services/dam-safety/documents/DamSafetyGuidelinesUpdate-Apr2016.pdf [accessed 28 July 2018].

Government of Saskatchewan. (1996). The Mineral Industry Environmental Protection Regulations, Government of Saskatchewan.

ICOLD Committee on Tailings Dams. (2013). Sustainable design and post-closure performance of tailings dams, Bulletin 153, International Committee on Large Dams (ICOLD).

ICOLD Committee on Tailings Dam and Waste Lagoons. (2001). Tailings Dams Risk of Dangerous Occurrences – Lessons learnt from practical experiences, Bulletin 121, International Committee on Large Dams (ICOLD).

MAC. (2017). A Guide to the Management of Tailings Facilities Third Edition, Mining Association of Canada (MAC), Ottawa, Ontario, Canada.

Ministerio de Mineria. (2015). Regula el cierre de faenas e instalaciones mineras, (Chile) Ley 20551, Gobierno de Chile, Santiago, Chile.

Ministry of Energy and Mines (MEM). (2015). Mount Polley Mine Tailings Storage Facility Breach August 4, 2014, Government of British Columbia, Victoria, British Columbia, Canada.

Ministry of Energy and Mines (MEM). (2016). Guidance Document Health, Safety and Reclamation Code for Mines in BC, Government of British Columbia, Victoria, British Columbia, Canada.

Ministry of Energy and Mines (MEM). (2017). Health, Safety and Reclamation Code for Mines in BC, Government of British Columbia, Victoria, British Columbia, Canada.

Ministry of Environment. (2008). Northern Mine Decommissioning and Reclamation Guidelines, Government of Saskatchewan, Regina, Saskatchewan, Canada.

Ministry of Energy and Resources. (2009). Institutional Control Program Post Closure Management of Decommissioned Mine/Mill Properties Located on Crown Land in Saskatchewan, Government of Saskatchewan, Regina, Saskatchewan, Canada.

Morgenstern, N. (2012). Oil Sands Mine Closure – the End Game: An Update. *In* Proceedings of the 3rd International Oil Sands Tailings Conference, Edmonton, Alberta, 2-5 December 2012.

OSTDC. (2014). De-licensing of Oil Sands Tailings Dams, Technical Guidance Document, Oil Sands Tailings Dam Committee (OSTDC).

Parliament of the Republic of South Africa. (2002). Mineral and Petroleum Resources Development Act, Parliament of the Republic of South Africa, Cape Town, South Africa.

Provincial Court of Alberta. (2017). Agreed Statement of Facts, Docket No. 151258456P1 &160061354P1. Available online: http://www1.aer.ca/compliancedashboard/enforcement/201706-04_AgreedStatementofFacts_PrairieMines_Obed_2013-006.pdf [accessed 20 June 2019].

Roberts, S., Viega, M. and Peiter, C. (2000). Overview of mine-closure and reclamation in the Americas, University of British Columbia, Vancouver, British Columbia, Canada.

Shanahan, J. (1995). How to rescue Superfund: Bringing common sense to the process, The Heritage Foundation Backgrounder, No. 1047.

World Bank and International Finance Corporation (IFC). (2002). It's not over when it's over: Mine closure around the world, mining and development series, International Finance Corporation, Washington, D.C., USA.

World Commission on Environment and Development. (1987). Our common future, Oxford University Press, Oxford, UK.

World Information Service on Energy Uranium Project (WISE). (2018). Chronology of Major Tailings Dam Failures (from 1960). Available online: http://www.wise-uranium.org/mdaf.html [accessed 31 July 2018].

STEWARDING DAM SAFETY IN ALBERTA: THE DAM INTEGRITY ADVISORY COMMITTEE (DIAC)

Jeremy Boswell, Paul Cavanagh and Larry Staples
Dam Integrity Advisory Committee, Alberta Chamber of Resources

ABSTRACT

After decades without a major failure in Alberta, the Obed Mountain Mine dyke breach and subsequent overtopping of their main tailings dam near Hinton in 2013, and the Mount Polley tailings dam breach in northern British Columbia in 2014 caused many engineers and dam safety specialists to ask: “Could another major dam failure like these happen again here?”

In response, the Alberta Chamber of Resources (ACR) convened a task group to carry out a high level evaluation of systemic risk. The top technical experts from eight resource companies met for a series of discussions about company practices, external reviews and regulatory oversight of the approximately 70 major dams in Alberta, including both tailings retention and water retention structures. The discussions culminated in a Briefing Note which concluded that the Alberta dam safety ‘system’ was fundamentally robust. Taking advantage of the collective wisdom of the technical experts, a two-day workshop was organized in November 2015 to identify and prioritize potential enhancements to make the dam safety system even more robust.

It became apparent that finding answers to such broad questions about dam safety was complex and could only be achieved through committed stewardship and consistent application of continuous improvement. The Dam Integrity Advisory Committee (DIAC) was formed, comprising senior technical staff from participating ACR Member Companies. The paper explains the components of a healthy dam safety system and highlights the unique role and mandate of DIAC in Alberta. The principal goals, initiatives and deliverables of DIAC in support of dam safety in Alberta are discussed in the context of the overall dam safety system.

INTRODUCTION

Major engineering failures, such as the Obed Mountain Mine dyke breach and subsequent overtopping of their main tailings facility in October 2013 (AER 2017) and the breach of the Mount Polley tailings facility in August 2014 (Morgenstern et al, 2015), invariably cause human anguish, environmental damage and economic loss. Within this dark cloud, a small but important silver lining is that failures sow the seeds of progress through questions like “Could another major failure like these happen again here?” or, “Really, how healthy are our engineering practices and safety systems?”

To provide an initial answer to these questions, the Alberta Chamber of Resources (ACR) pulled together senior technical experts from natural resources companies to prepare a Briefing Note (ACR 2015) on the health of dam safety in Alberta. The main conclusion of the review was that the dam safety ‘system’ – cultivated through the past five decades in Alberta – was among the best in the world. Managing the inescapable risks of major engineered structures means that proactively reducing the probability of dam failure as low as practically, or as reasonably, possible (ALARP, ECL 1949) presents a multi-faceted challenge which needs sustained stewardship and ongoing improvement.

Around the same time as the Briefing Note, in March 2015 the Alberta Office of Auditor General (OAG) released an assessment report (OAG 2015) which included recommendations for improvement of the dam safety regulatory framework in Alberta. Following these events and reviews, The ACR dam integrity task group decided to convene a two-day workshop in November 2015 comprising leading engineers and specialists in dam safety, to examine in more detail the components and conditions of the dam safety system in Alberta. The four strategic themes (shown in Figure 1) that emerged from the workshop were subsequently refined into prioritized objectives and supporting actions.

The dam integrity task group was transformed to the Dam Integrity Advisory Committee (DIAC),

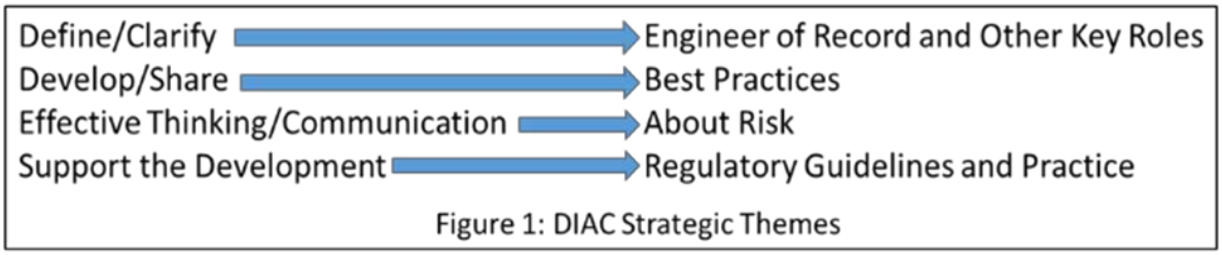

Figure 1: DIAC Strategic Themes

through a terms of reference and mandate (ACR 2016a), under the auspices of the ACR, to steward the follow-up actions in proactive pursuit of the desired goals. DIAC was founded on the established principles that eventual success could only be achieved through intentional stewardship of dam safety and continuous improvement of the dam safety system in Alberta.

THE DAM SAFETY SYSTEM IN ALBERTA

In order to understand DIAC's vision and role in dam safety, it was important to outline the purposes and interrelationships between the key components of the system. Figure 2 illustrates the model (ACR 2016b) developed by DIAC for the Alberta context.

This model demonstrates the importance of having a strong safety and integrity culture, top management support, resources, and technical expertise available for and working in harmony with regulators in the development of appropriate policies and regulations to establish and maintain the system. Some of the main components and supporting features include the following:

Top Management and Integrity Culture

- Active corporate risk management, review and assessment of dam safety
- Appropriate allocation of dedicated resources for dam safety management
- Aligning societal, regulatory and corporate dam safety principles and values

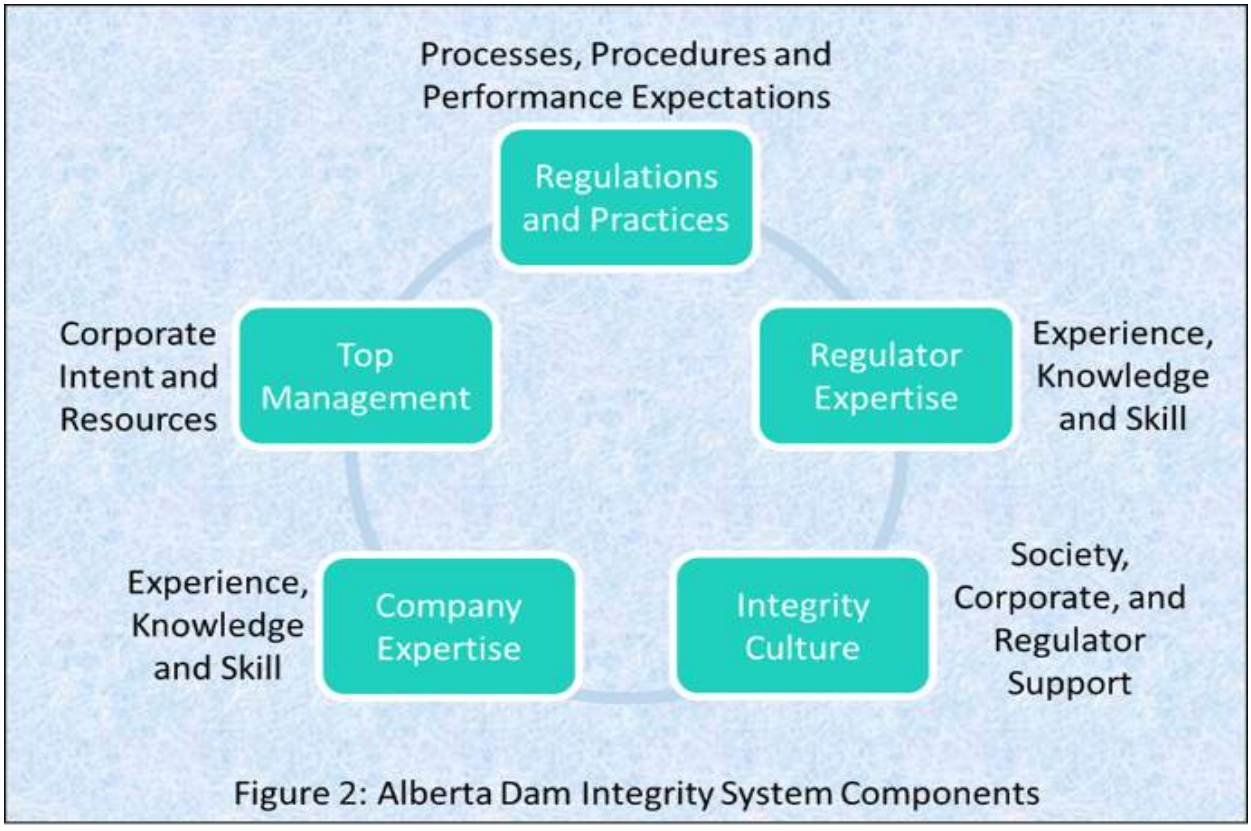

Figure 2: Alberta Dam Integrity System Components

Company and Regulator Expertise

- Active research and refinement of technical inputs and requirements
- Continuous training of personnel in new and improved methods of design, construction, operation and closure
- Succession plans for personnel engaged in dam safety management

Regulations and Procedures

- Incorporation of risk-informed methods in dam safety regulations and procedures
- Clear definition of roles, accountabilities and responsibilities for individuals
- Understanding how the state of practice compares with best practice

Consistent and reliable dam safety is achieved when each node is strong, incorporates robust processes, and all nodes are interacting and performing synergistically; should one node weaken temporarily, other strong nodes can compensate. However, the system would not be considered resilient or sustainable if there are acute or chronic weaknesses in one or more of the nodes or in the interactions between the nodes. Complacency with such a status quo could threaten the health of the overall system.

THE ROLES AND ACTIVITIES OF DIAC

DIAC was established to support the existing dam safety system across the natural resource sectors in Alberta and includes representation from the electricity generation, and coal and oil extraction and processing industries, where water and tailings containment dams are necessary infrastructure for successful operations. Considering the components and requirements of a healthy dam safety system, and in the light of recent events and observed trends, DIAC has taken on the following general objectives:

- Timely sharing of non-proprietary operating experiences and learnings
- Maintaining a global watching brief on dam safety issues, incidents and trends
- Identifying new technologies and facilitating their assessment and implementation
- Integrating implementation of Canadian Dam Association (CDA 2013) and Mining Association of Canada (MAC 2017a) guidelines for resource sector dams
- Facilitating discussions of mutual interest with regulators
- Developing recruitment strategies for the next generation of dam safety engineers, following the model of the ACR Mining Industry Advisory Committee (MIAC)

With respect to the individual components and/or their interactions, key DIAC activities focus on maintaining, strengthening, giving greater visibility to, or establishing broader understanding of the current components, policies, practices and procedures. These activities are aimed at stewarding and supporting the current dam safety system and culture by establishing broad-based understanding and effective implementation of existing standards and practices.

Additional activities focus on future trends and developments and are intended to identify and assess opportunities for positive change within the Alberta dam safety system. The main objective is to promote and facilitate implementation of innovations and continuous improvement.

Notable milestones, products, ongoing activities, and tasks of DIAC include the following:

Currently Completed Activities

- Articulated a conceptual model for dam safety in Alberta (Figure 2)
- Encouraged the University of Alberta to expeditiously organize the inaugural five-day course on tailings management, December 2015
- Catalogued an indexed reference list of 90 leading practice papers in dam safety (ACR 2017a)
- Prepared a white paper on roles and accountabilities for key positions responsible for management of dam safety in Alberta, with an initial focus on the Engineer of Record (ACR 2017b)
- Promoted the development of leading versus lagging indicators for assessing performance of dam safety and dam safety systems (Boswell and Sobkowicz 2018)

Ongoing Activities

- Prepare a white paper on thinking clearly and communicating effectively about dam safety and risk management

- Engage with Alberta Environment and Parks (AEP) and the Alberta Energy Regulator (AER) to provide industry feedback on the revision and updating of dam safety legislation
- Liaise with national and international dam safety organizations with similar interests (such as CDA, MAC, USSD, ICOLD, GBA and ASDSO)
- Encourage initiatives regarding engineering courses and career development seminars on dam integrity in the province (e.g. dam safety seminars; annual five-day course on tailings management at University of Alberta and the development of Masters level programs in tailings engineering)

Some of the significant insights, achievements and conclusions, to date, are:

- The dam owner is ultimately accountable for the safety of the dam and responsible for dam safety assurance, which is consistent with Alberta dam regulations.
- For owners that are unaware of these requirements, the engineer of record has a duty to apprise the owner of their accountabilities and responsibilities
- Within the context of owner accountability, effective dam safety is a team responsibility that requires role clarity and coordination of implementation and execution by numerous responsible groups and individuals
- The comprehensive reference list of preferred practices developed by DIAC is being used or cited by other organizations and agencies across North America
- Opportunities to update legislation and policy do not occur frequently; it is important to adopt a long-term view of change and continuous improvement
- There is a necessity for the conscious appreciation and application of the differences between engineering risk quantification and communication of the implications of those risks to stakeholders

It is also recognized that significant regulatory advances (Eaton et al. 2016) toward ensuring dam safety in Alberta have been implemented since 2014. Some of these advances include:

- Incorporation of risk-based approaches
- Emphasis on management practices
- Annual inspection and audit plans
- Holistic consideration of reviews, inspections and audits (now called safety assessments)
- Increased transparency and public reporting
- Better data management systems

The issues, goals and activities being addressed at DIAC are periodically prioritized and reviewed for progress. An example of the DIAC activity tracking tool is presented in Figure 3. It is clear from the

Goals and Actions	Status	Priority		Comments/Status
		Urgent	Important	
Define EOR and other Key Roles				
Define EOR, DOR, DSE, etc. – clarity of roles and responsibilities…	Complete	High	High	White paper
Owner commitment (e.g. at design application stage) to designating qualified engineer….	Underway	Med.	High	Communicate white paper
Update dam safety guidelines document…	Complete	Med.	High	See above
Roles and responsibilities in regulations …	Complete	High	High	See above
Develop and Share Best Practices				
Develop (non-prescriptive) best practice document….	Underway	Low	High	Assembled references papers
Annual workshop for dam integrity engineers – share best practices & learnings…	Underway	Low	High	Supported workshop in 2017
Advocacy of education opportunities and mentoring….	Underway	Med.	Med.	Letter support M.Eng. co-op
State of Practice manual for oil sands dam design ….	Upcoming	Low	High	
Update dam safety guidelines document	Upcoming	Low	High	
Explore the need to expand site characterization at design phase….	Upcoming	Med.	Med.	
DIAC follow up with others…	Underway	Low	High	Ongoing liaison
Think Clearly and Communicate Effectively About Risk				
Guidance for company to regulator communication (leading indicators)….	Underway	Med.	Med.	Assembled references
Standardize risk communication	Underway	Med.	Med.	Paper started above
Encourage regulators to establish formal process for communication…	Underway	High	High	Discussed with regulators
Support Regulators to Develop Guidelines and Processes				
Open discussion about principles underpinning water release criteria	Upcoming	Low	High	
Improve regulations with QPOs, DSRs, site investigation requirements, auditing….	Underway	High	High	Working with regulators
Process for auditing designs that rely on the observational approach…	Upcoming	Med.	High	
Encourage coordination between departments to facilitate implementation…	Underway	Med.	Med.	Reviews of regs and directives
Work with dam regulators to open discussion about principles for "de-licensing" of dams…	Underway	Low	Med.	

Figure 3: DIAC Activity Tracking Tool (Aug 2018)

recent scorecard that some important activities were started and completed but that additional work is necessary and ongoing.

ON THE SHOULDERS OF GIANTS

As the era of major Alberta water dams and tailings dams dawned in the latter half of the twentieth century, engineering leaders in the government and in industry demonstrated remarkable foresight in establishing high standards and embracing improved processes. For instance, the near-universal adoption of Independent Geotechnical Review Boards is the best known – but not the only – innovation which has provided confidence that the inherent risks of these large engineered structures are appropriately managed.

The Department of Civil & Environmental Engineering at the University of Alberta has played a unique role, firstly by recognizing the importance of geotechnical engineering generally, and dam engineering specifically, and attracting international leaders as faculty members such as Dr. Norbert Morgenstern, P. Eng., and others. They acted as expert advisors to industry and to governments; their research efforts addressed problems of both immediate and strategic significance, and they have shaped the minds of literally hundreds of students who now occupy positions of professional responsibility and executive leadership in companies and regulators. Their common foundation leading-edge learning and shared frame of reference have enabled the ready sharing of learnings and advancements across the industry.

Finally, comment is warranted on the degree to which the Alberta engineering community is connected to their national and international counterparts. Alberta practitioners are known not only as contributors and leaders in the Canadian Dam Association publications (CDA 2013) and the initiatives of the Mining Association of Canada (MAC 2017a, 2017b), but also as ready adopters of improved processes. Leading practices from Alberta are welcomed with interest from the Association of State Dam Safety Officials, the US Society on Dams and the Geoprofessional Business Association, and the reverse is also true.

Engineering professors and engineering consultants from Alberta are regularly called upon to serve on expert panels investigating major dam failures around the world. This is recognition of Alberta expertise; equally importantly, it provides direct connectivity of the Alberta dam engineering community to the *post mortem* learnings and the sense of engineering humility which arise from major failures.

DISCUSSION AND CONCLUSIONS

The initial outcome of the high-level review of dam safety in Alberta was a renewed sense of confidence that current engineering practices, corporate commitment and regulatory oversight are appropriately managing the risks inherent in operating major water and tailings dams. The second outcome was the realization that engineering practices, corporate commitment and regulatory oversight interact in a unique synergy in Alberta – a 'system' which is more robust than the sum of the component parts. The third outcome was the establishment of an honest broker, the Dam Integrity Advisory Committee, DIAC, through which this industry-wide system can be nurtured and improved.

DIAC sees its primary roles as providing stewardship, support, perspective, and facilitation of dam safety on behalf of owners and operators of major dams in Alberta. Forward-looking and future initiatives could include the definition, development and support for applying ALARP and performance-based, risk-informed principles and practices (Morgenstern 2018) to produce clear design, construction, operation, closure, decommissioning and de-licensing expectations and requirements.

While taking some pride in the robustness of the Alberta dam safety system and the unique role which DIAC plays, committee members are acutely aware of the imperative of avoiding professional hubris by embracing "generative unease" with the status quo. We are reminded of this imperative by the Obed Mountain and Mount Polley failures and more recently by the Fundão tailings dam failure in 2015 in Brazil (Morgenstern et al. 2016), which had devastating consequences. This sentiment was eloquently articulated in the report by the Independent Forensic Team (IFT 2018) while investigating the February 2017 failure of the spillway of the Oroville Dam in California:

> "Although the practice of dam safety has certainly improved since the 1970s, the fact that this incident happened to the owner of the tallest dam in the United States, under

> regulation by a federal agency, with repeated evaluations by reputable outside consultants, in a state with a leading dam safety program, is a wake-up call for everyone involved in dam safety."

DIAC is uniquely positioned to help advance dam safety in Alberta by working proactively with stakeholders, regulators, technical and engineering practitioners, educational institutions and the public. With its unique mandate, DIAC aims to perpetuate the conclusion from the ACR briefing note: the dam safety system in Alberta is one of the best in the world.

ACKNOWLEDGEMENTS

The authors thank the ACR for supporting the publication of this paper and the members of DIAC for their selfless contribution of time, expertise and experience in the pursuit of dam safety, including review of this paper. We also thank the many dedicated owners, regulators, stakeholders, engineers and technologists who ceaselessly pursue dam safety and make up the dam safety system in Alberta.

REFERENCES

Alberta Chamber of Resources. (2015). Orderly and Responsible Development, Briefing Note – Dam Integrity.

Alberta Chamber of Resources. (2016a). Dam Integrity Advisory Committee terms of Reference and Mandate.

Alberta Chamber of Resources. (2016b). The Alberta Dam Integrity System. DIAC Progress Report to the ACR.

Alberta Chamber of Resources. (2017a). Dam Integrity Advisory Committee Engineering Practice References Index.

Alberta Chamber of Resources. (2017b). Dam Integrity Advisory Committee Roles and Accountabilities for Dam Safety Management in Alberta.

Alberta Energy Regulator. (2017). Investigation Summary Report 2013-006: Coal Valley Resources.

Boswell, J. and Sobkowicz, J. (2018). Leading versus Lagging Indicators of Tailings Dam Integrity. Tailings and Mine Waste 2018.

Canadian Dam Association. (2013). Dam Safety Guidelines 2007 (revised 2013).

Eaton, T. and Paz, S. (2016). Alberta Energy Regulator Dam Safety Program. Canadian Dam Association Conference 2016.

English Case Law. (1949). Edwards v National Coal Board.

Independent Forensic Team. (2018). Independent Forensic Team Report – Oroville Dam Spillway Incident.

Mining Association of Canada. (2017a). A Guide to the Management of Tailings Facilities (Third Edition).

Mining Association of Canada. (2017b). Toward Sustainable Mining, TSM 101: A Primer.

Morgenstern, N. R., Vick, S. G. and Van Zyl, D. (2015). Independent Expert Engineering Investigation and Review Mount Polley Tailings Storage Facility Breach.

Morgenstern, N. R., Vick, S. G., Viotti, C. B. and Watts, B. D. (2016). Fundão Tailings Dam Review Panel Report on the Immediate Causes of the Failure of the Fundão Dam.

Morgenstern, N. R. (2018). Geotechnical Risk, Regulation, and Public Policy. 6th Victor de Mello Lecture, Soils and Rocks, São Paulo, **41**(2): 107-129.

Office of Auditor General of Alberta. (2015). Report from the Office of the Auditor General of Alberta to the Members of the Legislative Assembly of Alberta.

Session 9

TAILINGS MANAGEMENT

A CASE FOR ELIMINATION OF TAILINGS PONDS THROUGH IN-LINE TREATMENT USING A LOW COST, FLOCCULENT FREE APPROACH: RESULTS FROM TWO ON-SITE TRIALS

P. McEachern and D. Bromley
Purlucid Treatment Solutions Inc., Calgary, Canada

ABSTRACT

Managing tailings from oil sands mining has been a high cost, high liability endeavor. In part, this is because it has inherited a history driven by traditional mining and a focus on dewatering solids rather than water treatment. Combining the results from two extensive field trials, we show that tailings can be treated post production in a cost-effective manner. In-line treatment provides benefits by eliminating the need for multi-year settling in ponds, allowing hot water to return to extraction immediately and reducing the environmental footprint and cost of mine development.

The in-line treatment process consists of free oil removal, solids removal to 1 µm and subsequent ultrafiltration to remove fines to 0.01 µm in diameter. The approach has been proven in two separate on-site trials. The first trial operated for 2 months processing fresh tailings prior to discharge to a pond. The tailings were a combination of secondary extraction and froth flotation tails. Residual oil was recovered with flotation and coarse solids were removed using centripetal methods. The dry cake, 65-70%wt was suitable for deposition and quickly developed additional strength. Certain feed conditions made it possible to eliminate the need for flocculants and better cake was created without them.

The second trial operated for 8 months processing the ultra-fine clays that pass through centripetal and NST processes. Fines were removed using froth flotation followed by ultrafiltration. Turbidity of the treated water was consistently below < 0.5 NTU. The process did not require flocculent and consumed instead a charged surfactant at a rate of 0.003%v/v that promoted attachment of the fines to a high-density froth. The chemical costs were < $1/m3. The water quality following this simple step could be suitable for reuse without ultrafiltration. The trial targeted pre-treatment for reverse osmosis, hence ultrafiltration to remove emulsified oil and fine solids was required. Ultrafiltration deployed Replaceable Skin Layer (RSL™) membranes with flux rates of 550 lmh. The membranes consistently provided an oil and solids free permeate with < 3 SDI. The proposed treatment approach has the potential to greatly reduce the cost of tailings management, return high quality, high temperature water to extraction and eliminate the need for tailings ponds.

INTRODUCTION

Processing oil sands mine tailings is not dissimilar from the treatment of other fluid tailings in that these are vast deposits with two components; a fraction comprised of heavier solids that readily settle, and a free water component containing suspended and dissolved constituents that hamper reuse or make the fluid unsuitable for return to the environment without additional treatment. However, oil sands tailings are unique in that they have a bitumen fraction and contain heat both of which may have economic value if recovered during their production through inline treatment. While the current approach of deposition in large ponds may meet environmental liability concerns in the long term, the additional benefit of in-line processing to reduce environmental liability in the short term has additional benefits pertinent to the social license to operate.

In approaching these two components, the readily settled solids can be removed using centripetal force to immediately create the conditions that require months to accomplish in ponds. The subsequent or simultaneous removal of small colloidal materials including fine clays can be achieved with a number of existing water treatment technologies, chief among these being filtration. However, the volume of fluid that requires treatment in an oil sands tailings process combined with the integration of this flow with other water management requirements adds extreme variability of feed to the list of considerations for an in-line treatment process and anecdotally seems to be one of the major contributors to a lack of success in establishing a cost-effective in-line treatment

process. Here we present data from two field trials that separately attempted to deal with these two components and discuss the potential to combine these in a single process.

DESCRIPTION OF FEED

The feed waters for both projects were very different. In the one case, we received a portion of fresh tailings from a tailings deposition line approximately 100 m prior to its discharge to a tailings pond. This line, with a flow of ~ 2000 m3/hr, contained a combination of waters, primarily froth flotation tails consisting of fine clays but also included some coarse tails as well as recycle water pumped from other storage facilities on the mine site. As such, the feed was highly variable in solids content and size distribution (Fig. 1) as well as bitumen contents from less than 1% to as much as 17%, averaging 3.5%.

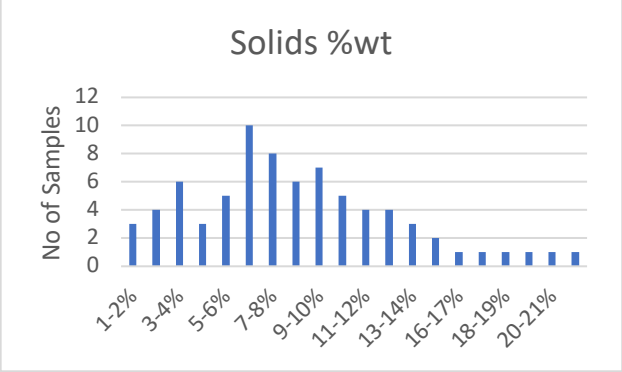

Figure 1. Percent solids (wt) for 76 samples collected over the run period. Samples were collected at the centrifuge feed line

The second source water considered here was the recycle water (RCW) from the free water cap of the CNRL Horizon mine tailings pond. RCW has above neutral pH, high alkalinity, low to moderate Total Suspended Solids (TSS) and turbidity with high Total Dissolved Solids (TDS), Total Organic Carbon (TOC) and Chemical Oxygen Demand (COD). TDS is primarily composed of sodium chloride, bicarbonate and sulfate. TOC is primarily composed of Naphthenic Acids (Table 1). Much like the previous source water, the RCW feed to the treatment system was variable, particularly for target water treatment parameters such as TSS, turbidity and hardness.

DESCRIPTION OF TREATMENT TECHNOLOGIES

Centripetal System

The in-line processing of fresh tailings was accomplished with standard technology currently deployed in the oil sands consisting of a dissolved air flotation skid, a centrifuge feed tank and a decanter scroll centrifuge all from common industrial suppliers. A skid containing 8 x 4 inch hydrocyclones was initially trialed after the centrifuge feed tank and before the centrifuge but this was removed when it was shown to have no benefit and could not be operated reliably under the cold weather conditions experienced during the field trial. The centrifuge had a hydraulic capacity of 700 gpm. The coagulants gypsum and alum and the flocculant A3338 were utilized over the trial period as indicated in Table 2. Trials consisted of a three by three matrix for back drive differential and bowl speed over three feed pump speeds resulting in 18 different trials for centrifuge conditions.

To reduce the number of total trials, pump speeds were held constant at 1200 rpm so that only 9 centrifuge conditions were applied to the 6 chemical manipulations used at three different dose rates. Each trial was performed for a minimum of 2 hours and the most successful condition within any given trial was run over the night shift.

Table 1. Characteristics of the feed water from the tailings free water cap over the four months of the treatment trial

Parameter	Units	Average	Max	Min	Std. Deviation
pH	SU	8.29	8.39	8.16	0.08
Total Alkalinity	mg/L as CaCO3	725	780	680	32
TSS	mg/L	359	880	ND	315
Turbidity	NTU	489	1000	100	312
Conductivity	µS/cm	2988	3200	2800	122
TDS	mg/L	2094	2500	1700	284
Total Sodium	mg/L	631	700	570	39
Chloride	mg/L	450	520	350	47
Bicarbonate	mg/L	876	930	830	32
Total Hardness	mg/L as CaCO3	47	56	36	6
TOC	mg/L	47	69	29	14
Oil & Grease	mg/L	25	32	14	6
Naphthenic Acids	mg/L	54	68	39	11
COD	mg/L	425	530	310	89

Table 2. Trial conditions

Centrifuge Parameters			
Pump Speed (rmp)	900	1200	1400
Back Drive %	15	25	38
Bowl Speed (rpm)	2200	2400	2800
Chemistry Trials			
No chemistry			
Polymer (g/t)	500	750	1000
Alum (g/t)	500	750	1000
Polymer & Alum (g/t)	500	750	1000
Gypsum (g/t)	500	750	1000
Polymer & Gypsum (g/t)	500	750	1000

Froth Flotation

The froth flotation system is a unique technology known as High Intensity Froth Flotation (HiFF). The HiFF system utilizes a surfactant and a patented high intensity froth generator and mixing system to create bubbles with an optimum size and surface charge to interact with the target colloids. The charged environment causes the collapse of the Electric Double Layer (EDL) around the colloidal solids. The solids then attach to the bubble in the froth. The bubble with the solids floats to the surface of a flotation chamber, which can be any standard flotation system. During regular operation of the system, froth was created by using water, air and an anionic surfactant. The froth was injected in the raw water line at 70 and 140 mL/L before the flotation tank, the higher dose resulted in better separation with up to 98.6% removal of turbidity (surfactant dose of 0.112 mL/L). The trial tested several coagulant aids, landing on PACl as the best performer and this was added upstream of the flotation tank at an optimized dose of 60 and 80 mg/L (as Al) where 96% and 99% reductions in turbidity were achieved, respectively at the 140 mL/L froth dosage rate.

Ultrafiltration

The combined flotation and ultrafiltration system operated at 5 m^3/hr. The submerged membrane system was composed of stainless steel tubes with 1 µm pore size. A powder precoat was applied to the membrane, the method and chemistry being the patented component of this unique system known as Replaceable Skin Layer (RSL) Membranes™. The RSL Membrane™ provides enhanced water treatment efficiency over two phases: during the repulsion phase the high charge and ionic strength of the powder RSL causes repulsion of the colloidal solids approaching the skin layer in a similar fashion as a conventional fixed membrane layer comprised the typical metal oxides such as aluminum oxide, Zirconium oxide or Titanium Oxide. This repulsion occurs as a result of a strong EDL on the surface of the membrane causing the colloidal solids to repel because of their own EDL. This high level of repulsion reduces the layering or caking of the solids on the surface of the skin layer. As the solids are repelled the concentration of solids increase on the feed side of the membrane. With increased concentrations (20000 to 30000 mg/l), the solids begin to penetrate the RSL powder initiating phase 2, EDL collapse and attachment of the solids to RSL powder. This

attachment causes the transmembrane pressure (TMP) to increase and the RSL powder layer fouls. At a TMP of 0.7 bar the RSL is backwashed off the surface of the membrane tube and a new powder RSL is applied. One of the major differences between the RSL Membrane™ and conventional attached skin layers is this second phase. With conventional membranes, there is a significant effort to avoid fouling of the membrane skin layer. Typical procedures to reduce membrane skin layer fouling are to backwash frequently (i.e. every 15 seconds) and use a high cross-flow over the surface of the membrane skin layer. The cross-flow option results in high pumping rates and energy consumption. Eventual fouling occurs and the system must be shut down where highly acidic and then basic solutions are used to clean the membrane skin layer (e.g. clean in place –CIP). In the RSL Membrane™ fouling is accepted as a normal operation as it is a key component in the separation of the solids from the water being treated. A fast 4-minute removal and replacement of the precoat eliminates the need for the energy intensive cross flow system. The highly charged environment within the pore spaces of the precoat creates a uniform compressive force that collapses the colloidal EDL. The collapse of the EDL allows van der waal forces to become dominant thereby causing the solids to aggregate and /or attach to the media. Solids and oil build up to high concentrations on the upstream side of the membrane, yet pressure loss across the membrane remains less than 70 kpa and flux rates remain consistently high (10 times conventional flux rates-200 lmh to 800 lmh). The technology provides an effluent similar to other ultrafiltration membrane technologies but requires significantly less energy and capital costs.

RESULTS

The centrifuge trials produced cake suitable for deposition and the subsequent development of strength consistent with Alberta Directive 085. The data have not been released so are only summarized generally here. Variability in centrifuge performance, as determined by cake %solids, was dominated by the variance in feed %solids making it difficult to determine the influence of bowl speed, back drive differential and pump speed. Pump speed appeared to have minimal impact while throughput and cake %solids were best at a back drive differential of 25%. Bowl speed also showed only modest differences across the trials with 2400 rpm producing the most consistent results.

Centrifuge solids, which were collected in paint cans and stored for processing by lab personnel on site, often released fluid to the surface while in the processing que. This made it difficult to assess the validity of measurements in the lab such as capillary suction time (CST) and vane sheer. Cake percent solids were analyzed immediately on sample collection and combined with centrate analyses, provided the simplest and most reliable measures for assessment. For example, cake CST values were highly variable ranging from low values of 15s to indeterminate values that exceeded two hours (7200s) when tests were stopped. Variability was extreme even among replicates of the same experimental conditions suggesting sample preparation for CST measurements had the predominant impact on the analysis. Results from vane shear analyses were more consistent with inter-replicate range typically less than 30% of the mean but also highly dependent on choices made by the lab technician on where to insert the vane in the bulk sample.

Cake percent solids ranged from 55% to 77% with lower percent solids when polymer was used but higher mineral capture rates. Gypsum provided the best cake strength and was similarly effective across all three doses. While gypsum also appeared to produce cake with the highest percent solids, the most important parameter for determining cake percent solids and strength was the percent solids in the feed and most importantly, whether a sand fraction was present. Centrate percent solids were as low as 4700 mg/L, which in this case could only be achieved with the use of polymer. However, gypsum combined with higher percent solids in the feed (>12%) and with the presence of coarse solids in the feed, did produce a cake with sufficient strength for immediate deposition 5 to 7 kPa and centrate with 7000 mg/L solids. This provides a context for subsequent processing of fluids in a water treatment process.

Treatment of tailings pond recycle water

The Nanoflotation system that was deployed to CNRL was previously described and a full report has been released (Epcor 2013) and subsequently published (Loganathan et al. 2015). Table 3 provides a summary from these published works and the mean values in the Lower Athabasca River calculated from the last 30 years of data.

The permeate had a consistent silt density index (SDI) below 3, making it suitable for subsequent treatment in an RO system (Loganathan et al. 2015). The HiFF system was surprisingly efficient at removing the stable suspended clays with 10-fold reduction in turbidity within seconds. Fig. 2 shows the results in water clarity that can be achieved in the flotation cell alone while total chemical costs to achieve these reductions were ~$0.50/m3.

While substantive reductions in several parameters were achieved, the permeate is likely unsuitable for discharge to the LAR without 1000-fold dilution due to the only marginally reduced concentrations of naphthenic acids.

The pilot system deployed at CNRL was the first generation of the Nanoflotation system. Since 2013, several developments have occurred that improve its application. Recent design improvements have focused on reducing silica and scale forming ions in highly concentrated waste waters. Some of these waters have had upwards of 25% solids following chemical manipulation to convert silica, calcium and magnesium, as well as other metals, into colloidal material for ultrafiltration. An example is provided in Table 4, where a highly concentrated waste stream from a SAGD facility where Strong Acid Cation Exchange regeneration waste (SAC Regen) and Evaporator Blowdown (EBD) was co-mingled and treated for subsequent disposal or reuse.

The success of implementing water treatment with high solids loading to ultrafiltration and without prior solids removal such as that offered by centripetal methods suggests it is possible to implement in-line treatment of middling and froth treatment tails without a centrifuge in pre-treatment. Fig. 3 shows a typical feed from the high TDS brine summarized in Table 4.

Exceptional reductions have been consistently achieved in selected parameters with better than expected reduction in TOC and colour (Fig. 4). TOC was reduced by 73% from 660 mg/L to 180 mg/L which appeared to be a result of pH adjustment downward to maximize silica removal as these high levels of TOC removal have not occurred when pH has been maintained at >10 for optimal calcium and magnesium removal.

Figure 2. RCW water (right) and result (left) after 23 seconds of froth separation

Figure 3a. Raw EBD entering the feed mix tank

Figure 3b. Treatment feed water of 50/50 EBD/SAC Regen with chemicals. Note high solids content

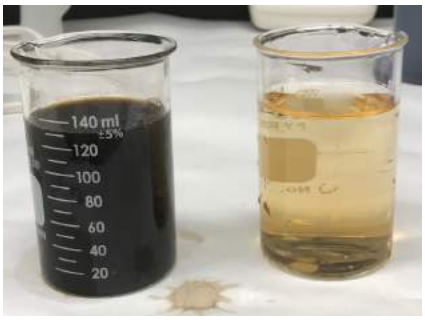

Figure 4a. Blowdown (left) and permeate following RSL treatment (right)

Figure 4b. Solids recovered from filter backwash after decanting only. The solids are suitable for trucking without further processing

Table 3. Results from treatment of the tailings pond free water cap (recycle water – RCW) through two treatment stages, froth flotation (HiFF) and ultrafiltration (RSL Permeate). Mean values for the Lower Athabasca River (LAR) are provided

Parameter	Units	RCW	Post HiFF	RSL Permeate	% Reduction	Mean LAR
pH (on-site lab)	SU	8.27	8.08	8.07	2.5%	7.61
Turbidity	NTU	115	12	0.2	98.3%	50.7
Electrical Conductivity	µS/cm	2983	2817	2850	4.5%	330
Total Dissolved Solids	mg/L	1750	1600	1650	5.7%	212
Hardness (as CaCO3)	mg/L	48	52	53	NA	146
Bicarbonate	mg/L	853	780	790	7.4%	168
Total Alkalinity (CaCO3)	mg/L	700	638	647	7.6%	138
Silica	mg/L	4.94	4.32	4.58	7.3%	4.38
Ammonia	mg/L	1.38	1.33	1.37	1.2%	0.03
Chloride	mg/L	473	443	452	4.6%	4.1
Sulphide	mg/L	0.0057	0.0022	0.0026	55.2%	0.01
TOC	mg/L	36	31	30	18.8%	8.95
DOC	mg/L	34	30	28	17.6%	8.32
Oil & Grease	mg/L	30	24	24	17.5%	
Naphthenic Acids	mg/L	63	55	56	11.1%	<0.1
Aluminum	mg/L	0.37	0.43	0.12	66.8%	1.26
Barium	mg/L	0.26	0.18	0.17	34.8%	0.08
Boron	mg/L	2.30	2.10	2.22	3.6%	0.03
Calcium	mg/L	10.3	11.8	11.8	NA	32.2
Iron	mg/L	0.30	0.26	0.26	15.0%	1.72
Magnesium	mg/L	5.30	5.33	5.67	NA	8.82
Manganese	mg/L	0.032	0.021	0.020	37.7%	0.008
Mercury	µg/L	0.001	0.001	0.001	31.0%	0.009
Phosphorus	mg/L	0.50	0.45	0.43	15.0%	0.05
Potassium	mg/L	10.2	9.2	9.9	2.5%	1.28
Silicon	mg/L	3.00	1.93	2.07	31.1%	
Sodium	mg/L	640	593	637	0.5%	16.6
Strontium	mg/L	0.30	0.28	0.29	3.3%	0.22
Sulfur	mg/L	30.5	28.8	30.2	1.1%	39.6 (sulfate)

Table 4. Ultrafiltration of 3 high mineral content brines from the Ft McMurray area. Raw is the feed water and Perm is the permeate after ultrafiltration

Scale Parameter	EBD1 Raw	EBD1 Perm	EBD2 Raw	EBD2 Perm	OTSG Raw	OTSG Perm
Total Silicon (mg/L)	1641	33	9200	71	120	22
Total Barium (mg/L)	14	4.9	5.5	0.6	32	<0.1
Total Strontium (mg/L)	67	34	13	5	0.21	<0.2
Fe-Dis (mg/L)	10	ND	<6	<0.6	<0.6	<0.6
Ca-Dis (mg/L)	1387	637	180	150	100	46
Mg-Dis (mg/L)	115	33	20	4.1	20	2
TOC (mg/L)			4800	3550	660	180
Turbidity (NTU)					8.5	2.2

DISCUSSION

While the two projects took entirely different approaches to the two fundamental components of oil sands mine tailings, it is a small logical proposition to combine the two treatment methods into a single process for in-line treatment that can deliver a water suitable for passive water treatment and subsequent discharge to the environment.

While centripetal methods achieved relatively good performance in terms of delivering a solid cake suitable for reclamation and a fluid suitable for further water treatment, we found the operation and economics of these methods, both hydrocyclones and centrifuges, problematic and potentially unnecessary. This was in large part due to the high variability in the solids content of the feed. The coarse solids were so readily separated that it was difficult to maintain them in suspension and very large differences between samples collected at the feed scroll and the centrifuge feed occurred due to settling in the DAF system where bitumen was initially recovered. Our assessment of the utility of hydrocyclones was limited due to solids settling in the initial froth flotation skid, and centrifuge feed tank, such that the hydrocyclones received far fewer coarse solids than anticipated and proved to have little positive benefit to the treatment process. Centrifuge performance depended on the solids content of the feed and rapidly degraded when solids contents dropped below 7% wt.

An alternative, proposed here, is to use a clarifier – air flotation combination to remove as much of the heavy solids, free oil and fine clays which occurred in the pre-treatment steps of the centrifuge trials. Instead of then feeding a decanting centrifuge, the subsequent feed should be suitable for direct ultrafiltration as demonstrated by the high solids loading the RSL system can process when treating blowdown waters.

Water quality following Nanoflotation did not meet the Alberta Surface Water Quality Guidelines and for several important parameters such as naphthenic acids, were unacceptably high to consider discharge to the LAR. However, the ultrafiltration permeate is suitable for consideration of passive treatment opportunities. One such opportunity is the use of treatment wetlands containing fluidized coke (Zubot et al. 2012). With the elimination of suspended solids and reduction in hydrocarbons offered by the ultrafiltration approach, the water is suitable for passage through a subsurface and surface wetland construct such as that proposed and now extensively tested in the oil sands (Zubot pers comm). These types of wetlands are effective in reducing naphthenic acids, total acid extractable organics, and nutrients sufficiently for release to the Lower Athabasca River.

Another option would be to treat the tailings water inline as discussed above. The treated water after the RSL membrane could then be used as a boiler feed water to produce high pressure steam. The high pressure steam would be used to produce electricity resulting in a high quality condensate that could be discharged.

REFERENCES

Epcor. (2013). CNRL Extraction Water Treatment Pilot Study: Nanoflotation Study Final Report. March 2013.

Loganathan, K., Bromley, D., Chelme-Ayala, P. and El-Din, M.G. (2015). A hybrid froth flotation-filtration system as a pretreatment for oil sands tailings pond recycle water management: Bench- and pilot-scale studies. *J. Environ. Man.*, **161**: 113-123.

Zubot, W., MacKinnon, M. D., Chelme-Ayala, P., Smith, D. W. and El-Din, M. G. (2012). Petroleum coke adsorption as a water management option for oil sands process-affected water. *Sci Total Env.*, 427–428: 364–372.

THE APPLICATION OF VERY LARGE PISTON DIAPHRAGM PUMPS FOR TAILINGS TRANSFER IN THE OIL SAND INDUSTRY

Hein Krimpenfort
Feluwa Pumps, Germany

ABSTRACT

The oil sand industry produces tailings in high volumes. Traditionally these tailings are transferred as a slurry through pipelines at low densities to storage facilities by means of large centrifugal type slurry pumps.

As pipelines are usually several kilometers long, pumping pressures mostly exceed 4.0 mPa (600 PSI), consequently these large centrifugal pumps need to be placed in trains consisting of several pumps in series at the plant and in multiple booster stations along the pipeline. Due to their low availability, standby pump trains are required. Consequently, a tailings pipeline is usually equipped with 20 or more of such large centrifugal pumps which operate at a relatively low mechanical efficiency.

In the mineral mining industry, very large piston diaphragm pumps (capacity 1,000 m³/hr) are in operation for similar applications. These pumps operate at a high mechanical efficiency and are capable of handling slurries at a solid concentration of 65% or more.

This paper will describe the use of such high capacity piston diaphragm pumps and compare them with centrifugal type slurry pumps on an imaginary 5.000 m³/hr (22,000 GPM) at 50 bar (725 PSI) oil sand tailings pipeline. In the paper CAPEX and OPEX will be compared and the amortization of the extra investment costs for the piston diaphragm will be calculated.

INTRODUCTION

The disposal of tailings in the oil sand industry always has presented considerable challenges.

Due to the enormous quantities of tailings and their rheological properties, over the years, large tailing ponds have been created which will remain in the same shape and consistency for many decades to come. New techniques are being developed to increase solid concentration which would reduce the flow of tailings, as well as improve the rheological properties. The implementation of these techniques however is quite difficult due to the quantities of tailings that needs to be thickened.

The transportation of these tailings currently takes place via pipelines to large tailings storage facilities (TSFs) powered by very large high-pressure centrifugal pumps. Up to a few years ago, these capacities could not be reached with other types of pumps. About 10 years ago however, high capacity piston diaphragm pumps, with a flow rate of up to 1,000 m³/hr, were developed which present a feasible alternative to these large centrifugal pumps.

PISTON DIAPHRAGM PUMPS

Materials

Piston diaphragm pump technology is already more than 40 years old and thousands of such pumps are in operation on various heavy-duty applications in the mineral mining industry. In the oil industry, high pressure piston pumps are also widely used for oil drilling to recirculate drilling mud. In the oil sand industry, however, piston pumps nor piston diaphragm pumps are very seldom in operation.

For those who are not familiar with this technology, the following is a short explanation of piston diaphragm pumps: when piston pumps are used for transferring abrasive slurries, the main pumping parts, such as pistons and cylinder liners are exposed to the slurry and subject to wear. As soon as these components are worn, slurry will start to leak over the pistons. Due to this leakage, the pump will not be able to reach its design pressure and capacity and the pump needs to be stopped.

In a piston diaphragm pump, the slurry is separated from the main pumping parts by a rubber diaphragm. The pistons pump hydraulic oil against the diaphragm which subsequently moves back and forth following the piston. As the pistons and

cylinder liners run in hydraulic oil, these components are not subject to wear. The only parts in contact with the slurry are the suction and discharge valves which are its only wearing parts. See also Fig. 1.

The extra costs for the addition of the diaphragm side to a piston pump are quickly amortized (depending on the abrasivity of the slurry) by the reduced wear part consumption.

Piston diaphragm pumps are available in various sizes, ranging from a few liters per hour, up to a thousand cubic meters per hour at pressures up to 500 bar or more, if required, see Fig. 2.

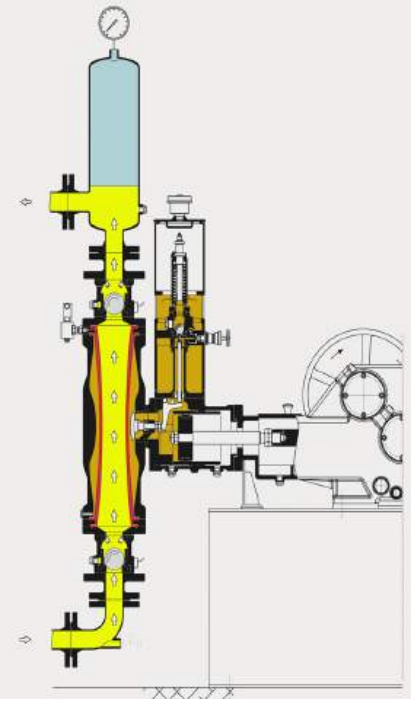

Figure 1. Cross section of a piston diaphragm pump

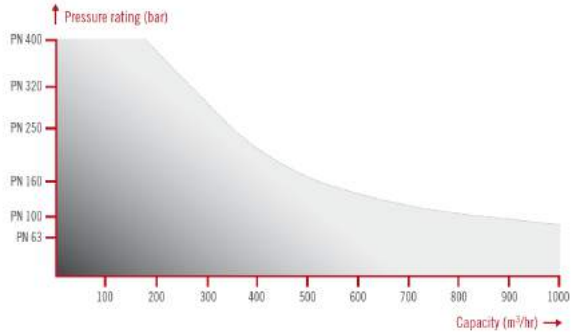

Figure 2. Performance range

Currently a number of these very large piston diaphragm pumps, with a rated capacity of 1,000 m³/hr) are in operation at a copper mine in Mexico where they transfer tailings through a 6 km long pipeline.

One of the few disadvantages of piston diaphragm pumps is their limited particle size handling capability. As the maximum particle size that can pass the suction and discharge valves is limited to a max of 8 to 10 mm, these pumps cannot be used for the transportation of oil sand slurry. The particles in tailings are usually very fine which makes these pumps especially suitable for pumping tailings slurry.

OPTIONS

For the transfer of high flow rates at elevated discharge pressures, a number of pumping alternatives are available:

Centrifugal Slurry Pumps

The first and most commonly used method is the application of centrifugal pumps in series. In order to reach an elevated discharge pressure (20 – 25 bar), typically, trains often consisting of up to 4 or 6 such pumps in series need to be installed in a station. In cases where even a higher pressure is required and even more pumps are needed, a booster station along the pipeline needs to be installed.

This is typically the case for the transfer of oil sand tailings where remote booster pump stations can be found along the pipeline.

Although the initial investment costs of these pumps are relatively low, their operating costs are usually quite high.

A large part of this higher cost is due to the relatively low efficiency of centrifugal slurry pumps when compared to PD pumps, when averaged over a complete wear cycle of the centrifugal pump, efficiency in most cases will fall in the range of 60 and 70%.

Another factor which results into high OPEX is the high wear parts consumption and associated down-time and costs. The abrasive slurry flows through the pump typically at an impeller tip speed of up to 25 m/sec. As the slurry is in direct contact with the

pump volute, wear plate and impeller, these components have to be replaced at regular intervals. Consequently, the availability of each individual pump is rather low. Since a pump train consists of multiple pump sets (see Fig. 3), the availability of a complete pump train is very low which is critical to ensure a reliable operation.

Another fact which contributes to the low availability of multiple pump trains, is that the shaft of centrifugal pumps needs to be flushed by a gland seal water system. The pressure of this system needs to increase at every stage in the train by 4 or 5 bar, which is difficult to control and makes the system vulnerable and potentially less unreliable.

The low availability of each pump set in combination with the vulnerability of the gland water system results in a very low system availability. In order guarantee a satisfactory availability, the majority of tailing pipelines are therefore equipped with at least 1 pump train of similar configuration. Some operators even prefer to have a third train of pumps to their disposal: 1 operating, 1 standby and 1 under repair.

The capacity of a centrifugal pump is dependent on its discharge pressure (further explained in chapter 6 of this paper), whenever pressure increases/capacity decreases, the possibility of settling of solids and the risk of a plug is considerable. For this reason, a positive displacement pump is often installed for deblocking purposes, which increases the total CAPEX of the entire system.

Figure 3. Centrifugal pumps in series

Medium Capacity Piston Diaphragm Pumps

An alternative for such centrifugal pumps in series, is the use of medium capacity piston diaphragm pumps (MCPD) of which the discharge pressure is in principle nearly unlimited. Therefore, booster stations along the pipeline are very seldom required. Traditionally, the capacity of such pumps is rather limited (typically 650 – 700 m^3/hr), in order to reach a high capacity, a number of such pumps need to be installed in parallel.

Obviously, the CAPEX of piston diaphragm pumps, when compared to centrifugal pumps, is relatively high. This is especially the case with conventional low to medium capacity PD pumps of which many units need to be used in parallel. These high CAPEX costs are however, depending on certain conditions, off-set by low their OPEX costs.

The mechanical efficiency of piston diaphragm pumps lies in the range of 85 and 90%, the difference with centrifugal pump systems is therefore at least 20%. This difference, especially when tailings pipelines are being used continuously and at high energy prices, leads to significantly lower annual energy costs for the piston diaphragm pump.

Furthermore, the wear part consumption of piston diaphragm pumps is much lower than for centrifugal pumps: as mentioned before, the abrasive slurry is separated from the main pump components by means of a rubber diaphragm, the only moving parts of the pump which are in contact with the slurry are the suction and discharge valves, consequently these are the only components subject to wear. The slurry flows through these valves at a velocity of less than 2 m/sec which is significantly lower than of centrifugal pumps mentioned earlier.

The combination of low energy costs and low wear parts cost lead to very low operating costs.

As the down time of piston diaphragm pumps required for replacement of wearing parts is very low, their availability is high (usually in excess of 98%), standby pumps are therefore not always required. Mostly however, such pumps are installed as an extra precaution.

Contrary to centrifugal pumps, the capacity of PD pumps is in principle independent of its discharge pressure. In case of an increasing discharge pressure, the capacity of the pump will remain

constant, as long as the same stroke rate is maintained. In case of a blocked pipeline therefore, a PD pump has the capability to remove plugs, without the need of an additional PD pump for this purpose. This benefits the CAPEX of the entire system.

High Capacity Piston Diaphragm Pumps

About 10 years ago, high capacity piston diaphragm pumps (HCPD) were introduced with a flow rate of 1,000 m³/hr (see Fig. 4). The operating principle and the advantages of these high capacity pumps are the same as for medium capacity piston diaphragm pumps described above. The OPEX therefore are very similar.

Figure 4. A 1.000 m³/hr Piston diaphragm pump

The difference lies in the fact that fewer high capacity pump units are required to reach the same flow rate.

As the price of these large pumps is lower (on a per m³ of pumping capacity) than of traditional piston diaphragm pumps, the initial investment of all pumps combined will also be lower.

The difference in pump CAPEX is further increased by the fact that also less auxiliary equipment (piping, cabling, valves and other infrastructure, also known as Balance of Plant, or BOP) will be needed. Also, less foundations are required and the entire pump station will have a smaller footprint. The total CAPEX of a HCPD pump station will therefore be lower.

For clarity, it should be noted that piston diaphragm pumps, regardless of their size, need a positive pressure on the suction side of the pump. This pressure is usually in between 1 and 3 bar and can either be provided by a sufficient static slurry level in the suction tank or (in most cases) by centrifugal type charge pumps. These charge pumps are of the same type as described above, with the same features (low efficiency, high wear part consumption, etc.). As the discharge pressure of these charge pumps is maximum 5 bar, only 1 pump is required, the influence on the CAPEX and OPEX of the piston diaphragm pump station is limited.

BASIC DATA

For the comparison in this paper, a tailings pipeline with a capacity of 5,000 m³/hr was selected with a discharge pressure of 5 mPa.

Multistage centrifugal pumps are mostly used on system pressure requirements of up to approximately 50 – 55 bar. It is generally accepted that above 55 bar the number of pumps required makes operation overly complicated and costly.

At pressures of 55 bar or more, historically piston diaphragm pumps are applied, it should be noted however, that depending on certain conditions, PD pumps also find application at pressures well below 50 bar.

For this comparison, a discharge pressure of 50 bar was chosen for which both centrifugal pumps can be used as well as piston diaphragm pumps.

Other operating parameters, such as solids concentration, viscosity, pipeline profile and such have not been considered in this comparison, only the basic pump data of 5,000 m³/hr at 50 bar are taken into consideration.

The subject pipeline obviously is located in the Athabasca region with arctic operating conditions, which require the need of a covered pump building to protect the pump and their operators from the weather conditions. Other data which are of importance are the abrasivity of the tailings, the price of power, cost of labor and water.

The abrasivity has an effect on the cost of wear parts for both types of pumps. Oil sand tailings are considered to consist mainly of silica sand which is extremely abrasive. Wear therefore will be high.

The price of power obviously has an important effect on the operating costs and supposed to be is C$ 0.10 per kWh.

For both the wear rate as well as the power price, different numbers will be compared which are summarized in a sensitivity analyses. The price of labor does not have a significant effect on the OPEX as wear part and power costs do. However, to be complete it has been included in the equitation at an hourly rate of C$ 100.00. Cost for gland water are C$ 0.40/m³. The number of operating hours per year is 8,500. These basic data are summarized in Table 1.

Table 1. Basic data

Pressure	bar	50
Capacity	m³/hr	5000
Price per kW hr	in C$	0.10
Operating hours	per year	8500
Labour cost per hour	in C$	100
Gland seal water costs per m³	in C$	40

PUMP ALTERNATIVES

For a flow rate of 5,000 m³/hr at a pressure of 50 bar, the previously mentioned pump types are considered. They are compared for this particular flow rate and pressure requirement.

Centrifugal Pumps

As mentioned before, the maximum discharge pressure of slurry type centrifugal pumps is usually limited to approximately 4 - 6 bar.

In order to reach a pressure of 50 bar, consequently 10 pumps in series are required. A train of 10 pumps in series in a single pump station is only possible with very special high pressure centrifugal pumps. Normally the casing pressure of these pumps does not allow pressures exceeding 30 bar. Therefore, such trains are usually divided over 2 pumps stations: one at the thickener and a second station at an appropriate intermediate point on the pipeline. This configuration is applied in this study.

As the availability of individual slurry centrifugal pumps is approximately 96%, the availability of a pump train with 5 pumps is limited to 77%. In order to ensure a maximum availability, a standby train will be required. Consequently, the centrifugal pump system will consist of 2 pump stations each equipped with an operating train with 5 pumps and an identical standby train.

The pumps selected for this application are 18/20 size slurry pumps with a capacity of 5,000 m³/hr, they are driven by 1,000 kW MV motors. In order to adjust the flow rate of each pump train, 1 out of 5 pumps per train are equipped with MV variable speed drives.

The average price for these pumps sets (pump, gearbox, motor) is quoted to be approximately C$ 600,000, including VFD the price is C$ 975,000.

The pumps require a large quantity of auxiliary equipment to keep them running satisfactorily. This auxiliary equipment consists of piping, cabling, switchgear, transformers, strainers, isolation valves etc. also called BOP.

Depending on the type of study, pipeline engineering companies use a “rule of thumb” factor to calculate the cost of the BOP, which is based on their experience in the design of these stations.

This factor varies from one engineering company to another, usually however a multiplier of 2 is applied to the accumulated price of the centrifugal pumps to estimate the price of the BOP. The BOP also includes the extra costs for the construction of 2 separate pump stations (rather than 1) and of extra cabling and gland water piping, etc. In the oil sand fields, however, the arctic like operating conditions require extra investments in heating, insulation and other precautions, therefore a multiplier of 2.5 is justified.

The efficiency of these large centrifugal pumps is estimated to average 70% over the wear life of the pump. As the slurry is considered to be very abrasive, the annual wear part consumption is estimated to be 100% of the CAPEX of the pumps. It should be noted that this percentage is applied over the price of the pump only, it excludes wear parts consumption of the gearbox, motor and VFD.

A factor which should not be ignored in these multistage systems, especially in arctic conditions, is the supply of gland water to the stuffing box of each slurry pump. This requires a complicated and vulnerable system, based on a small piston pump which supplies clean water to the shaft of the centrifugal pump.

At each stage in the pump train the pressure of the gland water needs to be higher than the discharge

pressure of the prior slurry pump. The vulnerability of this system, decreases the availability of the entire pump train.

This comparison is based on seal water consumption of 1.5 m³/hr per pump at an average total system pressure of 23 bar (slightly above the discharge pressure in the last stage 46 bar). In addition, also, the costs of gland water need to be considered: the cost of clean water (assumed to be C$ 40 per m³), based on a consumption of 1.5 m³/hr per pump by 10 operating pumps at 8,500 hours per year however are relatively minor.

Medium Capacity Piston Diaphragm Pumps

The maximum capacity of traditional (3-cylinder single acting) piston diaphragm pump is approximately 650 to 700 m³/hr, regardless of the discharge pressure. For higher capacities, the pump components would need to be too large and heavy to guarantee safe operating and maintenance conditions, as well as a low NPSHr.

For a total flow of 5,000 m³/hr, a total of 7 operating pumps would be required. Although the availability of these pumps is 98% or more, an extra standby pump needs to be installed to warrant a 100% availability of the system.

The pumping pressure of PD pumps is in principle unlimited, therefore only 1 pump station is required which is equipped with these 8 MCPD pumps.

As mentioned earlier, the PD pump need to be fed by a centrifugal type charge pump which is basically identical to the centrifugal pumps described in the previous section.

Also, these charge pumps require a gland water system which however consist only of 1 stage.

The gland water system is therefore much simpler and does not consume as much water and power. Each pair of 2 PD pumps can be fed by a single centrifugal type charge pump, a total of 4 centrifugal pumps therefore be required. In addition, an extra centrifugal pump needs to be available for standby purposes.

The average price of such medium capacity PD pumps is approximately C$ 3,450,000 which includes an external gearbox and a 1,400 kW MV motor with variable speed drive. The price for the charge pumps (1,500 m³/hr at 3 bar pressure) is estimated to be C$ 120,000, including gearbox and constant speed motor.

The overall efficiency of piston diaphragm pumps is typically in excess of 85%.

As the only wear parts in contact with the slurry are the suction and discharge valves, the annual wear parts costs (based on operational experience) is 4 to 5% of the CAPEX of the pumps. To cover the wearing parts costs of the charge pump, an extra 1% is added. As with centrifugal pumps, this percentage is applied only to the pump, not to the gearbox, motor and VFD.

The quantity of Balance of Plant (piping, valves, cablings, switchgear, etc.) required to keep these big pumps running is less than for centrifugal pumps, especially with 2 stations with 5 + 5 of such pumps in series. The rule of thumb factor that usually is applied to calculate the cost of the BOP is in between 1 and 1.5. In this comparison we have calculated with a factor of 1.2. It should however be considered that the CAPEX of PD pumps is much higher than of centrifugal pumps, even when there are 2 x 5 of such pumps in series in 2 pump stations. Floor space required (including maintenance area) for 8 pumps is estimated to be approximately 2,000 m².

High Capacity Piston Diaphragm Pumps

The pumps that are selected in this comparison as “High Capacity Piston Diaphragm pumps” are Feluwa type QGK500 double hose diaphragm pumps.

These are of 5-cylinder single acting configuration and are actually in operation very successfully at the Boleo Copper mine in Baja California, Mexico since 2013.

The pumps have a maximum capacity of 1,000 m³/hr, consequently only 5 of such pumps are required to transfer the total quantity of 5,000 m³/hr through the pipeline.

As with the MCPD pumps, also here an extra standby pump is required to guarantee maximum availability. The 6 pumps are fed by 3 charge pumps, plus 2 standby. The price for the 5-cylinder pump is approximately C$ 4,250,000, including MV motor and VFD. The other parameters (efficiency, wear part consumption) are the same as for the traditional MCPD pumps. As the charge pumps for the high capacity PD pumps are somewhat higher

than for the medium capacity pumps, the price is also higher.

Foot print for 6 of these pumps (including maintenance area) is approximately 1,400 m² which is 30% less than what is required for the smaller MCPD pumps. This difference can be explained by the fact that traditional piston diaphragm pumps are equipped with flat circular diaphragms which make the pump relatively wide.

The 5-cylinder pump has tubular diaphragms which makes this design much more compact. Due to the reduced number of pumps and their smaller footprint the pump station will be smaller. Consequently, a multiplier for Balance of Plant of 1 is included in the calculations.

CALCULATIONS AND RESULTS

A number of parameters which determine CAPEX and OPEX of each type of pump station is compared. In the tables below, these costs are summarized and the difference in costs between the systems is indicated.

CAPEX

The investments for pumps and Balance of Plant including pump housing, specified in Chapter 4 for each system are shown in Table 2. To cover the costs for EPCM, 12% has been added, an additional 15% has been added for contingencies. It is obvious that the CAPEX for centrifugal pumps is considerably lower than for PD pumps, however when Balance of Plant is included, this difference is significantly reduced, especially in the case of high capacity PD pumps.

OPEX (in C$)

The operating expenditure of these pump systems are mainly determined by power, wear parts and to a lesser extent, labour and gland seal water consumption. The cost for financing has not been considered.

Power Consumption

The power consumption and its cost of power is the biggest contributing factor to the total of operating costs. Depending on the efficiency of the pumps and the electricity price, cost of power, for centrifugal pumps, can contribute 75% to the OPEX.

Table 2. CAPEX comparison (in C$)

CAPEX	Centrifugal pumps	MCPD	HCPD
Capacity in m³/hr	5000	713	1000
Number of required pump units	20	8	6
Price per pump	675,000	3,450,000	4,200,000
Number of operating pumps	10	7	5
Number of standby pumps	10	1	1
Number of charge pumps for PD pumps		4	3
Number of standby charge pumps for PD pumps		2	2
Price per change pump		120,000	180,000
Total system pump CAPEX	13,500,000	28,320,000	26,100,000
CAPEX of BOP and pump station	33,750,000	33,984,000	26,100,000
Total direct costs	47,250,000	62,304,000	52,200,000
EPCM (12%)	5,670,000	7,476,480	6,264,000
Contingency (15%)	7,087,500	9,345,600	7,830,000
Total CAPEX pump station(s)	60,007,500	79,126,080	66,294,000
Difference in CAPEX		**19,118,580**	**6,286,500**

For PD pumps, the cost of power can be even as high as 90%, this is mainly caused by the fact that the other OPEX costs (especially wear parts) for these pumps are relatively low. In the Sensitivity Analyses section, the influence of a higher or lower kWh price is shown. Costs for power consumption are compared in Table 3.

Wear Parts Consumption

After the cost of power, costs for wear parts are the most important share of the OPEX of slurry pumps. Oil sand tailings consist mainly of silica sand which is considered to be extremely abrasive. In centrifugal pumps, this extremely abrasive slurry is

Table 3. Comparison power costs

	Centrifugal pump	MCPD	HCPD
Pressure	50	50	50
Capacity	5,000	5,000	5,000
Price per kW hr	0.1	0.1	0.1
Operating hours	8,500	8,500	8,500
Assumed efficiency in %	70	88	88
Calculation			
Absorbed power in kW	9,921	7,891	7,891
Hourly power cost	992	789	789
Annual power cost	**8,432,540**	**6,707,702**	**6,707,702**
Difference in power consumption per year		**1,724,838**	**1,724,838**

Table 4. Comparison wear parts costs

	Centrifugal pump	MCPD	HCPD
Parts consumption in % of purchase price	100	5	5
Calculation			
Annual pump wear parts cost	4,218,750	724,500	630,000
Difference in wear parts costs per year		**3,494,250**	**3,588,750**

Table 5. Comparison labour costs

	Centrifugal pump	MCPD	HCPD
Number of required pumps	20	8	6
Maintenance man hours per year per pump	300	200	250
Labour cost per hour	100	100	100
Calculation			
Annual labour costs	600,000	160,000	150,000
Difference in labour costs per year		**440,000**	**450,000**

in direct contact with the in contact with large and expensive pump components. Consequently, annual wear parts costs are about one third of the total operating expenditure of these pumps. The annual wear parts costs for centrifugal pumps is assumed to be 100% of the pump CAPEX.

For piston diaphragm pumps, only the suction and discharge valves are in contact with the slurry and wear parts costs are therefore approximately 4 - 5%. As mentioned before, the PD pumps are fed by centrifugal type charge pumps a total wear parts costs factor of 5% has been calculated with.

Other percentages for wear part consumption of centrifugal pumps are reviewed in the Sensitivity Analyses section.

Labour Costs

Labor costs play a relatively minor role in the operating costs for slurry pumps. In the oil sand industry, however, labor is quite expensive and surely needs to be considered.

The main components of centrifugal pumps need to be replaced frequently. This is, in addition to being expensive, is also time consuming.

The number of hours which need to be spent on maintenance and replacement on these pumps is therefore much higher than on PD pumps. As the quantity of centrifugal pumps is much higher, the labour costs for all of these pumps are considerably higher.

The difference in maintenance hours between the traditional and the high capacity PD pump can be explained by the fact that the traditional pump has 3 cylinders with 6 valves, whereas the 5-cylinder pump has 10 sets of valves. As only 6 of these high capacity pumps are required, rather than 8, the total labour costs pumps are still slightly less.

Varying labour costs have not been included in the sensitivity analyses, as the impact of these costs on the total OPEX is limited.

Gland Seal Water Costs

The cost for gland seal water (see Table 6) is, compared to power and wearing parts, very limited. The influence of the gland water system on the vulnerability of the centrifugal pump is much more important than its influence on the OPEX. Gland

Table 6. Comparison gland seal water costs

	Centrifugal pump	MCPD	HCPD
Power cost gland water pumps	9,563	3,825	2,869
Gland seal water consumption (at 1.5 m³/hr per pump)	127,500	51,000	38,250
Gland seal water cost (at C$ 0.40/m³)	51,000	20,400	15,300
Annual costs gland seal water system	60,563	24,225	18,169
Difference gland seal water costs per year		36,338	42,394

Table 7. Comparison summary

	Centrifugal pump	MCPD	HCPD
Annual power consumption	8,432,540	6,707,702	6,707,702
Annual spare parts costs	4,218,750	724,500	630,000
Annual labour costs	600,000	160,000	150,000
Annual gland water costs	60,563	24,225	18,169
Annual OPEX	13,311,852	7,616,427	7,505,871
Contingency (15%)	1,996,778	1,142,464	1,125,881
Total annual OPEX	15,308,630	8,758,891	8,631,751
Difference in OPEX per month		545,812	556,407
Total CAPEX	60,007,500	79,126,080	66,294,000
Amortization period	**in months**	**35**	**11**
	in years	**2.9**	**0.9**

Table 8. Result sensitivity analyses MCPD

		% of CAPEX for centrifugal pumps spare consumption				
		50%	80%	100%	120%	150%
Power cost in C$/kWh	8	5.1	3.7	3.1	2.7	2.2
	10	4.6	3.4	2.9	2.5	2.1
	12	4.2	3.2	2.8	2.4	2.0
	15	3.7	2.9	2.5	2.2	1.9

Table 9. Result sensitivity analyses HCPD

		% of CAPEX for centrifugal pumps spare consumption				
		50%	80%	100 %	120 %	150 %
Power cost in C$/kWh	8	1.6	1.2	1	0.9	0.7
	10	1.5	1.1	0.9	0.8	0.7
	12	1.4	1.0	0.9	0.8	0.7
	15	1.2	0.9	0.8	0.7	0.6

seal water consumption is based on 1.5 m³/hr per pump at a price of C$ 0.40 per m³.

Dilution of the tailings by the gland water has not been considered as this is only minor (in the case of centrifugal pumps only 15 m³/hr on a total flow of 5,000 m³/hr).

Summary

The result of the comparison of the above-mentioned parameter is summarized in Table 7. Based on the specified assumptions the amortization period for extra costs of the traditional PD pumps is 2.9 years. For the high capacity pumps, this is even reduced to 0.9 years which is mainly driven by the fact that fewer pumps are required with lower costs for Balance of Plant.

SENSITIVITY ANALYSES

As shown in Table 7, the main contributors to the OPEX of slurry pumps are the power and wear parts costs. Consequently, mainly these factors determine the amortization period of the extra costs for PD pumps when compared to centrifugal type slurry pumps.

For this reason, the cost of power and wear parts are subject to a sensitivity analyses where the price for electricity varies from C$ 0.08 to 0.15 per kWhr and the wear parts costs for the centrifugal pumps varies from 50 (for light abrasive slurries) to 150% (for very abrasive slurries) of the CAPEX of the centrifugal pumps.

The results of this analyses when compared to traditional PD Pumps can be seen in Table 8.

The same analyses regarding the amortization period of traditional PD pumps has been made for high capacity PD pumps. As can be expected, due to the lower CAPEX of these pumps, the payback

period is much shorter than with the traditional MCPD pumps (see Table 9).

TECHNICAL FEATURES

In addition to operational expenditure advantages, PD pumps also offer technical features which are advantageous when compared to centrifugal pumps. The most important one is based on the principle that the pumping capacity of PD pumps is independent of the discharge pressure. The only way to vary the flow rate of PD pumps, is to adjust the stroke rate. As known, with centrifugal pumps, when the system pressure increases, the pump follows its pump curve resulting in a reduced flow rate. A reduced flow rate results into a decrease in the velocity at which the slurry flows through the pipeline.

Every slurry has a deposition point, below which solid particles in the slurry will start to settle on the bottom of the pipeline. If the slurry velocity drops below the deposition point, a layer of particles will start to grow, reducing the pipeline diameter.

The reduced diameter will result in an increase in required discharge pressure, this in turn will again move the pump further back on the curve with a further reduction in flow rate as a consequence. This process can result in a vicious circle where the pump pressure ultimately will reach its closed valve position and does not produce any flow at all. This may be referred to as a pipeline blockage, but ss more accurately described as a system pressure exceeding the closed valve pressure capability of the pump.

As no slurry will be discharged from the pump, consequently, the build-up of particles may block the pipeline. See also Fig. 5.

Especially in remote locations, or arctic conditions, a plug in the pipeline can be difficult to remove which results into a long standstill of operations.

The PD pump has different characteristics: its capacity does not depend on its discharge pressure. As long as sufficient power to drive the pump is available, the pressure bearing components (discharge manifolds, valves, diaphragm housings, pulsation dampener), as well as the rod load of the crankshaft are suitable, the pressure can be increased without any reduction in flow rate or other consequences. For this reason, the risk of a blocked pipeline is substantially reduced.

In the unlikely event of a plug in the line, the PD pumps which are used to transfer the slurry, will be able to produce sufficient pressure for removal of the plug. An additional PD pump for this purpose will not be required.

Another feature of piston diaphragm pumps is that capacity does not vary with changes in slurry viscosity or specific gravity. This with previously mentioned stable capacity features, allows for designing reliable slurry systems with much higher solid concentrations than would be considered practical with centrifugal pumps. This makes this class of equipment ideally suited for higher density tailings systems and all of the benefits to cost and safety that these systems provide.

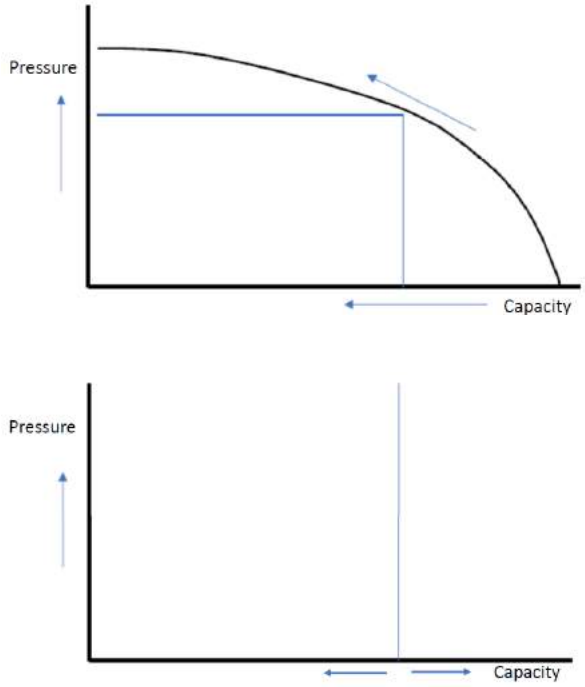

Figure 5. Curves of centrifugal and PD pumps

CONCLUSIONS

For this comparison, a pipeline application of 5,000 m³/hr at 50 bar has been selected. Although this may not represent the majority of existing tailings slurry transfer applications, there are already a number of pipelines in operation at similar conditions, especially in the oil sand fields.

Moreover, it can be expected that demand for such pipelines will increase for existing and future mines.

In this Paper, a number of operational cost factors have been considered such as power and water, cost for wear parts and labor as well as pump pricing and commonly used costing criteria for CAPEX, in a comparison between centrifugal pump system in series, traditional piston diaphragm pumps and high capacity piston diaphragm pumps in parallel.

Depending on price of electricity and the wear part consumption of pumps, the use of large piston diaphragm pumps for high flow rate slurry pipeline applications is proven to be feasible.

Payback period for the extra CAPEX of piston diaphragm pumps varies from 5.1 to 1.9 years for medium capacity piston diaphragm pumps, depending on wear part consumption and the price of power.

For high capacity piston diaphragm pumps, this period is even reduced to 1.6 to 0.6 year which makes this type of pump the most feasible option for high flow rate slurry pipelines.

In addition to commercial advantages, piston diaphragm pumps offer, the operational advantage that the risk of a blocked pipeline with these pumps is considerably less, than with centrifugal pumps.

ACCELERATED DEWATERING OF MATURE FINE TAILINGS THROUGH MICROBIAL INDUCED CALCIUM CARBONATE PRECIPITATION

Qianwen Liu[1], Brina Montoya[1] and Brian Martinez[2]
[1]North Carolina State University, Raleigh, United States
[2]Geosyntec Consultants Inc., CA, United States

ABSTRACT

Dewatering mature fine tailings (MFT) presents challenges to the oil sand industry due to the long-term stability of the MFT suspension. Microbial induced calcium carbonate precipitation (MICP) is investigated to accelerate the dewatering process of MFT. Hydrometer and column tests are conducted to evaluate the performance and mechanism of MICP treatments in MFT. Three stages of the dewatering process were observed in the MICP treated specimens, and after eight days the elevation of water-solids interface becomes relatively stable. The microstructure of the MFT before and after the MICP treatment was evaluated using cryo-SEM imaging. The results also show that the MICP process accelerates the dewatering process by creating pathways for the water to leave the MFT suspension as well as cementing solids.

INTRODUCTION

Alberta, Canada has the second largest deposit of oil sands, where 2.5 million barrels of crude bitumen were produced per day in 2016 (AER 2016/17 Annual Report). By the end of 2013, oil sand tailings, which are the by-product of crude oil production from oil sands, occupied an area of 220 km^2 (Steward 2015). Fluid fine tailings (FFT) are the deposit consisting of fine-grained sediment, sand, water, and bitumen. And within 2 to 5 years, when coarse sands have settled and the solids content of the suspension is greater than 30 % (weight of dry solids divided by the total weight), the stable suspension is termed mature fine tailings (MFT) (FTFC 1995, Liang et al. 2015).

The major extraction method, the Clark extraction process, uses a mixture of hot water, steam, and caustic to separate the bitumen from the oil sands, and generates tailings with a pH between 8 and 9 (FTFC 1995). Because of the extraction process and resulting high pH, the MFT demonstrates behavior consisting of extremely dispersed, high void ratio fabric, with large-strain consolidation, and low yield strength (Miller et al. 2010, Scott et al. 1985). A 25-year long study was conducted using a 10 m tall standpipe to demonstrate the compression behavior of the MFT (Jeeravipoolvarn et al. 2009). The results indicated the decrease in void ratio and interface settlement observed over the 25 years did not contribute to an increase in effective stress, and the pore pressure was measured to be as high as the total stress. This unique behavior of MFT demonstrates the need to find a treatment process to flocculate and densify the MFT. Once the MFT settles, the tailings can be dewatered and the water supernatant can be reused.

In recent years, many creative techniques have been suggested to accelerate the dewatering process. Yang et al. (2016) conducted research introducing *Tubifex* genus, which was known as sludge or sewage worms, to accelerate dewatering of fine tailings. By moving up and down to make channels as well as ingesting sediments and absorbing molecules through their body wall, *Tubifex* can accelerate the consolidation process of MFT in the last stage of the settlement process. In addition to the proposed treatment process using *Tubifex*, cationic and anionic flocculant polymers can be introduced into MFT to enhance dewatering. Li et al. (2015) used a thermos-sensitive polymer, named poly (n-isopropyl acrylamide) (PNIPAM) to dewater the oil sand fine tailings. PNIPAM worked well at 50 ℃ but did not demonstrate the ability to flocculate the MFT at room temperature because of its thermos-sensitive molecular properties. Nusri et al. (2016) proposed a method to increase the strength of MFT by using geopolmerization reactions to activate the surface minerals of MFT clay and increase the strength of MFT after 90 days of treatment. The high-molecular-weight flocculants or polymers can decant water from MFT by bridging the solids and enhancing the floc strength (Demoz and Mikula 2012, Li et al. 2015).

Precipitation of calcium carbonates from microbial induced calcium carbonate precipitation (MICP) can also provide cohesive bonds between soil particles (DeJong et al. 2013, Montoya and DeJong 2015). The typical water chemistry of MFT is also compatible with the MICP process, as calcium (17 to 25 mg/L) is the dominant cation (Proskin et al. 2012) and the pH is about 8 to 9, which is the preferred range for the alkalophilic soil bacterium *Sporosarcina pasteurii* (ATCC 11859) often used to induce MICP. The chemical reactions related to the MICP are shown below (Eq. 1 and 2) (DeJong et al. 2006).

$$NH_2\text{-}CO\text{-}NH_2+3H_2O \rightarrow 2NH_4^+ + 2OH^- + CO_2 \quad (1)$$

$$Ca^{2+} + HCO_3^- + OH^- \rightarrow CaCO_{3(s)} + H_2O \quad (2)$$

Liang et. al. (2015) demonstrated that MICP can be used to flocculate MFT, and their findings indicated that the ureolytic-driven MICP treatment method can increase the strength of MFT from 20 Pa to 790 Pa after 24 h of treatment. However, the test was only conducted for 24 hours and did not demonstrate the improvement mechanism of MICP on MFT. Moreover, currently most of the applications of MICP treatment are on sands (Ashkan and Montoya 2018, Cheng et al. 2016, van Paassen et al. 2010), but the utilization of MICP on extra soft soils is not clear. With abundant microbial species in the tailings ponds (Foght et al. 2017), the application of the MICP on MFT may be an effective and environmentally-friendly method. Hence, further tests are warranted. The objective of this study is to explore the dewatering process of the MFT using MICP treatments with different solutions and to explain the mechanism of the MICP process on MFT.

GENERAL PROPERTIES OF MATURE FINE TAILINGS

A phase diagram is commonly used in geotechnical engineering to aid in defining parameters and calculating mass-volume relationships for a soil. The presence of bitumen makes the phase diagram of MFT unique. In the MFT system, bitumen is represented as a solid because it can be absorbed on the soil surface and the high viscosity of bitumen prevents it from flowing (Scott et al. 1985). The phase diagram of MFT is shown in Figure 1. Figure 2 shows the solid phases of MFT before and after centrifugation. The layers after centrifugation (Figure 2(b)) are in accord with Proskin et al. (2010).

The presence of the bitumen as a part of solid requires a redefinition of some common geotechnical parameters (Dusseault and Scott 1983). It should be noted that mining engineering uses total mass in the denominator to express some indexes (Miller et al. 2010), while in geotechnical engineering, the indexes are expressed as dry mass. For example, in mining engineering the water content is defined as the mass of water divided by the total mass, while in geotechnical engineering it is defined as the mass of water divided by solid mass. In this paper, indexes are expressed in geotechnical engineering terms and the differences of the definition between these two disciplines are shown in Table 1.

MATERIAL AND METHODS

MFT were received from Syncrude Canada Ltd in Alberta, Canada. The MFT experienced partial dewatering during the shipment from Alberta, Canada to North Carolina, USA; therefore, the tailings were mixed for a half an hour to reestablish a consistent suspension.

The water content of MFT was determined following ASTM D2216 (2010) by oven-drying the material at 110 ℃ for 24 hours. In order to obtain the mass of soil (i.e., solids with the bitumen removed), the dried MFT sample was then mixed with toluene in flasks and shaken in an incubator for 24 hours. The residual solid was filtered and dried again to obtain the mass of soil; the mass of bitumen represented the difference in the dried masses (Holowenko et al. 2000). Specific surface area (SSA) was tested using the methylene blue spot test of the dry soil samples (Yukselen and Kaya 2006). Liquid limit, plastic limit, specific gravity and pH were tested using the Casagrande cup (ASTM D4318-10), rolling method (ASTM D4318-10), water pycnometer (ASTM D854-14) and pH strips, respectively. The calcite content was assessed through gravimetric acid washing (Choi et al. 2017, Montoya and DeJong 2015). The properties of the MFT are shown in Table 2.

Five tests groups were developed to evaluate the effect of MICP on the dewatering of MFT (Table 3) through hydrometer and column tests. The control (Group 1) provided a reference to compare all other treated specimens. Group 2 introduced the

bacteria and urea without calcium to evaluate if the MICP reaction could utilize the dissolved calcium within the tailings solution. Groups 3 through 5 provided calcium for the MICP reaction and varied the concentrations of urea and calcium to evaluate the effect of increased precipitation. Though the concentrations of urea and calcium chloride vary in Groups 3 through 5, the ratio between urea and calcium chloride remained constant at 3.33:1, which is similar to other MICP studies (e.g., Martinez et al. 2013). *Sporosarcina pasteurii* (ATCC 11859, DeJong et al. 2013) with 10^7 cells/mL was used for the MICP treatment process. The bacteria preparation process presented by Montoya and DeJong (2015) was followed herein.

Hydrometer tests (ASTM D7928-17) running for 24 hours were conducted to explore the particle size distributions of each group evaluated. Tailings were initially mixed with 200 mL deionized water in an empty beaker with a magnetic stir rod. The appropriate amount of urea and calcium chloride (Table 3) were mixed in another beaker. Then the tailings suspensions and mixed chemical solution were transferred into a hydrometer cylinder; any MFT adhering to the beakers was rinsed into the cylinder. Finally, the bacterial solution and residual amount of water was added to the cylinder to make a 1 L solution for each trial. A stopper was placed at the top of the cylinder and the cylinder was turned over 10 times. The self-weight consolidation processes of MFT with or without MICP treatment were investigated by column tests in the same sedimentation cylinders for a duration of a month. To decrease the disturbance of the tailings, the hydrometers remained in the cylinders for the entire duration. The volume of the solids was obtained from the graduations on the cylinders and the water-solids interface elevation was normalized as the volume of the solids divided by the area of the column (32.15 cm^2).

Due to the sensitive fabric of MFT, a cryo-scanning election micrograph (cryo-SEM) was used to evaluate the microstructure of the material at the termination of the treatment process. Cryo-SEM analyses were conducted using a JEOL JSM-7600 FE SEM (JEOL USA, Peabody, MA) outfitted with Alto-2500 (Gatan, Warrendale, PA). Samples were plunged frozen in liquid nitrogen slush, transferred under vacuum to the Alto-2500 preparation chamber and cryofractured. The fractured sample was etched for 5 min at - 95°C under 4 x 10^{-7} kPa vacuum to reveal the microstructure. Samples were allowed to cool down to -120°C. An in-situ cold magnetron coater was used to make a 5 nm thickness Au coating on etched samples. The SEM images were taken using 5 keV energy at 8 mm working distance under cryo-temperature. A limitation of the cryo-SEM device is that elemental composition analysis is unable to be conducted.

TEST RESULTS AND DISCUSSION

Hydrometer Test Results

Figure 3 shows the particle size distribution for each group where the lowest value of percent passing represents the material that was left in suspension after 24 hours. The control group, Group 1, has finest particle distribution compared to the other groups, with 42 % of the particles remaining in suspension after 24 hours. The MICP process appears to increase the particle size, creating a coarser particle distribution. There is a slight difference in particles size distribution between Group 2 and Groups 3 to 5. Group 2 has a finer distribution because only the in-situ calcium was available for calcium carbonate precipitation during the MICP process. There is little difference in particle size distribution between Groups 3 to 5, where both urea and calcium chloride were provided for the MICP process but at varying concentrations (Table 3).

Dewatering Column Test Results

The decrease in elevation of the interface between water and solids in the hydrometer cylinder provides further indication of the flocculation mechanism improved by MICP. Figure 4 shows the elevation decrease in the water-solid interface for four sets of photos captured at (a) the beginning of the experiment, (b) four hours, (c) one day, and (d) 31 days. By comparing the water-solids interface of Group 1 in Figure 4(a) and Figure 4(d), there is no obvious water-solids interface within the 31 days of testing, but the total volume of the solution is decreased by approximately 100 mL due to evaporation. However, for Groups 2 through 5, the water-solids interface is visually clear (Figure 4(b) to (d)).

The dewatering mechanism induced by MICP treatment was observed to occur in three distinct stages. Figure 5 shows measurements of the water-solids interface elevation versus time. Stage 1 of the dewatering process was observed from

0.03 days (0.72 hours) to 0.17 days (4 hours), which corresponds to the water-solids interface of each group dropping rapidly. The rate of dewatering decreases during Stage 2, from 0.17 days to 8 days, and after 8 days the water-solids interface elevation becomes stable, representing Stage 3. These three stages may relate to the behavior of slurries from sedimentation to consolidation (Bo 2008, Hawlader et al. 2007, Wong et al. 2008). In the first stage, the particles settle separately and gradually grow into clumps or flocculate. While in the second stage, the particles become more concentrated, crowded and connected to each other. Finally, in the third stage, soil structure gradually develops effective strength to support upper layers, which reaches a consolidation stage. The observed dewatering stages may also be a reflection of the ureolytic activity of the bacteria, where perhaps the transition between stages represents the depletion of urea. Additional tests are needed to further evaluate the observed phenomenon.

Gas bubbles were observed in Groups 2 through 5 during the column tests, likely due to the generation of carbon dioxide and/or ammonia during ureolysis. Cracks presented in Figure 6 are made by gas bubbles leaving the suspension; however, those cracks also create pathways for water to decant (Fedorak et al. 2003, Guo 2009). The supernatant in Groups 2 through 5 in Figure 4(b) is cloudy; however, after 20 hours the solution becomes clear and thin mineral precipitation layers can be observed on the surface of the soil layers for Groups 3 through 5.

Microstructure Observed by Scanning Electron Micrographs

It has been reported by researchers that a face-to-edge microstructure or a card-house structure is observed in MFT due to the repulsive and attractive forces of the clay particles (Botha and Soares 2015, Miller et al. 2010, Proskin et al. 2010). This highly ordered fabric allows for higher void ratio and larger water retention. Under a magnification of x2000, similar card-house structures of MFT (Figure 8) were observed from the cryo-SEM images. After MICP treatment a tighter arrangement of card-house structures were presented in Figure 8(b). A comparison of the fabric of MFT before and after MICP treatment (Figure 8(a) and Figure 8(b), respectively), indicates that MFT has been densified during the MICP treatment. Meanwhile, some round spherical structures are observed in Figure 8(b) at the face-to-edge points that could be the microbial cells (Foght et al. 2017), and the larger particles at the up right corner and bottom left corner may be the cemented solids by MICP treatment (Liang et al. 2015).

CONCLUSION

This paper presents hydrometer and column tests to demonstrate the effect of MICP treatments on the dewatering process of MFT. Without the MICP treatment, a significant amount of time is required for the MFT to decant. Based on the results presented herein, 42% of the particles remain in suspension after 24 hours in the control group (Group 1) suspension, and after a month of the self-slurry consolidation process no obvious water-solids interface was observed in Group 1. In contrast, the MFT specimens treated with the MICP process demonstrated dewatering behavior. Three stages of the dewatering process were observed and may be related to the sedimentation-consolidation behavior of slurries. Two different mechanisms may be used to explain the dewatering of MFT due to the MICP treatment. Gases are produced during the MICP reactions and the gases provide a pathway for water to exit the suspension. The SEM images indicate the MFT samples have been densified by the MICP treatment and some cemented solids are observed. This second mechanism is further strengthened by the hydrometers results of the MICP treated specimens, which indicates coarser particle distributions likely due to a combination of the precipitated calcium carbonate minerals bonding soil particles together and being attracted to the surface of the clayey particles.

ACKNOWLEDGEMENTS

Funding from the National Science Foundation (CMMI # 1554056) is appreciated. Any opinions, findings, and conclusions or recommendations expressed are those of the authors and do not necessarily reflect the views of the National Science Foundation. This work was performed in part at the Analytical Instrumentation Facility (AIF) at North Carolina State University, which is supported by the State of North Carolina and the National Science Foundation (ECCS #1542015). The AIF is a member of the North Carolina Research Triangle Nanotechnology Network

(RTNN), a site in the National Nanotechnology Coordinated Infrastructure (NNCI).

REFERENCES

AER (Alberta Energy Regulator). (2017). AER 2016/17 Annual Report. Alberta, Canada. See http://www.eub.gov.ab.ca/documents/reports/AER2016-17AnnualReportExecutiveSummary.pdf (accessed 19/03/2018).

ASTM D2216: 2010. Standard test method for measurement of laboratory determination of water (moisture) content of soil and rock by mass. ASTM International, West Conshohocken, PA, USA.

ASTM D4318: 2010. Standard test method for liquid limit, plastic limit and plasticity index of soils. ASTM International, West Conshohocken, PA, USA.

ASTM D854: 2014. Standard test methods for Specific gravity of soil solids by water pycnometer. ASTM International, West Conshohocken, PA, USA.

ASTM D7928: 2017. Standard Test Method for Particle-Size Distribution (Gradation) of Fine-Grained Soils Using the Sedimentation (Hydrometer) Analysis. ASTM International, West Conshohocken, PA, USA.

Bo, M. W. (2008). Compressibility of ultra-soft soil. World Scientific Publishing Company. Danvers, MA, USA, Chapter 2, pp. 6-11.

Botha, L. and Soares, J.B. (2015). The influence of tailings composition on flocculation. The Canadian Journal of Chemical Engineering **93**(9): 1514-1523.

Cheng, L., Shahin, M. A. and Mujah, D. (2017). Influence of Key Environmental Conditions on Microbially Induced Cementation for Soil Stabilization. Journal of Geotechnical and Geoenvironmental Engineering, **143**(1)**:** 04016083.

Choi, S. G., Park, S. S., Wu, S. and Chu, J. (2017). Methods for calcium carbonate content measurement of biocemented soils. Journal of Materials in Civil Engineering, **29**(11): 06017015.

DeJong, J. T., Fritzges, M. B. and Nüsslein, K. (2006). Microbially induced cementation to control sand response to undrained shear. Journal of Geotechnical and Geoenvironmental Engineering, **132**(11): 1381-1392.

DeJong, J. T., Soga, K., Kavazanjian, E. et al. (2013). Biogeochemical processes and geotechnical applications: progress, opportunities and challenges. Géotechnique, **63**(4): 287-301.

Demoz, A. and Mikula, R. J. (2011). Role of mixing energy in the flocculation of mature fine tailings. Journal of Environmental Engineering, **138**(1): 129-136.

Dusseault, M. B. and Scott, J. D. (1983). Tailings pond behavior and characterization of oil sand tailings sludge. Particulate Science and Technology, **1**(3): 295-309.

Fedorak, P. M., Coy, D. L., Dudas, M. J. et al. (2003). Microbially-mediated fugitive gas production from oil sands tailings and increased tailings densification rates. Journal of Environmental Engineering and Science, **2**(3): 199-211.

Fine Tailings Fundamentals Consortium (FTFC). (1995). Advances in oil sands tailings research. Alberta Department of Energy, Edmonton, AB, Canada, 1: 6-7, 79-80.

Foght, J. M., Gieg, L. M. and Siddique, T. (2017). The microbiology of oil sand tailings: past, present, future. FEMS Microbiology Ecology, **93**(5): 1-22.

Hawlader, B. C., Muhunthan, B. and Imai, G. (2008). State-dependent constitutive model and numerical solution of self-weight consolidation. Géotechnique, **58**(2): 133-141.

Jeeravipoolvarn, S., Scott, J. D. and Chalaturnyk, R. J. (2009). 10 m standpipe tests on oil sands tailings: long-term experimental results and prediction. Canadian Geotechnical Journal, **46**(8): 875-888.

Li, H., Zhou, J., Chow, R. et al. (2015). Enhancing treatment and geotechnical stability of oil sands fine tailings using thermo-sensitive poly (n-isopropyl acrylamide). The Canadian Journal of Chemical Engineering, **93**(10): 1780-1786.

Liang, J., Guo, Z., Deng, L. and Liu, Y. (2015). Mature fine tailings consolidation through microbial induced calcium carbonate precipitation. Canadian Journal of Civil Engineering, **42**(11): 975-978.

Miller, W. G., Scott, J. D. and Sego, D.C. (2010). Influence of the extraction process on the characteristics of oil sands fine tailings. Journal of Canadian Institute of Mining, Metallurgy and Petroleum, **1**(2): 93-112.

Martinez, B. C., DeJong, J. T., Ginn, T. R. et al. (2013). Experimental Optimization of Microbial Induced Carbonate Precipitation for Soil Improvement. ASCE Journal of Geotechnical and Geoenvironmental Engineering, **139**(4): 587-598.

Montoya, B. M. and DeJong, J. T. (2015). Stress-strain behavior of sands cemented by microbially induced calcite precipitation. Journal of Geotechnical and Geoenvironmental Engineering, **141**(6): 04015019.

Nafisi, A. and Montoya, B. M. (2018). A New Framework for Identifying Cementation Level of MICP-Treated Sands. In IFCEE 2018:37-47.

Nusri, S., Tan, X., Choi, P. and Liu, Q. (2016). Using surface geopolymerization reactions to strengthen Athabasca oil sands mature fine tailings. The Canadian Journal of Chemical Engineering, **94**(9): 1640-1647.

Proskin, S., Sego, D.C. and Alostaz M. (2010). Freeze–thaw and consolidation tests on Suncor mature fine tailings (MFT). Cold Regions Science and Technology, **63**(3): 110-120.

Scott, J. D., Dusseault, M. B. and Carrier, W. D. (1985). Behaviour of the clay/bitumen/water sludge system from oil sands extraction plants. Applied Clay Science, **1**(1-2): 207-218.

Steward, G. (2015). Tailings ponds a toxic legacy of Alberta's oil sands. See https://www.thestar.com/news/atkinsonseries/2015/09/04/tailings-ponds-a-toxic-legacy-of-albertas-oilsands.html.

van Paassen, L. A., Ghose, R., van der Linden, T. J., van der Star, W. R. and van Loosdrecht M. C. (2010). Quantifying biomediated ground improvement by ureolysis: large-scale biogrout experiment. Journal of Geotechnical and Geoenvironmental Engineering, **136**(12): 1721-1728.

Van Paassen, L. A. (2009). Biogrout, ground improvement by microbial induced carbonate precipitation. Doctoral dissertation, Delft University of Technology, Delft, Netherlands.

Wong, R. C., Mills, B. N. and Liu, Y. B. (2008). Mechanistic model for one-dimensional consolidation behavior of nonsegregating oil sands tailings. Journal of Geotechnical and Geoenvironmental Engineering, **134**(2): 195-202.

TABLES AND FIGURES

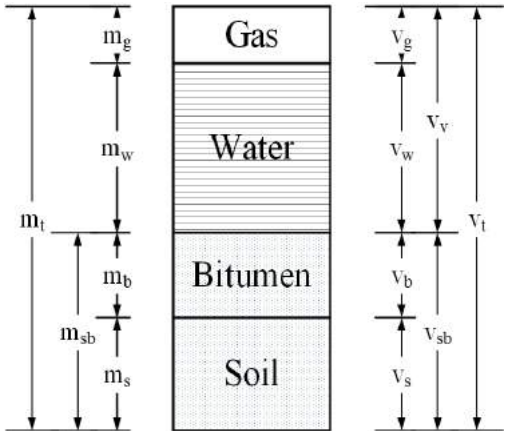

Figure 1. MFT phase diagram

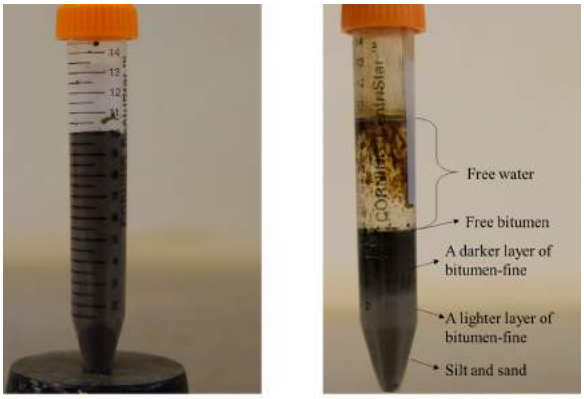

Figure 2. Solids phase before and after centrifugation

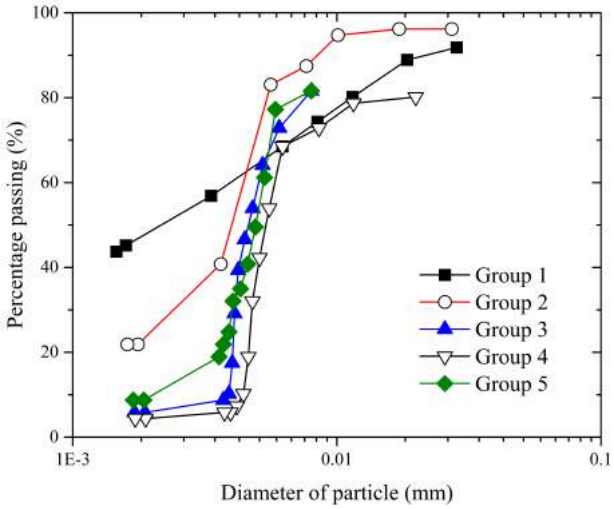

Figure 3. Particle size distribution of different test groups

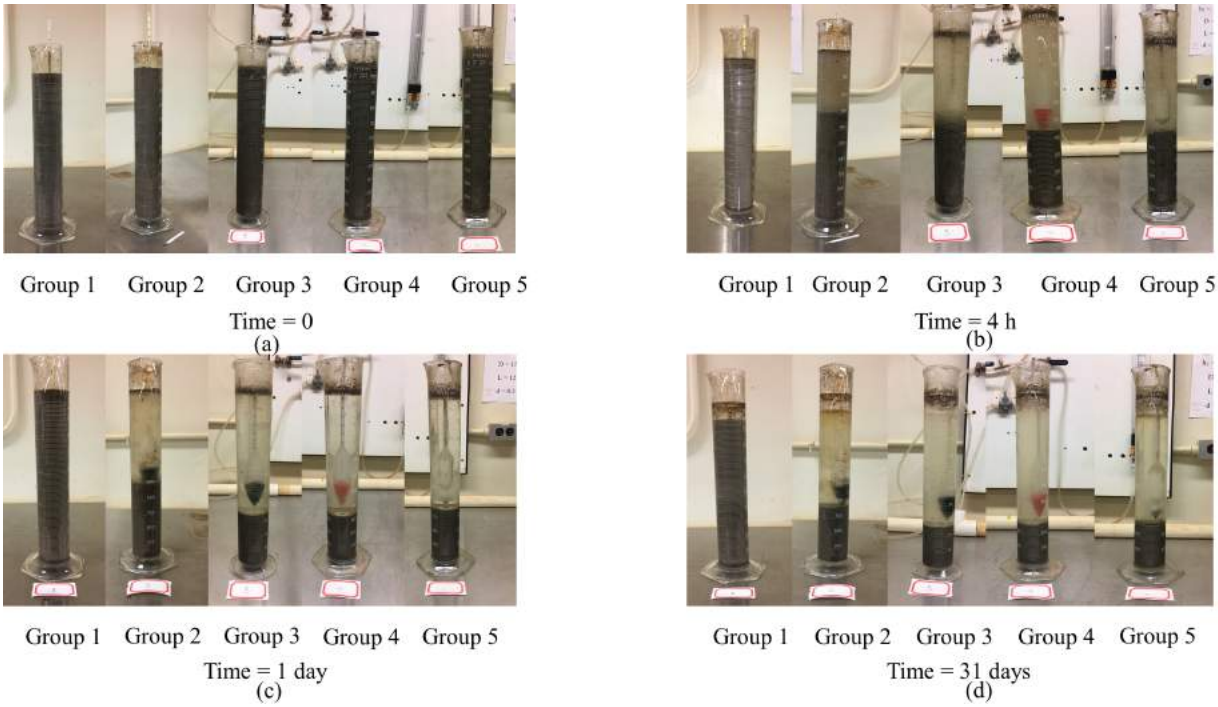

Figure 4. Photos of column test for each group (a) at the beginning of the experiment, (b) after four hours, (c) after one day, and (d) after 31 days

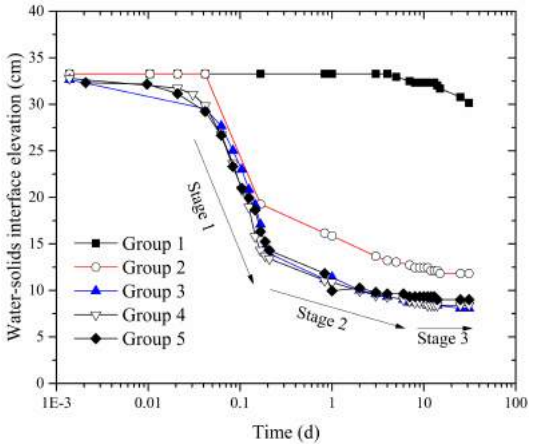

Figure 5. The water-solids interface

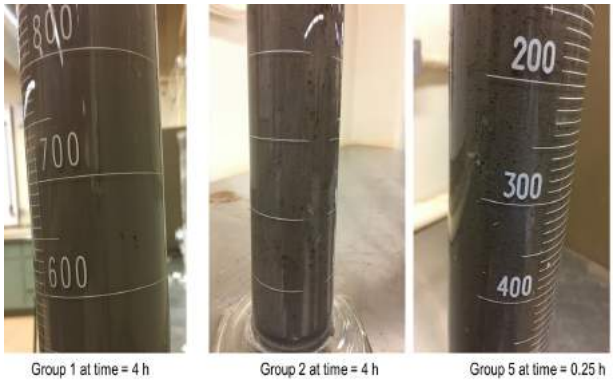

Figure 6. Cracks from gas generation in the MFT during MICP treatment

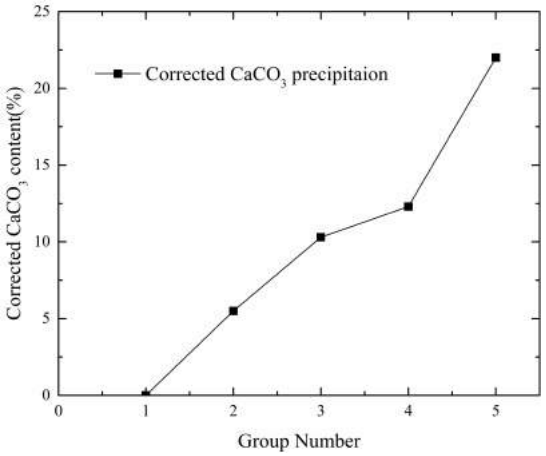

Figure 7. Corrected Calcium carbonate precipitation contents of each group

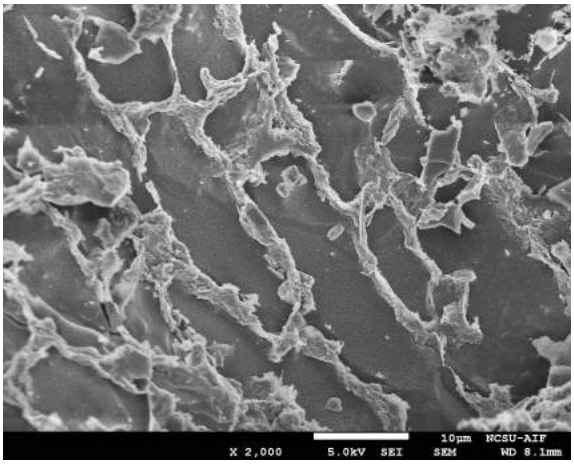

(a) MFT before MICP treatment

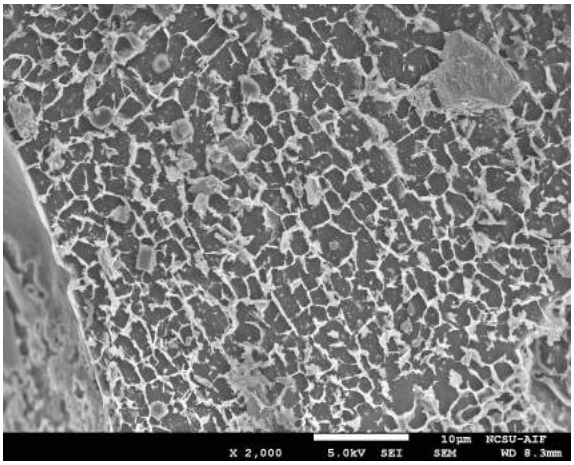

(b) MFT after MICP treatment (Group 5).

Figure 8. Scanning election micrographs of MFT at x2,000 magnification

Table 1. Indexes definition (after Dusseault and Scott 1983, Miller et al. 2010)

Type	Geotechnical definition	Mining definition
Solid	Soil + Bitumen; $m_{sb} = m_s + m_b$	Soil
Water content (%)	$w = \frac{m_w}{m_{sb}} \times 100\%$	$w = \frac{m_w}{m_t} \times 100\%$
Bitumen content (%)	$b = \frac{m_b}{m_{sb}} \times 100\%$	$b = \frac{m_b}{m_t} \times 100\%$
Specific gravity	$G_{solids} = \frac{\text{density of solids}}{\text{density of standard water}} = \frac{\rho_{sb}}{\rho_w}$	
Void ratio (e)	$e = \frac{V_v}{V_{sb}}$	NA

Table 2. MFT properties

Property	Test result
Water content (%)	196
Bitumen content (%)	13
Specific surface area (m^2/g)	122
Liquid limit	57
Plastic Index	23
Specific gravity	1.98
pH	8.0
Calcium carbonate content (%)	5.1

Table 3. Experimental trials

Group	Description	MFT mL	DI Water mL	*S. pasteurii* mL	Urea Stock (2.5 M) mL	$CaCl_2$ Stock (0.75 M) mL	Total volume mL
1	MFT Solution	200	800	0	0	0	1000
2	MFT + *S. pasteurii* + Urea	200	650	50	100	0	1000
3	MFT + *S. pasteurii* + Urea + $CaCl_2$	200	700	50	25	25	1000
4	MFT + *S. pasteurii* + Urea + $CaCl_2$	200	670	50	40	40	1000
5	MFT + *S. pasteurii* + Urea + $CaCl_2$	200	550	50	100	100	1000

Session 10

PHYSICAL MODELING OF OIL SAND TAILINGS

ASSESSMENT OF SELF-WEIGHT CONSOLIDATION OF CO-DEPOSITION DEPOSITS IN THE GEOTECHNICAL BEAM CENTRIFUGE

Gonzalo Zambrano Narvaez[1], Yazhao Wang[1], Rick Chalaturnyk[1], Atoosa Zahabi[2] and Dave Rennard
[1]University of Alberta, Edmonton, Canada
[2]Imperial, Calgary, Canada

ABSTRACT

The self-weight consolidation behavior of co-deposited tailings is not well understood at the field scale. Full assessment of the field performance of co-deposition techniques would take years to complete. Conventional laboratory tests can be carried out on individual materials, but the behavior at field scale of the co-deposition process has not been evaluated. Physical modelling of the co-deposition of thickened tailings and fluid fine tailings conducted in the **Geo**technical **C**entrifuge **E**xperimental **R**esearch **F**acility (**GeoCERF**) at the University of Alberta demonstrated the capabilities of using a geotechnical beam centrifuge to effectively and efficiently evaluate the self-weight consolidation of co-deposition deposits over a decades timeframe.

In the presented study, 20-years of consolidation of co-deposited pond tailings was simulated by conducting multi-day centrifuge experiments. In the first phase, the modelling of segregation investigated the dynamic segregation boundary of co-deposited tailings. Identical co-deposition models were tested in the centrifuge with incremental gravitational forces (G-forces). Solids content and sands to fine ratio profiles were obtained after each increment. Results indicated models remained unsegregated in the centrifuge environment up to 30 times the Earth's gravity (30G). In the second phase, the modelling of consolidation compared the long-term consolidation behavior of models with different co-deposition configurations. Twenty (20) years of prototype consolidation showed no major divergence in consolidation rate and total degree of settlement between "layered" and "homogenized" co-deposition models. The consolidation behavior indicated that there was no divergence in terms of the dewatering rate and the degree of settlement between the two co-deposition models.

INTRODUCTION

Tailings Co-Deposition Technique

The Kearl oil sands project (Kearl) is an oil sands mining, extraction, and processing operation in northern Alberta owned by Imperial Oil and ExxonMobil. The main tailings streams at Kearl are the Coarse Tailings (CST), Flotation Tailings (FT) and Fluid Fine Tailings (FFT) which is pumped from the tailings area. The KFTT (Kearl Flotation Tailings treatment) facility incorporates a two-stage process to treat FT+FFT: a thickener plus a 2nd chemical injection point. It was decided to treat the FFT using the 2nd chemical injection point to have more flexibility with treatment of tailings, to decouple the tailings treatment from bitumen production, and to treat more FFT over time. This will give Imperial a great opportunity to reduce FFT inventory and use the maximum capacity of their FFT barge. The flocculated FFT can then be deposited in the tailings area with the Thickened Tailings (TT). Due to the difference in nature of the two tailings streams, the co-deposition of FFT and TT could affect the displacement and run-off conditions. The frequency of flocculated FFT addition to the tailings area could also have a major impact on the overall performance of the tailings pond.

Centrifuge Modelling

The GeoCERF operates a 2-m radius geotechnical beam centrifuge. A geotechnical beam centrifuge can be used for modeling of large-scale nonlinear problems for which gravity is the primary driving force, including the self-weight consolidation of fine tailings materials. The fundamental principle of centrifuge modeling is based on the stress similarity between a prototype and a centrifuge model. Scaling laws for size and time are used to design the appropriate centrifuge operation. The research group at GeoCERF had conducted multiple physical modelling studies of the self-weight consolidation of oil sands tailings.

Equations 1 and 2 illustrate the scaling laws for size and time in a geotechnical centrifuge model when modelling large strain consolidation (Taylor 1995), such as the self-weight consolidation of tailings.

$$h_p = N * h_m \quad [1]$$
$$t_p = N^2 * t_m \quad [2]$$

h_p is the height of the prototype being simulated. h_m is the height of the centrifuge model. N is the multiple of earth gravity that the centrifuge model is subject to in the forms of centrifugal force. For example, testing a 20 cm thick tailings sample under 100 times earth's gravity can simulate a tailings deposit of 20 m as a prototype.

In Equation 2, t_p is the duration of the prototype being simulated and t_m is the duration of the centrifuge experiment. For example, 10 years of consolidation process can be simulated within 9 hours of centrifuge test at 100G.

The use of the geotechnical beam centrifuge in modelling oil sands tailings has been demonstrated as accurate as modelling soil slurries (Sorta 2015) and very effective for comparative modelling of tailings with unique treatment processes (Zambrano-Narvaez et al. 2018).

SEGREGATION AND CONSOLIDATION

The movement of sands within the tailings (particle segregation) is not well-understood in the centrifuge environment. Dynamic segregation could occur in higher G levels as the particles are exposed suddenly in a high-gravity environment, which does not occur in the field. The dynamic segregation boundary in a centrifuge is a function of G level, grain size of sand, the percentage fines and content of bitumen, solids and clay. TT materials contain particles above the size of 45 microns, which is defined as the boundary between sands and fines. Imperial supplied the TT and flocculated mature fine tailings materials (F-MFT) in this study. The initial average solids content of F-MFT and TT is 29% and 58%, respectively. The average sand to fine ratio (SFR) of F-MFT and TT is 0.03 and 1.73, respectively.

The long-term self-weight consolidation behavior of the co-deposition of F-MFT and TT is not well understood at the prototype/field scale. With the slow dewatering rate of tailings, field evaluation of co-deposition deposit performance would take years to assess. Conventional laboratory tests could be carried out on single materials, but the deposition configurations are difficult to duplicate in a laboratory environment, but the deposition techniques are difficult to scale in a laboratory environment. The advantages of centrifuge modelling include simulating the prototype stress field with a down-scaled model. The consolidation time is also significantly shortened.

In this study, the objective of the first set of five tests was to assess the dynamic segregation boundary on co-deposits of F-MFT and TT under a stage loading procedure (ramp up). Then, three additional samples with different layering configurations were used to assess the self-weight consolidation of 20 years of prototype performance.

METHODOLOGY

Modelling Co-Deposits Segregation

The focus of segregation modelling is to find the maximum G-force in centrifuge modelling that tailings material remains unsegregated.

Five identical co-deposition samples were prepared for segregation modelling and labeled Sample 1 to Sample 5. The samples were contained in identical consolidation cells (GeoCERF T-30, Figure 1). Each sample was made by depositing a 14.9 cm layer of TT over a 14.9 cm layer of F-MFT.

Figure shows the sample configurations.

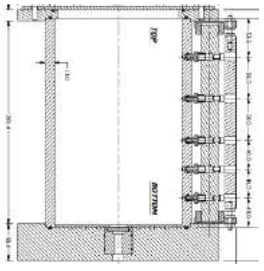

Figure 1. GeoCERF T-30 consolidation cell used in this study

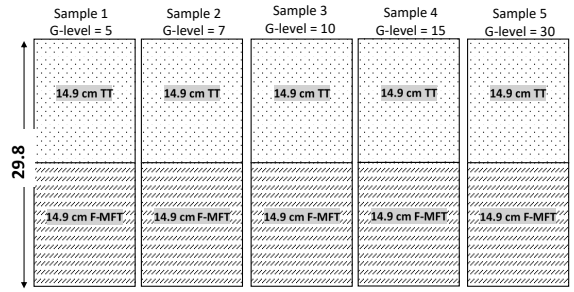

Figure 2. Schematics of co-deposition configurations for segregation modelling

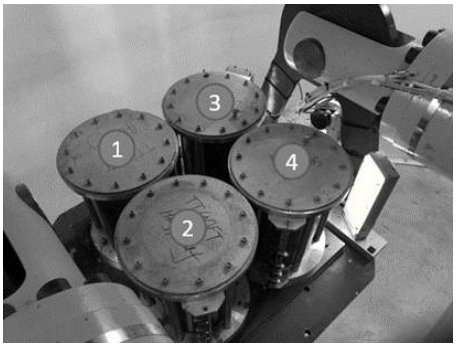

Figure 3. Sample positions for segregation modelling

Table 1. Centrifuge test plan for segregation modelling

Stage	G level	Incremental Hours	Incremental Prototype Time (Hour)	Cumulative Prototype Time (yr)	Samples on payload	Samples taken out from payload at the end of each stage
1	5	19	475	0.05	1,2,3,4	Sample 1
2	7	2	49	0.06	2,3,4	Sample 2
3	10	1	100	0.07	3,4	Sample 3
4	15	1	225	0.10	4	Sample 4
5*	30	1	900	0.20	-	Sample 5

**Sample 5 was tested separately*

A centrifuge test plan was made to investigate the dynamic segregation boundary for the co-deposits up to 30G. Sample 1 to Sample 4 were placed on the centrifuge test platform forming a square array (Figure). They were spun together at 5G for 19 hours. Then Sample 1 was taken out from the platform. The rest of samples were spun together at 7G for 2 hours. Then Sample 2 was taken out from the platform. The remaining two samples were spun at 10G for 1 hour. Then Sample 3 was taken out from the test platform. Sample 4 was spun for an additional one hour at 15G. Through the test, the samples remained in their respective positions. Sample 5 was tested separately and followed the same ramp up schedule to 15G as Sample 4. In addition, Sample 5 was tested at 30G for one hour. This ramp up plan allowed samples experience incremental G-force. Table shows the test matrix as well as the model and porotypes time for segregation modelling test.

After each sample was unloaded from the centrifuge platform, a post mortem analysis was conducted. Two columns of materials were transferred out using a Shelby tube and each column was further divided into 11 dices with equal thickness. Visual identification TT and F-MFT materials was made during the excavation as the two materials had different textures. One column of sample was used for solids content measurement. The other column for sample was wet-sieved with a 45-micron sieve for SFR measurement. Solids content and SFR profiles were therefore obtained for the co-deposits at incremental G-levels.

Modelling Co-Deposits Consolidation

The primary focus of consolidation modelling is to compare the consolidation behavior of tailings co-deposits with different co-deposition configurations.

Three samples were prepared for consolidation modelling and labeled Sample 6, 7 and 8. The same consolidation cells from segregation modelling were used. All samples shared the same height of 29.8 cm, but with different co-deposition configurations. Figure 4 shows the schematics of the configurations.

Sample 6 was prepared by layering F-MFT and TT materials in 2 cm intervals. The bottom layer was TT and the top layer was F-MFT. There was a total of 15 layers. The layers were individually placed by hand to minimize mixture. Sample 7 was prepared the same way as Sample 6, but it was later mixed by inserting and rotating a shear blade inside the consolidation cell. Sample 8 was prepared similarly as Sample 6, except that each layer was 4 cm thick. There was a total of 7 layers in Sample 8.

The primary focus of Consolidation modelling is to compare the long-term consolidation behavior between Sample 6 and Sample 7, which reflected the “layered” and “homogenized” co-deposition techniques. The purpose of Sample 8 is to allow for a better capture of solids content and SFR profiles for the “layered” configuration after consolidation.

The centrifuge test plan for consolidation modelling included spinning 3 samples together for a total prototype time of 20 years. During the test, the centrifuge followed similar incremental ramp-up schedule from segregation modelling, so that the samples were not immediately subjected to a high-G environment. A total modelling time of 10 days were used to carry out the test plan.

Sample 6 and Sample 7 were placed side by side on the centrifuge platform in front of a high-resolution camera (Figure 7). This allowed the settlement to be plotted with time for both samples.

Post mortem analysis was conducted for each sample after centrifuge stopped to obtain solids content and SFR profiles.

RESULTS AND ANALYSIS

Effect of Segregation

Five identical co-deposition samples were tested at incremental G-levels. Solids content and SFR profiles are shown from Figure to Figure for these samples. The normalized depth for each measurement is calculated as the ratio between the depth to the center of the measured sub-sample and the total depth of the sample. Visual identifications made during the post-mortem analysis are also marked in the plots. There was no distinct interface between F-MFT and TT as an area of transition was observed.

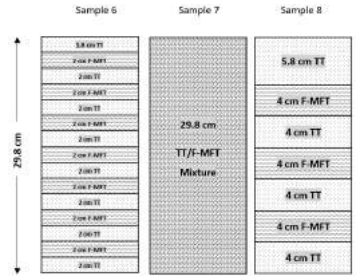

Figure 4. Schematics of samples for co-deposition modelling

Figure 5. Tracking the tailings settlement in-flight

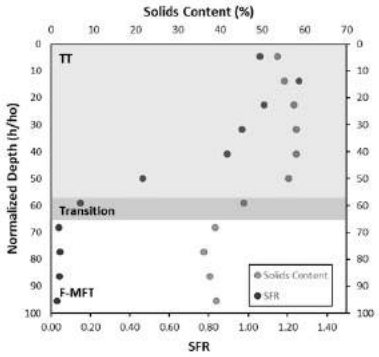

Figure 6. Solids content and SFR profiles of Sample 1 with maximum 5G

Solids content and SFR data show coherence with visual identifications. The original F-MFT material had a solids content of 29% and SFR of 0.036. The original TT material had a solids content of 58% and SFR of 1.73. Measured results indicate that there are no major deviations of either solids content or SFR from the original values, indicating no segregation had occurred during the centrifuge spinning up to 30G.

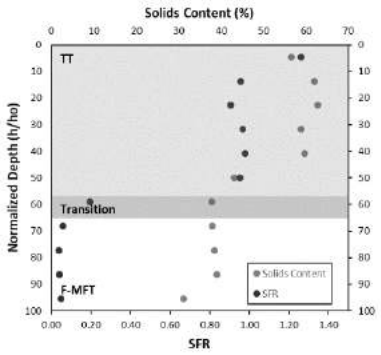

Figure 7. Solids content and SFR profiles of Sample 2 with maximum 7G

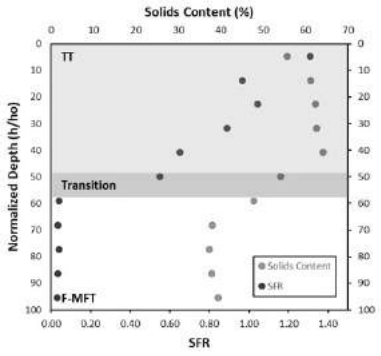

Figure 8. Solids content and SFR profiles of Sample 3 with maximum 10G

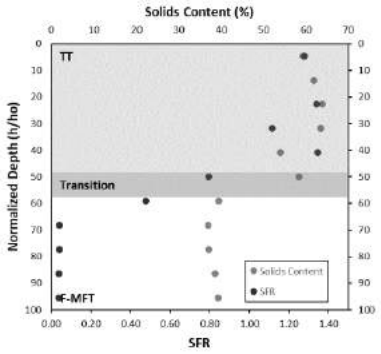

Figure 9. Solids content and SFR profiles of Sample 4 with maximum 15G

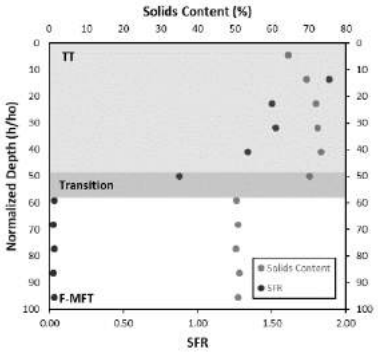

Figure 10. Solids content and SFR profiles of Sample 5 with maximum 30G

The segregation index (I_s) was calculated based on definition of Scott (2003).

$$I_s = \sum_{i=1}^{n} \left\{ \frac{1}{2} \left[\frac{S_i}{S_{avg}} - 1 \right] \left[\left(\frac{H}{H_f} \right)_{i+1} - \left(\frac{H}{H_f} \right)_{i-1} \right] \right\} * 100\%$$

where S_i is the integral solids content, S_{avg} is the average solids content, H is the integral height and H_f is the total height.

The segregation index was calculated individually for each F-MFT and TT layer (Table). With all segregation indices below 5, it indicated no segregation occurred and the dynamic segregation boundary for TT and F-MFT co-deposits was not reach in centrifuge environment up to 30G. Figure 11 summarizes the solids content profiles and segregation indices for each segregation modelling sample and their respective G-level.

Table 2. Segregation indices calculated from segregation modelling

	Segregation Indices, I_s				
G-level	5	7	10	15	30
TT	0.96	2.30	0.82	2.20	0.98
F-MFT	0.71	1.13	0.24	0.75	0.18
Sample #	1	2	3	4	5

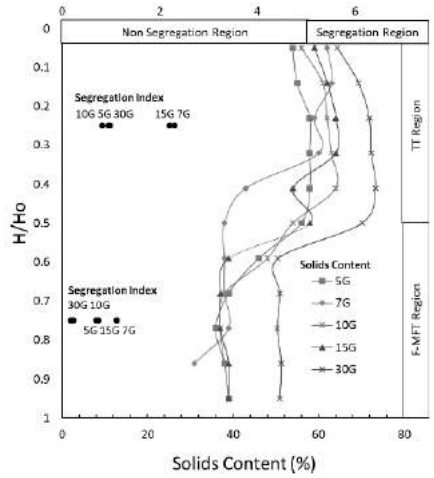

Figure 11. Segregation index profiles

Co-Deposits Consolidation

The prototype consolidation curves for Sample 6 and Sample 7 are shown in Figure 12. Both samples shared the same initial prototype height of 9 m. The final prototype height was also the same, at 4.8 m. Both samples settled 47% of its original thickness. The overlapping consolidation curve indicated that the “layered” or “homogenized” co-deposition configurations had no impact on the performance of long-term consolidation.

Figure 13 and Figure 14 shows the solids content and SFR profiles for Sample 6 and Sample 7, respectively. Solids content is increasing with depth for both samples, as significant settlement occurred during the test. The SFR distribution does not show a clear trend. Sample 6 profiles do not reflect the layered structure of TT and F-MFT, as the number of thin layers exceeded the post-mortem sampling resolution.

The thicker layers of Sample 8, even after large strain consolidation, was clearly reflected in solids content profile as shown in Figure . Readings of sub-samples fall in the 60% and 80% range categories, while exhibiting an upwards trend with depth. The SFR scatters around a lower value representing the F-MFT and a higher value representing the TT. This indicates the layered structure maintained despite undergoing large-strain consolidation.

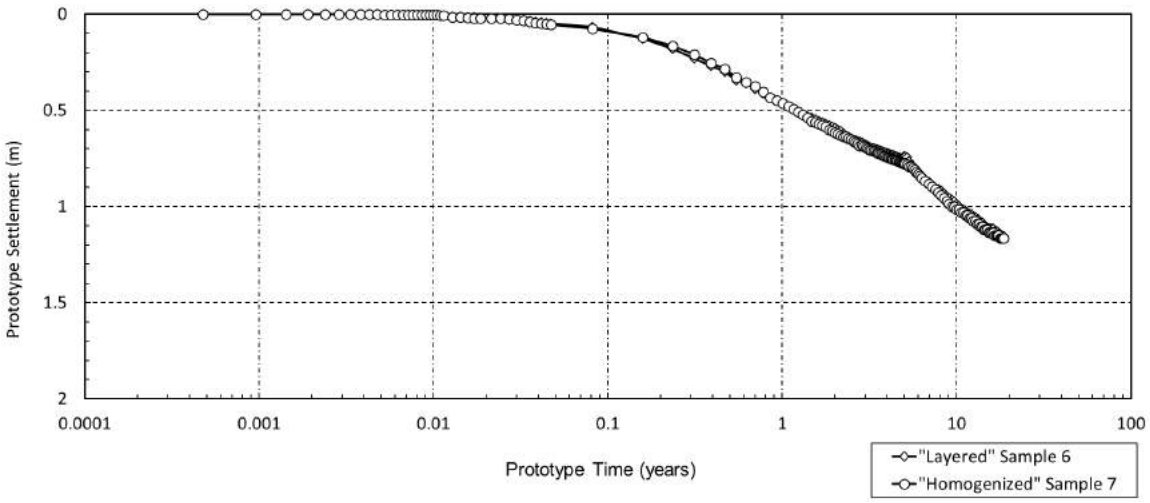

Figure 12. Prototype consolidation curves for consolidation modelling samples

DISCUSSIONS AND CONCLUSIONS

This research assessed tailings co-deposition technique in two key areas, segregation and long-term consolidation. Segregation modelling explored the segregation boundary of a co-deposition model of F-MFT and TT. Long-term consolidation modelling was conducted within the boundary and assessed the consolidation behavior of this co-deposition model.

The dynamic segregation boundary assessment analyzed five samples in the centrifuge environment with incremental G-levels. The TT and

F-MFT co-deposit tested in this program remained in the non-segregation region up to 30G. Consolidation modelling samples were therefore tested within the boundary.

Two samples (i.e. Samples 6 and Sample 7) were tested to assess the self-weight consolidation behavior of F-MFT and TT co-deposits. Sample 6 was configured to represent the “layered” deposition technique used in field operations. Sample 7 was built to represent the “homogenized” co-deposits as layered structures were sheared and mixed. The samples were tested in identical conditions. The consolidation curves developed after 20 prototype years were overlapping. The observed similarities indicated that the “layered” and “homogenized” co-deposition techniques had negligible impact in terms of long-term consolidation behavior. The developed solids content and SFR profiles of the “layered” co-deposits indicated that the layer structures existed after large-strain consolidation.

With the verification of segregation boundary and assessment of long-term consolidation behavior, the centrifuge co-deposition models demonstrated to be capable of simulating large-scale field co-deposition problems. The effectiveness of tailings co-deposition technique was experimentally verified in a matter of days instead of years of field study. Centrifuge modelling is proven to be an effective and highly-efficient experimental tool in assessing tailings treatment techniques.

REFERENCES

Taylor, R. N. (1995). Geotechnical centrifuge technology. London Blackie Academic and Professional.

Zambrano-Narvaez, G., Wang, Y. and Chalaturnyk, R. (2018). Comparative study of consolidation behavior of differently-treated mature find tailings specimens through centrifuge modelling at the GeoCERF in the University of Alberta, Canada. 9th ICPMG. London, U.K., July 17-20.

Sorta, A. R. (2015). Centrifugal modeling of oil sands tailings consolidation. PhD Thesis. Department of Civil and Environmental Engineering, University of Alberta, Edmonton.

Scott, J. D. (2013). Definitions and Convention Equations for Oil Sands Tailings.

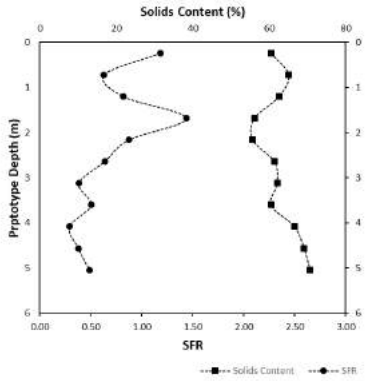

Figure 13. Solids content and SFR profiles for Sample 6

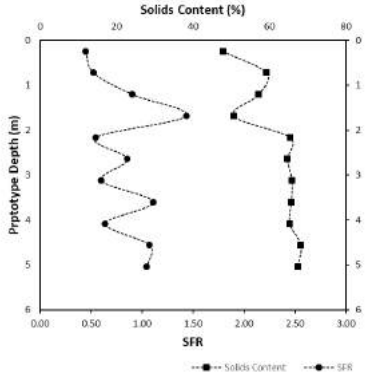

Figure 14. Solids content and SFR profiles for Sample 7

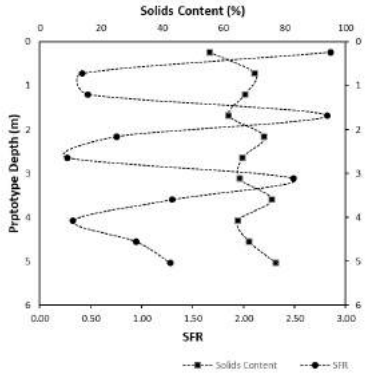

Figure 15. Solids content and SFR profiles for Sample 8

COMPARISON OF GEOTECHNICAL BEAM CENTRIFUGE PREDICTIONS TO FIELD DATA FROM 10M DEEP FFT CENTRIFUGE CAKE COLUMNS

Adedeji Dunmola[1], Nan Wang[1], Jim Lorentz[1], Rick Chalaturnyk[2], Gonzalo Zambrano[2] and Jason Song[3]
[1]Syncrude Canada Ltd., Edmonton, Canada
[2]University of Alberta, Edmonton, Canada
[3]O'Kane Consultants, Calgary, Canada

ABSTRACT

Geotechnical beam centrifuge (geotechnical centrifuge) modeling has been used to evaluate the sedimentation and self-weight consolidation behavior of cohesive oil sands tailings deposits. This is accomplished by spinning a physical model inside a geotechnical centrifuge, simulating the stress levels within a tailings pond or deposit. Understanding and predicting the long-term consolidation behavior of cohesive deposits is required for deposition planning and design, operation, management, capping, reclamation and closure. This paper compares the predictions from physical modeling of FFT centrifuge cake (cake) using the 50 g-tonne geotechnical beam centrifuge located at the University of Alberta, to field data from six 10m deep, 3m-diameter columns installed at the Syncrude mine site and filled with cake in 2014. The cake columns were designed to have various stress and boundary conditions, with only one of the six columns having the most similarity to the geotechnical centrifuge physical model. The results of a modeling of the model test to validate the scaling laws for cake is also presented. For the cake column with the most comparable boundary and stress conditions as the geotechnical centrifuge model, measured settlement and excess pore pressures were in general agreement with those of the physical model. As expected, for the other cake columns, settlement and excess pore pressures were not in agreement with the geotechnical centrifuge results. Also, the scaling laws for self-weight consolidation using the geotechnical centrifuge was successfully validated for cake. This paper demonstrates the viability of physical modeling using the geotechnical centrifuge in predicting the long-term consolidation behavior of cohesive oil sand tailings deposits such as cake.

INTRODUCTION

Background

Managing fines-dominated oil sands tailings as deep deposits is advantageous compared to thin-lift drying for a number of reasons. Such deep deposits allow for the minimization of the footprint required for the deposition, management and closure of oil sands tailings. This in turn maximizes the containment efficiency and cost effectiveness of engineered tailings structures. Also, deep deposits minimize the need for multiple re-handling of the same tailings material. In addition, localizing such soft tailings deposits may allow for a more efficient reclamation and closure operation as the footprint to be reclaimed and integrated into the final closure landscape becomes smaller.

Understanding the long-term consolidation performance of deep fines-dominated oil sands tailings deposits is critical for the efficient and successful reclamation and closure operations. Specifically, a knowledge of the magnitude and rates of settlement of these deposits is required for depositional planning, deposit management, capping as well as eventual reclamation and closure of these deposits.

A conventional method of assessing this long-term deposit performance is by numerical modeling. Numerical modeling involves the laboratory determination of consolidation parameters (such as compressibility and hydraulic conductivity functions), which are then input into an appropriate non-linear large-strain consolidation model. Depending on the testing method selected, it may take a significant amount of time (several months to 1 year) to determine these consolidation parameters. In addition, some analytical uncertainties are inherent with these laboratory testing methods. As a result, these uncertainties limit the accuracy of numerical prediction of long-term performance of deep tailings deposits. The

other option of constructing and monitoring field pilot deposits is obviously practically constrained from both cost and time requirement standpoints.

One alternate assessment technique is physical modeling using a geotechnical centrifuge. Geotechnical centrifuge modeling has been used in conventional geotechnical engineering and rock mechanics in several applications, including earthquake loading simulation and failure assessment of geotechnical and geo-mechanical structures such as foundations, tunnels, retaining walls, engineered slopes and off-shore rigs (Ng 2014).

Geotechnical centrifuge modeling involves the scaling of a model material both geometrically and temporally under elevated gravitational acceleration (*g*), in order to simulate an actual prototype. The model (in centimeters) is spun (in hours) under elevated *g* to simulate a prototype (in meters) undergoing self-weight consolidation in years. The technique is based on the principle of stress similarity between the model and the prototype. The model is scaled to the prototype in terms of geometry and time using the scaling relations expressed as:

$$H_m = H_p / N \quad [1]$$

$$T_m = T_p / N^2 \quad [2]$$

Where N is the geotechnical centrifuge acceleration level (N times the Earth's gravitational acceleration); H_m and T_m is the height and in-flight time of the model, respectively. Similarly, H_p and T_p is the height and equivalent consolidation time of the prototype, respectively.

There are numerous studies documenting the use of geotechnical centrifuge in modeling the consolidation behavior of phosphate clays (Beriswill et al. 1987, Bloomquist and Townsend 1984), gold mine tailings (Stone et al. 1994), soft soil (Mikasa and Takada 1984) and kaoline slurry (Croce et al. 1985). However, literature on the use of geotechnical centrifuge technique in modeling the consolidation behavior of oil sand tailings is limited (Sorta 2015, Theriault et al. 1995, Znidarcic et al. 2011).

Using a bench-top centrifuge, Theriault et al. (1995) investigated the dewatering behavior of various chemically-treated oil sands tailings with and without bitumen. The study concluded that while the ultimate settlement of the various amended tailings is independent of the chemical treatment, the only difference was in the rate of settlement. Znidarcic et al. (2011) also studied the self-weight consolidation of oil sands fluid fine tailings (FFT) using a geotechnical beam centrifuge, and compared the results to numerical model predictions. Numerical predictions agreed with the geotechnical centrifuge results, and the authors concluded that FFT behave like a conventional soil slurry, despite the presence of residual bitumen. Sorta (2015) investigated the self-weight consolidation of FFT using the geotechnical centrifuge, validated the scaling laws for centrifuge modeling, and concluded that the technique can be used successfully for oil sands tailings.

The current paper expands the existing literature demonstrating the utility of the geotechnical centrifuge technique in predicting the long-term performance of cake, a tailings product from a commercial FFT treatment technology implemented by Syncrude Canada Ltd (Syncrude). This paper presents the results from the modeling of the models conducted on cake produced at the Syncrude's Mildred Lake Mine site.

In addition, in order to further understand the long-term performance of cake, Syncrude constructed and filled ten low-friction wall columns (10m deep, 3m in diameter) with cake at the Mildred Lake site in 2014 and 2016. In this paper, the field performance of the six columns filled in 2014 is compared with the equivalent performance of the prototype modelled using the geotechnical beam centrifuge.

STUDY DESCRIPTION

Modeling of the Models Study of Cake with Geotechnical centrifuge

The geotechnical beam centrifuge located at the Geotechnical Centrifuge Experimental Research Facility (GeoCERF) of the University of Alberta (Figure 1) was used in the current study. The geotechnical centrifuge has a radius of 2m, and a maximum acceleration and payload of 150*g* and 500kg, respectively. The "modeling of the models" test was conducted to validate the scaling relationships (Equations 1 and 2) for cake, as well as to physically simulate the consolidation behavior of the 10m cake columns installed in the field as described in the next section. The details of the modeling of the models tests set up to simulate a

12m high prototype deposit of cake, are provided in Table 1.

The models were subjected to 1-way drainage, with a no-flow boundary at the base and a flow boundary at the top, where the release water from consolidation was allowed to accumulate throughout the flight. The three models subjected to geotechnical centrifuge testing were from the same batch of cake, but the three tests were conducted in sequence. During the geotechnical centrifuge test, the settlement of the model was tracked by means of a laser sensor mounted on the cell, complemented by an on-board high-resolution camera. The settlement of the model and equivalent prototype are expressed in terms of percent strain. Also, the pore pressures at various elevations along the depth of the model was tracked by means of specialized pressure transducers. At the end of the geotechnical centrifuge flight, the consolidated model was characterized with depth for water and solids contents.

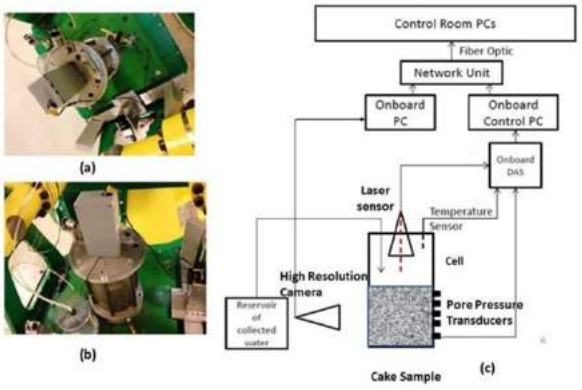

Figure 1. Equipment set up for the GeoCERF geotechnical centrifuge showing photos of the consolidation cell on the swing platform (a & b), and schematics of the cell and associated instrumentation (c)

Table 1. Testing parameters for the modeling of the models tests for FFT centrifuge cake

Physical Model	N (g)	Height		Time	
		Model (cm)	Prototype (m)	Model (Hours)	Prototype (Years)
Model 1	120	10	12	84	138
Model 2	100	12	12	120	137
Model 3	80	15	12	192	140

Field Centrifuge Cake Columns

A total of ten low-friction wall columns were installed by Syncrude at its Mildred Lake site in 2014. The columns were about 11m deep and 3m in internal diameter. Six of the columns were filled with cake in 2014, and the remaining four filled in 2016. The field columns were intended to track the long-term consolidation behaviour of cake. In addition, the cake columns were designed to assess the impact of various adaptive management options, including coke capping, under-drainage and wick drain installation, on the long-term performance of cake.

The cake columns were monitored for settlement by means of automated sensors, supplemented by occasional manual measurements. The settlement of the cake columns is also expressed in percent strain, consistent with the data from the geotechnical centrifuge testing. In addition, vibrating wire piezometers were installed along the full depth of the cake columns to track the pore water pressure response as the cake consolidates over time. In order to minimize disturbance of the cake deposit, in-situ core sampling was only done once for the cake columns, few months after the columns were filled.

The cake columns were sheltered to minimize the impact of atmospheric forcings on the cake deposits. The sheltered cake columns were also climate controlled in the winter, to minimize the potential for the cake undergoing freezing. However, as described later, there was evidence of atmospheric drying of the surface of some of the cake columns. Within the first year after placing the cake in the six columns (before placing the first coke cap on columns 2-6), the release water on top of the cake deposits was occasionally removed. This was discontinued after the first year. The first coke cap was placed on Columns 2, 3, 4, 5, and 6 after day 415, 408, 408, 396 and 396 since end of deposition, respectively. Columns 5 and 6 have a 1m thick sand under-drainage layer at the base (Figure 2), connected to the surface by a dewatering well. Water drained into the sand layer was occasionally pumped out via the dewatering well for the first year after deposition. Thereafter, pumping the under-drainage layer was discontinued. All six columns were situated on an overburden dump and the base plugged with bentonite grout to restrict unintended “under-drainage” to the native base.

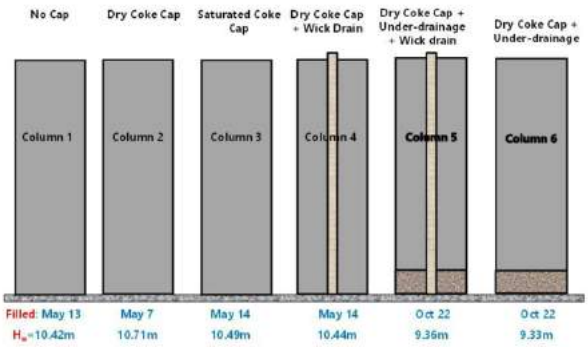

Figure 2. Schematic illustration of field Columns 1-6 filled with cake in May (Columns 1-4) and October (Columns 5 and 6) 2014

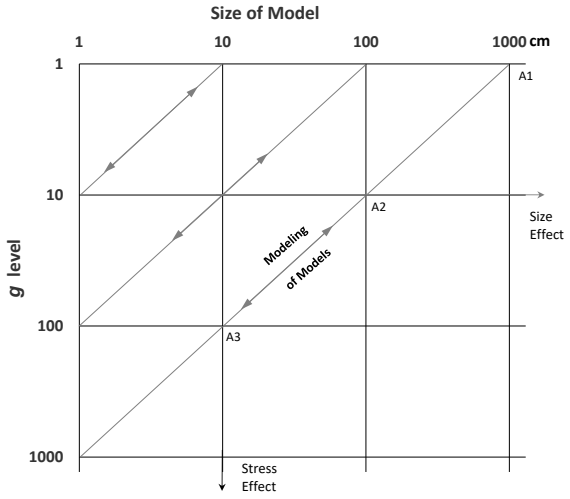

Figure 3. Principle of the modeling of the models (Ko 1998, Taylor 1995)

RESULTS

Validating the Geotechnical Centrifuge Scaling Laws for Centrifuge Cake

The modeling of the models tests were conducted to validate the scaling laws for centrifuge cake. The validation test is premised upon the fact that if the deformation, stress and flow conditions of the candidate material are captured appropriately within the geotechnical centrifuge environment, the relative response should be consistent at different scales (geometries) of the prototype. For example, as shown by points A1, A2 and A3 in Figure 3, a 10m-deep prototype can be represented by a physical model at full scale (10m, 1*g*), 10% of the full scale (1m, 10*g*), or at 1% of the full scale (0.1m, 100*g*), respectively.

Consistent with Equations 1 and 2, the scaling laws are validated in term of both geometry (settlement) and time. Given that the settlement of the model (and prototype) is directly related to the respective initial height, it follows from Equation 1 that:

$$S_m = S_p / N \quad [3]$$

Where S_m and S_p are the settlement of the model and prototype, respectively. Hence, for the scaling law with respect to geometry (Equation 3) to be valid, a plot of the final height of the model against 1/N should be a straight line passing through the origin. This is the case for the three geotechnical centrifuge tests completed for the cake as shown in Figure 4.

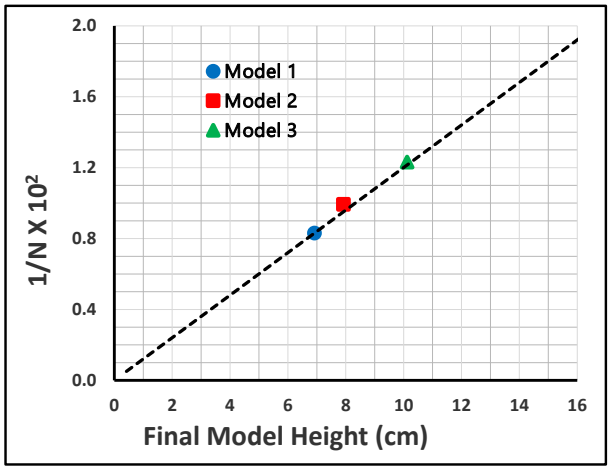

Figure 4. Scaling law with respect to geometry validated for centrifuge cake

Similarly, the scaling law with respect to time is validated in terms of t_{50} (time to 50% consolidation), with t_{50} determined from the deformation time series using the Cassagrande construction method. This is done by expressing Equation 2 as:

$$t_{50m} = t_{50p} / N^2 \quad [4]$$

Where t_{50m} and t_{50p} is the t_{50} for the model and prototype, respectively. Thus, for the scaling law with respect to time to be valid, a plot of $1 / N^2$ versus t_{50} for all 3 models should be on a straight line passing through the origin. This was the case when the data from geotechnical centrifuge tests for the centrifuge cake was plotted (Figure 5). The

settlement curves for all the 3 models, plotted in prototype scale, showing agreement (Figure 6) further validates the scaling law with respect to time. It is worthy of note that when t_{50} was determined based on the degree of excess pore pressure dissipation, the same result was obtained.

Hence, Figures 4, 5 and 6 showed the validity of the scaling laws for centrifuge cake. This implies that the geotechnical centrifuge modeling technique can be applied to assess the self-weight consolidation behavior of centrifuge cake.

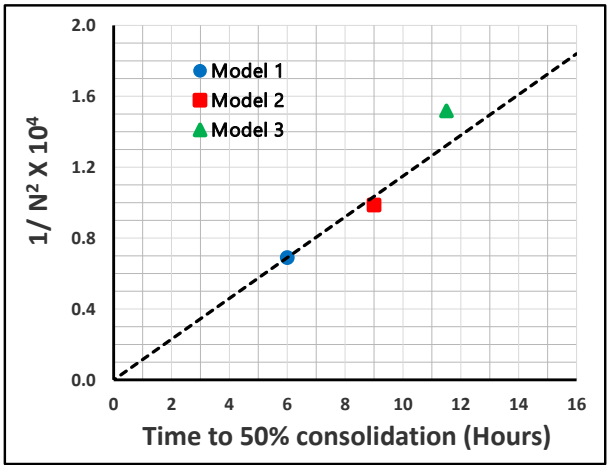

Figure 5. Scaling law with respect to time validated for centrifuge cake

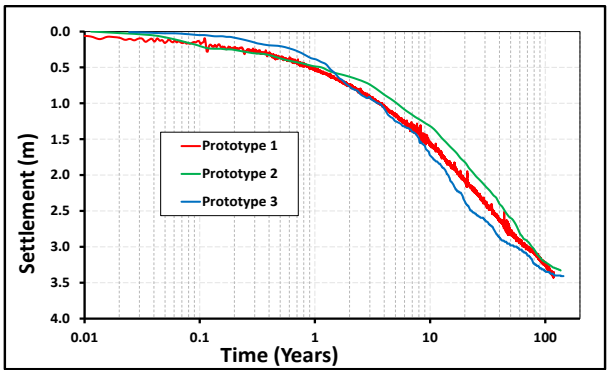

Figure 6. Scaling law with respect to time validated for centrifuge cake, using the settlement - time series curves in prototype scale.

Comparison of Consolidation Data for Geotechnical Centrifuge Test Prototypes to Field Cake Columns

The consolidation behavior of centrifuge cake deposited in the six field columns is compared with the equivalent prototype measured from the geotechnical centrifuge models in terms of both deformation and the dissipation of excess pore pressure with time. The data for the geotechnical centrifuge tests is presented in terms of the prototype behavior by converting the relevant model time to prototype time using the scaling law with respect to time (Equation 2) and the appropriate gravitational acceleration, N.

Deformation

The deformation data for the field cake columns is shown in Figure 7, compared with the equivalent prototype data for the 3 geotechnical centrifuge models. Of all the six field cake columns, Column 1 showed the best agreement with the geotechnical centrifuge prototypes. This is consistent with the fact that cake column 1 was the only column that had no adaptive management (no coke capping, no under-drainage and no wick drains), and is the most similar to the prototypes in terms of stress and flow conditions. The deformation measured for Column 1 matched the geotechnical centrifuge prototype data up till about 200 days since initial deposition (Figure 7). Afterwards, the deformation of cake column 1 began to slightly diverge from the equivalent prototype data. This can be explained by the observation that column 1, similar to the remaining five cake columns, experienced additional atmospheric drying as shown in Figure 8. This supplemental atmospheric drying would have contributed to the increased deformation observed. In contrast, the geotechnical centrifuge models were only subjected to self-weight consolidation, with the on-board temperature kept low enough to prevent evaporative drying of the model. In addition, the water released during consolidation was allowed to accumulate on top of the models, thus preventing any surficial drying of the models in-flight.

In a similar way, the deformation of the remaining cake columns (Column 2 - 6) closely agreed with the trend exhibited by the prototypes for a short duration following the end of deposition (Figure 7). Afterwards, the deformation recorded by all the five cake columns began to deviate from the consolidation trend shown by the prototypes. For the period prior the placement of the coke caps

(ranging from 396 to 415 days after deposition), this deviation can be attributed to additional dewatering from atmospheric drying and adaptive management options implemented, i.e. wick drains (Columns 4 and 5), and under-drainage (Columns 5 and 6) as shown in Figure 2. This is further enhanced afterwards by the placement of coke caps on Columns 2 - 6. In fact, columns 5 and 6 showed the most deviation from the prototypes in terms of deformation. This behaviour is consistent with these two columns having the most dewatering enhancements (atmospheric drying prior coke capping, coke capping and under-drainage) in addition to self-weight consolidation.

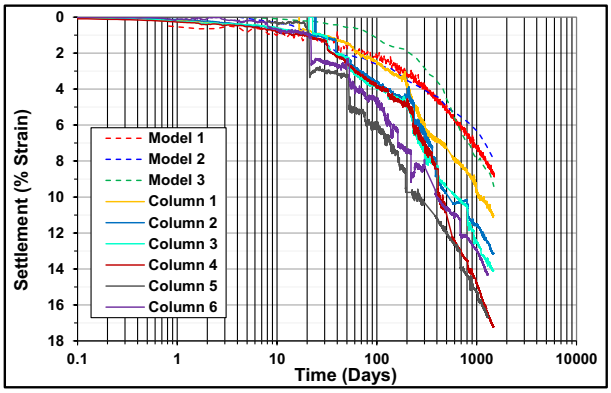

Figure 7. Deformation time series for the six cake columns (Columns 1-6) compared with the model data from the geotechnical centrifuge testing (Models 1 and 3)

Figure 8. Photographs of the surface of cake in Column 1 showing atmospheric drying, taken on: (a) April 2015; (b) July 2015; (c) September 2015; and (d) December 2015)

Excess Pore Pressures

The profiles of excess pore pressure for the field cake columns compared with the equivalent data for the geotechnical centrifuge models are shown in Figures 9 and 10. The comparative data for columns 3 and 4 are not shown, but are similar to the trend shown by Columns 2, 5 and 6. The closest agreement between the profiles of excess pore pressure measured in the field columns and the geotechnical centrifuge models is observed for Column 1 (Figure 9a). For Column 1, with the exception of normalized heights between 0.8 and 0.65, the profiles of excess pore pressures align well with the data for the geotechnical centrifuge model, especially for year 1. This close agreement for Column 1 is consistent with the column having the most similarity to the geotechnical centrifuge model. Beyond year 1, the excess pore pressure profiles for Column 1 diverged from the prototype measurements, exhibiting faster rate of excess pore pressure dissipation.

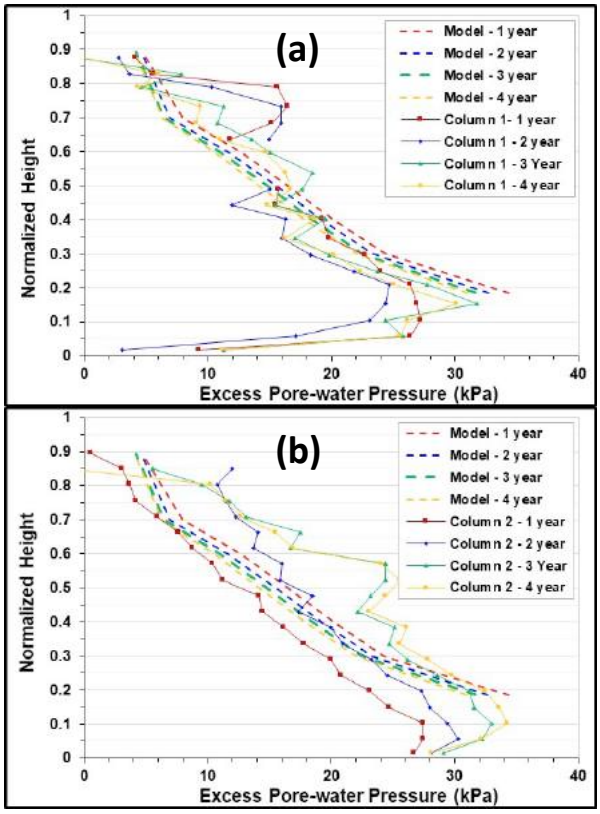

Figure 9. Profiles of excess pore pressures measured for the models and columns 1 (a) and 2 (b) over time. The vertical axis is presented as position of sensor relative to the initial height of model or column.

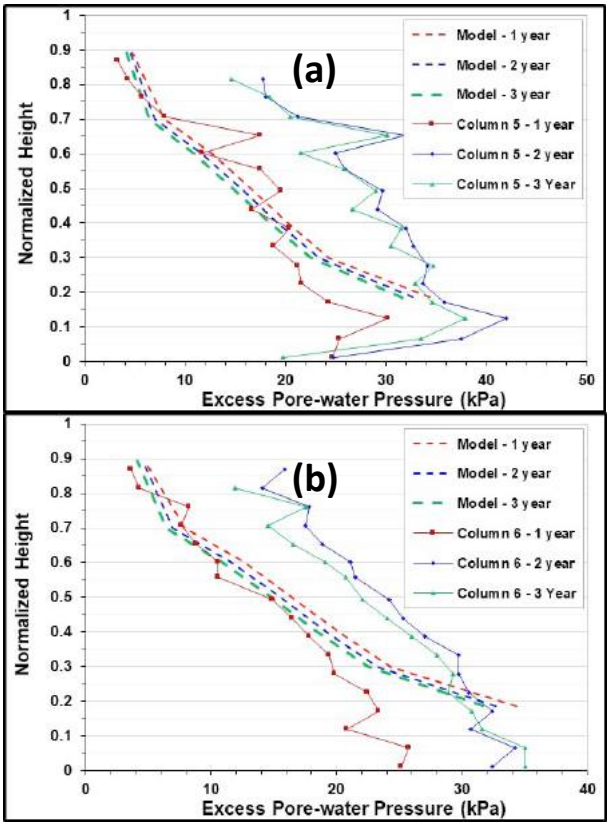

Figure 10. Profiles of excess pore pressures measured for the models and columns 5 (a) and 6 (b) over time. The vertical axis is presented as position of sensor relative to the initial height of model or column.

The remaining cake columns (Columns 2 - 6) diverged more from the prototype in terms of excess pore pressure profiles. This can be attributed to a number of reasons. One is the additional dewatering of the field cake columns due to atmospheric drying prior to coke cap placement. Second is the excess pore pressure response by the cake to the placement of coke caps. Also, the difference could have been an indication of the different flow conditions for columns 4, 5, and 6 (as a result of wick drains and under-drainage layer). The initial profile of excess pore pressure measured for all the cake columns and the model is shown to be identical as per Figure 11. Hence, the subsequent differences in excess pore pressure profiles can be validly attributed to the highlighted stress and flow boundary differences between the cake columns and the geotechnical centrifuge models.

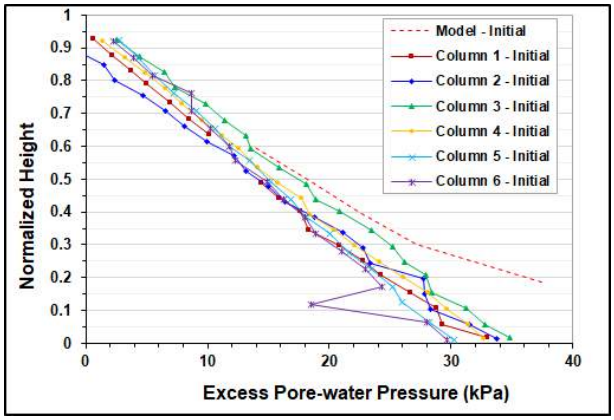

Figure 11. Initial profiles of excess pore pressures for the geotechnical centrifuge models and Columns 1-6. The vertical axis is presented as position of sensor relative to the initial height of model or column.

This overall consolidation pattern in terms of excess pore pressure profiles of the cake columns compared with the geotechnical centrifuge model, is consistent with the comparative behavior in terms of deformation (Figure 7). It is noted that the profiles of excess pore pressures for the cake columns indicate some under-drainage at the base for Columns 1, 2, 5 and 6, even though only columns 5 and 6 have a designed under-drainage sand layer at the base (Figure 2).

DISCUSSION

The modeling of the models test conducted for centrifuge cake validated the scaling laws in terms of both geometry and time. This indicates the theoretical justification for using the geotechnical centrifuge to simulate the physics of self-weight consolidation for a geo-material such as centrifuge cake. The current study is the first published instance of conducting this modeling of the models test specifically on oil sands centrifuge cake. Sorta (2015) is the only other publication that conducted this validation test on oil sands tailings, namely FFT and thickened tailings. The author concluded that the scaling laws are valid for these oil sands tailings in terms of both geometry and time.

To further test the validity of the geotechnical centrifuge modeling technique as a predictive tool, field measurements from cake columns were compared with equivalent data from geotechnical centrifuge testing in terms of both deformation and

excess pore pressure. Comparison in terms of deformation indicates that the self-weight consolidation of the centrifuge cake can be approximated using the geotechnical centrifuge modeling technique. The cake column with the most similarity in terms of boundary and stress conditions as the geotechnical centrifuge prototype (Cake column 1) exhibited the best agreement in terms of deformation. The same conclusion was proven in terms of the profiles of excess pore pressures for centrifuge cake.

To the authors' knowledge, the current paper represents the first publication demonstrating the validity of the geotechnical centrifuge physical modeling technique for predicting the long-term consolidation performance of a field deposit of oil sands tailings. In the absence of field verification of the geotechnical centrifuge technique for other types of oil sands tailings deposits, the results from this paper are significant. The geotechnical centrifuge technique would represent a valid alternative (or compliment) to the traditional numerical modeling technique for predicting the field behavior of oil sands tailings. This is particularly important considering the analytical uncertainties and length of time required for laboratory material characterization required for numerical modeling.

Also, constructing and spinning a physical model simulating a specific field deposit configuration may be easier to do using a geotechnical centrifuge compared to numerical modeling of such complex configuration. Of course, field construction and installation of such configuration would be more expensive and take a much longer time compared to geotechnical centrifuge modeling. Hence, physical modeling using a geotechnical centrifuge can allow for expeditious decision making regarding oil sands tailings treatment, deposition, deposit management, capping, reclamation and closure.

CONCLUSION

This paper demonstrates that physical modeling using geotechnical centrifuge is a viable way to assess the long-term self-weight consolidation behavior of a fine-grained geo-material such as centrifuge cake. The deformation and pore pressure response from the field cake columns were consistent with the results from the geotechnical centrifuge models, when the differences in the stress and flow boundary conditions are accounted for. Hence, the geotechnical centrifuge technique is an alternate approach to numerical modeling as a tool for assessing the long-term consolidation performance of centrifuge cake, and potentially, other fines-dominated oil sands tailings. Laboratory testing to derive the input parameters required for numerical modeling takes a long time and has associated analytical uncertainties. The quicker turnaround of the geotechnical centrifuge technique would allow for more efficient decision-making process related to tailings treatment technologies, tailings deposition and deposit management, as well as reclamation planning and operations.

It is important to note that the results presented here is specific for oil sands centrifuge cake, and may or may not be directly extrapolated to other types of fines-dominated oil sands tailings. Also, the impact of tailings treatment and residual bitumen on the validity of using geotechnical centrifuge modeling to assess the long-term consolidation behavior was not investigated in the current study. In addition, the potential impact of material heterogeneity that is characteristic of field deposits may limit the accuracy of prediction of long-term field behavior using geotechnical centrifuge modeling. These issues are recommended to be the subject for future research endeavor. Future geotechnical centrifuge modeling of the additional dewatering potential resulting from implementing adaptive management options like capping, wick drains and under-drainage would be a valuable complement to the field data presented in the current paper. Finally, in order to increase confidence in the design, construction, management and closure of deep fines-dominated oil sands tailings deposits, an optimal combination of numerical modeling, field piloting and physical modeling is recommended.

ACKNOWLEDGEMENT

The authors acknowledge Jonathan Spence and Geoff Halferdahl for reviewing an earlier version of this manuscript. Yazhao Wang assisted with the beam centrifuge and associated index property testing. Technical input from Drs. David Carrier and Ed McRoberts during the beam centrifuge testing is gratefully acknowledged.

REFERENCES

Beriswill, J. A., Bloomquist, D. and Townsend, F. C. (1987). Reclamation of phosphatic clay waste ponds by capping. Volume 5: Centrifugal model evaluation of the consolidation behavior of phosphatic clays and sand / clay mixes. Florida Institute of Phosphate Research, Bartow, FL, U.S.A. FIPR Publication # 02-030-075.

Bloomquist, D. G. and Townsend, F.C. (1984). Centrifuge modeling of phosphatic clay consolidation. In: Sedimentation consolidation models – predictions and validation (Yong, R.N. and Townsend, F.C. (eds). ASCE, New York, NY, U.S.A.

Croce, P., Pane, V., Znidarcic, D., Ko, H.-Y., Olsen, H. W. and Schiffman, R. L. (1985). Evaluation of consolidation theories by centrifuge modeling. In: Proceedings of the International Conference on Applications of centrifuge modeling to geotechnical design. Balkema, Rotterdam, Netherlands. Pp 380-401.

Ko, H.-Y. (1988). Summary of the state-of-the-art in centrifuge model testing. In: centrifuges in soil mechanics. (Eds W.H. Craig, R.G. James and A.N. Schofield). Pp. 11-18, Balkerma, Rotterdam.

Mikasa, M. and Takada, N. (1984). Self-weight consolidation of very soft clay by centrifuge. In: Sedimentation consolidation models – predictions and validation (Yong, R.N. and Townsend, F.C. (eds). ASCE, New York, NY, U.S.A. Pp 121-140.

Ng, W.W. (2014). The state-of-the-art centrifuge modeling of geotechnical problems at HKUST. J. of Zhejiang University SCIENCE A., **15**(1): 1-21.

Sorta, A. R. (2015). Centrifugal modeling of oil sands tailings consolidation. PhD Thesis. Department of Civil and Environmental Engineering, University of Alberta, Edmonton. 315 Pages.

Stone, K. J. L., Randolph, M. F., Toh, S. and Sales, A. A. (1994). Evaluation of consolidation behavior of mine tailings. J. Geotechnical Engineering, ASCE, **120**(3): 473-490.

Taylor, R. N. (1995). Geotechnical centrifuge technology. London Blackie Academic and Professional.

Theriault, Y., Masliyah, J. H., Fedorak, P. M., Vazquez-Duhalt, R. and Gray, M. R. (1995). The effect of chemical, physical and enzymatic treatments on the dewatering of tar sand tailings. Fuel, **74**(9): 1404-1412.

Znidarcic, D., Miller, R., van Zyl, D., Fredlund, M. and Wells, S. (2011). Consolidation testing of oil sands fine tailings. In: Proceedings, Tailings and Mine Waste Conference, Vancouver, British Columbia, Canada.

INFLUENCE OF FILL SCHEME ON SLURRY CONSOLIDATION MODELLING IN A GEOTECHNICAL CENTRIFUGE

Taylor Hall, Nicholas A. Beier and Rick J. Chalaturnyk
University of Alberta, Edmonton, Canada

ABSTRACT

A geotechnical beam centrifuge is used to model the consolidation behaviour of a flocculated oil sands tailings material and a kaolinite slurry. The objective of these centrifuge tests is to determine the effect of fill scheme on centrifuge modelling of high void ratio materials. A single and a layered fill scheme were utilized for both test materials, and the results were compared. Interface settlement curves, void ratio profiles and pore pressure profiles are presented for all tests. In both the kaolinite and flocculated oil sands tailings models, the layered fill models resulted in greater settlement, though this value was small (<3%) and may lie within the bounds of experimental error. The void ratio-effective stress curves for the kaolinite tests were developed from the final test results. Flocculated oil sands tailings models settled significantly without developing appreciable effective stress.

INTRODUCTION

In Alberta's oil sands, synthetic crude oil is produced from the mining and processing of bitumen. This extraction process leaves behind large quantities of tailings materials composed of water, sands, silt, clay and residual bitumen. These tailings are deposited in tailings ponds but have poor consolidation behaviour and take many decades or even centuries to settle (Chalaturnyk et. al. 2002). Significant research has been conducted on improving and understanding the consolidation of oil sands tailings materials. Physical modelling using a geotechnical centrifuge can significantly decrease the time required to test new tailings treatment methods and research the long-term performance of tailings deposits (Sorta 2015). In this paper, a geotechnical centrifuge is used to physically model the consolidation of a treated oil sands tailings material and a kaolinite slurry.

The geotechnical centrifuge is a useful tool for modelling the consolidation of high void ratio materials such as clay slurries and mine tailings. The geotechnical centrifuge operates by increasing the self-weight stresses of a model with centrifugal acceleration beyond those experienced by the model at Earth's gravitational acceleration of 1 G. The desired self-weight stresses can be achieved in the centrifuge model by accelerating to the desired speed, which results in the model experiencing N times Earth's gravity. The formula for calculating G-level in a geotechnical centrifuge is given by

$$N = \frac{rR^2}{895}$$

Where N is the centrifugal acceleration level (number of Earth's gravities), r is the centrifuge radius, and R is the rotational speed of the centrifuge (revolutions per minute).

In centrifuge modelling, model height is scaled by a factor of 1/N as compared to prototype (field scale) height. Consolidation time is scaled by a factor of $1/N^2$ when converting between model and prototype scale for slurry consolidation modelling (Taylor 1995). This scalability allows researchers to maintain equal stress levels (including pore pressures) between model and prototype, and significantly reduce testing time, which is particularly useful in modelling consolidation of oil sands tailings.

The purpose of this experimental program is to determine the effect of fill scheme on consolidation modelling using a geotechnical centrifuge. Current test procedures for centrifuge consolidation modelling use a single fill of the consolidation cell which is then spun at the desired G-level and time to model consolidation of a prototype. This modelling technique can be used to estimate the long-term performance of slurry deposits such as oil sands tailings ponds (Sorta et al. 2016, Zambrano-Narveaz et al. 2014). Using a single fill scheme, however, does not represent how tailings are deposited in the field. This fill scheme would represent a tailings deposit that is instantly deposited to its full height. In the field, tailings are continuously deposited and undergo consolidation during fill cycles. By using a layered fill scheme, deposition of material in the centrifuge model is more representative of how material is being

deposited at the prototype scale. The layered fill tests model material being added over time, with consolidation occurring between each layer addition. This process more closely follows how material is deposited in the field, as compared to completely filling the consolidation cell at the start of testing. In this paper, results obtained from the single and layered fill schemes are compared for a kaolinite slurry and a flocculated oil sands fine tailings material.

TEST MATERIALS

A kaolinite slurry and flocculated oil sands tailings were chosen for these tests. The kaolinite slurry was prepared by mixing Edgar Plastic Kaolin (EPK) clay with distilled water to the desired solids content. Mixing was done using a mud mixer in a 20L pail until thoroughly mixed.

The oil sands tailings for these tests was sourced from the Oil Sands Tailings Research Facility (OSTRF) located in Devon, Alberta. The tailings arrived in 20L pails, untreated, at 52% solids content. The raw tailings material was diluted with process water and flocculated before being loaded into the centrifuge test cells. The flocculant used was FLOPAM A3338 at a dosage of 785 g/T. The flocculant dosage was chosen to line up with ongoing research on similar tailings samples. The purpose of this research was to compare fill schemes, not identify optimal flocculant treatment dosages. The tailings were flocculated using a stand mixer with a specially designed mixing blade at a set RPM to ensure consistent flocculation of the material.

The kaolinite used in these tests had a fines content (<45µm) of 98% and a specific gravity (G_s) of 2.65 (Sorta et al. 2016). The oil sands tailings had a fines content of 85%, clay content of 42%, G_s of 2.2 and a Methylene Blue Index of 7.50meq/100g.

The kaolinite slurry was mixed to 39.0% solids (e = 4.06) and 38.4% solids (e = 4.17) in the single and layered fill tests, respectively. The flocculated oil sands tailings were mixed to 42.6% solids (e = 3.16) and 42.3% solids (e = 3.01) in the single and layered fill tests, respectively. Materials for the four tests were prepared in separate batches and can explain the discrepancy between the initial solids contents between the single and layered fill tests.

TEST PROCEDURES AND EQUIPMENT

Equipment

The centrifuge used for these experiments is a 2m radius 50-g ton beam centrifuge located at the University of Alberta in Edmonton, Alberta, Canada. Details of the beam centrifuge facility can be found in (Zambrano-Narveaz & Chalaturnyk 2014). The beam centrifuge is part of the Geomechanical Reservoir Experimental Facility (GeoREF) at the University of Alberta.

The centrifuge consolidation cell used for these tests consists of a plexiglass cylinder with an internal diameter of 177mm and a height of 297mm. The cell is instrumented with five pore pressure sensors mounted on the wall of the consolidation cell. An externally mounted HD camera is used to monitor the interface settlement of the materials in-flight. The centrifuge consolidation cell used in these tests is shown in Figure 1.

Single Fill Test Procedure

In the single fill tests, kaolinite slurry and flocculated oil sands tailings were loaded into individual consolidation cells and mounted to the centrifuge platform. The single fill tests were conducted at 100 G for 24 hours total. The testing conditions for the single fill tests is given below in Table 1.

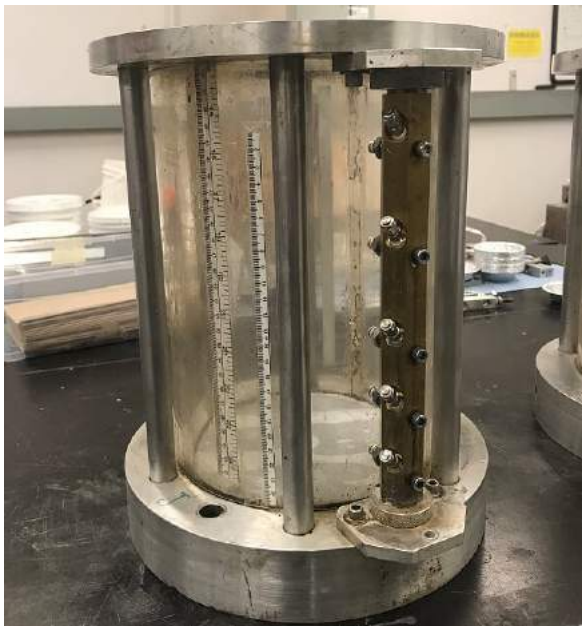

Figure 1. Centrifuge Consolidation Cell

Table 1. Single Fill Test Conditions

Material	Model Height (cm)	Model Time (hrs)	Prototype Height (m)	Prototype Time (years)
Kaolinite	28.4	24.1	28.4	27.6
Tailings	27.3	24.1	27.3	27.6

Figure 2. Push Tube Sampling Technique. a) Push tubes are inserted into sample; b) Push tubes are removed from sample; c) Push tubes samples are extruded in equal heights; d) Six samples obtained from push tubes prior to oven-drying

After centrifuge flight, the consolidation cells are removed from the centrifuge platform and sampled to determine the solids content profile of the consolidated material. The discharge water is decanted from the surface and push tubes are inserted into the sample. Samples obtained from the push tubes are divided into six equal slices, weighed and oven dried to determine the solids content of each slice. The push tube sampling technique is shown in Figure 2.

Interface settlement is monitored in-flight using the externally mounted HD camera. Scales are attached to the inside wall of the consolidation cells and the cells are photographed at set intervals to

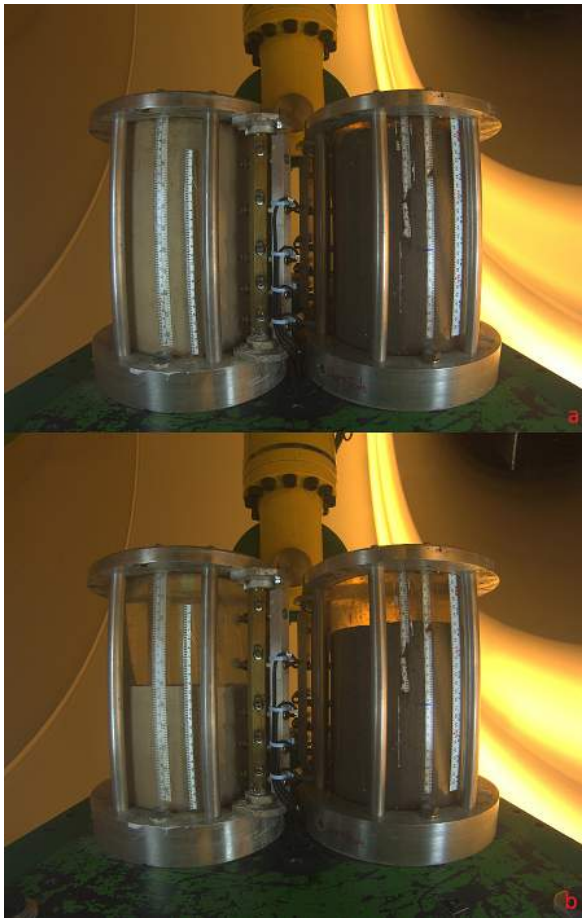

Figure 3. Single Fill Tests of Kaolinite (Left) and Tailings (Right) at Start (a) and End (b) of Testing

generate the interface settlement curves. Sample photos from the HD camera are shown in Figure 3. Pore pressure readings are taken at set intervals throughout testing and recorded via an external data acquisition system (DAS).

Layered Fill Test Procedure

In the layered fill tests, material was loaded into the consolidation cells in six layers. After addition of a new layer, the cells were spun in the centrifuge for one hour at 100 G. Each layer represented approximately 5m of placement and one year of consolidation at the prototype scale. After spinning each layer, the consolidation cell cap was removed, discharge water decanted, and a new layer was added. This process was repeated until all six layers had been added to the consolidation cells. Once all six layers had been added, the centrifuge was spun for the targeted amount of time. In the layered tests, the kaolinite sample was spun for a total of 24 hours,

whereas the tailings sample was spun for 48 hours. The tailings sample was spun for an additional 24 hours to allow the material to consolidate further, as consolidation in the single fill tests was observed to be significantly slower than the kaolinite sample. The test conditions for the layered fill tests is shown below in Table 2.

Table 2. Layered Fill Test Conditions

Material	Model Height (cm)	Model Time (hrs)	Prototype Height (m)	Prototype Time (years)
Kaolinite	29.1	23.9	29.1	24.2
Tailings	28.8	48.4	28.8	51.4

The kaolinite slurry was added to the consolidation cell by funneling the material. The kaolinite slurry flowed easily due to its low solids content (38.4%). Funneling of the kaolinite slurry into the consolidation cell is shown in Figure 4.

A new dispensing device, developed in-house by members of the GeoREF team, was used to dispense the flocculated tailings material into the consolidation cell. The dispenser was designed for tailings and high solids content materials that do not easily flow. The dispenser is shown in Figure 5.

Figure 4. Funneling Kaolinite Slurry into Consolidation Cell

Figure 5. Dispensing Tailings Material to the Consolidation Cell. a) Material is added to the dispenser; b) Dispenser is secured to the consolidation cell; c) Dispenser shown inside consolidation cell; d) Dispensed material in the consolidation cell

Interface settlement monitoring, pore pressure data and push tube sampling for the layered tests followed the same procedure as outlined in the single fill test procedures.

RESULTS

Interface Settlement

The settlement curves for the kaolinite tests are presented in Figure 6. In the single fill test, settlement of the kaolinite slurry was complete after ten years of prototype time. In the layered fill tests, significant settlement occurred in each layer after one year of prototype time, and settlement was complete within ten years prototype time. The total settlement of the single and layered kaolinite models were 13.5cm (47.5%) and 14.6cm (50.2%), respectively.

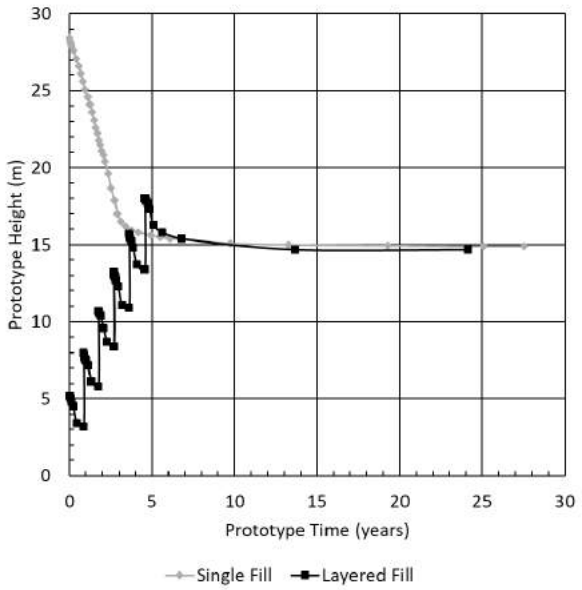

Figure 6. Kaolinite Interface Settlement

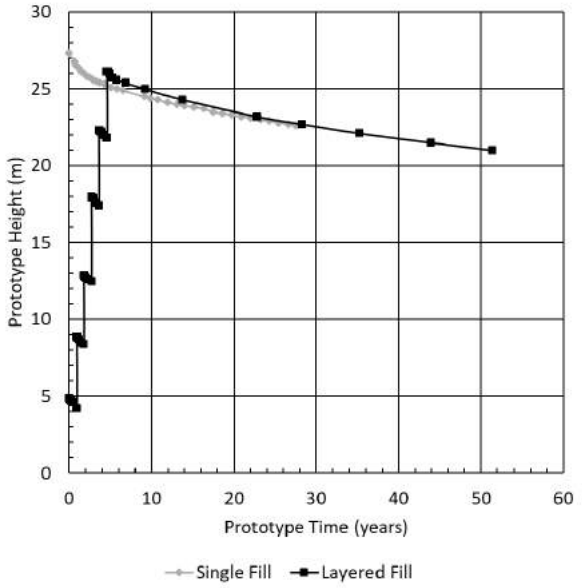

Figure 7. Tailings Interface Settlement

The settlement curves for the tailings tests are presented in Figure 7. Settlement of the single fill model did not complete after 27.6 years of prototype time. The layered fill tests were spun for an additional 24 hours in the centrifuge for a total of 51.4 years of prototype settlement time. Even with the additional spin time, settlement did not complete in the layered fill tests. Settlement occurred in each layer of the layered tailings model as they were added to the cell, as expected. The total settlement of the single and layered tailings models were 4.7cm (17.2%) and 7.9cm (27.4%), respectively. After 24.5 years of prototype time, the layered fill model settled 5.8cm (20.1%).

Void Ratio Profiles

The final void ratio profiles for the kaolinite tests are shown in Figure 8. Void ratios for the bottom four layers were similar between the single and layered models. The topmost layers had a final void ratio of 2.87 and 2.09 in the single and layered fill models, respectively.

The final void ratio profiles for the tailings tests are shown in Figure 9. As expected, the void ratio was lower at all sample points in the layered fill model. This was due to the additional spin time in the layered fill model.

Pore Pressure Profiles

The pore pressure profiles for the four models are presented in the following figures. In the figures, port 1 refers to the lowest pore pressure port, and port 4 refers to the topmost pore pressure port. Hydrostatic pore pressure values are presented on the figures as dashed lines. The hydrostatic values are calculated theoretical values and may differ from the actual reading of the pore pressure sensors inside the cell. Technical difficulties were encountered with some of the pore pressure sensors during testing, and these values are omitted from the results presented here.

The pore pressure profiles for the kaolinite tests are shown in Figure 10 and Figure 11. In both tests, the excess pore pressure dissipation with time is clearly visible. The addition of each layer is visible in the layered fill pore pressure profile (Figure 11).

The pore pressure profiles for the tailings tests are shown in Figure 12 and Figure 13. As shown by these results, little to no excess pore pressure dissipation occurred in either the single or layered fill models. This suggests that the tailings models did not develop any appreciable effective stresses during settlement.

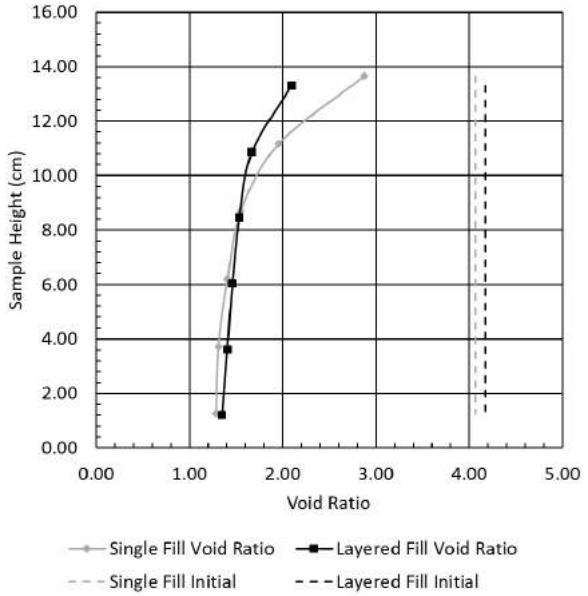

Figure 8. Kaolinite Void Ratio Profiles at End of Testing

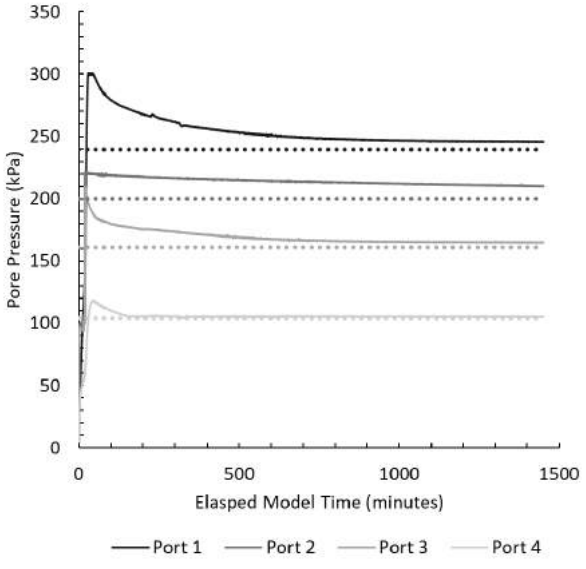

Figure 10. Kaolinite Pore Pressures (Single Fill Model)

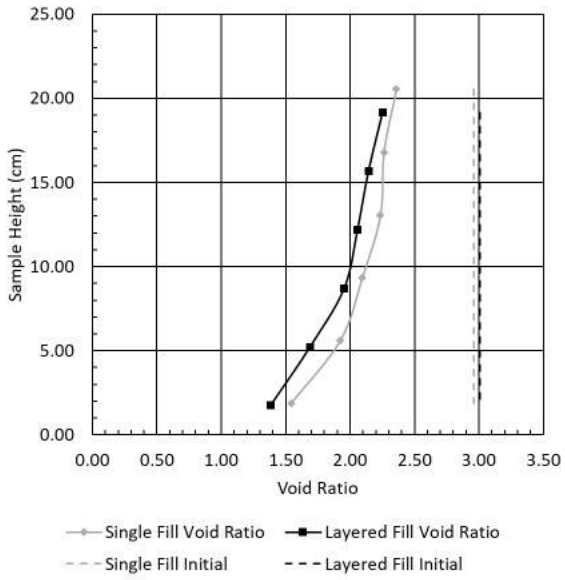

Figure 9. Tailings Void Ratio Profiles at End of Testing

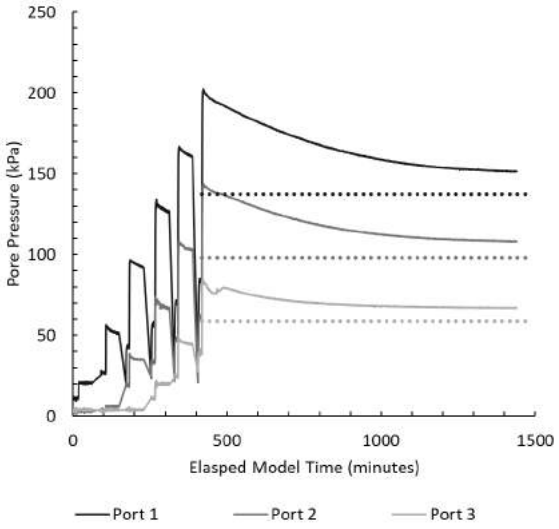

Figure 11. Kaolinite Pore Pressures (Layered Fill Model)

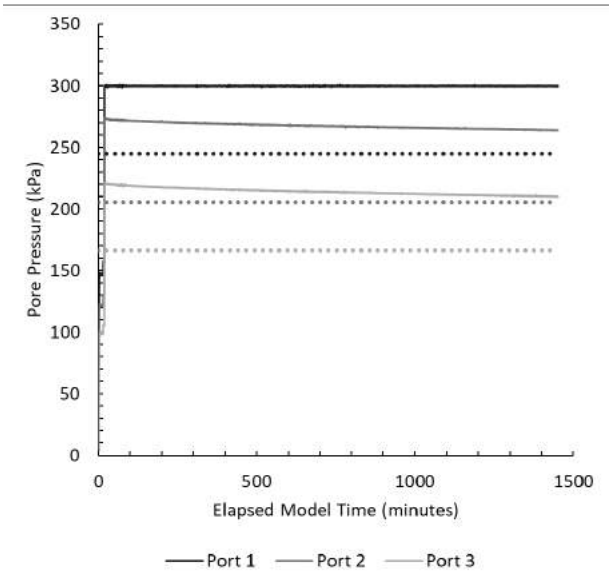

Figure 12. Tailings Pore Pressures (Single Fill Model)

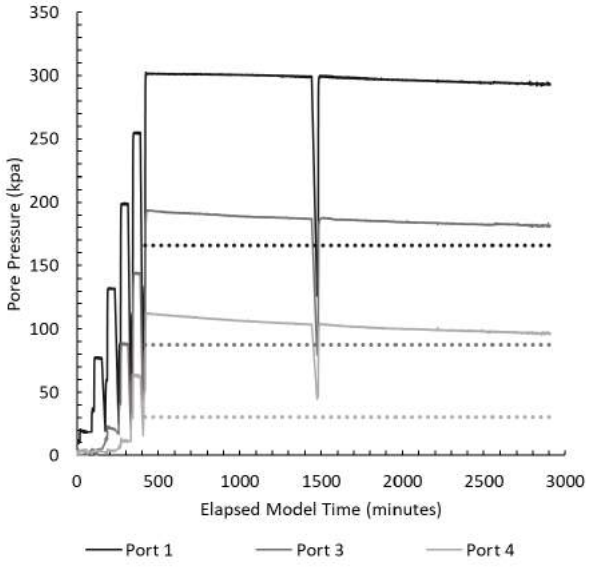

Figure 13. Tailings Pore Pressures (Layered Fill Model)

Effective Stress Curves

Void ratio effective stress curves were developed from the kaolinite test results. Pore pressure data was used to create an effective stress profile with depth in the final kaolinite results, and this was matched to the final void ratio profile to generate the void ratio-effective stress curve. These results are

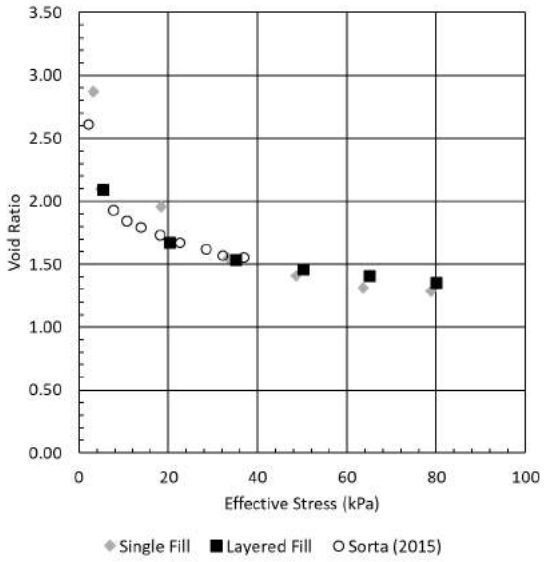

Figure 14. Kaolinite Void Ratio Effective Stress Curves

shown in Figure 14. The void ratio effective stress curves could not be made for the tailings models as they did not develop any appreciable effective stress during testing.

DISCUSSION

In the kaolinite tests, the single fill model had an initial solids content of 39.0% and settled 13.5cm (47.5%) after 27.6 years of prototype time. In the layered fill model, the initial solids content was 38.4% and settled 14.6cm (50.2%) after 24.2 years of prototype time. When referring to the settlement graph of the kaolinite tests (Figure 7), settlement of both models was complete after approximately ten years of prototype time. Therefore, the additional 3.4 years of prototype settlement time in the single fill test should be negligible. As demonstrated by the final void ratio profiles, it is shown that the layered model had a lower void ratio (higher solids content) in the top sample layers as compared to the single fill model. These results suggest additional settlement in the layered model occurred in the top two layers. These results, along with the interface settlement observations, suggest that the layered addition of material in the kaolinite model resulted in more settlement overall as compared to the single fill approach, although this value is small (2.7%).

Similar observations can be made in the tailings tests. The single fill model had an initial solids content of 42.6% and settled 4.7cm (17.2%) after

27.6 years of prototype time. The layered fill model had an initial solids content of 42.3% and settled 7.9cm (27.4%) after 51.4 years of prototype time and 5.8cm (20.1%) after 24.5 years of prototype time. Therefore, at a similar solids content and prototype time, the layered model settled 2.9% more than the single fill model. This value would represent an additional 0.9m of settlement when modelling a 30m deposit with the centrifuge.

The tailings models underwent significant settlement after 27.6 years of prototype time in the single fill model and 51.4 years of prototype time in the layered fill models. These models, however, did not appear to develop any appreciable levels of effective stress as indicated by the pore pressure readings. A similar phenomenon was observed by (Jeeravipoolvarn 2004) during large-scale settling column tests conducted at the University of Alberta on oil sands fine tailings.

Void ratio-effective stress curves were created for the kaolinite models using pore pressure readings and solids content sampling without the use of additional instrumentation. These void ratio-effective stress curves, along with permeability-void ratio curves, can be used as inputs for large strain consolidation numerical models as demonstrated by (Sorta et al. 2016). Data interpretation from these tests is ongoing, and permeability-void ratio curves are not yet available.

CONCLUSIONS

In this paper, a series of consolidation tests were completed on a kaolinite slurry and treated oil sands tailings. The goal of the research program was to determine the effect of fill scheme on the consolidation test results using a geotechnical centrifuge. The conclusions from these tests can be summarized as follows.

Test materials were able to be successfully loaded into centrifuge consolidation cells in a layered fill scheme to more closely replicate how these materials are deposited in the field. A new dispensing device was developed by the GeoREF research team to load treated oil sands tailings into the consolidation cells.

Using a layered fill scheme in consolidation tests for slurry materials (including oil sands tailings) in the geotechnical centrifuge may lead to greater settlement compared to a single fill scheme, though this value is small (<3%). This increased settlement from the layered tests may have implications for future test programs where total interface settlement is the primary interest. Void ratio-effective stress curves were developed from the final tests results of the kaolinite tests. Data interpretation is ongoing and permeability-void ratio curves are not yet available. Void ratio-effective stress curves were not developed for the oil sands tailings materials, as these models did not develop appreciable effective stress during testing.

ACKNOWLEDGEMENTS

The authors would like to thank the Natural Sciences and Engineering Research Council of Canada (NSERC), Canada's Oil Sands Innovation Alliance (COSIA) and Alberta Innovates – Energy and Environment Solutions for their financial support.

The authors would also like to thank Dr. Gonzalo Zambrano-Narvaez and Yazhao Wang of the GeoREF laboratory for their insights and assistance with the experimental program.

REFERENCES

Chalaturnyk, R. J., Scott, J. D. and Ozum, B. (2002). Management of oil sands tailings. Petroleum Science and Technology, **20**(9 & 10): 1025-1046.

Jeeravipoolvarn, S. (2004). Compression behaviour of thixotropic oil sands tailings (Master). Available from University of Alberta.

Sorta, A. R. (2015). Centrifugal modelling of oil sands tailings consolidation (PhD). Available from University of Alberta.

Sorta, A. R., Sego, D. C. and Wilson, G. W. (2016). Physical modelling of oil sands tailings consolidation. International Journal of Physical Modelling in Geotechnics, 16(2), 47-64.

Taylor, R. N. (1995). Geotechnical centrifuge technology. London: Blackie Academic & Professional.

Zambrano-Narveaz, G. and Chalaturnyk, R. J. (2014). The new GeoREF geotechnical beam centrifuge at the University of Alberta, Canada. Proceedings of the 8th International Conference on Physical Modelling in Geotechnics. 163-167.

Zambrano-Narveaz, G., Scott, J. D. and Chalaturnyk, R. J. (2014). Modeling tailings consolidation with the GeoREF geotechnical beam centrifuge. Paper presented at the 7th International Conference on Environmental Geotechnics, Melbourne, Australia. 926-933.

Session 11

TAILINGS TREATMENT PROCESSES

CATIONICALLY GRAFTED NATURAL FLOCCULANT FOR DEWATERING OF MATURE FINE TAILINGS

Sarang P. Gumfekar[1], Mohammed Ghuzi[1], Saurabh C. Patankar[2],
Scott Renneckar[2] and João B. P. Soares[1]
[1]University of Alberta, Edmonton, Canada
[2]University of British Columbia, Vancouver, Canada

ABSTRACT

This work reports the use of a two-stage modification of chitosan for the flocculation and dewatering of mature fine tailings (MFT). First, chitosan was oxidized to enhance its solubility in MFT, and then 2-methacryloyloxy ethyltrimethyl ammonium chloride (MATMAC) monomer was in-situ polymerized onto the as-oxidized chitosan. The cationic modification was pursued to enhance the flocculation performance of the flocculants via charge neutralization. The chitosan was oxidized using a novel, recyclable, magnetically-supported catalyst, which was reused for further oxidation experiments. Further, MATMAC was grafted onto oxidized chitosan using free radical polymerization. We investigated the effect of flocculant dosage on flocculation performance of cationically-modified chitosan in MFT. The flocculant dosage was varied from 1000 to 6000 ppm. Flocculation performance was evaluated in terms of initial settling rate (ISR), capillary suction time (CST), supernatant turbidity, and the sediment solid content (SSC). Settling did not induce until 4000 ppm dosage due to insufficient bridging and intermolecular forces. We obtained the highest ISR of 0.75 m/h, lowest CST of ~ 11 s, the lowest supernatant turbidity of ~3 NTU, and highest SSC of 14 wt. %. In all experiments carried out in this study, effective flocculation occurred at 6000 ppm polymer dosage. This study demonstrated the application of cationic, chitosan-based natural flocculant with novel process of chitosan oxidation for MFT flocculation.

INTRODUCTION

The second largest oil sands reserves in the world can be found in Northern Alberta, Canada. The oil sands provide extensive benefits to the Canadian economy and have worldwide importance as energy deposits. Typically, bitumen is extracted from the oil sands by modified variants of the Clark hot water extraction process over the past few decades. (Clark and Pasternack 1932) The extraction process uses hot alkaline water and hydrocarbon solvents, producing fluid wastes that are composed of an aqueous suspension of fine clays, dissolved salts, unrecovered bitumen, and solvents. The waste by-product is alkaline, brackish, and toxic to the environment due to high concentrations of organic acids leached from the bitumen during extraction, called as fluid fine tailings (FFT). Over the approximate duration of two years, larger particles in the FFT settle to form a fluid of yogurt-like consistency, called as MFT. MFT have poor consolidation under natural conditions, taking many decades to release water. 840 billion liters of MFT have been produced and deposited in enormous tailings ponds covering approximately 176 km^2. (Zhu et al. 2017)

Effective dewatering and consolidation of oil sands tailings are of extreme importance to reduce the environmental contamination caused by bitumen extraction operations. Consolidated tailings and paste technology are the most widely used dewatering methods for oil sands tailings. (Masliyah et al. 2004) Consolidated tailings (CT) is a process where fresh tailings are mixed with MFT and a coagulant, such as a gypsum, to form denser solid phase with sand and fine clay particles, releasing free water. (Beier et al. 2013) The high concentration of divalent cations in the recovered water using the consolidated tailings process impedes the re-utilization of this water in the bitumen extraction process. On the other hand, paste technology uses polymers to thicken the oil sands tailings and remove the water that can be used in the bitumen extraction process. (Li et al. 2007) Accumulation of ions does not occur in the case of paste technology; but this technology, similar to the consolidated tailings process, recovers only part of the water from tailings and produces sediments with a high water content that still requires special storage.

Recently, natural polymeric flocculants are being studied for water treatment because of their ability to bridge the particles in suspension. (Pennetta de Oliveira et al. 2018) Natural polymers may be of

noteworthy interest because they are non-toxic, renewable, and easily available. (Sharma et al. 2006) Usually, flocculants based on natural polymers are made up of starch, chitosan, cellulose, konjac glucomanna, tamarind kernel, alginate, guar gum etc. (Dao et al. 2016) Natural polymeric flocculants have the ability to biodegrade, but unfortunately, exhibit poor flocculation performance and storage life. In this work, we describe the performance of chitosan-based cationic flocculant to treat MFT. The performance of chitosan can be improved when it is modified with suitable functional groups that can alter its functional properties. Previously, chitosan-based flocculants have been synthesized and tested with wastewater contaminated with dissolved and undissolved inorganic, organic, and biological contaminants, including suspended solids, heavy metals, humic acid, dyes, algae, and bacteria. (Jia et al. 2016) These flocculants exploit the free amines and hydroxyl groups on the backbone of the chitosan chain that can be linked to various functional groups.

Taking the advent of the aforementioned factors, we synthesized cationically-modified chitosan-based flocculants. The synthesized flocculants were employed to dewater the MFT, and to study the dewatering performance. The performance of flocculants is measured in terms of the initial settling rate (ISR) of MFT, the turbidity of supernatant and capillary suction time (CST) and sediments solid content (SSC).

EXPERIMENTAL

Materials

Chitosan, NaBr, sodium hypochlorite solution, [2-(methacryloyloxy) ethyl] trimethyl ammonium chloride (MATMAC), ammonium persulfate (APS) were purchased from Sigma-Aldrich. The magnetically separable catalyst was prepared according to the procedure described elsewhere. (Patankar and Renneckar 2017) MFT was provided by Syncrude Canada Ltd.

Synthesis

Chitosan was first oxidized and then MATMAC was grafted onto it using free radical polymerization. The oxidation of chitosan was performed using a TEMPO-attached magnetic catalyst in presence of NaBr and NaOCl at 70 °C. The oxidized chitosan was washed and then dried using lyophilizer. In the second step, MATMAC was grafted onto oxidized chitosan using 0.01 M ammonium persulfate initiator. The reaction was performed overnight and the product was precipitated in acetone. Figure 1 shows the chemical structure of cationically modified chitosan.

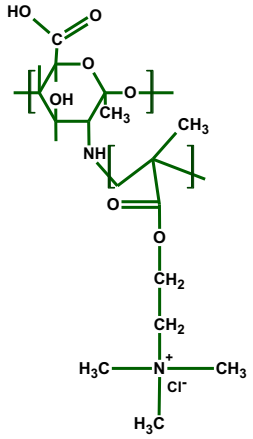

Figure 1. Chemical structure of cationically-modified chitosan

Characterization

Chitosan, oxidized chitosan, and cationically-modified chitosan were characterized using Fourier transform infrared (FTIR) spectroscopy in the range of 400 to 4000 cm^{-1} wavenumber. The composition of MFT was determined using Dean-Stark method (Table 1).

Table 1. Composition of MFT

Compound	Weight %
Solid	39.55
Water	55.13
Bitumen	5.32

Flocculation Tests

As-received MFT was diluted to 5 wt% using DI water for flocculation experiments. The polymer stock solution of 0.8 wt% was prepared in DI water and used immediately to avoid the degradation of polymeric chains. The desired volume of polymer solution from stock solution was added into 100 g of diluted MFT in a beaker. The mixing was performed at 200 rpm for 1 min. Then, the CST was immediately measured to evaluate the dewaterability of the suspension. Remaining

suspension was transferred to 100 mL cylinder for settling test. The supernatant was collected after 24 h of settling and the turbidity was measured using turbidimeter. The sediment solids content (SSC) was gravimetrically determined to evaluate the effectiveness of the flocculant.

RESULTS AND DISCUSSION

Synthesis and characterization

Generally, chitosan is water insoluble at neutral and alkaline pH. In order to use it effectively, it should be soluble in MFT, which exhibits pH of 8-9. Cationic flocculants are more effective in flocculation of MFT because cations neutralize the negatively charged clay particles. To perform the cationic modification in an aqueous environment, chitosan should be soluble in water. Thus, we first oxidized the chitosan using TEMPO-attached magnetic catalyst, which was recovered after the oxidation reaction. Further, MATMAC was grafted onto oxidized chitosan. The purpose of the cationic modification was to introduce cationicity so that a better colloidal destabilization can be achieved through the compression of electrical double layers, charge neutralization, and polymer bridging.

FTIR spectroscopy was performed to confirm the oxidization of chitosan and further grafting of MATMAC onto the oxidized chitosan. Figure 2 shows the FTIR spectra of chitosan, oxidized chitosan, and cationically-modified chitosan.

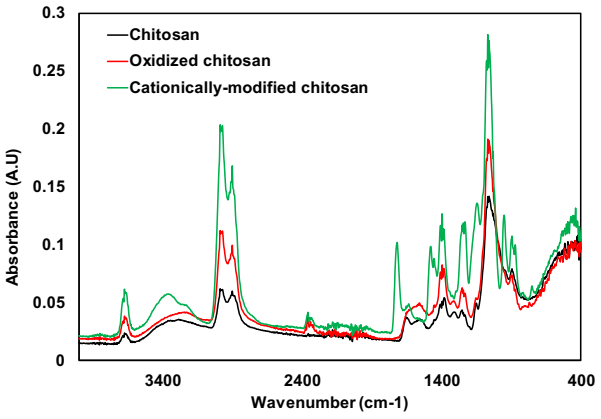

Figure 2. FTIR spectra of chitosan, oxidized chitosan, and cationically-modified chitosan

Since chitosan has abundant hydroxyl groups on its backbone, the corresponding peak was observed at 3350 cm-1. Other characteristic peaks at 2900, 1560, and 1065 cm-1 were also confirmed. (Bordenave et al. 2008) Further, oxidation of chitosan was confirmed by the presence of COO- at 1394 cm-1 and carboxylic acid OH at 2356 cm-1. Finally, the peaks at 1713, 1634, and 1478 cm-1 confirmed the grafting of MATMAC onto oxidized chitosan. (Vold and Christensen 2005)

Settling tests

In this study, we flocculated 5 wt% MFT suspensions and the flocculant dosage was varied from 1000 to 10000 parts per million (ppm). It is worthwhile to note that the flocculant dosage is expressed on the basis of the weight of solids in the slurry, not the volume. The mudline height against time was recorded over a period of 60 min to determine the ISR. ISR was calculated from the slope of an initial linear portion of the settling curves. Figure 3 shows how ISR varies as a function of flocculant dosage. At low polymer dosages (1000 and 2000 ppm), the solid-liquid interface was barely visible because the dosage did not induce floc formation in MFT to sufficiently distinguish the solid-liquid interface. However, the settling in MFT was induced when the flocculant dosage increased to 4000 ppm, indicating that sufficient charge density required for the distinct solid-liquid interface was achieved. At 6000 ppm, the highest ISR was achieved within the dosage range studied in this work.

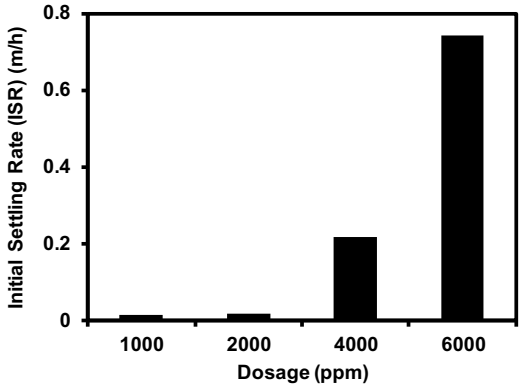

Figure 3. The initial settling rate of MFT as a function of polymer dosage

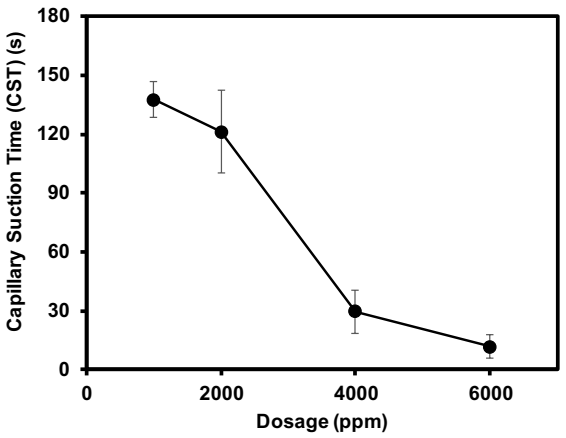

Figure 4. Capillary suction time of MFT with an increase in polymer dosage

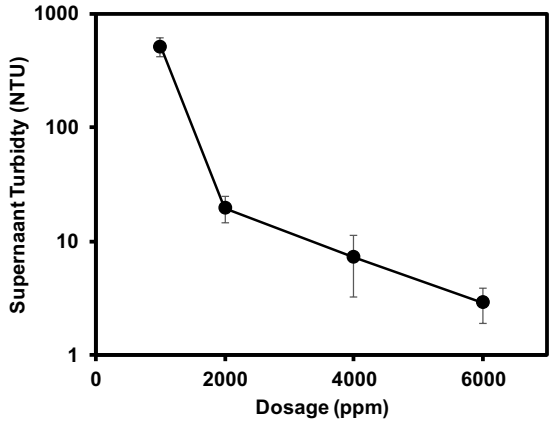

Figure 5. The turbidity of the supernatant as a function of dosage

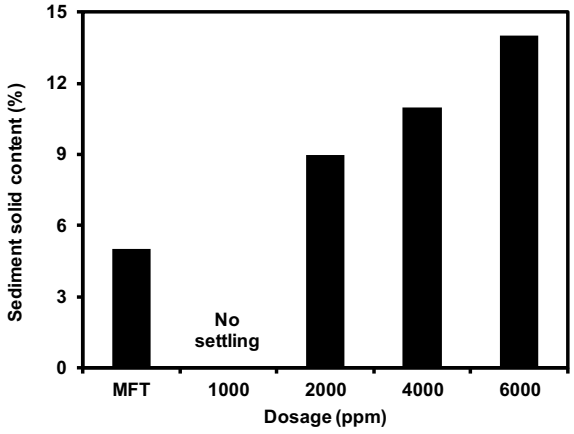

Figure 6. Sediment solids content obtained after flocculation as a function of dosage

The dewaterability of the flocculated MFT was measured using CST measurements, where lower CST corresponds to higher (faster) dewaterability. Figure 4 shows the effect of the polymer dosage on the CST with their associated standard errors. The CST decreased with the increase of the polymer dosage, noting that the unflocculated MFT has a CST of 364 s ± 13.8 s. At lower dosages, namely 1000 ppm and 2000 ppm, within the standard error, the flocculant exhibited similar dewaterability performance corroborating the observations of ISR at lower dosages. With further increase in dosage, CST rapidly decreased to 7 s indicating faster dewaterability of the sediments.

The turbidity of the supernatant was measured to determine the quality of the recovered water after settling for 24 h. Figure 5 shows the effect of polymer dosage on the supernatant turbidity. At 1000 ppm, the MFT treated with flocculant suffered from the poorest clarity, suggesting that a greater portion of fine particles remained in the released water. The supernatant obtained using polymer dosages of 4000 and 6000 ppm was significantly clear suggesting the destabilization and bridging of particles by neutralization of the charges and formation of flocs, which agreed well with the ISR results.

Sediment solids content (SSC) was measured gravimetrically after 24h of settling to evaluate the compaction effectiveness of the flocculant. Figure 6 shows the SSC as a function of polymer dosage. We could not measure SSC after polymer dosing of 1000 ppm because the solid-liquid interface was unclear due to insufficient floc formation. Further increase of dosage increased the SSC from 5 wt% (starting MFT) to 14 wt% at 6000 ppm. The results indicated that the increase of dosage increased the compaction of sediment solids, expelling more water out of sediments.

CONCLUSIONS

Chitosan-based flocculant was synthesized using a two-step approach. First, the chitosan was oxidized using a magnetically-separable catalyst. Oxidation increased the solubility of chitosan at neutral and alkaline pH. Further, cationic monomer MATMAC was grafted onto oxidized chitosan using free radical polymerization. The cationically-modified flocculant was tested on 5 wt% MFT in the dosage range of 1000 to 6000 ppm. The best flocculation performance of the flocculant in terms of ISR, CST,

turbidity, and the solids content was observed at 6000 ppm. In general, our results provide new insights into the development of novel excellent green flocculants, which require further systematic research on scale-up synthesis.

REFERENCES

Beier, N., Wilson, W., Dunmola, A. and Sego, D. (2013). Impact of flocculation-based dewatering on the shear strength of oil 1007, 1001–1007.

Bordenave, N., Grelier, S. and Coma, V. (2008). Advances on selective C-6 oxidation of chitosan by TEMPO. Biomacromolecules, **9**: 2377–2382. https://doi.org/10.1021/bm800375v

Clark, K. A. and Pasternack, A. N. D. D. S. (1932). Hot Water Separation of Bitumen from Alberta Bituminous Sand. Ind. Eng. Chem., **24**: 1410–1416.

Dao, V. H., Cameron, N. R. and Saito, K. (2016). Synthesis, properties and performance of organic polymers employed in flocculation applications. Polym. Chem., **7**: 11–25. https://doi.org/10.1039/C5PY01572C

Jia, S., Yang, Z., Yang, W., Zhang, T., Zhang, S., Yang, X., Dong, Y., Wu, J. and Wang, Y. (2016). Removal of Cu(II) and tetracycline using an aromatic rings-functionalized chitosan-based flocculant: Enhanced interaction between the flocculant and the antibiotic. Chem. Eng. J., **283**: 495–503. https://doi.org/10.1016/j.cej.2015.08.003

Li, H., Long, J., Xu, Z. and Masliyah, J. (2007). Flocculation of kaolinite clay suspensions using a temperature-sensitive polymer. AIChE J., **53**: 479–488. https://doi.org/10.1002/aic

Masliyah, J., Zhou, Z. J., Xu, Z., Czarnecki, J. and Hamza, H. (2004). Understanding Water-Based Bitumen Extraction from Athabasca Oil Sands. Can. J. Chem. Eng., **82**: 628–654. https://doi.org/10.1002/cjce.5450820403

Patankar, S. C. and Renneckar, S. (2017). Greener synthesis of nanofibrillated cellulose using magnetically separable TEMPO nanocatalyst. Green Chem., **19**: 4792–4797. https://doi.org/10.1039/C7GC02383A

Pennetta de Oliveira, L., Gumfekar, S. P., Lopes Motta, F. and Soares, J. B. P. (2018). Dewatering of Oil Sands Tailings with Novel Chitosan-Based Flocculants. Energy & Fuels, **32**: 5271–5278. https://doi.org/10.1021/acs.energyfuels.7b03634

Sharma, B. R., Dhuldhoya, N. C. and Merchant, U. C. (2006). Flocculants—an Ecofriendly Approach. J. Polym. Environ., **14**: 195–202. https://doi.org/10.1007/s10924-006-0011-x

Vold, I. M. N. and Christensen, B. E. (2005). Periodate oxidation of chitosans with different chemical compositions. Carbohydr. Res., **340**: 679–684. https://doi.org/10.1016/j.carres.2005.01.002

Zhu, Y., Tan, X. and Liu, Q. (2017). Dual polymer flocculants for mature fine tailings dewatering. Can. J. Chem. Eng., **95**: 3–10. https://doi.org/10.1002/cjce.22628

FILTER PRESS MODIFICATION TO ASSESS DEWATERING PERFORMANCE OF FLUID FINE TAILINGS

Yunhui Li[1], Heather Kaminsky[1], Nikolas Romaniuk[2] and Mike Tate[3]
[1]Northern Alberta Institute of Technology, Edmonton, Canada
[2]Nikolas Romaniuk Consulting, Alberta, Canada
[3]Graymont Inc., Genoa, Ohio, USA

ABSTRACT

The standard resistance to filtration (SRF) test is a standard test used primarily to assess the filtration resistance of drilling muds. This test has also been used to screen the filtration performance of tailings for the potential application to pressure filtration. In both cases, direct air pressure is applied to a tailings sample and the rate of water release measured either for a fixed portion of time or until the cake dewaters sufficiently to crack (thereby short circuiting the test). The cake cracking limits the ability to test the dewaterability of different tailings as they approach their plastic limit. NAIT has modified this test set up to use a piston cylinder in between the gas and the sample. This allows the same gas pressure to be applied to the sample but removes the limitation on dewatering time due to cracking. This permits an assessment of dewatering performance of different treatments at much higher solids contents.

NAIT used this modification to assess the impact of lime, gypsum and polymer treatment on the dewatering performance of fluid fine tailings (FFT) under pressure. The lime treated tailings generated a much denser filter cake than either the gypsum or polymer treated tailings for the same filtration time in the modification set up indicating a potential benefit of lime addition in filtration applications.

INTRODUCTION

The oil sands in northern Alberta, Canada, represent the 3rd largest proven global oil reserve with a bitumen reserve equivalent to 1.6 trillion barrels of oil (Alberta Energy 2013). Bitumen is extracted by the Clark Hot Water Extraction process, leaving behind a combination of sand, silt, clay, water and residual bitumen known as tailings. The tailings in the Athabasca oil sands region covered 1,206 million m^3 by 2016 (AER 2016a), despite past regulatory efforts requiring operators to treat the FFT. In 2016 the Alberta Energy Regulator (AER) released Directive 85 which requires operators to ensure that all fluid tailings are returned to a reclamation ready state ten years after the end of mine life (AER 2016b). Current industry methods are estimated to cost in the rage of $5 to $10 per cubic meter, representing a multi-billion dollar liability for the industry (Klohn Crippen Berger 2017).

Significant efforts have been devoted to fluid tailings treatment technology, such as thin lift drying or tailings reduction operation (TRO) by Suncor, composite tailings (CT) and centrifuge by Syncrude, thickened tailings (TT) by Imperial Oil, and non-segregating tailings (NST) by CNRL (AER 2016a).

Filtration is one of the most traditional methods for solid-liquid separation and it has been widely used in other industries. Filtration is also one of consolidation methods achieving dry tailings through a mechanical driving force process. Filtration of coarse oil sands tailings was evaluated in the mid-1990s during the pilot-scale tests on different bitumen extraction processes (Sury and Stone 1995). Flocculated oil sands tailings with different treatments were assessed by many researchers using pressure filtration (Alamgir et al. 2012, Loerke et al. 2017, Xu et al. 2008, Zhu 2015) and vacuum filtration (Liu et al. 1980, Zhu 2015). But filtration has never been implemented by the oil sands industry (Xu et al. 2008) due to the high capital cost relative to alternatives (Davies 2011, Krester 2018), low filter constant (Suthaker and Scott 1996, Vedoy and Soares 2015), and filter media fouling and blockage by residual bitumen in tailings (Loerke et al. 2017, Wang et al. 2018). With the pressure and incentive by the Alberta government (AER 2016b), filtration might be an option for dry tailings disposal.

Graymont Western Canada Inc. (Graymont) is an emerging global leader in the supply of lime and limestone products. Graymont can potentially help

manage the large oil sands tailings inventories in Alberta by treating FFT with lime prior to filtration.

Specific Resistance to Filtration (SRF) is a measure of the filterability by measuring the resistance of the formation cake to the flow of the filtrate. The SRF calculation is based on a theoretical filtration model derived from Darcy's equation (Coulson 1991). High SRF value indicates low filterability. The SRF of a sample is a critical parameter to evaluate the performance of a flocculant, coagulant, or coagulant/flocculant combination as a filtration aid. It was found that only the filtration of very coarse tailings (<4% fines) was applicable, and flocculation of tailings improved the filterability significantly by reducing the filtration resistance three orders of magnitude (Xu et al. 2008).

During the filtration process, shrinkage cracking is frequently encountered resulting in a restriction on further desaturation (Anlauf et al. 1985, Wakeman et al. 1974). Lloyd et al. (1972) suggested that the filter cake cracking may be due to the internal stress development during compression (Lloyd et al. 1972). It was determined in that study that the filter cake cracking could be eliminated through careful control of key input parameters such as initial slurry concentration, fine particle content, surfactant addition, et al. (Barua 2014). It is not desired, however, to change the original properties of the testing materials.

This study introduced a modified gas pressure filtration setup by inserting a cylinder piston between the sample and high pressure gas which could avoid filter cake cracking without changing the original properties of the testing materials. With the modification of the filter press, the sample is dewatered through a single drainage path under a desaturated condition without encountering cake cracking. This allows us to achieve a highest consolidated cake in a short time by applying a strong force. Therefore, this modified filter press could be a good option as a rapid indicator of long-term consolidation behavior.

In addition, the thickness of the compressed cake and the force applied could be adjusted by changing the amount of sample and the pressure. In this study, dewatering performance of untreated FFT, coagulated FFT and flocculated FFT was investigated using the modified pressure filtration setup under a constant gas pressure.

EXPERIMENTAL

The study was performed at Centre for Oil Sands Sustainability (COSS) at Northern Alberta Institute of Technology (NAIT), Edmonton, Alberta.

Materials

FFT from an oil sands tailings pond was characterized by Dean and Stark (D&S) for bitumen, solids, and water (BSW) contents (Dean and Stark 1920), methylene blue index (MBI) and particle size distribution (PSD) (Table 1). The D&S extraction was performed by NAIT in the range of 21 to 24 hours to ensure complete removal of bitumen from the solids. The wt% of fines with less than 44 micron for the D&S cleaned solids was 96.8%. The clay content calculated by MBI was 101 wt%. The calculated clay to water ratio (CWR) was 0.34.

Table 1. Average MBI, %Fines, D&S data for bitumen, solids and water, and calculated CWR

Bitumen (wt%)	Mineral (wt%)	Water (wt%)	MBI (meq/100 g solids)	Clay content in Solids (wt%)	CWR	Fines %
1.2	24.7	73.6	14.1	101%	0.34	84.2

The simulated process water was prepared based on chemicals and masses in Table 2. The target ion concentration is shown in Table 3. The pH of the simulated process water was adjusted to 8.4 using acid or base in order to be consistent with the industrial process water.

The simulated process water was used to prepare the additive slurry or solution and diluted FFT in this study. The high calcium hydrated lime was provided by Graymont Inc. Gypsum was purchased from Sigma-Aldrich.

Methods

Slurry and Solution Preparation. Lime slurry of 5 wt%, gypsum slurry of 12 wt%, NaOH solution of 10 wt%, and polymer (SNF A3338) of 0.45 wt% were prepared by mixing lime, gypsum, NaOH, and polymer with simulated process water under 300 rpm.

FFT was homogenized prior to testing. For untreated FFT, the material was mixed for 30 minutes using an overhead mixer at high speed before subsampling. Diluted FFT was prepared by

Table 2. Simulated process water preparation.

Salt	$CaCl_2.2H_2O$	$MgCl_2.6H_2O$	KCl	NaCl	$NaHCO_3$	Na_2SO_4
CAS	10043-52-4	7791-18-6	7447-40-7	7647-14-5	144-55-8	7757-82-6
Purity	100%	100%	100%	100%	100%	100%
Mole (mol)	0.07	0.07	0.07	1.68	1.92	0.56
Molecular weight (g/mol)	147.02	203.3	74.55	58.44	84.007	142.04
Mass to be added (g)	9.90	15.06	5.15	98.12	161.10	79.85

Table 3. The composition of the prepared simulated process water.

Ions	Ca	Mg	K	Na	Cl	HCO_3^-	SO_4^{2-}
Targetted ion concentration (ppm)	15	10	15	600	400	650	300
Mass to be added (g)	2.7	1.8	2.7	108	72	117	54
Molucular mass (g)	40.08	24.31	39.10	22.99	35.45	61.01	96.06
Mole (mol)	0.07	0.07	0.07	4.70	2.03	1.92	0.56

mixing a desired amount of simulated process water and FFT.

FFT Treatment with Additives. FFT treatment with lime, gypsum, and NaOH was conducted using a Phipps & Bird-700 Gang mixer with an adjustable paddle. The desired amounts of FFT and additive slurry or solution were introduced into a beaker or metal cup with the stirring speed of 300 rpm. The combined fluid was mixed for 5 minutes.

The dosages of lime in this study were all based on the wet sample weight. The conversion of wet sample based dosages to solid based dosages for the FFT used is shown in Table 4.

Table 4. Dosage conversion of lime used

Nominal Lime dose (ppm)	Mass of lime/mass of solids in FFT (g/tonne)
2000	8097
3000	12146
4000	16194
5000	20243

A pulsed mixing technique (0-320 rpm) was used to form flocculated FFT using polymer A3338 (Li et al. 2016).

Filter Press Test. An OFITE's Multi-Unit filter press was used for the SRF measurement (Figure 1). It consists of 6 stainless-steel cylinders. The filter medium used was Whatman 42 filter paper with a 2.5 µm pore size and a filtration area of 50.27 cm^2. The samples were fed into the cylinder through an opening on the top of the cylinder. Each cylinder was connected to a compressed air line and the pressure was adjusted to 100 psi through a regulator. There was a water drain valve at the bottom of each cylinder and the filtrate (release water) was collected in a graduate cylinder.

The cumulative volume of filtrate (mL) was plotted as a function of filtration time (t), which was 30 minutes or 60 minutes. The performance of filtration was evaluated in terms of filtration rate, i.e. the slope of the linear portion of the filtration curve based on the theoretical filtration model (Coulson et al. 1991). Typical filtration curves, t/V against V, were plotted and the slope of the trend lines were determined. Assuming that the filter cake is incompressible during filtration and the initial volume of filtrate is 0 at time 0, the slope values can be used to calculate the SRF as in Equation 1.

Figure 1. Specific Resistance to Filtration (SRF) setup (Figure adopted from OFITE website)

Equation 1. SRF calculation

$$SRF = (2 \cdot P \cdot A^2) \times b/(\mu_f \cdot c)$$

Where SRF = specific resistance to filtration
ΔP = Pressure drop = 100 psi = 689476 Pa
A = Area of filter = 50.27×10^{-4} m^2
μ_f = viscosity of filtrate = 1×10^{-3} Pa·s (assume the viscosity of filtrate be the same as water)
c = Concentration of solid in suspension (kg/m3)

$$= \frac{Mass\ of\ solids\ (kg)}{volume\ of\ water\ (m^3) + volume\ of\ solids\ (m^3)}$$

$$= \frac{24.7}{\frac{100-24.7}{1000} + \frac{24.7}{2650}}$$

= 291.89 kg/m^3
Density of water = 1000 kg/m^3
Density of solids = 2650 kg/m^3
b = slope of t/V against V plot = t/V^2
V = volume of filtrate after time t (m^3)

RESULTS AND DISCUSSION

The Original SRF Setup

The SRF equipment as purchased presses the high pressure gas directly onto the sample as illustrated in Figure 2. With the pressure on the sample, the solids content of the sample increases and the surface desaturates. As a result, the plastic limit of the desaturated location is reached and the compressed cake cracks (Figure 3) resulting a great internal stress and unsaturated system. Therefore, the filter press test was stopped.

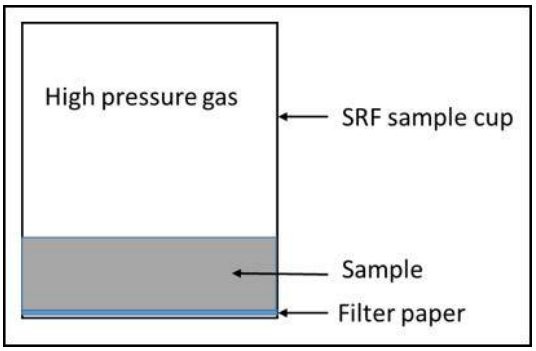

Figure 2. Schematic diagram of unmodified SRF setup

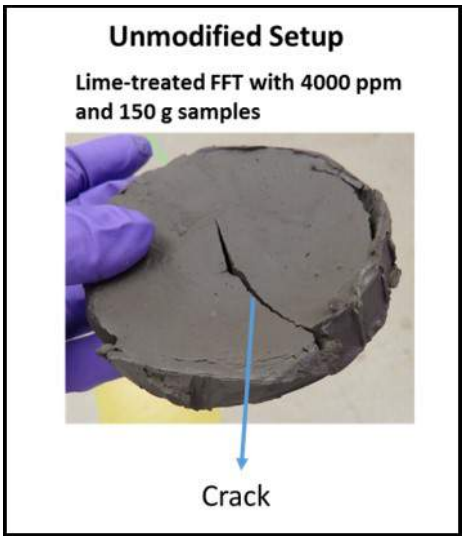

Figure 3. The photo of cracked cake after filtering press by an unmodified SRF setup

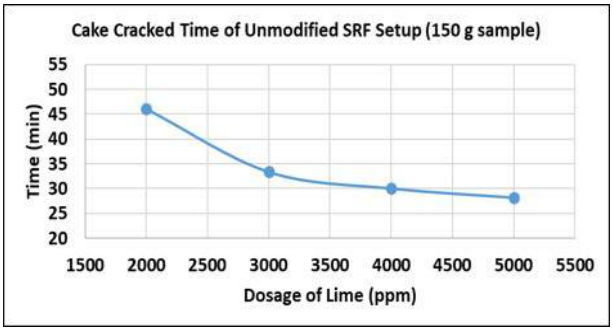

Figure 4. Cake cracked time after filtration using the unmodified SRF setup

In the case of 150 g of lime-treated FFT samples, the cake cracked, stopping the test less than one hour (25-50 minutes) into pressing (Figure 4). The higher the dosage of lime used in the treated FFT, the more quickly the cake cracked. The 150 g of FFT samples without lime treatment did not crack throughout the 60 minutes of pressure using the original setup.

The Modified Filter Press Setup

In order to avoid compressed sample cake cracking resulting in a premature end to the test, a Teflon piston cylinder was inserted into the SRF sample cup between the sample and the high-pressure gas (Figure 5). The diameter of the piston was designed slightly smaller than the SRF sample cup to reduce friction losses due to binding between the piston and the cylinder. The O-ring on

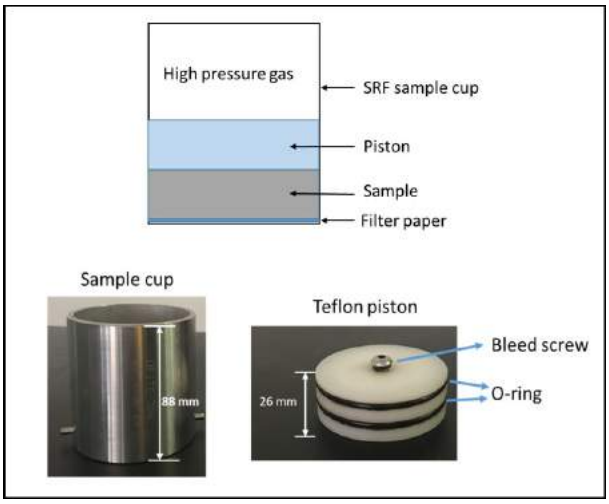

Figure 5. Schematic diagram of modified SRF setup

the piston was used to eliminate the gas leak between the sample cup and the piston. Lubricant was put on the O-rings before each test to reduce friction losses.

FFT has a heterogeneous nature resulting in zones of easy-cracking. The air pressure directly applied before any cracking is likely to be reasonably even across the sample surface, and will then only short-circuit when a cracking feature develops. Whereas the piston is insensitive to any cracking features on the surface as it applies pressure evenly throughout the experiment by design.

In the case of 150 g of lime-treated FFT samples, the cake cracking resulting from the uneven gas compression was not observed on the cake obtained by the modified setup (Figure 6). Figure 7 compares the solids contents in the cakes obtained by modified setup with 1 hour pressing and unmodified setup by pressing until cake cracked. The modified setup produced higher solids content and more consistent results than the unmodified setup. The cake solids contents showed the optimal dosage of lime to treat FFT was 4000 ppm.

SRF Test on 150 g of Lime-Treated FFT

Lime-treated FFT with different dosages (2000-5000 ppm) were tested using the SRF. The dosages of lime in this study were all based on the wet sample weight and conversion of wet sample based dosages to solid based dosages is shown in Table 4. Two sample weights (150 g and 300 g)

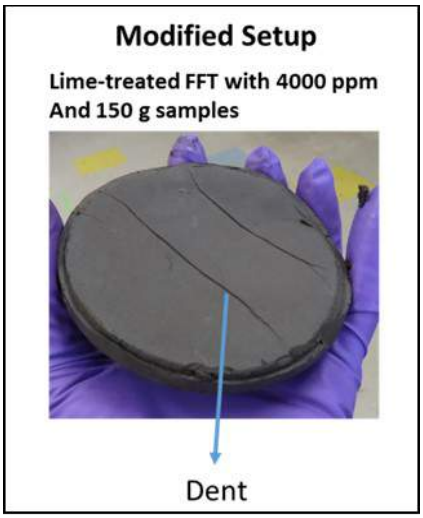

Figure 6. The photo of the cake after 60 min filtering press by a modified SRF setup

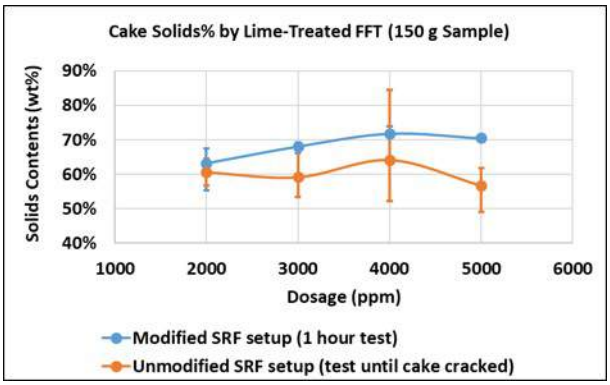

Figure 7. Cake solids% comparison produced by lime-treated FFT (150 g samples) using modified and unmodified filter press setups

were used to test the capability of the bench-scale SRF equipment.

Figure 8 shows the plots of filtrate flow rates obtained by modified SRF setup on 150 g of samples. The amount of the filtrate increases as the test was run at constant gas pressure (100 psi). The filtrate flow rates produced by untreated FFT and lime-treated FFT with 2000 and 3000 ppm dosages increased approximately linearly during the 60 minute SRF test. The filtrate flow rates produced by lime-treated FFT with 4000 and 5000 ppm dosages increased linearly until the 30 minute time mark after which the curves flattened.

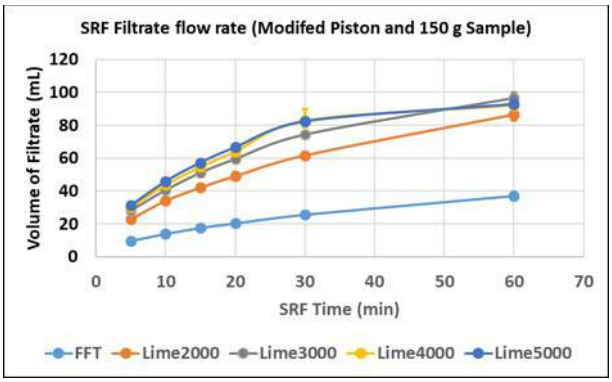

Figure 8. Filtrate flow rate of lime-treated FFT obtained by modified SRF setup with 150 g of sample

The calculated SRF values are determined by the b value according to Equation 1, where b is the slope of t/V against V plot. Figure 9 shows the plots of t/V against V of lime-treated FFT for 60 minute SRF tests. Table 5 shows the calculated SRF values for the 60 minute SRF tests. The slope (b value) of each curve was obtained from the linear trend line. The closer to 1 of the R-square value, the better fit of the regression line. Since the assumptions in the SRF equation require linearity to provide meaningful results, a non-linear curve (i.e. low R-square value) means the SRF is not consistent throughout the whole test period, but changed (mostly increased) at a certain test time. In the case of lime-treated FFT, the SRF is consistent throughout the 60 min test with 2000 ppm dosages, but that is greatly increased after 30 min with the dosages of 4000 and 5000 ppm.

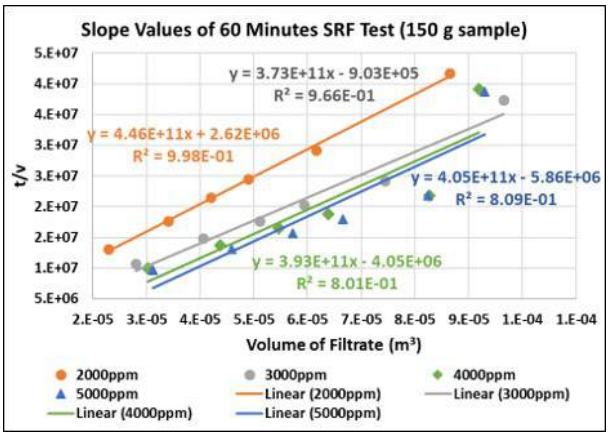

Figure 9. Plot of t/V against V with 60 minutes of SRF test using modified setup and 150 g samples

Table 5. Calculated SRF values with 60 minutes SRF tests

Dosage of Lime (ppm)	60 Minutes SRF Test Data		
	b value	R^2 value	Average SRF
0	2.39E+12	0.999	3.85E+14
2000	4.46E+11	0.998	5.32E+13
3000	3.73E+11	0.966	4.45E+13
4000	3.93E+11	0.801	4.69E+13
5000	4.05E+11	0.809	4.83E+13

The performance of filtration was then compared in terms of the slope of the first linear portion of the filtration curve – 30 minutes of SRF test data (Figure 10 and Table 6). The R-squared values of all lime dosages were close to 1 indicating that the calculated SRF values using 30 minutes data were best applied to comparing filtration experiments in the linear water release regimes.

Table 6. Calculated SRF values with 30 minutes SRF tests

Dosage of Lime (ppm)	30 Minutes SRF Test Data		
	b value	R^2 value	Average SRF
0	2.39E+12	0.999	3.85E+14
2000	4.20E+11	0.998	5.01E+13
3000	2.90E+11	0.998	3.46E+13
4000	2.28E+11	0.985	2.72E+13
5000	2.38E+11	1.00	2.84E+13

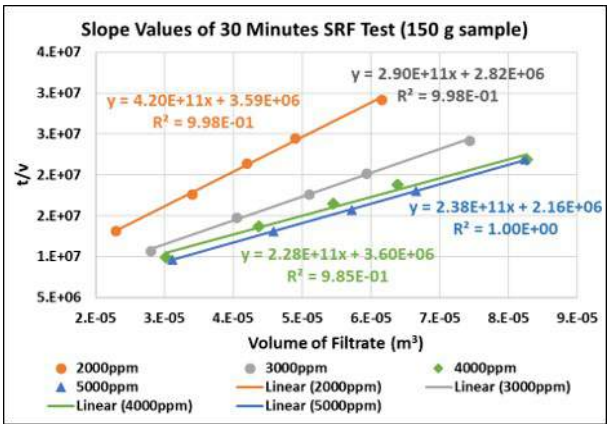

Figure 10. Plot of t/V against V with 30 minutes of SRF test using modified setup and 150 g samples

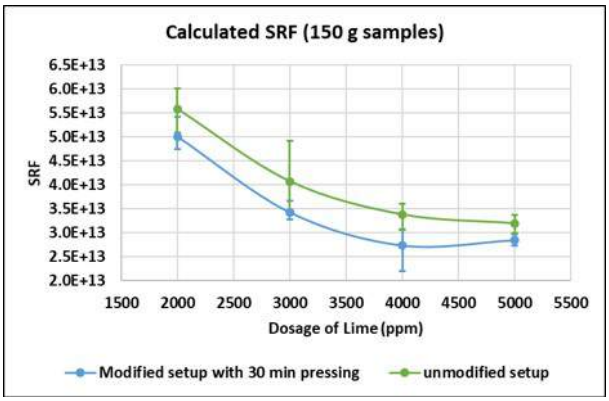

Figure 11. Calculated SRF values comparison obtained by modified setup with 30 min pressing and unmodified setup until cake cracks

Figure 12. Photos of SRF cakes obtained by 300 g of treated FFT with 60 minutes test and unmodified setup

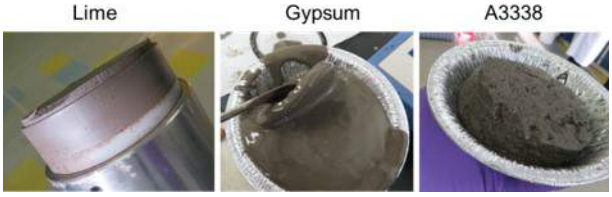

Figure 13. Photos of compressed cakes obtained by 300 g of treated FFT with 60 minutes SRF test and modified setup

Lime treatment greatly decreased the SRF value of FFT compared to the raw FFT. The SRF values decreased with the increase of lime dosages from 2000-4000 ppm and then slightly increased with the 5000 ppm of lime according to the 30 min data (Figure 11). Therefore, 4000 ppm was the optimal dosage of lime for the filtration application. This was consistent with the results determined by the solids content in the compressed cakes.

The SRF values obtained by using the unmodified SRF setup and 150 g samples were calculated using the time and filtrate volumes when the compressed cake cracked (Figure 11). The trend of SRF values from the unmodified setup was similar to that from the modified setup using 30 minutes data. This confirmed that 4000 ppm was the optimal dosage of lime for the filtration test. The unmodified setup produced less water than the modified setup resulting in higher calculated SRF values compared to the modified setup. This was likely due to the rigid piston providing a more consistent compression on the FFT surface compared to gas alone.

SRF Test on 300 g Sample

The optimal dosage of lime (4000 ppm) determined by the SRF test on the 150 g samples was also tested on 300 g samples in order to test the capability of the SRF equipment. Gypsum is used as a coagulant in commercial consolidated tailings (CT) technologies (Matthews 2002). Gypsum-treated FFT using the equivalent Ca^{2+} dosage to 4000 ppm of lime was also tested on the SRF to compare the Ca^{2+} effect on filtration performance. Polymer A3338 is a popular flocculant in the oil sands tailings treatment, and hence the polymer A3338-treated FFT using the optimal A3338 dosage was also tested.

Lime, gypsum and polymer A3338 produced different structures of cakes with the 60 minute test time using unmodified or modified setups. The cake obtained by lime treatment using the unmodified setup was less compacted with a muddy top layer (Figure 12). The solids wt% of lime-treated FFT using the unmodified setup is ~42 wt%. The gypsum treatment produced one thin layer of solid cake (~51 wt%) and left the rest sample fluid (~27 wt%) using the same setup. A3338 treatment produced sponge-like SRF cake (~41 wt%) and continued to release water which was a similar result to using the modified setup.

Compared to the unmodified SRF setup, the cake obtained by lime treatment with the modified setup was relatively dry and well compacted with the ~55 wt% solids content (Figure 13). This indicated that the inserted piston could enhance the filtration under the same gas pressure due to the even pressure on the cake.

Using the modified setup, and similar to the unmodified SRF setup, gypsum treatment produced two layers of cake with the modified SRF setup: the bottom layer was compacted (~49 wt% solids), while the top layer was fluid (~28 wt%

solids). Polymer A3338 treatment produced sponge-like cake (~40 wt% solids) which continued to release water after the SRF testing was complete. Unlike the lime-treated FFT, the solids content of the compressed cake obtained by the gypsum and A3338 treatment were not affected by the different SRF setup (with 60 minutes of test time and 300 g of samples).

The lime-treated FFT generated a much denser filter cake than either the gypsum or polymer-treated FFT for the same filtration time indicating a potential benefit of lime addition in filtration applications.

The amount of filtrate obtained by the modified setup with 60-90 minutes of testing increased approximately linearly with the increase of the testing period for all the lime, gypsum and A3338 treated FFT samples (Figure 14). Lime-treated FFT produced the highest volume of filtrate, indicating the lowest SRF values (Figure 15). Gypsum-treated FFT produced the lowest volume of filtrate, resulting in the highest SRF values. With the 300 g of samples, the SRF values were approximately consistent throughout the 90 minutes.

With modified SRF setup for 60 minutes of pressure, the behavior of polymer A3338-treated FFT was consistent with Jelly-donut behavior seen in the field and long consolidation times predicted from large strain consolidation (LSC) and seepage induced consolidation test (SiCT) (Boxill 2016, Stianson et al. 2016) Gypsum treatment and raw FFT also showed similar behaviors observed in the field – crusting and long consolidation times. Lime treatment was the only treatment to produce a filter cake with a consistency closer to the plastic limit of the 300 g of materials in 60 minutes.

Long-Time SRF Tests

SRF tests were also performed for a long time duration until no filtrates were collected in order to predict the long-term consolidation behavior. Lime-treated FFT required the least time (3-4 hours) compared to raw FFT and other treatments (~20 hours). When the lime-treated FFT was filter pressed for the same period with other treatments (~20 hours), the solids content in the compressed cake was 91.2wt% with a corresponding CWR of 10.4 wt%. Gypsum and polymer treatments and raw FFT required longer filtration time (~20 hours) to achieve comparable cake solids with lime treatment after 3-4 hours. This solids content

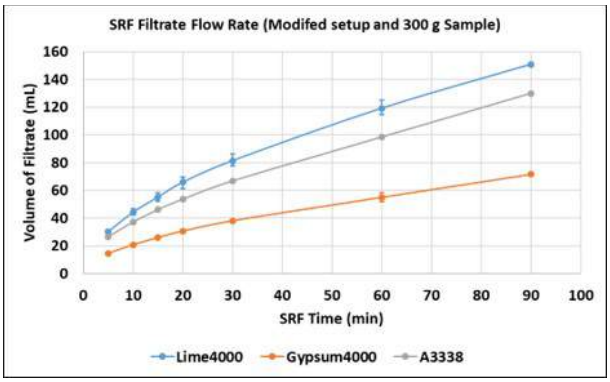

Figure 14. Filtrate flow rate of treated FFT obtained by modified filter press setup with 300 g of sample

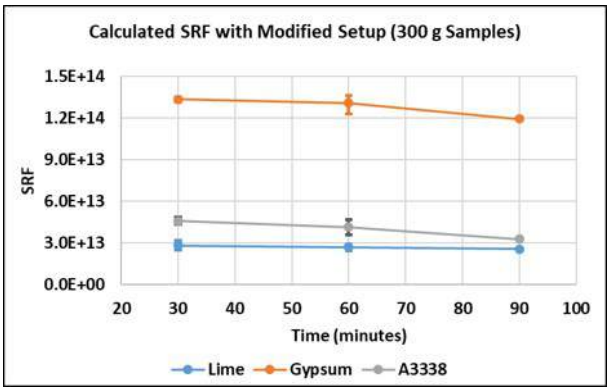

Figure 15. Calculated SRF values comparison of treated FFT using modified SRF setup and 300 g of samples

Table 7. The solids content and CWR of compressed cake and the required filter press time

Additive	Required filter pressing time (hours)	Compressed Cake of Long-Time Pressing			
		Average solids% (wt%)	STDEV of solids% (wt%)	Average CWR	STDEV of CWR
A3338	~20	76.33%	0.08%	3.22	0.01
Gypsum	~20	76.67%	0.11%	3.29	0.02
Lime	~3.5	71.30%	1.35%	2.49	0.16
none	~20	75.33%	0.87%	3.06	0.14

corresponded to the point where no further water was expressed from the cake, as determined by no change in water released after 30 minutes.

The dramatic reduction in filtration time for the lime treatment indicates that lime treatment may be an option for reducing the consolidation time of FFT. Alternatively the lime-treatment may be suitable for pressure filtration.

CONCLUSIONS

A modified SRF setup was designed and manufactured by inserting a Teflon piston cylinder into the SRF sample cup between the gas and the testing sample. The modified SRF setup could effectively press the sample and avoid compressed cake cracking resulting in the premature end of the test.

According to the SRF test with the modified setup, the lime dosage of ~16,000 g/tonne solids produced highest solids content in the compressed cake and lowest SRF values indicating the optimal lime dosage for the FFT tested.

Lime-treated FFT provided better filtration performance and formed a more compact cake compared to gypsum- and polymer-treated FFT for the same filtration time in the modification setup.

The long-time filtration test indicates that lime addition would be a potential benefit in fluid fine tailings filtration applications.

ACKNOWLEDGEMENTS

The authors acknowledge the support of the Natural Sciences and Engineering Research Council of Canada (NSERC).

REFERENCES

Alamgir, A., Harbottle, D., Masliyah, J. and Xu, Z. (2012). Al-PAM assisted filtration system for abatement of mature fine tailings. Chemical Engineering Science, **80**: 91-99.

Alberta Energy. (2013). Alberta's oil sands: January fact-sheet. Government of Alberta, Edmonton, Alberta.

Alberta Energy Regulator. (2016a). Mineable oil sands tailings status report, 2016.

Alberta Energy Regulator. (2016b). Fluid tailings management for oil sands mining projects.

Anlauf, H., Bott, R., Stahl, W. and Krebber, A. (1985). The formation of shrinkage cracks in filter cakes during dewatering of fine sized ores. Aufbereitungs Technik, **26**(4): 188-196.

Barua, A. (2014). Experimental study of filter cake cracking during deliquoring. Department of Chemical Engineering & Chemical Technology, Imperial College of Science, Technology and Medicine, London.

Boxill, L. (2016). The impact of fabric and surface characteristics on the engineering behavior of polymer-amended mature fine tailings. The University of British Columbia.

Coulson, J. M., Richardson, J. F., Backhurst, J. R. and Harker, J. H. (1991). Particle technology and separation processes. Chem. Eng., Vol. 2, 4th ed. Pergamon, Chapter 7.

Davies, M. (2011). Filtered dry stacked tailings – the fundamentals. Proceedings of the 15th International Conference on Tailings and Mine Waste: Tailings and Mine Waste 2011. Norman B. Keevil Institute of Mining Engineering, University of British Columbia, Vancouver, Canada.

Dean, E. W. and Stark, D. D. (1920). A convenient method for the determination of water in petroleum and other organic emulsions. Ind. Eng. Chem., **12**: 486-490.

Kaminsky, H. (2014). Demystifying the methylene blue index. International Oil Sands Tailings Conference, Banff, Alberta, Canada.

Klohn Crippen Berger. (2017). Study of tailings management technologies. Report of Mine Environment Neutral Drainage (MEND) Project.

Kretser, R. G. (2018). Tailings filtration: risk reduction through understanding and designing for variability. Paste, Perth, Australia, pp 63-74.

Li, Y., Currie, R., Kaminsky, H., Sedgwick, A. and Qureshi, T. (2016). The effects of flocculation on the methylene blue index. Proceedings of Fifth International Oil Sands Tailings Conference, pp 242-248.

Liu, J. K., Lane, S. J. and Cymbalisty, L. M. (1980). Filtration of hot water extraction process whole tailings. Patent US4225433A.

Lloyd, P. J. and Dodds, J. A. (1972). Liquid retention in filter cakes. Filtration & Separation. Jan/Feb: 91-96.

Loerke, R., Tan, X. and Liu, Q. (2017). Dewatering of oil sands mature fine tailings by dual polymer flocculation and pressure plate filtration. Energy Fuels, **31**(7): 6986-6995.

Matthews, J., Shaw, W., Mackinnon, M. and Cuddy, R. (2002). Development of composite tailings technology at Syncrude. International Journal of Surface Mining Reclamation and Environment, **16**: 24-39.

Stianson, J., Mahood, R., Fredlund, D. G. and Sun J. (2016). Large-strain consolidation modeling to determine representative tailings consolidation properties from two meso-scale column tests. Proceedings of International Oil Sands Tailings Conference, Lake Louise, Alberta, pp 40-50.

Sury, K. and Stone, J. (1995). Non-Clark extraction process and their tailings characteristics. Alberta Department of Energy, Oil Sands and Research Division.

Suthaker, N. N. and Scott, J. D. (1996). Measurement of hydraulic conductivity in oil sands tailings slurries. Canadian Geotechnical Journal, **33**(4): 642-653.

Vedoy, D. R. L. and Soares, J. B. P. (2015). Water-soluble polymers for oil sands tailings treatment: a review. The Canadian Journal of Chemical Engineering, **93**(5): 888-904.

Wakeman, R. J. (1974). The role of internal stresses in filter cake cracking. Filtration & Separation. Jul/Aug: 357-360.

Wang, C., Najafi, A., Masliyah, J., Liu, Q. and Xu, Z. (2018). Flocculation-assisted dewatering of fluid fine tailings using a volume screw press. The Canadian Journal of Chemical Engineering, **9999**: 1-10.

Xu, Y., Dabros, T. and Kan, J. (2008). Filterability of oil sands tailings. Process Safety and Environment Protection, **86**: 268-276.

Zhu, Y. (2015). Cationic and anionic dual polymer pairs for mature fine tailings flocculation and dewatering (MSc Thesis). University of Alberta, Edmonton, AB, Canada.

ACCELERATED OIL SANDS TAILINGS DEWATERING WITH THICKENING AND REFLOCCULATION

Wei Ren and Sidantha Weerakone
Imperial, Calgary, Canada

ABSTRACT

Several technologies are employed by oil sands operators for tailings treatment at commercial scales. Process performance and deposit dewatering are impacted by the tailings' processability with varying feed, especially with varying fines/clay content. Effective fines treatment technology provides efficient storage volume and produces a reclaimable deposit in a timely fashion. The operation envelope determines the process scheme design. This work by Imperial shows operation envelopes for different operating scenarios with an empirical model that predicts long term deposit performance at preferred operation window using a 1-D consolidation model. A combination of thickening and reflocculation provides two stages of water recovery, one at the plant and one in the deposition area. Enhanced thickened tailings performance with reflocculation produces favorable properties that suggest the deposit can be reclaimed in a reasonable time. This work presents the process and deposition performance, including thickened tailings (TT) dewatering capability, flow behavior (e.g. beach above / below slopes, flow lengths and flow patterns) in conjunction with feed properties such as sand/fines ratio and clay content. The optimum operation envelope and feed properties are identified for targeted thickened tailings solids content gain and effective storage volume usage. Implications of atmospheric drying for dewatering of thicken tailings, with alternate deposition strategies, are also recognized in a commercial scale deposition.

INTRODUCTION

In the oil sands mining industry, Tailings are major byproducts of bitumen production, producing significant volumes requiring treatment before they can be reclaimed. In the extraction processes, hot water and caustic are often used to assist bitumen separation. With the addition of caustic, fines/clay are dispersed and suspended in the water, which results in slow settlement and consolidation in deposits. When tailings streams are transported to the deposition area, the tailings stream further dewaters. Water released from the plant and the deposits is recovered and reused in oil extraction. The fines not captured on the beaches and in cells form fluid fine tailings (FFT), which contains 55 wt% - 70 wt% water. Without further treatment, the water remains trapped and with time, the FFT becomes mature fine tailings (MFT).

Several technologies have been employed to treat oil sands tailings at commercial scales (Boswell & Davachi 2012). For example: Consolidated tailings (CT) are produced by combining a coarse tailings stream and fines tailings stream with gypsum; In-line flocculation of MFT with thin lift drying; Centrifuge polymer treated MFT; and mixing thickened tailings with the coarse sand tailings stream to produce non-segregated tailings (NST). In general, process performance and deposit dewatering capability are highly impacted by the tailings operability of the chemical treatment and the processability with varying feed properties, particularly varying fines/clay content. Polymer and chemical usage are related to the fines/clay content in feed. For higher fines/clay content feed, more chemical or polymer is needed, resulting in higher operation cost and slower dewatering. Technology selection along with corresponding operational envelopes are critical for a cost effective tailing treatment process and for producing a timely reclaimable deposit.

OPERATIONAL ENVELOPE FOR EFFECTIVE FINES TREATMENT AND EFFICIENT STORAGE VOLUME

Before selecting a technology and designing a process for fines treatment, it is necessary to evaluate the efficiency of each considered technology. Normally, untreated and un-captured fines exist in the form of FFT (defined as fine tailings material that consists of less than 5kPa undrained shear strength and greater than 5% solids content). FFT often contains 60 wt% (or higher) fines content. One main requirement of treatment technologies is

that the expected deposit should, within a reasonable time, achieve a higher solids content and a higher undrained shear strength than FFT. Ideally, treated tailings should be capped soon after deposition is complete and achieve a traversable conditions within a few years of deposition. An efficient treatment technology should considerably improve tailings properties compared to raw FFT.

Tailings containment and storage volume also need to be considered during process selection, which are major components in tailings planning. Creating and maintaining above grade tailings facilities poses long term liability and risk for operations. If the selected tailings treatment technology is efficient, it should be able to store fines in a smaller volume than that of raw FFT storage, including using dedicated deposit areas and/or in-pit tailings areas.

Governing Phenomenon

The presence of clay particles in FFT is an impediment to improve properties of treated tailings deposit. It is difficult to convert FFT with high clay contents to a high solids or high strength material and doing so requires long time periods for consolidation. As clay content is one of the governing factors of treated tailings properties, understanding how clay content impacts treated tailings properties is critical. Laboratory and commercial scale deposit data were collected to build a correlation between clay content and immediate solids content (up to one year after flocculation and deposition)

The clay content was determined by Methylene Blue Index (MBI) as calculated using Equation 1 (Omotoso & Melanson 2014):

$$CC = \frac{\left(\frac{meq}{100g} + 0.04\right)}{0.14} \quad \text{Eq. (1)}$$

where, $\frac{meq}{100g}$ – Methylene blue index

Figure 1 illustrates the data and developed correlations between laboratory and commercial scale deposit information. Both lab and field data show a strong linear correlation and that the flocculated tailings solids content decreases as clay content increases.

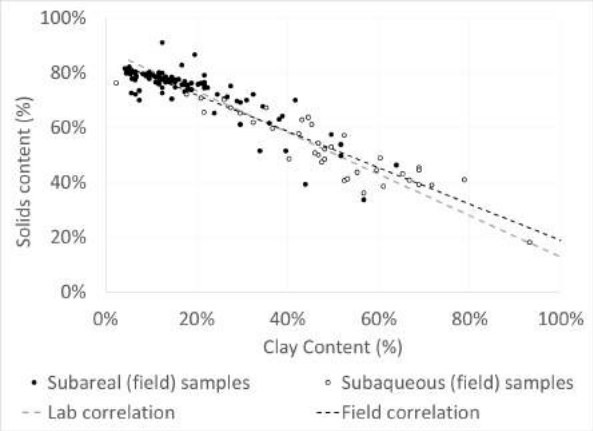

Figure 1. Deposit solids content vs. clay content correlation after flocculation

Table 1 shows the lab and field data of deposit solids content and clay content. The clay content needs to be less than ~30% in order to achieve 65 wt% + solids content from both lab testing and field sampling data. Similarly, the material should be less than ~40% clay content to achieve 60 wt% + solids content. At lower clay content (e.g. less than 40%), lab test results are consistent with field data, except in that the field results show more scattering due to process variability. At higher clay contents, average solids content in the field shows slightly better than that found in the lab data due to loading factor and atmospheric drying, etc.

Table 1. Deposit clay content vs solids content data after 7 days in the lab and up to one year in the field

Clay content	7 days Deposit Solids Content (Lab)	Deposit Solids Content (Field)
10%	81%	79%
15%	77%	75%
20%	73%	72%
25%	69%	69%
30%	66%	65%
35%	62%	62%
40%	58%	59%
45%	54%	55%
50%	51%	52%
55%	47%	49%
60%	43%	45%
65%	39%	42%
70%	35%	39%

The correlation developed from field data was used to evaluate the efficiency of different fine tailings treatment technologies, considering corresponding solids content gain and storage volume.

The following equations were used to calculate the deposit solids content and storage volume with respect to treatment of 1Mt of fines.

$$SC = -0.664 \times CC + 0.8515 \quad \text{Eq. (2)}$$

$$V = \frac{W_m}{\rho_m} + \left[\left(\frac{W_m}{SC} - W_m\right)/\rho_w\right] \quad \text{Eq. (3)}$$

where;
SC – wt% solids content; *CC* – wt% clay content;
W_m - Mineral mass; ρ_m – Mineral density
ρ_w – Water density; *V* – Deposit volume

Table 2. Additional assumptions used in calculation of deposit volume and solids content

Sand Fine Ratio (SFR) of MFT	0.1
MFT clay content [%]	66%
MFT solids content (%)	35%
Fresh tailings clay content [%]	13%
Fresh tailings clay/fines ratio	0.33
Mineral density [Kg/m3]	2650
Water density [Kg/m3]	1000

Treatment Technology Evaluation

Due to the high clay content and very fine nature of the material, the industry acknowledges that the treatment of pure FFT/MFT often requires substantial consolidation times and/or the use of additional effort (e.g. using mechanical force through centrifuge or air drying through thin lift deposits) to achieve desired solids content and strength due to high clay content and very fine nature of the material. However, improved FFT/MFT treatment and deposit performance can be achieved by combining FFT/MFT with other tailings streams. Different process schemes will generate different properties in the deposit. Therefore, understanding the deposit properties generated by different "recipes" is critical to determining the most effective process scheme configuration and operational envelope. The preferred tailings treatment technology will have an efficient tailings storage volume and accelerated tailings sedimentation and consolidation.

In this study, multiple cases are considered with different fresh tailings and FFT/MFT mixes. In each case, the solids content gain, change in SFR in the deposit and the deposit volume were calculated for relatively short deposit periods (e.g. up to one year).

Case 1: Fresh Tailings with SFR of 1.5

In Case 1, different mixes of FFT/MFT and fresh tailings of SFR 1.5 were studied. Figure 2 illustrates the modeling results of solids content, deposit SFR and volume change for different mixes. The solid line provides the deposit storage volume, starting from storing pure FFT/MFT without treatment (vertical grey dash line), and then varying the SFR by mixing with fresh tailings. The dashed line shows the FFT ratio in deposit, as SFR increases. The dotted circle line describes the increased deposit solids content with different mixtures of SFR. For example, the black dashed line starts from 100% FFT/MFT, with an SFR of 0.1. As the FFT/MFT ratio decreases, when mixing with fresh tailings of SFR 1.5, the mixture concentration of SFR increases. At the end of the dashed line, the FFT/MFT mixture ratio is reduced to zero and deposit SFR is the same as the original tailings SFR. The dotted circle line shows that solids content increases with increased deposit SFR. Similarly, the solid line describes the deposit volume changes with deposit SFR.

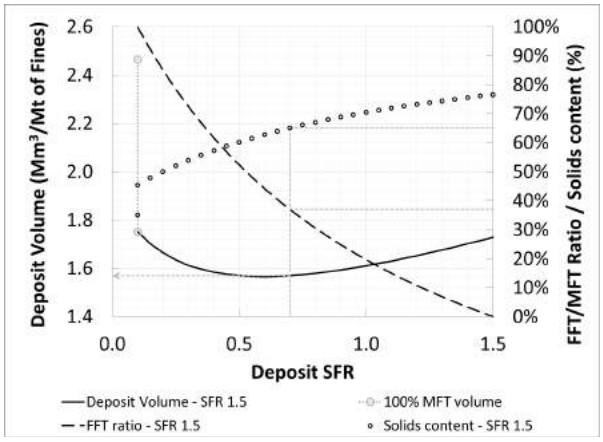

Figure 2. Volume and SC variation for different mixes of MFT and fresh tailings (SFR 1.5)

When drawing a vertical line at a given SFR (e.g. SFR of 0.7), the deposit volume is 1.6 Mm^3 per 1Mt of fines and solids content is 65%, after dewatering, and the corresponding FFT/MFT mix ratio is about 37%.

The solid content of the flocculated tailings increases with increasing SFR, while volume of the

deposit decreases at lower SFR and increases at high SFR. The minimum storage volume is achieved at a preferred SFR range of 0.5 – 0.8. When the mixture of tailings stream SFR is below the preferred range, the higher deposit storage volume is most likely due to water bonding with the higher clay content. When the mixture of tailings stream SFR is above the preferred range, e.g., the MFT content is below 20%, the higher deposit storage volume is most likely due to the sand material in the deposit occupying the storage volume by its grain size.

Case 1 demonstrates that fresh tailings with 1.5 SFR, alone or mixed with FFT/MFT, can achieve 65% solids content with a minimum storage volume after flocculation. Flotation tailings generally possess SFR in this range. While achieving solids content of 65% within one year deposition, the tailings treatment technology will likely produce timely reclaimable material.

Case 2: Fresh Tailings SFR Between 1 and 2.5

One challenge for commercial scale tailings processing is the varying properties of fresh tailings. Even though an average flotation tailings SFR is expected to be around 1.5, it can vary between 1 and 2 or 2.5. This variation can be caused by mine feed fines variation, process/operational variability, etc. To account for the variability of SFR, similar model results to those in Case 1 were generated for fresh tailings having SFRs of 1 and SFRs of 2.5 to define the potential operational envelop.

As shown in Figure 3, flotation tailings with an SFR of 1 (grey lines) could achieve 65% solids content using a 30% MFT mix. At this mix, however, the storage volume (~1.5Mm^3) is not the minimum volume and likewise the solids content is not the highest. Further reduction of the MFT ratio will reduce volume as well as increase solids content. The lowest volume mix can be achieved at ~17% MFT, which generates 70% solids content. Therefore, if targeting 65% solids content, the optimum “recipe” for SFR 1 fresh tailings is a 30% MFT mix.

The other lines illustrate the behavior of deposit for flotation tailings with SFR 2.5 (black lines). The mix of this material with SFR of 0.9 and ~41% MFT creates a result of 65% solids content. While this mix does not produce the lowest deposit volume, it is a balance between storage volume and solids content gain. Therefore, increased MFT contribution helps to reduce deposit volume, but,

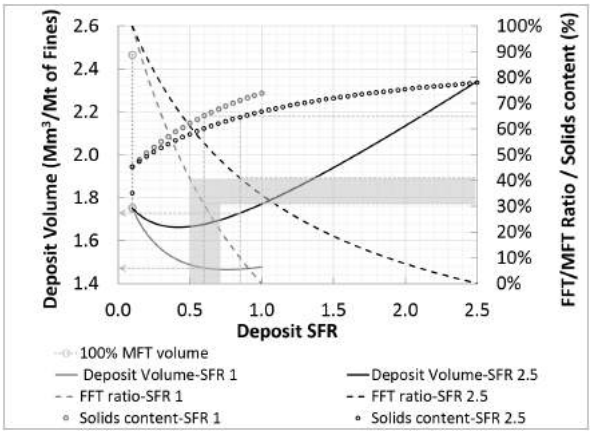

Figure 3. Volume and solids content variation for different deposit mixes of MFT and fresh tailings (SFR 1 – 2.5)

as a tradeoff, would not achieves just 65% solids content (due to the high clay coming from the increased MFT material). Using this mix may also result in longer consolidation requirements.

The operational envelop for optimum deposit performance can be determined by considering both deposit composition and further dewatering capability, e.g. both storage volume and solids content gain. To achieve 65% solids content, the MFT mix ratio can vary between 30% and 40%, based on fresh tailings SFR between 1 and 2.5. In other words, the optimum deposit (mix) SFR should be between 0.6 and 0.8. This preferred SFR range could be expanded to 0.5 - 1.0 for operations flexibility.

Case 3: Use of Coarse Tailings or a Combination of Coarse / Fines Tailings as Fresh Tailings

Cases 1 and 2 examined two operational scenarios of mixing FFT/MFT and fine tailings stream, e.g. middling stream of PSC, also known as flotation tailings. The other possibility for generating a tailings stream is to mix coarse sand tailings or whole tailings or course/fine tailings streams together with FFT/MFT. The SFR of these tailings streams is usually high and can vary between 5 and 15. Figure 4 shows the deposits results of mixing MFT and SFR of 8 and 13 fresh tailings mix.

These deposit mixes demonstrated the operation scenario of adding up to ~ 45% of MFT to get 65% solids content. These mixes, however, consume higher storage volume. At SFR of 1, the treated tailings consumed approximately 15% higher volume (~1.9Mm^3) than the optimum volume

(~1.7Mm^3 at SFR of 0.3). The potential of these mixes to achieve higher solids content and increased treatment of MFT is offset by the high deposit volume required.

Long Term Consolidation

The modeling work above represents a short term (or up to one year) deposit behavior of tailings with different compositions. In addition to the short term behavior, it is important to evaluate long term consolidation impacts to determine appropriate tailings treatment technology and optimum composition of treating materials. Thus, the long term consolidation behavior is modelled for the preferred SFR range (0.5-1.0) and for high SFR (4) material.

Compressibility and hydraulic conductivity parameters are two main inputs for self-weight consolidation processes. Re-flocculated thickened tailings slurry samples with different compositions were tested in large strain consolidation apparatus to evaluate those parameters. Using several lab test results, representative compressibility and hydraulic conductivity curves were developed for SFR 0.5, 0.7, 1 and 4 slurry samples. Figures 5 and 6 show the determined compressibility and hydraulic conductivity parameters, respectively.

Figure 7 shows the deposit height change over time for four different tailings types. In each case, deposition was modelled assuming treatment of same amount of fines in total and same annual solids treatment capacity. To store the same amount of fines, High SFR tailings will take a longer time for treatment and depositing, and additionally requires of high storage volume. While material of SFR between 0.5 and 1 demonstrates low storage volume requirement in the short term, and SFR 1 material shows better consolidation the long term.

The modelled deposit was presumed to be capped with 5m coarse sand tailings after a 20/30-year time period (after deposition is completed). Predicted deposit conditions were evaluated at the end of deposition for four different cases. Results are shown in Figure 8.

Based on the modeling results, at expected capping time SFR 4 material achieves over ~80% solids content cross deposit and should not have any capping problems. The modelled material with SFR 1 gained about 75% solids content on the top of the deposit and gradually reaches 80% at bottom of deposit. At this point, placing capping material on

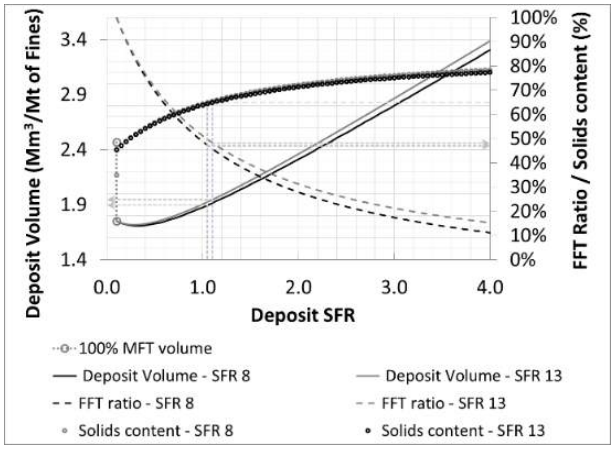

Figure 4. Volume and solids content variation for different deposit mixes of MFT and fresh tailings (SFR 8 - 13)

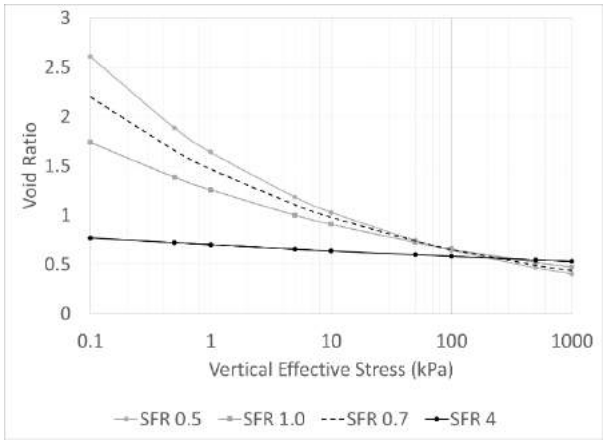

Figure 5. Compressibility parameters for consolidation modelling

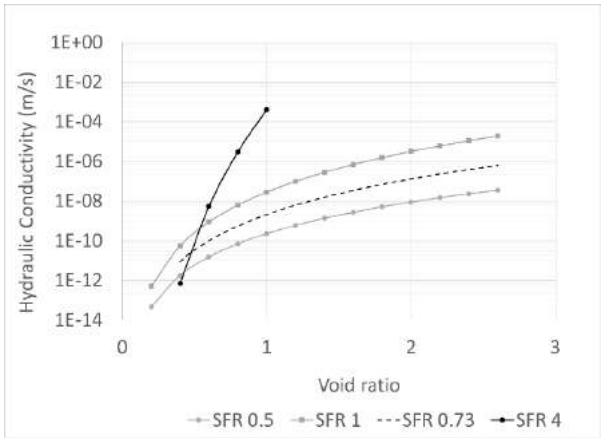

Figure 6. Hydraulic conductivity parameters for consolidation modelling

top of this treated tailings deposit is also feasible. The other two cases (with SFR 0.5 and SFR 0.7) show that the top of the deposit, and several meters below the top, retain solid contents concentrations similar to the initial value at time of deposit. It should be noted that this modelling work only considered self-weight consolidation. Natural phenomenon (such as atmospheric drying or freeze-thaw), as well as engineered techniques (e.g. installing wick drains, adding water absorbent polymer, etc.) offer opportunities to increase strength of the top surface of the deposit to place capping material. In addition, understating of the correct recipe (SFR, FFT/MFT mix ratio, clay content etc.) to create a sufficiently strong layer on top of the deposit can be used to purposely produce material with desired composition during last few meters of the deposit.

In summary, the deposit performance can be categorized as three regions: high SFR and sand dominated material (e.g. SFR > 2), low SFR and fine/clay dominated material (e.g. SFR < 0.5), and medium SFR and sand/fines balanced material (e.g. SFR ~1). Material with high SFR gains higher strength rapidly, but with little or no post deposition consolidation, and will be ready for capping material at end of deposition. The resulting material will, however, have relatively lower fines/clay content and require a longer time to treat the same amount fines and need high storage volume. Materials with medium SFR will gain a good strength, deposition settlement and consolidation, and will be ready to be capped on time. Material with lower SFR will take a much longer time to gain strength, as it contains a high portion of clay or FFT/MFT material. We can use these generalities to design and build the deposit for short-term volume management and fines capture with a consideration of a long-term performance in terms of consolidation and strength gain.

The self-weight consolidation process for the selected material range was continued up to one hundred years to determine long term consolidation. Solids content results for those simulations are shown in Figure 9. Results indicated that material in the high end of the SFR range perform acceptable dewatering behavior and material in the lower end of the range possesses relatively poor dewatering behavior.

Overall, consolidation results demonstrated the challenging dewatering nature of oil sands tailings material. However, material in medium SFR range demonstrates potentials of timely capping without compromising fines treatment capabilities.

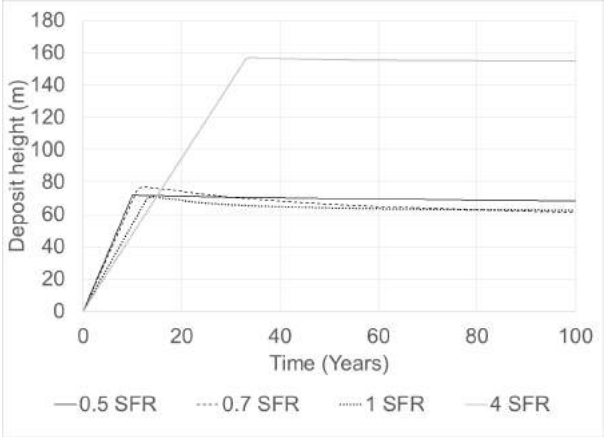

Figure 7. Deposit height variation with time for different SFR material

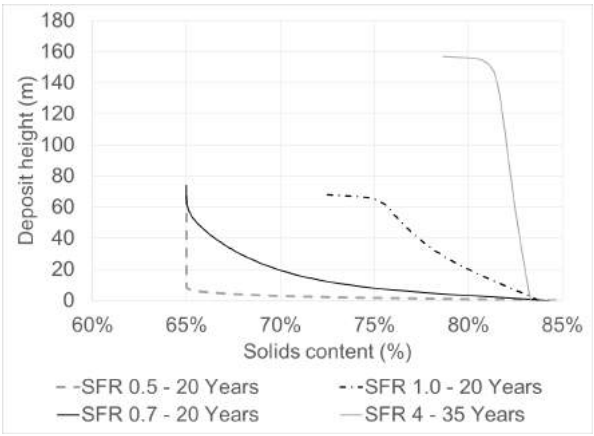

Figure 8. Deposit solids content at expected capping time

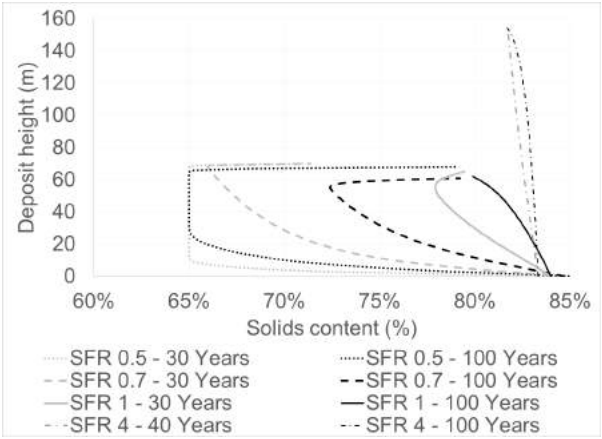

Figure 9. Deposit solids content gain with a long term consolidation

PREFERRED PROCESS SCHEME AND OPERATIONAL WINDOW

Based on the cases above, the preferred tailings mixture will add FFT/MFT into fresh tailings stream with an SFR below 2.5. Any coarse tailings addition will increase the storage volume. To achieve solids content of 60% and 70%, the material clay content should be in a range of ~25% to ~40%, the preferred corresponding SFR of blended tailings feed is between 0.5 and 1.0. If there is no volume limitation, the preferred SFR range can be increased between 0.8 and 1.2, which produces more favorable properties for consolidation, but reduces the fines treatment efficiency. There are several tailing technologies that can be considered to process these fine tailings streams, e.g. thickener, centrifuge, in-line flocculation, filtration, etc. It is challenging to achieve high production rates with existing centrifuges and filter press scales. Mechanical drying also requires additional operational costs and increases maintenance complicity. Thickeners may prove to be more suitable for treating fine tailings within the preferred operational envelopes.

Thickener

Thickeners are widely used in the mining industry for tailings treatment and water recovery. A thickener is a gravity settling vessel that de-waters slurry and separates liquid from the solids. Water is recovered through overflow and can be reused. Concentrated slurry is generated from thickener underflow and is able to be transported to the deposition area hydraulically. The particle size range in thickeners feed is generally from 0.5 mm to a few microns. The finer the particle size, the slower settling and compaction rate. At the thickener design stage, the size of thickener is generally determined by feed particle size distribution, floc settling behavior and flux rate based on selected flocculant. The type of thickener (e.g. traditional thickener, high rate thickener, paste thickener, etc.) is selected based on specific applications. With a high rate thickener, the slurry can be thickened to achieve underflow solids densities of 40 – 50 wt% solids content from 10 – 20 wt% solids content feed. A typical thickener feed is ranging from 5% solids to 10% solids (by weight) after dilution (Laros et al. 2002).

A thickening process is a combination of mixing feed with flocculent, forming floc agglomeration and sedimentation. Flocculants and optional coagulants can be injected to the feed slurry and the turbulent flow and feed well design provides the mixing needed. The increased particle size after flocculation causes the solids to fall towards the thickener bottom under gravitational force. The bed level of a thickener depends on the solids loading rate and underflow discharge rate. The underflow density can be controlled by adjusting the bed level and residence time.

A thickener is often equipped with a rake and scraper blades on the bottom, which slowly rotates to create water channels in the slurry bed to let water migrate to the top, while at the same time pushing solids towards the cone. Once the solids enter the cone discharge, they are removed by underflow pumps, pumping to the next process or deposition area.

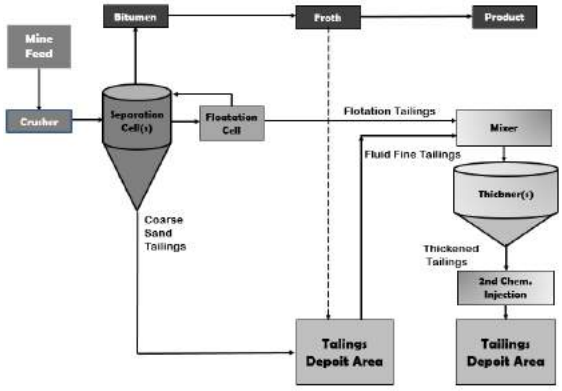

Figure 10 Process scheme of thickening and reflocculation

Key Process Indicators of Thickening

The purpose of a thickener is to recover water and produce concentrated slurry. Thus, the overflow clarity and underflow density/solids content are key process indicators to measure the success of thickening processes. Additionally, other process variables to be monitored include:

1. Feed composition: volumetric flow and solids content, solids rate, particle size distribution, clay content and bitumen content
2. Underflow composition: volumetric flow, solids rate, particle size distribution, clay content, bitumen content and yield stress if needed
3. Bed level, pressure and density gradient
4. Rake torque reading
5. Flocculant dosage and concentration

Operational Envelope

As the thickener is intended to treat finer particles, the sand to fine ratio is often targeted at a range of 0.5 to 1.2 or extended upper limit at design phase. Based on the feed particle size distribution, the operational envelope can be expanded to a higher range: e.g. up to SFR of 3. High SFR material will settle faster at the same solids loading rate. When operating at high SFR feed, the torque reading, overflow water clarity and underflow density should be closely monitored. As well, sufficient flocculant should be added into the system to avoid sanding the thickeners due to segregation.

Thickener Performance

Due to the bitumen content in tailings streams, and varying clay content in thickener feed, operational challenges for a continuous thickener operation could include:

- Feed variability: solids loading rate and composition
- Minimum underflow volumetric flow rates to maintain hydraulic requirements
- Desired underflow density to meet deposit requirement

To avoid producing off-spec thickened tailings when solids loading rate is consistently low, a Semi-Continuous operation mode has been developed and implemented (Ren 2018). There are critical factors impacting the thickener performance:

- Stable feed and feed variability management
- Reliable and operable facilities
- Instrumentation and control system

Thickeners performance at Kearl met the design target. Table 4 summarizes the data for 2017.

Table 4. Kearl thickener performance

Solids Content (%)	Expected Properties	Observed Average Properties
Thickener Underflow	40-50%	Avg. 41%
Thickener Overflow	<1%	<0.5%

Reflocculation

In general, thickener plants are built close to other production facilities and far from the deposition areas. The thickened tailings are sheared through pumps and pipeline during transportation. Shear thinning loops are generally designed and installed at the thickener underflow to reduce the yield of thickened tailings so that they can be transported easily. Therefore, when sheared thickened tailings are pumped to the deposition area, the resulting material often has small floc size, weak flocculation structure, and lower permeability, less yield strength and dewaters slowly. In order to improve the thickened tailings performance, a second flocculant is added to the pipeline before it is discharged to the deposition area.

The benefits of having a second chemical injection are (Ren et al. 2014):

- Rebuilding the floc structure and enhancing the thickened tailings permeability (shown in Figure 11).
- Accelerated thickened tailings (TT) dewatering reduces the footprint and volume for thickened tailings storage.
- Increasing the yield stress slowly at discharge and allowing the thickened tailings to flow out the deposit area and gain strength after further dewatering.

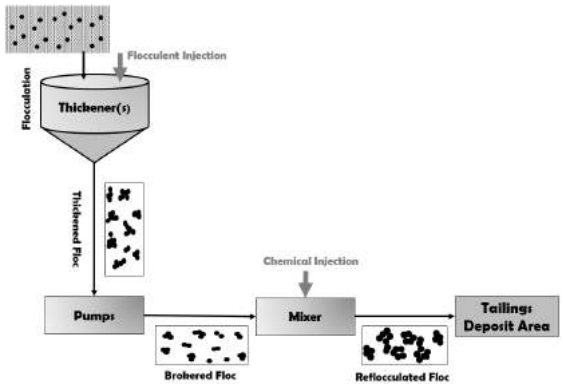

Figure 11. Thickening and Re-flocculation process

Figure 12 shows hydraulic conductivity variation with void ratio for TT and reflocculated TT. After reflocculation, hydraulic conductivity is greatly improved at a void ratio of 1.5 (63% solids content) and above. When void ratio is approaching 1, conductivity is similar between these two materials. With high permeability of reflocculated TT, the timing to achieve a void ratio of 1 will be much shorter compared to regular TT.

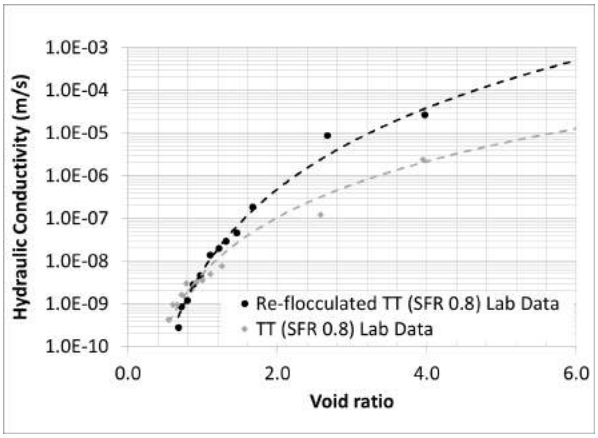

Figure 12. Hydraulic conductivity variation with void ratio for TT and re-flocculated TT

Key Process Indicators of Reflocculation

As with thickeners, optimal floc dosage and appropriate mixing energy is needed for re-flocculation. The optimal floc dosage is determined by thickened tailings compositions (fines/clays content) with given water chemistry. The mixing energy required depends on solids rate, thickened tailings volumetric flow and density, pipeline shear and injector design. With a given injector, it has been found that the mixing energy required is more impacted by thickened tailings density than the volumetric flow. Thus, the density should be controlled in a desired range to minimize the impacts of mixing.

As the floc size and structure are critical for flocculation performance, capillary suction time (CST) provides a good measurement of dewaterability for flocculated material. The key process indicators are:

- Capillary suction time
- Initial yield stress and yield stress gain after 24hrs and 7 days deposit
- Solids content gain in 24hrs and 7 days

Additionally, the thickened tailings density, flow and floc dosage should be monitored to ensure the generated tailings are on spec.

DEPOSIT PERFORMANCE

Based on the above investigation, it appears that material produced by thickening and re-flocculation processes is capable of achieving approximately 60% or 65% solids content within one year, using the desired SFR feed. However these materials need to be further de-watered before capping and reclamation. As this consolidation process takes a long time, ideally, material should be deposited at the final designated location contained with engineered structure. Kearl is building just such a deep deposit of re-flocculated thickened tailings. Observations of the young deposit are given below.

Flow Characteristics

Flow characteristics of treated tailings (such as beach above water (BAW) slope, beach below water (BBW) slope, flow distance, flow extent) are important when designing and planning a treated tailings deposition facility. Data from monthly satellite captures has been used to evaluate beach slopes and flow patterns and extent.

The beach slope varies with the physical properties of the slurry, such as yield strength, initial solids content, discharge velocity etc. It is generally difficult to evaluate beach slope variation with those physical parameters as the properties of treated tailings material change over time and as the composition of the deposit changes. After analyzing multiple satellite images, beach slope appears to vary between 0.5% and 2.5%. In the first few 100 meters, the slope is generally 2.5%-1%. One explanation for a steeper slope could be the original ground profile. Beyond 0.5 km, the beach tends to be as flat as 0.5%. 1% beach slope is a good approximation for designing and planning a tailing deposition facility. Figure 13 illustrates a typical beach profile obtained from satellite data.

Determining the slope of the beach below water is challenging. Existing survey techniques are not

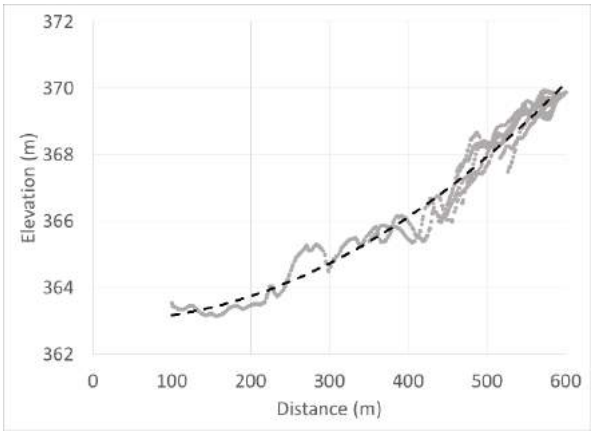

Figure 13. Typical beach slope profile of treated tailings deposit

capable of detecting below water soft deposit behavior. Physical sampling and testing of the deposit is required to provide insights for BBW slope. Figure 14 illustrates the typical section developed from pond sampling information of the deposit. For 40% (and higher) solids content, beach slope below water was estimated as 1%.

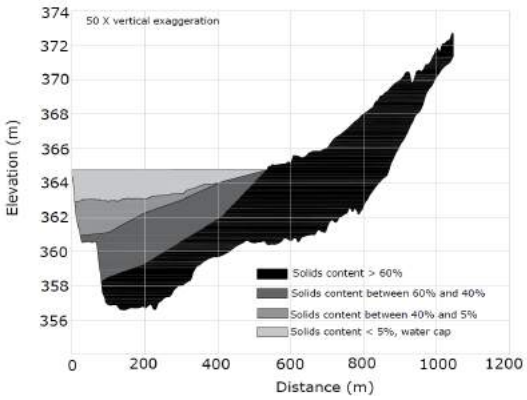

Figure 14. Typical cross section of treated tailings

Frequent satellite imaging of the active deposit is one of the most useful methods of monitoring flow behavior of commercial scale operation. Figure 15 shows an image of commercial scale TT deposition. Continuous monitoring of such images illustrated that re-flocculated TT was capable of flowing 600-700 m and spread over 500 m laterally. Initially, slurry flow creates flow channels through the lowest locations of the deposit. When the flow channel fills up with material, the flow path gradually shifts. Eventually the flow channel moves throughout the low laying region and builds up the deposit.

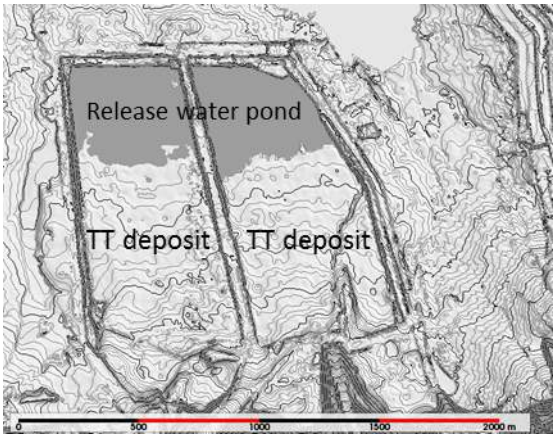

Figure 15. Stellate data of the tailings deposit which shows the flow extent

Impact of Atmospheric Drying

Materials with favorable properties, such as low clay content and high SFR, will dewater without the need for assistance of any environmental phenomena. When material properties are not conducive to unassisted dewatering, atmospheric drying enhances the solids content (dewatering) of the material within a relatively short period of time. Figure 16 shows deposit solids content differences between SFRs located in subaerial (beach above) and subaqueous (beach below) environments. Similar SFR samples, located on beaches above water zones, show relatively high solids content due to atmospheric drying.

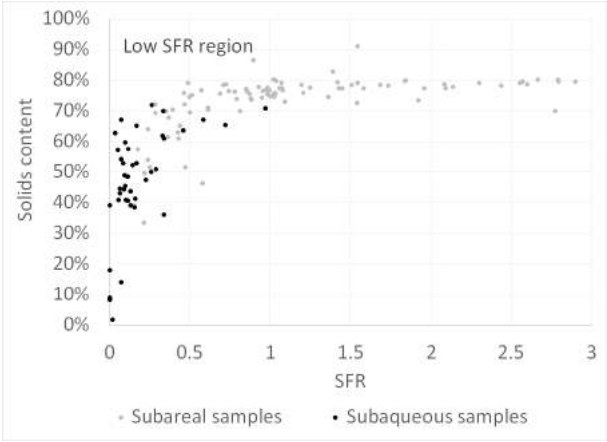

Figure 16. Impact of atmospheric drying for similar clay content samples

CONCLUSIONS

Oil sands tailings treatment has engineering challenges. Selected tailings treatment technologies should be able to treat fines tailings at an acceptable rate while maintaining short term and long term dewatering capabilities. Reduction of clay or FFT/MFT in treated tailings deposits can improve short and long term dewatering capability. FFT/MFT ratio reduction in tailings feed, however, will also reduce fines treatment efficiency. Optimal mixes of fresh tailings and FFT/MFT can enhance dewatering while maintaining efficient fines storage volume. This work introduces a methodology of identifying optimum operation envelope for tailings treatment to determine the process scheme design. In general, tailings mixtures of medium SFR (preferred~1), with approximately 30-40% MFT, was identified as the optimum composition for short term dewatering and long term consolidation.

Identification of the correct recipe should consider both efficient fines treatment and creating reclaimable deposit in a relatively short time. An application of selected treatment envelope, with thickening and re-flocculation process, can produce favorable deposit properties for timely reclamation and was discussed in detail with key process performance indicators and successful commercial scale deposit performance. Most importantly the study illustrated that the treated tailings deposit can be successful in both short and long term time periods with a range of feed variability.

REFERENCES

Boswell, J. R. and Davachi, M. (2012). Oil sands tailings technology deployment roadmap, Project Report, **5**.

Omotoso, O. and Melanson, A. (2014). Influence of clay minerals on the storage and treatment of oil sands tailings. Paste 2014, Proceedings of the 17th International Seminar on Paste and Thickened Tailings, pp. 269-280.

Laros, T., Slottee, S. and Baczek F. (2002). Testing, sizing, and specifying sedimentation equipment. Mineral Processing Plant Design, Practice, and Control: Proceedings, **1**: 1295-1312.

Ren, W. (2018). Expanded operational envelope of thickening and reflocculation through Semi-continuous operation. 2018 Oil Sands Innovation Summit, June 7-8, Calgary, Alberta, Canada.

Ren, W., Sury, K. and Clingman, S. (2014). Enhanced thickened tailings performance via additional chemical treatments. Paste 2014, Proceedings of the 17th International Seminar on Paste and Thickened Tailings, pp. 245-255.

ZERO WATER INTAKE TECHNOLOGY FOR TREATMENT OF MINING TAILINGS

Morgan Tizzotti[1], Scott Ramey[2], Kirk Thomas[2], George Tichenor[2] and Trong Dang-Vu[3]
[1]SNF France
[2]SNF US
[3]SNF Canada

ABSTRACT

Treatment of mine tailings commonly utilizes water soluble polymers to enhance solid-liquid separation. The preparation of these polymer solutions requires a significant volume of water which, depending on the application, is recovered very slowly or may not be recovered at all due to evaporative losses. In addition, low quality (high fine solids content) water can potentially have a detrimental effect on polymer performance.

As a solution to this challenge, SNF has been developing a new Zero Water Intake Technology using a unique SNF polymer product which allows recycling of water recovered from treated tailings directly to polymer make-down systems. This eliminates the need of fresh water for preparing a new polymer solution. The laboratory test results, conducted on a number of tailings including coal and oil sands tailings, demonstrate that with a new single polymer treatment sufficient quantities of water can be recovered at a high rate with little to no remaining fine solids and its reuse for preparing new polymer solutions has impact on neither polymer performance nor water chemistry. The new zero water intake approach effectively eliminates the need for water from other sources to be used for the polymer make-down, offering significant reductions in water consumption and capex and opex related to pipeline and water pumping energy.

INTRODUCTION

The oil sands deposits in northern Alberta, Canada, constitute one of the world's largest oil reserves. Currently, a significant portion of this bitumen is extracted using the Clark Hot Water Extraction process (Masliyah et al. 2004). This process uses significant amounts of water, consuming approximately three barrels of water for each barrel of bitumen produced (Kaperski and Mikula 2011). This requires oil sands facilities to draw large quantities of fresh water from the Athabasca River, which could potentially affect the aquatic ecosystem, particularly during low winter flows (Allen 2008). The mineral portion of the oil sands ore contains sand as well as fine clays, which are separated from the bitumen and are discharged from the process as tailings slurry. Coarse sand tailings settle quickly and form beaches, but fine tailings separate and run into the pond, forming a slurry. These fines gradually settle to form a material known as Mature Fine Tailings (MFT) or Fluid Fine Tailings (FFT). A significant portion of the water used for extraction of bitumen remains trapped in the MFT due to its extremely slow consolidation. This results in significant accumulation of fine tailings at oil sands mining operations. A number of processes have been developed to treat these tailings so that tailings volumes can be reduced and tailings ponds can be reclaimed. These processes include beach drying, centrifugation and blending coarse and fine tailings streams into a non-segregative mixture (COSIA 2017). The majority of tailings treatment processes in oil sands utilize synthetic polymer flocculants to allow water to be more easily separated from the MFT or other tailings.

A number of studies have determined that treatment performance using a single flocculant can be improved by the application of two flocculants/coagulants in sequence. Yuan and Shaw (2007) investigated the effect of adding anionic flocculant and cationic coagulant in different sequences to oil sands tailings. They determined that the best performance was achieved by treating with flocculant first, then coagulant, and then another smaller addition of flocculant. Tizzotti et al. (2014) proposed a simpler dual treatment, replacing cationic coagulant with anionic flocculant, and demonstrated the advantages of cationic flocculants over coagulants. Vedoy et al. (2016) also found that MFT treatment could be improved with the application of two polymers in sequence. Studies have also been conducted that demonstrate the effectiveness of dual treatment on thickener

applications (Dang-Vu et al. 2014). In addition, Dang-Vu et al. (2016) developed a novel MFT deposition process in which flocculated MFT is deposited and then capped with coarse tailings. Dual polymer treatment was found to be the most effective treatment for this application as well. However, dual polymer treatments suffer from one main drawback that severely hinders their industrial implementation: the need of two products instead of one. Such treatment process increases both OPEX (higher overall polymer dosage is typically required) and CAPEX (separate polymer dissolution units, storage tanks, etc) as blending an anionic and a cationic polymers would lead to the irreversible formation of strong and insoluble polymer aggregates unable to allow subsequent flocculation of the tailings.

Depending on the application, polymer treatment can require a significant amount of water for polymer solution preparation. Furthermore, this water may be recovered very slowly, or may not be recovered at all due to evaporative losses. In addition, low quality (high fine solids content) and chemistry change of the water can potentially have a detrimental effect on polymer performance. Therefore, it would be advantageous if water could be recovered very rapidly and with sufficient quality to allow re-use for polymer make-down (Klein et al. 2018). SNF has developed a new chemistry enabling a single treatment process and allowing fast and positive Net Water Release.

MATERIALS AND METHODS

A sample of Mature Fine Tailings (MFT) was obtained from an oil sands operator. The properties of the MFT sample were determined in SNF's laboratory located in Edmonton, Alberta, and are shown in Table 1. The composition was measured using Dean-Stark extraction. A fines content was measured by wet sieving with a 45 µm-opening sieve and clay content was determined from methylene blue index. An anionic flocculant with medium charge density and low molecular weight was used as the reference product for the treatment of MFT. Product solutions used for the treatment of MFT were prepared at a concentration of 0.4 wt% in process water.

Table 1. MFT sample properties

Dean Stark extraction			MBI		PSD Laser		
Mineral (wt%)	Water (wt%)	Bitumen (wt%)	MBI (no units)	% clay	d90 (µm)	d50 (µm)	D10 (µm)
39.9	57.9	2.2	13	91	53.3	10.0	2.1

A sample of coal thickener underflow (UF) was obtained from a coal mining operator. Solids content of the UF sample, 29.6%, was determined in SNF's laboratory located in Edmonton, Alberta.

Gravity Drainage Tests

Tailings (MFT and Coal thickener UF) were homogenized and 400 g aliquots were subsampled for flocculation tests. These aliquots were mixed with selected dosages of polymer solution until the desired flocculated structure was formed. Then the flocculated tailing was deposited on a 1 mm mesh screen and the amount of release water collected was measured over time. In every case, the polymer solution was added in a single injection.

The water chemistry of the process and released waters were measured by a third party laboratory (Maxxam Analytics).

RESULTS AND DISCUSSION

Figure 1 shows the effect of two single polymer treatments on the quantity of water released from MFT by gravity drainage. For this MFT, single polymer treatment with the reference product at the optimum dosage of 2000 g of polymer per dry tonne of solid material caused minimal release of water after 10 minutes. Net Water Release (NWR) was about 10% after 1 hour and 20% after 24 h, while treatment with Product A at 1800 g/t allowed a 25% NWR after only 10 minutes and 30% after 24 hours. These results demonstrate the potential of this recently developed chemistry to not only increase the dewatering rate of MFT, but also to significantly accelerate it. The total suspended solids (TSS) concentration of the release water from treatment with the reference product and Product A were 0.07% and 0.08%, respectively. This demonstrated that Product A provides filtrate similar in quality to the reference product, but faster and in greater quantity.

The released water obtained after MFT dewatering with Product A was collected and used as-is to prepare a fresh solution of Product A of similar

concentration. This solution of Product A in recycle water was used to treat MFT and positive NWR values of 20%, 30% and 35% were obtained after 10 minutes, I hour and 24 hours, respectively. Note that the recycle water affected neither (i) the dosage of flocculant A nor (ii) the dissolution of Product A whatsoever. A homogeneous solution was obtained within 40 minutes, just as for the original process water.

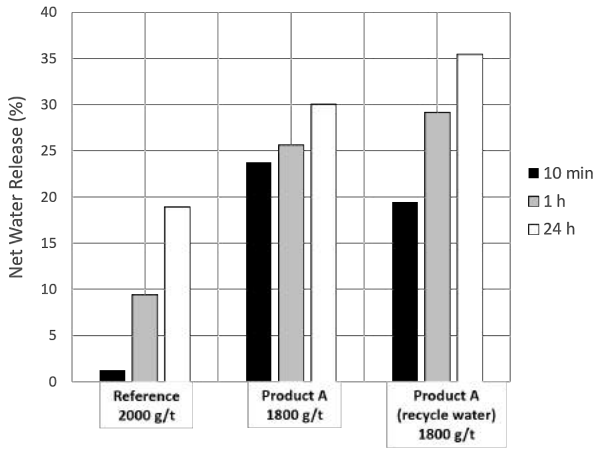

Figure 1. Effect of various polymer treatments on MFT dewatering

The effect of the single treatment with Product A on released water chemistry was investigated and the results are presented in Table 2. It has been observed that process water chemistry can have a significant effect on flocculation of tailings, particularly pH, as well as calcium and magnesium concentrations (Sworska et al. 2000). Comparison of the water chemistry of process water used for initial polymer make-down and water chemistry of the resulting released water from treated MFT with Product A shows insignificant variation in ion concentrations (Table 2). These results indicate that released water obtained after treatment with Product A could be used again to prepare a new flocculant solution, thus significantly reducing the consumption of fresh water.

This new chemistry was also tested on a different type of mineral tailing. Figure 2 shows the effect of two single polymer treatments on the quantity of water released by gravity drainage from a coal mine refuse thickener underflow (UF). The reference product quickly led to more than 40% NWR after only 10 minutes, then 45% and 48% after 1h and 24h, respectively. Product B did not further increase NWR but led to similar performance at half the dosage. Product B also significantly improved the quality of the released water as the TSS dropped from 0.21% with the reference product to 0.02% with Product B.

The released water obtained after coal thickener UF dewatering with product B was collected and used as-is to prepare a fresh solution of Product B of similar concentration in recycle water. This solution of Product B in recycle water was used to treat coal UF; NWR values were not impacted by the use of recycled water to prepare the polymer solution.

Table 2. Water chemistry of process and released waters: Treatment of MFT with product A

Ion	Concentration (mg / L)		
	Oil Sands Process Water	Release water (1st treatment)	Release water (2nd treatment)
Na^+	333	363	369
K^+	19.7	21.4	20.9
Ca^{2+}	20.8	22.6	22.7
Mg^{2+}	11.5	13	12.4
Cl^-	179.5	182.1	183.6
HCO_3^-	510	580	575
SO_4^{2-}	271	281.7	278.4
CO_3^{2-}	15	36	37
pH	8.52	8.64	8.59

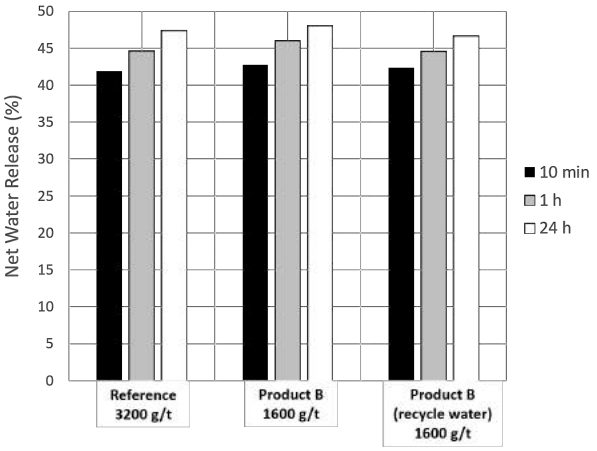

Figure 2. Effect of various polymer treatments on coal tailing dewatering

The effect of the single treatment with Product B on released water chemistry was investigated and the results are presented in Table 3. As observed earlier with the MFT, similar released water chemistries were found after 2 cycles of UF dewatering with Product B.

Table 3. Water chemistry of process and released waters: Treatment of Coal UF with product B

Ion	Concentration (mg / L)		
	Coal UF Process Water	Release water (1st treatment)	Release water (2nd treatment)
Na^+	126	124	127
K^+	8.3	8.3	8.5
Ca^{2+}	84.8	87.3	86.3
Mg^{2+}	14.1	14.5	14.7
Cl^-	119.1	120.5	120.2
HCO_3^-	130	130	132
SO_4^{2-}	300.5	301.8	302.1
CO_3^{2-}	<1.0	<1.0	<1.0
pH	8.22	8.21	8.21

CONCLUSIONS

The conclusions can be summarized as follows:

- A novel chemistry compatible with a single process has been developed.
- This chemistry allows increase of the dewatering rate and/or decrease of the dosage compared to conventional flocculants.
- Release water chemistry is not significantly affected by the treatment and can be used again to prepare more flocculant solution without impacting the dewatering performances.
- These results demonstrate the viability of a zero water intake process for polymer make-down in tailings treatment.

REFERENCES

Allen, E. (2008). Process water treatment in Canada's oil sands industry: I. Target pollutants and treatment objectives. Journal of Environmental Science, **7**: 123-138.

COSIA. (2017). Tailings projects. Retrieved January 15, 2018, from: http://www.cosia.ca/initiatives/tailings/tailings-projects

Dang-Vu, T., Salehi, R. and Ramey, S. (2014). Oil sands mature fine tailings spiking for thickener applications. Proceedings of the Fourth International Oil Sands Tailings Conference, Lake Louise, Alberta, Canada, December 7-10, 2014.

Dang-Vu, T., Keele, H., Lacoste-Bouchet, P., Salehi, R., Najafi, A., Klein, C., Nelson, A. and Ramey, S. (2016). In-situ deposition of treated tailings. Proceedings of the Fifth International Oil Sands Tailings Conference, Lake Louise, Alberta, Canada, December 4-7, 2016.

Kasperski, K. L. and Mikula, R. J. (2011). Waste streams of mined oil sands: Characteristics and remediation. Elements, **7**: 387-392.

Klein, C., Tizzotti, M., Thomas, K. and Dang-Vu, T. (2018). A new zero water intake technology for chemical treatment of mining tailings. Proceedings of Mine Water Solutions, Vancouver, British Columbia, Canada, June 12-15, 2018.

Masliyah, J., Zhou, Z., Xu, Z., Czarnecki, J. and Hamza, H. (2004). Understanding water-based bitumen extraction from Athabasca Oil Sands, Canadian Journal of Chemical Engineering, **82**(4): 628-654.

Sworska, A., Laskowski, J. S. and Cymerman, G. (2000). Flocculation of the Syncrude fine tailings, Part 1: Effect of pH, polymer dosage and Mg^{2+} and Ca^{2+} cations. International Journal of Mineral Processing, **60**(2): 143-152.

Vedoy, D., Botha, L. and Soares, J. (2016). Filtering mature fine tailings flocculated with single and dual anionic/cationic polymers. Proceedings of the 19th International Seminar on Paste and Thickened Tailings, Santiago, Chile, July 5-8, 2016.

Tizzotti, M., Frédéric, P. and Dang-Vu, T. (2014). Dual polymeric flocculants treatment for the dewatering of whole oil sands tailings. Proceedings of the 2014 World Heavy Oil Congress, New Orleans, Louisiana, USA, March 5-7, 2014.

Yuan, X. S. and Shaw, W. (2007). Novel processes for treatment of Syncrude fine transition and marine ore tailings. Canadian Metallurgical Quarterly, **46**(3): 265-272.

Session 12

SAND CAPPING OF OIL SAND TAILINGS DEPOSITS

EVALUATION OF SUBAQUEOUS GRANULAR CAP SUCCESS CONDITIONS AND FAILURE POTENTIAL ON TREATED FINE TAILINGS

Jed Greenwood, Jim Langseth, Raul Velasquez, Farzaan Abbasy and Phil Solseng
Barr Engineering and Environmental Science Canada Limited, Calgary, Canada

ABSTRACT

Conventional practice limits sand cap placement to tailings that have already achieved trafficable strengths. Most fine tailings deposits in the oil sands industry will not achieve this strength until they have consolidated and dewatered for some time. Sand cap or sand layer placement using hydraulic delivery methods offers great potential as a cost-effective, technically feasible capping method for treated fine tailings of the oil sands industry. In this work, 2D FLAC (Fast Lagrangian Analysis of Continua) models were developed to predict the potential for tailings to fail as a hydraulically-placed cap is advanced. The modeling showed the limits of cap layer thickness for tailings of various strengths for subaqueous cap placement. The work is an important step in establishing a foundation for an engineering and design approach for sand cap placement and a better understanding of how to execute one of the most cost-effective methods of sand capping soft fines-dominated tailings deposits. A future step will include modeling subaerial cap placement and application of the results of physical tests used to observe the various failure mechanisms. The preliminary models will be calibrated against these observations and used to identify critical factors for establishing necessary corrections for commercial-scale applications.

INTRODUCTION

Background

Conventional practice limits mechanical sand cap placement to tailings that have already achieved trafficable strengths, i.e., 25 kPa (McKenna et al. 2016). Most fine tailings deposits in the oil sands industry will not achieve this strength until they have consolidated and dewatered for some time. Sand cap or sand layer placement using hydraulic delivery methods (such as sand raining or rainbowing) represents a potentially cost-effective, technically feasible fine tailings management method for the oil sands industry (OSTC 2012) that warrants further study. The purpose of this sand capping is to increase consolidation, trafficability, and reclamation of soft tailings in oil sands tailings basins.

The oil sands industry is nearly universally treating their fine tailings, producing centrifuged tailings, thickened tailings, flocculated tailings, and other treated tailings, which are stronger than the mature fine tailings (MFT) considered in the OSTC feasibility study. These treated fine tailings can be expected to support a sand cap placed using hydraulic delivery techniques that can be adapted to mine operating conditions.

This paper is part of a collaborative project funded by the University of Alberta Institute for Oil Sands Innovation, Canada's Oil Sands Innovation Alliance, and Alberta Innovates. The research team consists of Barr Engineering and Environmental Science Canada Limited, Deltares, and Itasca Consulting Group, Inc (the creators of the geomechanics program used for this work). The project, "Evaluation of Granular Cap Success Conditions and Failure Potential on Treated Fine Tailings," represents a first phase of defining conditions for sand capping success. The program involves three steps: 1) develop a model of granular capping of soft tailings to predict the potential for tailings failure as the cap is placed; 2) bench scale testing intended to illustrate the potential for treated oil sands tailings to support a sand cap; and 3) identify critical factors to consider during scale-up to pilot-scale test programs such that testing at larger scales will form a firm basis for successful commercial application.

There are currently no tools accepted by the industry for assessing the behaviour of the fine tailings deposit as a granular layer is advanced across it. The current study, using the advanced geomechanics modeling program FLAC (Fast Lagrangian Analysis of Continua) for numerical simulation of this capping process, is intended as an initial step toward development of such a tool that also could be used for field trials and full-scale implementation of granular layer placement.

This paper presents the subaqueous capping modeling results. Future work will address subaerial capping. This paper summarizes the tailings properties, tailings deposit geometry, cap material properties, cap geometry, and advancement for FLAC modelling. Also summarized are the various FLAC cases that were modelled and the associated success and failure conditions.

TAILINGS PARAMETERS

The tailings material selected for capping in this work was based on the COSIA Capping Challenge Accelerated Dewatered Tailings (ADW), whose properties are listed below.

- Undrained Shear Strength, s_u [Pa]: 300–2,500 (1)
- Solids Content - Geotechnical, s [%]: 40 (1) (2)
- Fines Content - Geotechnical I, f [%]: 85 (1) (2)
- Clay Content, c [%]: 25 (1)
- Bitumen Content, b_m [%]: 5 (1) (2)
- Plastic Limit, PL [%]: 30
- Liquid Limit, LL [%]: 60
- Specific Gravity - Solids, G_s: 2.30 (2)
- Specific Gravity - Fines, G_f: 2.65 (2)
- Specific Gravity - Bitumen, G_b : 1.03 (2)
- Degree of Saturation, S_r : 1.00 (2)
- Water Density, ρ_w [kg/m^3]: 1,020

1 COSIA Challenge, Appendix 1, table

2 Scott, J.D. (2013). Multiphase Mass Volume Relationships for Tailings, Department of Civil and Environmental Engineering, University of Alberta, Revised April 14, 2003.

For purposes of this study, the geotechnical relationships representing ADW material were gathered from several sources of data for similarly flocculated MFT. These relationships between various parameters are described in later sections.

The solids content profile was assumed to increase with depth at a rate of 25% over a depth of 15 m. Furthermore, the pore pressure profile at the beginning of cap advancement was assumed to be 20 percent above the hydrostatic pore pressure profile. These are broadly consistent with the flocculated MFT “deep stack” properties, aged one year, shown in the Muskeg River Mine 2014 Annual Report submitted to the AER (MRM 2014).

Undrained Shear Strength

Undrained shear strength was used as the primary input parameter and all other parameters were correlated back to this value. The initial undrained shear strengths at the mudline and associated solids contents that were considered in the FLAC simulations, are shown in Table 1.

Table 1. Initial undrained shear strengths and associated solids contents

Undrained Shear Strength (kPa)	0.1	0.25	0.5	0.75	1.0	2.0
Solids content (%)	32	40	46	49	51	56

It should be noted that for FLAC to execute properly, a fixed, initial solids content profile, increasing linearly with depth (25% increase in 15 m), was used for each initial undrained shear strength case. The “input” undrained shear strengths named above are the values at the top of the fine tailings deposit (mudline), and the undrained shear strength increased from this value according to the relationship described in the following sections.

It should be noted that while the initial undrained shear strength listed was used as a starting point for each FLAC simulation, the modeling resulted in changes to void ratio and effective stress. This subsequently altered the undrained shear strength profile as a function of time and space with consolidation (provided the rate of sand cap advancement and permeability allowed for consolidation to occur).

Other Parameters

As stated above, undrained shear strength was used as the primary input parameter and all other parameters were correlated back to this value. However, the initial conditions after the model had been brought to equilibrium included an initial effective stress profile that increased with depth. Given that all parameters are correlated together, including undrained shear strength and effective stress, this resulted in a non-uniform initial undrained shear strength profile before the cap started to advance across the tailings.

The FLAC model uses FISH functions to represent relationships that require recomputation as the model runs. FISH is an embedded scripting language in the software that enables the user to define new variables and functions. The sections below describe the FISH function relationships that were used for the initial input parameters in addition to the parameters that were computed during advancement of the sand cap.

Void Ratio vs. Effective Stress [$e = f(\sigma')$]

To ensure that the model was in static equilibrium before the start of sand cap advancement, a void ratio vs. effective stress relationship was developed for each initial undrained shear strength profile and each cap thickness (the cap thickness governed the thickness of the underlying fine tailings used in the modeling of that case). A typical example is shown in Figure 1. The curvature matches the shape that has been observed for other flocculated MFT materials.

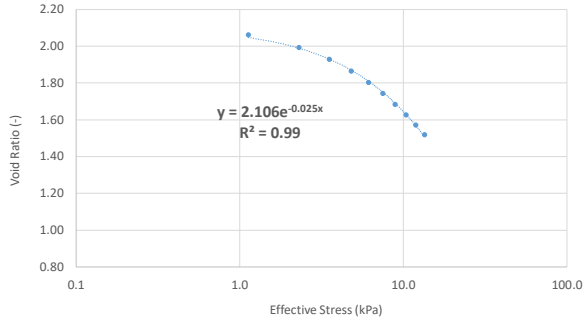

Figure 1. Typical void ratio vs. effective stress relationship from FLAC initial equilibrium run

Undrained Shear Strength vs. Liquidity Index [$s_u = f(LI)$]

The liquidity index (LI) is defined as:

$$LI = \frac{\frac{e}{G_s} * 100 - PL}{LL - PL} \qquad \text{Eq. 1}$$

Where e = void ratio, and the rest of the parameters are as defined in the Tailings Parameters section, above.

The flocculated MFT relationship between undrained shear strength and liquidity index is shown on Figure 2, adapted from Beier et al. (2013), using a LL of 60% and PL of 30%.

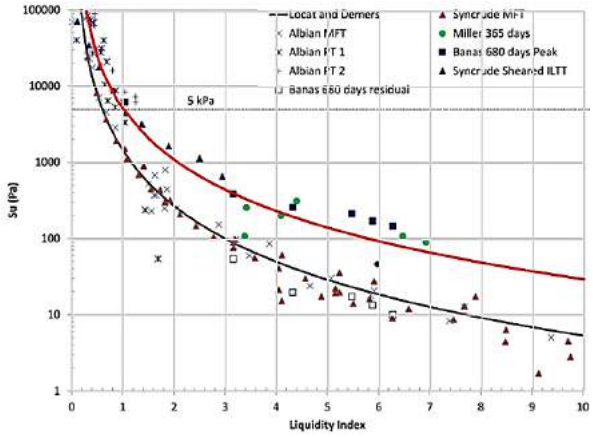

Figure 2. Undrained shear strength of oil sand fine tailings as a function of liquidity index (after Beier et al. 2013)

The area of interest for this study is primarily in the liquidity index range of 1 to 3, where the curve is not at its steepest. Note the clear distinction between MFT and Flocculated MFT in the range of interest.

Although the PL and LL for flocculated fines-rich tailings can range widely, the difference is often around 30 to 35, and thus 30 was considered a representative value for the plasticity index (LL-PL).

The resulting relationship used for modelling is as follows:

$$s_u = (45/LI)^{2.25} \qquad \text{Eq. 2}$$

Where the undrained shear strength, s_u, is in Pa.

Fines Void Ratio vs. Solids Content [$e_f = f(s)$]

The relationship between fines void ratio and solids content is defined as:

$$e_f = \frac{\left(\frac{1}{s} - 1\right) \cdot G_f}{(S_r \cdot G_w \cdot f)} \qquad \text{Eq. 3}$$

Where the parameters are as defined in the Tailings Parameters section, above.

Hydraulic Conductivity vs. Fines Void Ratio [$k = f(e_f)$]

As described in Hockely (2017), the hydraulic conductivity of fines-dominated deposits can be represented as a function of the fines void ratio. This modeling effort adapted the flocculated tailings hydraulic conductivity reported in Dunmola et al.

(2013) as a function of fines void ratio as shown in Figure 3.

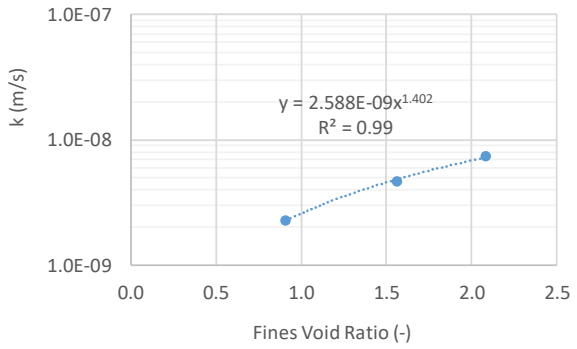

Figure 3. Hydraulic conductivity of oil sand fine tailings as a function of fines void ratio (after Dunmola et al. 2013)

The resulting relationship used in the modelling is as follows:

$$k = 5.704 \cdot 10^{-11} \cdot e_f^{3.776} \qquad \text{Eq. 4}$$

Where k = hydraulic conductivity in m/s and e_f is the fines void ratio.

CAP PROFILES AND CAP ADVANCEMENT

Cap profiles were separated into subaqueous and subaerial cases. This paper presents only subaqueous. The cap thickness, front slope, and cap/barge rate of advance were varied in this modeling effort. For each run, the cap exhibited a uniform thickness (horizontal surface) with a front slope. Cap thicknesses modeled were 20, 50, and 100 cm. The three front slopes shown in Figure 4 were considered for each cap thickness. The cap advance rate was based on the concept of a barge depositing about a 10-m-wide swath of cap through a 3-metre water cover over the tailings. Itasca developed a FISH function for use in the FLAC modeling to represent the cap advance.

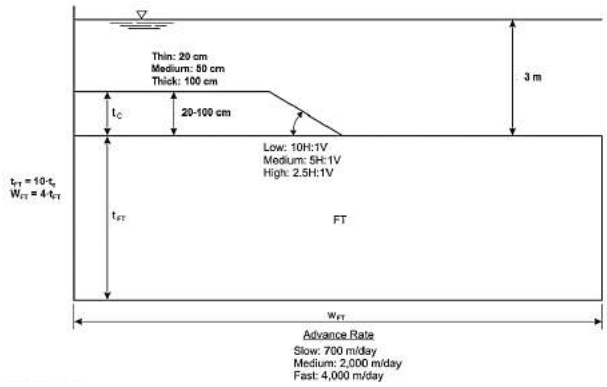

Figure 4. Geometry and input parameters for subaqueous FLAC runs

CAP MATERIAL PARAMETERS

The cap material modeled for this work consists of sand; future work will also consider coke. The following properties were used for sand material based on the authors's experience.

- Dry density: 1,485 kg/m^3
- Saturated density: 1,935 kg/m^3
- Porosity: 0.45
- Specific gravity: 2.70
- Shear modulus (small-strain): 10,000 kPa
- Drained Poisson's ratio: 0.30
- Peak friction angle: 30°
- Hydraulic conductivity: 8.0x10^{-4} cm/s (assumed)

MODELING METHODOLOGY

As stated above, the modeling was carried out using FLAC. This section describes the modeling procedure, the definition of failure, and the simplifications and assumptions.

Modeling Procedure, Assumptions, and Simplifications

Modeling was performed to show the response of the tailings to a cap advancing across a submerged tailings surface of a defined strength. The surface strength defined the solids content at the mudline, as summarized in Table 1. The model used a fixed, initial solids content profile for the tailings. Based on the solids content profile and the relationships defined above, the other elastic, hydraulic conductivity parameters and profile of undrained shear strength with depth were calculated.

While it is recognized that the moisture content of the tailings modeled for this work was often above the liquid limit, the modeling effort assumed that effective stresses had been developed within the fine tailings. A related assupmtion is that the shear modulus of the material was not zero, indicating that the material is in the “soil mechanics regime” and not the fluid mechanics/sedimentation regime. These assumptions are reasonable for the range of solids contents modeled.

Prior to initiating cap advance, the model was brought to initial equilibrium. Generally more than one iteration of equilibrium calculations were needed to establish internal consistency of the parameters.

After deposit equilibration, the cap was advanced across the tailings.

The model accounts for fluid-mechanical interaction (i.e., solves equations of equilibrium and groudwater flow). The FLAC model mesh for the fine tailings was not allowed to deform, which means that the gridpoints remained fixed as the cap advanced across the surface of the fine tailings. Deformations were computed but the mesh itself was not allowed to distort in order to match the computed deformations. Thus, the model calculations were performed in small-strain mode.

The model advanced the cap across the fine tailings at a constant rate, updating the undrained shear strength and hydraulic conductivity parameters based on the relationships defined above. The cap continued to advance until either the cap had moved across the entire deposit domain, or the tailings had failed and the cap did not succeed.

This procedure was carried out to cover the range of cap thickness, front slope, and advance rate conditions shown in Figure 4. Modelling indicated which conditions induced failure of the cap for the various initial undrained shear strength profiles (solids content profiles).

Initial Model State

Figure 5 shows the following parameters as a function of depth for an initial undrained shear strength of 0.75 kPa (at mudline), just before the cap began to advance:

- Total vertical stress
- Pore pressure (hydrostatic, note 3 m of clear water)
- Pore pressure (including excess pore pressure, also note 3 m of clear water)
- Effective vertical stress
- Undrained shear strength

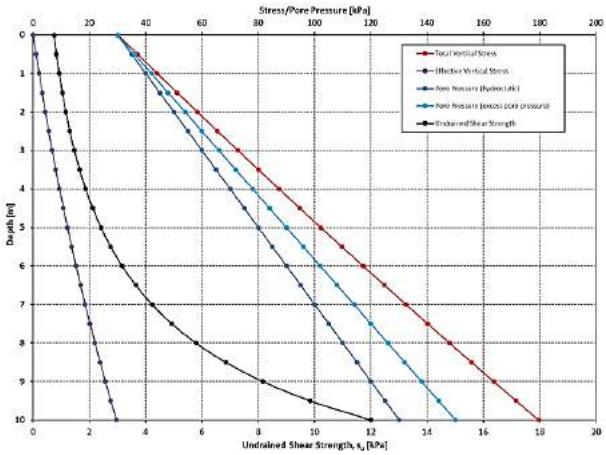

Figure 5. Initial conditions for a typical subaqueous FLAC run (su=0.75 kPa)

Definition of Failure

The definition of failure is an important consideration for this modeling effort. In general terms, it is defined as failure of the cap. It is known that deformation of the cap will occur due to instantaneous deformation and consolidation of the underlying fine tailings and typical sedimentation processes. However, failure would not be considered to have occurred if the cap layer remains continuous even if it deforms somewhat.

Failure is defined as follows:

- Slope instability (plastic shear deformation) of the cap and underlying fine tailings in which the failure surface extends as far into the fine tailings vertically as the thickness of the cap.
- Punching failure in which the vertical shear deformation in the cap is greater than the thickness of the cap. In other words, the cap would be sheared through and no longer be continuous. This failure mode was not observed in the modelling.
- Other failure mechanisms in which the integrity of the cap is compromised and the continuity of the cap is broken. One of these could be squeezing in which the fine tailings squeeze out faster than the cap advances, leading to sinking of the cap and causing difficulties for practical capping of the deposit. However, the squeezing mechanism requires a “hard” bottom and the bottom of the model has been established deep

enough that this particular failure mechanism was not observed.

It should be noted that success or failure of cap advancement was determined based on model convergence. For example, in cases where cap failure occurred and the model did not converge, displacements could become very high, often on the order of kilometers. Given that these are obviously erroneous displacements and the model would not converge, these were flagged as failing cases. On the other hand, displacements (especially vertical displacements) were less than the cap thickness for the successful cases in which the model converged throughout the cap advancement process.

RESULTS

The subaqueous capping model results are shown in Table 2. The cap thickness, front slope, and advance rate were varied for various initial undrained shear strengths. The green sections of the table indicate successful capping (Pass) while red areas of the table indicate unsuccessful capping (Fail). As stated above, the success or failure of a cap advance was determined based on model convergence. It should be noted that some cases were inferred by extrapolation and not by a specific model run, for which the P_e and F_e symbols were used.

Table 2. Results of FLAC simulations for subaqueous sand cap advancement

SAND																										
Cap Thickness [m]	1.0									0.5									0.2								
Front Slope	2.5H:1V			5H:1V			10H:1V			2.5H:1V			5H:1V			10H:1V			2.5H:1V			5H:1V			10H:1V		
Advance Rate [m/day]	4000	2000	700	4000	2000	700	4000	2000	700	4000	2000	700	4000	2000	700	4000	2000	700	4000	2000	700	4000	2000	700	4000	2000	700
s_u [kPa]																											
2.0	P	P	P	P_e	P_e	P_e	P_e	P_e	P_e	P_e	P_e	P_e	P_e	P_e	P_e	P_e	P_e	P_e	P_e	P_e	P_e	P_e	P_e	P_e	P_e	P_e	P_e
1.0	F	F_e	F	P	P_e	P	P	P_e	P	P	P	P	P_e	P_e	P_e	P_e	P_e	P_e	P_e	P_e	P_e	P_e	P_e	P_e	P_e	P_e	P_e
0.75	F_e	F_e	F_e	F_e	F_e	F	P	P_e	P	P	P	P	P_e	P_e	P_e	P_e	P_e	P_e	P_e	P_e	P_e	P_e	P_e	P_e	P_e	P_e	P_e
0.50	F_e	F_e	F_e	F_e	F_e	F_e	F_e	F_e	F_e	F	F_e	F_e	F_e	F_e	F	P	P_e	P_e	P	P_e	P_e	P_e	P_e	P_e	P_e	P_e	P_e
0.25	F_e	F_e	F_e	F_e	F_e	F_e	F_e	F_e	F_e	F_e	F_e	F_e	F_e	F_e	F_e	F_e	F_e	F_e	F	F	F	F_e	F_e	F_e	F	F	F
0.10	F_e	F_e	F_e	F_e	F_e	F_e	F_e	F_e	F_e	F_e	F_e	F_e	F_e	F_e	F_e	F_e	F_e	F_e	F_e	F_e	F_e	F_e	F_e	F_e	F	F	F
*P- Pass, F- Fail, P_e - Pass Extrapolation, F_e- Fail Extrapolation																											

The modelling results are broadly consistent with reported capping of soft deposits. For instance, the Ijburg project (De Leeuw 2002) placed a 0.5 m subaqueous sand cap on clay-rich sediments of 0.7 to 1 kPa undrained shear strength. The Ijburg cap was placed with 5H:1V slopes on the front and edges.

The following observations can be made from the modelling and the results in Table 2:

1. The model is providing reasonable results - the overall pattern of success and failure is consistent with experience and expectations; stronger tailings are required to support thicker caps.

2. Capping tailings weaker than 0.5 kPa with a 0.2 m sand cap does not appear practical, even using subaqueous placement methods. To cap such tailings, lighter-weight granular materials or sand lifts thinner than 0.2 m should be explored.

3. The front slope can be a very important factor near the cap thickness limits that a tailings strength can support.

4. Cap advance rate is a very small factor for success. The reason for this is that the subaqueous advance rates are very fast relative to the hydraulic conductivity of the fine tailings, even the “slow” advance rate of 700 m/day. This leads to very little consolidation and strength gain during cap advancement, thus resulting in very little difference in the performance of the various advance rates.

A typical successful case is shown in Figure 6. This is the case with the following geometry and material strength:

- Cap thickness: 1 m
- Front slope: 10H:1V
- Advance rate: 4,000 m/day
- Undrained shear strength: 0.75 kPa

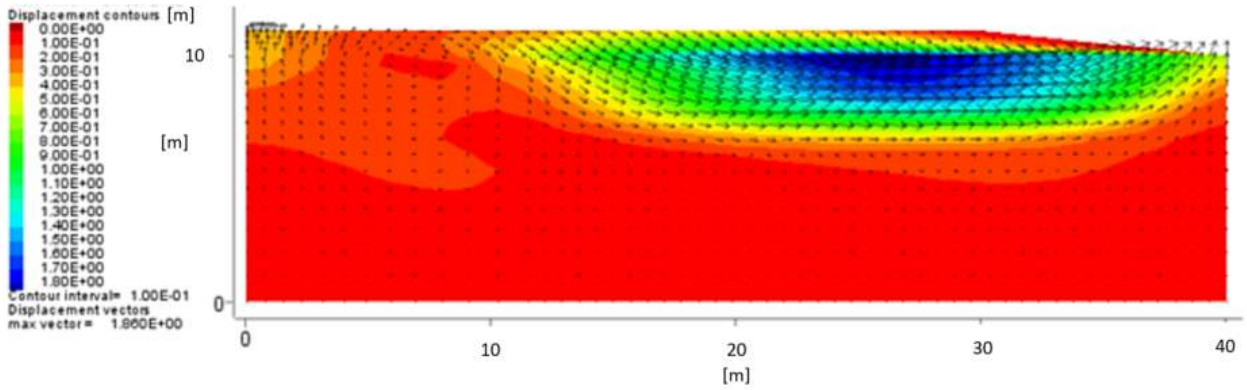

Figure 6. Total displacement contours and displacement vectors for a typical successful FLAC run

Figure 6 shows the cap as a trapezoidal shape above 10 m while the fine tailings occupy the lower 10 m of the geometry. In this illustration, the cap has advanced all the way across the fine tailings from left to right and the toe of the front slope has touched the right boundary. The color contours are total cumulative displacement (resultant of horizontal and vertical displacements) in units of meters and the arrows are displacement vectors. Most of the deformation is horizontal out in front of the cap advance; as the cap is placed, the tailings in the vicinity of the front of the cap deform forward and upward. As the cap overruns that "bulge," the tailings deform back down, and are even displaced downward some centimeters below their original elevation due to the loading from the cap. The details of how the model tracks displacement account for apparent differences in displacement between the cap and the tailings.

Figures 7 and 8 depict results from the same run but show only horizontal and vertical displacements, respectively. The only other difference is that the mesh is shown instead of displacement vectors.

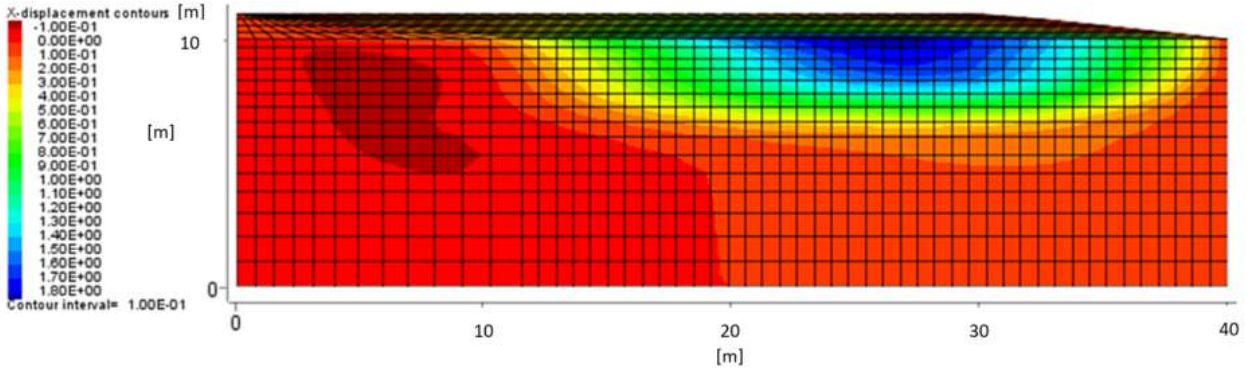

Figure 7. Horizontal displacement contours and mesh for a typical successful FLAC run

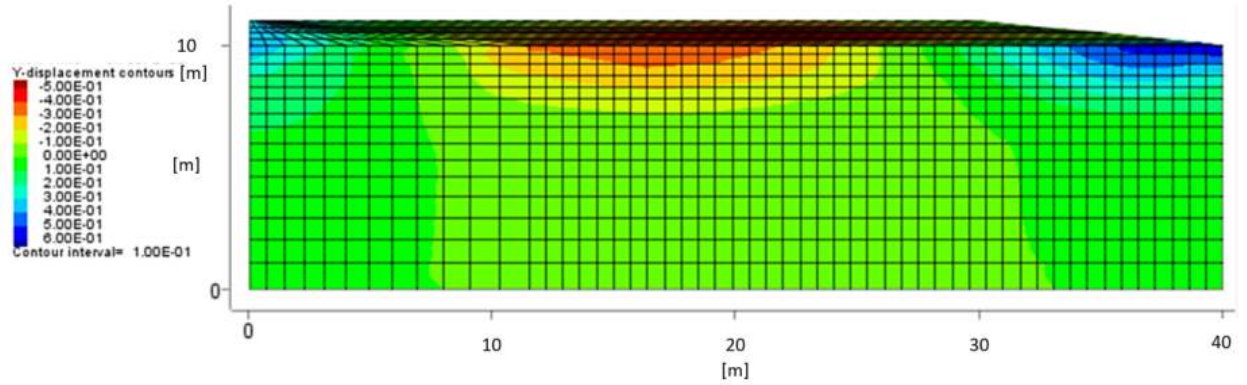

Figure 8. Vertical displacement contours and mesh for a typical successful FLAC run

FLAC modelling outputs for the successful case example shown in Figures 6-8 represent expected kinematics of a physically stable capping process where both vertical and horizontal deformations are within a reasonable range (e.g., vertical displacements in cap are less than cap thickness, upward movement of tailings in front of cap advancement are not excessive).

A typical unsuccessful case is shown in Figure 9. This case had the following inputs:

- Cap thickness: 1 m
- Front slope: 5H:1V
- Advance rate: 4,000 m/day
- Undrained shear strength: 0.75 kPa

Note this case is identical to the successful case described above except that the front slope is 5H:1V rather than 10H:1V.

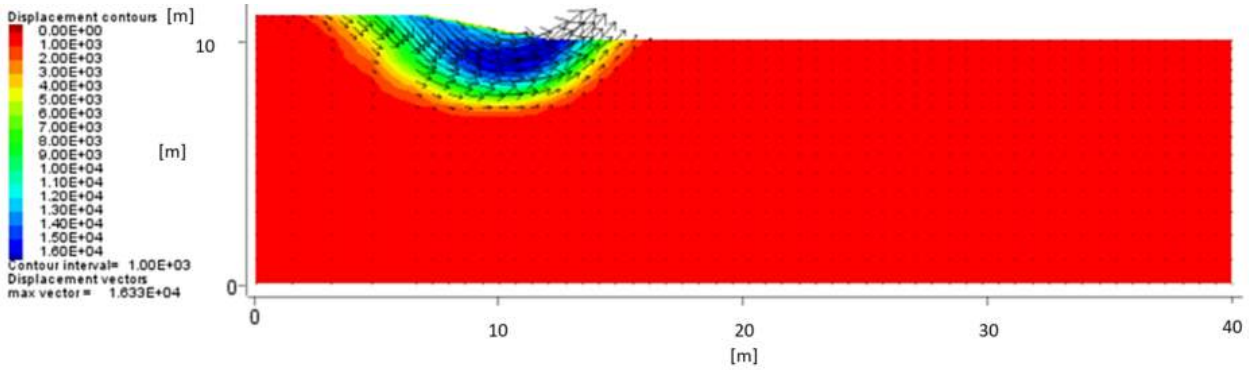

Figure 9. Total displacement contours for a typical unsuccessful FLAC run

As in the previous figures, the total displacements are in units of meters. Of note is the displacement of 1.6 km (1.60E+04), indicating that the deformations are unrealistically large (i.e., kinematics of an un-stable capping process). Furthermore, the model stopped running shortly after this total displacement output, indicating non-convergence.

SUMMARY AND CONCLUSIONS

Numerical modeling of sand cap or sand layer placement by subaqueous hydraulic delivery has been examined. Subaerial hydraulic delivery will be examined in a similar way and reported at a later date.

The current study has used the FLAC finite difference formulation to simulate the capping process with the intent of establishing the behaviour of the tailings as a cap is placed.

The results of the modeling have shown consistency with experience and expectations; stronger tailings are required to support thicker caps. It was shown that capping of very weak tailings (less than 0.5 kPa) does not appear practical with a 0.2 m sand cap. Lighter-weight granular materials or sand lifts thinner than 0.2 m should be explored for tailings like these. Additionally, it was seen that front slope of the cap can be a very important factor when cap thicknesses are approaching the limit that can be supported by the underlying tailings. Cap advance rate was shown to be a very small factor for cap success. This is because advance rates are very fast relative to the hydraulic conductivity of the fine tailings, which leads to little consolidation and strength gain during the rapid cap advancement.

The work presented is an important step in establishing a foundation for an engineering and design approach for sand cap placement and a better understanding of how to execute one of the most cost-effective methods of sand capping soft fines-dominated tailings deposits. Future work includes modeling subaerial cap placement and application of the results of physical tests to observe the various failure mechanisms. The preliminary models will be calibrated against these observations and then used to identify critical factors for establishing necessary corrections for commercial-scale applications.

ACKNOWLEDGEMENTS

The authors would like to acknowledge the valuable contributions to the success of this project by the industry Stewards: Reza Moussavi Nik, PhD., P.Eng., Paul Cavanagh, P.Eng., Nan Wang, P.Eng., and Adedeji Dunmola, PhD. Other members of the team have contributed significantly to the work reported here, including Dirk Luger of Deltares, Branko Damjanac of Itasca and Nav Dhadli, P.Eng, of Barr.

REFERENCES

Beier, N., Sort, A., Wilson, W., Sego, D. and Dunmola, A. (2012). Geotechnical Aspects of Flocculation-based Technologies for Dewatering Mature Fine Tailings, 65th Canadian Geotechnical Conference, Winnipeg, Manitoba, October 1 to 3, 2012.

Canada's Oil Sands Innovation Alliance. (2012). Subaqueous Sand Capping of Soft Oil Sands Tailings, Evaluation, by Barr Engineering and Environmental Science Canada Ltd., Deltares, Anchor QEA, and Royal Boskalis Westminster. December 2012.

Canada's Oil Sands Innovation Alliance. (2017). COSIA Challenge, Soft Tailings Capping Technology, Appendix 1. COSIA's Tailings EPA. September 28, 2017.

De Leeuw, H. A., Smits, E. P. T., Mathijssen, F. A. J. M. and Estourgie, A. L. Ph. (2002). "Reclamation on Soft Subsoil by Spraying Thin Layers of Sand: the 'Ijburg' Project near Amsterdam," International Association of Dredging Companies, Terra et Aqua International Journal on Public Works, Ports & Waterways Developments, Number 89 – December 2002.

Dunmola, A., Dhadli, N., Freeman, G., Kolstad, D., Fasking, T., Song, J. and Langseth, J. (2013). Geotechnical Benefits of Flocculation in Dewatering of Oil Sands Mature Fine Tailings. 66th Canadian Geotechnical Conference, Montreal, Quebec, September 30 to October 3, 2013.

Hockley, D. (2017). Clay Effects on Tailings Geotechnical Properties. Introduction to Oil Sands Clays, Clay Mineral Society Workshop Lectures. 4th June 2017, NAIT, Edmonton, Canada.

McKenna, G., Mooder, B. and Jamieson A. (2016). Shear Strength and Density of Oil Sands Fine Tailings for Reclamation to a Boreal Forest Landscape. International Oil Sands Tailings Conference, Lake Louise, Alberta, December 4 to 7, 2016

Muskeg River Mine (2014). Annual Report. Submitted to Alberta Energy Regulator.

Shell Canada. (2015). 2014 Annual Report – Approval 8512G, Section 4.0 –Tailings Research. Submitted to Alberta Energy Regulator.

Scott, J. D. (2003). Multiphase Mass Volume Relationships for Tailings, Department of Civil and Environmental Engineering, University of Alberta, Revised April 14, 2003.

PRELIMINARY STUDY FOR SAND CAPPING OF TREATED TAILINGS

Murray Fredlund[1], Nam Pham[1], Matt Donaldson[1] and Monica Ansah-Sam[2]
[1]SoilVision Systems Ltd., Saskatoon, Canada
[2]Canadian Natural Resources Limited, Calgary, Canada

ABSTRACT

This paper describes activities used to numerically model the process of sand cap placement on the surface of a deep deposit. The design concept is to allow for sand capping of a deep deposit filled with centrifuged product. The concept involves allowing the upper surface of the tailings to dry and a crust to form through the evaporative process. The added strength contribution from the crust will allow the placement of a sand cap in thin layers such as to avoid problems with inversion of the denser sand material. The intent of this study is to determine through preliminary numerical modeling, if this concept has theoretical justification.

The main objective is to determine the potential rate of sand cap placement in terms of sand cap lift thickness and frequency of layer placement which would be allowed. The present investigation focuses strictly on an uncalibrated numerical estimation by a variety of numerical methods to determine reasonable bounds on the placement of a sand cap over top of centrifuged deposit.

INTRODUCTION

Background

The placement of sand covers over oil-sand centrifuged deposit has little practical precedent. Previous numerical modeling studies have focused largely on the consolidation properties of the tailings material itself and ignored the shear-strength issues surrounding the placement of various cover materials on the tailings. Numerical models and experience has shown that the process of large-strain consolidation begins from the bottom up on a deep deposit. If climatic evaporation / densification is ignored or not present, then the highest void ratios remain at the surface of the deposit which reduces trafficability for many years. The evaporation process has been shown to produce a working crust of a limited thickness for oil-sand tailings (Barr & O'Kane 2015, SoilVision 2015). These evaporative crusts have increased densities and shear strengths, and potentially allow the placement of a sand cap of limited thickness on the top of the oil-sand tailings. Canadian Natural modelled the process of sand cap placement on the surface of a deep deposit. The design concept is to allow for sand capping of a deep deposit filled with centrifuged product. The historical difficulty with sand cap placement over oil-sand tailings is that the density of sand is higher than that of tailings. Therefore, problems related to inversion of the sand and tailings can occur. The concept involves allowing the upper surface of the tailings to dry and a crust to form through the evaporative process. The added strength contribution from the crust is hoped to allow the placement of a sand cap in thin layers to avoid problems with inversion of the denser sand material. The intent of the present study is to determine through preliminary numerical modeling if this concept has theoretical justification.

The ultimate intent is to determine the potential rate of sand cap placement in terms of sand cap lift thickness which would be practically allowed.

Purpose

Numerical modeling related to a proposed design for a deep deposit was performed. The established numerical analysis work scope was therefore comprised of the following tasks:

- Predict crust thickness and shear strength for elapsed times of 0, 2, and 5 years of evaporation cycles
- Develop a numerical model to analyze bearing capacity of crusted centrifuge deposit for sand capping
- Determine sand cap load rates for different crust thickness and strength relationships for elapsed times of 0, 2, and 5 years, and maximize lift thickness and time between lift placement

This study predates any detailed field or laboratory testing program to provide comprehensive data for such a study, and must therefore be considered a preliminary study. The present investigation focuses strictly on an uncalibrated numerical estimation by a variety of numerical methods to determine reasonable bounds on the placement of a sand cap over top of centrifuged deposit.

CONCEPTUAL MODELS AND THEORETICAL APPROACH

Numerical methods varying from simple to complex are to be used in the present study. In order to utilize such numerical models, the scenarios under examination must be clearly articulated. The scenarios receiving analysis are described as follows.

The first conceptual model aims to examine the bearing capacity of a sand cap load over top of a crust and tailings in the simplest format. The height of the crust, Hc, and the height of the sand cap, Hs, will be varied such that a sensitivity analysis will determine reasonable limits of bearing capacity for a simplified sand cap load. The concept of this bearing capacity loading can be seen in Figure 1.

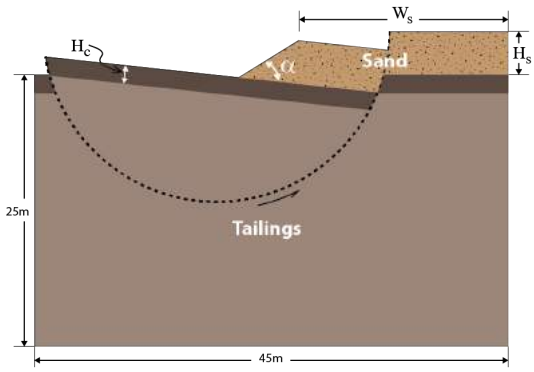

Figure 1. Bearing capacity failure

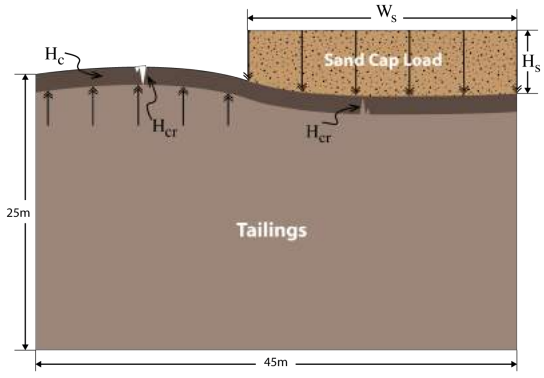

Figure 2. Deformation failure

The deformation conceptual model examines the effect of the sand cap on deformation. The focus of the numerical modeling will be on the potential deformations and bulging next to the sand cap. It is also noted that deformations can produce cracking in the tailings crust which will affect the amount of vertical surface area available to obtain shear resistance. The deformation conceptual model can be seen in Figure 2.

MATERIAL PROPERTIES

Material properties required for the present study are shear strength properties for the bearing capacity and rotational failure mechanisms. Data from a consolidation test are utilized for the deformation modeling. It is recognized that triaxial data might be better for deformation modeling, but such data was presently unavailable and therefore consolidation test data was used.

Shear strength properties were required for the centrifuge deposit, the crust, and the sand cap material for the present modeling exercise. The present analysis included ranges of reasonable sensitivity parameters which were established.

Centrifuge Deposit Composite Sample

Homogeneous material properties were assumed for the Centrifuge Cake material deposited in the deep deposit. The compressibility constitutive relationship relating the void ratio to effective stress was defined through use of a Weibull function written as:

$$e = A - B\exp(-E\sigma'^{F}) \qquad [1]$$

where e is void ratio, σ' is effective stress (kPa), and A, B, E, and F are data fitting parameters.

The compressibility curve for the Centrifuge deposit is shown in Figure 3.

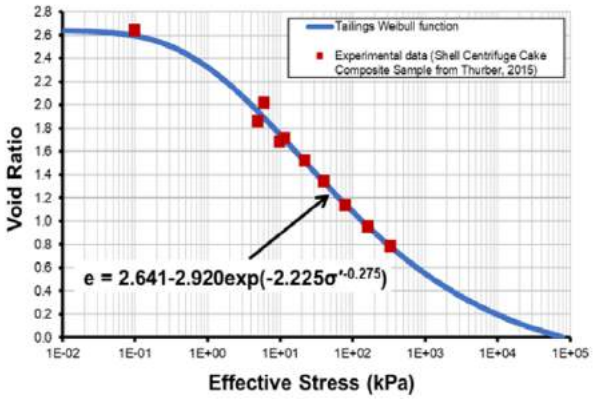

Figure 3. Compressibility of Centrifuge Deposit (Thurber 2015)

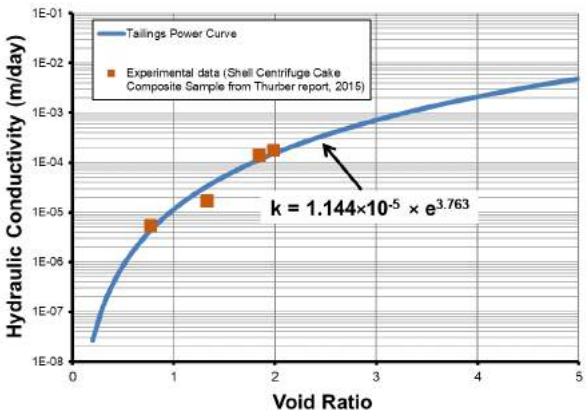

Figure 4. Hydraulic conductivity of Centrifuge Deposit (Thurber 2015)

The hydraulic conductivity data is fitted with a Power function as shown in Figure 4. The relationship between hydraulic conductivity and void ratio using a Power function can be written as:

$$k = C\, e^{D} \qquad [2]$$

where k is hydraulic conductivity (m/s), e is void ratio, and C and D are data fitting parameters.

Crust Material Properties

Material properties for the crust were derived from the Centrifuge deposit material properties since the Centrifuge deposit has a higher solids content due to evaporation. A solids content of 66% was chosen as a representative value based on the solids content values observed by another operator at an Oil Sands site. The hydraulic conductivity constitutive relationship for the crust was not changed from the Centrifuge deposit relationship shown in Figure 4. The compressibility constitutive relationship for the crust was modified so that the initial void ratio at an effective stress 0.1 kPa was consistent with a solids content of 66%. Please note that observations have been made that crusts with much higher solids content can be formed under conditions such as additives, evaporative drying and thickness of deposit; and these may correspond to desiccation cracking that can potentially reduce the strength along the vertical planes. The initial void ratio corresponding to 66% solids content is 1.3 based on the following equation:

$$sc = \frac{G_s}{e + G_s} * 100\% \qquad [3]$$

where Gs =2.49 is specific gravity, e is void ratio, and sc is solids content.

The Centrifuge deposit laboratory data points corresponding to an effective stress greater than 100 kPa were left unchanged. The remaining laboratory data points were scaled to provide a smooth transition between the initial void ratio at 0.1 kPa and the data points with an effective stress greater than 100 kPa. The resulting compressibility data and best-fit Power function to the data can be seen in Figure 5. The original Centrifuge deposit laboratory data points and best-fit curve are also shown for comparison purposes.

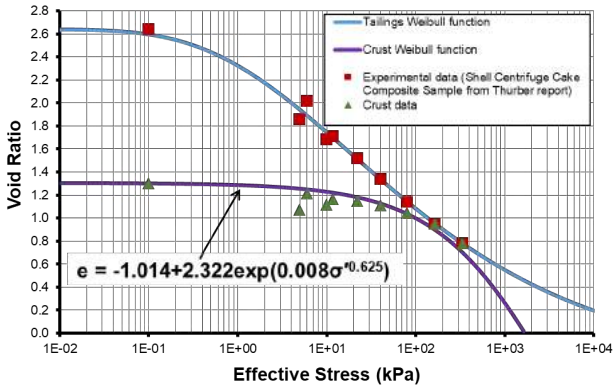

Figure 5. Compressibility of Shell centrifuge deposit

SAND CAP SINGLE-LAYER LOADING RATES

The purpose of this study was to theoretically determine the approximate sand cap layer thickness which could be placed on top of the tailings material. This section examines the placement of a single sand cap layer. Numerical methods varying from simple to complex were considered. The hierarchy of numerical methods for a single sand cap layer can be seen in Figure 6. The results for each of the numerical methods are described in the following sections.

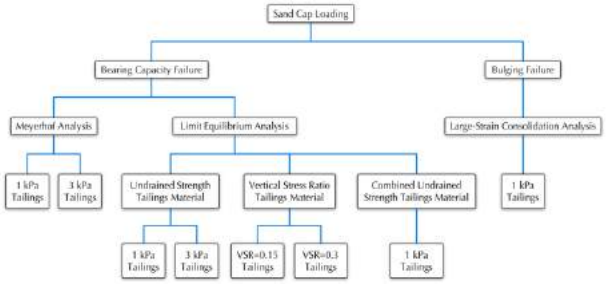

Figure 6. Hierarchy of numerical methods for a single layer sand cap

A Meyerhof analysis represents a total stress analysis and therefore is likely to yield sand loading thicknesses which may be higher than experienced in the field. The present analysis ideally represents the centrifuged deposit as an undrained loading scenario given the low permeability of the material. Therefore, several types of undrained analyses are selected to provide context to the numerical modeling in the present study. Representing the centrifuged deposit with an undrained strength model is performed as well as representing the material with an Undrained (Vertical) Strength Ratio (USR) strength model. The USR method estimates shear strength based on a vertical effective stress calculated through depth from the surface. The vertical effective stress is calculated assuming 100% consolidation and therefore means the USR method is likely to yield sand cap thicknesses higher than experienced in the field.

The deformation failure is represented by a coupled large-strain consolidation model. The low hydraulic conductivities of the centrifuged deposit mean the numerical model largely represents undrained loading conditions.

Bearing Capacity of Sand Cap Loading

The next step in the analysis was to determine the bearing capacity of a 2-layer system of a stronger layer over a weaker layer (Figure 7). The Meyerhof and Adams (1968) punching method of analysis was selected for the present study and an overview of the method is presented in the following sections.

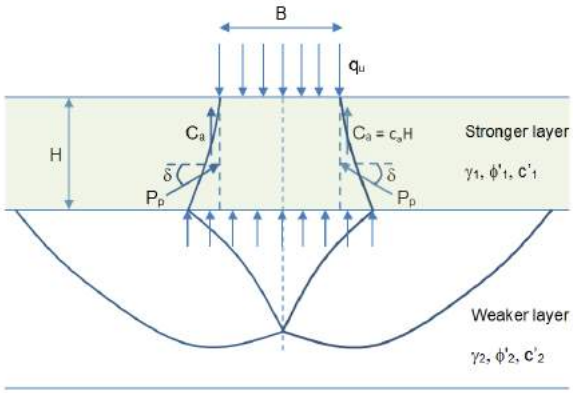

Figure 7. Failure mechanism of two-layer soil below footing on top of strong soil

Results of the Meyerhof (Meyerhof & Adams 1968) bearing capacity analysis of a two-layer system are presented in Figure 8 and Figure 9. The results presented in these graphs assume an undrained shear strength response for both the crust and tailings. The undrained strength for the crust was varied between 5 and 30 kPa and the undrained strength for the tailings is varied between 1 and 3 kPa. Relating undrained shear strength and solids content, an approximate solids content of 50% corresponds to an undrained tailings strength of 1 kPa and an approximate solids content of 59% corresponds to an undrained tailings strength of 3 kPa. It should be noted that this analysis considers only a static two-layer system and the rate of deposition is not considered. In these figures, the lines represent a factor of safety (FOS) equal to 1.0. The Meyerhof analysis can be considered to analyze the bearing capacity conceptual model (Figure 1).

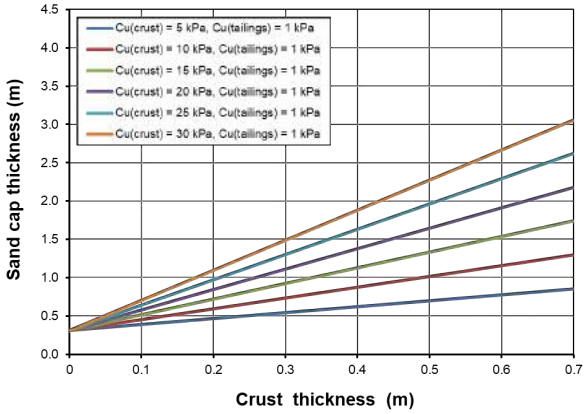

Figure 8. Bearing capacity with varied undrained crust strengths and undrained tailings strength of 1 kPa

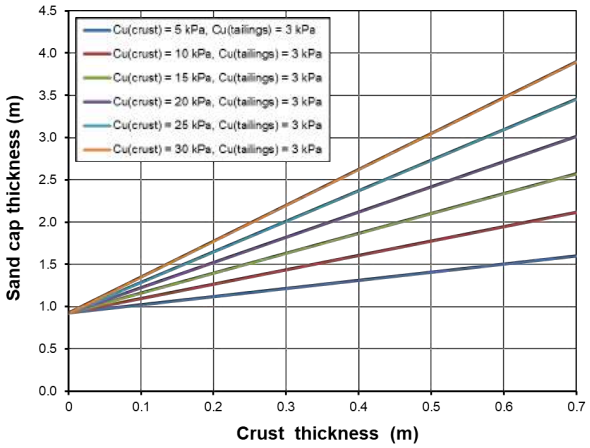

Figure 9. Bearing capacity with varied undrained crust strengths and undrained deposit strength of 3 kPa

Limit Equilibrium Analysis

A limit equilibrium analysis using SVSLOPE® was used to explore the possibility of a rotational failure as noted in the bearing failure conceptual model (Figure 1). The centrifuge deposit are represented with either an Undrained Stress Ratio (USR) constitutive model or with an undrained strength constitutive model. The strength of the tailings is varied to be either 1 kPa or 3 kPa. The typical range of USR values for normally consolidated clay and silt materials was compiled by Ladd (1991). In the USR constitutive model an undrained stress ratio of 0.15 is chosen to represent the lower end of the typical USR range and a vertical stress ratio of 0.3 is chosen to represent the higher end of the typical USR range. The sand is represented with a Mohr-Coulomb constitutive model. The crust is represented with an undrained strength constitutive model with strength equal to 5 kPa.

Undrained Strength Constitutive Model

The results of the limit equilibrium analysis when representing the centrifuge deposit with an undrained strength constitutive model with strength of 1 kPa are shown in Table 1. For any crust thickness, the maximum possible sand cap thickness is 0.25 m. A sand cap thickness of 0.25 m, when no crust is present, is consistent with the Meyerhof analysis. For a fixed sand cap thickness, as the crust thickness increases the FOS also increases indicating less likelihood of a failure occurring. However, because of the limitation of the minimum sand cap thickness increment of 0.25 m, a thicker sand cap is not achieved for a thicker crust. Sand cap thickness greater than 0.25 m and less than 0.5 m would be possible for crust thicknesses of 0.3 m and 0.7 m were it not for the limitation of a sand cap thickness of 0.25 m.

The results of the limit equilibrium analysis when representing the tailings material with an undrained strength constitutive model with a strength of 3 kPa are shown in Table 2. For any crust thickness the maximum possible sand cap thickness is 0.75 m. A sand cap thickness of 0.75 m when no crust is present is consistent with the Meyerhof analysis.

Based on the results in Table 1 and Table 2, the dominant factor for the undrained strength constitutive model is the strength of the centrifuge deposit. The crust thickness has little effect on the maximum sand cap thickness.

Table 1. Limit equilibrium analysis FOS and maximum sand cap thickness results with 1 kPa undrained tailings

FOS ≥ 1
FOS < 1

Sand Cap Thickness (m)	Crust Thickness (m) 0	0.3	0.7
0.25	1.106	1.210	1.247
0.50	0.552	0.579	0.626
Max. sand thickness (m):	0.25	0.25	0.25

Table 2. Limit equilibrium analysis FOS and maximum sand cap thickness results with 3 kPa undrained tailings

FOS ≥ 1
FOS < 1

Sand Cap Thickness (m)	Crust Thickness (m) 0	0.3	0.7
0.75	1.098	1.112	1.125
1.00	0.824	0.834	0.842
Max. sand thickness (m):	0.75	0.75	0.75

Undrained Stress Ratio Constitutive Model

The results of the limit equilibrium analysis when representing the strength of the tailings material with USR = 0.15 are shown in Table 3. It can be seen that a sand cap thickness of 0.25 m

corresponding to a crust thickness of 0 m, a sand cap thickness of 0.5 m corresponding to a crust thickness of 0.3 m, and a sand cap thickness of 0.75 m corresponding to a crust thickness of 0.7 m are consistent with the Meyerhof analysis with an undrained crust strength of 5 kPa and an undrained tailings strength of 1 kPa.

The results of the limit equilibrium analysis when representing the strength of the centrifuge deposit with a USR = 0.3 are shown in Table 4. It can be seen that a sand cap thickness of 0.75 m corresponding to a crust thickness of 0 m, a sand cap thickness of 1.25 m corresponding to a crust thickness of 0.3 m, and a sand cap thickness of 1.75 m corresponding to a crust thickness of 0.7 m are consistent with the Meyerhof analysis with an undrained crust strength of 5 kPa and an undrained tailings strength of 3 kPa.

Table 3. Limit equilibrium analysis FOS and maximum sand cap thickness results with tailings USR = 0.15

FOS ≥ 1
FOS < 1

Sand Cap Thickness (m)	Crust Thickness (m) 0	0.3	0.7
0.25	1.234		
0.50	0.749	1.271	
0.75		0.945	1.076
1.00			0.991
Max. sand thickness (m):	0.25	0.50	0.75

Table 4. Limit equilibrium analysis FOS and maximum sand cap thickness results with tailings USR = 0.3a

FOS ≥ 1
FOS < 1

Sand Cap Thickness (m)	Crust Thickness (m) 0	0.3	0.7
0.75	1.102		
1.00	0.962		
1.25		1.044	
1.50		0.898	
1.75			1.036
2.00			0.936
Max. sand thickness (m):	0.75	1.25	1.75

Deformation Failure Sand Cap Loading

There is difficulty in defining "failure" in the Deformation Failure Sand Cap Loading Scenario. When a sand cap is placed over weak tailings material there is a bulging that occurs because of the added load. The bulging may be controlled and may not indicate complete failure conditions. If the bulging becomes excessive then failure conditions exist. Evidence of failure may become apparent in different ways in the numerical model. Cracking of the crust surface is simply one possible criterion. When the effective stresses become increasingly negative along the surface of the bulge over time this represents cracking of the crust and will cause convergence failure in the numerical solver since the effective stresses become too negative.

The approach used with the present stress-deformation analysis was to simulate the sand cap loading process with a 2-D combined large-strain stress/deformation and flow code SVFLUX/SVSOLID™ (i.e., large-strain consolidation). The model was loaded until deformation conditions became so excessive that model convergence failure occurred in a manner similar to that of the shear strength reduction (SSR) methodology. The sand cap was modeled as a surcharge applied to the crust with the measured unit weight. As in the limit equilibrium analysis the surcharge was varied in increments equivalent to a sand cap thickness of 0.25 m. It is more likely that a failure may occur during deposition of the sand cap because of the bulging effect (as opposed to after the entire sand cap has been deposited and the bulge is no longer present). For this reason, the sand cap was placed across only a portion of the width of the numerical model. Once the sand cap has been added the model is left to consolidate over time under self-weight and the surcharge due to the sand cap load. It is also assumed that the crust exists at the start of the numerical model (i.e., the crust formation was not modeled).

It is intuitive to consider that when a sand load is placed on the tailings that the pore-water squeezes out from beneath the sand cap and creates pressure / bulging beside the sand load. It was noted in the numerical modeling that the hydraulic conductivity of the centrifuge deposit is low enough that pore-water flow can be considered to be approximately stationary for the time-scale involved in sand-capping. Bulging may occur ahead of the sand cap placement, but it was found to be strictly because of the natural loading of a material with low shear strength. An example of a typical loading

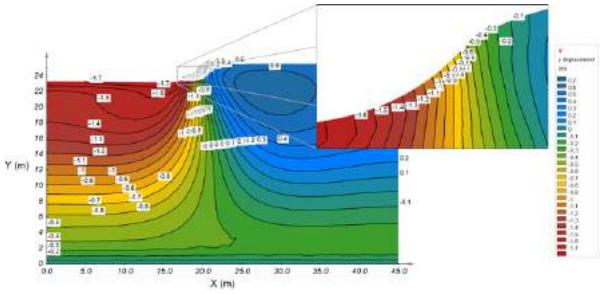

Figure 10. Stress/deformation results after a sand capping scenario

scenario is seen in Figure 10. The results in shown in this figure are at an elapsed time of 5 years, a sand cap thickness of 0.5 m, and a crust thickness of 0.3 m.

The deformation results due strictly to the sand cap loading (i.e., no effect of consolidation is included) are shown in Table 5. The maximum negative displacement and maximum positive displacement in the finite element mesh are given for each sand cap thickness and crust thickness. As shown in Figure 10, the maximum negative displacement occurs below the sand cap load and the maximum positive displacement occurs in the area of the bulge. Note that the figure includes the effect of consolidation; however, the location of the maximum displacement remains unchanged compared to the deformations without consolidation. As expected, a thinner sand cap gives smaller deformations than a thicker sand cap. The range of negative displacement varies from -0.5 m to -2.1 m. The range of positive displacement varies from 0.5 m to 1.6 m. Also, the range of displacement for a given sand cap thickness is independent of the crust thickness.

Table 5. Maximum displacement due to sand cap loading without considering consolidation

		Crust Thickness (m)					
		0		0.3		0.7	
		Max. neg. disp. (m)	Max. pos. disp. (m)	Max. neg. disp. (m)	Max. pos. disp. (m)	Max. neg. disp. (m)	Max. pos. disp. (m)
Sand Cap Thickness (m)	0.25	-0.5	0.5	-0.5	0.5	-0.5	0.5
	0.50	N/A	N/A	-1.1	1.0	-1.1	1.0
	0.75	N/A	N/A	N/A	N/A	-2.1	1.6

The deformation results due to the loading scenario including the effect of consolidation are shown in Table 6. The vertical displacement values were taken after an elapsed consolidation time of 5 years, i.e., the sand cap load was placed immediately with the tailings and crust left to consolidate over a period of 5 years. The range of negative displacement varies from -1.1 m to -3.3 m. The range of positive displacement varies from 0.2 m to 1.3 m. Therefore, at a time of 5 years the effect of consolidation alone accounts for approximately 40% - 60% of the total vertical displacement observed in the numerical model.

Table 6. Maximum displacement due to sand cap loading with consolidation included at time = 1825 days

		Crust Thickness (m)					
		0		0.3		0.7	
		Max. neg. disp. (m)	Max. pos. disp. (m)	Max. neg. disp. (m)	Max. pos. disp. (m)	Max. neg. disp. (m)	Max. pos. disp. (m)
Sand Cap Thickness (m)	0.25	-1.1	0.2	-1.1	0.2	-1.1	0.2
	0.50	N/A	N/A	-1.7	0.6	-1.7	0.7
	0.75	N/A	N/A	N/A	N/A	-3.3	1.3

Summary of Sand Cap Single-Layer Loading Rates

Several different numerical methods were examined for determining the maximum sand cap thickness that can be placed on top of the tailings. These methods ranged from simple to complex methodologies and varied in terms of how the failure mechanism was defined. Despite significant differences in the theoretical basis for each of the numerical methods, the results are remarkably similar.

The graph of maximum sand cap thickness versus crust thickness for all numerical methods on 1 kPa tailings presented in the previous sections is shown in Figure 11. For 5 kPa of undrained strength in the crust the Meyerhof analysis, the limit equilibrium analysis with a USR constitutive model for the tailings, and the 2-D large-strain consolidation analysis give the same maximum sand cap thickness when considering that the minimum thickness increment for the sand cap is 0.25 m. The limit equilibrium analysis with undrained tailings and crust resulted in the lowest predicted sand cap thickness at 0.25 m for all crust thicknesses.

For 3 kPa centrifuge deposit, the graph of the maximum sand cap thickness versus crust thickness for all numerical methods presented in the previous sections is shown in Figure 12. For 5 kPa of undrained strength in the crust, the Meyerhof analysis and the limit equilibrium analysis with a USR constitutive model for the tailings give the same maximum sand cap thickness when considering that the minimum thickness increment

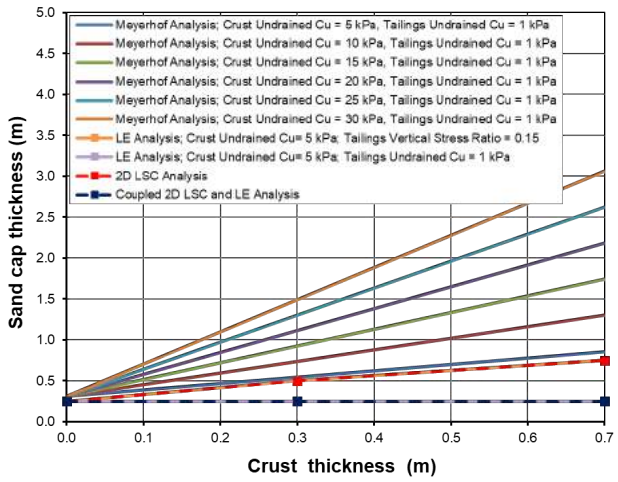

Figure 11. Summary of maximum single layer sand cap thickness for 1 kPa tailings

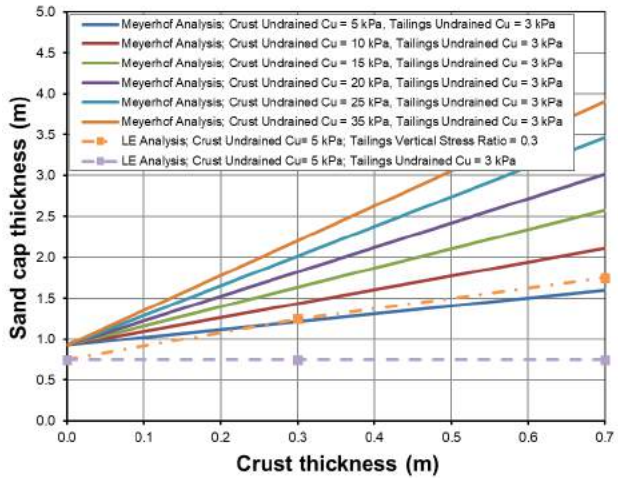

Figure 12. Summary of maximum single layer sand cap thickness for 3 kPa tailings

for the sand cap is 0.25 m. The limit equilibrium analysis with undrained tailings and crust resulted in the lowest sand cap thickness at 0.75 m for all crust thicknesses. The 2-D large-strain consolidation analysis was not included because the data from the consolidation test results for the centrifuge deposit was not consistent with 3 kPa strength conditions.

SUMMARY AND CONCLUSIONS

This paper has presented the results of preliminary numerical modeling to determine the potential loading rates for sand capping tailings material with a crust present. Even though this numerical modeling is theoretical it is possible to draw the following preliminary conclusions from the analyses:

- The results of a Meyerhof bearing capacity analysis indicated that a sand cap thickness **between 0.54 m and 1.49 m** was possible if we assume the undrained strength of the tailings material is 1 kPa with a crust thickness of 0.3 m and undrained crust strength between 5 kPa to 30 kPa respectively. If the crust thickness increases to 0.7 m then a sand cap thickness between **0.85 m to 3.1** m is possible for the same undrained crust strength.

- The results of the limit equilibrium analysis when representing the tailings material with an undrained strength constitutive model indicated that a sand cap thickness of **0.25 m** for 1 kPa tailings and **0.75 m** for 3 kPa tailings could be placed. In this analysis, the thickness of the crust did not affect the maximum sand cap thickness.

- The results of the limit equilibrium analysis when representing the strength of the tailings material with a USR = 0.15 are shown in Table 3. It was seen that a sand cap thickness of **0.5 m** corresponding to a crust thickness of 0.3 m and a sand cap thickness of **0.75 m** corresponding to a crust thickness of 0.7 m are consistent with the Meyerhof analysis.

- The results of the loading scenario coincide closely with the previous three analyses. The analysis indicated that the maximum sand cap thickness for a crust of 0.3 m is **0.5 m**. Likewise; a crust of 0.7 m could potentially support a sand layer of **0.75 m**.

The results of the combined 2-D large-strain consolidation and limit equilibrium analyses indicated that the added strength at the top of the tailings layer was not sufficiently high to allow for any additional sand compared to the tailings with a constant undrained strength throughout the layer, i.e., the maximum sand cap thickness in the single and two sand cap combined analyses were the same as in the non-combined undrained analyses.

ACKNOWLEDGEMENTS

Sincere appreciation and thanks to Robert Donahue formerly of Shell Canada who had significant input into the study.

REFERENCES

Barr and O'Kane. (2015). Atmospheric Fines Drying (AFD) Deposition Optimization: Multi-lift versus Deep Stacking Project Progress Report, Prepared for Shell Canada Limited, March.

BGC Engineering Inc. (2014). Perimeter Ditch Pilot 1 Trial, 2013 Performance Monitoring Update, Submitted to Syncrude Canada Limited, April.

Golder Associates Ltd. (2014). East ETA Polymer Treated Thickened Tailings Deposit – Capping Options Assessment, Submitted to Imperial Oil Resources Ltd., April 29.

Jeeravipoolvarn, S. (2010). Geotechnical Behavior of In-line Thickened Oil Sands Tailings. Ph.D. Thesis, University of Alberta, Edmonton, Alberta, Canada.

Ladd, C. (1991). Stability Evaluation during Staged Construction. Journal of Geotechnical Engineering, **117**(4): 540-615.

Meyerhof, G. and Adams, G. (1968). The Ultimate Uplift Capacity of Foundations. Canadian Geotechnical Journal, **5**(4): 225-244.

Meyerhof, G. and Hanna, A. (1978). Ultimate Bearing Capacity of Foundations on Layered Soils Under Inclined Load. Canadian Geotechnical Journal, **15**(4): 565-572.

SoilVision Systems Ltd. (2014). Calibration of Centrifuge Cake with Gypsum Data. Report submitted to Syncrude Research Centre. Edmonton, Alberta, Canada.

SoilVision Systems Ltd. (2015). Calibration of Rim Ditch Dewatering Pilot with Large-Strain Consolidation, Sedimentation, Continuous Filling, Evaporation and Thaw Strain. Report submitted to Syncrude Research Center. Edmonton, Alberta, Canada.

Syncrude Canada Ltd. (2012). Results of Large Strain Consolidation Testing and Triaxial Testing of Gypsum Treated Polymer Flocculated Centrifuge Cake by SNC-LAVALIN INC., Saskatoon, Saskatchewan, Canada.

Thurber Engineering Ltd. (2015). Large Strain Consolidation with Constant Head Hydraulic Conductivity Test, Draft report submitted to Shell Canada, October 22.

DETERMINING BEARING CAPACITY FOR SAND CAP PLACEMENT AT JACKPINE MINE DDA1

Murray Fredlund[1], Nam Pham[1], Matt Donaldson[1] and Monica Ansah-Sam[2]
[1]SoilVision Systems Ltd., Saskatoon, Canada
[2]Canadian Natural Resources Limited, Calgary, Canada

ABSTRACT

There has been interest in recent years to determine the thickness and shear strength requirements to support tailings surface layer improvements. The intent of this analysis was to determine the required surface improvements in order to place a sand cap on the Designated Disposal Area 1 (DDA1) above-ground tailings storage facility.

The design of the DDA1 facility is an above-ground storage facility, in which the oil-sand tailings material is contained by retaining structures, where the tailings is allowed to consolidate over time. The successful management of the tailings facility will require engineered solutions that take into consideration the amount of surface improvement as well as the application methodology to be established in order to place the sand cap.

Sensitivity analysis were performed. The proposed modeling applies knowledge obtained during the calibration of an existing centrifuged deposit test plot. The intent of the present study is to extend the previous calibration modeling analysis to determine the depth and shear strength requirements for top layer of the tailings, such that a sand cap can be supported. A flat tailings surface as well as the top surface sloped at a 1% grade were considered.

INTRODUCTION

Background

Engineering decisions related to placing the sand cap are complicated by i) the low solids contents and subsequent low shear strength at the surface of current oil-sand tailings deposits as well as, ii) the higher density of the sand used for hydraulic or mechanical capping.

The intent of the planned analysis is to determine the required surface improvements in order to place a sand cap on the DDA1 above-ground tailings storage facility.

This paper provides insight into the bearing capacity related to placement of a sand cap. The proposed modeling applies knowledge obtained during the calibration to the existing centrifuged deposit test plot at Jackpine Mine (JPM) site. The intent of this study is to extend the previous calibration modeling analysis to determine the depth and shear strength requirements for the top layer of tailings that can be supported by a sand cap.

Objective

The main objective of the project was to perform bearing capacity sensitivity numerical analysis to determine surface improvement requirements necessary for placing a sand cap on the DDA1 facility. The sensitivity analysis focused on determining the depth and shear strength requirements necessary for a range of target sand cap thicknesses. The analysis took the form of a sensitivity analysis to determine ranges of surface improvement layer thickness and shear strength which will be required for sand cap placement.

The sensitivity analysis considers a rotational failure mechanism that uses the Limit Equilibrium Method (LEM). The SVSLOPE® computer software is used in the present project for both 2-D and 3-D modes of bearing capacity failure.

The numerical modeling results relate the thickness of the surface improvement layer and the required shear strength of the layer for sand cap thicknesses between 3 m and 5 m.

CONCEPTUAL MODELS AND THEORETICAL APPROACH

A typical surface crust is formed mainly due to the evaporation of water at the tailings surface to a limited thickness of up to 1 m in oil-sands tailings.

Freeze-thaw cycles can also induce a crust layer of oil-sands tailings surface. Field measurement values of shear strength and thickness of the crust layer depends on environmental variables (i.e., air temperatures, solar radiation, wind speed and other factors). The installation of wick drains in tailings also has the potential for the improvement of strength in the 5-15 m layer for oil-sand tailings.

This study does not include "how" an improved strength upper zone is achieved in an oil-sand tailings facility but rather "assumes" a range of thicknesses and shear strengths for the purpose of demonstrating the strength requirements for supporting a sand cap. The required shear strength and thickness of the improved layer is determined for a given sand cap thickness. The models are all run and the results calculated assuming a factor of safety (FOS) of 1.0.

The analysis was performed using a limit equilibrium method (LEM) analysis which only considers failure conditions and not potential deformations during installation of the sand cover. Failure is therefore defined as a potential rotational failure.

It is possible that during field placement of a particular cover scenario, limit equilibrium conditions are met but excessive deformations may limit the ability of the sand cover to function properly. The expected deformations of the installation of a particular cover was not considered in this analysis.

Several conceptual models were considered in this study and the purpose of each of them was to simulate scenarios that could occur in the field at various thicknesses and strengths of the improved layer corresponding to the sand cap thickness between 3 m and 5 m. Conceptual model #1 simulates typical cover placement using hydraulic methods. Conceptual model #2 is to simulate the assumed placement of the sand cover by mechanical spreading. The scenarios analyzed are described as follows:

Conceptual Models

There are four conceptual scenarios simulated in this study using LEM in order to develop a relationship between improved layer thickness versus shear strength for a given sand cap thickness and factor of safety (FOS).

Conceptual Model #1: This conceptual model represents the general scenario of a hydraulically pumped sand cap with a sloping angle of 1.5 % in 2-D. The thickness of the tailings plus the improved layer is 30 m and the improved thickness is simulated for values between 1 m and 15 m (Figure 1).

Conceptual Model #2: This conceptual model represents the case of a locally formed sand cap slope at an angle of 36°. Other dimensional variables are similar to those used for conceptual model #1. This conceptual model simulates the placement of the sand cap by mechanical placement methods (Figure 2).

Conceptual Model #3: This conceptual model is similar to conceptual model #1 but with a local steep slope of 36°, which is formed in the middle of the general slope (Figure 3).

Conceptual Model #4: This conceptual model is an extension into 3-D of conceptual model #2, in which the sand cap occupies one quadrant of the geometry (Figure 4).

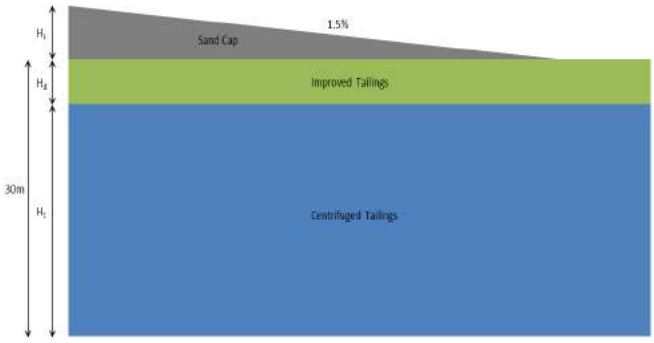

Figure 1. Conceptual model #1 – Hydraulic placement of sand

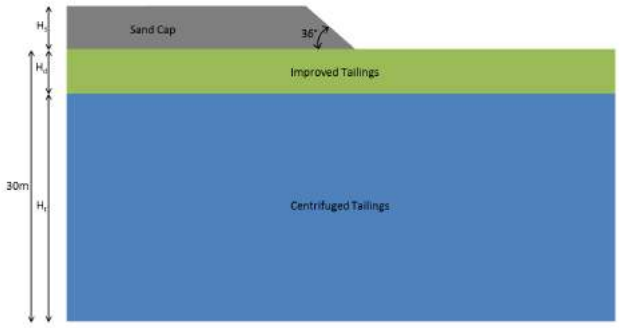

Figure 2. Conceptual model #2 – Mechanical placement of sand

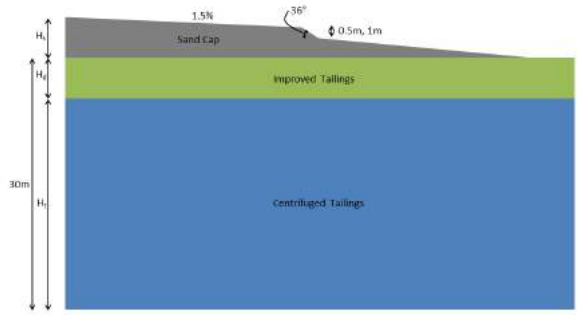

Figure 3. Conceptual model #3 – Hydraulic placement of sand with an anomaly

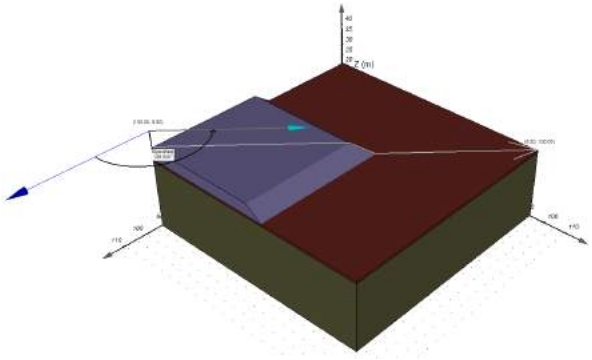

Figure 4. Conceptual model #4 – 3-D Mechanical placement of sand (assumed slip direction line is the grey arrow)

MATERIAL PROPERTIES

The strength parameters and unit weight required for all materials are shown in Table 1. The field test results using field vane shear tests from the JPM Centrifuge deposit Pilot indicated the peak undrained shear strength, s_u, of 1 kPa can be achieved at a solids content around 50%. At s_u = 1 kPa, the tailings water content is less than the liquid limit (at the liquid limit, s_u ~ 2 kPa for fine-grained soils as reported by Terzaghi et al., 1996). A study by Daliri et al. (2015) reported that at a solids content of 50%, the peak values of s_u can vary significantly between 0.1 kPa and 1 kPa. The remolded s_u is generally less than 1 kPa at this solids content.

Table 1. Material properties (SoilVision 2016)

Material name	Peak undrained shear strength (kPa)		Unit weight (kN/m^3)
Centrifuged Tailings	1		13.83
Improved Tailings	To be defined		17.79
	Cohesion (kPa)	**Friction angle (deg.)**	
Sand cap	0	31	19.5

SIMULATION RESULTS AND DISCUSSIONS

Simulations were run for the above-mentioned scenarios at a given improved layer thickness, H_d, and sand cap thickness, H_s. The undrained shear strength, s_u, of the improved layer was calibrated so that the resulting FOS varies generally between 0.8 and 1.3. In the simulations, the water table is assumed to be at the base of the improved layer. The increased pore-water pressure due to the sand cap load was not included in the anlayses since it does not influence the FOS in an undrained analysis.

Conceptual Model #1

The typical critical slip surface for conceptual model #1 is shown in Figure 5. This slip surface is deep (typically hits the lowest base allowed) and wide due to the low value for the shear strength of the tailings (Merifield et al. 1999).

Figure 6 and Figure 7 show the relationship between an improved layer thickness and the undrained shear strength for various sand cap thicknesses between 3 m and 5 m for a FOS = 1 and 1.3, respectively. These figures indicate that the relationship between the improved layer thickness and undrained shear strength is nonlinear. The values of the required s_u increase rapidly for an improved layer thickness, H_d < 5 m.

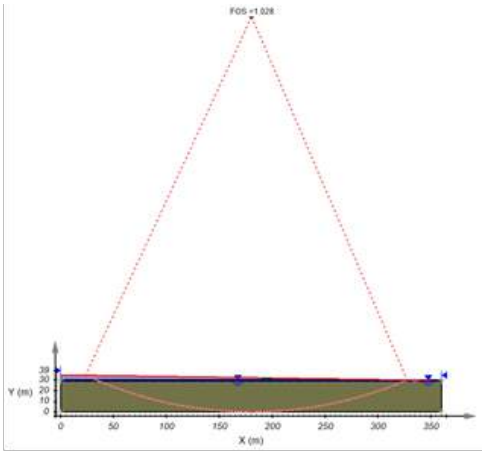

Figure 5. Typical critical slip surface of conceptual model #1

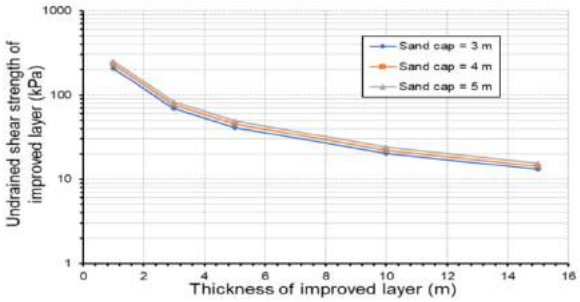

Figure 6. The relationship between improved layer thickness and undrained shear strength at various sand cap thickness for FOS = 1 (Conceptual model #1)

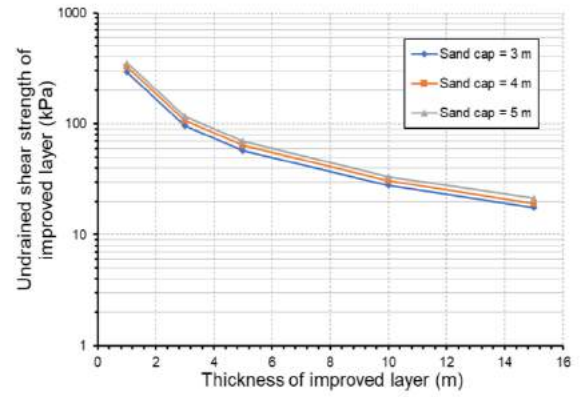

Figure 7. The relationship between improved layer thickness and undrained shear strength at various sand cap thickness for FOS = 1.3 (Conceptual model #1)

Conceptual Model #2

The typical critical slip surface for conceptual model #2 is shown in Figure 8. The results of the relationship between H_d and s_u are shown in Figure 9 and Figure 10. Table 2 presents the results utilizing strengths of 1 and 5 kPa undrained shear strength for the centrifuged deposit. The required undrained shear strength for the improved layer decreases marginally with the 5 kPa assumption of centrifuged tailings strength. The required s_u varies significantly depending on the thickness of sand cap and the improved layer.The relationship between H_d and s_u are nonlinear for both FOS = 1 and 1.3 at a given sand cap thickness. For a sand cap of 3 m, the required s_u changes between 270 kPa (H_d = 1 m) and 28 kPa (H_d = 15 m) for FOS = 1 Figure 9; and between 365 kPa (H_d = 1 m) and 37 kPa (H_d = 15 m) for a FOS = 1.3 (Figure 10). When a thin sand cap H_s = 0.5 m is constructed, the required s_u = 26 kPa for a 1 m improved layer thickness with FOS = 1.

This conceptual model is similar to the case of a 2-layer clay soil (the applied load is the sand cap load) in which a stronger clay layer (improved layer) is placed over a soft clay layer (tailings). The failure mechanism for this 2-layered soil bearing capacity depends on both the improved layer thickness and the relative strength of the two layers. Merifield at al. (1999) defined two failure mechanisms for this case; namely, partial and full punching shear through the strong layer. Full punching shear occurs when there is complete vertical separation of the top layer and the rigid soil column punches through the soft layer. Detailed analytical and numerical model (Finite Element Method – FEM) results were presented in studies by Chen (1975), Meyerhof and Hanna (1978), Merifield at al. (1999) and SoilVision (2016, 2017).

Table 2. Undrained shear strength of improved layer, s_u (kPa), for a critical FOS = 1 (Conceptual model #2): Centrifuged tailings-vane test

Improved Layer Thickness (m)	Sand Cap Thickness (m)				
	0.5	1	3	4	5
1	71.5	133.2	329.8	459.5	679.8
3	24.5	42.1	128.2 (117)*	190.2	276.7 (223)*
5	15.9	26.3	78.8 (74)*	126.1	167.2 (134)*
10	8.5	14.5	51.7	67.8	81.3
15	7.5	13.4	35.4	42.8	50.9

* Values in the brackets corresponds to 5 kPa of tailings

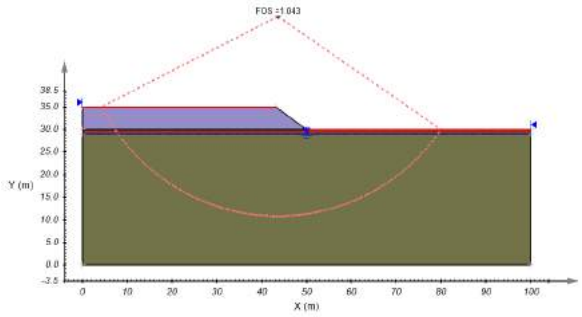

Figure 8. Typical critical slip surface of conceptual model #2

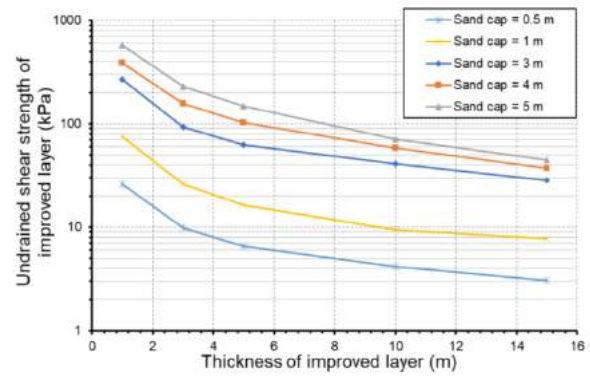

Figure 9. The relationship between improved layer thickness and undrained shear strength at various sand cap thickness for FOS = 1 (Conceptual model #2)

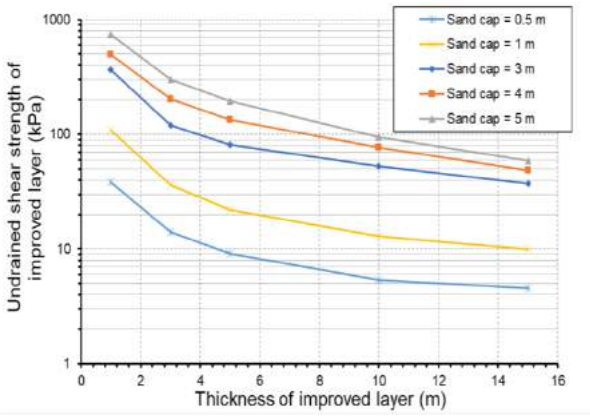

Figure 10. The relationship between improved layer thickness and undrained shear strength at various sand cap thickness for FOS = 1.3 (Conceptual model #2)

Conceptual Model #3

The typical critical slip surface for conceptual model #3 is shown in Figure 11. The results of this conceptual model are shown in Figure 12 (FOS = 1) and Figure 13 (FOS = 1.3). These figures clearly indicate that the required s_u is greater in this conceptual model due to the local steep slope (36°) (in comparison to the results of conceptual model #1 as presented in Figure 6 and Figure 7. These conceptual model results are generally insensitive to the thickness of the sand cap (between 3 m and 4 m).

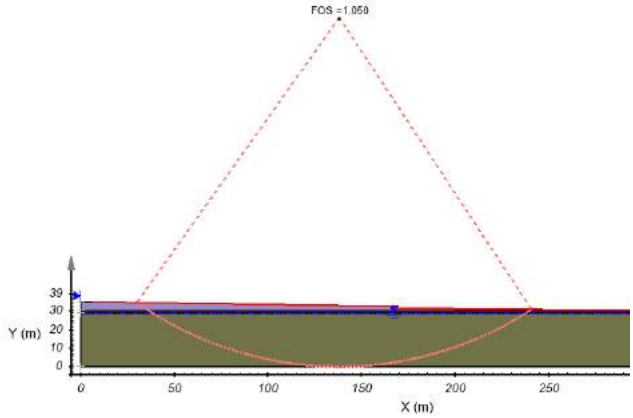

Figure 11. Typical critical slip surface of conceptual model #3

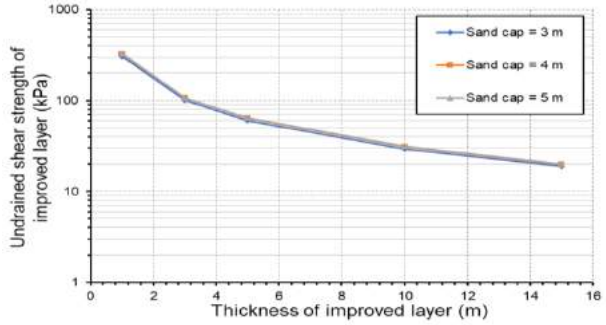

Figure 12. The relationship between improved layer thickness and undrained shear strength at various sand cap thickness for FOS = 1.0 (Conceptual model #3)

The required s_u is between 310 kPa and 330 kPa for a FOS = 1 (Figure 12) and between 420 kPa and 460 kPa for a FOS = 1.3 (Figure 13) With H_d = 1 m. As the values of H_d increase to 3 m, the required s_u reduces to around 110 kPa for a FOS = 1 and 150 kPa for a FOS = 1.3.

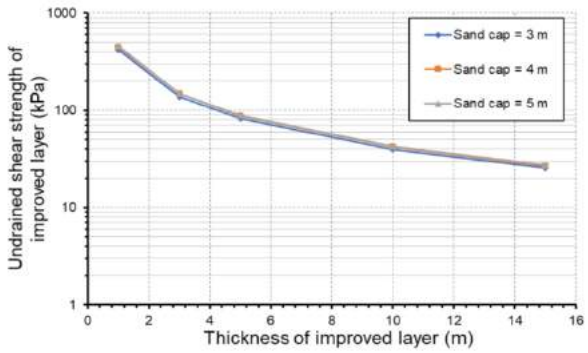

Figure 13. The relationship between improved layer thickness and undrained shear strength at various sand cap thickness for FOS = 1.3 (Conceptual model #3)

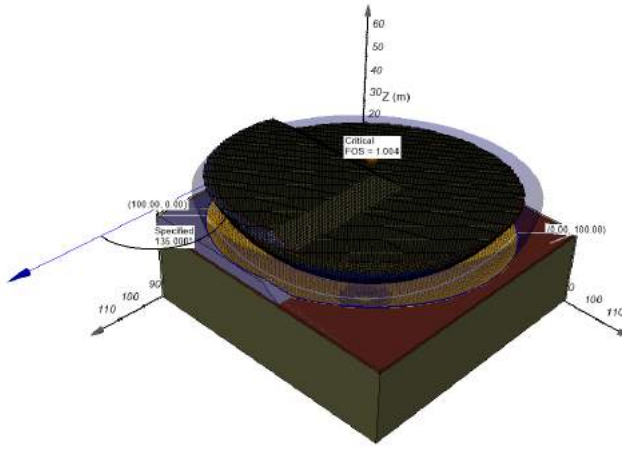

Figure 14. Typical critical slip surface of conceptual model #4

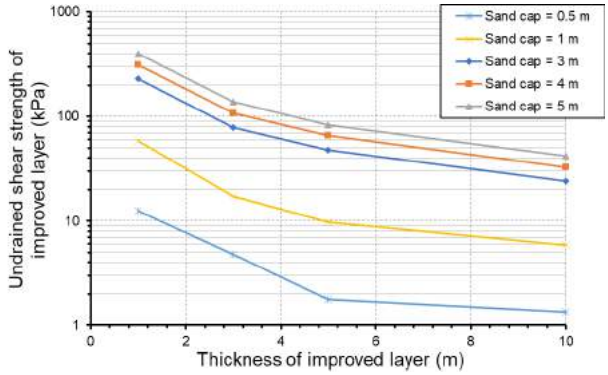

Figure 15. The relationship between improved layer thickness and undrained shear strength at various sand cap thickness for FOS = 1 (Conceptual model #4)

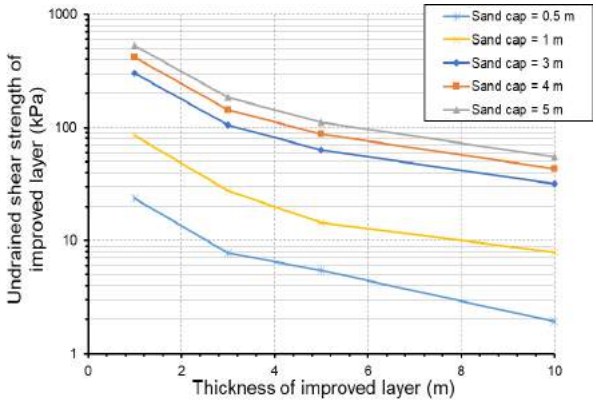

Figure 16. The relationship between improved layer thickness and undrained shear strength at various sand cap thickness for FOS = 1.3 (Conceptual model #4)

Conceptual Model #4

The typical critical slip surface for conceptual model #4 is shown in Figure 14. The results of this conceptual model are shown in Figure 15 (FOS = 1) and Figure 16 (FOS = 1.3).

This conceptual model is a 3-D extension of conceptual model #2 with the sand cap constructed in one quadrant of the geometry. The relationship between improved layer thickness and improved layer undrained strength are non-linear and the slope changes significantly at H_d = 3 m. With H_d = 1 m and a FOS = 1, the required s_u varies significantly from 13 kPa to 400 kPa for sand cap thickness from 0.5 m to 5 m, respectively (Figure 15). For a FOS = 1.3, the required s_u increases to 24 kPa and 530 kPa for sand cap thickness from 0.5 m to 5 m, respectively (Figure 16). With H_d = 3 m, the required s_u values are from 5 kPa to 140 kPa for a FOS = 1 and from 8 kPa to 184 kPa for a FOS = 1.3.

In general, the 2-D slope analysis (that assumes plane strain conditions) yields a conservative FOS (Duncan, 1992 cited by Stark, 2012) in comparison to 3-D results. The values for the ratio of the 3-D/2-D factors of safety can generally vary between 1.17 and 1.72 (or 17% to 72% higher). In the majority of cases the values vary between 1.17 and 1.5 (17% to 50% higher). These values are consistent with an increase of 29% obtained by Gitirana et al. (2008). Reyes and Parra (2014) reported the 3-D/2-D FOS ratio around 1.18 in the slope analysis of a mine waste dump using the SVSLOPE 2D/3D software. An extensive study conducted by Chaudhary et al.

(2016) for convex, concave and planar 3-D slope showed that the increase in FOS was from 10% to 40%, with the 3-D FOS for concave slopes showing increases greater than those of convex slopes.

DISCUSSIONS OF THE RESULTS

There are several processes that can increase the thickness and strength of the improved (or densified) layer, (e.g. freeze-thaw cycles, evaporative drying or accelerated consolidation using wick drains). Under freeze-thaw cycles the micro-structure of tailings changes due to formation of ice during freezing. Upon thawing, the water from the ice thaws and drains away to decrease the water content and increase shear strength, permeability and solids content. The post-thaw tailings is over-consolidated and the effective stress path during freeze-thaw cycles was described by Nixon and Morgensterm (1973). Caldwell et al. (2014) found that the peak undrained shear strength of post-thaw tailings can reach from 8 to 12 kPa under proper drainage of the thaw-water. With the increased undrained shear strength, the post-thaw tailings is still considered to be a very soft clay (Table 3). Under the climatic conditions in Fort McMurray, Alberta, the maximum freezing depth would be between 1 m and 1.5 m depending on the solids content. When the solids content is higher, the freezing depth is greater. With increased thickness and strength caused by the freeze-thaw cycles, the maximum calculated sand cap thickness is around 1 m for conceptual model #4.

Another physical process that can increase the shear strength of the tailings surface is surface evaporation. Using thin-lift drying method of polymer-flocculated MFT, Caldwell et al. (2014) reported that a densified layer thickness between 0.5 m to 0.75 m could be achieved. A field measurement of peak undrained shear strength of densified centrifuged deposit has been shown to reach 15 kPa. The improved layer thickness and undrained shear strength due to evaporation are somewhat similar due to freeze-thaw cycles.

In summary, both freeze-thaw process and evaporative drying can produce an improved layer thickness of around 1 m and a peak undrained shear strength around 12 kPa. To achieve a greater improved layer, wick drains installation or mixing centrifuge deposit with sand may be required (Ansah-Sam et al. 2018).

Table 3. Strength of clay (Das and Sobhan 2013, Lambe and Whitman 1969)

Consistency	Undrained Shear Strength (kPa)
Very soft	< 12.5
Soft	12.5 – 25
Medium	24 – 50
Stiff	50 – 100
Very Stiff	100 – 200
Hard	> 200

SUMMARY AND CONCLUSIONS

LEM analyses were used to determine the thickness of an improved layer and required undrained shear strength for various sand cap thicknesses. The 2-D conceptual models (#1, #2 and #3) and the 3-D conceptual model (#4) were simulated using a LEM sensitivity analyses. The sand cap thicknesses used in the conceptual models were up to 5 m and the improved layer thickness was up to 15 m.

- In the case of the 2-D conceptual model #1 (Figure 1), with an improved thickness H_d = 1 m, the required s_u is between 207 kPa and 250 kPa for a FOS = 1 and between 290 kPa and 360 kPa for a FOS = 1.3. When H_d increases to 3 m, the required s_u reduces to between 68 kPa and 83 kPa for a FOS = 1; and between 96 kPa and 117 kPa for a FOS = 1.3. The analysis is largely insensitive to sand cap thicknesses between 3-5 m.

- For a sand cap of 3 m for the 2-D conceptual model #2, the required s_u varies between 270 kPa (H_d = 1 m) and 28 kPa (H_d = 15 m) for a FOS = 1; and between 365 kPa (H_d = 1 m) and 37 kPa (H_d = 15 m) for a FOS = 1.3. When a thin sand cap, H_s = 0.5 m is constructed, the required s_u = 26 kPa for 1 m improved layer thickness with a FOS = 1. The required s_u decreases marginally with a 5 kPa assumed strength of the centrifuged mine tailings.

- With H_d = 1 m for the 2-D conceptual model #3, the required s_u is between 310 kPa and 330 kPa for a FOS = 1 (Figure 12) and between 420 kPa

and 460 kPa for a FOS = 1.3 (Figure 13). As the values of H_d increased to 3 m, the required s_u reduces to around 110 kPa for a FOS = 1 and 150 kPa for a FOS = 1.3

- For the 3-D conceptual model #4, H_d = 1 m and FOS = 1, the required s_u varies significantly from 13 kPa to 400 kPa for sand cap thickness from 0.5 m to 5 m, respectively. For a FOS = 1.3, the required s_u increases to 24 kPa and 530 kPa for a sand cap thickness varying from 0.5 m to 5 m, respectively. With H_d = 3 m, the required s_u reduces from 5 kPa to 140 kPa for a FOS = 1 and from 8 kPa to 184 kPa for a FOS = 1.3.

The results from this study provide guidance for DDA1 facility which is planned for a minimum cap of 3 m. Results indicate that if construction is managed to maximise 3-D effects during mechanical or hydraulic capping, at least an improved layer of about 30 kPa (up to 10 m in the deposit) may be required to support a 3 m minimum sand cap. The impact of an improved layer to the underlying soft deposits needs to be considered prior to use of this guideline. Please note that the results will be different if there is a shear strength increase with depth due to consolidation in the deposit.

ACKNOWLEDGEMENTS

Sincere appreciation and thanks to Scott Martens and Catherine Isaka for their significant contribution to the work reported in this paper.

REFERENCES

Caldwell, J., Revington, A., McPhail, G. and Charlebois, L. (2014). Optimised seasonal deposition for successful management of treated mature fine tailings. In Proceedings of the 17th International Seminar on Paste and Thickened Tailings, Australian Centre for Geomechanics, Perth, pp. 371-379

Chaudhary, K., Domingos, V., Gitirana, G., Fredlund, M. and Lu, H. (2016). Three-Dimensional Slope Stability: Geometry Effects. Tailings and Mine Waste, Keystone, Colorado.

Chen, W. F. (1975). Limit Analysis and Soil Plasticity, Developments in Geotechnical Engineering. Elsevier Scientific Pub. Co. 638 pp.

Daliri, F., Jeeravipoolvarn, S. and Masala, S. (2015). Geotechnical behavior of oil-sands tailings. Obtained on May 18, 2017 at www.ptac.org/attachments/1648/download.
Das, B. M. and Sobhan, K. (2013). Principles of Geotechnical Engineering. Cengage Learning.

Duncan, J. M. (1992). State-of-the-Art: Static Stability and Deformation Analysis. Proceedings of Stability and Performance of Slopes and Embankments-II, ASCE, **1**: 222-266.

Gitirana, G. Jr., Santos, M. A. and Fredlund, M. (2008). Three-Dimensional Analysis of the Lodalen Landslide, GeoCongress 2008, March 9 - 12, 2008, New Orleans, LA, USA.

Merifield, R. S., Sloan, S. W. and Yu, H. S. (1999). Rigorous plasticity solutions for the bearing capacity of two-layered clays. Geotechnique, **49**(4): 471-490.

Meyerhof, G. G. and Hanna, A. M. (1978). Ultimate bearing capacity of foundations on layered soils under inclined load. Canadian Geotechnical Journal, **15**(4): 565-572.

Reyes, A. and Parra, D. (2014). 3-D slope stability analysis by the limit equilibrium method of a mine waste dump. In Proceedings 18th International Conference on Tailings and Mine Waste (pp. 257-271).

Stark, T. D. (2012). Three-dimensional slope stability methods in geotechnical practice. 51st Annual Geotechnical Engineering Conference, University of Minnesota.

Terzaghi, K., Peck, R. B. and Mesri, G. (1996). Soil Mechanics in Engineering Practice. John Wiley & Sons.

SAND CAPPING OF TREATED TAILINGS: INSIGHTS FROM FIELD TRIALS ON DDA1 CENTRIFUGE DEPOSITS

Monica Ansah-Sam[1], Adam Thompson[1], Ben Sheets[2] and Jim Langseth[2]
[1]Canadian Natural Resources Limited, Calgary, Canada
[2]Barr Engineering and Environmental Science Limited, Calgary, Canada

ABSTRACT

Hydraulic sand capping is a potentially economical and safe method to accelerate consolidation, trafficability, and reclamation of soft tailings in oil sands tailings basins. Compared to placing a sand cap through a water cover (raining or rainbowing), placing a cap subaerially on exposed treated soft tailings may reduce costs significantly and minimize risk from working over water. The sand slurry and soft tailings properties suitable for subaerial hydraulic capping, however, are poorly understood. We present insights gained from a series of coarse sand tailings (CST) placement trials conducted at the Canadian Natural Jackpine Mine in 2015, 2016, and winter 2017. The intent of these trials was to understand the interaction between CST and treated (centrifuged) soft tailings, and whether sand capping would be possible with relatively high-discharge rate and high-solids content of CST slurry. Analysis of the deposit conditions before and after the trials indicates that the predominant CST behaviour involves beach creation and mixing of sand into soft tailings, producing regions of densified soft tailings and mixed CST/soft tailings, which are stronger than the original deposit. The trials indicate that significant challenges exist with implementation of hydraulic capping technology, but provide important insight into the conditions necessary for success.

INTRODUCTION

The placement of centrifuge product into the Jackpine Mine (JPM) Dedicated Disposal Area (DDA1) is a component of reducing the fluid fine tailings inventory at JPM. This is part of the Canadian Natural Upgrading Ltd's (Canadian Natural) program to meet the requirements of the Tailings Management Framework (TMF) issued by the Government of Alberta in March 2015 (Ansah-Sam et al. 2017). The centrifuge product has average solids content of 45%, produced from fluid fine tailings (about 25% solids) dredged from a tailings pond at JPM. The centrifuged material is being deposited in an external tailings facility to create a deep deposit at the JPM DDA1. Additional details on the centrifugation process at JPM are provided in Graham et al. (2016).

Characterization of tailings deposits provides necessary information to support reclamation and closure designs (Ansah-Sam et al. 2016). Annual tailings investigations have been conducted since the start of centrifuge operations in 2013 at JPM DDA1 to monitor the volume and material properties of the centrifuged tailings deposit (centrifuge deposit), and also to assess the potential to co-deposit sand and thickened tailings with the centrifuge deposit. The annual tailings investigations also provide an understanding of the historic behavior and current conditions, as well as the ability to predict the long-term geotechnical behaviour of the deposit. Another step towards the closure and reclamation goal for the JPM DDA1 was to understand the feasibility of sand capping of the centrifuge deposit.

In general, the main goals of placing a cap are:

1. Enhance consolidation (provide load, manage release water etc.);
2. Provide and maintain long and short-term trafficability (allow access for placement of other loads; allow access for wick drains installation etc.);
3. Provide a buffer between the reclamation cover and the deposit;
4. Manage surface water;
5. Provide nutrients for plants and animals; and
6. Minimize acid mine or rock drainage, by creating water-capped deposits or end pit lakes.

The first and second points are the main geotechnical drivers for successful sand placement on treated tailings deposits (Ansah-Sam et al. 2017).

Canadian Natural identified hydraulic and mechanical sand capping as a technical gap when the base technology in the tailings plan was

changed from non-segregated tailings to centrifuge product. Three areas of opportunity were discussed:

- Hydraulic capping of centrifuge at DDA1;
- Mechanical capping of Atmospheric Fines Drying (AFD) Deep Stack; and
- Capping of 5 m Centrifuge Test Cell.

deposition of CST over and into the centrifuged material. In addition, modelling studies were also performed to evaluate mechanical and hydraulic sand placement methods, and the JPM DDA1 was identified for subsequent hydraulic sand placement trials.

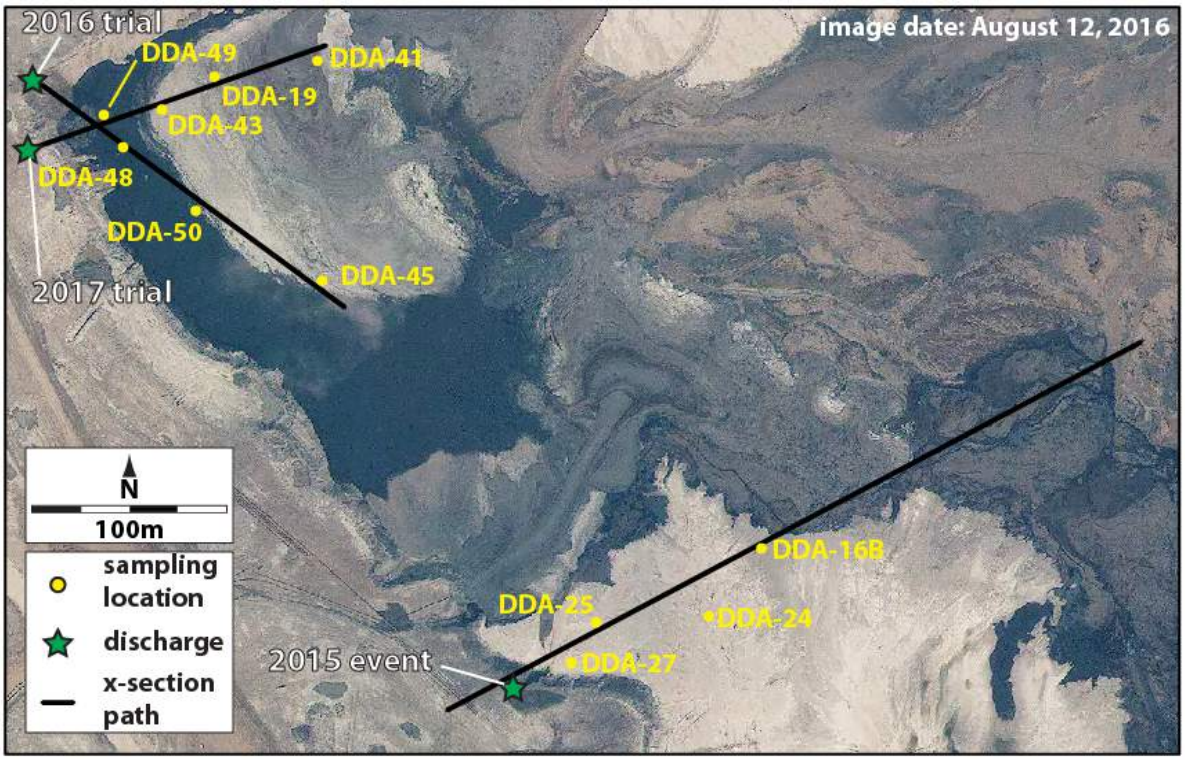

Figure 1. JPM DDA1 aerial photograph showing locations of event/trial discharges, sampling locations, and cross-section transects for Figure 2

Prior to these areas of opportunity being identified, an opportunistic overboard event with Coarse Sand Tailings (CST) occurred. In October 2015, CST was poured over and into the centrifuge deposit along the western margin of DDA1. Based on observations and sampling of deposits associated with this event, significant mixing occurred between the CST and centrifuge deposit, producing a mixed deposit with higher strength and solids content than pure centrifuge deposit. A CST beach was formed, and in some areas a CST cap appeared to have formed over the centrifuge deposit that was not displaced by the CST.

These results provided further justification for a program to investigate the potential for capping, mixing, or increasing the strength and solids content of the centrifuge deposit via intentional

Two additional trials were conducted, a summer 2016 capping trial, and a winter 2017 capping trial (from two discharge locations). These trials (along with the 2015 event) are summarized in Table 1.

The DDA1 deposits were physically sampled and tested with cone penetration testing (CPT) during the annual investigation program in 2015, 2016, and 2017. In addition to standard annual sampling, supplementary sampling and testing was completed after the summer 2016 and winter 2017 trials. Comparison between pre-trial and post-trial deposit characteristics was made using recurrent sampling locations before and after the trials. The centrifuged material added between trials was assumed to have properties consistent with those observed in areas undisturbed by the trial.

Table 1. Capping event summary

Event	Duration (hr.)	CST Slurry Volume (m^3)	Deposition Conditions
2015 Oct. 24	6	45,000	CST overboarding onto centrifuge deposit
2016 Aug. 24-25	7	54,000	CST multi-port outfall trial onto centrifuge deposit
2017 part 1 Mar. 21-22	14	107,000	CST spoon outfall trial onto ice-covered centrifuge deposit
2017 part 2 Mar. 29	5	30,000	CST multi-port outfall trial onto ice-covered centrifuge deposit

Tailings Property Definitions

For the purposes of this paper, we defined three types of deposit:
1. "Pure" centrifuge deposit;
2. CST beach; and
3. Mixed deposit of centrifuge product and CST.

Figure 2 shows shaded interpretation of post-trial deposits into these broad categories.

In general, pure centrifuge deposits are characterized by fines content in excess of 90% and solids content between 40 and 50%, as shown in the data from sampling location DDA-45 in the middle panel of Figure 2. Centrifuge deposit typically shows strength less than 1 kPa, and SFR well below 1 (approx. 0.1).

CST beach deposits comprise almost exclusively sand with minimal fines, showing fines contents below 10%, as indicated in sampling location DDA-24 on the top panel of Figure 2. Solids content typically exceeds 75%. The CST beach has strength, typically exceeding a friction angle of 31, with sand to fines ratio (SFR) values of 13 and higher.

Between centrifuge deposit and CST beach, the mixed zones show intermediate, and variable with depth, values of all parameters. Sampling location DDA-16B, on the top panel of Figure 2, shows a good example of mixed deposits. These mixed deposits are characterized by variable fines and solids contents, strength, and SFR that reflect their origin as combinations of CST and pure centrifuge deposit. Most importantly, however, these deposits have strength significantly higher than pure centrifuge deposit; often several kPa, with modest increase in sand content over pure centrifuge deposit.

CST CAPPING EVENTS AND TRIALS

2015 Overboard Event

The CST over boarding opportunity, in which dyke-construction CST was released onto the centrifuge deposit, occurred on October 24, 2015 along the western edge of DDA1 (see Figure 1 for location). The event lasted approximately 6 hours, and released an estimated 45,000 m^3 of CST slurry. A representative cross section of the resulting deposit conditions in DDA1 is shown on Figure 2.

2015 Overboard Event Observations

In areas where there was CST discharge onto the centrifuge deposit, a significant portion of the centrifuge deposit was displaced and was pushed farther out into the pond. The CST discharge also caused both mixing and interlayering of CST and centrifuge deposit, which led to increased deposit strength in certain areas. Significant capping of 'pure' centrifuge deposit was not observed, though sampling indicated that some CST deposited over a mixture of sand-enriched centrifuge deposit towards the distal extent of CST sand at sampling location DDA-16B (Figure 2).

The overall deposit geometry resulting from the 2015 overboarding event shows that introduction of CST led predominantly to displacement of pre-existing centrifuge deposit. However, introduction of sand to the centrifuge deposit led to the creation of a significant mixed zone, which extends many tens of metres in length along the primary direction of deposition, and over the entire 5 m depth of the pre-existing centrifuge deposit. These mixed deposits are significantly stronger than the pre-existing centrifuge deposit.

2016 Capping Trial

As noted above, the presence of significantly mixed deposits with improved reclamation characteristics compared to pure centrifuged deposits was a promising result. In order to better understand the potential of sand introduction to centrifuge deposits, CST was discharged from a

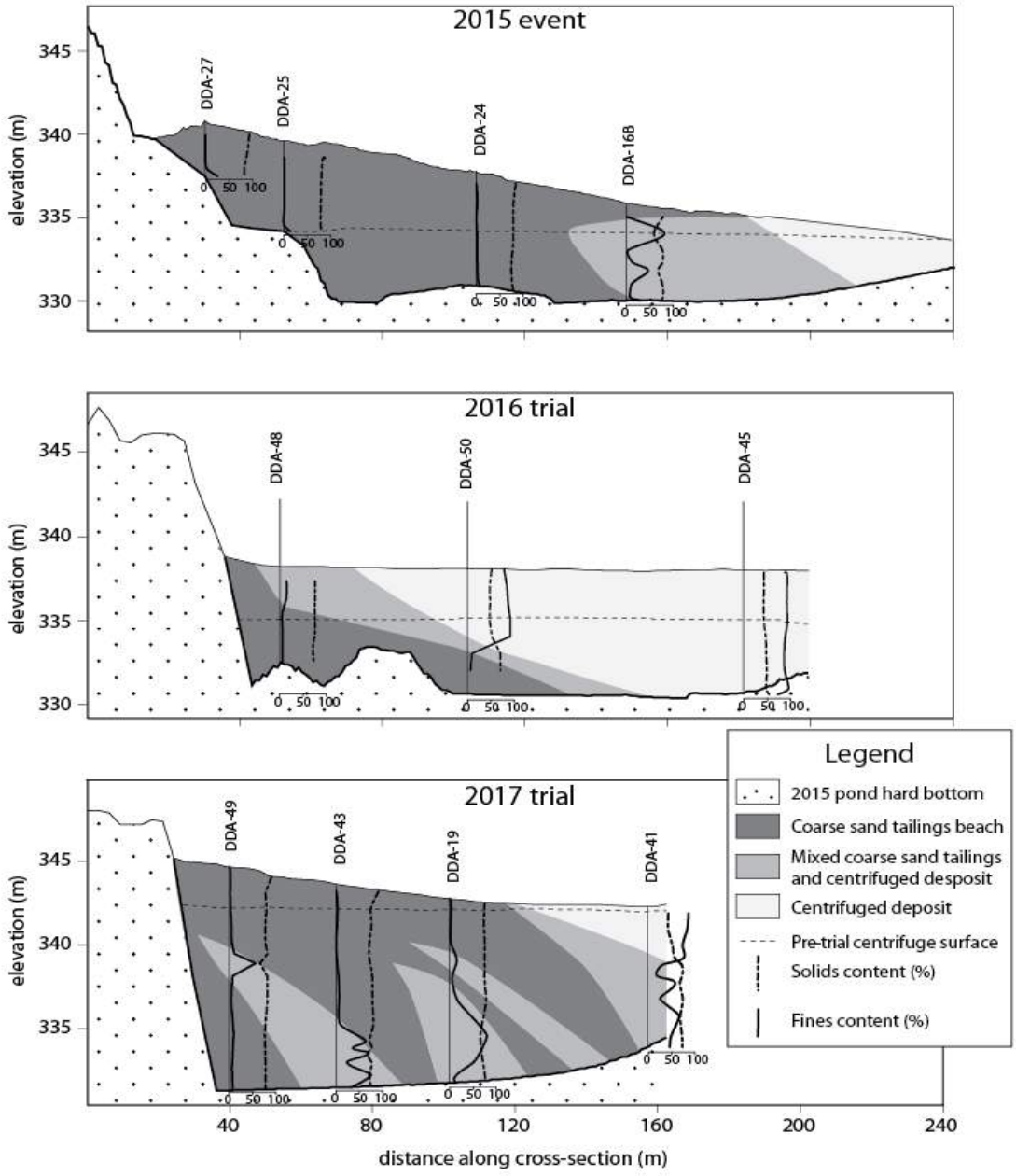

Figure 2. Cross-sections along predominant flow direction for the 2015, 2016, and 2017 trials. Cross-section locations shown in Figure 1

multi-port diffuser into the northwest corner of DDA1 (Figure 1) at 7700 m^3/hr. for approximately seven hours (split over the course of August 24 and 25, 2016).

The middle panel of Figure 2 shows a simplified cross-section through the northwest corner of DDA1, approximately along the primary direction of CST flow during the 2016 trial.

2016 Capping Trial Observations

As shown on Figure 2, and discussed in greater detail by Ansah-Sam et al. (2017), CST formed a sand-dominated beach near the discharge, which

extended below and displaced the centrifuge deposit. A mixed zone was formed overlying the CST and underlying the centrifuge deposit. In the mixed zone, sand concentrations diminish with distance from the discharge. The mixed zone overlying the CST is thickest near the discharge and tapers with distance into the pond. The wedge of mixed material was, in turn, overlain by centrifuge deposit. The mixed material showed a higher solids content and strength than pure centrifuge deposit.

The post 2016 trial sampling did not show significant capping of centrifuge deposit with CST. In assessing the conditions that produce capping or mixing for a centrifuge deposit such as this, Ansah-Sam et al. (2016) showed that mixing behaviour is strongly related to the relative bulk density of the materials, as well as pre-existing deposit strength (correlated with solids content). In this trial, the CST bulk density ranged between 1,520 to 1,664 kg/m^3 which were approximately 54 to 63% solids content. The centrifuge deposit bulk density was 1,400 kg/m^3 which is approximately 46% solids content. Ansah-Sam et al. (2016) concluded through observations and numerical modeling that:

1. If CST density is greater than centrifuge density, the CST will plunge and create a mixed zone along the margins of the CST beach,
2. Significant strengthening of the deposit occurs when sand is mixed with the centrifuge deposit,
3. A CST stream of this density likely would cap the centrifuge deposit if the deposit had a minimum of 65% solids content (based on centrifuge deposit density required to support CST), and
4. When CST bulk density is less than centrifuge deposit density, a cap can form, with a mixed zone immediately below.

2017 Winter Capping Trial

The objective of the winter 2017 CST pour was to test the potential to cap an ice-covered centrifuge deposit and also potentially frozen centrifuge deposit. Trials with two separate outfall systems were performed with a “spoon” and a multi-port diffuser outfall. Approximately ½ m of ice-cover was present on the centrifuge deposit during the trials.

On March 21-22, 2017, CST was discharged using a spoon outfall near the northwest corner of DDA1 (see Figure 1). The CST flowrate averaged about 7,480 m^3/hr. and ran for 14 hours and 20 minutes. The total volume of CST slurry was 107,000 m^3, with an average density of 1,626 kg/m^3 which provided an estimated 103,000 tonnes of sand. The average air temperature was -6.4°C on March 21 and -1.8°C on March 22.

CST was observed to plunge through the ice and into the centrifuge deposit within 10 minutes of start of CST slurry discharge. The beach at the outfall expanded, and after about ½ an hour, water streams emerged through holes 30 to 40 m from the outfall. On March 29, 2017, CST was discharged using a multi-port diffuser outfall. The CST flowed at 6,100 m^3/hr. for 4 hours and 48 minutes. The total volume discharged was 30,000 m^3 at an average density of 1,600 kg/m^3, delivering 27,000 tonnes of sand. The average air temperature on March 29 was 4.5°C, though the centrifuge deposit remained ice-covered.

The CST was observed to briefly ‘run’ over the ice, but then began to plunge into the centrifuge deposit at the outfall.

2017 Winter Capping Trial Observations

The lower panel of Figure 2 shows the typical outcome of the 2017 trial: the CST plunged into the centrifuge deposit, displacing, rearranging, burying, and mixing with the prior materials. In general, the CST did not cap the centrifuge deposit in a conventional way, and there is no evidence that the CST ran over the ice for any extended distance. However, the mixed deposits formed in this trial are found not only above the CST beach, but interlayered between CST-dominated zones.

The winter 2017 trial did not achieve any significant capping of centrifuge deposit, despite the presence of an ice cap. In addition to the deposit sampling results shown on Figure 2, which indicate plunging of sand, field observations during the trial suggested that the relatively warm and dense CST was able to plunge through the ice cap quickly. The reasons for this have not been fully evaluated, but it is most likely that the high CST density and deposition rate was not supported by the thickness of the ice cap. Thermodynamic computations suggest that temperature difference alone is not sufficient to explain the observed behaviour.

DISCUSSION

The three trials presented above suggested a number of general behaviours, regardless of whether conventional capping was achieved. What was observed was that, whether or not hydraulically placed sand forms a cap over a pre-existing soft tailings deposit, a mixed deposit of centrifuge and sand is a likely outcome. The properties of these mixed deposits are considerably better from a reclamation perspective than those of the original soft tailings deposit.

The geometry of the mixing zones observed in these trials depended on trial duration, with the shorter trials (2015, 2016) leading to relatively simple wedge-like geometries situated above an evolving CST beach. In contrast, the longer-duration (2017 trial) led to a more complex interlayering of CST and mixed deposits. This interlayered pattern suggests development of processes not obvious in the 2015 and 2016 trials.

One possibility is that the 2017 system evolved over a long enough time, and was spatially large enough, that channelization of flow across the CST beach led to alternate periods of rapid sand delivery and relative quiescence. This phenomenon is common in distributary sediment depositional systems, such as river deltas, where sandy coarse layers inter-finger and alternate with layers of finer-grained silt and mud-sized grains.

An additional consequence of this more complex interaction is a more variable character in the 2017 mixed zones when compared with the shorter trials. Figure 3 shows a detail of sampling location DDA-43, in which the upper 7 – 8 metres comprise a CST beach. Below the CST, however, a mixed layer is found, in which several data points show both high fines content and high solids content, such as that just above elevation 332 m. These layers are interspersed with mixed layers of deposit similar to those found in the 2015 and 2016 trials, where fines contents are below 50%.

This observation suggests that the more complex mixing environment of the longer 2017 test led to not only mixing of CST sand into centrifuge deposit, but also trapping and densification of high-fines content centrifuge deposit. While pure centrifuge deposit typically shows solids content of 50% and below, these densified layers show solids contents in excess of 70%.

Capping Feasibility

Despite a lack of observed capping in these trials, subaerial hydraulic capping seems promising, and should be considered at centrifuge deposit solids contents above 65%, even with the CST slurry bulk density seen in these trials (Ansah-Sam et al. 2016). This previous finding is corroborated by the presence of CST beach over mixed and densified centrifuge deposit observed in the 2017 trial.

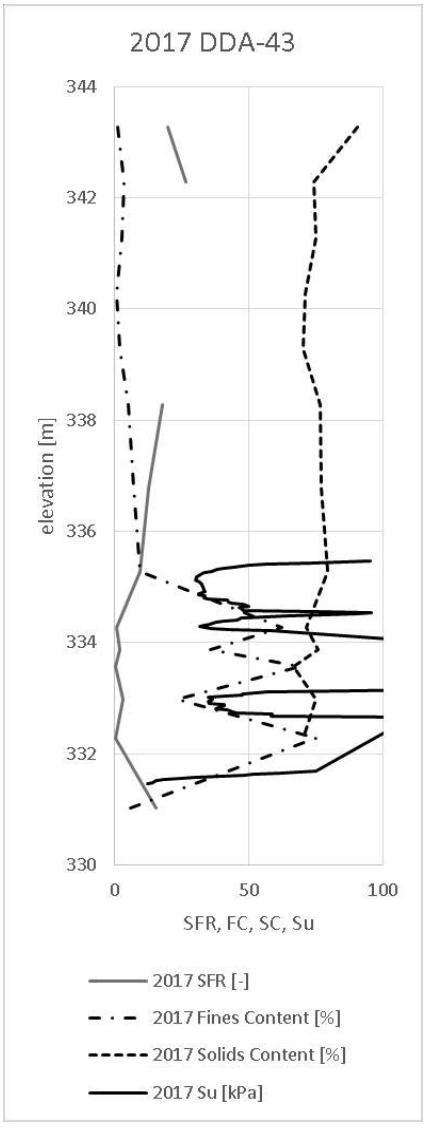

Figure 3. 2017 Sampling and CPT data from location DDA-43. Note that solids and fines content also appear on the lower panel of Figure 2

In the absence of attaining a higher solids content centrifuge deposit, other approaches to making hydraulic capping practical include making the CST slurry less dense and/or making the surface of the centrifuge deposit tougher. It is likely that multiple techniques would have to be combined to achieve robust hydraulic capping of centrifuge deposit.

The bulk density of the capping slurry could be reduced by lowering the slurry sand content and/or using lower specific gravity granular material in the slurry (e.g., coke, a silt slurry, or substitution of lightweight fibres in a portion of the sand slurry). Ideas for toughening the centrifuge deposit surface include allowing for desiccation, promoting vegetation growth, mixing a modest quantity of sand into the surface via sand raining, or having a thicker ice layer before placing a cap.

One promising approach suggested by the trials discussed in this study is that the centrifuge deposit could be strengthened by mixing in CST, such that a 'true' cap could be placed later. As seen in the 2017 trial, mixing is more complex, and possibly more effective using cyclic deposition. Such complexity could be promoted via "natural" alternation, as was observed here, or intentional movement of discharge points.

It is possible that other outfall designs could be used to moderate the focusing and plunging of CST observed in these trials, for instance, an outfall system that more effectively spreads the capping slurry over a wide area. However, as long as the local bulk density of the CST exceeds that of the centrifuge deposit, mixing and plunging of the CST will be difficult to avoid.

As with any technology development, the above concepts would be better understood and implemented after lab-scale tests and numerical modelling to determine conditions likely to succeed. The most successful options should be pilot tested in the field to overcome laboratory scale limitations. Laboratory testing would help explain the relationship between CST bulk density, discharge rate, and centrifuge deposit characteristics that could lead to capping, as the trials presented here only proved a handful of data points describing the plunging case.

A range of challenges will remain even after demonstrating that CST can cap the centrifuge deposit, particularly if systems to cap a weak centrifuge deposit are pursued. These challenges include developing effective approaches to hydraulic placement, such as placing sand in desired locations, addressing the distance the sand can effectively advance over a deposit, and the practicalities of deploying the sand distribution system. Other challenges include getting consistent flows and densities from the plant to match the needs of the capping program and managing the excess water from hydraulic cap placement.

CONCLUSIONS

The intent of these trials was to assess the potential effectiveness of sand capping by CST, and resultant improvements in deposit density, solids content, or strength. Only minimal capping was observed, but significant mixing of sand with centrifuge deposit occurred. The properties of these mixed deposits are significantly better from a reclamation perspective relative to pure centrifuge deposit.

The overall findings of these trials are:

1. The capping trials did not result in significant capping of centrifuge deposit with CST, regardless of end of pipe device or with the presence of ice cover. Rather, there was beach formation and mixing.

2. The absence of capping behaviour is due to two aspects of these trials: The CST delivery was too rapid for soft tailings to support the sand plunging; and the CST at normal solids content (60% +/-) was too dense to be supported by lower bulk density centrifuge deposit (40 – 50% solids content).

3. Mixed CST and centrifuge deposits were stronger and had higher solids content than centrifuge deposit alone. The mixed deposit generally exceeded 10 kPa strength, with some as low as 5 kPa when centrifuge deposit was predominant in the mix.

4. In the longer-duration 2017 trial, complex mixing patterns led to trapping and densification of centrifuge deposit.

5. The mixing zone geometry can be expected to relate to pour duration and soft tailings strength, with the longer-duration trial showing more complex inter-fingering between CST beach and mixed deposits. The shorter-

duration trials showed a simpler wedge-shaped mixing zone adjacent to the CST beach.

6. Capping of centrifuge deposit should be possible via some combination of reduced-density CST slurry, strengthened centrifuge deposit, or careful management of sand delivery onto the centrifuge deposit.

7. There is a significant argument that a mixed deposit of centrifuge and sand can be capped compared to a 'pure' centrifuge deposit.

ACKNOWLEDGEMENT

Sincere appreciation and thanks to Scott Martens for his contribution to the work reported in this paper.

REFERENCES

Ansah-Sam, M., Hachey, L., McKenna, G. and Mooder, B. (2016). The DBM approach for setting engineering decision criteria for an oil sand mine closure plan, in: D. Sego, N. Beier, and G.W. Wilson (eds.). Proc. 5th International Oil Sands Tailings Conference, Lake Louise, Alberta, Canada, Dec. 4-7, 2016, 163-167p.

Ansah-Sam, M., Sheets, B., Langseth, J., Sittoni, L. and Hanssen, J. (2017). *Delft3D Modelling of Sand Placement on an Oil Sands Treated Tailings Deposit*. Tailings and Mine Waste Conference, Nov. 6-8, 2016. Banff, Alberta. 10p.

Graham, M., Bodtker, S., McMinn, N. and Wanstrom, C. (2016). Pipeline transport of centrifuge product, in: D. Sego, N. Beier, and G.W. Wilson (eds.). Proc. 5th International Oil Sands Tailings Conference, Lake Louise, Alberta, Canada, Dec. 4-7, 2016, 387-393p.

The Oil Sands Tailings Research Facility (OSTRF) was established in 2003 as a direct response to the global need for improved tailings management. Through extensive interaction and collaboration with other distinguished research groups, the OSTRF provides the novel research required to develop environmentally superior tailings disposal options. With the flexibility to support concurrent interdisciplinary research projects, the facility attracts the brightest minds in the field and trains early-career, technically competent scientists and engineers—the future leaders, consultants and regulators for the oil sands industry. The OSTRF is pioneering the way to innovative, environmentally conscientious solutions for future generations.

Drs. Nicholas A. Beier, G. Ward Wilson and David C. Sego, through the OSTRF, lead instrumental initiatives to bring together academia, industry and government agencies to find environmentally sustainable solutions for oil sands development. One such initiative is the International Oil Sands Tailings Conference (IOSTC), which is held every two years, and provides a forum for mine waste managers, engineers, regulators and researchers to present new ideas and to discuss the latest developments in the field.

The Sixth International Oil Sands Tailings Conference offers the most recent developments in oil sands tailings and management through invited speakers and select technical presentations. IOSTC'18 will also feature research from the NSERC/COSIA Senior Industrial Research Chair (IRC) in Oil Sands Tailings Geotechnique held by Dr. G. Ward Wilson. The IRC enables the oil sands industry to combine its efforts with those of leading researchers at the University of Alberta to develop novel technologies and methods to manage oil sands tailings in Alberta. The IRC program will advance the scientific community's fundamental understanding of the behaviour of fluid find tailings and mature fine tailings through focusing on the following research themes:

Theme 1: Unsaturated Soil Mechanics for Oil Sands Tailings Deposition
Theme 2: Consolidation Processes for Mature Fine Tailings
Theme 3: Assessing and Improving Tailings Deposition
Theme 4: Tailings Simulation Modelling and Long-term Behaviour of Fine Tailings

For more information about the University of Alberta Geotechnical Centre's current oil sand tailings research projects and initiatives, including the NSERC/COSIA IRC in Oil Sands Tailings Geotechnique, please visit www.ostrf.com or uab.ca/geotech.

International Oil Sands Tailings Conference

The UofA Geotechnical Centre

Proceedings cover photo courtesy of Syncrude Canada Ltd.